

EMERGING INFECTIOUS DISEASES®



Respiratory Infections

November 2023



Ralph Steadman (1936–) *Viral Menace*, 2020. Water, ink, and paint on paper, 35.25 in. x 24.5/89.5 cm x 62.23 cm. © Ralph Steadman Art Collections Ltd., Maidstone, Kent, England.

EMERGING INFECTIOUS DISEASES®

EDITOR-IN-CHIEF

D. Peter Drotman

ASSOCIATE EDITORS

Charles Ben Beard, Fort Collins, Colorado, USA
 Ermias Belay, Atlanta, Georgia, USA
 Sharon Bloom, Atlanta, Georgia, USA
 Richard Bradbury, Melbourne, Victoria, Australia
 Corrie Brown, Athens, Georgia, USA
 Benjamin J. Cowling, Hong Kong, China
 Michel Drancourt, Marseille, France
 Paul V. Effler, Perth, Western Australia, Australia
 Anthony Fiore, Atlanta, Georgia, USA
 David O. Freedman, Birmingham, Alabama, USA
 Isaac Chun-Hai Fung, Statesboro, Georgia, USA
 Peter Gerner-Smidt, Atlanta, Georgia, USA
 Stephen Hadler, Atlanta, Georgia, USA
 Shawn Lockhart, Atlanta, Georgia, USA
 Nina Marano, Atlanta, Georgia, USA
 Martin I. Meltzer, Atlanta, Georgia, USA
 David Morens, Bethesda, Maryland, USA
 J. Glenn Morris, Jr., Gainesville, Florida, USA
 Patrice Nordmann, Fribourg, Switzerland
 Johann D.D. Pitout, Calgary, Alberta, Canada
 Ann Powers, Fort Collins, Colorado, USA
 Didier Raoult, Marseille, France
 Pierre E. Rollin, Atlanta, Georgia, USA
 Frederic E. Shaw, Atlanta, Georgia, USA
 Neil M. Vora, New York, New York, USA
 David H. Walker, Galveston, Texas, USA
 J. Scott Weese, Guelph, Ontario, Canada

Deputy Editor-in-Chief

Matthew J. Kuehnert, Westfield, New Jersey, USA

Managing Editor

Byron Breedlove, Atlanta, Georgia, USA

Technical Writer-Editors

Shannon O'Connor, Team Lead;
 Dana Dolan, Thomas Gryczan, Amy Guinn,
 Tony Pearson-Clarke, Jill Russell, Jude Rutledge,
 Cheryl Salerno, P. Lynne Stockton, Susan Zunino

Production, Graphics, and Information Technology Staff

Reginald Tucker, Team Lead; William Hale, Tae Kim,
 Barbara Segal

Journal Administrators J. McLean Boggess, Alexandria Myrick,
 Susan Richardson (consultant)

Editorial Assistants Claudia Johnson, Denise Welk

Communications/Social Media Sarah Logan Gregory,
 Team Lead; Heidi Floyd

Associate Editor Emeritus

Charles H. Calisher, Fort Collins, Colorado, USA

Founding Editor

Joseph E. McDade, Rome, Georgia, USA

EDITORIAL BOARD

Barry J. Beaty, Fort Collins, Colorado, USA
 David M. Bell, Atlanta, Georgia, USA
 Martin J. Blaser, New York, New York, USA
 Andrea Boggild, Toronto, Ontario, Canada
 Christopher Braden, Atlanta, Georgia, USA
 Arturo Casadevall, New York, New York, USA
 Kenneth G. Castro, Atlanta, Georgia, USA
 Gerardo Chowell, Atlanta, Georgia, USA
 Christian Drosten, Berlin, Germany
 Clare A. Dykewicz, Atlanta, Georgia, USA
 Kathleen Gensheimer, College Park, Maryland, USA
 Rachel Gorwitz, Atlanta, Georgia, USA
 Patricia M. Griffin, Decatur, Georgia, USA
 Duane J. Gubler, Singapore
 Scott Halstead, Westwood, Massachusetts, USA
 David L. Heymann, London, UK
 Keith Klugman, Seattle, Washington, USA
 S.K. Lam, Kuala Lumpur, Malaysia
 John S. Mackenzie, Perth, Western Australia, Australia
 Jennifer H. McQuiston, Atlanta, Georgia, USA
 Nkuchia M. M'ikanatha, Harrisburg, Pennsylvania, USA
 Frederick A. Murphy, Bethesda, Maryland, USA
 Barbara E. Murray, Houston, Texas, USA
 Stephen M. Ostroff, Silver Spring, Maryland, USA
 Christopher D. Paddock, Atlanta, Georgia, USA
 W. Clyde Partin, Jr., Atlanta, Georgia, USA
 David A. Pegues, Philadelphia, Pennsylvania, USA
 Mario Raviglione, Milan, Italy, and Geneva, Switzerland
 David Relman, Palo Alto, California, USA
 Connie Schmaljohn, Frederick, Maryland, USA
 Tom Schwan, Hamilton, Montana, USA
 Wun-Ju Shieh, Taipei, Taiwan
 Rosemary Soave, New York, New York, USA
 Robert Swanepoel, Pretoria, South Africa
 David E. Swayne, Athens, Georgia, USA
 Kathrine R. Tan, Atlanta, Georgia, USA
 Phillip Tarr, St. Louis, Missouri, USA
 Duc Vugia, Richmond, California, USA
 Mary Edythe Wilson, Iowa City, Iowa, USA

Emerging Infectious Diseases is published monthly by the Centers for Disease Control and Prevention, 1600 Clifton Rd NE, Mailstop H16-2, Atlanta, GA 30329-4027, USA. Telephone 404-639-1960; email, eideditor@cdc.gov

The conclusions, findings, and opinions expressed by authors contributing to this journal do not necessarily reflect the official position of the U.S. Department of Health and Human Services, the Public Health Service, the Centers for Disease Control and Prevention, or the authors' affiliated institutions. Use of trade names is for identification only and does not imply endorsement by any of the groups named above.

All material published in *Emerging Infectious Diseases* is in the public domain and may be used and reprinted without special permission; proper citation, however, is required.

Use of trade names is for identification only and does not imply endorsement by the Public Health Service or by the U.S. Department of Health and Human Services.

EMERGING INFECTIOUS DISEASES is a registered service mark of the U.S. Department of Health & Human Services (HHS).

EMERGING INFECTIOUS DISEASES®

Respiratory Infections

November 2023



On the Cover

Ralph Steadman (1936–) *Viral Menace*, 2020. Water, ink, and paint on paper, 35.25 in x 24.5 / 89.5 cm x 62.23 cm]. © Ralph Steadman Art Collections Ltd. Maidstone, Kent, England

About the Cover p. 2411

Synopses



Campylobacter fetus Invasive Infections and Risks for Death, France, 2000–2021

C. fetus Bacteremia is associated with a high mortality rate, mainly among persons who are elderly, immunocompromised, or have underlying conditions.

S. Zayet et al.

2189

Congenital Mpox Syndrome (Clade I) in Stillborn Fetus after Placental Infection and Intrauterine Transmission, Democratic Republic of the Congo, 2008

D.A. Schwartz et al.

2198



Group A *Streptococcus* Primary Peritonitis in Children, New Zealand

We describe 20 pediatric cases from 2010–2022 and review the literature on previous cases.

A. Tayler et al.

2203

Detection of Novel US *Neisseria meningitidis* Urethritis Clade Subtypes in Japan

H. Takahasi et al.

2210

Clinical Manifestations and Genomic Evaluation of Melioidosis Outbreak among Children after Sporting Event, Australia

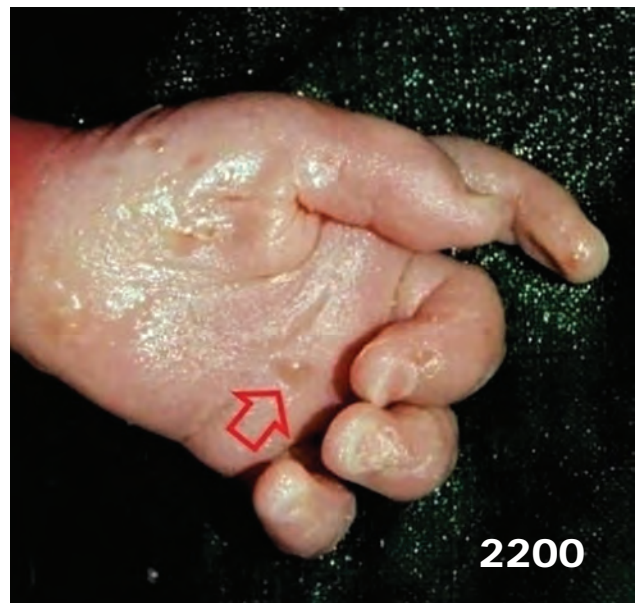
S. Smith et al.

2218

Outbreak of *Pandoraea commovens* Infections among Non–Cystic Fibrosis Intensive Care Patients, Germany, 2019–2021

T. Kruis et al.

2229



2200



Research

- Micro-Global Positioning Systems for Identifying Nightly Opportunities for Marburg Virus Spillover to Humans by Egyptian Rousette Bats**
B.R. Amman et al. 2238
- Global Phylogeography and Genomic Epidemiology of Carbapenem-Resistant *bla*_{OXA-232}-Carrying *Klebsiella pneumoniae* Sequence Type 15 Lineage**
Y. Wu et al. 2246
- SARS-CoV-2 Reinfection Risk in Persons with HIV, Chicago, Illinois, USA, 2020–2022**
R.A. Teran et al. 2257
- Evolution of *Klebsiella pneumoniae* Sequence Type 512 during Ceftazidime/Avibactam, Meropenem/Vaborbactam, and Cefiderocol Treatment, Italy**
G. Arcari et al. 2266
- Neurologic Effects of SARS-CoV-2 Transmitted among Dogs**
D.-H. Kim et al. 2275
- Environmental Persistence and Disinfection of Lassa Virus**
M. Shaffer et al. 2285



EMERGING INFECTIOUS DISEASES®

November 2023

- Simulation Study of Surveillance Strategies for Faster Detection of Novel SARS-CoV-2 Variants**
S. Patel et al. 2292
- Human Salmonellosis Outbreak Linked to *Salmonella* Typhimurium Epidemic in Wild Songbirds, United States, 2020–2021**
K. Patel et al. 2298
- Prevalence of Undiagnosed Monkeypox Virus Infections during Global Mpxv Outbreak, United States, June–September 2022**
F.S. Minhaj et al. 2307
- Duration of Enterovirus D68 RNA Shedding in the Upper Respiratory Tract and Transmission among Household Contacts, Colorado, USA**
H. Nguyen-Tran et al. 2315
- Risk Factors for Recent HIV Infections among Adults in 14 Countries in Africa Identified by Population-Based HIV Impact Assessment Surveys, 2015–2019**
D.W. Currie et al. 2325
- Systematic Review and Meta-Analysis of Deaths Attributable to Antimicrobial Resistance, Latin America**
A. Ciapponi et al. 2335
- ## Dispatches
- Monkeypox Virus in Wastewater Samples from Santiago Metropolitan Region, Chile**
M. Ampuero et al. 2345
- Three Cases of Tickborne *Francisella tularensis* Infection, Austria, 2022**
F. Heger et al. 2349
- Racial and Socioeconomic Equity of Tecovirimat Treatment during the 2022 Mpxv Emergency, New York, New York, USA**
M.K. Lash et al. 2353
- Hepatitis C Virus Elimination Program among Prison Inmates, Israel**
L. Eisen et al. 2358
- Trends of Enterovirus D68 Concentrations in Wastewater, California, USA, February 2021–April 2023**
A.B. Boehm et al. 2362
- Erythema Migrans Caused by *Borrelia spielmanii*, France**
P. del Giudice et al. 2366



Genetic Characterization of Extensively Drug-Resistant *Shigella sonnei* Infections, Spain, 2021–2022
C. Jacqueline et al. 2370

Research Letters

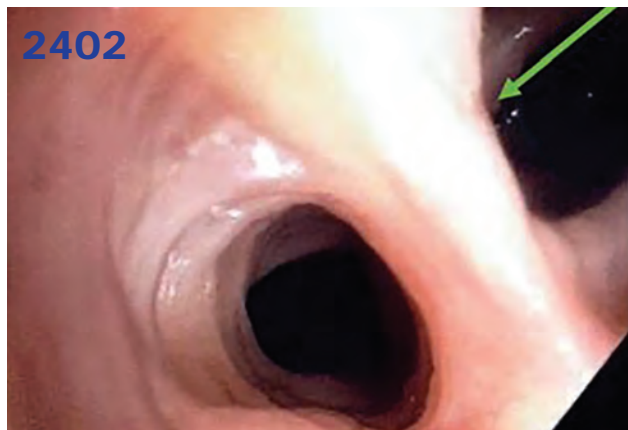
Severe *Rickettsia typhi* Infections, Costa Rica
D. Chinchilla et al. 2374

New SARS-CoV-2 Omicron Variant with Spike Protein Mutation Y451H, Kilifi, Kenya, March–May 2023
M.J. Mwanga et al. 2376

Genomic Sequencing Surveillance to Identify Respiratory Syncytial Virus Mutations, Arizona, USA
L.A. Holland et al. 2380

Domestically Acquired NDM-1–Producing *Pseudomonas aeruginosa*, Southern California, USA, 2023
H.K. Gray et al. 2382

***Plasmodium vivax* Prevalence in Semiarid Region of Northern Kenya, 2019**
W. Prudhomme O'Meara et al. 2385



Case Report and Literature Review of Prosthetic Cardiovascular Mucormycosis
B. Hoellinger et al. 2388

Changes in Group A *Streptococcus emm* Types Associated with Invasive Infections in Adults, Spain, 2023
A. Bellés-Bellés et al. 2390

SARS-CoV-2 Infection in Wrestlers after International Tournaments, April 2021
S.T. Kuribayashi et al. 2393

Case of Carbapenem-Resistant *Salmonella* Typhi Infection, Pakistan, 2022
S. Nizamuddin et al. 2395

Ceftazidime/Avibactam Resistance in Carbapenemase-Producing *Klebsiella pneumoniae*
Q. Cui et al. 2398

Refractory *Microascus* Bronchopulmonary Infection Treated with Olorofim, France
E. Faure et al. 2401

Tuberculosis Variant with Rifampicin Resistance Undetectable by Xpert MTB/RIF, Botswana
C. Modongo et al. 2403

***Scedosporium* Infection in Recipients of Kidney Transplants from Deceased Near-Drowning Donor**
D. Choudhary et al. 2406

Comment Letter

Investigation of Possible Link between Interferon- α and Lyme Disease
A. Alaedini et al. 2409

Books and Media

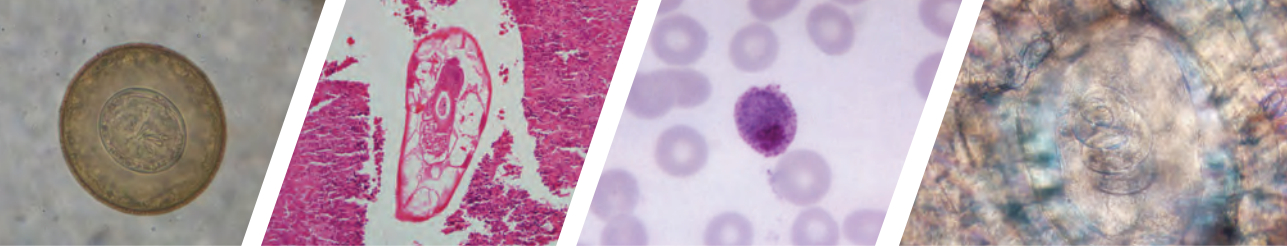
Viruses: A Natural History
S.S. Morse 2410

About the Cover

A Turbulent Cloud, a Viral Menace
B. Breedlove 2411

Correction

Vol. 29, No. 3 2410
The author order was incorrect in Multicenter Retrospective Study of Vascular Infections and Endocarditis Caused by *Campylobacter* spp., France



Diagnostic Assistance and Training in Laboratory Identification of Parasites

A free service of CDC available to laboratorians, pathologists, and other health professionals in the United States and abroad



Diagnosis from photographs of worms, histological sections, fecal, blood, and other specimen types



Expert diagnostic review



Formal diagnostic laboratory report



Submission of samples via secure file share

Visit the DPDx website for information on laboratory diagnosis, geographic distribution, clinical features, parasite life cycles, and training via Monthly Case Studies of parasitic diseases.

www.cdc.gov/dpdx
dpdx@cdc.gov



**U.S. Department of
Health and Human Services**
Centers for Disease
Control and Prevention

Campylobacter fetus Invasive Infections and Risks for Death, France, 2000–2021

Souheil Zayet, Timothée Klopfenstein, Vincent Gendrin, Jean-baptiste Vuillemenot, Julie Plantin, Lynda Toko, Nour Sreiri, Pierre-Yves Royer



In support of improving patient care, this activity has been planned and implemented by Medscape, LLC and Emerging Infectious Diseases. Medscape, LLC is jointly accredited with commendation by the Accreditation Council for Continuing Medical Education (ACCME), the Accreditation Council for Pharmacy Education (ACPE), and the American Nurses Credentialing Center (ANCC), to provide continuing education for the healthcare team.

Medscape, LLC designates this Journal-based CME activity for a maximum of 1.00 **AMA PRA Category 1 Credit(s)**[™]. Physicians should claim only the credit commensurate with the extent of their participation in the activity.

Successful completion of this CME activity, which includes participation in the evaluation component, enables the participant to earn up to 1.0 MOC points in the American Board of Internal Medicine's (ABIM) Maintenance of Certification (MOC) program. Participants will earn MOC points equivalent to the amount of CME credits claimed for the activity. It is the CME activity provider's responsibility to submit participant completion information to ACCME for the purpose of granting ABIM MOC credit.

All other clinicians completing this activity will be issued a certificate of participation. To participate in this journal CME activity: (1) review the learning objectives and author disclosures; (2) study the education content; (3) take the post-test with a 75% minimum passing score and complete the evaluation at <http://www.medscape.org/journal/eid>; and (4) view/print certificate. For CME questions, see page 2414.

NOTE: It is Medscape's policy to avoid the use of Brand names in accredited activities. However, in an effort to be as clear as possible, the use of brand names should not be viewed as a promotion of any brand or as an endorsement by Medscape of specific products.

Release date: October 17, 2023; Expiration date: October 17, 2024

Learning Objectives

Upon completion of this activity, participants will be able to:

- Distinguish the most common *Campylobacter* species isolated in a hospital record system
- Compare clinical characteristics among patients with *C. fetus* bacteremia and infection with *C. fetus* without bacteremia
- Identify the most common source of secondary localization of *C. fetus* infection
- Evaluate outcomes of *C. fetus* infection in the current study

CME Editor

P. Lynne Stockton Taylor, VMD, MS, ELS(D), Technical Writer/Editor, Emerging Infectious Diseases. *Disclosure:* P. Lynne Stockton Taylor, VMD, MS, ELS(D), has no relevant financial relationships.

CME Author

Charles P. Vega, MD, Health Sciences Clinical Professor of Family Medicine, University of California, Irvine School of Medicine, Irvine, California. *Disclosure:* Charles P. Vega, MD, has the following relevant financial relationships: served as an advisor or consultant for Boehringer Ingelheim Pharmaceuticals, Inc.; GlaxoSmithKline; Johnson & Johnson Pharmaceutical Research & Development, L.L.C.

Authors

Souheil Zayet, MD; Timothée Klopfenstein, MD; Vincent Gendrin, MD; Jean-baptiste Vuillemenot, MD; Julie Plantin, MD; Lynda Toko, MD; Nour Sreiri, MD; and Pierre-Yves Royer, MD.

Author affiliation: Nord Franche-Comté Hospital, Trévenans, France

DOI: <https://doi.org/10.3201/eid2911.230598>

Campylobacter fetus accounts for 1% of *Campylobacter* spp. infections, but prevalence of bacteremia and risk for death are high. To determine clinical features of *C. fetus* infections and risks for death, we conducted a retrospective observational study of all adult inpatients with a confirmed *C. fetus* infection in Nord Franche-Comté Hospital, Trevenans, France, during January 2000–December 2021. Among 991 patients with isolated *Campylobacter* spp. strains, we identified 39 (4%) with culture-positive *C. fetus* infections, of which 33 had complete records and underwent further analysis; 21 had documented bacteremia and 12 did not. Secondary localizations were reported for 7 (33%) patients with *C. fetus* bacteremia, of which 5 exhibited a predilection for vascular infections (including 3 with mycotic aneurysm). Another 7 (33%) patients with *C. fetus* bacteremia died within 30 days. Significant risk factors associated with death within 30 days were dyspnea, quick sequential organ failure assessment score ≥ 2 at admission, and septic shock.

Campylobacter is a genus of microaerophilic, fastidious, gram-negative, occasionally partially anaerobic, non-spore forming, motile bacteria with a characteristic spiral or corkscrew-like appearance (1). Such morphology enables the bacteria to colonize the mucosal surfaces of the gastrointestinal tract in humans and other animal species (2). In France, *C. fetus* is the most commonly isolated *Campylobacter* species, after *C. jejuni* and *C. coli*, found in fecal samples during diarrheal episodes in humans (3), and the leading species recovered from invasive infections, such as bacteremia and secondary localizations; both *C. jejuni* and *C. coli* have been identified in 43% of cases (4).

Earlier reports have revealed the incidence, clinical characteristics, and outcomes of bacteremia caused by *C. fetus* (4,5). Disease severity and risk for death from *C. fetus* systemic infection are of concern for clinicians; fatality rate is $\approx 15\%$ (4,5). *C. fetus* is also known to have a predilection for vascular endothelium, causing mycotic aneurysms, thrombophlebitis, endocarditis (including infections of prosthetic heart valves), and multivisceral complications (4–11). A bactericidal antimicrobial drug treatment based on use of a β -lactam (such as amoxicillin/clavulanic acid or a carbapenem) should be favored (4).

Using data for January 2000–December 2021, we conducted a retrospective observational and descriptive study in Nord Franche-Comté Hospital, located in eastern France. Our primary objective was to describe clinical and paraclinical features (including antimicrobial susceptibility) in patients with *C. fetus* infections by comparing patients with and without

bacteremia. Our secondary objective was to evaluate the risk factors for 30-day mortality in patients with bacteremia caused by *C. fetus*.

Patient consent was obtained by sending patients a letter informing them of the use of their medical data for research purposes and receiving no objection by 30 days later. Because of the retrospective nature of the study, with no patient involvement and use of already available data, the local Ethics Committee of Nord-Franche-Comte Hospital determined that patient consent was sufficient. The confidentiality of participant data has been respected in accordance with the Declaration of Helsinki.

Methods

Study Population and Design

Nord Franche-Comté Hospital has a capacity of 1,216 beds across all sites. The Nord-Franche-Comté Hospital practice has $\approx 100,000$ visits to its emergency rooms and $\approx 3,600$ deliveries per year (12,13). Our study included all adults (≥ 18 years of age) with a *C. fetus* infection, defined by identification of *C. fetus* in a microbiological sample (blood, fecal, or other site culture) of hospitalized patients over a 21-year period (January 1, 2000–December 31, 2021).

Data Collection

We collected clinical data regarding demographic and baseline characteristics and underlying conditions from patients' medical records. We also extracted laboratory and imaging findings, outcomes, and results of antimicrobial susceptibility to amoxicillin, amoxicillin/clavulanic acid, imipenem, gentamicin, azithromycin, doxycycline, and fluoroquinolones (ofloxacin and ciprofloxacin).

Definitions

We defined secondary localizations as a positive result on biopsy, graft, blood culture samples (or a combination of those) or evocative images on computed tomography or ^{18}F -fluorodeoxyglucose-positron emission tomography/computed tomography (^{18}F -FDG PET/CT). Endocarditis, also considered as a secondary localization, was defined by a positive valvular biopsy sample, blood culture, or both, associated with evocative images on echocardiography, ^{18}F -FDG PET/CT, according to the European Society of Cardiology 2015 modified criteria for diagnosing infective endocarditis (14).

According to the Third International Consensus Definitions for Sepsis and Septic Shock (Sepsis-3) (15), adult patients with suspected infection can be rapidly identified as being more likely to have poor outcomes

typical of sepsis if they have ≥ 2 of the following clinical criteria that together constitute a new bedside clinical score termed quick sequential (sepsis-related) organ failure assessment: respiratory rate of ≥ 22 minutes, altered mentation, or systolic blood pressure of ≤ 100 mm Hg.

Microbiological Diagnosis

Until November 2016, strains were identified to the species level by biochemical tests associated with culture conditions and antimicrobial susceptibility and then by matrix-assisted laser desorption/time-of-flight ionization mass spectrometry methods (Microflex; Bruker Daltonics, <https://www.bruker.com>). Antimicrobial susceptibility was determined by using the disk-diffusion method; we reinterpreted susceptibility for this study according to guidelines of the Comité de l'Antibiogramme de la Société Française de Microbiologie (CA-SFM)/European Committee on Antimicrobial Susceptibility Testing (EUCAST) 2021 version 1. CA-SFM/EUCAST is a version of EUCAST translated into French and adjusted for practices in France (16). We considered antimicrobial treatment to be appropriate if the strain was susceptible to >1 of the drugs prescribed, according to the CA-SFM/EUCAST recommendations (17). *C. fetus* is naturally resistant to third-generation cephalosporins, ticarcillin, and piperacillin, so we considered those drugs to be inappropriate. Some strains were tested by automated broth microdilution system (Vitek-2; bioMérieux, <https://www.biomerieux.com>), and results could not be reinterpreted according to current recommendations.

Data Analysis

Unless otherwise indicated, we expressed discrete variables as numbers and percentages and continuous variables as mean/average, SD, and 95% CI. We performed comparisons among patients with and without *C. fetus* bacteremia by using a χ^2 or Fisher exact test for qualitative variables and a Student *t* or Wilcoxon test for quantitative data. Risk factors for death are expressed as odds ratios (ORs), and statistical analysis was performed by using univariate logistic regression. We used a significance level of $p > 0.05$ and performed all analyses by using R version 4.2.1 (The R Project for Statistical Computing, <https://www.r-project.org>). We defined a significant trend as $p \leq 0.06$.

Results

We considered conventional methods to be the standard combined with matrix-assisted laser desorption/

time-of-flight ionization mass spectrometry identification, which enabled us to identify 991 *Campylobacter* species. The main species found was *C. jejuni* (823 [83%]), followed by *C. coli* (70 [7%]). The third most frequently found species was *C. fetus* (39 [4%]) and the fourth was *C. upsaliensis* (12 [1%]). *Campylobacter* species were not identified in 47 (5%) isolates.

During the study period, we identified 39 patients with culture-positive *C. fetus* infections; of those, 33 had complete records and underwent further analysis, 21 with documented bacteremia and 12 without (Figure 1). Among bacteremic patients, fecal cultures were negative for 20 (95.3%). For only 1 patient were simultaneous peripheral blood and stool cultures positive, isolating *C. fetus*, and that patient was included in the bacteremia group. With regard to patients without documented bacteremia, most (11 of 12) isolates were from fecal samples; gastroenteritis was reported for 10 (83%) patients, of which 9 had liquid diarrhea. Peripheral blood cultures were performed for 8 (66%) of 12 patients without documented *C. fetus* bacteremia and were negative.

Demographic and Epidemiologic Data

The mean prevalence of *C. fetus* infection was 1.5 cases/year. During the study, the highest incidence rate was noted in 2011 (6 [18%] cases) (Figure 2). The mean age of the study population was 73 (SD 18) years, and male patients (54%) were predominant. Patients with *C. fetus* bacteremia were older than patients without bacteremia, but the difference was not significant (77 [SD 16] vs. 66 [SD 19] years; $p = 0.12$). Immunosuppression was more frequent in patients with *C. fetus* bacteremia, and the trend was significant (52% [11/21] vs. 16% [2/12]; $p = 0.06$); malignancy/cancers were the leading cause (7/21 [33%]). Among the 21 patients with bacteremia, the main underlying conditions were cardiovascular disease (15 [71%]), diabetes mellitus (7 [33%]), renal failure (6 [29%]), and prosthetic heart valves (4 [19%]); no significant difference compared with patients without documented *C. fetus* bacteremia was noted. Not represented by our study population were pregnancy, contact with livestock, poultry consumption, and similar cases in the household (Table 1).

Clinical Features, Laboratory Data, and Imaging Findings

The predominant clinical sign was fever; no significant difference was found between the 2 groups (62% [13/21] vs. 73% [8/11]; $p = 0.7$). Gastrointestinal signs/symptoms were more common among patients with no bacteremia (abdominal pain, 58%

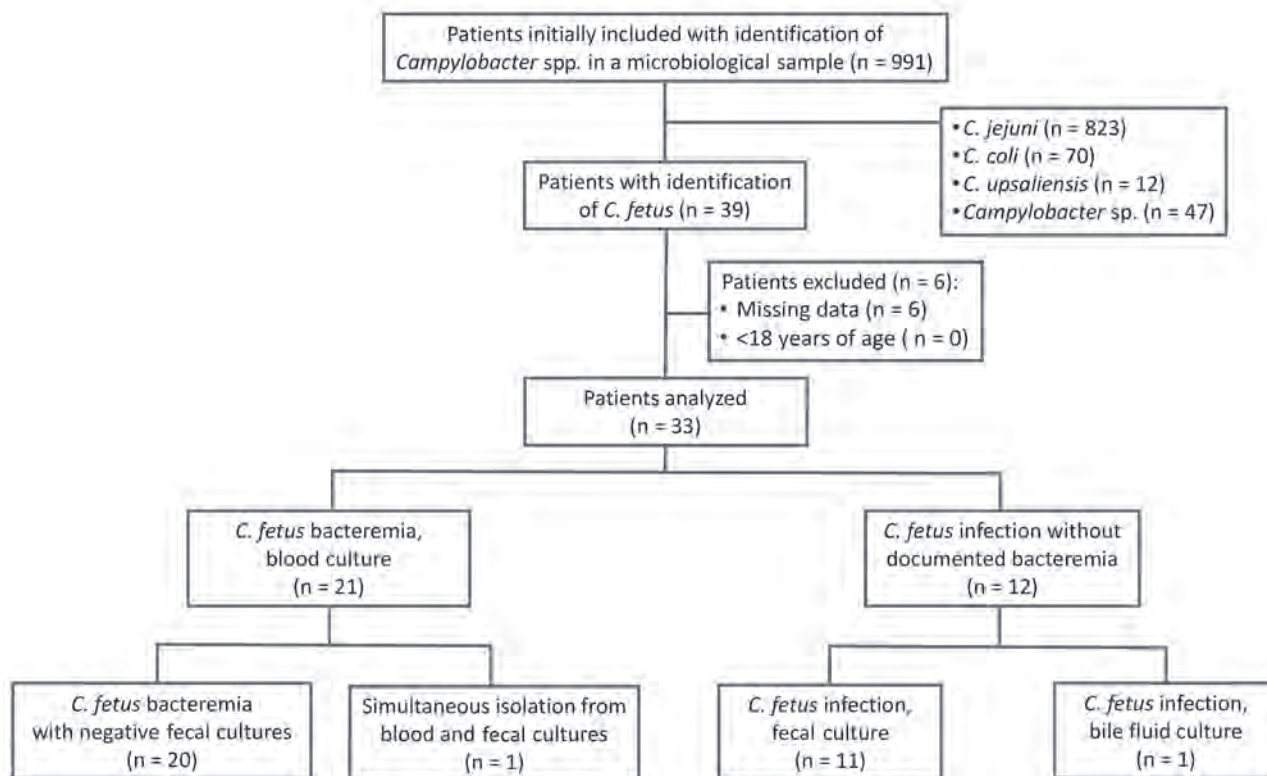


Figure 1. Flowchart of patient enrollment in study of *Campylobacter fetus* invasive infections and risks for death, Nord Franche-Comté Hospital, France, 2000–2021.

vs. 19%; $p = 0.052$; diarrhea, 75% vs. 24%; $p = 0.009$); the difference was significant. At admission, average leukocyte count was higher for patients with *C. fetus* bacteremia (13,550 [SD 7.57] cells/mm³) than without bacteremia (9,950 [SD 3.31] cells/mm³); the difference was not significant ($p = 0.076$). C-reactive protein level was equivalent in both groups (116 [SD 93] mg/L vs. 120 [±52] mg/L; $p = 0.9$). Transthoracic echocardiography (TTE) and ¹⁸F-FDG PET/CT were performed for 3 bacteremic patients. TTE indicated 1 case of prosthetic valve endocarditis and revealed typical oscillating vegetation. ¹⁸F-FDG PET/CT confirmed the diagnosis of mycotic aneurysm in 3 other patients (Table 1).

Secondary Localizations

Secondary localizations were exclusively observed in one third of patients with *C. fetus* bacteremia (7/21 [33%]; $p = 0.03$). A predilection for vascular infections was noted for 5 patients (3 with mycotic aneurysm, 2 with percutaneous implantable port-related infection/thrombophlebitis), and 1 had endocarditis, and 1 had septic arthritis (Table 2).

Therapeutic Management and Outcomes

Among 29 patients receiving antimicrobial therapy, the most commonly used drug was amoxicillin/clavulanic acid (12 [41%]). The most common choice for treating *C. fetus* bacteremia was dual-regimen therapy (8/20

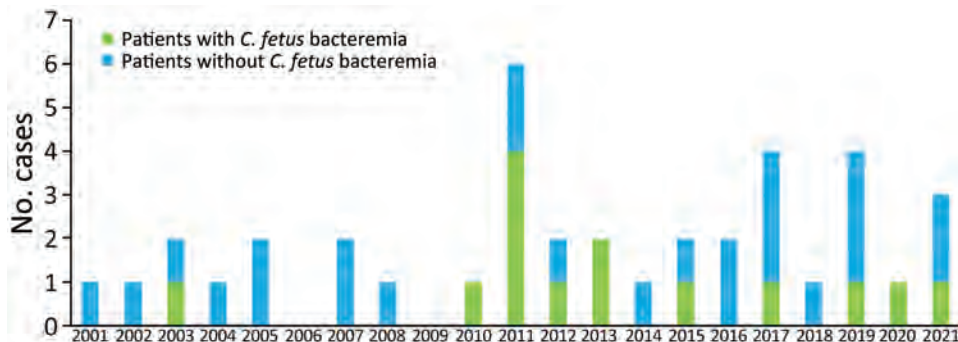


Figure 2. Distribution over time of bacteremia in 33 patients with *Campylobacter fetus* infection, Nord Franche-Comté Hospital, France, 2000–2021.

Table 1. Baseline characteristics, clinical features, and laboratory, and imaging findings for patients with *Campylobacter fetus* infections, Nord Franche-Comté Hospital, Trévenans, France, 2000–2021*

Characteristics	All patients, n = 33	Patients without documented <i>C. fetus</i> bacteremia, n = 12†	Patients with documented <i>C. fetus</i> bacteremia, n = 21	p value
Baseline				
Sex				0.7
M	18/33 (54)	6/12 (50)	12/21 (57)	
F	15/33 (45)	6/12 (50)	9/21 (43)	
Age, y (SD)	73 (±18)	66 (±19)	77 (±16)	0.12
Underlying comorbidities	27/33 (82)	8/12 (67)	19/21 (90)	0.2
Immunosuppression	13/33 (39)	2/12 (16)	11/21 (52)	0.06
Malignancy/cancers	8/33 (24)	1/12 (8.3)	7/21 (33)	0.2
Transplantation	0/33	0/12	0/21	
Cirrhosis	1/33 (3.0)	0/12	1/21 (4.8)	>0.9
HIV infection	0/33	0/12	0/21	
Connective tissue disease‡	3/33 (9.0)	1/12 (8.3)	2/21 (9.5)	>0.9
Other§	1/33 (3.0)	0/12 (8.3)	1/21 (29)	>0.9
Prosthetic heart valves	8/33 (24)	4/12 (33)	4/21 (19)	0.4
Renal failure	7/33 (21)	1/12 (8.3)	6/21 (29)	0.2
Diabetes mellitus	12/33 (36)	5/12 (42)	7/21 (33)	0.7
Cardiovascular disease¶	20/33 (61)	5/12 (42)	15/21 (71)	0.14
Recent abdominal surgery	1/33 (3.0)	0/12	1/21 (4.8)	>0.9
Pregnancy	0/33	0/12	0/21	
Contact with livestock/cattle	0/31	0/11	0/20	
Poultry consumption	0/31	0/11	0/20	
Recent travel#	1/31 (3.2)	1/11 (9.1)	0/20	0.4
Similar cases in household/entourage	0/31	0/11	0/20	
Recent abdominal trauma injury	4/31 (13)	2/11 (18)	2/20 (10)	0.6
Transmission or contamination, food or pet	2/31 (6.5)	0/11	2/20 (10)	0.5
Clinical features				
Fever	21/32 (66)	8/11 (73)	13/21 (62)	0.7
Headache	1/32 (3.1)	0/11	1/21 (4.8)	>0.9
Asthenia/anorexia	16/33 (48)	4/12 (33)	12/21 (57)	0.3
Abdominal pain	11/33 (33)	7/12 (58)	4/21 (19)	0.052
Confusion	8/31 (26)	2/10 (20)	6/21 (29)	>0.9
Dyspnea, respiratory rate >22 cycles/min	8/31 (26)	1/10 (10)	7/21 (33)	0.2
Hypotension, systolic pressure <100 mm Hg	7/31 (23)	1/10 (10)	6/21 (29)	0.4
qSOFA score				0.4
0	20/31 (65)	8/10 (80)	12/21 (57)	
1	3/31 (10)	1/10 (10)	2/21 (10)	
2	6/31 (19)	0/10	6/21 (29)	
3	2/31 (6.5)	1/10 (10)	1/21 (4.8)	
Sepsis: qSOFA ≥2	8/31 (26)	1/10 (10)	7/21 (33)	0.22
Diarrhea, n = 33				
Total	16/33 (48)	10/12 (83)	6/21 (29)	0.004
Liquid	14/33 (42)	9/12 (75)	5/21 (24)	0.009
Bloody	2/33 (6.1)	1/12 (8.3)	1/21 (4.8)	>0.9
Laboratory and imaging findings				
Leukocyte count, cells/mm ³ (SD); reference range 4,000–10,000 cells/mm ³	12,387 (6,665)	9,949 (3,307)	13,548 (7,571)	0.076
CRP, mg/L (SD), reference range <5 mg/L	118 (79)	120 (52)	116 (93)	0.9
Peripheral blood culture				
No. (SD)	NA	NA	2.52 (1.63)	NA
Negatiation, d (SD)	NA	NA	2.89 (3.14)	NA
Transthoracic echocardiography**	4/32 (12)	1/11 (9.1)	3/21 (14)	>0.9
¹⁸ F-FDG PET/CT	3/32 (9.4)	0/11 (0)	3/21 (14)	0.5

*Values are no./total (%) except as indicated. Boldface indicates $p < 0.05$ or a significant trend defined by $p \leq 0.06$. Blank cells for p values indicate no p value was calculated. ¹⁸F-FDG PET/CT, ¹⁸F-fluorodeoxyglucose-positron emission tomography/computed tomography; CRP, C-reactive protein; qSOFA, quick sequential organ failure assessment; NA, not applicable.

†*Campylobacter fetus* was isolated from 11 fecal cultures and from 1 bile fluid culture; only 1 patient had simultaneous positive peripheral blood and fecal cultures in which *C. fetus* was isolated with the same antimicrobial testing susceptibility pattern.

‡All patients with connective tissue diseases (bacteremia; n = 2) had multiple sclerosis.

§Defined by hematologic diseases, long-term steroid therapy, or immunomodulatory treatment.

¶Defined by cardiac failure, arrhythmia, coronary heart disease, stroke, peripheral arterial obstructive disease and thromboembolic disease.

#28-y-old patient sought care for bloody diarrhea without fever 8 d after a travel in Spain.

**The 3 patients who underwent transthoracic echocardiography were different patients than those who underwent ¹⁸F-FDG PET/CT. No patient had both endocarditis and mycotic aneurysm.

Table 2. Secondary localizations, therapeutic management, and outcomes of patients with *Campylobacter fetus* infections among patients with and without bacteremia, Nord Franche-Comté Hospital, Trévenans, France, 2000–2021*

Characteristics	All patients, n = 33	Patients with no <i>C. fetus</i> bacteremia, n = 12	Patients with <i>C. fetus</i> bacteremia, n = 21	p value
Secondary localizations†				
Site infection				
Total	7/33 (21)	0/12	7/21 (33)	0.03
Mycotic aneurysm	3/33 (9.0)	0/12	3/21 (14.3)	0.28
Endocarditis	1/33 (3.0)	0/12	1/21 (4.8)	>0.9
Infection associated with a medical device	1/33 (3.0)	0/12	1/21 (4.8)	>0.9
Thrombophlebitis	1/33 (3.0)	0/12	1/21 (4.8)	>0.9
Bone or joint infection	1/33 (3.0)	0/12	1/21 (4.8)	>0.9
Skin or soft tissue/abscesses	0/33 (0)	0/12	0/21 (0)	NA
Meningitis	0/33 (0)	0/12	0/21 (0)	NA
Antimicrobial therapy				0.6
Amoxicillin	0/29 (0)	0/9	0/20 (0)	
Amoxicillin–clavulanic acid	12/29	2/9	10/20 (50)	
Imipenem	2/29 (6.9)	0/9	2/20 (10)	
Gentamicin	3/29 (10)	0/9	3/20 (15)	
Azithromycin	1/29 (3.4)	1/9 (11)	0/20 (0)	
Ciprofloxacin	3/29 (10)	2/9 (22)	1/20 (5.0)	
Other	11/29 (38)	3/9 (33)	8/20 (40)	
No. antimicrobial drugs/patient				0.065
0	4/29 (17)	2/9 (22)	2/20 (10)	
1	11/29 (38)	5/9 (56)	6/20 (30)	
2	10/29 (34)	2/9 (22)	8/20 (40)	
3	4/29 (14)	0/9	4/20 (20)	
Dual-therapy regimens				
Amoxicillin/clavulanic acid + gentamicin	3/10 (30)	0/2	3/8 (38)	
Amoxicillin/clavulanic acid + azithromycin	1/10 (10)	0/2	1/8 (12)	
Amoxicillin/clavulanic acid + ciprofloxacin	2/10 (20)	0/2	2/8 (25)	
Amoxicillin/clavulanic acid + doxycycline	3/10 (30)	2/2 (100)	1/8 (12)	
Imipenem + gentamicin	1/10 (10)	0/2	1/8 (12)	
Treatment duration, d (SD)	8 (8)	5 (5)	9 (8)	0.2
Outcomes and mortality rates				
Long-term complications, n = 33				
Total	1/33 (3.0)	0/12	1/21 (4.8)	>0.9
Aneurysmal rupture/aortic dissection	1/33 (3.0)	0/12	1/21 (4.8)	>0.9
Acute coronary syndrome	0/33 (0)	0/12	0/21 (0)	NA
Irritable bowel syndrome	0/33 (0)	0/12	0/21 (0)	NA
GBS (polyradiculoneuritis)	0/33 (0)	0/12	0/21 (0)	NA
Surgery‡	5/31 (16.1)	1/10	4/21 (19)	0.6
Relapse§	2/33 (6)	0/12	2/21 (9.5)	0.5
Transfer to intensive care	4/33 (12)	0/12	4/21 (19)	0.3
Septic shock	4/33 (12)	0/11	4/21 (19)	0.3
Infection-related mortality	6/29 (21)	1/8 (12)	5/21 (24)	0.6
30-day mortality rate¶	10/33 (30)	3/12 (25)	7/21 (33)	0.9

*Values are no./total (%) except as indicated. Boldface indicates $p < 0.05$ or a significant trend defined by $p \leq 0.06$. Blank cells for p values indicate no p value was calculated. GBS, Guillain-Barré syndrome; NA, not applicable.

†Mycotic aneurysm (n = 3) with infectious native aortic aneurysm (n = 2); prosthetic aortic valve and a positive culture of the aneurysm after surgery (n = 1); prosthetic valve endocarditis (n = 1) with typical oscillating vegetation (15 mm) confirmed by transthoracic echocardiography; abdominal aorta thrombophlebitis (n = 1); hematogenous medical device infection with a percutaneous implantable port-related infection (n = 1); osteoarticular (n = 1) with glenohumeral shoulder arthritis and a positive culture of the articular fluid after surgery, suggesting a contiguous infection.

‡Four patients with bacteremia caused by *C. fetus* underwent surgery: mycotic aneurysm (n = 2), endocarditis (n = 1), and septic arthritis (n = 1).

§Two patients exhibited a relapse with fever after 26 and 50 d; the second patient died of septic shock during the second episode. The first patient received ciprofloxacin orally for 5 d, and the second patient received IV vancomycin for 7 d.

¶Among the 7 bacteremic patients who died, 2 died in the context of evolutive/expanding malignancy (independently of the bacteremia).

[40%]). Amoxicillin/clavulanic acid was prescribed for 7 (88%) of 8 patients with bacteremia treated with dual-regimen therapy. We found no significant difference in mean duration of treatment between the 2 groups (9 [SD 8] vs. 5 [SD 5] days; $p = 0.2$). Five patients underwent surgery, including 4 with bacteremia (2 for mycotic aneurysm, 1 for prosthetic valve endocarditis, and 1 for septic arthritis). Four patients were

transferred to an intensive care unit for septic shock. Two patients experienced a relapse with fever as the main clinical sign after 26 and 50 days; 1 patient died of septic shock during the second episode.

Antimicrobial Susceptibility Testing

Among patients with *C. fetus* bacteremia, the rate of resistance was 10% (2/20) to both amoxicillin and

Table 3. Antimicrobial resistance of *Campylobacter fetus* strains isolated from patients with and without bacteremia, Nord Franche-Comté Hospital, Trévenans, France, 2000–2021*

Antimicrobial tested	All patients, no. (%), n = 33	Patients with no <i>C. fetus</i> bacteremia, no. (%), n = 12	Patients with <i>C. fetus</i> bacteremia, no. (%), n = 21	p value
Amoxicillin†	3/28 (10.7)	1/8 (12)	2/20 (10)	0.3
Amoxicillin–clavulanic acid	0/28	0/8	0/20	
Imipenem	0/28	0/8	0/20	
Gentamicin	0/27	0/8	0/19	
Azithromycin	2/29 (6.9)	0/9	2/20 (10)	>0.9
Fluoroquinolones: ofloxacin and ciprofloxacin‡	8/27 (30)	2/9 (22)	6/18 (33)	0.7
Doxycycline	7/29 (24)	1/9 (11)	6/20 (30)	0.4

*Values are no. resistant/no. tested (%) except as indicated. Blank cells for p values indicate no p value was calculated.

†Susceptibility to amoxicillin was intermediate (susceptible with high doses) for 2 strains.

‡Susceptibility to ofloxacin and ciprofloxacin was the same for all strains.

azithromycin and 33% (6/18) to fluoroquinolones. No resistance to amoxicillin/clavulanic acid, imipenem, and gentamicin was noted (Table 3).

Mortality Rate

The global 30-day mortality rate was estimated at 30% (10/33); no significant difference between the 2 groups was noted (33% [7/21] vs. 25% [3/12]; $p = 0.9$) (Figure 3). Seven (33%) patients with *C. fetus* bacteremia died within 30 days. Among them, 2 patients died of evolutive/expanding neoplasia, independent of the *C. fetus* bacteremia. Significant risk factors associated with the 30-day mortality rate were dyspnea (OR 15.0, 95% CI 1.9–186.4; $p = 0.017$), quick sequential organ failure assessment score at admission ≥ 2 (OR 4.9, 95% CI 1.6–21.9; $p = 0.012$), and septic shock (OR not applicable; $p = 0.006$). Protective factors were initial prescription of amoxicillin–clavulanic acid (OR 0.09; 95% CI 0–0.75; $p = 0.05$) and use of dual antimicrobial therapy (OR not applicable; $p = 0.001$) (Table 4).

Discussion

The most commonly detected cause of *Campylobacter* bacteremia is *C. fetus* (5,6). However, cohorts or large case series exclusively involving patients with *C. fetus* bacteremia remain scarce. *C. fetus* is usually isolated from blood samples and is less frequently associated with enteritis (18,19). The *Campylobacter* Study (4), a retrospective multicentric study of *Campylobacter* spp. bacteremia in France, also showed that one of the regions with the highest rate of *Campylobacter* spp. infection is the Franche-Comté region.

Our study comprised 33 patients with *C. fetus* infection; the 21 patients with bacteremia were older than the patients without bacteremia, in keeping with data in the literature and previous reports. According to the medical literature of patients with *Campylobacter* bacteremia in one of the largest retrospective cohorts ($n = 592$), patients were elderly (median age 68 years) and most had underlying conditions, mainly immunosuppression

(4). In our cohort, immunosuppression was more frequent among patients with bacteremia caused by *C. fetus* than among patients with no bacteremia; the trend was significant ($p = 0.06$). The leading cause was malignancy or cancer (33%) (1,20). Two patients with documented *C. fetus* bacteremia had systemic sclerosis, which seems to be a predisposing condition among connective tissue diseases (1,21). Pacanowski et al. (5) showed that, compared with patients with bacteremia caused by other *Campylobacter* species, patients with *C. fetus* bacteremia were older and had underlying comorbidities (e.g., cardiovascular diseases, diabetes mellitus). That finding is consistent with our results and those of other reports (20,22).

Among patients with *C. fetus* bacteremia, one third exhibited secondary localizations with a predilection for vascular infections. A recent multicenter study in France (252 patients with *C. fetus* bacteremia) found that 11.5% patients had vascular localization and 4.4% had endocarditis (6). In our study population, we found more vascular localizations but less endocarditis. However, secondary endovascular localizations were not systematically searched and might have been underdiagnosed.

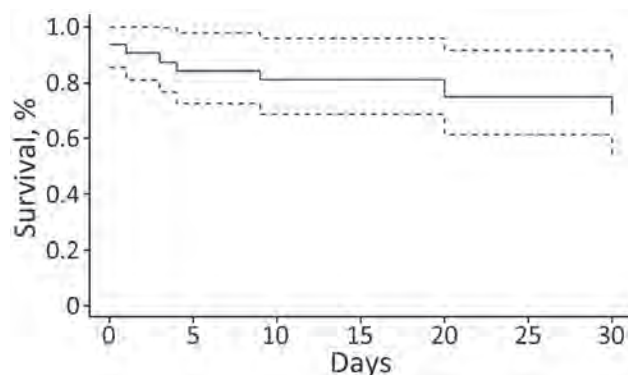


Figure 3. Kaplan-Meier survival curve for 33 patients with *Campylobacter fetus* infection, with and without bacteremia, Nord Franche-Comté Hospital, France, 2000–2021. Dashed lines indicate 95% CIs.

Table 4. Risk factors for death within 30 d after *Campylobacter fetus* bacteremia, Nord Franche-Comté Hospital, Trévenans, France, 2000–2021*

Variable	Total, n = 21	Survival, n = 14	Death, n = 7	p value†	OR (95% CI)
Dyspnea, respiratory rate >22 cycles/min	7/21 (33)	2/14 (14)	5/7 (71)	0.017	15.0 (1.9–186.4)
qSOFA score				0.017	NA
0	12/21 (57)	11/14 (79)	1/7 (14)		
1	2/21 (10)	1/14 (7.1)	1/7 (14)		
2	6/21 (24)	2/14 (14)	4/7 (57)		
3	1/21 (4.8)	0/14	1/7 (14)		
qSOFA score				0.012	4.9 (1.6–21.9)
Sepsis: qSOFA score \geq 2	7/21 (33)	2/14 (14)	5/7 (71)	0.021	13.7 (1.7–171.4)
Septic shock	4/21 (19)	0/14	4/7 (57)	0.006	NA
Transfer to intensive care	4/21 (19)	0/14	4/7 (57)	0.006	NA
Treated with amoxicillin/clavulanic acid	10/21 (48)	9/14 (64)	1/7 (14)	0.05	0.09 (0.0–0.75)
Antimicrobial drugs/patient				0.001	NA
0	3/21 (14)	0/14	3/7 (43)		
1	6/21 (29)	5/14 (36)	1/7 (14)		
2	8/21 (38)	8/14 (57)	0/7		
3	4/21 (19)	1/14 (7.1)	3/7 (43)		
Antimicrobial drugs/patient, median	1.6	1.7	1.4	0.519	0.7 (0.2–1.9)
Infection-related mortality	5/21 (24)	0/14	5/7 (71)	0.001	NA

*Values are no./total (%) except as indicated. Blank cells for p values indicate no p value was calculated. qSOFA, quick sequential organ failure assessment; NA, not applicable; OR, odds ratio.

†p \leq 0.05 indicates significance.

In our study, TTE and ^{18}F -FDG PET/CT were each performed for only 14% of patients with bacteremia, which is a major limitation. We suggest performing those radiologic examinations early for patients with *C. fetus* bacteremia (6,23). Late radiologic examination may partially explain the high mortality rate among patients with aneurysm rupture or endocarditis.

One of the major problems associated with *C. fetus* infection is empiric treatment. Infection with those fastidious bacteria is uncommon, and recommendations for treatment of bacteremia are lacking. The standard choice for empiric treatment of *Campylobacter* spp. enteritis remains fluoroquinolones and macrolides (18). However, in our cohort, 33% of bloodstream isolates were resistant to fluoroquinolones, and 10% were resistant to azithromycin. No strain was resistant to amoxicillin/clavulanic acid, aminoglycoside, or imipenem. The initial empiric treatment should be dual antimicrobial therapy (including amoxicillin/clavulanic acid or imipenem with an aminoglycoside) (6,22,24). In our cohort, all dual-therapy regimens consisted of amoxicillin/clavulanic acid (7/8 [88%]) or imipenem (1/8 [12%]) with a second agent. We conclude that initial prescription of amoxicillin/clavulanic acid and use of dual antimicrobial therapy were protective factors. Failure to administer appropriate antimicrobial therapy is strongly associated with fatal outcomes (4,5).

Other independent risk factors for death were immunosuppression, cancers, and surgery (5,6). In our cohort, risk factors for death within 30 days after *C. fetus* bacteremia were dyspnea, quick sequential

organ failure assessment score at admission \geq 2, and septic shock. We found no significant difference between survivors and nonsurvivors with regard to antimicrobial therapy duration (p = 0.8), which could be explained by the longstanding clinician behavior of avoiding short antimicrobial regimens, even for patients who have positive fecal cultures without bacteremia.

In our cohort, the mortality rate was high (33% of patients with *C. fetus* bacteremia). It should be noted that among those 7 patients, 2 died in the context of evolutive/expanding malignancy and 1 died in the context of recurrent bacteremia with septic shock. In addition, 3 of 7 bacteremic patients who died were receiving 3 antimicrobial drugs, which suggests that in some cases, the number of antimicrobial drugs may have been a marker of illness severity.

Among the limitations of our study were the retrospective method used and the limited number of patients. A prospective study might confirm and support our results. As we previously mentioned, secondary localizations are probably underdiagnosed because of lack of knowledge of this disease and therefore nonperformance of investigations.

In summary, we found that *C. fetus* bacteremia mainly affects patients who are elderly, are immunocompromised, or have underlying conditions. Infections are associated with high mortality rates, especially if no dual antimicrobial therapy including amoxicillin/clavulanic acid is prescribed. For patients with bacteremia caused by *C. fetus*, screening for secondary localizations may be warranted by performing TTE and ^{18}F -FDG PET/CT.

Acknowledgment

We thank all participants in this study and Charlotte Bourgoin, Florence Braun, and Emmanuel Siess for their help.

We declare no conflict of interest. This research received no external funding. Because of privacy restrictions, the data presented in this case study are available only on request from the corresponding author.

About the Author

Dr. Zayet is a specialist in the Infectious Diseases Department of Nord Franche-Comte Hospital, Trevenans, France. His primary research interests focus on hepatitis and tuberculosis, especially in HIV-infected patients and COVID-19 patients.

References

- Liu YH, Yamazaki W, Huang YT, Liao CH, Sheng WH, Hsueh PR. Clinical and microbiological characteristics of patients with bacteremia caused by *Campylobacter* species with an emphasis on the subspecies of *C. fetus*. *J Microbiol Immunol Infect*. 2019;52:122–31. <https://doi.org/10.1016/j.jmii.2017.07.009>
- Wagenaar JA, van Bergen MAP, Blaser MJ, Tauxe RV, Newell DG, van Putten JPM. *Campylobacter fetus* infections in humans: exposure and disease. *Clin Infect Dis*. 2014;58:1579–86. <https://doi.org/10.1093/cid/ciu085>
- Bessède E, Solecki O, Sifré E, Labadi L, Mégraud F. Identification of *Campylobacter* species and related organisms by matrix assisted laser desorption ionization-time of flight (MALDI-TOF) mass spectrometry. *Clin Microbiol Infect*. 2011;17:1735–9. <https://doi.org/10.1111/j.1469-0691.2011.03468.x>
- Tinévez C, Velardo F, Ranc AG, Dubois D, Pailhoriès H, Codde C, et al.; Campylobacteremia Study Group. Retrospective multicentric study on *Campylobacter* spp. bacteremia in France: the Campylobacteremia Study. *Clin Infect Dis*. 2022;75:702–9. <https://doi.org/10.1093/cid/ciab983>
- Pacanowski J, Lalande V, Lacombe K, Boudraa C, Lesprit P, Legrand P, et al.; CAMPYL Study Group. *Campylobacter* bacteremia: clinical features and factors associated with fatal outcome. *Clin Infect Dis*. 2008;47:790–6. <https://doi.org/10.1086/591530>
- Tinévez C, Lehours P, Ranc AG, Belaroussi Y, Cazanave C, Puges M, et al.; Campylobacteremia Study Group. Multicenter retrospective study of vascular infections and endocarditis caused by *Campylobacter* spp., France. *Emerg Infect Dis*. 2023;29:484–92. <https://doi.org/10.3201/eid2903.221417>
- Coustillères F, Hanoy M, Lemée L, Le Roy F, Bertrand D. *Campylobacter fetus* bacteremia complicated by multiple splenic abscesses and multivisceral signs in a renal transplant recipient: a case report and review of the literature. *Braz J Infect Dis*. 2022;26:102336. <https://doi.org/10.1016/j.bjid.2022.102336>
- Seong YJ, Lee SH, Kim EJ, Choi YH, Kim TJ, Lee WG, et al. *Campylobacter fetus* subspecies *venerealis* meningitis associated with a companion dog in a young adult: a case report. *BMC Infect Dis*. 2021;21:1280. <https://doi.org/10.1186/s12879-021-07007-5>
- Nakatani R, Shimizu K, Matsuo T, Koyamada R, Mori N, Yamashita T, et al. *Campylobacter fetus* bacteremia and meningitis in an acute lymphoblastic leukemia patient undergoing maintenance therapy: a case report. *BMC Infect Dis*. 2021;21:680. <https://doi.org/10.1186/s12879-021-06364-5>
- Lynch CT, Buttner C, Epping L, O'Connor J, Walsh N, McCarthy C, et al. Phenotypic and genetic analyses of two *Campylobacter fetus* isolates from a patient with relapsed prosthetic valve endocarditis. *Pathog Dis*. 2022;79:ftab055.
- Dobrović K, Fila B, Janeš A, Civljak R. *Campylobacter fetus* bacteremia related to vascular prosthesis and pseudoaneurysm infection: a case report and review. *Pathogens*. 2022;11:1536. <https://doi.org/10.3390/pathogens11121536>
- Zayet S, Gendrin V, Gay C, Selles P, Klopfenstein T. Increased COVID-19 severity among pregnant patients infected with SARS-CoV-2 Delta variant, France. *Emerg Infect Dis*. 2022;28:1048–50. <https://doi.org/10.3201/eid2805.212080>
- L'Hopital Nord Frances-Compté. Key figures [in French] [cited 2023 Jul 11]. <https://www.hnfc.fr/encart-presentation,245,248.html>
- Adler Y, Charron P, Imazio M, Badano L, Barón-Esquivias G, Bogaert J, et al.; ESC Scientific Document Group. 2015 ESC Guidelines for the diagnosis and management of pericardial diseases: The Task Force for the Diagnosis and Management of Pericardial Diseases of the European Society of Cardiology (ESC) endorsed by: The European Association for Cardio-Thoracic Surgery (EACTS). *Eur Heart J*. 2015;36:2921–64. <https://doi.org/10.1093/eurheartj/ehv318>
- Singer M, Deutschman CS, Seymour CW, Shankar-Hari M, Annane D, Bauer M, et al. The Third International Consensus Definitions for Sepsis and Septic Shock (Sepsis-3). *JAMA*. 2016;315:801–10. <https://doi.org/10.1001/jama.2016.0287>
- Société Française de Microbiologie. CASFM/EUCAST April 2021 V1.0 [in French] [cited 2023 Jul 11]. <https://www.sfm-microbiologie.org/2021/04/23/casfm-avril-2021-v1-0>
- European Committee on Antimicrobial Susceptibility Testing. Clinical breakpoints – breakpoints and guidance [cited 2023 Jul 11]. https://www.eucast.org/clinical_breakpoints
- Donner V, Croxatto A, Tissot F. Invasive *Campylobacter* infection [in French]. *Rev Med Suisse*. 2021;17:722–5. <https://doi.org/10.53738/REVME.2021.17.734.0722>
- Blaser MJ. *Campylobacter fetus* – emerging infection and model system for bacterial pathogenesis at mucosal surfaces. *Clin Infect Dis*. 1998;27:256–8. <https://doi.org/10.1086/514655>
- Cypierre A, Denes E, Barraud O, Jamilloux Y, Jacques J, Durox H, et al. *Campylobacter fetus* infections. *Med Mal Infect*. 2014;44:167–73. <https://doi.org/10.1016/j.medmal.2014.02.001>
- Moffatt CRM, Kennedy KJ, O'Neill B, Selvey L, Kirk MD. Bacteraemia, antimicrobial susceptibility and treatment among *Campylobacter*-associated hospitalisations in the Australian Capital Territory: a review. *BMC Infect Dis*. 2021;21:848. <https://doi.org/10.1186/s12879-021-06558-x>
- Gazaigne L, Legrand P, Renaud B, Bourra B, Taillandier E, Brun-Buisson C, et al. *Campylobacter fetus* bloodstream infection: risk factors and clinical features. *Eur J Clin Microbiol Infect Dis*. 2008;27:185–9. <https://doi.org/10.1007/s10096-007-0415-0>
- Charbonnel A, Carmoi T, Lecoules S, Bonnefoy S, Algayres JP. Vascular manifestations due to *Campylobacter fetus* subsp. *fetus* infection: report of two cases [in French]. *Rev Med Interne*. 2012;33:643–5. <https://doi.org/10.1016/j.revmed.2012.08.011>
- Bastos L, Gomes R, Pocinho S, Baptista T, Mansinho K. *Campylobacter fetus* cellulitis. *Cureus*. 2023;15:e35328.

Address for correspondence: Souheil Zayet, Nord Franche-Comte Hospital, 100 route de Moval, Trevenans 90400 Belfort CEDEX, France; email: souhail.zayet@gmail.com

Congenital Mpox Syndrome (Clade I) in Stillborn Fetus after Placental Infection and Intrauterine Transmission, Democratic Republic of the Congo, 2008

David A. Schwartz,¹ Placide Mbala-Kingebeni, Kerry Patterson, John W. Huggins, Phillip R. Pittman¹

We report the autopsy pathology findings of a 21-week stillborn fetus with congenital mpox syndrome that occurred in the Democratic Republic of the Congo in 2008. The fetus acquired mpox from the mother after intrauterine transplacental monkeypox virus transmission. We confirmed monkeypox virus infection in the mother, fetus, and placenta by using a monkeypox virus–specific quantitative PCR. Subtyping of the virus was not performed, but the mother and fetus were almost certainly infected with the clade I variant that was endemic in the Democratic Republic of the Congo at the time. Risk for intrauterine infection appears to differ between virus clades, but clinicians should be aware of potential for intrauterine monkeypox virus transmission among pregnant persons during ongoing and future mpox outbreaks.

Monkeypox virus, which causes mpox, is the most medically concerning member of the genus *Orthopoxvirus*. Monkeypox virus is related to the variola virus, the etiologic agent of smallpox before its eradication. Mpox has caused illness and death in endemic countries of Central and West Africa, where it infects thousands of persons annually. In 2022, a global outbreak of mpox occurred that has resulted in >87,000 infections, most of which have occurred in nonendemic countries (1). We describe a case of stillbirth

caused by congenital mpox after transplacental transmission that occurred in the Democratic Republic of the Congo (DRC) in 2008. Although some aspects of this case have been previously reported (2–4), the onset of the 2022–2023 global mpox outbreak prompted reevaluation of the case for additional placental and perinatal pathology information.

Methods

To examine the clinical and epidemiologic aspects of monkeypox virus, the Institut National de Recherche Biomédicale (Kinshasa, DRC) and the US Army Medical Research Institute of Infectious Diseases jointly designed and conducted a prospective study at the Kole Hospital in Kole, located in the Sankuru District of Kasai-Oriental Province in DRC (2). The Kole Hospital is the sole health facility in the region where persons infected with mpox are hospitalized and treated. The region is rural and consists of areas of savanna and tropical rainforest with interspersed traditional agricultural fields. The inhabitants are members of a subtribe of the Nkutu (or Okutshu) ethnic group and are mostly hunters and subsistence farmers who are dependent on wildlife, predominantly monkeys and rodents, for their main source of protein. The inhabitants reside in small villages of ≤100 persons in clearings and have a communal lifestyle composed of extended family groups of ≤15 persons living in simple wattle and daub houses. Because participants for the study were not actively recruited, some mpox cases might have occurred in the region but not been included in the study, and other cases might not have

Author affiliations: Perinatal Pathology Consulting, Atlanta, Georgia, USA (D.A. Schwartz); Institut National de Recherche Biomédicale, Ministère de la Santé Publique, Kinshasa, Democratic Republic of the Congo (P. Mbala-Kingebeni); US Army Medical Research Institute of Infectious Diseases, Fort Detrick, Maryland, USA (K. Patterson, J.W. Huggins, P.R. Pittman)

DOI: <https://doi.org/10.3201/eid2911.230606>

¹These senior authors contributed equally to this article.

been detected because the relative isolation of the region limits access to medical care and hospitalization.

As part of the original study, in 2008, a 22-year-old G3P2 pregnant person was seen at 19 weeks' gestation. She was well-nourished and had a positive malaria status but had no allergies or obstetric-related underlying conditions. At enrollment, the mother had moderate mpox with a maculopapular rash and lesion count of 113, accompanied by fever and submandibular lymphadenopathy, but no genital lesions. Mpox infection was confirmed by quantitative PCR (qPCR). She had become febrile at 18 weeks' gestation and had mpox viremia confirmed by virus-specific qPCR. Two weeks after enrollment, she noted absence of fetal movement, which was confirmed both clinically and by 2 sequential obstetrical ultrasounds, leading to diagnosis of intrauterine fetal death.

Maternal viremia rose rapidly from 10^2 to 10^6 viral copies/mL over a 3-day period after cessation of fetal movement. Transcutaneous amniocentesis was positive for mpox virus. Labor was induced by using oxytocin. After membrane rupture, a 21-week gestation stillborn female fetus was delivered vaginally. Umbilical vein blood was positive for mpox virus by qPCR. Oral and written autopsy consent was obtained in the native language from the mother, per the study protocol, which included photography and use of all body specimens, including tissue samples, for further study and publication. After the delivery, the mother was monitored in the hospital; although depressed, she recovered from the mpox infection and was discharged to home in good health. She was well when she returned for her 75-day postpartum follow-up visit.

Fetal Autopsy

The fetal autopsy was performed in a surgical operating suite at the Hôpital General du Référence in Kinshasa. The lighting was suboptimal for photography, and equipment for measuring organ weights and taking dictation was not available. Photographs of the fetus were taken by using a digital Stylus 790 SW camera (Olympus, <https://explore.omsystem.com>).

The female fetus was macerated and had an estimated weight of 300–350 g. Body measurements were crown-heel length 27 cm, crown-rump length 16 cm, arm span 20 cm, head circumference 17–18 cm, and abdominal circumference 30 cm. The outer canthal distance and interpupillary distance were normal. No evidence of either symmetric or asymmetric fetal growth restriction was noted. The fetus displayed nonimmune hydrops fetalis, an abnormal accumulation of fluid in ≥ 2 body areas. The eyelids were closed

and appeared swollen and edematous. The skin of the scalp and face showed multiple distinctive pale pink to white maculopapular lesions (pox) involving the right nostril, upper mid-lip, forehead, right cheek, and temporoparietal regions of the scalp. The lesions on the head were not as well developed as lesions on other parts of the body. Many maculopapular lesions, varying from 0.3–0.5 cm in size, were noted on the skin of the extremities, including the soles of the feet and palms of the hands bilaterally, back, chest, shoulders, abdomen, and buttocks (Figure 1). Many of the lesions were bright red surrounded by white halos, and some had superficial ulcerations. Results of internal organ examination were unremarkable except for the liver, which demonstrated hepatomegaly and measured $8 \times 6 \times 4$ cm (Figure 2, panel A). No pox lesions were noted on any surfaces of the internal organs of the chest or abdomen. Ascites was present and was sampled for viral analysis. The placenta was examined at the time of autopsy, was of normal shape, and weighed ≈ 250 g. The maternal surface was abnormal, showing multiple punctate hemorrhages varying from 0.4–0.8 cm in diameter (Figure 2, panel B). The amniotic surfaces of the umbilical cord, extra-placental membranes, and placental disc had no pox-like lesions.

Microscopic Findings

Because fetal organs had extensive postmortem autolysis, the only slides available for histological examination were from the fetal skin, liver, and placenta. We stained those formalin-fixed specimens by using immunohistochemistry with vaccinia virus antibodies. Because vaccinia virus is also an orthopoxvirus agent, its antibodies have strong cross-reactivity to monkeypox virus. Strong immunohistochemical positivity for poxvirus was detected in the skin, liver, and placental tissues. In particular, the placenta was re-evaluated by a perinatal pathologist during the global 2022–2023 mpox outbreak. It demonstrated extensive and diffuse positive staining of villous stromal cells that were consistent with Hofbauer cells, the native population of villous macrophages (Figure 3). Those cells were increased in number within the chorionic villi, a finding termed Hofbauer cell hyperplasia. We searched for Guarnieri bodies, intracytoplasmic inclusions consisting of aggregates of orthopoxvirus virions often seen in infected epithelial cells, but none were definitively identified.

Viral Analysis

Results of quantitative PCR testing for monkeypox virus were positive from multiple samples: fetal

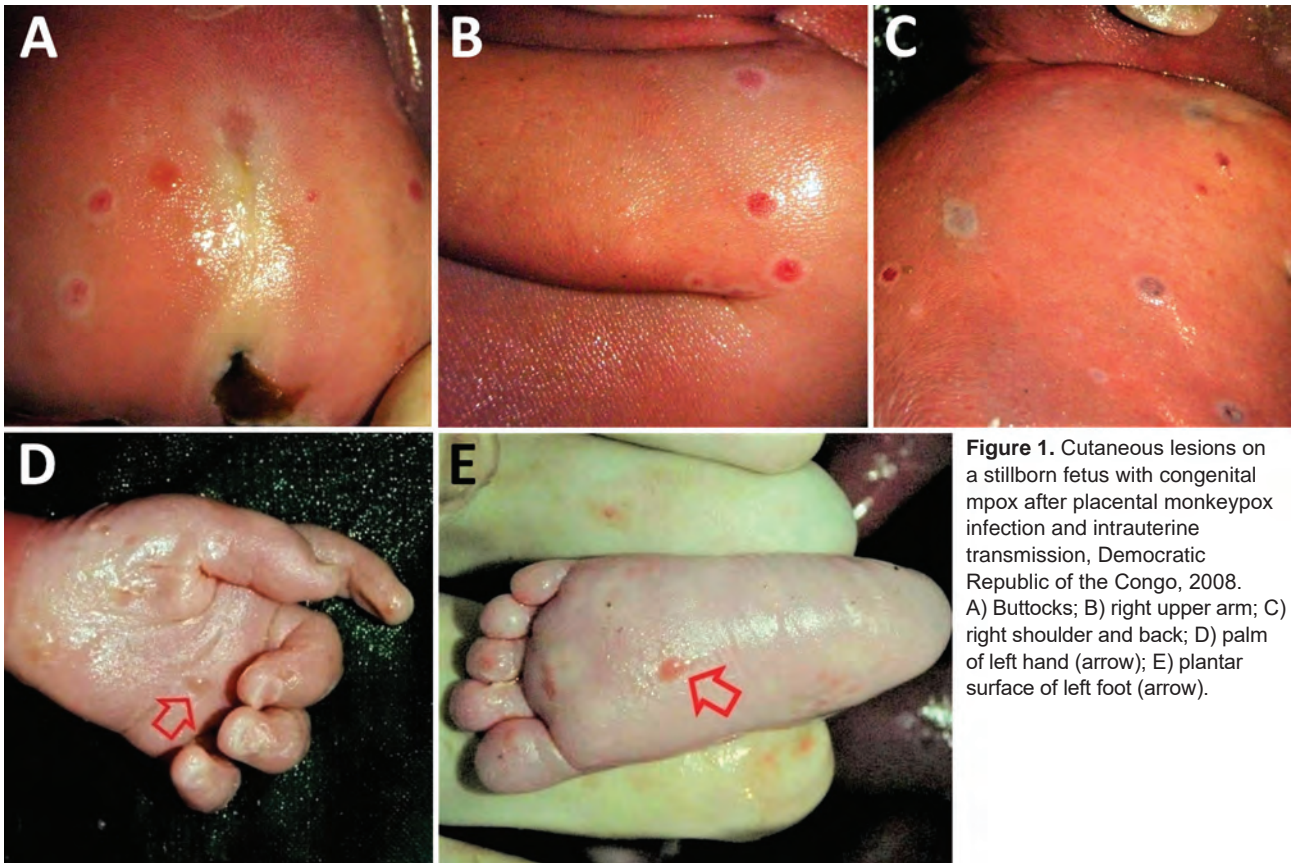


Figure 1. Cutaneous lesions on a stillborn fetus with congenital mpox after placental monkeypox infection and intrauterine transmission, Democratic Republic of the Congo, 2008. A) Buttocks; B) right upper arm; C) right shoulder and back; D) palm of left hand (arrow); E) plantar surface of left foot (arrow).

organs, skin lesions, sterile peritoneal fluid, umbilical cord blood, and placenta. Tissue obtained from the fetus at autopsy had 1.7×10^7 genome copies/mL, the placenta had 2.4×10^7 genome copies/mL, and fetal blood obtained from the umbilical cord vein blood had 2.5×10^7 genome copies/mL. During autopsy, sterile peritoneal fluid was obtained from the fetus and found to contain 1.6×10^3 genome copies/mL of monkeypox virus. Although subtyping of the virus was not performed, the mother and fetus were almost certainly infected with the clade I mpox variant that was endemic in DRC at the time.

Discussion

Most of our knowledge of the effects of mpox in pregnancy is derived from investigations reported as part of the Kole Human Monkeypox Infection Study in the Sankuru Province of DRC during March 2007–July 2011 (2,3). Among a cohort of 222 symptomatic mpox patients (36% female, 64% male) who were seen at the General Hospital of Kole in DRC, 4 were pregnant persons with mpox infection. One pregnancy resulted in birth of an uninfected healthy infant, 2 pregnancies resulted in first trimester miscarriage, and the fourth pregnancy (described in this report) resulted

in intrauterine fetal death at 21 weeks' gestation. Unfortunately, no information is available on the other 2 stillborn fetuses, except that both mothers had active mpox disease.

A case of suspected congenital mpox occurred in DRC in the 1980s, in which a pregnant woman developed a rash, was confirmed to have mpox, and subsequently delivered a live-born 24-week gestation neonate, who at the time of delivery exhibited a generalized rash that was consistent with mpox (5). In Nigeria, fetal losses associated with maternal mpox infection during 2017–2018 were reported at 16- and 21-weeks' gestation, but no fetal studies were performed (6,7).

The microscopic findings in the placenta of our case were remarkable, consisting of diffuse and intense immunohistochemical positivity for orthopoxvirus antigen in villous stromal cells that were consistent with Hofbauer cells and virus-positive staining in the skin and liver. No definitive Guarnieri bodies were identified. Unlike in cases of smallpox, in which those intracytoplasmic aggregates of viral material often were identified, much less is known regarding their occurrence in monkeypox-infected tissues, but similar structures have been identified in infected cutaneous lesions (8).

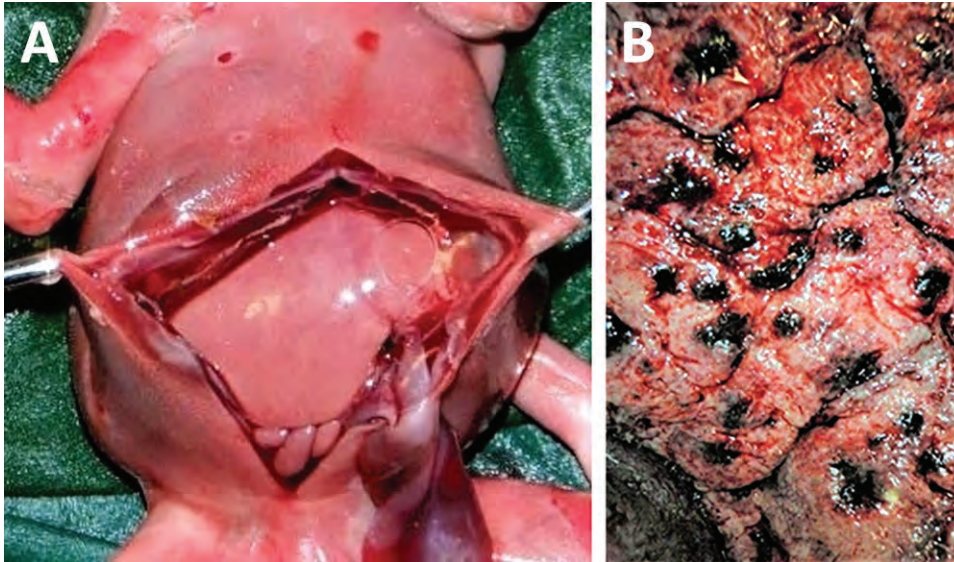


Figure 2. Evidence of congenital mpox syndrome from a stillborn fetus after placental monkeypox infection and intrauterine transmission, Democratic Republic of the Congo, 2008. A) Marked hepatomegaly demonstrating liver twice normal size for gestational age, ascites, and hydrops. B) The maternal surface of the placenta had numerous discrete punctate hemorrhages.

This report adds additional details to the previously published autopsy pathology findings on a stillborn fetus with confirmed congenital mpox syndrome (2,4). This case report adds new information on confirmed fetal intrauterine mpox infection and serves as an example of the characteristic macroscopic presentation of congenital mpox. The occurrence of cutaneous pox lesions diffusely extant on all parts of the body is similar that those seen in cases of congenital smallpox infection before its eradication (4). The finding of poxvirus antigen staining within the chorionic villi of the placenta in this stillborn fetus is indicative of intrauterine transplacental transmission and is similar to that seen in placentas from viral TORCH (an acronym for toxoplasmosis, other agents, rubella, cytomegalovirus, and herpes simplex) infections, including cytomegalovirus, Zika virus, and SARS-CoV-2 (9–11). As with those viral diseases, the chorionic villi of the placenta in our case were found to be infected, providing a potential pathway for crossing the maternal–fetal interface. The death of the fetus in this case was the result of infection with monkeypox virus clade I (formerly the Congo Basin clade). Risk for adverse perinatal outcomes appears to differ depending on virus clades. According to published literature, clade I virus has a 75% perinatal fatality rate (2). In contrast, at least 58 cases (likely more) of pregnant women infected with mpox occurred during the 2022–2023 global mpox outbreak, but no confirmed cases of fetal infection or intrauterine transmission were reported (4,12,13).

Phylogenetic analysis identified the 2022–2023 mpox outbreak strain to be an offshoot of the clade II (West African) virus and that it had sufficient novel

mutations to be classified as a new subclade, clade IIb (14). The absence of perinatal disease from clade IIb corresponds to the <0.1% overall case-fatality rate among nonpregnant persons (13,15). Clade IIb has produced less severe disease than have the mpox clade I or IIa variants (13), but the large predominance of men who have sex with men that were infected during the 2022–2023 outbreak might also play a role. The difference in perinatal death between the various mpox clades might be analogous to the differences in the frequency of miscarriage and stillbirth associated with differing variants of SARS-CoV-2 during the COVID-19 pandemic (16).

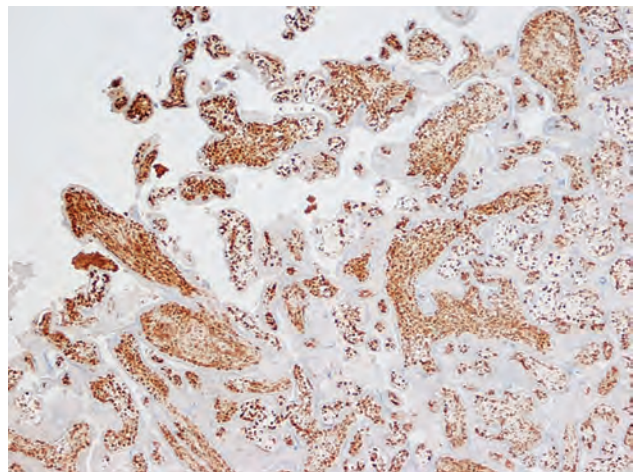


Figure 3. Immunohistochemistry of placenta from a stillborn fetus after placental monkeypox infection and intrauterine transmission, Democratic Republic of the Congo, 2008. Microscopic findings show diffuse and intense positive staining for orthopoxvirus antigen in Hofbauer cells in the chorionic villi. Immunohistochemistry with antibody to vaccinia virus counterstained with hematoxylin and eosin. Original magnification $\times 10$.

In conclusion, we report a case of fetal death after placental infection and intrauterine transmission of monkeypox virus clade I in the Democratic Republic of the Congo in 2008. Risk for intrauterine infection appears to differ between virus clades. Nonetheless, clinicians should be aware of potential for placental infection and intrauterine transmission of monkeypox virus among pregnant persons during ongoing and future mpox outbreaks.

Opinions, interpretations, conclusions, and recommendations are those of the authors and are not necessarily endorsed by the US Army or US Department of Defense.

About the Author

Dr. Schwartz is a global maternal health specialist, pathologist, and medical epidemiologist at Perinatal Pathology Consulting in Atlanta, GA, USA, and has subspecialties in obstetric, fetal, and perinatal pathology; emerging infectious diseases; and maternal-child health. His research interests include investigating the epidemiology, pathology, and public health aspects of emerging infectious diseases as they affect pregnant women, placentas, fetuses, and infants.

References

- Centers for Disease Control and Prevention. 2022 mpox global outbreak map [cited 2023 Apr 26]. <https://www.cdc.gov/poxvirus/mpox/response/2022/world-map.html>
- Mbala PK, Huggins JW, Riu-Rovira T, Ahuka SM, Mulembakani P, Rimoin AW, et al. Maternal and fetal outcomes among pregnant women with human monkeypox infection in the Democratic Republic of Congo. *J Infect Dis.* 2017;216:824–8. <https://doi.org/10.1093/infdis/jix260>
- Schwartz DA, Pittman PR. Monkeypox and pregnancy: correspondence. *Am J Obstet Gynecol.* 2023;228:365. <https://doi.org/10.1016/j.ajog.2022.10.034>
- Schwartz DA, Ha S, Dashraath P, Baud D, Pittman PR, Waldorf KA. Monkeypox virus in pregnancy, the placenta and newborn. *Arch Pathol Lab Med.* 2023; 147:746–5. <https://doi.org/10.5858/arpa.2022-0520-SA>
- Ježek Z, Fenner F. Human monkeypox. Basel (Switzerland): S. Karger; 1988.
- Ogoina D, Iroezindu M, James HI, Oladokun R, Yinka-Ogunleye A, Wakama P, et al. Clinical course and outcome of human monkeypox in Nigeria. *Clin Infect Dis.* 2020;71:e210–4. <https://doi.org/10.1093/cid/ciaa143>
- Yinka-Ogunleye A, Aruna O, Dalhat M, Ogoina D, McCollum A, Disu Y, et al.; CDC Monkeypox Outbreak Team. Outbreak of human monkeypox in Nigeria in 2017–18: a clinical and epidemiological report. *Lancet Infect Dis.* 2019;19:872–9. [https://doi.org/10.1016/S1473-3099\(19\)30294-4](https://doi.org/10.1016/S1473-3099(19)30294-4)
- Stagles MJ, Watson AA, Boyd JF, More IA, McSeveney D. The histopathology and electron microscopy of a human monkeypox lesion. *Trans R Soc Trop Med Hyg.* 1985;79:192–202. [https://doi.org/10.1016/0035-9203\(85\)90333-5](https://doi.org/10.1016/0035-9203(85)90333-5)
- Schwartz DA. Viral infection, proliferation, and hyperplasia of Hofbauer cells and absence of inflammation characterize the placental pathology of fetuses with congenital Zika virus infection. *Arch Gynecol Obstet.* 2017;295:1361–8. <https://doi.org/10.1007/s00404-017-4361-5>
- Schwartz DA, Baldewijns M, Benachi A, Bugatti M, Bulfamante G, Cheng K, et al. Hofbauer cells and COVID-19 in pregnancy. *Arch Pathol Lab Med.* 2021;145:1328–40. <https://doi.org/10.5858/arpa.2021-0296-SA>
- Dashraath P, Alves MP, Schwartz DA, Nielsen-Saines K, Baud D. Potential mechanisms of intrauterine transmission of monkeypox virus. *Lancet Microbe.* 2023;4:e14. [https://doi.org/10.1016/S2666-5247\(22\)00260-9](https://doi.org/10.1016/S2666-5247(22)00260-9)
- Oakley LP, Hufstetler K, O'Shea J, Sharpe JD, McArdle C, Neelam V, et al.; CDC Mpxo Analytics Team. Mpxo cases among cisgender women and pregnant persons – United States, May 11–November 7, 2022. *MMWR Morb Mortal Wkly Rep.* 2023;72:9–14. <https://doi.org/10.15585/mmwr.mm7201a2>
- Schwartz DA, Pittman PR. Mpxo (monkeypox) in pregnancy: viral clade differences and their associations with varying obstetrical and fetal outcomes. *Viruses.* 2023;15:1649. <https://doi.org/10.3390/v15081649>
- Bosmeny MS, White AA, Pater AA, Crew J, Geltz J, Gagnon KT. Global mpox lineage discovery and rapid outbreak tracking with nanopore sequencing. *Virol J.* 2023;20:90. <https://doi.org/10.1186/s12985-023-02059-2>
- Vogel L. Making sense of monkeypox death rates. *CMAJ.* 2022;194:E1097. <https://doi.org/10.1503/cmaj.1096012>
- Schwartz DA, Mulkey SB, Roberts DJ. SARS-CoV-2 placentitis, stillbirth, and maternal COVID-19 vaccination: clinical-pathologic correlations. *Am J Obstet Gynecol.* 2023;228:261–9. <https://doi.org/10.1016/j.ajog.2022.10.001>

Address for correspondence: David A. Schwartz, Perinatal Pathology Consulting, 490 Dogwood Valley Dr, Atlanta, GA 30342, USA; email: davidalanschwartz@gmail.com

Group A *Streptococcus* Primary Peritonitis in Children, New Zealand

Amanda Taylor, Brodie M. Elliott, John Atkinson, Sally Roberts, Lesley Voss, Emma J. Best, Rachel Webb



In support of improving patient care, this activity has been planned and implemented by Medscape, LLC and Emerging Infectious Diseases. Medscape, LLC is jointly accredited with commendation by the Accreditation Council for Continuing Medical Education (ACCME), the Accreditation Council for Pharmacy Education (ACPE), and the American Nurses Credentialing Center (ANCC), to provide continuing education for the healthcare team.

Medscape, LLC designates this Journal-based CME activity for a maximum of 1.00 **AMA PRA Category 1 Credit(s)**™. Physicians should claim only the credit commensurate with the extent of their participation in the activity.

Successful completion of this CME activity, which includes participation in the evaluation component, enables the participant to earn up to 1.0 MOC points in the American Board of Internal Medicine's (ABIM) Maintenance of Certification (MOC) program. Participants will earn MOC points equivalent to the amount of CME credits claimed for the activity. It is the CME activity provider's responsibility to submit participant completion information to ACCME for the purpose of granting ABIM MOC credit.

All other clinicians completing this activity will be issued a certificate of participation. To participate in this journal CME activity: (1) review the learning objectives and author disclosures; (2) study the education content; (3) take the post-test with a 75% minimum passing score and complete the evaluation at <http://www.medscape.org/journal/eid>; and (4) view/print certificate. For CME questions, see page 2415.

NOTE: It is Medscape's policy to avoid the use of Brand names in accredited activities. However, in an effort to be as clear as possible, the use of brand names should not be viewed as a promotion of any brand or as an endorsement by Medscape of specific products.

Release date: October 16, 2023; Expiration date: October 16, 2024

Learning Objectives

Upon completion of this activity, participants will be able to:

- Analyze clinical characteristics of pediatric cases of Group A *Streptococcus* primary peritonitis in the current study
- Assess microbiologic findings in the current series of pediatric cases of Group A *Streptococcus* primary peritonitis
- Evaluate clinical outcomes of Group A *Streptococcus* primary peritonitis among children

CME Editor

Jill Russell, BA, Technical Writer/Editor, Emerging Infectious Diseases. *Disclosure: Jill Russell, BA, has no relevant financial relationships.*

CME Author

Charles P. Vega, MD, Health Sciences Clinical Professor of Family Medicine, University of California, Irvine School of Medicine, Irvine, California. *Disclosure: Charles P. Vega, MD, has the following relevant financial relationships: served as consultant or advisor for Boehringer Ingelheim Pharmaceuticals, Inc.; GlaxoSmithKline; Johnson & Johnson.*

Authors

Amanda Taylor, MBChB; Brodie M. Elliott, MBChB; John Atkinson, MBChB, FRACS; Sally Roberts, MBChB, FRACP, FRCPA; Lesley Voss, MBChB, FRACP; Emma J. Best, MBChB, FRACP, MMED; and Rachel Webb, MBChB, FRACP, MD.

Author affiliations: Starship Children's Hospital, Auckland, New Zealand (A. Taylor, B.M. Elliott, J. Atkinson, L. Voss, E.J. Best, R. Webb); The University of Auckland, Auckland (A. Taylor, E.J. Best, R. Webb); LabPLUS, Auckland City Hospital,

Auckland (S. Roberts); Kidz First Hospital, Counties Manukau, Auckland (R. Webb)

DOI: <https://doi.org/10.3201/eid2911.230211>

Group A *Streptococcus* (GAS) primary peritonitis is a rare cause of pediatric acute abdomen (sudden onset of severe abdominal pain); only 26 pediatric cases have been reported in the English language literature since 1980. We discuss 20 additional cases of pediatric primary peritonitis caused by GAS among patients at Starship Children's Hospital, Auckland, New Zealand, during 2010–2022. We compare identified cases of GAS primary peritonitis to cases described in the existing pediatric literature. As rates of rates of invasive GAS increase globally, clinicians should be aware of this cause of unexplained pediatric acute abdomen.

Streptococcus pyogenes, or group A *Streptococcus* (GAS), causes a wide spectrum of disease ranging from superficial skin infection and pharyngitis to invasive infections, such as sepsis, empyema, necrotizing fasciitis, meningitis, osteomyelitis, and septic arthritis (1). GAS is responsible for the toxin-mediated complications of scarlet fever and streptococcal toxic shock syndrome, as well as the postinfectious sequelae rheumatic fever and poststreptococcal glomerulonephritis (2).

Primary peritonitis is defined as a bacterial infection within the peritoneal cavity in the absence of ascites or an intraabdominal source of infection, such as appendicitis (3,4). Primary peritonitis is an uncommon manifestation of invasive GAS (iGAS) disease; a 2016 report found it accounted for 4.6% of children with iGAS in Finland (5). Pediatric primary peritonitis itself is rare, reportedly accounting for 1%–3% of children experiencing acute abdomen (sudden onset of severe abdominal pain), and is most commonly caused by *S. pneumoniae*, gram-negative organisms, and staphylococcal species (3).

In late 2022, the United Kingdom, United States, Australia, and several countries in Europe reported unexpectedly high rates of iGAS and scarlet fever, particularly in children <10 years of age (6–10). Rates of iGAS in the United Kingdom during this period are reported to be higher than in the years before the COVID-19 pandemic (2017–2019) and substantially higher than those reported during 2020–2021 (11). With increased GAS circulation, media coverage, and heightened community awareness, clinicians globally should be aware of the vast spectrum of invasive disease caused by GAS, including primary peritonitis.

In New Zealand, iGAS disease is not notifiable to Public Health authorities (12). Surveillance relies on individual laboratories sending clinically relevant iGAS isolates to the Institute of Environmental Science and Research (ESR) for typing (13). The most recent ESR report (2016) describes an iGAS incidence of 9.0/100,000 population in New Zealand;

rates were inequitably high among New Zealand Māori (23.5/100,000 population) and Pacific peoples (73.9/100,000 population) compared with rates among persons of European or other ethnicities (4.3/100,000 population) (13). Incidence of iGAS is highest in children <1 year of age (13). Although ESR laboratory surveillance provides some information on the burden of iGAS in New Zealand, its passive nature suggests that reported rates are likely to be an underestimate.

Consistent with the high burden of iGAS disease in children in New Zealand, clinicians at Starship Children's Hospital in Auckland have observed that GAS is a major cause of primary peritonitis in the pediatric population. We evaluated the incidence, clinical features, and management of children admitted to this tertiary pediatric center with GAS primary peritonitis during January 1, 2010–June 30, 2022, to provide a better understanding of the clinical features of GAS primary peritonitis in a contemporary setting with a high burden of iGAS disease. In addition, we reviewed and compared identified cases with reports in the English language literature.

Methods

We performed a retrospective observational study of children admitted to Starship Children's Hospital with GAS primary peritonitis during January 1, 2010–June 30, 2022. Starship Children's Hospital is a tertiary hospital with a surgical department that primarily serves Auckland and northern New Zealand. It contains the country's only pediatric intensive care unit (PICU), and complex cases from across New Zealand are frequently transferred to the facility for surgical management.

We included children <15 years of age who had primary peritonitis, defined as bacterial infection within the peritoneal cavity in the absence of ascites or an intraabdominal source of infection either confirmed on abdominal imaging (typically free intraabdominal fluid and peritoneal enhancement with small bowel dilation and bowel wall thickening) (14) or operative findings (free fluid in the abdomen without intraabdominal or gynecological pathology) (3); and from whom GAS had been isolated from culture or molecular methods from blood culture, peritoneal fluid, peritoneal tissue, or intraoperative peritoneal swab samples (3,4). We excluded children with peritonitis secondary to preexisting ascites or an indwelling peritoneal dialysis catheter or device; children in whom an intraabdominal source of infection, such as a perforated viscus, acute appendicitis, or gynecological pathology, had been identified; or in whom

another bacterial cause of primary peritonitis had been identified, by culture or molecular method, from any of blood culture, peritoneal fluid, peritoneal tissue, or intraoperative peritoneal swab sample.

A.T. reviewed electronic notes, imaging, operative findings, and microbiology of all possible cases to determine whether persons met the study criteria. A multidisciplinary team of the remaining authors then discussed possible cases; the team consisted of pediatric surgeons, pediatric infectious disease specialists, and a clinical microbiologist.

We reviewed 4 data sources for case ascertainment. The first source was Pediatric Infectious Diseases (ID) daily handover lists from the Starship Pediatric ID service inpatient consultation service, which are Microsoft Word documents stored in a password-protected folder on the Starship hospital server. They are manually updated each day by the Starship Pediatric ID team with a summary of all active referrals, including patient diagnosis and relevant microbiology. We searched all handover lists during the study period were electronically searched for the terms "peritonitis," "group A *Streptococcus*," "GAS" and/or "*Streptococcus pyogenes*." Second, we searched for codes from the International Classification of Diseases, 10th Revision (ICD-10), from discharge summaries of patients at Starship Children's Hospital during the study period for primary diagnosis peritonitis or acute peritonitis (codes K65.-, P78.0, P78.1, N73.3, N73.4, N73.5, K35.2, K35.3, K57.0-, K57.2-, K57.4-, K57.8-), with or without secondary group A streptococcus (codes B95.0, A40.0). Third, we requested national reference laboratory data from the New Zealand ESR for children <15 years of age with iGAS isolates sent from LabPLUS (Starship Hospital laboratory service) for *emm* typing. All laboratories in New Zealand are asked to send clinically relevant iGAS isolates to ESR for typing. Clinically relevant iGAS isolates are defined as GAS from a normally sterile body site (e.g., blood, cerebrospinal fluid, pleural fluid, peritoneal fluid, synovial fluid) consistent with the US Centers for Disease Control and Prevention definition of iGAS (13). Last, we reviewed LabPLUS microbiology data for children with GAS culture-positive or molecular test-positive peritoneal or abdominal aspirates, tissue, or peritoneal swab samples and GAS-positive blood cultures.

We subsequently conducted a review of the English literature from 1980 onward using PubMed and the search terms "streptococcus pyogenes" [MeSH] OR "group A streptococc*" OR "streptococcal infection*" OR "invasive GAS" OR "invasive group A streptococc*" AND primary peritonitis

[MeSH]. We identified additional cases by reviewing references and citations of articles identified from the initial PubMed search. We excluded cases in which a primary etiology of peritonitis (e.g., peritoneal dialysis, gynecological or abdominal pathology) had been identified.

This study received Auckland Health Research Ethics Committee approval (AH24823). We performed data collection and descriptive analyses using Microsoft Excel.

Results

We identified 253 possible cases at the hospital during the study period. Of those, 20 cases met the study inclusion criteria for GAS primary peritonitis (Appendix Table, <http://wwwnc.cdc.gov/EID/article/29/11/23-0211-App1.pdf>). Only 2/20 (10%) were identified from all 4 data sources and 5/20 (20%) were notified to ESR by LabPLUS. We compared patient demographics and clinical features to features described in previous case reports (Table).

Ethnicity was recorded as New Zealand Māori for 3/20 (15%) children and Pacific peoples for 8/20 (40%) children. Comorbidities were present in 3 children: 1 child was born at 29 weeks' gestation with hypoxic ischemic encephalopathy, 1 had suspected immunodeficiency, and 1 child had a periodic fever syndrome.

Median symptom duration before admission was 3.5 days (range 1–8 days). We reviewed clinical notes to identify possible skin or pharyngeal sources. A possible skin source was identified in 5/20 (25%) children; sources were a foot wound with cellulitis, a leg wound with cellulitis, vaginal erythema and discharge, groin cellulitis, and scrotal erythema with discharge. Skin swab samples were culture-positive for GAS in 4/5 children with possible skin sources. One child was documented as having pharyngitis the week before admission, although no throat swab sample was collected. Although the presence of skin or pharyngeal infection in household contacts was infrequently documented, 1 child's father had confirmed GAS pharyngitis the week before the child's hospitalization.

Of the 22 cases identified as primary peritonitis on ICD-10 codes, 13/22 had positive microbiology. GAS was cultured from 11/22 (50%). One case each of *S. pneumoniae* and *S. anginosus* primary peritonitis was identified.

A total of 19/20 cases of GAS primary peritonitis were culture-positive for GAS from blood or intraoperative peritoneal samples. In 3/19 cases, GAS was cultured from blood or peritoneal samples at the original hospital before the patient was transferred to

SYNOPSIS

Table. Comparison of characteristics of cases of pediatric GAS primary peritonitis at Starship Children's Hospital, New Zealand, 2010–2022, to previously described cases*

Pediatric GAS primary peritonitis	Cases from literature review, 1980–2022, n = 26 [3,4,14–30]	Cases from Starship Hospital, Jan 1, 2010–Jun 30, 2022, n = 20
Median age (range)	7 y (2 wk–16 y)	2 y (3 wk–13 y)
Sex		
F	16/19 (84)	11/20 (55)
M	3/19 (16)	9/20 (45)
Preceding throat or skin infection		
Pharyngitis	4/18 (22)	1/20 (5)
Skin	3/18 (17)	5/20 (25)
STSS	7/18 (39)	6/20 (30)
Microbiology		
Peritoneal fluid or tissue	25/26 (96)	17/20 (85)
Blood culture	5/26 (19)	9/20 (45)
Other	1/26†	4/20 (20)‡
Molecular method (16S)	3/25 (12)	0/20
Culture	22/25 (88)	19/20 (95)
Surgery		
Laparoscopy or laparotomy	21/25 (84%)§	19/20 (95)
VATS only	NA	1/20 (5)
Median antibiotic duration (range), d	14 (10–61)	21 (14–42)
Clindamycin treatment	4/14 (29)	4/20 (20)
IVIG treatment	3/14 (21)	1/20 (5)
Median length of hospital stay (range), d	10 (4–47)	13 (5–31)
Deaths	0/19	0/20
<i>emm</i> types	3.1 (n = 1)	88 (n = 1), 65/69 (n = 1), 114 (n = 2), 118 (n = 1)§
M-type	M3 (n = 1), M81 (n = 1), M2 (n = 1)	NA

*Values are no. (%) except as indicated. IVIG, intravenous immunoglobulin; NA, not available; STSS, streptococcal toxic shock syndrome; VATS, video-assisted thoracoscopic surgery.

†From pleural aspirate.

‡From skin swab samples; 3/4 GAS-positive skin swabs also had a positive blood or intraoperative peritoneal culture.

§5/20 isolates were sent for *emm* typing.

Starship Hospital. In 7/20 cases, both blood culture and peritoneal culture were GAS-positive (on tissue, aspirate, or intraoperative swab sample). Two of 20 cases were blood culture-positive and peritoneal culture-negative. Half (10/20) were peritoneal culture-positive and blood culture-negative. No patients were identified by molecular methods.

We included 1 patient despite negative blood and peritoneal cultures because intraoperative and imaging findings were consistent with primary peritonitis and because GAS was cultured from a swab sample of vaginal discharge taken at admission. That patient had 2 intraoperative peritoneal swab samples (obtained after antimicrobial treatment) that were culture-negative but demonstrated gram-positive cocci. No molecular method could be performed on the swabs. It was the multidisciplinary team's consensus opinion that this patient should be included as a probable case of GAS primary peritonitis.

One quarter (5/20) of iGAS isolates from this series were sent to ESR from LabPlus for typing and surveillance. In total, primary peritonitis represented 4.6% (5/108) of pediatric iGAS isolates sent to ESR from LabPLUS during the study period.

US Centers for Disease Control and Prevention criteria for streptococcal toxic shock syndrome (STSS)

were met in 6/20 cases (30%), and 10/20 (50%) patients were admitted to the PICU; 5/10 (50%) patients required ventilation and 6/10 (60%) required inotropes (9). A total of 4/20 (20%) patients were given adjunctive clindamycin, and 1/20 received intravenous immunoglobulin. Of those who received clindamycin, 2 patients had STSS, 1 had presumed β -lactam-induced neutropenia, and 1 had clindamycin added to their existing treatment for evolving empyema. The average duration of total antibiotic treatment in our series was 21 days (range 14–42 days), and the average hospital stay was 13 days (range 5–31 days). No deaths occurred within 90 days of hospital admission. One patient was readmitted to the hospital because of intolerance of oral antibiotics.

Discussion

GAS primary peritonitis is a rare but noteworthy cause of pediatric acute abdomen; only 26 pediatric cases have been reported in the English literature since 1980 (Table) (3,5,14–30). We describe a large single-center pediatric cohort of 20 cases in patients admitted to Starship Children's Hospital, New Zealand, during 2010–2022. This study contributes to existing knowledge of the clinical manifestations, treatment, and trajectory of children with GAS primary peritonitis.

In the context of increasing rates of iGAS globally, our case series should increase awareness among clinicians of this manifestation of iGAS disease.

In our series, GAS was the most common pathogen isolated from children with an ICD-10 discharge code of primary or acute peritonitis. This finding contrasts with previous reports that found more common pediatric primary peritonitis causes were *S. pneumoniae*, staphylococci, and gram-negative organisms (3). Although this retrospective, observational study did not aim to assess the causative pathogens of all primary peritonitis cases, key pathogens could have changed over time; this possibility should be the focus of further study. Our findings could be explained by the high burden of iGAS in New Zealand children, particularly among Māori and Pacific peoples, who were overrepresented in our case series (accounting for 55% of cases).

Postulated causes of GAS primary peritonitis include hematogenous spread from the skin or respiratory tract, ascending infection from the female genital tract, and gastrointestinal translocation (4,30). Although GAS is known to colonize the throat, skin, and female genital tract, it is not typically present in intestinal flora (30). Among previously reported pediatric cases, a possible skin or throat source was found in 50% of cases (14). In our cohort, a skin or throat source was identified in a similar proportion of cases (30%). Because of the retrospective nature of our study, clinical records were not always complete. Future studies would benefit from standardized, prospective collection of cases detailing recent pharyngeal, skin, or genitourinary infections (1,3).

Previous reports have suggested that girls are disproportionately affected by GAS primary peritonitis because of ascending genitourinary infection; in 84% (16/19) of previous pediatric case reports where sex was given, the child was a girl (30). This effect was not seen in our cohort, where the median age was younger than that previously reported and 55% of case-patients were girls, suggesting that this route might be less common in younger children (30).

As in previous reports, symptoms of children in our cohort were abdominal pain, nausea, vomiting, and diarrhea. Several cases were initially diagnosed as viral gastroenteritis before deteriorating into peritonism and sepsis (3,14). Of the children in our cohort, 30% met STSS criteria, which is comparable with previous case reports that found an overall STSS incidence of 39% (5,14,15).

Although adult clinical practice guidelines advise nonoperative management, particularly in persons with underlying ascites, previous case reports found

that most (83%) pediatric patients undergo surgery to rule out secondary peritonitis (14,30). This practice was also demonstrated in our series; 95% of patients underwent laparoscopy or laparotomy. Surgical management might aid source control, particularly in patients with STSS where reduction of bacterial load plays a major role (4,14,31). Operative management has also been hypothesized to decrease the duration of illness: a 2020 case report describes a child who was managed nonoperatively and in whom a multiloculated abscess developed that required multiple drains and 61 days of antibiotics (30).

The median total duration of antibiotic treatment in our cohort was 21 days (range 14–42 days), which is 1 week longer than the median duration of 14 days (range 10–61) seen in previous case reports. The additional benefit of clindamycin or intravenous immunoglobulin in the management of GAS primary peritonitis remains unclear; however, those adjunct treatments might have a role in patients with STSS.

Observational case reports alone make it difficult to comment on the importance of operative management or the optimal duration of antibiotic treatment for GAS primary peritonitis; however, despite substantial rates of severe illness in our series (10 cases [50%] required PICU admission), no deaths occurred, and only 1 patient required readmission to the hospital. Furthermore, no deaths have been reported in any pediatric case report of GAS primary peritonitis since the 1980s (14). As such, shorter durations of antibiotics may be reasonable for patients with less severe clinical manifestation, particularly when early surgical source control is achieved.

Although this report describes iGAS infection in a population with an identified high burden of GAS infection, as reports emerge from Europe, the United Kingdom, and the United States describing an increase in iGAS and scarlet fever, pediatricians should be aware of this cause of acute abdomen (6). Identifying iGAS promptly enables antibiotic treatment to be rationalized to penicillin and might enable STSS to be recognized earlier. The international rise in iGAS cases might also provide an opportunity to evaluate the best treatment approach for GAS primary peritonitis and how best to manage close contacts. In New Zealand, no guidelines exist around routine assessment of household contacts of persons with iGAS. The risk for secondary iGAS disease in household contacts is estimated to be 2,000 times higher than the general population risk, substantially higher than that reported for meningococcal disease (500–800 times), which is a notifiable condition in New Zealand (32).

Therefore, identifying highly transmissible iGAS should prompt timely review, collection of throat swab specimens, and consideration of chemoprophylaxis for high-risk household contacts through existing public health communicable disease control services for meningococcal disease and other high-priority close contact infectious diseases (32).

During the study period, GAS primary peritonitis accounted for 4.2% of pediatric iGAS isolates sent to the national reference laboratory from Starship Children's Hospital for *emm*-typing and surveillance. Although this is comparable with a 2016 national surveillance study of pediatric iGAS disease in Finland, which reported a primary peritonitis incidence of 4.6% (7/151) (5), in our series only 5/20 patients with GAS primary peritonitis had their isolates sent for *emm*-typing and surveillance. Starship Hospital is a tertiary referral center, and 3/19 iGAS isolates were cultured at other hospitals in New Zealand. Those isolates could have been sent to ESR by those hospital laboratories, but our observation that only a small number of culture-positive samples at our hospital were sent to ESR suggests that passive surveillance is likely to underestimate the true burden of iGAS in New Zealand. This case series highlights the difficulties of case ascertainment, disease surveillance, and the ability to monitor circulating *emm*-types when a disease is not monitored through prospective national surveillance. In a time of increasing global rates of iGAS disease, the results of this study strengthen calls for enhanced, prospective, national iGAS surveillance (1,6,12,32). Although this cohort is small, strengths include robust case ascertainment from multiple data sources and comprehensive classification of cases through detailed review by a multidisciplinary team of clinicians.

In conclusion, GAS primary peritonitis is an uncommon cause of iGAS disease in children but can cause severe illness. This contemporary case series describes 20 children over a 12.5-year period, 30% of whom met the criteria for STSS and 50% of whom required PICU admission. Our findings reflect the substantial burden of GAS disease in New Zealand. In a time of increasing iGAS rates globally, GAS primary peritonitis should be considered in children experiencing unexplained acute abdomen.

About the Author

Dr. Taylor, a PhD candidate with The University of Auckland, completed this work while employed as a pediatric infectious diseases fellow at Starship Children's Hospital. Her research interests include group A *Streptococcus* and acute poststreptococcal glomerulonephritis.

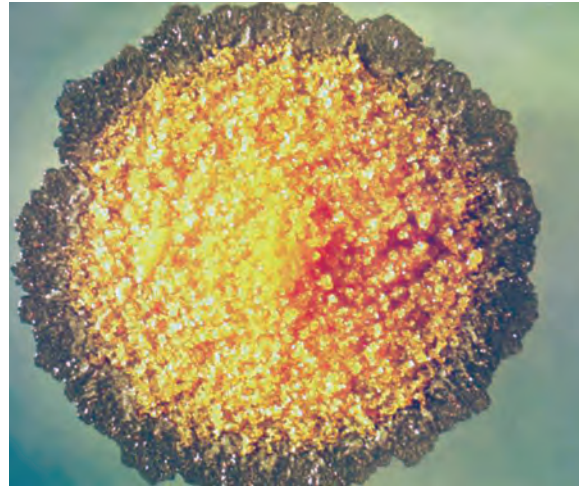
References

1. Miller KM, Lamagni T, Cherian T, Cannon JW, Parks T, Adegbola RA, et al. Standardization of epidemiological surveillance of invasive group A streptococcal infections. *Open Forum Infect Dis*. 2022;9:S31–40. <https://doi.org/10.1093/ofid/ofac281>
2. Safar A, Lennon D, Stewart J, Trenholme A, Drinkovic D, Peat B, et al. Invasive group A streptococcal infection and vaccine implications, Auckland, New Zealand. *Emerg Infect Dis*. 2011;17:983–9. <https://doi.org/10.3201/eid1706.100804>
3. Sharp EA, Linn A, Zitelli BJ. Group A streptococcal pharyngitis associated with primary peritonitis. *BMJ Case Rep*. 2019;12:e229186. <https://doi.org/10.1136/bcr-2019-229186>
4. Westwood DA, Roberts RH. Management of primary group A streptococcal peritonitis: a systematic review. *Surg Infect (Larchmt)*. 2013;14:171–6. <https://doi.org/10.1089/sur.2012.038>
5. Tapiainen T, Launonen S, Renko M, Saxen H, Salo E, Korppi M, et al. Invasive group A streptococcal infections in children: a nationwide survey in Finland. *Pediatr Infect Dis J*. 2016;35:123–8. <https://doi.org/10.1097/INF.0000000000000945>
6. World Health Organization. Increased incidence of scarlet fever and invasive Group A Streptococcus infection – multi-country [cited 2023 Apr 6]. <https://www.who.int/emergencies/disease-outbreak-news/item/2022-DON429>
7. UK Health Security Agency. Group A streptococcus in children – interim clinical guidance summary [cited 2023 Apr 28]. <https://nhs.uk/Downloads/aboutus/medicines-management/Other%20Guidelines/PRN00058-group-a-streptococcus-in-children-interim-clinical-guidance-december-2022.pdf>
8. Cobo-Vázquez E, Aguilera-Alonso D, Carrasco-Colom J, Calvo C, Saavedra-Lozano J, Calvo C, et al. Increasing incidence and severity of invasive group A streptococcal disease in Spanish children in 2019–2022. *Lancet Reg Health Eur*. 2023;27:100597.
9. Guy R, Henderson KL, Coelho J, Hughes H, Mason EL, Gerver SM, et al. Increase in invasive group A streptococcal infection notifications, England, 2022. *Euro Surveill*. 2023;28:2200942. <https://doi.org/10.2807/1560-7917.ES.2023.28.1.2200942>
10. MacPhail A, Lee WJL, Kotsanas D, Korman TM, Graham M. A rise in invasive and non-invasive group A streptococcal disease case numbers in Melbourne in late 2022. *Med J Aust*. 2023;218:378–9. <https://doi.org/10.5694/mja2.51909>
11. UK Health Security Agency. Group A streptococcal infections: report on seasonal activity in England, 2022 to 2023 [cited 2023 May 30]. <https://www.gov.uk/government/publications/group-a-streptococcal-infections-activity-during-the-2022-to-2023-season/group-a-streptococcal-infections-report-on-seasonal-activity-in-england-2022-to-2023>
12. Bennet J, Moreland N, Birrell J, Webb R, Kvalsvig A, Roberts S, et al. Likely rise in invasive strep infections in NZ requires a strategy. *Public Health Communication Centre Aotearoa* [cited 2023 Jun 15]. <http://hdl.handle.net/10523/15125>
13. Institute of Environmental Science and Research Ltd (ESR). Invasive group A streptococcal infection in New Zealand, 2016 [cited 2023 May 19]. https://surv.esr.cri.nz/PDF_surveillance/InvasiveGAS/InvGASinfectioninNewZealand2016.pdf
14. Holtestaut T L-BABM. Group A streptococcal primary peritonitis in an otherwise healthy adolescent female. *J Pediatr Surg Case Rep*. 2021;64:101729. <https://doi.org/10.1016/j.epsc.2020.101729>
15. Liang TC, Lu CY, Lu FL, Lee PI, Huang LM. Streptococcal toxic shock syndrome manifesting as peritonitis in a child. *J Formos Med Assoc*. 2002;101:509–13.

16. Goepel JR, Richards DG, Harris DM, Henry L. Fulminant streptococcus pyogenes infection. *BMJ*. 1980;281:1412. <https://doi.org/10.1136/bmj.281.6252.1412>
17. Freij BJ, Votteler TP, McCracken GH Jr. Primary peritonitis in previously healthy children. *Am J Dis Child*. 1984;138:1058–61.
18. Harnden A, Lennon D. Serious suppurative group A streptococcal infections in previously well children. *Pediatr Infect Dis J*. 1988;7:714–8. <https://doi.org/10.1097/00006454-198810000-00010>
19. Torres-Martínez C, Mehta D, Butt A, Levin M. Streptococcus associated toxic shock. *Arch Dis Child*. 1992;67:126–30. <https://doi.org/10.1136/adsc.67.1.126>
20. Watson WJ, Powers KS. Primary peritonitis associated with streptococcal toxic shock-like syndrome. *Clin Pediatr (Phila)*. 1999;38:175–7. <https://doi.org/10.1177/000992289903800310>
21. Gillespie RS, Hauger SB, Holt RM. Primary group A streptococcal peritonitis in a previously healthy child. *Scand J Infect Dis*. 2002;34:847–8. <https://doi.org/10.1080/0036554021000026944>
22. Dann PH, Amodio JB, Rivera R, Fefferman NR. Primary bacterial peritonitis in otherwise healthy children: imaging findings. *Pediatr Radiol*. 2005;35:198–201. <https://doi.org/10.1007/s00247-004-1304-7>
23. Sewrey H, Bryant PA. Group A streptococcus causing primary peritonitis in a healthy infant. *Pediatr Infect Dis J*. 2009;28:1146. <https://doi.org/10.1097/INF.0b013e3181b1bd9f>
24. Demitrack J. Primary group A streptococcal peritonitis in a previously healthy child. *Pediatr Infect Dis J*. 2012;31:542–3. <https://doi.org/10.1097/INF.0b013e31824f1b0d>
25. Holden R, Wilmer A, Kollman T. Primary peritonitis due to group A *Streptococcus* in a previously healthy pediatric patient. *Can J Infect Dis Med Microbiol*. 2012;23:e69–70. <https://doi.org/10.1155/2012/105850>
26. Patel RV, Kumar H, More B, Rajimwale A. Primary group A streptococcal septic shock syndrome simulating perforated appendicitis in a previously healthy girl. *BMJ Case Rep*. 2013;2013:bcr2013009502. <https://doi.org/10.1136/bcr-2013-009502>
27. Benidir A, Lim R. Case 1: a 16-year-old female with left lower-quadrant abdominal pain. *Paediatr Child Health*. 2014;19:19–20. <https://doi.org/10.1093/pch/19.1.19>
28. Filan E, Abbas M. Abdominal pain, fever, and infection secondary to an unusual source in a previously healthy child. *Clin Pediatr (Phila)*. 2014;53:607–9. <https://doi.org/10.1177/0009922814526987>
29. Chomton M, Emeriaud G, Bidet P, Rallu F, Ovetchkine P, Gaschignard J. Group A streptococcal primary peritonitis in a healthy girl. *J Paediatr Child Health*. 2017;53:615–6. <https://doi.org/10.1111/jpc.13584>
30. Haskett H, Delair S, Neemann K. Primary group A streptococcal peritonitis in a previously healthy female teenage patient. *Glob Pediatr Health*. 2020;7:2333794X20957647.
31. Sumiyama F, Sakaguchi T, Yamamichi K, Sekimoto M. Peritonitis caused by group A streptococcus: a case report and literature review. *Int J Surg Case Rep*. 2022;92:106839. <https://doi.org/10.1016/j.ijscr.2022.106839>
32. Oliver J, Thielemans E, McMinn A, Baker C, Britton PN, Clark JE, et al. Invasive group A *Streptococcus* disease in Australian children: 2016 to 2018 – a descriptive cohort study. *BMC Public Health*. 2019;19:1750. <https://doi.org/10.1186/s12889-019-8085-2>

Address for correspondence: Amanda Taylor, Pediatric Infectious Diseases Department, Starship Children's Hospital, 2 Park Road, Grafton, Auckland, 1023, New Zealand; email: ATaylor@adhb.govt.nz

EID Podcast *Mycobacterium marinum* Infection after Iguana Bite in Costa Rica



Zoonotic infections associated with animal bite injuries are common and can result in severe illness. Approximately 5 million animal bites occur annually in North America, and 10 million injuries occur globally from dog bites alone. Pathogens causing infections after dog or cat bites are well described; pathogens from other animal bites are less well defined, although their oral microbiota are known.

In this EID podcast, Dr. Niaz Banaei, a professor of pathology and medicine at Stanford University in California, discusses *Mycobacterium marinum* infection after an iguana bite in Costa Rica.

Visit our website to listen:
<https://bit.ly/3Jh2FSI>

**EMERGING
INFECTIOUS DISEASES®**

Detection of Novel US *Neisseria meningitidis* Urethritis Clade Subtypes in Japan

Hideyuki Takahashi, Masatomo Morita, Mitsuru Yasuda, Yuki Ohama, Yoshitomo Kobori, Munekado Kojima, Ken Shimuta, Yukihiko Akeda, Makoto Ohnishi

Neisseria meningitidis causes invasive meningococcal diseases and has also been identified as a causative agent of sexually transmitted infections, including urethritis. Unencapsulated sequence type 11 meningococci containing the gonococcal *aniA-norB* locus and belonging to the United States *N. meningitidis* urethritis clade (US_NmUC) are causative agents of urethral infections in the United States, predominantly among men who have sex with men. We identified 2 subtypes of unencapsulated sequence type 11 meningococci in Japan that were phylogenetically close to US_NmUC, designated as the Japan *N. meningitidis* urethritis clade (J_NmUC). The subtypes were characterized by PCR, serologic testing, and whole-genome sequencing. Our study suggests that an ancestor of US_NmUC and J_NmUC urethritis-associated meningococci is disseminated worldwide. Global monitoring of urethritis-associated *N. meningitidis* isolates should be performed to further characterize microbiologic and epidemiologic characteristics of urethritis clade meningococci.

Neisseria meningitidis causes invasive meningococcal diseases (IMDs), such as meningitis and septicemia. *N. meningitidis* is classified into 12 defined serogroups; however, most IMDs are associated with the serogroups A, B, C, W, X, and Y (1). Serogrouping is critical for IMD control because meningococcal vaccines have serogroup-specific effects (2). Whole-genome sequencing (WGS)-based typing, such as high-resolution core genome multilocus sequence typing (MLST), is the most powerful method for analyzing meningococcal isolates. However,

standard MLST, which identifies sequence types (STs) of isolates according to the unique allelic profiles of 7 housekeeping genes, is still applied to meningococcal epidemiology studies because the most invasive isolates belong to a limited number of clonal complexes (CCs). For example, ST11 and the locus variants comprising CC11 meningococci are well-known hypervirulent *N. meningitidis* strains that have caused many pandemics (3), including IMD outbreaks that predominately occurred among men who have sex with men (MSM) (4–9).

N. gonorrhoeae is also a human pathogen capable of infecting the urethra, cervix, rectum, and oropharynx. Most gonococcal infections manifest clinically as urethritis in men or cervicitis in women, both of which are sexually transmitted infections (STI). Meningococcus and gonococcus are generally regarded as distinct taxa that cause specific diseases; however, recent findings suggest a greater overlap than was originally reported. *N. gonorrhoeae* is rarely identified as a causative agent of systemic infection; *N. meningitidis* has been reported to cause STIs, such as urethritis. An outbreak of meningococcal urethritis predominantly among MSM was reported in multiple cities in the United States (10). Causative agents were identified as CC11 *N. meningitidis* isolates with several unique features and classified as US *N. meningitidis* urethritis clade (US_NmUC) (11–14). The capsular polysaccharide (*cps*) locus in US_NmUC meningococci is disrupted by insertion sequence (IS) 1301 that replaced *ccaA*, *cssB*, and *cssC* genes and part of the *csc* gene causing loss of encapsulation (12). That genetic mutation also caused the loss of wild-type lipooligosaccharide sialylation, which appeared to increase mucosal surface adherence (15). Moreover, the factor H binding protein (fHbp), which binds to human factor H and inhibits the alternative complement activation pathway in the human immune system (16),

Author affiliations: National Institute of Infectious Diseases, Tokyo, Japan (H. Takahashi, M. Morita, Y. Ohama, K. Shimuta, Y. Akeda, M. Ohnishi); Sapporo Medical University, Sapporo, Japan (M. Yasuda); Private Care Clinic Tokyo, Tokyo (Y. Kobori); Nagoya Urology Hospital, Aichi, Japan (M. Kojima)

DOI: <https://doi.org/10.3201/eid2911.231082>

was highly expressed in US_NmUC *N. meningitidis* isolates and might promote evasion from immune responses in the human urogenital tract (12). The most unique feature of US_NmUC meningococci is their acquisition of the *N. gonorrhoeae* denitrification apparatus that comprises gonococcal alleles encoding nitrate reductase AniA and nitric oxide reductase NorB and the intergenic promoter region, which confers survival in the urogenital tract (12,17).

Most US_NmUC isolates have been recovered from patients with urethritis in the United States. However, 2 US_NmUC meningococci isolates were identified in 2019 in rectal swab samples from MSM in the United Kingdom (18), and 19 US_NmUC meningococci were isolated in Vietnam in 2019 and 2020 (19). US_NmUC meningococci have not yet been reported in other countries. We report the genomic and phenotypic features of 3 unencapsulated ST11 urethritis-associated *N. meningitidis* strains isolated in Japan that were phylogenetically close to US_NmUC but classified as novel urethritis meningococcus clade subtypes.

Methods

N. meningitidis Isolates

Although IMDs are legally notifiable diseases in Japan, STIs caused by *N. meningitidis* are not. In Japan, meningococcal isolates from patients with STIs are typically collected as part of the country-wide gonococcal surveillance program (headed by M.Y.). Urethral swab samples from male patients suspected of having urethritis and cervical swab samples from female patients suspected of having cervicitis were sent to Sapporo Medical University from ≈100 clinics across Japan. We isolated strains by selective growth on Thayer-Martin medium and analyzed those isolates by using Biotyper matrix-assisted/laser desorption time-of-flight mass spectrometry (Beckman Coulter, <https://www.beckmancoulter.com>) and commercially available mass spectrometry profiles to identify species. We collected >1,000 gonococcal isolates annually and isolated ≈10 *N. meningitidis* strains under the gonococcal surveillance program, in which no misidentification of *N. meningitidis* as *N. gonorrhoeae* has occurred. We characterized 3 *N. meningitidis* isolates at the National Institute of Infectious Diseases by using serologic and genetic analyses.

Typing and Antimicrobial Drug Susceptibility Tests

We performed serogrouping by using PCR (20) and slide agglutination tests with meningococcal rabbit

antiserum (Remel, <http://www.remel.com>, or Difco/Becton Dickinson, <https://www.bd.com>) and a commercial latex agglutination kit (Pastorex Meningitis assay; Bio-Rad Laboratories, <https://www.bio-rad.com>). We conducted MLST by using the standard method (21). We performed antimicrobial drug susceptibility tests by using E-tests (bioMérieux, <https://www.biomerieux.com>) and Mueller-Hinton agar with 5% sheep blood (Becton Dickinson), which we interpreted according to the Clinical and Laboratory Standards Institute criteria for agar dilution, as previously described (22).

WGS, Genome Assembly, and Phylogenetic Analysis

We extracted genomic DNA by using the MagMAX DNA Multi-Sample Ultra 2.0 Kit, which we then purified by using the KingFisher Duo Prime Purification System and measured concentrations by using a Qubit dsDNA HS assay kit (all from Thermo Fisher Scientific, <https://www.thermofisher.com>). We prepared genomic libraries for short read sequencing by using the QIAseq FX DNA Library Kit (QIAGEN, <https://www.qiagen.com>) and sequenced 300-bp paired-end reads on a MiSeq instrument (Illumina, <https://www.illumina.com>). For long-read sequencing on a MinION sequencer (Oxford Nanopore Technologies, <https://nanoporetech.com>), we prepared genomic libraries by using a Rapid Barcoding Kit (Oxford Nanopore Technologies) and sequenced them by using an R9.4.1 flow cell. We basecalled raw data by using Guppy 6.5.7 (23) and removed adaptors before assembly by using Porechop 0.2.3 (<https://github.com/rrwick/Porechop>). We generated draft genome sequences for both long and short reads by using Unicycler version 0.5.0 in conservative mode (24) and performed annotations of complete genomes and genome assemblies by using the DDBJ Fast Annotation and Submission Tool (<https://dfast.ddbj.nig.ac.jp>) (25). We used draft genome assemblies for PorA and FetA typing and determining the Meningococcal Deduced Vaccine Antigen Reactivity Index through PubMLST (<https://www.pubmlst.org>). We performed phylogenetic analyses of *N. meningitidis* from urethritis patients by using 26 publicly available genomes and constructed core gene alignments by using Roary version 3.12.0 and the -s and -e-mafft options (26), which were subject to SNP-sites version 2.5.1 (27) to extract single-nucleotide variants. We constructed the phylogenetic tree by using IQ-TREE version 2.0.3 (<http://www.iqtree.org>) with 1,000 ultrafast bootstrap replicates and visualized the tree by using iTOL (28).

Repositories

We deposited the short reads sequence data for NIID835, NIID836, and NIID838 in the DDBJ Sequence Read Archive (<https://www.ddbj.nig.ac.jp>) under accession nos. DRR494404 (NIID835), DRR494405 (NIID836), and DRR494406 (NIID838) and in the PubMLST database under nos. 135430 (NIID835), 135431 (NIID836), and 135432 (NIID838). The annotated complete genome assemblies of NIID835, NIID836, and NIID838 strains are also available in the GenBank, EMBL (<https://www.ebi.ac.uk>), and DDBJ databases under accession nos. AP028680 (NIID835), AP028681 and AP028682 (NIID836), and AP028683 (NIID838).

Results

The 3 J_NmUC *N. meningitidis* strains (NIID835, NIID836, and NIID838) were isolated from 3 men with urethritis that developed 4–5 days after contact with commercial sex workers for oral sexual services (Appendix 1 Table, <https://wwwnc.cdc.gov/EID/article/29/11/23-1082-App1.xlsx>). Although *N. meningitidis* strains from patients with urethritis in Japan are typically classified as ST11026, which is also isolated from healthy carriers (29), or ST23, which is also isolated from IMD patients and healthy carriers (30), we identified all 3 J_NmUC *N. meningitidis* strains as ST11 (Appendix 1 Table). To further characterize the 3 J_NmUC *N. meningitidis* isolates as urethritis clade meningococci, we performed WGS, phylogenetic, and serologic analyses.

aniA-norB Locus

We conducted phylogenetic analysis of the 3.5-kb *aniA-norB* gene sequence (Appendix 2 Figure 1, <https://wwwnc.cdc.gov/EID/article/29/11/23-1082-App2.pdf>) for 3 J_NmUC *N. meningitidis* isolates from Japan, 2 *N. meningitidis* US_NmUC isolates, *N. gonorrhoeae* FA1090 (GenBank accession no. NC_002946.2), *N. meningitidis* MC58 (31), and 6 *N. meningitidis* serogroup C isolates from IMD patients in United States that were genetically very close to US_NmUC (32) (Figure 1). Moreover, we included 3 ST23 *N. meningitidis* isolates (NM001, NM003, and NIID574) from Japan harboring the gonococcal *aniA-norB* locus (30), designated as J_NmUC-II (Figure 1). The *aniA-norB* locus in the 3 ST11 J_NmUC isolates was 100% identical to that in US_NmUC meningococci (12,17), indicating the *aniA-norB* locus in the 3 J_NmUC strains was of gonococcal origin. In the 3 ST11 J_NmUC and 3 J_NmUC-II isolates, the *aniA-norB* locus was located between *gpxA* and NMB1624 genes (Appendix 2 Figure 1), which was identical to that in US_NmUC *N. meningitidis* strains (12). Collectively, those results indicated that the 3 ST11 J_NmUC isolates acquired the gonococcal *aniA-norB* locus, similar to US_NmUC meningococci.

Serogrouping and *cps* Locus Analysis

Although we initially identified the 3 ST11 J_NmUC *N. meningitidis* strains as serogroup C meningococci (MenC) by PCR (20), the strains were agglutination negative when we tested with serogroup C-specific antiserum. To clarify this discrepancy, we characterized

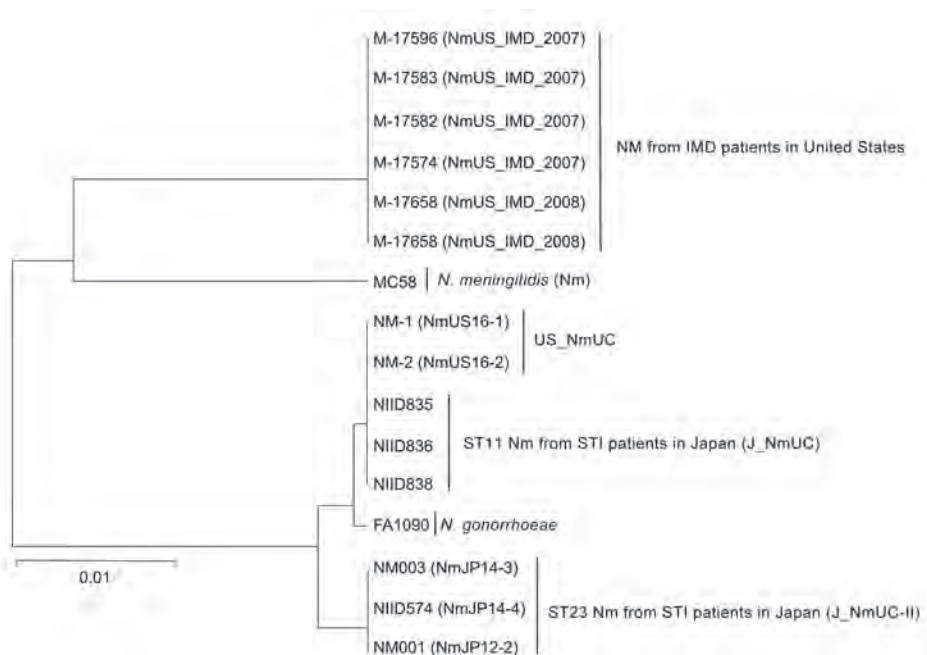


Figure 1. Phylogenetic analysis of the 3.5-kb *aniA-norB* gene locus of *Neisseria* spp. isolates in study detecting novel US *N. meningitidis* urethritis clade subtypes in Japan. Tree was constructed by using the unweighted pair group method with arithmetic mean and 1,000 bootstrap replicates. The gonococcal *aniA-norB* locus was derived from *N. gonorrhoeae* FA1090 (GenBank accession no. NC_002946.2); all others are from *N. meningitidis* isolates. Scale bar indicates nucleotide substitutions per site. IMD, invasive meningococcal disease; Nm, *N. meningitidis*; ST, sequence type; STI, sexually transmitted infection.

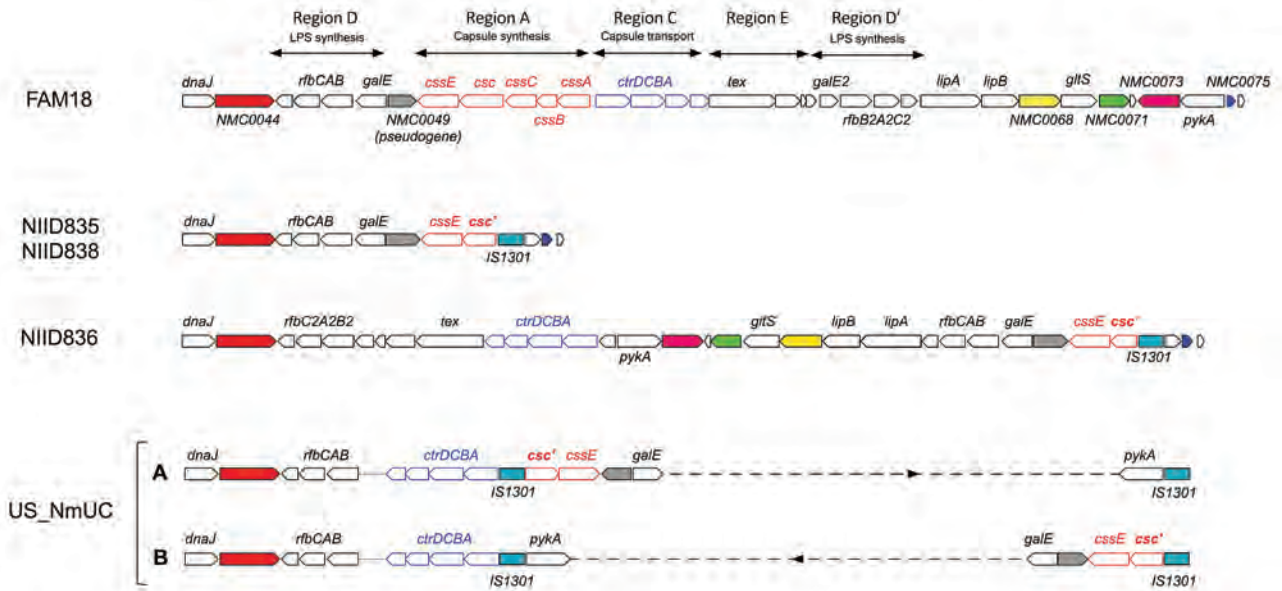


Figure 2. Organization of genes within the *cps* locus of *Neisseria meningitidis* isolates in study of detection of novel US *N. meningitidis* urethritis clade subtypes in Japan. *N. meningitidis* isolates from Japan (NIID835, NIID836, NIID838) and United States (US_NmUC) were compared with *N. meningitidis* strain FAM18 (GenBank accession no. AM421808). Open red arrows indicate the *cssA*, *cssB*, *cssC*, *csc*, and *cssE* genes in region A responsible for capsule synthesis and open blue arrows the *ctrD*, *ctrC*, *ctrB*, and *ctrA* genes (in that order) in region C responsible for capsule transport. Insertion sequence IS1301 is indicated. Open reading frames identical to NMC0044 (solid red), NMC0049 (gray), NMC0068 (yellow), NMC0071 (green), NMC0073 (pink), and NMC0075 (blue) in FAM18 are shown for each isolate. Partial deletion is indicated for the *csc* gene (*csc**). The *cps* locus for US_NmUC had 2 configurations created by a ~20-kb genome inversion between 2 IS1301 sequences (designated as A and B). Gene alignments in the region between the 2 IS1301 sequences have been omitted and are indicated by the dashed line. Although *ctrD*, *ctrC*, *ctrB*, and *ctrA* genes were shown to be proximal to *dnaJ* (12), contigs containing the *dnaJ*-*rfbC*, *rfbA*, and *rfbB* genes and the *ctrD*, *ctrC*, *ctrB*, and *ctrA* genes (shown on the left side of A and B), as well as 2 IS1301 and *pykA* genes (shown on the right side of A and B), were not connected by our analysis because of the absence of US_NmUC long-read sequences. Therefore, unidentified connections of the 2 contigs are indicated by a dotted line.

the *cps* gene locus (Figure 2). In NIID835 and NIID838 isolates, *cssA*, *cssB*, and *cssC* genes, and part of the *csc* gene (region A) were deleted and replaced with IS1301, but the *ctrABCD* gene cluster (region C) was also deleted. In contrast to 2 copies of IS1301 in US_NmUC isolates (12), only 1 copy of IS1301 was found in the *cps* locus of NIID835 and NIID838 isolates. In the NIID836 J_NmUC isolate, deletions of *cssA*, *cssB*, *cssC*, *csc* genes were identical to those in NIID835 and NIID838, but the *ctrABCD* gene cluster remained, containing the *pylA*, *gltS*, *lipA*, and *lipB* genes, which are typically proximal to the *csc* and *cssE* genes. Furthermore, 2 copies of the *rfbC*, *rfbA*, and *rfbB* gene cluster were identified in the NIID836 J_NmUC isolate; only 1 copy was found in NIID835 and NIID838 isolates. Although the *cps* locus in the 3 J_NmUC meningococcal strains were not identical to that in US_NmUC meningococci, the J_NmUC meningococci were genotypically nongroupable. All of the genetic features within the *cps* and *aniA*-*norB* loci confirmed that the 3 nongroupable ST11 J_NmUC meningococci were classified into the urethritis clade.

fHbp Locus

In US_NmUC meningococci, fHbp was speculated to be highly expressed because the *fHbp* promoter sequence belonged to high fHbp-expressing promoter clade I (33). In the 3 ST11 J_NmUC *N. meningitidis* isolates, the *fHbp* promoter sequence, fHbp peptide, and *fHbp* allele were identical to those in US_NmUC meningococci strains (Appendix 2 Figure 2), suggesting fHbp might also be highly expressed in J_NmUC meningococci (12).

Phylogenetic Analysis by Using WGS

To gain insights into the origin of J_NmUC meningococci, we performed phylogenetic analysis by using WGS to compare 9 ST11 IMD isolates from Japan (29), 1 STI isolate (NmJP12-1) (30), and 7 IMD MenC isolates from the United States that were genetically close to US_NmUC (32) (Figure 3). ST23 J_NmUC-II, ST11 serogroup W meningococci SK001 (NmJP12-1), 8 IMD MenC, and 5 STI MenC (30) isolates were genetically separate from J_NmUC and US_NmUC meningococci; 7 US IMD MenC that were close to US_NmUC (32) were also genetically close to J_NmUC.

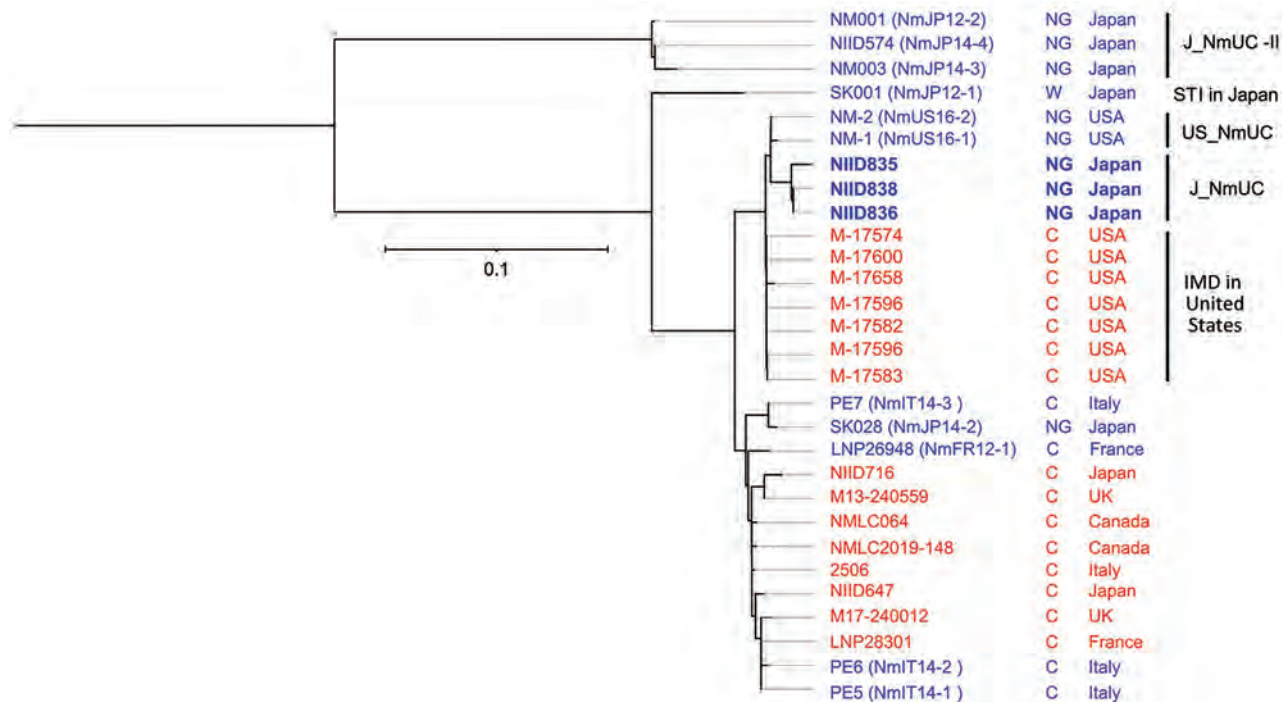


Figure 3. Phylogenetic analysis of *Neisseria meningitidis* from different countries in study of detection of novel US *N. meningitidis* urethritis clade subtypes in Japan. Strains isolated from patients with IMD (red font) or STI (blue font), serogroup (NG or C), and country of origin are indicated. US_NmUC, J_NmUC, and J_NmUC-II *N. meningitidis* isolates have detailed profiles (Appendix 1 Table, <https://wwwnc.cdc.gov/EID/article/29/11/23-1082-App1.xlsx>). We included 1 sequence type 11 *N. meningitidis* strain isolated in Japan from a patient with an STI (SK028) and 4 serogroup C meningococci (MenC) that were phylogenetically close to SK028 (PE5, PE6, PE7, and LNP26948) (29). Moreover, we included 7 MenC phylogenetically close to US_NmUC (IMD strains in the United States) (31), 2 sequence type 11 MenC isolated from IMD patients during 2003–2020 in Japan (NIID647 and NIID716) (28), and 6 MenC phylogenetically close to the 2 MenC from Japan (28). Scale bar indicates nucleotide substitutions per site. C, serogroup C; IMD, invasive meningococcal disease; NG, nongroupable; STI, sexually transmitted infection.

However, J_NmUC strains were the phylogenetically closest to US_NmUC, eliminating the possibility that J_NmUC was originally derived from MenC strains in Japan.

Susceptibility to Antimicrobial Drugs

Antimicrobial resistance in *N. meningitidis* is considered to be acquired by transmission of genetic material from *N. gonorrhoeae*, such as the gonococcal *aniA-norB* locus (14). However, US_NmUC meningococci isolated in the United States were susceptible to the third-generation cephalosporin ceftriaxone, ciprofloxacin, and rifampin, whereas ≈75%–85% of US_NmUC meningococci were nonsusceptible (intermediate susceptibility) to penicillin G (34,35). The 3 J_NmUC meningococci were susceptible to most antimicrobial drugs tested, except the NIID836 strain had intermediate susceptibility to penicillin G, similar to US_NmUC meningococci (34,35). Those results suggest that genetic material related to antimicrobial resistance genes might not be transmitted into J_NmUC *N. meningitidis* isolates. Of note, the NIID835

strain was susceptible to penicillin G and ceftriaxone despite having the *penA327* allele, which typically reduces susceptibility to penicillin G and third-generation cephalosporins (36).

Discussion

Meningococcus and gonococcus generally colonize distinct niches in humans causing systemic (meningococcus) and sexually transmitted (gonococcus) disease; few cases exist that identify *N. meningitidis* as a causative agent for STI (14). Meningococcal urethritis is symptomatically indistinguishable from gonococcal urethritis; one of the main problems in clinical and public health is that meningococcal urethritis cannot be diagnosed by the existing nucleic acid amplification test, a standard method for STI diagnosis (14,34). Urethritis clade meningococci, such as US_NmUC and J_NmUC, have been isolated only from urethritis patients (10), rectal swab samples of asymptomatic MSM (18), and 1 neonatal patient with conjunctivitis (37); virulence was considered equal to gonococci. However, urethritis clade meningococci were also

speculated to colonize the upper respiratory tracts of sexual partners of persons who eventually manifested urethritis. No published studies exist regarding carriage of urethritis clade meningococci in the upper respiratory tract; thus, the public health threat of urethritis clade meningococci is unclear, and emergence of this clade should be continuously monitored.

Although deletion of the *cps* locus or genes within this locus, which results in loss of encapsulation, is a main feature of urethritis clade meningococci (12,14), the pattern of deletion within the *cps* locus was different between J_NmUC and US_NmUC isolates, despite the identical junctions between the *csc* gene and IS1301 sequences. Because meningococcal loss of encapsulation enhances adherence to human cells (15,38–44), loss of the capsule might promote *N. meningitidis*-induced urethritis. However, some cases of meningococcal urethritis might be caused by encapsulated *N. meningitidis* isolates (30). Therefore, the relationship between loss of encapsulation by deletions within the *cps* locus in *N. meningitidis* and meningococcal urethritis should be further examined.

Acquisition of the gonococcal *aniA-norB* locus (12) was another main feature of urethritis clade meningococci (Figure 1). In some *N. meningitidis* strains, such as M-17541 (Appendix 2 Figure 1), the meningococcal *aniA* gene was disrupted by an insertion or missense mutation (45,46). Moreover, if the meningococcal *aniA* gene was intact, expression was lower than that of gonococcal *aniA* genes (45). However, the gonococcal *aniA-norB* locus was not detected in some *N. meningitidis* isolates from patients with meningococcal urethritis (30), suggesting that acquisition of the gonococcal *aniA-norB* locus was advantageous (12,13,17) but not essential to cause urethritis.

A phylogenetic analysis using WGS data supports the hypothesis that US_NmUC and J_NmUC might be derived from the same ancestor (Figure 3). US_NmUC appears to have originated during 2006–2012 in the United States (32), and the ancestral strain might have been imported into Japan during the same period. However, MenC, serogroup W, and CC11 meningococci have rarely been detected in Japan for >40 years, even in IMD patients (29,47,48). Although CC11 meningococci have never been identified as a causative agent for meningococcal urethritis in Japan (29), J_NmUC meningococci, as well as the ST11 ancestral strain, might be dormant in the urethra or pharynx of persons in Japan. Therefore, further analyses of meningococcal isolates from healthy carriers and patients with urethritis will provide insights into dissemination of the *N. meningitidis* urethritis clade among the human population in Japan.

In conclusion, few studies have attempted to estimate the prevalence of meningococcal infections, including the urethritis clade. J_NmUC meningococci identified in this study are new subtypes of US_NmUC, and microbiologic characteristics, such as virulence and transmissibility, remain unclear. Continuous monitoring and analyses of J_NmUC meningococci will elucidate more precise features, including transmissibility and pathogenicity. Moreover, detection of J_NmUC in Japan suggests potential dissemination of several types of urethritis clade meningococci (US_NmUC and J_NmUC) worldwide. Global monitoring of urethritis-associated *N. meningitidis* isolates should be required to reveal further microbiologic and epidemiologic aspects of urethritis clade meningococci and to improve laboratory diagnostic testing for urethritis.

This work was supported by a grant from the Japan Agency for Medical Research and Development (grant no. JP21fk0108605) and Ministry of Healthcare and Labour of Japan (grant no. JPMH22HA1007 to H.T.).

This publication made use of the PubMLST website (<https://pubmlst.org>) developed by Keith Jolley and Martin Maiden (49); the website is located at the University of Oxford. The development of that site has been funded by The Wellcome Trust and European Union.

About the Author

Dr. Takahashi is the chief of the urogenital infection laboratory, Department of Bacteriology I, National Institute of Infectious Diseases, Japan. His research interests focus on meningococcal epidemiology and molecular pathogenesis as well as the gonococcal equivalents.

References

1. Acevedo R, Bai X, Borrow R, Caugant DA, Carlos J, Ceyhan M, et al. The Global Meningococcal Initiative meeting on prevention of meningococcal disease worldwide: epidemiology, surveillance, hypervirulent strains, antibiotic resistance and high-risk populations. *Expert Rev Vaccines*. 2019;18:15–30. <https://doi.org/10.1080/14760584.2019.1557520>
2. Taha MK, Martinon-Torres F, Köllges R, Bonanni P, Safadi MAP, Booy R, et al. Equity in vaccination policies to overcome social deprivation as a risk factor for invasive meningococcal disease. *Expert Rev Vaccines*. 2022;21:659–74. <https://doi.org/10.1080/14760584.2022.2052048>
3. Mustapha MM, Marsh JW, Harrison LH. Global epidemiology of capsular group W meningococcal disease (1970–2015): multifocal emergence and persistence of hypervirulent sequence type (ST)-11 clonal complex. *Vaccine*. 2016;34:1515–23. <https://doi.org/10.1016/j.vaccine.2016.02.014>
4. Schmink S, Watson JT, Coulson GB, Jones RC, Diaz PS, Mayer LW, et al. Molecular epidemiology of *Neisseria*

- meningitidis* isolates from an outbreak of meningococcal disease among men who have sex with men, Chicago, Illinois, 2003. *J Clin Microbiol*. 2007;45:3768–70. <https://doi.org/10.1128/JCM.01190-07>
5. Marcus U, Vogel U, Schubert A, Claus H, Baetzing-Feigenbaum J, Hellenbrand W, et al. A cluster of invasive meningococcal disease in young men who have sex with men in Berlin, October 2012 to May 2013. *Euro Surveill*. 2013;18:20523. <https://doi.org/10.2807/1560-7917.ES2013.18.28.20523>
 6. Kratz MM, Weiss D, Ridpath A, Zucker JR, Geevarughese A, Rakeman J, et al. Community-based outbreak of *Neisseria meningitidis* serogroup C infection in men who have sex with men, New York City, New York, USA, 2010–2013. *Emerg Infect Dis*. 2015;21:1379–86. <https://doi.org/10.3201/eid2108.141837>
 7. Taha MK, Claus H, Lappann M, Veyrier FJ, Otto A, Becher D, et al. Evolutionary events associated with an outbreak of meningococcal disease in men who have sex with men. *PLoS One*. 2016;11:e0154047. <https://doi.org/10.1371/journal.pone.0154047>
 8. Nanduri S, Foo C, Ngo V, Jarashow C, Civen R, Schwartz B, et al. Outbreak of serogroup C meningococcal disease primarily affecting men who have sex with men—Southern California, 2016. *MMWR Morb Mortal Wkly Rep*. 2016;65:939–40. <https://doi.org/10.15585/mmwr.mm6535e1>
 9. Folaranmi TA, Kretz CB, Kamiya H, MacNeil JR, Whaley MJ, Blain A, et al. Increased risk for meningococcal disease among men who have sex with men in the United States, 2012–2015. *Clin Infect Dis*. 2017;65:756–63. <https://doi.org/10.1093/cid/cix438>
 10. Bazan JA, Peterson AS, Kirkcaldy RD, Briere EC, Maierhofer C, Turner AN, et al. Notes from the field: increase in *Neisseria meningitidis*-associated urethritis among men at two sentinel clinics—Columbus, Ohio, and Oakland County, Michigan, 2015. *MMWR Morb Mortal Wkly Rep*. 2016;65:550–2. <https://doi.org/10.15585/mmwr.mm6521a5>
 11. Toh E, Gangaiah D, Batteiger BE, Williams JA, Arno JN, Tai A, et al. *Neisseria meningitidis* ST11 complex isolates associated with nongonococcal urethritis, Indiana, USA, 2015–2016. *Emerg Infect Dis*. 2017;23:336–9. <https://doi.org/10.3201/eid2302.161434>
 12. Tzeng YL, Bazan JA, Turner AN, Wang X, Retchless AC, Read TD, et al. Emergence of a new *Neisseria meningitidis* clonal complex 11 lineage 11.2 clade as an effective urogenital pathogen. *Proc Natl Acad Sci U S A*. 2017;114:4237–42. <https://doi.org/10.1073/pnas.1620971114>
 13. Bazan JA, Stephens DS, Turner AN. Emergence of a novel urogenital-tropic *Neisseria meningitidis*. *Curr Opin Infect Dis*. 2021;34:34–9. <https://doi.org/10.1097/QCO.0000000000000697>
 14. Burns BL, Rhoads DD. Meningococcal urethritis: old and new. *J Clin Microbiol*. 2022;60:e0057522. <https://doi.org/10.1128/jcm.00575-22>
 15. Bartley SN, Tzeng YL, Heel K, Lee CW, Mowlaboccus S, Seemann T, et al. Attachment and invasion of *Neisseria meningitidis* to host cells is related to surface hydrophobicity, bacterial cell size and capsule. *PLoS One*. 2013;8:e55798. <https://doi.org/10.1371/journal.pone.0055798>
 16. Yee WX, Barnes G, Lavender H, Tang CM. Meningococcal factor H-binding protein: implications for disease susceptibility, virulence, and vaccines. *Trends Microbiol*. 2023;31:805–15. <https://doi.org/10.1016/j.tim.2023.02.011>
 17. Tzeng YL, Sannigrahi S, Berman Z, Bourne E, Edwards JL, Bazan JA, et al. Acquisition of gonococcal AniA-NorB pathway by the *Neisseria meningitidis* urethritis clade confers denitrifying and microaerobic respiration advantages for urogenital adaptation. *Infect Immun*. 2023;91:e0007923. <https://doi.org/10.1128/iai.00079-23>
 18. Brooks A, Lucidarme J, Campbell H, Campbell L, Fifer H, Gray S, et al. Detection of the United States *Neisseria meningitidis* urethritis clade in the United Kingdom, August and December 2019—emergence of multiple antibiotic resistance calls for vigilance. *Euro Surveill*. 2020;25:2000375. <https://doi.org/10.2807/1560-7917.ES.2020.25.15.2000375>
 19. Nguyen HT, Phan TV, Tran HP, Vu TTP, Pham NTU, Nguyen TTT, et al. Outbreak of sexually transmitted nongroupable *Neisseria meningitidis*-associated urethritis, Vietnam. *Emerg Infect Dis*. 2023;29:2130–2134. <https://doi.org/10.3201/eid2910.221596>
 20. Taha MK. Simultaneous approach for nonculture PCR-based identification and serogroup prediction of *Neisseria meningitidis*. *J Clin Microbiol*. 2000;38:855–7. <https://doi.org/10.1128/JCM.38.2.855-857.2000>
 21. Maiden MC, Bygraves JA, Feil E, Morelli G, Russell JE, Urwin R, et al. Multilocus sequence typing: a portable approach to the identification of clones within populations of pathogenic microorganisms. *Proc Natl Acad Sci U S A*. 1998;95:3140–5. <https://doi.org/10.1073/pnas.95.6.3140>
 22. Saito R, Nakajima J, Prah I, Morita M, Mahazu S, Ota Y, et al. Penicillin- and ciprofloxacin-resistant invasive *Neisseria meningitidis* isolates from Japan. *Microbiol Spectr*. 2022;10:e0062722. <https://doi.org/10.1128/spectrum.00627-22>
 23. Wick RR, Judd LM, Holt KE. Performance of neural network basecalling tools for Oxford Nanopore sequencing. *Genome Biol*. 2019;20:129. <https://doi.org/10.1186/s13059-019-1727-y>
 24. Wick RR, Judd LM, Gorrie CL, Holt KE. Unicycler: resolving bacterial genome assemblies from short and long sequencing reads. *PLOS Comput Biol*. 2017;13:e1005595. <https://doi.org/10.1371/journal.pcbi.1005595>
 25. Tanizawa Y, Fujisawa T, Nakamura Y. DFAST: a flexible prokaryotic genome annotation pipeline for faster genome publication. *Bioinformatics*. 2018;34:1037–9. <https://doi.org/10.1093/bioinformatics/btx713>
 26. Page AJ, Cummins CA, Hunt M, Wong VK, Reuter S, Holden MT, et al. Roary: rapid large-scale prokaryote pan genome analysis. *Bioinformatics*. 2015;31:3691–3. <https://doi.org/10.1093/bioinformatics/btv421>
 27. Page AJ, Taylor B, Delaney AJ, Soares J, Seemann T, Keane JA, et al. SNP-sites: rapid efficient extraction of SNPs from multi-FASTA alignments. *Microb Genom*. 2016;2:e000056. <https://doi.org/10.1099/mgen.0.000056>
 28. Letunic I, Bork P. Interactive Tree Of Life (iTOL) v5: an online tool for phylogenetic tree display and annotation. *Nucleic Acids Res*. 2021;49(W1):W293–6. <https://doi.org/10.1093/nar/gkab301>
 29. Takahashi H, Morita M, Kamiya H, Fukusumi M, Sunagawa M, Nakamura-Miwa H, et al. Genomic characterization of Japanese meningococcal strains isolated over a 17-year period between 2003 and 2020 in Japan. *Vaccine*. 2023;41:416–26. <https://doi.org/10.1016/j.vaccine.2022.10.083>
 30. Ma KC, Unemo M, Jeverica S, Kirkcaldy RD, Takahashi H, Ohnishi M, et al. Genomic characterization of urethritis-associated *Neisseria meningitidis* shows that a wide range of *N. meningitidis* strains can cause urethritis. *J Clin Microbiol*. 2017;55:3374–83. <https://doi.org/10.1128/JCM.01018-17>
 31. Tettelin H, Saunders NJ, Heidelberg J, Jeffries AC, Nelson KE, Eisen JA, et al. Complete genome sequence of *Neisseria meningitidis* serogroup B strain MC58. *Science*. 2000;287:1809–15. <https://doi.org/10.1126/science.287.5459.1809>

32. Retchless AC, Kretz CB, Chang HY, Bazan JA, Abrams AJ, Norris Turner A, et al. Expansion of a urethritis-associated *Neisseria meningitidis* clade in the United States with concurrent acquisition of *N. gonorrhoeae* alleles. *BMC Genomics*. 2018;19:176. <https://doi.org/10.1186/s12864-018-4560-x>
33. Biagini M, Spinsanti M, De Angelis G, Tomei S, Ferlenghi I, Scarselli M, et al. Expression of factor H binding protein in meningococcal strains can vary at least 15-fold and is genetically determined. *Proc Natl Acad Sci U S A*. 2016;113:2714–9. <https://doi.org/10.1073/pnas.1521142113>
34. Sukhum KV, Jean S, Wallace M, Anderson N, Burnham CA, Dantas G. Genomic characterization of emerging bacterial uropathogen *Neisseria meningitidis*, which was misidentified as *Neisseria gonorrhoeae* by nucleic acid amplification testing. *J Clin Microbiol*. 2021;59:e01699-20. <https://doi.org/10.1128/JCM.01699-20>
35. Bazan JA, Tzeng YL, Bischof KM, Satola SW, Stephens DS, Edwards JL, et al. Antibiotic susceptibility profile for the US *Neisseria meningitidis* urethritis clade. *Open Forum Infect Dis*. 2023;10:ofac661. <https://doi.org/10.1093/ofid/ofac661>
36. Willerton L, Lucidarme J, Walker A, Lekshmi A, Clark SA, Walsh L, et al. Antibiotic resistance among invasive *Neisseria meningitidis* isolates in England, Wales and Northern Ireland (2010/11 to 2018/19). *PLoS One*. 2021;16:e0260677. <https://doi.org/10.1371/journal.pone.0260677>
37. Kretz CB, Bergeron G, Aldrich M, Bloch D, Del Rosso PE, Halse TA, et al. Neonatal conjunctivitis caused by *Neisseria meningitidis* US urethritis clade, New York, USA, August 2017. *Emerg Infect Dis*. 2019;25:972–5. <https://doi.org/10.3201/eid2505.181631>
38. Virji M, Makepeace K, Ferguson DJ, Achtman M, Sarkari J, Moxon ER. Expression of the Opc protein correlates with invasion of epithelial and endothelial cells by *Neisseria meningitidis*. *Mol Microbiol*. 1992;6:2785–95. <https://doi.org/10.1111/j.1365-2958.1992.tb01458.x>
39. Stephens DS, Spellman PA, Swartley JS. Effect of the (alpha 2→8)-linked polysialic acid capsule on adherence of *Neisseria meningitidis* to human mucosal cells. *J Infect Dis*. 1993;167:475–8. <https://doi.org/10.1093/infdis/167.2.475>
40. McNeil G, Virji M, Moxon ER. Interactions of *Neisseria meningitidis* with human monocytes. *Microb Pathog*. 1994;16:153–63. <https://doi.org/10.1006/mpat.1994.1016>
41. Kolb-Mäurer A, Unkmeir A, Kämmerer U, Hübner C, Leimbach T, Stade A, et al. Interaction of *Neisseria meningitidis* with human dendritic cells. *Infect Immun*. 2001;69:6912–22. <https://doi.org/10.1128/IAI.69.11.6912-6922.2001>
42. Hill DJ, Griffiths NJ, Borodina E, Virji M. Cellular and molecular biology of *Neisseria meningitidis* colonization and invasive disease. *Clin Sci (Lond)*. 2010;118:547–64. <https://doi.org/10.1042/CS20090513>
43. Sutherland TC, Quattroni P, Exley RM, Tang CM. Transcellular passage of *Neisseria meningitidis* across a polarized respiratory epithelium. *Infect Immun*. 2010;78:3832–47. <https://doi.org/10.1128/IAI.01377-09>
44. Takahashi H, Kim KS, Watanabe H. Differential in vitro infectious abilities of two common Japan-specific sequence-type (ST) clones of disease-associated ST-2032 and carrier-associated ST-2046 *Neisseria meningitidis* strains in human endothelial and epithelial cell lines. *FEMS Immunol Med Microbiol*. 2008;52:36–46. <https://doi.org/10.1111/j.1574-695X.2007.00342.x>
45. Stefanelli P, Colotti G, Neri A, Salucci ML, Miccoli R, Di Leandro L, et al. Molecular characterization of nitrite reductase gene (*aniA*) and gene product in *Neisseria meningitidis* isolates: is *aniA* essential for meningococcal survival? *IUBMB Life*. 2008;60:629–36. <https://doi.org/10.1002/iub.95>
46. Barth KR, Isabella VM, Clark VL. Biochemical and genomic analysis of the denitrification pathway within the genus *Neisseria*. *Microbiology (Reading)*. 2009;155:4093–103. <https://doi.org/10.1099/mic.0.032961-0>
47. Takahashi H, Kuroki T, Watanabe Y, Tanaka H, Inouye H, Yamai S, et al. Characterization of *Neisseria meningitidis* isolates collected from 1974 to 2003 in Japan by multilocus sequence typing. *J Med Microbiol*. 2004;53:657–62. <https://doi.org/10.1099/jmm.0.45541-0>
48. Fukusumi M, Kamiya H, Takahashi H, Kanai M, Hachisu Y, Saitoh T, et al. National surveillance for meningococcal disease in Japan, 1999–2014. *Vaccine*. 2016;34:4068–71. <https://doi.org/10.1016/j.vaccine.2016.06.018>
49. Jolley KA, Maiden MCJ. BIGSdb: scalable analysis of bacterial genome variation at the population level. *BMC Bioinformatics*. 2010;11:595. <https://doi.org/10.1186/1471-2105-11-595>

Address for correspondence: Hideyuki Takahashi, Department of Bacteriology I, National Institute of Infectious Diseases, Toyama 1-23-1, Shinjuku-ku, Tokyo 162-8640, Japan; email: hideyuki@niid.go.jp

Clinical Manifestations and Genomic Evaluation of Melioidosis Outbreak among Children after Sporting Event, Australia

Simon Smith, Tonia Marquardt, Amy V. Jennison, Andrew D'Addona, James Stewart, Trent Yarwood, Jennifer Ho, Enzo Binotto, Julian Harris, Mark Fahmy, Juliet Esmonde, Megan Richardson, Rikki M.A. Graham, Richard Gair, Lawrence Ariotti, Annie Preston-Thomas, Sally Rubenach, Siobhan O'Sullivan, Darren Allen, Thomas Ragh, Sachjuan Grayson, Sophie Manoy, Jeffery M. Warner, Ella M. Meumann, Jennifer M. Robson, Josh Hanson

Melioidosis, caused by the environmental gram-negative bacterium *Burkholderia pseudomallei*, usually develops in adults with predisposing conditions and in Australia more commonly occurs during the monsoonal wet season. We report an outbreak of 7 cases of melioidosis in immunocompetent children in Australia. All the children had participated in a single-day sporting event during the dry season in a tropical region of Australia, and all had limited cutaneous

disease. All case-patients had an adverse reaction to oral trimethoprim/sulfamethoxazole treatment, necessitating its discontinuation. We describe the clinical features, environmental sampling, genomic epidemiologic investigation, and public health response to the outbreak. Management of this outbreak shows the potential benefits of making melioidosis a notifiable disease. The approach used could also be used as a framework for similar outbreaks in the future.

Melioidosis, caused by the environmental gram-negative bacterium *Burkholderia pseudomallei*, is endemic in northern Australia (1). The most common clinical manifestation of the infection is pneumonia, with or without bacteremia, but almost any organ can be involved, including the liver, spleen, prostate, skin, bones, joints, and central nervous system (2). *B. pseudomallei* is an opportunistic pathogen that usually affects adults, ≈90% of whom have underlying conditions that predispose them to developing the disease (1,3).

Melioidosis is uncommon in children. In a large prospective series from northern Australia, children represented only 4% of cases (1). The infection is usually subclinical in children, and a case series from Thailand estimated that only 1 in 4,600 antibody-

producing exposures resulted in symptomatic disease (4). When clinical disease occurs, children with melioidosis usually have limited cutaneous disease; however, invasive disease, including bacteremia and meningoenzephalitis, also can occur, particularly in children with underlying conditions (5–8).

B. pseudomallei is saprophytic and is in soil of endemic tropical and subtropical areas. During the dry season, the organism is found at soil depths of ≥30 cm, but during the wet season, monsoonal rains cause the rising water table to bring bacteria to the surface where they proliferate (9), increasing the risk for human exposure to the organism. That bacterial cycle also explains the strong seasonality of the disease (10–12).

Author affiliations: Cairns Hospital, Cairns, Queensland, Australia (S. Smith, J. Stewart, T. Yarwood, J. Ho, E. Binotto, J. Harris, M. Fahmy, S. O'Sullivan, T. Ragh, S. Grayson, S. Manoy, J. Hanson); Cairns & Hinterland Health Service, Cairns (T. Marquardt, A. D'Addona, J. Esmonde, M. Richardson, R. Gair, A. Preston-Thomas, S. Rubenach); Forensic and Scientific Services, Brisbane, Queensland, Australia (A.V. Jennison, R.M.A. Graham, L. Ariotti); University of Queensland, Herston, Queensland, Australia (T. Yarwood); James Cook University,

Cairns (T. Yarwood, J. Ho); Royal Brisbane and Women's Hospital, Brisbane, Queensland, Australia (D. Allen); James Cook University, Townsville, Queensland, Australia (J.M. Warner); Sullivan Nicolaides Pathology, Bowen Hills, Queensland, Australia (E.M. Meumann, J.M. Robson); Menzies School of Health Research, Darwin, Northern Territory, Australia (E.M. Meumann); University of New South Wales, Sydney, Australia (J. Hanson)

DOI: <https://doi.org/10.3201/eid2911.230951>

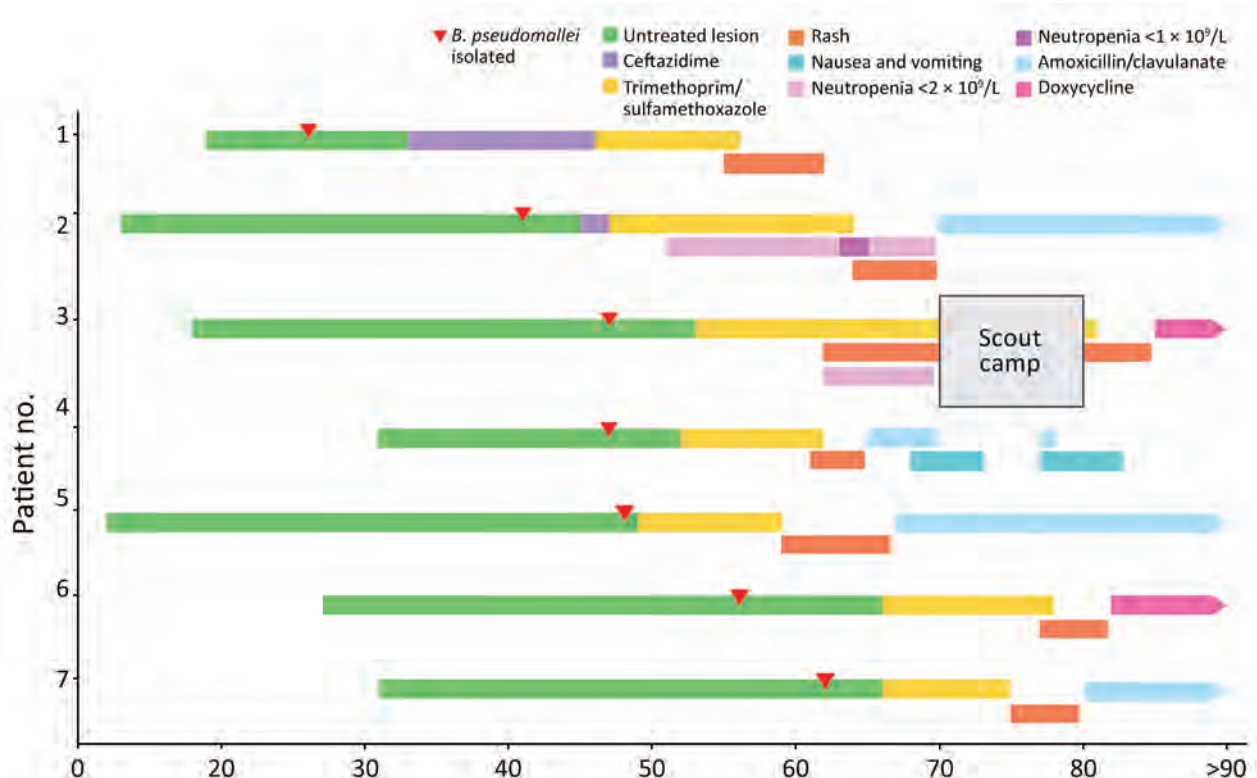


Figure 1. Timeline of clinical manifestations and treatment of melioidosis among 7 children after sporting event, Australia. Limited cutaneous melioidosis developed in children after crawling through a mud pit on an obstacle course in a tropical region of Queensland. All children experienced an adverse drug reaction to trimethoprim/sulfamethoxazole, the preferred oral antimicrobial agent. All case-patients had good clinical outcomes, suggesting that a shorter duration of antimicrobial drugs might be appropriate for limited cutaneous melioidosis in some children.

Melioidosis is usually acquired through percutaneous inoculation, inhalation of contaminated dust, or ingestion of contaminated water (1,13). Although inoculation events are often not evident, many infected persons report recent recreational activities, such as gardening, or occupational exposure to soil or surface water (1). In Far North Queensland, a tropical area of Australia, the incidence of melioidosis in the region’s main city has increased 10-fold in the past 22 years (14). The reasons for the increase are not completely understood but could be related to the local construction of major infrastructure and the expansion of the urban-rural fringe (14).

Cases of melioidosis acquired through sporting activities are exceptionally rare, even in endemic areas where soil sampling confirms the presence of *B. pseudomallei* on sports fields, likely because sports participants lack predisposing conditions for melioidosis (15). Although sporadic melioidosis cases have been linked to sporting events, no outbreaks have been genomically linked to the site of the sporting event. We report the clinical characteristics, case management,

and patient outcomes, as well as genomic evaluation and the public health response, for a melioidosis outbreak among children after a sporting event in a tropical region of Australia.

Methods

Sporting Event

On 1 day in November 2022, children in a primary school in Queensland participated in a sporting event. The event occurred at the end of the region’s dry season, when cases of melioidosis are uncommon, and minimal rain had fallen in the preceding months (16). The sporting event involved an obstacle course on the school grounds that included crawling through a mud pit.

Nineteen days after the event, an 8-year-old female child (case 1) was seen by her general practitioner for a 2-cm pustular lesion on her left arm. She received oral cefalexin for 5 days, but the lesion persisted, and further lesions appeared on her left leg, right leg, and back. *B. pseudomallei* was isolated from a swab of one of the lesions.



Figure 2. Site of exposure in an outbreak of limited cutaneous melioidosis among children after a sporting event, Australia. A) Mud pit site when not in use for the sporting event; members of a wallaby troupe surround the site. B) Mud pit site when not in use for the sporting event; water pooling is evident.

Public Health Response

Melioidosis is a notifiable disease in Queensland, which expedited the public health response. Pathology providers directly alerted the local public health team after culture confirmation, enabling the prompt alert of the school, the children's parents, and health-care providers. Those notifications encouraged parents of affected children to seek healthcare, particularly for nonhealing skin lesions.

A total of 7 melioidosis cases were detected among children who participated in the obstacle course event (Figure 1). Besides the case-patients, ≈ 265 other students also participated in the event, which included a mud pit. The pit had been formed 10 years previously and was dug each year to a depth of ≈ 50 cm and filled with water. After each year's event, the soil was returned to the pit. When not in use, the pit site had become a shallow depression that allowed water to pool (Figure 2). The rest of the obstacle course was located

on undisturbed sports fields. For the November 2022 event, the pit had been filled with chlorinated tap water. All 7 case-patients had crawled through the pit multiple times during the event (Figure 3).

All 7 infected children were immunocompetent. All had limited cutaneous disease (Figure 4), and 4 were aware of a pre-existing lesion, usually insect bites, before participating in the event. None reported sustaining an injury during the event.

Wallabies, marsupials in the Macropodidae family, had been observed on the school grounds. The wallaby troupe had increased to ≈ 200 members during the previous 5 years and were often seen near the site of the mud pit (Figure 2, panel A). Wallabies previously have been hypothesized to spread melioidosis through fecal shedding (17). None of the case-patients reported any notable interaction with the wallabies. Construction has previously been hypothesized to increase the risk of melioidosis, likely by the inhalation route (14),

and 6 of the 7 case-patients regularly walked past roadworks taking place at the edge of the school grounds on their journey to school.

Antimicrobial Drug Treatments

The clinical management of melioidosis usually consists of 2 phases: an intensive phase consisting of intravenous meropenem or ceftazidime for a minimum of 14 days, then an eradication phase of oral trimethoprim/sulfamethoxazole (TMP/SMX) for a minimum of 12 weeks (18). Case-patient 1 received intravenous ceftazidime for 14 days, then TMP/SMX. However, 9 days after commencing TMP/SMX, a widespread, erythematous, pruritic rash developed (Figure 5, panel A). Her antibiotics were ceased, and her rash improved after 5 days. Case 2 also had an adverse reaction to TMP/SMX (Figure 5, panel B). The remaining cases also had adverse reactions to TMP/SMX, necessitating cessation of the drug and prompting an investigation of the adverse drug event (Figure 1).

In all, 5 children received oral therapy only, and 1 received only 2 days of intravenous therapy (Appendix, <https://wwwnc.cdc.gov/EID/article/29/11/23-0951-App1.pdf>). Because of the adverse reactions to TMP/SMX, amoxicillin/clavulanate (AMOX/CLAV) was the predominant antibiotic used in 4 cases (Table 1).

Adverse Drug Event Investigation

When a skin reaction developed in the second patient, the Therapeutic Goods Administration was notified by the hospital pharmacist involved in the care of the patient. Liquid chromatography quadrupole time-of-flight mass spectrometry of 1 patient's urine sample detected TMP/SMX but no unexpected additional compounds. TMP/SMX tablets from separate batches, all of which had been given to the case-patients, were sent to the Therapeutic Goods Administration for further investigation, but only controlled impurities within the control limit specified in the pharmacopeia monograph were identified.

Environmental Sampling and Analysis

We hypothesized that the mud pit was the source of the outbreak and performed environmental sampling 13 weeks after the obstacle course event. Sampling occurred during the region's wet season. We used international recommendations for sampling, but laboratory capacity limited the number of samples that we could process (9). In total, we obtained 18 environmental samples from various areas of the obstacle course event: 14 soil samples, 2 bore water samples from the source used to irrigate the field, and 2 separate

collections of wallaby scat weighing 100 g each (Table 2; Figure 6).

We performed culture of soil and wallaby scat, as previously described (8). In brief, we placed 10 g of soil or scat into 10 mL Ashdown's selective broth (Oxoid–Thermo Fisher Scientific, <https://www.thermo-fisher.com>). For bore water, we filtered 1 L through a 0.45 µm filter (Pall Life Sciences, <https://www.pall.com>), then transferred to 10 mL Ashdown's selective broth. We vigorously vortexed the broth, then incubated at 37°C for 48 hours and subcultured to Ashdown's solid medium plates (Edwards Microbiology, <https://www.edwards.com>). We reviewed plates for *B. pseudomallei* morphotypes and screened up to 5 suspect colonies by using Biotyper (Bruker Corporation, <https://www.bruker.com>) matrix-assisted laser desorption/time-of-flight (MALDI-TOF) mass spectrometry to capture potential strain variation.

Of the 18 environmental samples, we isolated *B. pseudomallei* from 12 (67%), which included 49 individual isolates. We screened those 49 isolates and 29



Figure 3. Images of participants immediately after a sporting event that resulted in an outbreak of limited cutaneous melioidosis, Australia. The sporting event was held in a tropical region of Queensland and involved crawling through a mud pit on an obstacle course. Children are extensively covered in mud immediately after participating in the event. Neither of the pictured children contracted melioidosis. However, *Burkholderia pseudomallei* was isolated in soil samples from the mud pit and genomically linked to *B. pseudomallei* isolated from cutaneous lesions on 7 children who participated in the event and had melioidosis diagnoses.

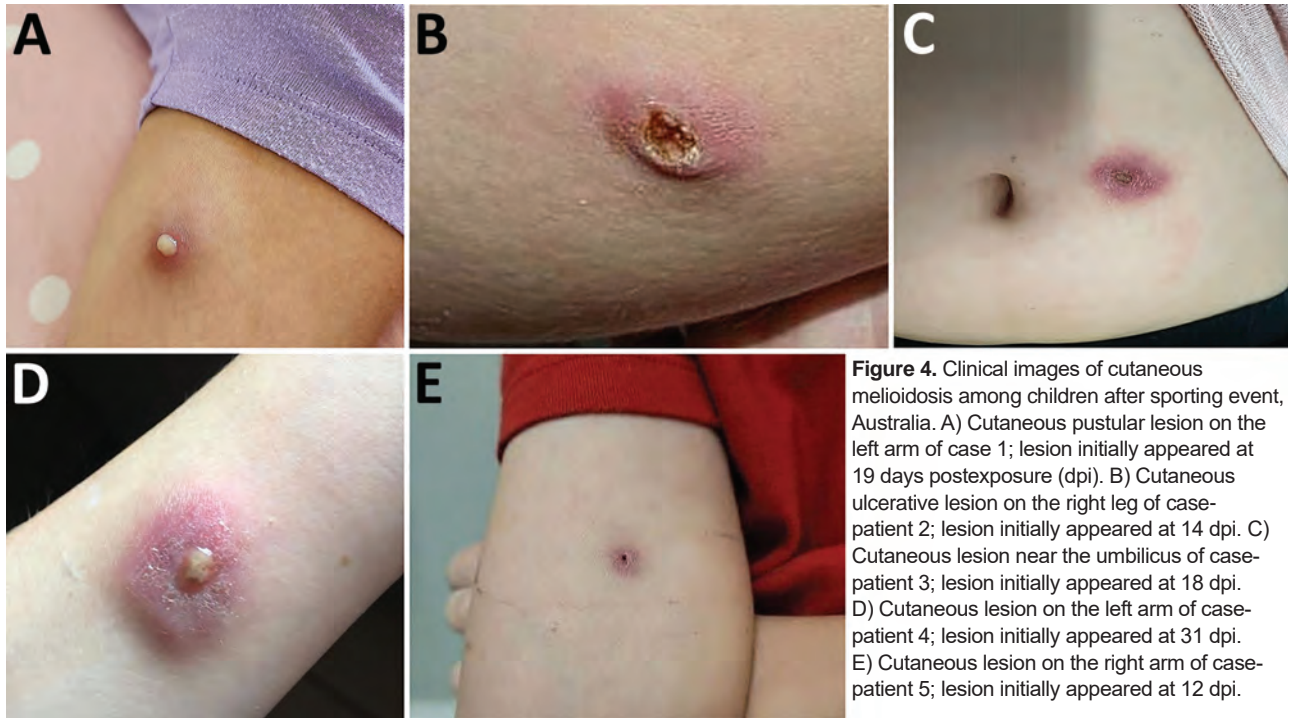


Figure 4. Clinical images of cutaneous melioidosis among children after sporting event, Australia. A) Cutaneous pustular lesion on the left arm of case 1; lesion initially appeared at 19 days postexposure (dpi). B) Cutaneous ulcerative lesion on the right leg of case-patient 2; lesion initially appeared at 14 dpi. C) Cutaneous lesion near the umbilicus of case-patient 3; lesion initially appeared at 18 dpi. D) Cutaneous lesion on the left arm of case-patient 4; lesion initially appeared at 31 dpi. E) Cutaneous lesion on the right arm of case-patient 5; lesion initially appeared at 12 dpi.

returned a result of *B. thailandensis* using the MALDI Biotyper Library (Bruker), an in vitro diagnostic (IVD) database, which cannot distinguish between *B. thailandensis* and *B. pseudomallei*. We further analyzed all IVD spectral profiles using a curated *B. pseudomallei* library and confirmed that all 29 *B. thailandensis* isolates were actually *B. pseudomallei*. The other 20 isolates returned no identification using the IVD library, but we subsequently confirmed those as *B. pseudomallei* by using the curated library. The 49 colonies dis-

played minimal colony variation, and we selected 32 colonies for further testing.

Genomic Investigation

We performed whole-genome sequencing on all 7 clinical isolates and 32 environmental isolates. We extracted and prepared DNA from the isolates for sequencing, as previously described (20). In brief, we prepared DNA by using the Nextera XT Kit (Illumina, <https://www.illumina.com>) and sequenced



Figure 5. Clinical images of adverse reactions secondary to trimethoprim/sulfamethoxazole among children treated for cutaneous melioidosis after a sporting event, Australia. A) Widespread, erythematous, pruritic rash in case-patient 1 that began 9 days after commencing trimethoprim-sulfamethoxazole. B) Lip swelling and a widespread erythematous rash in case-patient 2 that began 16 days after commencing trimethoprim/sulfamethoxazole.

Table 1. Clinical features, antimicrobial drug treatment, and outcomes of limited cutaneous melioidosis among children after sporting event, Australia*

Case no.	Age, y/sex	Location of cutaneous lesion(s)	No. swabs†	Immunocompetent	Disseminated foci excluded‡	Intensive phase duration	Eradication phase duration§	Primary antimicrobial drug#	Outcome
1	8/F	Left arm, right leg, low back	1	Y	Y	14 d	9 d	Ceftazidime	Recovered
2	8/F	Right leg, left leg	2	Y	Y	2 d	12 wk	AMOX/CLAV	Recovered
3	10/F	Abdomen	1	Y	Y	NA	8 wk	Doxycycline	Recovered
4	7/M	Left arm	1	Y	Y	NA	17 d	AMOX/CLAV	Recovered
5	7/M	Right arm	2	Y	Y	NA	12 wk	AMOX/CLAV	Recovered
6	7/F	Right arm	1	Y	Y	NA	9 wk	Doxycycline	Recovered
7	9/F	Right hip	1	Y	Y	NA	12 wk	AMOX/CLAV	Recovered

*AMOX/CLAV, amoxicillin/clavulanate. NA, not applicable.

†Number of swab samples collected before *Burkholderia pseudomallei* was cultured.

‡Defined by no *B. pseudomallei* growth in blood cultures, and no evidence of infection on chest radiograph and abdominal ultrasound.

§Defined as total duration of antimicrobial drug course, excluding treatment interruptions.

#Antimicrobial drug used for longest time.

on the NextSeq 500 using the NextSeq 500 Mid Output Version 2 Kit (Illumina) at 300 cycles, according to the manufacturer’s instructions. We used Trimmomatic version 0.36 to trim sequences (21), and quality checked sequences by using FastQC version 0.11.5 (Babraham Bioinformatics, <https://www.bioinformatics.babraham.ac.uk>) and MultiQC version 1.1 (<https://multiqc.info>) (22). We used SPAdes as-

sembler version 3.12.0 (23) to perform de novo assembly of sequences into contigs. We performed multi-locus sequence type (MLST) and core genome MLST (cgMLST) analysis by using Ridom SeqSphere+ version 8.4 (Ridom Bioinformatics, <https://www.ridom.de>) and publicly available schemes at PubMLST (24). We uploaded sequence data to GenBank (BioProject accession no. PRJEB61871).

Table 2. Environmental sample selections and sampling methods in an investigation of melioidosis among children after sporting event, Australia

Sample site	Rationale for site selection	Sampling method	No. samples
Mud pit	Epidemiologic review suggested the mud pit used during the event was the most plausible source of infection	Soil samples were collected at a minimum of 2.5 m apart and in a grid format	8
	Because this was the likely point of acquisition, the greatest number of samples were taken here	Two additional samples taken in the center of the mud pit	
Earth works	Determine whether earth works brought into the site introduced <i>B. pseudomallei</i>	Area was condensed rock and soil, which was a barrier to reaching 30 cm depth. Soil was also well drained	1
	Identify whether runoff from this site affected other parts of the school, sports field, or mud pit area	Sample was collected at a random spot in the earth works area due to limited laboratory capacity	
	Identify whether this area had similar contamination as other areas		
Drainage area adjacent to earth works	Identify whether runoff or sediment from earthworks or school grounds contained <i>B. pseudomallei</i>	Samples were collected at random spots in sample area due to limited laboratory capacity	3
	Determine if the stormwater diversion drains were introducing <i>B. pseudomallei</i> to the school site	Sample location was identified because areas where runoff and sediment from the earthworks site and school might collect and settle	
Side sports field stormwater runoff	Area appeared to hold water runoff from earthworks site and sports field	Samples were collected at random spots in sample area due to limited testing ability	2
	Detection of <i>B. pseudomallei</i> might have supported theory that <i>B. pseudomallei</i> was introduced to the school site through earthworks	Sample location was identified as an area where water runoff from earthworks site and sports field collected and pooled	
Wallaby scat	Evidence that wallabies can carry <i>B. pseudomallei</i> that might have been spread across the site through their feces (17)	Surface sampling of wallaby feces in areas witnessed to have a high population of wallabies grazing during sampling visit	2
		Scat collected from multiple droppings to meet the 100 g sample requirement Scat collected from ground	
Bore water pump	Evidence that bore water has been found to contain <i>B. pseudomallei</i> (19)	Two water samples taken, a first flush sample and then a sample after the bore had run for a 2-min period. Samples required a minimum of 1 L collected into sterile containers	2

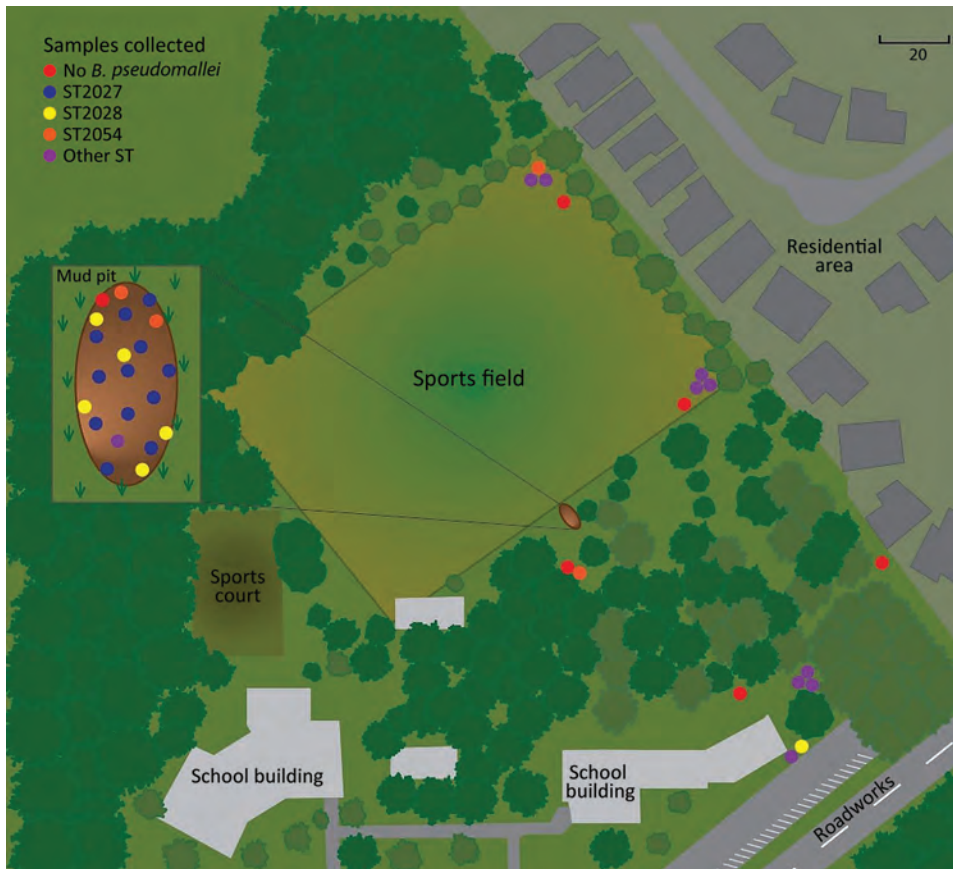


Figure 6. Location of sporting event that resulted in an outbreak of limited cutaneous melioidosis, Australia. The sporting event involved crawling through a mud pit on an obstacle course. Inset shows detail of the mud pit area. Colored dots indicate environmental sampling sites and *Burkholderia pseudomallei* STs detected from samples. Among participants, 7 children who crawled through the mud pit had clinical manifestations of melioidosis. *Burkholderia pseudomallei* isolated in soil samples from the mud pit were later genomically linked to isolates from cutaneous lesions on 7 children. ST, sequence type.

Among the clinical isolates, we found 3 different sequence types (STs): ST2027 in 5 cases, ST2028 in 1 case, and ST2054 in 1 case. Environmental isolates showed much more diversity; we found 9 different STs, 3 of which matched STs of the clinical isolates (Table 3; Figure 7). Genomic analysis of cgMLST showed isolates of all 3 STs from the mud pit and the children had 0–2 cgMLST allele difference, a level of genetic similarity consistent with the mud pit being the source of the exposure (25).

We used BLAST (<https://blast.ncbi.nlm.nih.gov>) analysis to investigate the *fhaB3* gene, a virulence factor involved in host cell attachment and associated with bacteremia, against full-length

fhaB3 genes from the *B. pseudomallei* K96243 genome (GenBank accession no. NZ_CP009537) (26). Of the clinical cases, we found ST2028 isolates had the full-length *fhaB3* gene, but other STs had a truncated version of *fhaB3* that reduced the peptide length from 3,103 to 739 amino acids in ST2027 and to 3,008 amino acids in ST2054 (Figure 7). We are uncertain of the potential functionality of these truncated versions but suspect they might not have the same functionality as the full-length version.

Discussion

This outbreak of melioidosis originating from a sporting event is striking for several reasons. Although

Table 3. Microbiological and genomic results from environmental testing of *Burkholderia pseudomallei* from investigation of melioidosis outbreak among children after sporting event, Australia

Sample site	No. samples collected	No. samples growing <i>B. pseudomallei</i>	No. <i>B. pseudomallei</i> isolates	Sequence type								
				2027*	2028*	2054*	994	2052	2053	2049	2050	1952
Mud pit	8	7	20	12	5	2	1					
Earth works, including drainage	4	2	5		1		1	2	1			
Sports field	2	2	6			1					2	2
Wallaby scat	2	0	0									1
Bore water	2	1	1			1						

*Sequence type genetically matching a clinical case.

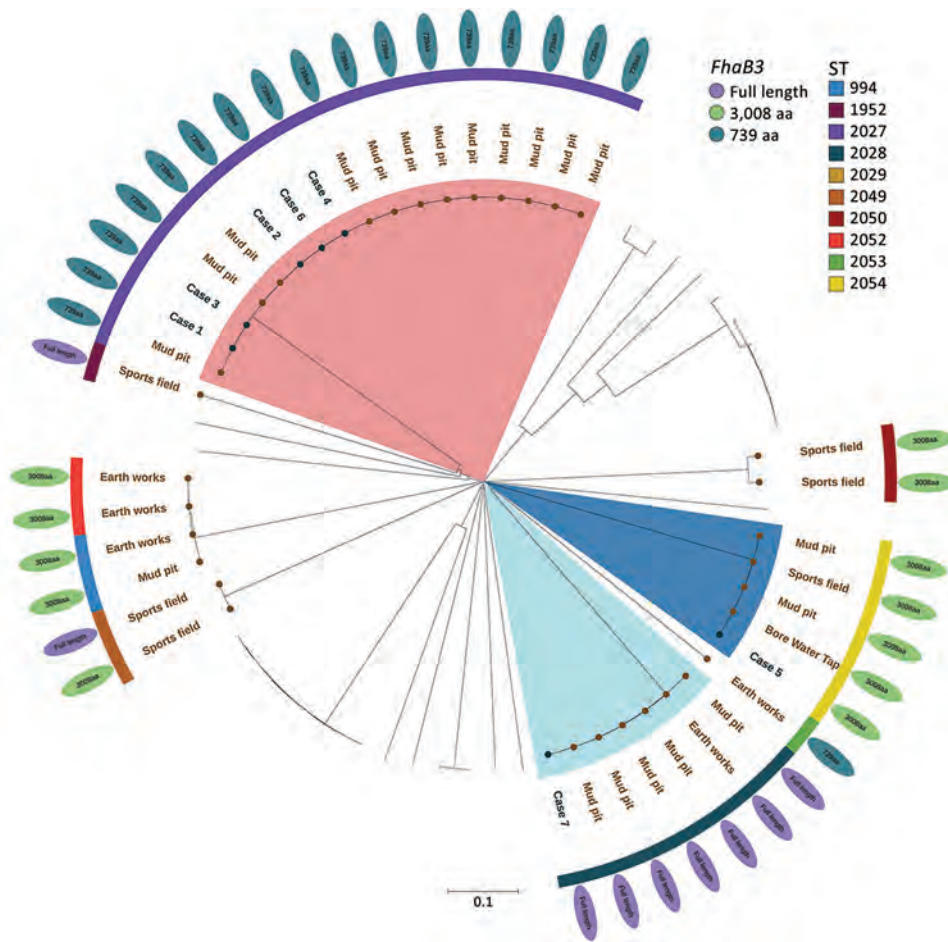


Figure 7. Core multilocus sequence typing of *Burkholderia pseudomallei* isolated in an outbreak of melioidosis among children after a sporting event, Australia. The phylogenetic neighbor-joining tree shows the relationships between environmental and clinical isolates; isolate sources are noted. The tree was constructed by using SeqSphere version 9.0.8 (Ridom, <https://www.ridom.de>) on the *fhaB3* gene and iTOL (<https://itol.embl.de>) was used to add the annotations. Identified *B. pseudomallei* STs are noted. Scale bar indicates nucleotide substitutions per site. ST, sequence type.

the outbreak occurred in an endemic area, the attack rate was 2.6%, much higher than the 0.02% rate of symptomatic disease reported in seropositive children in Thailand (4). The difference could partly be explained by the higher rates of seropositivity generally seen in children in Thailand, which potentially results from increased exposure to *B. pseudomallei* from ingestion of unchlorinated tap water in early life (27,28). In the outbreak we describe, existing abrasions and minor skin trauma sustained during the obstacle course might have enabled inoculation in the mud pit. Our environmental testing was not able to quantify *B. pseudomallei* in the mud pit samples, but a larger inoculum, which can contribute to the development of disease, might be partly responsible for the increased number of cases (29). The full and truncated *fhaB3* gene or other undefined virulence factors also might have contributed to the higher attack rate, although absence the *fhaB3* gene has previously been correlated with cutaneous disease (26). In addition, limited cutaneous melioidosis in immunocompe-

tent children occasionally will heal spontaneously (6). Public health messaging and greater awareness in this outbreak might have improved the detection of cases in persons who otherwise would not have sought medical attention.

The exposure event occurred at the end of the region’s dry season, when cases of melioidosis are uncommon, highlighting that human modification of the environment can increase exposure to *B. pseudomallei* (30,31). MLST matching of the children’s *B. pseudomallei* isolates to those found in the mud pit confirmed that the pit was the source of the outbreak. Contaminated unchlorinated bore water supplies have been implicated in other melioidosis outbreaks (19). In this outbreak, bore water was used regularly on the school’s sports fields, but it had not been used to fill the mud pit. However, sampling of the bore water did identify an MLST that matched 1 child and 2 samples from the pit, suggesting that both the pit and the bore might have become contaminated by organisms from the surrounding soil. For this sporting event, the pit had been filled with chlorinated tap

water, but we were unable to ascertain if a different water source was used in previous years. In addition, because of resource limitations, we were unable to collect extensive environmental samples, including from irrigation equipment that might have been used to fill the pit.

In 2 of the children, an initial swab sample tested negative. Culture of *B. pseudomallei* remains the standard for diagnosing melioidosis, and those cases highlight that even in well-equipped laboratories, multiple or repeat swab samples from skin lesions might be needed to confirm the diagnosis (32). When melioidosis is clinically suspected or a history of soil or water exposure exists, clinicians should advise the laboratory so that appropriate selective and differential media can be used.

Although the same pit had been used in the obstacle course for 9 years before this outbreak, participation in the event had not previously been associated to any confirmed melioidosis cases. However, repeated use and subsequent ground sinkage and water pooling could have resulted in greater soil water content, creating an optimal environment for *B. pseudomallei* growth (33). No *B. pseudomallei* was detected in the 2 wallaby scat samples, making the presence of a large troupe of wallabies an unlikely explanation for the outbreak. However, testing of further samples would be required to fully exclude wallabies as the source of *B. pseudomallei* (17).

The clinical management of melioidosis usually consists of an intensive phase of intravenous meropenem or ceftazidime for a minimum of 14 days, then an eradication phase of oral TMP/SMX for a minimum of 12 weeks (18). However, an eradication phase-only regimen using oral TMP/SMX has been proposed for limited cutaneous disease in children without risk factors for invasive disease and without disseminated foci (6). In our series, 5 children received oral therapy only, and 1 received only 2 days of intravenous therapy. Also, because of the adverse reactions to TMP/SMX, AMOX/CLAV was the predominant antibiotic used in 4 cases. In adults, AMOX/CLAV is associated with higher relapse rates than TMP/SMX-based regimens (34), but AMOX/CLAV has been successfully used as eradication therapy in some children (28). However, the recommended dosing of 20 mg/kg amoxicillin and 5 mg/kg clavulanate 3 times a day could influence tolerability and adherence (35). In 2 cases, doxycycline was the predominant antimicrobial drug therapy, and both children recovered. Doxycycline has previously been avoided in children <8 years of age because of concerns about dental staining, but

durations ≤ 21 days are considered safe in any age group. Rarely, longer courses of doxycycline can be required in children when no suitable alternative is available (36). However, adverse events, such as erosive esophagitis and photosensitivity, particularly in tropical climates, require consideration. In our cases, a doxycycline dose of 2 mg/kg twice daily was administered and was well tolerated by the children.

The clinical course of the children in this outbreak supports recommendations that oral antibiotics alone are appropriate for children with limited cutaneous melioidosis (6). Although TMP/SMX remains first-line therapy, alternative agents can be substituted if TMP/SMX is not tolerated. A 3-month course is recommended for limited cutaneous disease, but recovery is possible with shorter durations (6,28). In this outbreak, 4 cases received substantially less than 3 months of oral therapy, suggesting that, in immunocompetent children without signs of dissemination, a shorter duration could be sufficient (37).

Melioidosis is extant throughout tropical regions of the world, and outbreaks could occur in areas not yet considered endemic for the disease. However, acquiring melioidosis from participation in sporting activities remains exceptionally uncommon, and the risk to children playing in mud or surface water in melioidosis endemic areas is infinitesimally small. Furthermore, that none of the 7 cases in this outbreak developed into invasive disease and that all case-patients had a good clinical outcome is reassuring. Nonetheless, these cases highlight some of the challenges in the diagnosis and management of melioidosis, and the adverse reactions to TMP/SMX illustrate the potential risks associated with this antimicrobial agent (18). These cases also suggest that a shorter duration of antibiotics for limited cutaneous melioidosis might be appropriate for some children, and the use of doxycycline, a drug often avoided in children, could be useful in children with melioidosis if TMP/SMX is not tolerated. As a result of this outbreak, Far North Queensland guidelines have been updated to include advice about the risk to participants of events that include exposure to deeper layers of soil, and consideration of risk assessment for such activities.

In conclusion, the management of this outbreak highlights the virtue of making melioidosis a notifiable disease. The approach used for the public health response, environmental sampling, and genomic investigation of a melioidosis outbreak provided here could be used as a framework for similar outbreaks in the future.

Acknowledgments

We thank the staff members, parents, and children of the school for their support and understanding during this investigation. We also thank Clement Chao for help with the chemical analysis of medications.

About the Author

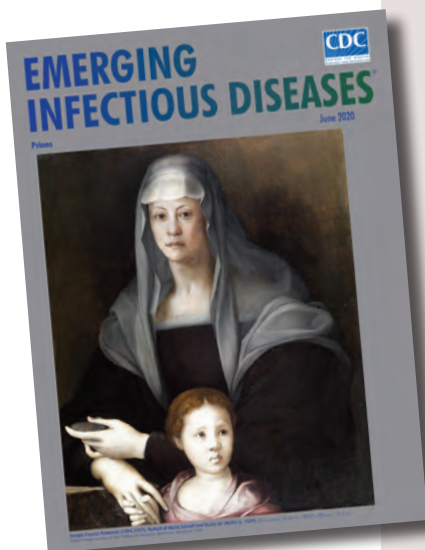
Dr. Smith is an infectious diseases and general internal medicine physician at Cairns Hospital in Cairns, Queensland, Australia. His interests include melioidosis, leptospirosis, and the management of severe clinical manifestations of tropical diseases.

References

- Currie BJ, Mayo M, Ward LM, Kaestli M, Meumann EM, Webb JR, et al. The Darwin Prospective Melioidosis Study: a 30-year prospective, observational investigation. *Lancet Infect Dis*. 2021;21:1737–46. [https://doi.org/10.1016/S1473-3099\(21\)00022-0](https://doi.org/10.1016/S1473-3099(21)00022-0)
- Smith S, Hanson J, Currie BJ. Melioidosis: an Australian perspective. *Trop Med Infect Dis*. 2018;3:27. <https://doi.org/10.3390/tropicalmed3010027>
- Hanson J, Smith S, Stewart J, Horne P, Ramsamy N. Melioidosis—a disease of socioeconomic disadvantage. *PLoS Negl Trop Dis*. 2021;15:e0009544. <https://doi.org/10.1371/journal.pntd.0009544>
- Cheng AC, Wuthiekanun V, Limmathurotsakul D, Chierakul W, Peacock SJ. Intensity of exposure and incidence of melioidosis in Thai children. *Trans R Soc Trop Med Hyg*. 2008;102(Suppl 1):S37–9. [https://doi.org/10.1016/S0035-9203\(08\)70010-5](https://doi.org/10.1016/S0035-9203(08)70010-5)
- Smith S, Stewart JD, Tacon C, Archer N, Hanson J. Children with melioidosis in Far North Queensland are commonly bacteraemic and have a high case fatality rate. *Commun Dis Intell Q Rep*. 2017;41:E318–21.
- McLeod C, Morris PS, Bauert PA, Kilburn CJ, Ward LM, Baird RW, et al. Clinical presentation and medical management of melioidosis in children: a 24-year prospective study in the Northern Territory of Australia and review of the literature. *Clin Infect Dis*. 2015;60:21–6. <https://doi.org/10.1093/cid/ciu733>
- Young A, Tacon C, Smith S, Reeves B, Wiseman G, Hanson J. Case report: fatal pediatric melioidosis despite optimal intensive care. *Am J Trop Med Hyg*. 2017;97:1691–4. <https://doi.org/10.4269/ajtmh.17-0650>
- Gora H, Hasan T, Smith S, Wilson I, Mayo M, Woerle C, et al. Melioidosis of the central nervous system; impact of the *bimA_{bm}* allele on patient presentation and outcome. *Clin Infect Dis*. 2022;ciac111. <https://doi.org/10.1093/cid/ciac111>
- Limmathurotsakul D, Dance DA, Wuthiekanun V, Kaestli M, Mayo M, Warner J, et al. Systematic review and consensus guidelines for environmental sampling of *Burkholderia pseudomallei*. *PLoS Negl Trop Dis*. 2013;7:e2105. <https://doi.org/10.1371/journal.pntd.0002105>
- Gassiep I, Armstrong M, Norton R. Human melioidosis. *Clin Microbiol Rev*. 2020;33:e00006-19. <https://doi.org/10.1128/CMR.00006-19>
- Kaestli M, Grist EPM, Ward L, Hill A, Mayo M, Currie BJ. The association of melioidosis with climatic factors in Darwin, Australia: a 23-year time-series analysis. *J Infect*. 2016;72:687–97. <https://doi.org/10.1016/j.jinf.2016.02.015>
- Fairhead LJ, Smith S, Sim BZ, Stewart AGA, Stewart JD, Binotto E, et al. The seasonality of infections in tropical Far North Queensland, Australia: a 21-year retrospective evaluation of the seasonal patterns of six endemic pathogens. *PLoS Glob Public Health*. 2022;2:e0000506. <https://doi.org/10.1371/journal.pgph.0000506>
- Currie BJ, Ward L, Cheng AC. The epidemiology and clinical spectrum of melioidosis: 540 cases from the 20 year Darwin prospective study. *PLoS Negl Trop Dis*. 2010;4:e900. <https://doi.org/10.1371/journal.pntd.0000900>
- Smith S, Horne P, Rubenach S, Gair R, Stewart J, Fairhead L, et al. Increased incidence of melioidosis in Far North Queensland, Queensland, Australia, 1998–2019. *Emerg Infect Dis*. 2021;27:3119–23. <https://doi.org/10.3201/eid2712.211302>
- Hill AA, Mayo M, Kaestli M, Price EP, Richardson LJ, Godoy D, et al. Melioidosis as a consequence of sporting activity. *Am J Trop Med Hyg*. 2013;89:365–6. <https://doi.org/10.4269/ajtmh.12-0744>
- Australian Bureau of Meteorology. Daily rainfall Cairns Aero [cited 2023 Jun 30]. <http://www.bom.gov.au/climate/data>
- Höger AC, Mayo M, Price EP, Theobald V, Harrington G, Machunter B, et al. The melioidosis agent *Burkholderia pseudomallei* and related opportunistic pathogens detected in faecal matter of wildlife and livestock in northern Australia. *Epidemiol Infect*. 2016;144:1924–32. <https://doi.org/10.1017/S0950268816000285>
- Sullivan RP, Ward L, Currie BJ. Oral eradication therapy for melioidosis: important but not without risks. *Int J Infect Dis*. 2019;80:111–4. <https://doi.org/10.1016/j.ijid.2019.01.019>
- McRobb E, Kaestli M, Mayo M, Price EP, Sarovich DS, Godoy D, et al. Melioidosis from contaminated bore water and successful UV sterilization. *Am J Trop Med Hyg*. 2013;89:367–8. <https://doi.org/10.4269/ajtmh.13-0101>
- Graham RMA, Hiley L, Rathnayake IU, Jennison AV. Comparative genomics identifies distinct lineages of *S. Enteritidis* from Queensland, Australia. *PLoS One*. 2018;13:e0191042. <https://doi.org/10.1371/journal.pone.0191042>
- Bolger AM, Lohse M, Usadel B. Trimmomatic: a flexible trimmer for Illumina sequence data. *Bioinformatics*. 2014;30:2114–20. <https://doi.org/10.1093/bioinformatics/btu170>
- Xue G, Wang Q, Yan C, Jeoffreys N, Wang L, Li S, et al. Molecular characterizations of PCR-positive *Mycoplasma pneumoniae* specimens collected from Australia and China. *J Clin Microbiol*. 2014;52:1478–82. <https://doi.org/10.1128/JCM.03366-13>
- Bankevich A, Nurk S, Antipov D, Gurevich AA, Dvorkin M, Kulikov AS, et al. SPAdes: a new genome assembly algorithm and its applications to single-cell sequencing. *J Comput Biol*. 2012;19:455–77. <https://doi.org/10.1089/cmb.2012.0021>
- Jolley KA, Bray JE, Maiden MCJ. Open-access bacterial population genomics: BIGSdb software, the PubMLST.org website and their applications. *Wellcome Open Res*. 2018;3:124. <https://doi.org/10.12688/wellcomeopenres.14826.1>
- Lichtenegger S, Trinh TT, Assig K, Prior K, Harmsen D, Pesl J, et al. Development and validation of a *Burkholderia pseudomallei* core genome multilocus sequence typing scheme to facilitate molecular surveillance. *J Clin Microbiol*. 2021;59:e0009321. <https://doi.org/10.1128/JCM.00093-21>
- Sarovich DS, Price EP, Webb JR, Ward LM, Voutsinos MY, Tuanyok A, et al. Variable virulence factors in *Burkholderia pseudomallei* (melioidosis) associated with human disease.

- PLoS One. 2014;9:e91682. <https://doi.org/10.1371/journal.pone.0091682>
27. Tiyawisutsri R, Peacock SJ, Langa S, Limmathurotsakul D, Cheng AC, Chierakul W, et al. Antibodies from patients with melioidosis recognize *Burkholderia mallei* but not *Burkholderia thailandensis* antigens in the indirect hemagglutination assay. *J Clin Microbiol*. 2005;43:4872–4. <https://doi.org/10.1128/JCM.43.9.4872-4874.2005>
 28. Lumbiganon P, Chotechuangnirun N, Kosalaraksa P, Teeratakulpisarn J. Localized melioidosis in children in Thailand: treatment and long-term outcome. *J Trop Pediatr*. 2011;57:185–91. <https://doi.org/10.1093/tropej/fmq078>
 29. Cheng AC, Currie BJ. Melioidosis: epidemiology, pathophysiology, and management. *Clin Microbiol Rev*. 2005;18:383–416. <https://doi.org/10.1128/CMR.18.2.383-416.2005>
 30. Stewart JD, Smith S, Binotto E, McBride WJ, Currie BJ, Hanson J. The epidemiology and clinical features of melioidosis in Far North Queensland: implications for patient management. *PLoS Negl Trop Dis*. 2017;11:e0005411. <https://doi.org/10.1371/journal.pntd.0005411>
 31. Kaestli M, Harrington G, Mayo M, Chatfield MD, Harrington I, Hill A, et al. What drives the occurrence of the melioidosis bacterium *Burkholderia pseudomallei* in domestic gardens? *PLoS Negl Trop Dis*. 2015;9:e0003635. <https://doi.org/10.1371/journal.pntd.0003635>
 32. Hoffmaster AR, AuCoin D, Baccam P, Baggett HC, Baird R, Bhengsri S, et al. Melioidosis diagnostic workshop, 2013. *Emerg Infect Dis*. 2015;21:e141045.
 33. Palasatien S, Lertsirivorakul R, Royros P, Wongratanacheewin S, Sermswan RW. Soil physicochemical properties related to the presence of *Burkholderia pseudomallei*. *Trans R Soc Trop Med Hyg*. 2008; 102(Suppl 1):S5–9. [https://doi.org/10.1016/S0035-9203\(08\)70003-8](https://doi.org/10.1016/S0035-9203(08)70003-8)
 34. Rajchanuvong A, Chaowagul W, Suputtamongkol Y, Smith MD, Dance DA, White NJ. A prospective comparison of co-amoxiclav and the combination of chloramphenicol, doxycycline, and co-trimoxazole for the oral maintenance treatment of melioidosis. *Trans R Soc Trop Med Hyg*. 1995;89:546–9. [https://doi.org/10.1016/0035-9203\(95\)90104-3](https://doi.org/10.1016/0035-9203(95)90104-3)
 35. Cheng AC, Chierakul W, Chaowagul W, Chetchotisakd P, Limmathurotsakul D, Dance DA, et al. Consensus guidelines for dosing of amoxicillin-clavulanate in melioidosis. *Am J Trop Med Hyg*. 2008;78:208–9.
 36. Cherry CC, Kersh GJ. Pediatric Q fever. *Curr Infect Dis Rep*. 2020;22:10. <https://doi.org/10.1007/s11908-020-0719-0>
 37. Lumbiganon P, Chotechuangnirun N, Kosalaraksa P. Clinical experience with treatment of melioidosis in children. *Pediatr Infect Dis J*. 2004;23:1165–6. <https://doi.org/10.1097/01.inf.0000145477.29311.71>

Address for correspondence: Simon Smith, Department of Medicine, Cairns Hospital, 165 The Esplanade, Cairns, QLD 4870, Australia; email: simon.smith2@health.qld.gov.au



Originally published
in June 2020

etymologia revisited

Scrapie

[skra'pe]

Scrapie is a fatal neurodegenerative disease of sheep and goats that was the first of a group of spongiform encephalopathies to be reported (1732 in England) and the first whose transmissibility was demonstrated by Cuille and Chelle in 1936. The name resulted because most affected sheep develop pruritis and compulsively scratch their hides against fixed objects. Like other transmissible spongiform encephalopathies, scrapie is associated with an alteration in conformation of a normal neural cell glycoprotein, the prion protein. The scrapie agent was first described as a prion (and the term coined) by Stanley Prusiner in 1982, work for which he received the Nobel Prize in 1997.

References:

1. Brown P, Bradley R. 1755 and all that: a historical primer of transmissible spongiform encephalopathy. *BMJ*. 1998;317:1688–92.
2. Cuillé J, Chelle PL. The so-called “trembling” disease of sheep: is it inoculable? [in French]. *Comptes Rendus de l'Académie Sciences*. 1936;203:1552.
3. Laplanche J-L, Hunter N, Shinagawa M, Williams E. Scrapie, chronic wasting disease, and transmissible mink encephalopathy. In: Prusiner SB, editor. *Prion biology and diseases*. Cold Spring Harbor (NY): Cold Spring Harbor Laboratory Press; 1999. p. 393–429.
4. Prusiner SB. Novel proteinaceous infectious particles cause scrapie. *Science*. 1982;216:136–44.

https://wwwnc.cdc.gov/eid/article/26/6/et-2606_article

Outbreak of *Pandoraea commovens* Infections among Non-Cystic Fibrosis Intensive Care Patients, Germany, 2019–2021

Tassilo Kruis, Peter Menzel, Rolf Schwarzer, Solveigh Wiesener, Felix Schoenrath, Frank Klefisch, Miriam Stegemann, Frieder Pfäfflin

Pandoraea spp. are gram-negative, nonfermenting rods mainly known to infect patients with cystic fibrosis (CF). Outbreaks have been reported from several CF centers. We report a *Pandoraea* spp. outbreak comprising 24 non-CF patients at a large university hospital and a neighboring heart center in Germany during July 2019–December 2021. Common features in the patients were critical illness, invasive ventilation, antimicrobial pretreatment, and preceding surgery. Complicated and relapsing clinical courses were observed in cases with intraabdominal infections but not those with lower respiratory tract infections. Genomic analysis of 15 isolates identified *Pandoraea commovens* as the genetically most similar species and confirmed the clonality of the outbreak strain, designated *P. commovens* strain LB-19-202-79. The strain exhibited resistance to most antimicrobial drugs except ampicillin/sulbactam, imipenem, and trimethoprim/sulfamethoxazole. Our findings suggest *Pandoraea* spp. can spread among non-CF patients and underscore that clinicians and microbiologists should be vigilant in detecting and assessing unusual pathogens.

The widespread use of matrix-associated laser desorption/ionization time-of-flight (MALDI-TOF) mass spectrometry, 16s rRNA sequencing, and whole-genome sequencing (WGS) have improved diagnostic accuracy. However, in using those methods, microbiologists and clinicians can be confronted with uncommon gram-negative, nonfermenting bacteria. Those microorganisms originate from the environment,

and their pathogenic potential is often unclear. When they are cultured from a clinical specimen, determining whether such a finding represents a true pathogen or a contaminant can be difficult.

One example is the genus *Pandoraea*, which was described in 2000 when researchers reclassified several *Burkholderia*- or *Ralstonia*-like organisms cultured from specimens of patients with cystic fibrosis (CF) (1). *Pandoraea* spp. are found in soil and water habitats, where the bacteria contribute to soil formation and cycling of elements necessary for plant growth. By 2022, at least 29 species had been identified within the genus, 19 of which were detected in clinical samples, most often from CF patients (2). Those species are *P. anapnoica*, *P. anhela*, *P. aquatica*, *P. apista*, *P. bronchicola*, *P. capi*, *P. captiosa*, *P. cepalis*, *P. commovens*, *P. communis*, *P. faecigallinarum*, *P. iniqua*, *P. morbifera*, *P. nosoerga*, *P. norimbergensis*, *P. pneumonica*, *P. pnomenusa*, *P. pulmonicola*, and *P. sputorum* (2).

Pandoraea spp. can trigger inflammatory responses and interleukin 6 and 8 elevation in cultures of lung epithelial cells and bacteria from some isolates are capable of crossing lung epithelial cell monolayers (3,4). In an in vivo model for killing *Galleria mellonella* larvae, virulence of some *Pandoraea* strains was comparable to that of *Burkholderia cenocepacia* (3,4). Various other virulence and resistance factors found in other pathogens also can be found in *Pandoraea* spp. (5,6).

Knowledge on the clinical significance of *Pandoraea* spp. is based on case reports and case series. *Pandoraea* spp. can chronically colonize lungs of CF patients and evolve over time by sequential mutations, leading to an adaptation to the CF host niche (7–10). Worsening lung function in CF patients has been linked to *Pandoraea* spp. colonization, but because CF patients often carry multiple other relevant pathogens, causality between

Author affiliations: Labor Berlin Charité Vivantes GmbH, Berlin, Germany (T. Kruis, P. Menzel, R. Schwarzer); German Heart Center Berlin, Berlin (S. Wiesener, F. Schoenrath); Paulinenkrankenhaus, Berlin (F. Klefisch); Charité–Universitätsmedizin Berlin, Berlin (M. Stegemann, F. Pfäfflin)

DOI: <https://doi.org/10.3201/eid2911.230493>

Pandoraea spp. colonization and clinical deterioration is not always clear (9,11,12). The potential of *Pandoraea* spp. to cause acute illnesses has been exemplified by bloodstream and other life-threatening infections in CF patients and patients who received solid organ transplantation (7,13–15).

Single cases of *Pandoraea* spp. infections in patient populations other than those with CF or solid organ transplantation have been documented. Cases have occurred among persons without apparent immunodeficiency, causing illnesses such as nosocomial pneumonia, including infections associated with COVID-19, as well as localized hemodialysis catheter infections, prosthetic valve endocarditis, and skull base osteomyelitis (16–22). Nosocomial acquisition and antimicrobial pretreatment seem to be common features among affected patients (16–22).

Pandoraea outbreaks have been documented in CF centers in Denmark and France, each comprising 6 patients (9,12). One in-depth analysis described a large *P. apista* cluster affecting 18 CF patients serviced at the pediatric and adult CF centers in a city in Scotland and 1 other patient from south England (6). We report a *Pandoraea* spp. outbreak during July 2019–December 2021 at a large university hospital and the directly neighboring heart center in Berlin, Germany, involving 24 non-CF patients colonized or infected with a novel *P. commovens* strain.

Methods

Patient Data

We retrospectively extracted patient data from hospital records. Data included length of hospital stay, time to isolate *Pandoraea* spp., antimicrobial drug treatment, intensive care unit (ICU) admission, renal dialysis, solid organ transplantation, underlying conditions exemplified by the Charlson Comorbidity Index (CCI) scores, and patient outcome. We classified patients as either colonized or infected according to the judgment of 2 infectious disease consultants. Detection of *Pandoraea* spp. from otherwise sterile sites, such as blood, or from intraabdominal specimens was considered as infection. Culture from nonsterile sites (e.g., respiratory samples) was considered colonization if further assessment of antibiotic prescriptions, physicians' notes, laboratory values, and radiology and pathology findings did not reveal evidence of infection. For the diagnosis of pneumonia, ≥ 1 of the following criteria had to be met: new or progressive infiltrate, new or worsening respiratory signs and symptoms, or rising inflammatory markers and assessment of pneumonia by the treating physician. For difficult cases, 2 clinicians

discussed and then agreed on a classification for each case (Appendix, <https://wwwnc.cdc.gov/EID/article/29/11/23-0493-App1.pdf>).

Microbiology

All microbiological investigations were performed by Labor Berlin–Charité Vivantes GmbH in accordance with German Quality Standards for the Microbiological Diagnosis of Infectious Diseases (<https://www.dghm.org>). To detect aerobic bacteria, we plated clinical specimens on conventional solid media, then incubated in ambient air and 5% CO₂ enriched atmosphere at 37°C. We read plates after 24 h and 48 h incubation. We tested suspicious gram-negative microorganisms on oxidase and catalase activity and identified microorganisms by using the VITEK 2 System (bioMérieux, <https://www.biomerieux.com>), VITEK MALDI-TOF mass spectrometry (bioMérieux), or both. Per our clinical routine, we performed antimicrobial susceptibility testing of *Pandoraea* spp. by using the VITEK 2 AST GN-233 card, GN-248 card, or both. In addition, we subjected several isolates to further genomic analyses. For those isolates, we performed broth microdilution by using MICRONAUT-S test plates (MERLIN Diagnostika GmbH, <https://www.merlin-diagnostika.de>), and tested the following antimicrobial agents: piperacillin, piperacillin/tazobactam, temocillin, ceftazidime, cefepime, ceftolozane/tazobactam, ceftazidime/avibactam, meropenem, imipenem, ertapenem, aztreonam, aztreonam/avibactam, ciprofloxacin, levofloxacin, gentamicin, tobramycin, amikacin, trimethoprim/sulfamethoxazole (TMP/SMX), fosfomycin, colistin, minocycline, and tigecycline. We used MIC strips (Liofilchem, <https://www.liofilchem.com>) to solve discrepancies or to test antimicrobial agents that failed or were not included in VITEK 2 or MICRONAUT-S panels. Were interpreted results according to non-species-related pharmacokinetic/pharmacodynamic (PK/PD) breakpoints published by the European Committee on Antimicrobial Susceptibility Testing (23).

We also conducted environmental investigations for a point source of *P. commovens*. For environmental investigations, we probed respiratory tubes, nebulizers, suction catheters, washing gloves, toothbrushes, nutrition solutions, inhalation solutions, oral medications such as painkillers in solution, eye and nasal ointments, and eye drops.

Genomic Sequencing and Analysis

For exact species identification and determination of clonality, we subjected 15 clinical outbreak isolates to WGS, by using either the Nextera Flex (Illumina, <https://www.illumina.com>) or QIASeq FX

(QIAGEN, <https://www.qiagen.com>) library preparation kits, according to the manufacturers' protocols. In brief, we extracted and enzymatically fragmented 10–100 ng of DNA by using DNeasy PowerSoil Pro Kit (QIAGEN). We added indexed adapters and amplified libraries in limited-cycle PCRs. After clean-up, we quantified, normalized, and pooled sequence-ready libraries before sequencing by using 2× 250 cycles paired-end sequencing on a MiSeq (Illumina).

To close the genome, we performed nanopore sequencing on genomic DNA from isolate LB-19-202-79 from our outbreak on GridION (Oxford Nanopore Technologies, <https://nanoporetech.com>) using an R9.4 flow cell (Oxford Nanopore). We prepared the sequencing library by using the SQK-LSK109 Ligation Sequencing Kit (Oxford Nanopore), according to the manufacturer's protocol. We performed basecalling by using Guppy version 5.0.11 (Oxford Nanopore) on the SUP accuracy setting in GridION.

After adapter-trimming the Illumina sequencing reads by using fastp version 0.20.0 (24), we performed de novo genome assemblies by using SPAdes assembler version 3.15.5 (25). For the assembly of nanopore sequencing reads, we tried several protocols using ont-assembly-snake version 1.0 (P. Menzel, unpub. data, <https://doi.org/10.20944/preprints202208.0191.v1>) and eventually chose the protocol that showed the least differences with *P. commovens* strain LMG 31010 (National Center for Biotechnology Information [NCBI] RefSeq accession no. GCF_902459615.1). For that protocol, we used Filtong (<https://github.com/rrwick/Filtong>) to quality-filter nanopore reads that passed the basecalling quality filter to the top 500 megabases and assembled reads using Flye version 2.9 (26). Then, we polished the initial assembly with the ONT reads by using Racon version 1.4.20 (27) and Medaka version 1.4.3 (<https://github.com/nanoporetech/medaka>) and polished the Illumina reads by using Polypolish version 0.5.0 (28). We rotated the final assembly to start at the *dnaA* gene.

We screened the genome assembly of LB-19-202-79 against all available *Pandoraea* spp. assemblies in the NCBI RefSeq database (29) as of July 21, 2022, by using mash-screen version 2.3 (30). We calculated average nucleotide identity (ANI) between genome assemblies by using FastANI version 1.33 (31). We used andi version 0.12 (32) to calculate pairwise genetic distances between the assembled genomes, from which we constructed a phylogenetic tree comprising the isolate assemblies and the closest *Pandoraea* spp. by using the neighbor joining method of the ape package version 5.6 (33).

We uploaded the genome assembly to GenBank for annotation by using the NCBI Prokaryotic Genome Annotation Pipeline (34). The uploaded assembly was then automatically annotated by the Bacterial and Viral Bioinformatics Resource Center (BV-BRC) pipeline (<https://www.bv-brc.org>).

Ethics, Consent, and Permissions

The study was approved by the internal review board of Charité-Universitätmedizin Berlin (registry no. EA4/145/21). The need for informed consent was waived because the study was retrospective.

Results

During July 2019–December 2021, we registered phenotypically identical *Pandoraea* spp. isolates in specimens from 24 patients, which is 8 times the number of all *Pandoraea* spp. detected at our laboratory in the 3 previous years (2016–2018). The cases clustered at Charité Campus Virchow Klinikum (CVK) and Deutsches Herzzentrum Berlin (DHZB), 2 neighboring institutions that are on the same grounds; staff and patients regularly move between the 2 institutions. Thirteen patients were treated at DHZB and 9 were treated at CVK. One other patient was treated at Charité Campus Benjamin Franklin and 1 at Unfallkrankenhaus Berlin, a major trauma center; both of those institutions are in different districts of the city. A total of 7 ICUs, 3 at DHZB and 4 at Charité CVK, and 3 regular wards were affected by the outbreak. Cases were first observed at Charité CVK, then the outbreak shifted after a patient was transferred to 2 ICUs at DHZB. Since late August 2019, nearly all isolates have been recovered on those 2 ICUs (Figure 1). Environmental investigations performed at those ICUs in September 2019 did not reveal any point source.

Patient Information and Outcomes

Among the 24 patients whose cultures grew *Pandoraea* spp., the median age was 67 (range 45–81) years; 50% were male and 50% female. Clinical data were available on 23 patients. Median time from admission to *Pandoraea* spp. detection was 22 days; 22 (96%) of the 23 patients were treated in ICUs. Patients had numerous underlying conditions, and the median CCI was 6 (range 0–13). All patients had received antimicrobial drug treatment during their hospital stays before *Pandoraea* spp. detection, 65% had undergone surgery, and 65% received mechanical ventilation (Table 1).

We considered 12 patients colonized and 10 patients infected. For 2 cases, we were unable to make a classification. All 10 of the infected patients were on mechanical ventilation, compared with only 4 (33%)

colonized patients. Among infected patients, 8 had lower respiratory tract infections and 2 had intraabdominal infections. In 5 infected patients, *Pandora* spp. was part of a polymicrobial culture, and in the other 5 infected patients, no other pathogens were detected. *Pandora* spp. infections were treated with imipenem in 8 patients and meropenem in 2 patients. TMP/SMX was administered as stepdown therapy in 1 patient after initial treatment with imipenem. All respiratory tract infections resolved, whereas the 2 patients with intraabdominal infections had complicated clinical courses that involved several surgical interventions and protracted administration of various antimicrobial agents in both cases (Appendix).

Among the 10 infected patients, 4 died during hospitalization. None of those deaths were judged to be directly related to the *Pandora* spp. infections (Table 2, <https://wwwnc.cdc.gov/EID/article/29/11/23-0493-T2.htm>).

Microbiology Results

During July 2019–December 2021, *Pandora* spp. was cultured from 43 clinical specimens, including throat

swabs, respiratory secretions, bile, ascites, intraabdominal specimens, and wound swabs. Numerous blood cultures were collected from 19 of the 24 patients. However, *Pandora* spp. was only detected in 1 blood culture from a patient with a complicated intraabdominal infection. *Pandora* spp. isolates grew readily after overnight culture on commercial solid media, such as Columbia blood or MacConkey agars. Single colonies appeared pale to grayish, displayed weak oxidase activity, and were catalase negative. Neither a mucoid phenotype nor small colony variants were observed.

Using the VITEK 2 GN ID card, identification was possible only to the genus level. In 4 of 17 tested isolates, a reliable discrimination between *Pandora* spp. and *Bordetella hinzii* could not be made by VITEK 2. In the remaining 13 isolates, we identified *Pandora* spp. with probabilities ranging from 95% to 99%. All 36 isolates tested by VITEK MALDI-TOF mass spectrometry were identified as *P. sputorum* with a score of 99.9. We were able to perform WGS to differentiate *P. commovens* from *P. sputorum* on isolates from patients 7, 9–11, and 14–24, as described in the next

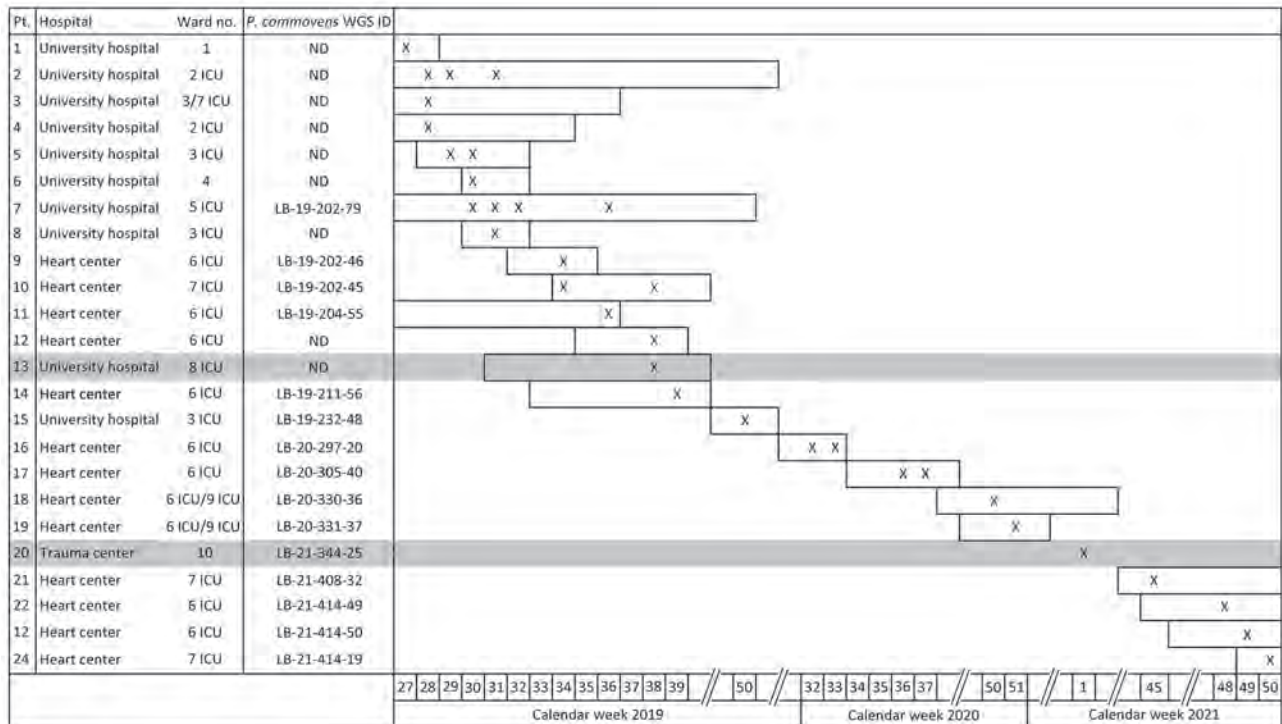


Figure 1. Timeline of an outbreak of *Pandora* *commovens* among non-cystic fibrosis intensive care patients, Germany, 2019–2021. The cases clustered at Charité Campus Virchow Klinikum (university hospital) and Deutsches Herzzentrum Berlin (heart center), 2 neighboring institutions that are on the same grounds and staff and patients regularly move between the 2 institutions. Wards 1–7 are located at the same grounds; wards 8 and 10 are located in facilities elsewhere in Berlin (indicated by grey background). X symbols indicate calendar weeks with detection of *P. commovens*; horizontal bars in timelines indicate length of stay. ICU, intensive care unit; ND not done; Pt., patient; WGS ID, whole-genome sequencing identification number corresponding to the numbering in phylogenetic tree (Figure 2).

section. Because of the local and temporal relationship, identical colony morphology and antimicrobial susceptibilities, we assumed that the correct species identification was *P. commovens* in all patients reported in this outbreak and that *P. sputorum* was a misidentification resulting from limitations in the VITEK mass spectrometry database.

We performed susceptibility testing on 35 isolates. For susceptibility testing methods, agreement between VITEK 2 and MICRONAUT-S broth microdilution plates was good for most tested antimicrobial agents. According to EUCAST PK/PD breakpoints, MICs obtained for ampicillin/sulbactam and imipenem were consistently found to be susceptible at standard dosing levels. MICs for TMP/SMX were ≤ 20 mg/L in all tested isolates. Cephalosporins including ceftazidime/avibactam, ceftolozane/tazobactam, and cefiderocol tested resistant, as did fluoroquinolones, aminoglycosides, tetracyclines, and colistin (Table 3).

Discrepancies between VITEK 2 and microdilution were apparent for piperacillin and piperacillin/tazobactam; higher MICs were detected using VITEK 2 (range 16 to ≥ 128 mg/L for both) than with microdilution (range ≤ 4 to 32 mg/L for piperacillin and ≤ 1 to 2 mg/L for piperacillin-tazobactam). MICs for meropenem and ertapenem were also higher in VITEK 2 (range 4–8 mg/L and 1 to ≥ 8 mg/L, respectively) than in microdilution (range 1–4 mg/L and ≤ 0.5 to 1 mg/L, respectively).

Genomic Characterization and Phylogeny

We screened the genome assemblies from 15 isolates from our outbreak against genomes in RefSeq. We found the genome assembly GCF_902459615.1 of *P. commovens* strain LMG 31010 to be the most similar, then *P. sputorum* strain ATCCBAA64, and *P. oxalatio-orans* strain DSM 23570. The average genome-wide nucleotide identity between isolate LB-19-202-79 and GCF_902459615.1 was 99.5% and identity between LB-19-202-79 and *P. sputorum* GCF_900187205.1 was 94.1%. Thus, we designated our strain as *P. commovens* strain LB-19-202-79. The phylogenetic tree derived from the pairwise phylogenetic distances showed that all our isolates are closely related to each other and distinct from *P. commovens* strain LMG 31010 and other *Pandoraea* spp. (Figure 2). We concluded that the outbreak isolates were from a single origin.

The assembly of isolate LB-19-202-79 (NCBI BioSample no. SAMN30015177) from nanopore sequencing data yielded 1 circular chromosome of 5.9-megabase length (GC content 57%; GenBank accession no. CP102780) and 1 plasmid of 80.7 kb length (GC content 63%, 2 copies; GenBank accession no. CP102779).

Table 1. Patient characteristics in an outbreak of *Pandoraea commovens* among non-cystic fibrosis intensive care patients, Germany, 2019–2021*

Characteristics	Value†	IQR
Sex		
M	12 (50)	NA
F	12 (50)	NA
Age, y	67 (45–81)	61–69
Length of stay, d	51 (0–131)	32–105
Discharged alive	17 (74)	NA
Time to detect <i>P. commovens</i> , d	22 (0–131)	11–45
Intensive care unit admission	22 (96)	NA
Invasive ventilation	15 (65)	NA
Renal replacement therapy	7 (30)	NA
Surgery	15 (65)	NA
Antimicrobial drug therapy		
During hospitalization	23 (100)	NA
During previous 3 mo	14 (82)	NA
Immunosuppressed	5 (22)	NA
Charlson Comorbidity Index	6 (0–13)	3–6
Vascular disease or disorder		
Myocardial infarction	4 (17)	NA
Congestive heart failure	14 (61)	NA
Peripheral vascular disease	3 (13)	NA
Cerebrovascular accident	3 (13)	NA
Chronic lung disease	6 (26)	NA
Peptic ulcer disease	1 (4)	NA
Moderate to severe liver disease	3 (13)	NA
Moderate to severe CKD	9 (39)	NA
Diabetes mellitus	5 (22)	NA
Diabetes mellitus with end-organ damage	4 (17)	NA
Cancer		
Solid tumor	2 (9)	NA
Leukemia	2 (9)	NA
Lymphoma	2 (9)	NA

*Data reflect 23 cases, except for sex, median age, and median length of hospitalization (n = 24). CKD, chronic kidney disease.

†Values are no. (%) or median (range).

A search of the plasmid sequence against the NCBI BLAST nucleotide database (<https://blast.ncbi.nlm.nih.gov>) revealed several alignments to the plasmid of *Burkholderia aenigmatica* strain CMCC(B)23010 (GenBank accession no. CP091649.1), totaling ≈ 22 kb and $\approx 99.9\%$ sequence identity. That strain is a member of the *Burkholderia cepacia* complex and was originally isolated from water purified for pharmaceuticals. Apart from that, we only found alignments to transposase genes in *Klebsiella pneumoniae* plasmids.

The annotation of the LB-19-202-79 chromosome yielded 2 β -lactamase family proteins that are also found in the *P. commovens* strain LMG 31010 genome assembly and have $>99\%$ amino acid identity. The β -lactamase with locus tag NTU39_20675 was identified as an oxacillinase (OXA) 62 family carbapenem-hydrolyzing class D enzyme and now is denoted as allele *bla*OXA-1149 in the NCBI Reference Gene Catalog. The β -lactamase with locus tag NTU39_00730 was identified as a class C β -lactamase. We analyzed the complete resistome

Table 3. Antimicrobial susceptibilities of *Pandoraea commovens* isolates in an outbreak among non-cystic fibrosis intensive care patients, Germany, 2019–2021

Antimicrobial drugs tested	MIC, mg/L	Breakpoints, mg/L	
		Susceptible	Resistant
Ampicillin	≥32	<2	>8
Ampicillin/sulbactam	≤2	<2	>8
Piperacillin	8 to ≥128	≤8	>16
Piperacillin/tazobactam	≤1 to ≥128	≤8	>16
Temocillin	≥128	IE	IE
Cefotaxime	8–16	<1	>2
Ceftazidime	≥64	≤4	>8
Cefepime	≥64	≤4	>8
Ceftolozane/tazobactam	16 to ≥256	<4	>4
Ceftazidime/avibactam	16 to ≥256	≤4	>8
Cefiderocol	≥256	<2	>2
Meropenem	1–8	<2	>8
Imipenem	≤0.25 to 1	<2	>4
Imipenem/relebactam	≤1	<2	>2
Ertapenem	<0.5 to ≥8	≤0.5	>0.5
Aztreonam	32 to ≥128	<4	>8
Aztreonam/avibactam	≥128	NA	NA
Ciprofloxacin	≥4	<0.25	>0.5
Moxifloxacin	≥8	≤0.25	>0.25
Gentamicin	8 to ≥16	<0.5	>0.5
Tobramycin	≥16	≤0.5	>0.5
Amikacin	≥64	1	>1
TMP/SXT	≤20	IE	IE
Fosfomycin	128 to ≥256	IE	IE
Colistin	≥16	IE	IE
Minocycline	1–4	IE	IE
Tigecycline	1	≤0.5	>0.5
Doxycycline	≥16	IE	IE

*MIC results are from susceptibility testing of 35 *Pandoraea* spp. isolates. The table comprises results of different test methods VITEK 2 (bioMérieux, <https://www.biomerieux.com>), MICRONAUT-S broth microdilution (MERLIN Diagnostika GmbH, <https://www.merlin-diagnostika.de>), and MIC strips (Liofilchem, <https://www.liofilchem.com>). IE, insufficient evidence, no breakpoints available; NA, not applicable; TMP/SXT, trimethoprim/sulfamethoxazole.

†According to pharmacokinetic/pharmacodynamic (non-species related) breakpoints from European Committee on Antimicrobial Susceptibility Testing Clinical Breakpoint Tables version 11.0, 2021 (<http://www.eucast.org>).

comprising all genes associated with antimicrobial resistance as determined by the BV-BRC genome annotation (Appendix Table). The complete genome annotation is available at BV-BRC (accession no. 2508289.5; <https://www.bv-brc.org/view/Genome/2508289.5>).

Discussion

We describe a large *Pandoraea* spp. outbreak comprising 24 non-CF patients. In contrast to earlier outbreaks that took place uniformly among CF patients (6,9,12), none of the patients in this outbreak had CF. However, all but 1 patient were treated in an ICU immediately before or during the time when *P. commovens* was isolated. All patients had received antimicrobial drugs before *P. commovens* isolation, and all likely acquired the pathogen in the hospital. Most of the patients had undergone surgery or were on mechanical ventilation, and their overall CCI was high (median 6, range 0–13). Those

observations align with earlier case reports on *Pandoraea* spp. infections among non-CF patients (16–21).

As described by others (35), we experienced difficulties in correctly identifying the species of the outbreak strain. In several cases, *P. commovens* was misidentified as *B. hinzii* by biochemical means. Because *P. commovens* was not identified as a separate species before November 2019 (2), VITEK MALDI-TOF mass spectrometry analysis misidentified the outbreak strain as *P. sputorum*.

Pandoraea spp. can harbor multiple antimicrobial resistance and biodegradation genes, enabling the pathogen to persist in the hospital environment (6). Our resistome analyses and the course of this outbreak that lasted for 2.5 years suggest that *P. commovens* LB-19-202-79 is equipped with such an armament.

Pandoraea spp. exhibit resistance to most antimicrobial agents, including penicillins, cephalosporins, fluoroquinolones, aminoglycosides, and colistin, but frequently are susceptible to imipenem and TMP/SMX (14,36,37). Resistance is mediated by different efflux pumps and β -lactamases with a carbapenem-resistant phenotype observed in isolates carrying OXA-62 or a homologue to OXA-153, both carbapenem-hydrolyzing oxacillinases. OXA-62 hydrolyzes meropenem more efficiently than imipenem, but expanded-spectrum cephalosporins are only poor substrates (5,6,38). Among the β -lactamase family proteins detected in our strain, one was identified as an OXA-62 family carbapenem-hydrolyzing class D β -lactamase, now denoted as OXA-1149. However, all our *P. commovens* isolates were susceptible to imipenem but showed elevated MICs (1–8 mg/L) for meropenem, corresponding to susceptible to increased exposure according to EUCAST PK/PD non-species related breakpoints. The high-level resistance of *P. commovens* to all cephalosporins might at least in part be mediated by the expression of a class C β -lactamase (39). Although all 8 patients with respiratory tract infections recovered with a single course of antimicrobial drugs, the 2 patients with *P. commovens* intraabdominal infections had relapsing courses of disease. *Pandoraea* spp. are environmental bacteria and can thrive in wet settings, such as an abdominal area undergoing multiple surgeries. Under such circumstances, armed with a class D carbapenemase, *P. commovens* LB-19-202-79 might withstand even prolonged targeted antimicrobial treatment, as noted in patient 7 (Appendix).

The assessment of the clinical significance of detection of *P. commovens* in the patients in this outbreak was not always straightforward, especially in cases where *Pandoraea* spp. was cultured from respiratory secretions. Some cases could easily be classified

as colonization, such as when only throat swab samples were positive and patients had no other signs and symptoms of infection. However, *P. commovens* was part of polymicrobial cultures in some patients, and its role in those cases was difficult to estimate. *P. commovens* was the only relevant pathogen that could be detected in 5 of 8 patients with nosocomial pneumonia; however, it was only detected in low to intermediate quantities. Those cases were classified as infections because patients had nosocomial pneumonia, which cleared after administration of targeted antimicrobial drug treatment for *P. commovens*. The pathogenicity of *P. commovens* in the 2 patients with complicated intraabdominal infections seemed evident. *P. commovens* was the predominant pathogen and was repeatedly isolated from different materials, even from blood culture in 1 case.

The first limitation of this study is that we were not able to sequence all *Pandora* spp. isolates from the outbreak. Some uncertainty remains about whether all isolates belonged to the outbreak strain *P. commovens* LB-19-202-79. However, given the identical phenotypic features and the temporal and spatial relationship, we assume the same strain was responsible for all

cases. Second, we were not able to find an environmental source. Third, detection of *Pandora* spp. could not easily be classified as colonization or infection in several patients; however, that is a well-known dilemma when low-virulent pathogens are cultured from non-sterile sites, such as the respiratory tract.

In conclusion, our sequence analysis highlights the advantage of bacterial WGS for exact species identification and typing of outbreak isolates. On the basis of these findings, we conclude that *Pandora* spp. are not only capable of spreading among CF patients, as described before, but also to non-CF patients. The bacteria can also cause outbreaks on ICUs, in particular affecting patients with a history of intensive antimicrobial pretreatment, multiple abdominal surgeries, and mechanical ventilation. This outbreak report underscores the critical role of vigilance among both clinicians and microbiologists when unusual pathogens occur and the need for access to modern molecular sequencing techniques in hospital laboratories.

All sequencing data are available from the NCBI under BioProject no. PRJNA849608.

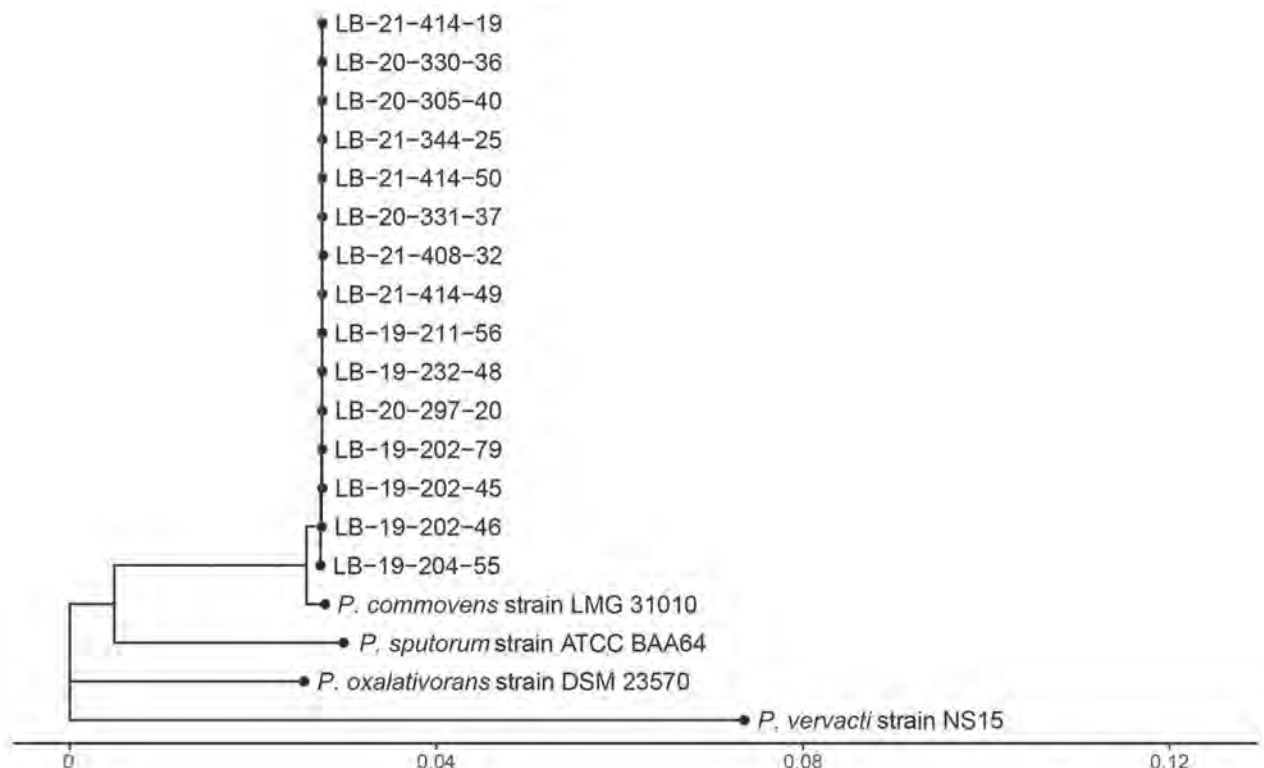


Figure 2. Phylogenetic tree of isolates from an outbreak of *Pandora* *commovens* among non-cystic fibrosis intensive care patients, Germany, 2019–2021. Genome assemblies from 15 isolates (labeled LB) compared with *Pandora* spp. genomes in the National Center for Biotechnology Information RefSeq database (<https://www.ncbi.nlm.nih.gov>) found the genome assembly GCF_902459615.1 of *P. commovens* strain LMG 31010 was the most similar. The tree was created by using neighbor joining the calculated pairwise phylogenetic distances between genome assemblies and available database sequences. Scale bar indicates nucleotide substitutions per site.

About the Author

Dr. Tassilo Kruis is an internist and medical microbiologist at Labor Berlin Charité Vivantes GmbH, Berlin, Germany. His research interests focus on clinical infectious diseases.

References

- Coenye T, Falsen E, Hoste B, Ohlén M, Goris J, Govan JR, et al. Description of *Pandoraea* gen. nov. with *Pandoraea apista* sp. nov., *Pandoraea pulmonicola* sp. nov., *Pandoraea pnomenus* sp. nov., *Pandoraea sputorum* sp. nov. and *Pandoraea norimbergensis* comb. nov. *Int J Syst Evol Microbiol*. 2000; 50:887–99. <https://doi.org/10.1099/00207713-50-2-887>
- Peeters C, De Canck E, Cnockaert M, De Brandt E, Snauwaert C, Verheyde B, et al. Comparative genomics of *Pandoraea*, a genus enriched in xenobiotic biodegradation and metabolism. *Front Microbiol*. 2019;10:2556. <https://doi.org/10.3389/fmicb.2019.02556>
- Caraher E, Collins J, Herbert G, Murphy PG, Gallagher CG, Crowe MJ, et al. Evaluation of in vitro virulence characteristics of the genus *Pandoraea* in lung epithelial cells. *J Med Microbiol*. 2008;57:15–20. <https://doi.org/10.1099/jmm.0.47544-0>
- Costello A, Herbert G, Fabunmi L, Schaffer K, Kavanagh KA, Caraher EM, et al. Virulence of an emerging respiratory pathogen, genus *Pandoraea*, in vivo and its interactions with lung epithelial cells. *J Med Microbiol*. 2011;60:289–99. <https://doi.org/10.1099/jmm.0.022657-0>
- Lim Y-L, Ee R, Yong D, Yu C-Y, Ang G-Y, Tee K-K, et al. Complete genome sequence analysis of *Pandoraea pnomenus* type strain DSM 16536(T) isolated from a cystic fibrosis patient. *Front Microbiol*. 2016;7:109. <https://doi.org/10.3389/fmicb.2016.00109>
- Kenna DTD, Coward A, Perry C, Pike R, Schaefer U, Turton J, et al. Investigation of a *Pandoraea apista* cluster common to adult and paediatric cystic fibrosis patients attending two hospitals in the same city. *J Med Microbiol*. 2019;68:1081–95. <https://doi.org/10.1099/jmm.0.001010>
- Pimentel JD, MacLeod C. Misidentification of *Pandoraea sputorum* isolated from sputum of a patient with cystic fibrosis and review of *Pandoraea* species infections in transplant patients. *J Clin Microbiol*. 2008;46:3165–8. <https://doi.org/10.1128/JCM.00855-08>
- Fernández-Olmos A, Morosini MI, Lamas A, García-Castillo M, García-García L, Cantón R, et al. Clinical and microbiological features of a cystic fibrosis patient chronically colonized with *Pandoraea sputorum* identified by combining 16S rRNA sequencing and matrix-assisted laser desorption ionization-time of flight mass spectrometry. *J Clin Microbiol*. 2012;50:1096–8. <https://doi.org/10.1128/JCM.05730-11>
- Degand N, Lotte R, Decondé Le Butor C, Segonds C, Thouverez M, Ferroni A, et al. Epidemic spread of *Pandoraea pulmonicola* in a cystic fibrosis center. *BMC Infect Dis*. 2015;15:583. <https://doi.org/10.1186/s12879-015-1327-8>
- Greninger AL, Streithorst J, Golden JA, Chiu CY, Miller S. Complete genome sequence of sequential *Pandoraea apista* isolates from the same cystic fibrosis patient supports a model of chronic colonization with in vivo strain evolution over time. *Diagn Microbiol Infect Dis*. 2017;87:1–6. <https://doi.org/10.1016/j.diagmicrobio.2016.10.013>
- Pugès M, Debelleix S, Fayon M, Mégraud F, Lehours P. Persistent infection because of *Pandoraea sputorum* in a young cystic fibrosis patient resistant to antimicrobial treatment. *Pediatr Infect Dis J*. 2015;34:1135–7. <https://doi.org/10.1097/INF.0000000000000843>
- Jørgensen IM, Johansen HK, Frederiksen B, Pressler T, Hansen A, Vandamme P, et al. Epidemic spread of *Pandoraea apista*, a new pathogen causing severe lung disease in cystic fibrosis patients. *Pediatr Pulmonol*. 2003;36:439–46. <https://doi.org/10.1002/ppul.10383>
- Johnson LN, Han J-Y, Moskowitz SM, Burns JL, Qin X, Englund JA. *Pandoraea* bacteremia in a cystic fibrosis patient with associated systemic illness. *Pediatr Infect Dis J*. 2004;23:881–2. <https://doi.org/10.1097/01.inf.0000136857.74561.3c>
- Stryjewski ME, LiPuma JJ, Messier RH Jr, Reller LB, Alexander BD. Sepsis, multiple organ failure, and death due to *Pandoraea pnomenus* infection after lung transplantation. *J Clin Microbiol*. 2003;41:2255–7. <https://doi.org/10.1128/JCM.41.5.2255-2257.2003>
- Xiao X, Tian H, Cheng X, Li G, Zhou J, Peng Z, et al. *Pandoraea sputorum* bacteremia in a patient who had undergone allogeneic liver transplantation plus immunosuppressive therapy: a case report. *Infect Drug Resist*. 2019;12:3359–64. <https://doi.org/10.2147/IDR.S227643>
- Lin C, Luo N, Xu Q, Zhang J, Cai M, Zheng G, et al. Pneumonia due to *Pandoraea apista* after evacuation of traumatic intracranial hematomas: a case report and literature review. *BMC Infect Dis*. 2019;19:869. <https://doi.org/10.1186/s12879-019-4420-6>
- Monzón T, Valga F, Reichert J, López C. Hemodialysis catheter colonized by *Pandoraea sputorum*. *Nefrologia (Engl Ed)*. 2018;38:662–4. <https://doi.org/10.1016/j.nefro.2018.06.013>
- Bodendoerfer E, Personnic N, Mestres CA, Wilhelm MJ, Meyer L, Hasse B. Possible prosthetic valve endocarditis by *Pandoraea pnomenus* and specific virulence mechanisms. *Infect Drug Resist*. 2021;14:1319–24. <https://doi.org/10.2147/IDR.S301138>
- Gawalkar AA, Kasinadhuni G, Kanaujia R, Rajan P, Vijay J, Revaiah PC, et al. Prosthetic aortic valve dehiscence following infective endocarditis by a rare bacterium - *Pandoraea pnomenus*. *J Cardiol Cases*. 2021;24:27–9. <https://doi.org/10.1016/j.jccase.2020.12.003>
- Patil NR, Tripathi M, Charaya K, Angrup A, Ahuja C, Mohindra S. Skull base osteomyelitis by *Pandoraea apista*: an unusual pathogen at unusual location – a case report. *Surg Neurol Int*. 2021;12:447. https://doi.org/10.25259/SNI_472_2021
- Singh S, Sahu C, Patel SS, Garg A, Ghoshal U. *Pandoraea apista* bacteremia in a COVID-positive man: a rare coinfection case report from north India. *J Lab Physicians*. 2021;13:192–4. <https://doi.org/10.1055/s-0041-1730847>
- Dlewati MM, Aung PP, Park K, Rodriguez JA, Poon KK. Meropenem-resistant *Pandoraea* pneumonia in a critically ill patient with COVID-19. *Cureus*. 2021;13:e19498. <https://doi.org/10.7759/cureus.19498>
- European Committee on Antimicrobial Susceptibility Testing. EUCAST Clinical Breakpoint Tables version 11.0, 2021 [cited 2021 Dec 31]. https://www.eucast.org/fileadmin/src/media/PDFs/EUCAST_files/Breakpoint_tables/v_11.0_Breakpoint_Tables.pdf
- Chen S, Zhou Y, Chen Y, Gu J. fastp: an ultra-fast all-in-one FASTQ preprocessor. *Bioinformatics*. 2018;34:i884–90. <https://doi.org/10.1093/bioinformatics/bty560>
- Prijbelski A, Antipov D, Meleshko D, Lapidus A, Korobeynikov A. Using SPAdes de novo assembler. *Curr Protoc Bioinformatics*. 2020;70:e102. <https://doi.org/10.1002/cpbi.102>
- Kolmogorov M, Yuan J, Lin Y, Pevzner PA. Assembly of long, error-prone reads using repeat graphs. *Nat Biotechnol*. 2019;37:540–6. <https://doi.org/10.1038/s41587-019-0072-8>

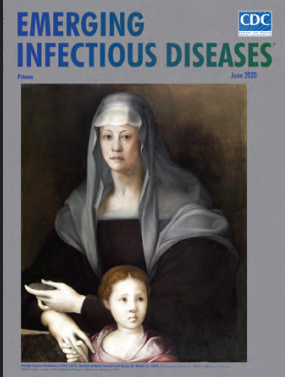
27. Vaser R, Sović I, Nagarajan N, Šikić M. Fast and accurate de novo genome assembly from long uncorrected reads. *Genome Res.* 2017;27:737–46. <https://doi.org/10.1101/gr.214270.116>
28. Wick RR, Holt KE. Polypolish: short-read polishing of long-read bacterial genome assemblies. *PLoS Comput Biol.* 2022; 18:e1009802. <https://doi.org/10.1371/journal.pcbi.1009802>
29. O’Leary NA, Wright MW, Brister JR, Ciufo S, Haddad D, McVeigh R, et al. Reference sequence (RefSeq) database at NCBI: current status, taxonomic expansion, and functional annotation. *Nucleic Acids Res.* 2016;44:D733–45. <https://doi.org/10.1093/nar/gkv1189>
30. Ondov BD, Starrett GJ, Sappington A, Kostic A, Koren S, Buck CB, et al. Mash Screen: high-throughput sequence containment estimation for genome discovery. *Genome Biol.* 2019;20:232. <https://doi.org/10.1186/s13059-019-1841-x>
31. Jain C, Rodriguez-R LM, Phillippy AM, Konstantinidis KT, Aluru S. High throughput ANI analysis of 90K prokaryotic genomes reveals clear species boundaries. *Nat Commun.* 2018;9:5114. <https://doi.org/10.1038/s41467-018-07641-9>
32. Haubold B, Klötzl F, Pfaffelhuber P. andi: fast and accurate estimation of evolutionary distances between closely related genomes. *Bioinformatics.* 2015;31:1169–75. <https://doi.org/10.1093/bioinformatics/btu815>
33. Paradis E, Schliep K. ape 5.0: An environment for modern phylogenetics and evolutionary analyses in R. *Bioinformatics.* 2019;35:526–8. <https://doi.org/10.1093/bioinformatics/bty633>
34. Li W, O’Neill KR, Haft DH, DiCuccio M, Chetvernin V, Badretdin A, et al. RefSeq: expanding the prokaryotic genome annotation pipeline reach with protein family model curation. *Nucleic Acids Res.* 2021;49:D1020–8. <https://doi.org/10.1093/nar/gkaa1105>
35. Martina PF, Martínez M, Frada G, Alvarez F, Leguizamón L, Prieto C, et al. First time identification of *Pandoraea sputorum* from a patient with cystic fibrosis in Argentina: a case report. *BMC Pulm Med.* 2017;17:33. <https://doi.org/10.1186/s12890-017-0373-y>
36. Daneshvar MI, Hollis DG, Steigerwalt AG, Whitney AM, Spangler L, Douglas MP, et al. Assignment of CDC weak oxidizer group 2 (WO-2) to the genus *Pandoraea* and characterization of three new *Pandoraea* genomospecies. *J Clin Microbiol.* 2001;39:1819–26. <https://doi.org/10.1128/JCM.39.5.1819-1826.2001>
37. Fernández-Olmos A, Morosini MI, Lamas A, García-Castillo M, García-García L, Cantón R, et al. Clinical and microbiological features of a cystic fibrosis patient chronically colonized with *Pandoraea sputorum* identified by combining 16S rRNA sequencing and matrix-assisted laser desorption ionization-time of flight mass spectrometry. *J Clin Microbiol.* 2012;50:1096–8. <https://doi.org/10.1128/JCM.05730-11>
38. Schneider I, Queenan AM, Bauernfeind A. Novel carbapenem-hydrolyzing oxacillinase OXA-62 from *Pandoraea pnomensis*. *Antimicrob Agents Chemother.* 2006;50:1330–5. <https://doi.org/10.1128/AAC.50.4.1330-1335.2006>
39. Philippon A, Arlet G, Labia R, Iorga BI. Class C β -lactamases: molecular characteristics. *Clin Microbiol Rev.* 2022;35:e0015021. <https://doi.org/10.1128/cmr.00150-21>

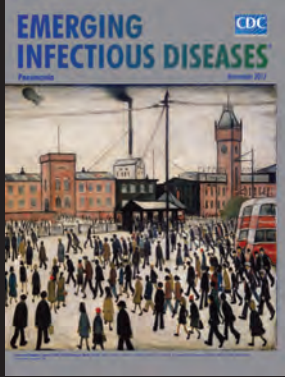
Address for correspondence: Tassilo Kruiis, Charité Vivantes GmbH, Sylter Str. 2, Berlin 13353, Germany; email: tassilo.kruiis@laborberlin.com

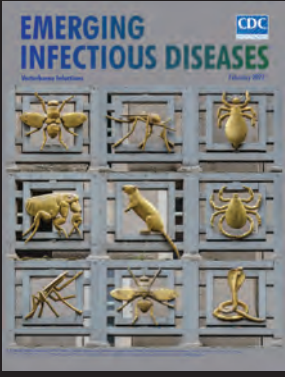
EID Podcast

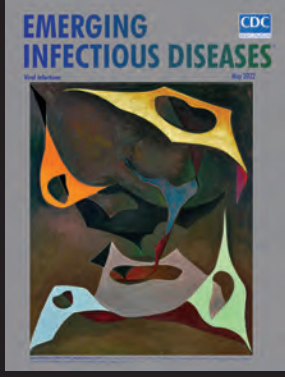
Emerging Infectious Diseases Cover Art

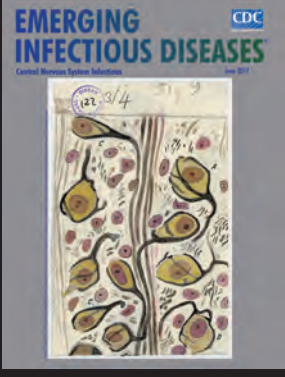
Byron Breedlove, managing editor of the journal, elaborates on aesthetic considerations and historical factors, as well as the complexities of obtaining artwork for Emerging Infectious Diseases.

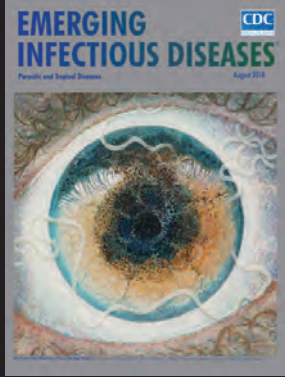












Visit our website to listen:

<https://www2c.cdc.gov/emerging-infectious-diseases/podcasts/player.asp?f=8646224>

Micro–Global Positioning Systems for Identifying Nightly Opportunities for Marburg Virus Spillover to Humans by Egyptian Rousette Bats

Brian R. Amman, Amy J. Schuh, Gloria Akurut, Kilama Kamugisha, Dianah Namanya, Tara K. Sealy, James C. Graziano, Eric Enyel, Emily A. Wright, Stephen Balinandi, Julius J. Lutwama, Rebekah C. Kading, Patrick Atimnedi, Jonathan S. Towner

Marburg virus disease, caused by Marburg and Ravn orthommarburgviruses, emerges sporadically in sub-Saharan Africa and is often fatal in humans. The natural reservoir is the Egyptian rousette bat (ERB), which sheds virus in saliva, urine, and feces. Frugivorous ERBs discard test-bitten and partially eaten fruit, potentially leaving infectious virus behind that could be consumed by other susceptible animals or humans. Historically, 8 of 17 known Marburg virus disease outbreaks have been linked to human encroachment on ERB habitats, but no linkage exists for the other 9 outbreaks, raising the question of how bats and humans might intersect, leading to virus spillover. We used micro-global positioning systems to identify nightly ERB foraging locations. ERBs from a known Marburg virus–infected population traveled long distances to feed in cultivated fruit trees near homes. Our results show that ERB foraging behavior represents a Marburg virus spillover risk to humans and plausibly explains the origins of some past outbreaks.

Marburg virus (MARV) and Ravn virus (RAVV) (family Filoviridae, genus and species *Orthommarburgvirus marburgense*) are the causative agents of Marburg virus disease (MVD). The prototypical filovirus and close relative of Ebola virus, MARV was identified in Germany and the former Yugoslavia in 1967 when laboratory workers had MVD develop after handling

infected African green monkeys (*Cercopithecidae: Chlorocebus tantalus*) imported from Uganda (1,2). Since then, 16 additional MVD outbreaks have been reported, with case-fatality rates of 23%–90% (3). A reported large MVD outbreak in Africa (>100 cases) occurred at the Gorumbwa mine in eastern Democratic Republic of the Congo during 1998–2000, followed nearly a decade later by 2 small outbreaks, at the Kitaka mine in southwest Uganda in 2007 (4,5) and Python Cave in Queen Elizabeth National Park, ≈32 km from Kitaka mine, in 2008 (6).

Subsequent ecologic investigations identified the Egyptian rousette bat (ERB; *Rousettus aegyptiacus*), a cave-dwelling fruit bat, as the MARV natural reservoir based on the repeated detection or isolation of MARV and RAVV directly from ERBs captured at those and other locations (7–15). This conclusion is further supported by experimental infection studies showing that ERBs are capable of shedding MARV for up to 3 weeks, the highest amounts in oral secretions and urine and to a lesser extent in feces (16–18), and that sustained bat-to-bat MARV transmission is possible under laboratory conditions in the absence of any other animals or arthropods normally found in their natural habitat (18).

Many MVD outbreaks were associated with direct human encroachment into ERB roosts and presumably exposure to infectious ERB material such as urine or feces. However, more than half (9/17) of historic MARV spillover events are epidemiologically unlinked to ERB cave habitats or infected secondary hosts. Because ERBs in Africa prefer to roost in unpopulated forested areas, pinpointing the intersections between ERBs and humans is difficult. Moreover, human infection with MARV occurs through broken skin or mucous membranes such as the eyes, nose, or mouth, implying the

Author affiliations: Centers for Disease Control and Prevention, Atlanta, Georgia, USA (B.R. Amman, A.J. Schuh, T.K. Sealy, J.C. Graziano, J.S. Towner); Uganda Wildlife Authority, Kampala, Uganda (G. Akurut, K. Kamugisha, D. Namanya, E. Enyel, P. Atimnedi); Oak Ridge Institute of Science and Education, Oak Ridge, Tennessee, USA (E.A. Wright); Uganda Virus Research Institute, Entebbe, Uganda (S. Balinandi, J.J. Lutwama); Colorado State University, Fort Collins, Colorado, USA (R.C. Kading)

DOI: <https://doi.org/10.3201/eid2911.230362>

need for direct or indirect contact with an infected bat or infectious bodily fluids.

The question remains then, how do MVD outbreaks that are geographically distant from and epidemiologically unlinked to caves or mines get started? One possibility is suggested by virus stability studies showing that MARV remains viable for up to 5 days on surfaces such as wool and glass (19) or up to 6 hours on the surfaces of banana and mango, favorite foods among wild ERBs (20). This level of virus stability might provide sufficient time for humans, nonhuman primates (NHPs), or other potentially susceptible wildlife or domestic animals to be infected by indirect contact with contaminated surfaces or by consumption of fruits soiled with infectious ERB urine, feces, or saliva. ERBs routinely test bite and discard unwanted fruit or spit out masticated fruit pulp in the tree or on the ground (21,22), providing another means for releasing infectious virus into the environment. This behavior of test biting fruit most likely extends to all ERBs throughout their distribution in sub-Saharan Africa, where multiple other MVD outbreaks have occurred (Figure 1). We used micro-global positioning systems (micro-GPS) to track nightly movements of ERBs in Uganda to identify opportunities for MARV spillover to humans.

Methods

Ethics and Biosafety

All animal work was performed with approval of the Centers for Disease Control and Prevention Institutional Animal Care and Use Committee (protocol no. 3063AMMBATX-A2) and with permissions from the Uganda National Counsel for Science and Technology (NS 614) and the Uganda Wildlife Authority (COD96/05) and through collaborations with Uganda Wildlife Authority and Uganda Virus Research Institute. All personnel wore appropriate personal protective equipment while performing all bat handling aspects of this field study as described (23). Those materials and procedures included disposable gowns or Tyvek coveralls, double gloves (including bite-resistant gloves if necessary), face shields, and respiratory protection.

Bat Capture and Processing

To determine if ERBs, originating from a known MARV-infected population, routinely travel long distances to forage in cultivated fruit crops near homes, we fitted 100 male bats from Python Cave in Maramagambo Forest, part of Queen Elizabeth National Park in Uganda, with micro-GPS units and tracked their nightly movements. This process was performed over 2 separate capture sessions, once in February 2022 and again in August 2022,

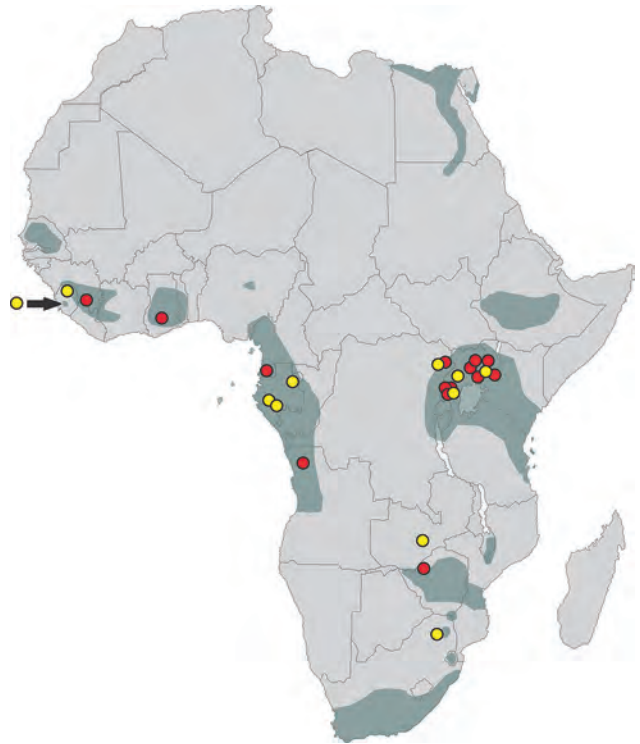


Figure 1. Distribution of *Roussettus aegyptiacus* bats in Africa (dark gray shading), showing locations of known Marburg virus disease spillover events into humans (red dots) and Egyptian rousette bats (*R. aegyptiacus*) that previously tested positive for Marburg or Ravn viruses (yellow dots). The bat distribution was adapted from the International Union for Conservation of Nature and Natural Resources Red List of Threatened and Endangered Species distribution maps (<https://www.iucnredlist.org>), except for the shaded area in Sierra Leone indicated by the yellow dot and black arrow, which represents a range extension for Egyptian rousette bats not shown on the Red List website (7).

marking 50 bats each time. We selectively captured the bats by using handheld sweep nets. Only adult male bats were used in this study, to avoid burdening pregnant female bats with the GPS units.

As part of an ongoing zoonotic virus surveillance effort at Python Cave, an additional 50 bats were captured for destructive sampling. The bats were humanely euthanized under anesthesia and necropsied following procedures outlined in Amman et al. (23). Tissues harvested were cardiac blood, liver, spleen, heart, lung, kidney, salivary gland, and axillary lymph node; tissues were either flash frozen in liquid nitrogen for storage or placed in of virucidal lysis buffer and homogenized (100 mg tissue in 1 mL MagMax Lysis Buffer; Life Technologies, <https://www.thermofisher.com>) for RNA extraction and downstream PCR analysis. When handling bats and performing necropsies, all personnel wore appropriate personal protective equipment that included disposable gowns, double gloves (including bite-resistant

gloves if necessary), and powered air-purifying respiratory protection.

Viral Detection

We extracted RNA from 125 μ L of tissue homogenate on the MagMAX Express-96 Deep Well Magnetic Particle Processor (Thermo Fisher Scientific, <https://www.thermofisher.com>) from homogenized tissues by using the MagMAX Total RNA Isolation Kit (Thermo Fisher Scientific). We then tested the extracted RNA by quantitative reverse transcription PCR (qRT-PCR) targeting the MARV protein 40 gene (VP40; see Amman et al. [7] for primer and probe sequences) and the eukaryotic 18S rRNA gene (Eukaryotic 18S rRNA Endogenous Control Kit; Thermo Fisher) by using the SuperScript III Platinum One-Step qRT-PCR Kit (Thermo Fisher Scientific).

GPS Tracking and Data Analysis

We attached small (≤ 7 g) micro-GPS units (Telemetry Solutions, <https://www.telemetrysolutions.com>) to an area of the bat's dorsum just between the scapulae (Figure 2) by using a veterinary adhesive (America's Acres Inc., <https://americasacres.com>). We used male bats weighing >100 g (mean 161.0 g, range 118.0–188.0 g) to keep the total percentage of unit weight to body-weight ratio $<10\%$. We kept bats fitted with GPS units in a screenhouse for several minutes to ensure a good GPS fit and unincumbered flight before release. The GPS units were preprogrammed to begin collecting data at 5-minute intervals beginning at 7:00 PM and stopping at 5:00 AM the next morning for the duration of the



Figure 2. Micro–global positioning system placement on an adult male Egyptian rousette bat (*Rousettus aegyptiacus*). Micro–global positioning system units (≤ 7 g; Telemetry Solutions, <https://www.telemetrysolutions.com>) were attached to the dorsum of male bats weighing >100 g.

battery life. We placed a base station capable of wireless data download (Telemetry Solutions) just inside the entrance of Python Cave so that the entire cave interior was within line-of-sight. To preserve GPS battery life, we used a repeater antenna outside the cave to transmit satellite signal to the GPS units on the bats inside the cave.

We collected the base station 5–7 days after the last GPS unit was deployed and downloaded the data to the Collar software (Telemetry Solutions) where it was converted to KML (Keyhole Markup Language) file format and viewed on Google Earth Pro version 7.3.4.8642 (<https://www.google.com>) to locate foraging sites and generate minimum convex polygons. We calculated average flight distance by using ArcGIS Pro 2.9.2 (Environmental Systems Research Institute, Inc., <https://www.esri.com>) to estimate movement by converting multiple KML layers to shapefiles and using the Generate Near Table Tool (<https://pro.arcgis.com>) with the Geodesic method selected for the Method parameter to calculate distances between the furthest 2 GPS locations. We defined foraging sites as areas where the GPS-fitted bats remained in the area, presumably feeding, for >30 minutes. We examined GPS trajectories to locate bat visits within 0–30 m from houses, cultivated crops, or forest patches near farms or cultivated crops outside the contiguous forest preserve.

Results

MARV Circulation in ERBs

Analysis of samples acquired from the ongoing viral zoonoses surveillance has shown that MARV continues to circulate in the ERB population roosting in Python Cave. Of the 50 bats captured for destructive sampling, 2 (4.0%) of 50 had detectable MARV RNA identified by qRT-PCR.

GPS Tracking

Of the 100 ERBs fitted with GPS units, data from 70 bats were ultimately usable. Data from the other 30 units either were never received or were not usable because the data points were so few that no discernable flight pattern could be determined. We suspect that complete GPS failures were caused by the unit being pulled off by the bat or its roost mates or by the bat not returning to that roost, preventing the wireless download of data to the base station. Other reasons might include failure of the unit, including the battery; failure of the adhesive; or predation by one of the many snakes living in the cave or some other predator, such as birds of prey, in the surrounding area.

Plotting the bat GPS coordinates onto satellite imagery showed that over a maximum battery life span

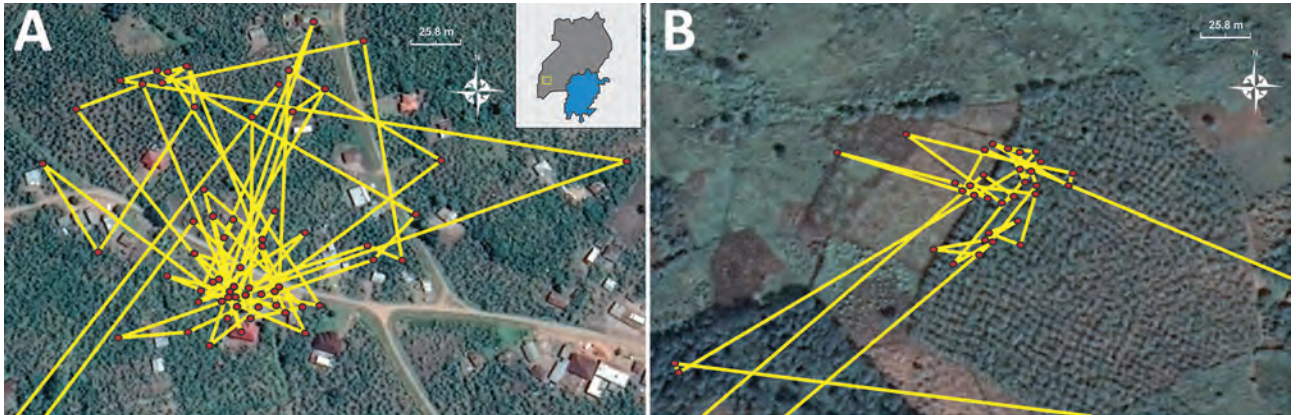


Figure 3. Google Earth Pro (<https://www.google.com/earth/versions>) images of Egyptian roussette bat (*Rousettus aegyptiacus*) foraging activity, southwest Uganda, February 2022. Both images show micro-global positioning system locations of Egyptian roussette bats from a population of known Marburg virus-infected bats foraging in fruiting trees and cultivated crops near homes in southwest Uganda. Red dots indicate individual global positioning system points taken at 5-minute intervals, connected by yellow lines indicating the track from one point to another. A) Home with mango, avocado, papaya, and banana crops ≈ 12 km northeast of Python Cave visited by bat MV19. Total time spent at this site was 5 hours and 35 minutes (10:35 PM–4:10 AM) overnight on February 12, 2022. Inset map shows study area in Uganda (yellow square). B) Banana crop visited by bat MV18 200 m northwest of a farm, ≈ 49 km south-southwest of Python Cave. Total time spent at this site was 1 hour and 30 minutes (02:00 AM–3:30 AM) on February 13, 2022, and again for 1 hour and 20 minutes (2:40 AM–4:00 AM) on February 14, 2022.

of 4 days (range 1.5–4 days), ERBs from Python Cave had an average flight distance of 60.18 km (range 0.83–1,176.10 km) and visited 6 different homes and 34 independent cultivated crop localities in the surrounding agricultural communities. In some instances, bats visited the same location on consecutive nights. In total, 68/70 bats with GPS data (97.14%) made at least 1 visit to a house, a cultivated crop, or a forest patch near a farm or home in an agricultural area outside of the forest preserve surrounding Python Cave.

We assessed the accuracy of the GPS data by performing ground truthing, a method used to compare data from field measurements to data collected remotely, at 2 locations in August 2022 at sites where bats visited, presumably foraging, for extended periods on consecutive nights. At 1 house, bat MV19 visited for 5 hours and 35 minutes (10:35 PM–4:10 AM) overnight on February 12–13, 2022 (Figure 3, panel A). There, mango, papaya, avocado, and bananas were directly observed growing in the yard and along the sides of the house (Figure 4, panel A). Furthermore, a young pig (*Sus scrofa*) was observed rooting under the mango tree (Figure 4, panel B, C). An interview with the homeowner confirmed that the mango tree was fruiting in February 2022 when the GPS-tagged bat foraged in the tree. At a second site, bat MV18 spent 1 hour and 30 minutes (2:00 AM–3:30 AM) on February 13, 2022, and then foraged again at the same site for 1 hour and 20 minutes (2:40 AM–4:00 AM) the following night (Figure 3, panel B). The crops visited at this second site were predominantly bananas but also mangos. We have not published GPS coordinates for those locations to protect the privacy of the property owners.

Movement Area

To quantify the estimated minimum movement area where the ERBs appeared to forage nightly, we created a minimum convex polygon (MCP) (24–27) by using the outermost peripheral sites ($n = 9$) where the GPS-fitted bats foraged for >30 minutes (homes, crops, and forest patches) for both February and August 2022. In total, the area of bat foraging activity encompassed by this MCP was 1,887 km², of which 44.8% (846 km²) was in agricultural or community areas outside the forest (Figure 5). Even though the shortest distance from Python Cave and the forest preserve to an agricultural area was just >0.5 km, the longest distance traveled by a single bat in 1 night was 57 km, suggesting a theoretical foraging zone radiating >50 km in any direction from an ERB roost. The GPS data also showed that several ERBs came within 10 km of Kitaka mine, where, in 2007, 2.8% of an ERB colony containing $>100,000$ animals, or $\approx 5,000$ bats total, were found to be actively infected with either MARV or RAVV (13).

Discussion

Analysis of the tissues from the bats euthanized as part of ongoing zoonotic viral surveillance determined that MARV continued to circulate in Python Cave almost 15 years after 2 tourists were infected there, once in December 2007 and again in July 2008 (6,28). Moreover, the level of active infection was consistent with that found among adult bats during previous studies at Python Cave (8), albeit with a much smaller sample size. The data reported showed that ERBs at Python Cave, a forest-bound roost of $>40,000$ bats (8), routinely travel distances

up to 57 km to forage in peripheral agricultural areas where they have easy access to human cultivated fruits and wild fruiting trees opportunistically used by humans and domestic livestock. Given the known distribution of ERBs in Africa, overlaid by locations of past MVD outbreaks and MARV-positive ERBs (Figure 1), the potential area in Africa at risk for virus spillover is considerable but, on a fine scale, might be limited to foraging range of ERB roosts. This behavior presents a previously underappreciated geographic range and potential mechanism of MARV spillover that might explain the origins of MVD outbreaks, such as those most recently in Guinea in 2021, Ghana in 2022, and Equatorial Guinea and Tanzania in 2023. In all instances, ERBs were reported near the index case, but ensuing epidemiologic investigations produced no links between the primary cases and known ERB colonies.

At Python Cave, 6 of the 70 GPS-tagged ERBs foraged in fruiting trees near houses, sometimes on consecutive nights by the same bat; 1 house was later confirmed to have both mangoes and bananas growing within a few meters of the structure. In that instance, the ERB stayed at the location for >5.5 hours, vacating the

area just 2 hours before sunrise, leaving a period of up to 4 hours after sunrise for humans to encounter infectious virus shed in ERB excreta or oral secretions.

The role of secondary animal hosts must also be considered, and at the time of ground truthing, a young pig was observed rooting under the same mango tree the ERB visited, not far from children playing in the yard. Pigs are known to be susceptible to ebolavirus (Reston and Ebola virus) infection (29,30), which suggest a potential susceptibility to MARV infection. Given that experimental infection studies of ERBs have shown that $>10^4$ 50% tissue culture infectious doses/mL of MARV can be shed intermittently in oral secretions for up to 19 days after infection (16,18,31), this mechanism of bat-to-human MARV transmission is plausible, as well as potential transmission events involving intermediate hosts such as pigs or NHPs. Such competition for cultivated fruit could draw ERBs and other animals together in time and space when they otherwise might not interact.

MVD and Ebola disease outbreaks have been initiated through hunting or scavenging of infected sick, dying, or recently dead animals or by unwitting importation of diseased NHPs for research (1,2,32–34). Both

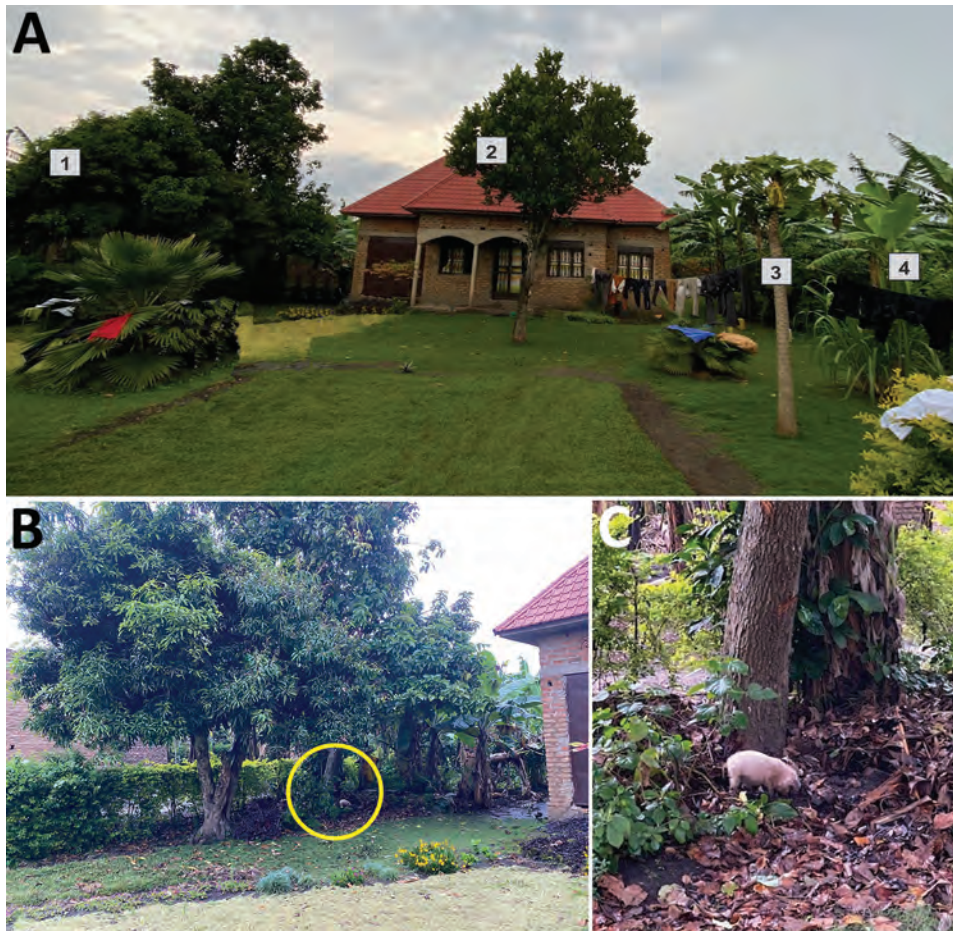


Figure 4. House visited by Egyptian rousette bat (*Rousettus aegyptiacus*) MV19, southwest Uganda, February 2022. A) Front view of the house where bat MV19 spent 10:35 PM–4:10 AM on February 12 and 13, 2022, foraging: 1, mango tree; 2, avocado tree; 3, papaya tree; 4, banana crop. B) Pig rooting underneath a mango tree (yellow circle). C) Enlargement of yellow circled area from panel B.

Reston virus, an ebolavirus, and Nipah virus, a paramyxovirus carried by multiple species of *Pteropus* bats, have emerged in pigs (35,36), and Reston virus emerged in NHPs imported from the Philippines to the United States in 1989 (37). Moreover, domestic pigs were believed to have been infected with Nipah virus by eating fruit dropped by bats that was contaminated with bat excreta (38), and infectious MARV was recovered from experimentally inoculated banana and mango up to 6 hours postinoculation (20).

Although the exact number of bats visiting the areas identified by the GPS units is unknown, newly independent juvenile ERBs have been shown to use the same navigation routes and foraging areas as their mothers (39). Therefore, it is probable that older juvenile bats, the age cohort with the highest incidence of MARV infection (8), forage on the same cultivated crops as their male GPS-fitted ERB counterparts. This result is supported by findings that human-generated land use changes are linked to increases in the abundance of zoonotic reservoir species, along with decreases in nonreservoir species (40). This loss in biodiversity correlates with increased human exposure to zoonotic pathogens (41–43). It is therefore not difficult to picture the remnants of a forest surrounded by drastically altered agricultural areas as having much reduced biodiversity, leading to increased prevalence of ERBs practicing foraging patterns learned from older ERBs, thereby continuing to circulate MARVs in the surrounding altered habitat areas.

The GPS data showed that several ERBs came close to Kitaka mine, which supports earlier published accounts that infected ERBs at Python Cave, ≈ 32 km from Kitaka mine, routinely travel between roosts, effectively creating a small scale metapopulation within 2 forest preserves (8). Combined with twice yearly breeding and seasonal pulses of up to 12% MARV infection in juvenile ERBs, this finding could help explain how such a large amount of MARV genetic diversity is maintained at those 2 locations (8,13,44). The foraging data also suggest that other homes and agricultural areas in Uganda, beyond what is shown here, are frequented by ERBs. To get a sense of the overall potential for ERB-human interactions, we can consider that 8.5% (6/70) marked bats visited fruit trees near homes over an ≈ 4 -day period. Extending those values to an ERB population of 40,000 bats, 2.8% of which are actively infected, translates to 95 home visits by MARV-infected bats every 4 days, or 8,668 infected bat visits per year. Although highly consequential if infection does occur, those numbers also suggest that, despite the large geographic zone of risk surrounding ERB roosts, actual spillover events that result in outbreaks are rare, probably requiring an alignment of multiple circumstances,



Figure 5. Minimum convex polygons (MCP) of Egyptian rousette bat (*Rousettus aegyptiacus*) total foraging area, southwest Uganda, February and August 2022. Yellow lines indicate MCP of foraging area overall (1,887 km²); orange lines indicate MCP of foraging area in agricultural communities (846 km²). Red dots for all MCPs indicate the outermost peripheral sites where the bats fitted with micro-global positioning system units foraged for >30 minutes. MCPs are shown in relation to Python Cave, where the Egyptian rousette bats roost and were fitted with the micro-global positioning system; the house visited by bat MV19; and Kitaka Mine, the site of a 2007 Marburg virus outbreak.

including seasonal fruiting periods, akin to that proposed for how Hendra virus spills over into horses (45). Nevertheless, a successful transmission event of this batborne virus or others, even if extremely rare, can be devastating. Examples include the recent Ebola outbreak in West Africa during 2013–2016 that infected >28,000 persons, primarily in Guinea, Sierra Leone, and Liberia, and, more recently, the COVID-19 pandemic caused by SARS-CoV-2, a batborne coronavirus that spilled over into humans, possibly from a horseshoe bat (*Rhinolophus affinis*) (46).

We report findings of visits to cultivated fruit crops near homes and farms by a known MARV natural

reservoir, the ERB. Although this information has public health usefulness, the study has several limitations, including battery limitations of the GPS units, shorter time frames for recording foraging activity, and that only male bats have been fitted with GPS units to this point in the study. Investigations of female and older juvenile bats ≥ 100 g, which are the more actively infected cohort of the population (8), will be useful. Longer monitoring periods with fewer data points collected to preserve battery life and increase the number of days the bats will be tracked will also be useful.

Acknowledgments

We thank David Apollo, the Uganda Wildlife Authority Park Rangers, the Centers for Disease Control and Prevention Uganda, and Brian Harcourt for providing assistance during this study.

This study was supported in part by an appointment to the Research Participation Program at the Centers for Disease Control and Prevention administered by the Oak Ridge Institute for Science and Education through an interagency agreement between the US Department of Energy and the Centers for Disease Control and Prevention and the US Federal Government Defense Threat Reduction Agency grant (HDTRA1033036) and core funding from the Centers for Disease Control and Prevention.

The authors declare that all data supporting the findings of this study are available within the article and its supplementary information files or from the authors upon request.

B.R.A and J.S.T. conceptualized the study; B.R.A, A.J.S., T.K.S, G.A., D.N., K.K. and E.A.W. performed formal analysis; B.R.A., A.J.S., G.A., K.K., D.N., T.K.S., J.C.G., E.P.A., and J.S.T. performed investigations; B.R.A. and S.B. performed logistics; J.J.L. and R.C.K. obtained financial support; B.R.A, A.J.S., G.A., K.K., D.N., and T.K.S. performed methods; B.R.A., A.J.S., G.A., T.K.S., and E.A.W. performed data curation; B.R.A. and J.S.T. wrote and prepared the original draft; and B.R.A., A.J.S., G.A., K.K., D.N., T.K.S., J.C.G., E.A.W., E.E., S.B; J.J.L, R.C.K., P.A., and J.S.T. wrote, reviewed, and edited the paper.

All authors have read and agreed to the published version of this manuscript.

About the Author

Dr. Amman is a disease ecologist in the Viral Special Pathogens Branch, Virus Host Ecology Unit, Division of High-Consequence Pathogens and Pathology, National Center for Emerging and Zoonotic Infectious Diseases, Centers for Disease Control and Prevention, Atlanta, GA. His primary research interests include investigating the ecology of, and relationships between, emerging zoonotic viruses and their reservoirs.

References

1. Luby JP, Sanders CV. Green monkey disease ("Marburg virus" disease): a new zoonosis. *Ann Intern Med*. 1969;71:657–60. <https://doi.org/10.7326/0003-4819-71-3-657>
2. Siegert R, Shu HL, Slenczka HL, Peters D, Müller G. The aetiology of an unknown human infection transmitted by monkeys (preliminary communication). *Ger Med Mon*. 1968;13:1–2.
3. Centers for Disease Control and Prevention. Marburg disease outbreaks. February 23, 2023 [cited 2023 10 Nov]. <https://www.cdc.gov/vhf/marburg/outbreaks/chronology.html>
4. Adjemian J, Farnon EC, Tschiko F, Wamala JF, Byaruhanga E, Bwire GS, et al. Outbreak of Marburg hemorrhagic fever among miners in Kamwenge and Ibanda Districts, Uganda, 2007. *J Infect Dis*. 2011;204(Suppl 3): S796–9. <https://doi.org/10.1093/infdis/jir312>
5. Bausch DG, Nichol ST, Muyembe-Tamfum JJ, Borchert M, Rollin PE, Sleurs H, et al.; International Scientific and Technical Committee for Marburg Hemorrhagic Fever Control in the Democratic Republic of the Congo. Marburg hemorrhagic fever associated with multiple genetic lineages of virus. *N Engl J Med*. 2006;355:909–19. <https://doi.org/10.1056/NEJMoa051465>
6. Timen A, Koopmans MP, Vossen AC, van Doornum GJ, Günther S, van den Berk mortel F, et al. Response to imported case of Marburg hemorrhagic fever, the Netherlands. *Emerg Infect Dis*. 2009;15:1171–5. <https://doi.org/10.3201/eid1508.090015>
7. Amman BR, Bird BH, Bakarr IA, Bangura J, Schuh AJ, Johnny J, et al. Isolation of Angola-like Marburg virus from Egyptian Rousette bats from West Africa. *Nat Commun*. 2020;11:510. <https://doi.org/10.1038/s41467-020-14327-8>
8. Amman BR, Carroll SA, Reed ZD, Sealy TK, Balinandi S, Swanepoel R, et al. Seasonal pulses of Marburg virus circulation in juvenile *Rousettus aegyptiacus* bats coincide with periods of increased risk of human infection. *PLoS Pathog*. 2012;8:e1002877. <https://doi.org/10.1371/journal.ppat.1002877>
9. Kajihara M, Hang'ombe BM, Changula K, Harima H, Isono M, Okuya K, et al. Marburg virus in Egyptian fruit bats, Zambia. *Emerg Infect Dis*. 2019;25:1577–80. <https://doi.org/10.3201/eid2508.190268>
10. Paweska JT, Jansen van Vuren P, Kemp A, Storm N, Grobelaar AA, Wiley MR, et al. Marburg Virus infection in Egyptian Rousette bats, South Africa, 2013–2014. *Emerg Infect Dis*. 2018;24:1134–7. <https://doi.org/10.3201/eid2406.172165>
11. Pourrut X, Souris M, Towner JS, Rollin PE, Nichol ST, Gonzalez JP, et al. Large serological survey showing cocirculation of Ebola and Marburg viruses in Gabonese bat populations, and a high seroprevalence of both viruses in *Rousettus aegyptiacus*. *BMC Infect Dis*. 2009;9:159. <https://doi.org/10.1186/1471-2334-9-159>
12. Swanepoel R, Smit SB, Rollin PE, Formenty P, Leman PA, Kemp A, et al.; International Scientific and Technical Committee for Marburg Hemorrhagic Fever Control in the Democratic Republic of Congo. Studies of reservoir hosts for Marburg virus. *Emerg Infect Dis*. 2007;13:1847–51. <https://doi.org/10.3201/eid1312.071115>
13. Towner JS, Amman BR, Sealy TK, Carroll SA, Comer JA, Kemp A, et al. Isolation of genetically diverse Marburg viruses from Egyptian fruit bats. *PLoS Pathog*. 2009; 5:e1000536. <https://doi.org/10.1371/journal.ppat.1000536>
14. Towner JS, Pourrut X, Albariño CG, Nkogwe CN, Bird BH, Grand G, et al. Marburg virus infection detected in a common African bat. *PLoS One*. 2007;2:e764. <https://doi.org/10.1371/journal.pone.0000764>

15. Makenov MT, Boumbaly S, Tolno FR, Sacko N, N'Fatoma LT, Mansare O, et al. Marburg virus in Egyptian Rousettus bats in Guinea: investigation of Marburg virus outbreak origin in 2021. *PLoS Negl Trop Dis*. 2023;17:e0011279. <https://doi.org/10.1371/journal.pntd.0011279>
16. Amman BR, Jones ME, Sealy TK, Uebelhoer LS, Schuh AJ, Bird BH, et al. Oral shedding of Marburg virus in experimentally infected Egyptian fruit bats (*Rousettus aegyptiacus*). *J Wildl Dis*. 2015;51:113–24. <https://doi.org/10.7589/2014-08-198>
17. Pawęska JT, Storm N, Markotter W, Di Paola N, Wiley MR, Palacios G, et al. Shedding of Marburg virus in naturally infected Egyptian Rousette bats, South Africa, 2017. *Emerg Infect Dis*. 2020;26:3051–5. <https://doi.org/10.3201/eid2612.202108>
18. Schuh AJ, Amman BR, Jones ME, Sealy TK, Uebelhoer LS, Spengler JR, et al. Modelling filovirus maintenance in nature by experimental transmission of Marburg virus between Egyptian rousette bats. *Nat Commun*. 2017;8:14446. <https://doi.org/10.1038/ncomms14446>
19. Belanov EF, Muntianov VP, Kriuk VD, Sokolov AV, Bormotov NI, P'iankov OV, et al. Survival of Marburg virus infectivity on contaminated surfaces and in aerosols [in Russian]. *Vopr Virusol*. 1996;41:32–4.
20. Amman BR, Schuh AJ, Albariño CG, Towner JS. Marburg virus persistence on fruit as a plausible route of bat to primate filovirus transmission. *Viruses*. 2021;13:2394. <https://doi.org/10.3390/v13122394>
21. Jacobsen NH, Du Plessis E. Observations on the ecology and biology of the Cape fruit bat *Rousettus aegyptiacus leachi* in the Eastern Transvaal. *S Afr J Sci*. 1976;72:270–3.
22. Kwiecinski GG, Griffiths TA. *Rousettus aegyptiacus*. *Mamm Species*. 1999;611:1–9. <https://doi.org/10.2307/3504411>
23. Amman BR, Schuh AJ, Towner JS. Ebola virus field sample collection. In: Hoenen T, Groseth A, editors. *Methods in molecular biology*. Clifton (NJ): Humana Press; 2017. p. 373–93.
24. Amman BR, Cossaboom CM, Wendling NM, Harvey RR, Rettler H, Taylor D, et al. GPS tracking of free-roaming cats (*Felis catus*) on SARS-CoV-2-infected mink farms in Utah. *Viruses*. 2022;14:2131. <https://doi.org/10.3390/v14102131>
25. Amman BR, Manangan AP, Elietstra TD, Calisher CH, Carroll DS, Wagoner KD, et al. Association between movement and Sin Nombre virus (*Bunyaviridae: Hantavirus*) infection in North American deer mice (*Peromyscus maniculatus*) in Colorado. *J Wildl Dis*. 2013;49:132–42. <https://doi.org/10.7589/2012-02-041>
26. Newton-Fisher NE. The home range of the Sonso community of chimpanzees from the Budongo Forest, Uganda. *Afr Ecol*. 2003; 41:150–6. <https://doi.org/10.1046/j.1365-2028.2003.00408.x>
27. Ribble DO, Wurtz AE, McConnell EK, Buegge JJ, Welch KC Jr. A comparison of home ranges of two species of *Peromyscus* using trapping and radiotelemetry data. *J Mammal*. 2002;83:260–6. [https://doi.org/10.1644/1545-1542\(2002\)083<0260:ACOHRO>2.0.CO;2](https://doi.org/10.1644/1545-1542(2002)083<0260:ACOHRO>2.0.CO;2)
28. Centers for Disease Control and Prevention (CDC). Imported case of Marburg hemorrhagic fever – Colorado, 2008. *MMWR Morb Mortal Wkly Rep*. 2009;58:1377–81.
29. Pan Y, Zhang W, Cui L, Hua X, Wang M, Zeng Q. Reston virus in domestic pigs in China. *Arch Virol*. 2014;159:1129–32. <https://doi.org/10.1007/s00705-012-1477-6>
30. Kobinger GP, Leung A, Neufeld J, Richardson JS, Falzarano D, Smith G, et al. Replication, pathogenicity, shedding, and transmission of Zaire ebolavirus in pigs. *J Infect Dis*. 2011;204:200–8. <https://doi.org/10.1093/infdis/jir077>
31. Paweska JT, Jansen van Vuren P, Fenton KA, Graves K, Grobbelaar AA, Moolla N, et al. Lack of Marburg virus transmission from experimentally infected to susceptible in-contact Egyptian fruit bats. *J Infect Dis*. 2015;212(Suppl 2):S109–18. <https://doi.org/10.1093/infdis/jiv132>
32. Amman BR, Swanepoel R, Nichol ST, Towner JS. Ecology of filoviruses. In: Mühlberger E, Towner J., editors. *Current topics in microbiology and immunology*. New York: Springer; 2017. p. 23–61.
33. Judson SD, Fischer R, Judson A, Munster VJ. Ecological contexts of index cases and spillover events of different ebolaviruses. *PLoS Pathog*. 2016;12:e1005780. <https://doi.org/10.1371/journal.ppat.1005780>
34. Weyer J, Grobbelaar A, Blumberg L. Ebola virus disease: history, epidemiology and outbreaks. *Curr Infect Dis Rep*. 2015;17:480. <https://doi.org/10.1007/s11908-015-0480-y>
35. Barrette RW, Metwally SA, Rowland JM, Xu L, Zaki SR, Nichol ST, et al. Discovery of swine as a host for the Reston ebolavirus. *Science*. 2009;325:204–6. <https://doi.org/10.1126/science.1172705>
36. Chua KB, Goh KJ, Wong KT, Kamarulzaman A, Tan PS, Ksiazek TG, et al. Fatal encephalitis due to Nipah virus among pig-farmers in Malaysia. *Lancet*. 1999;354:1257–9. [https://doi.org/10.1016/S0140-6736\(99\)04299-3](https://doi.org/10.1016/S0140-6736(99)04299-3)
37. Jahrling PB, Geisbert TW, Dalgard DW, Johnson ED, Ksiazek TG, Hall WC, et al. Preliminary report: isolation of Ebola virus from monkeys imported to USA. *Lancet*. 1990; 335:502–5. [https://doi.org/10.1016/0140-6736\(90\)90737-P](https://doi.org/10.1016/0140-6736(90)90737-P)
38. Chua KB, Chua BH, Wang CW. Anthropogenic deforestation, El Niño and the emergence of Nipah virus in Malaysia. *Malays J Pathol*. 2002;24:15–21.
39. Goldshtein A, Harten L, Yovel Y. Mother bats facilitate pup navigation learning. *Curr Biol*. 2022;32:350–360.e4. <https://doi.org/10.1016/j.cub.2021.11.010>
40. Gibb R, Redding DW, Chin KQ, Donnelly CA, Blackburn TM, Newbold T, et al. Zoonotic host diversity increases in human-dominated ecosystems. *Nature*. 2020; 584:398–402. <https://doi.org/10.1038/s41586-020-2562-8>
41. Keesing F, Ostfeld RS. Impacts of biodiversity and biodiversity loss on zoonotic diseases. *Proc Natl Acad Sci U S A*. 2021;118:e2023540118. <https://doi.org/10.1073/pnas.2023540118>
42. Letko M, Seifert SN, Olival KJ, Plowright RK, Munster VJ. Bat-borne virus diversity, spillover and emergence. *Nat Rev Microbiol*. 2020;18:461–71. <https://doi.org/10.1038/s41579-020-0394-z>
43. Olival KJ, Hosseini PR, Zambrana-Torrel C, Ross N, Bogich TL, Daszak P. Host and viral traits predict zoonotic spillover from mammals. *Nature*. 2017;546:646–50. <https://doi.org/10.1038/nature22975>
44. Amman BR, Nyakarahuka L, McElroy AK, Dodd KA, Sealy TK, Schuh AJ, et al. Marburgvirus resurgence in Kitaku Mine bat population after extermination attempts, Uganda. *Emerg Infect Dis*. 2014;20:1761–4. <https://doi.org/10.3201/eid2010.140696>
45. Plowright RK, Eby P, Hudson PJ, Smith IL, Westcott D, Bryden WL, et al. Ecological dynamics of emerging bat virus spillover. *Proc Biol Sci*. 2015;282:20142124. <https://doi.org/10.1098/rspb.2014.2124>
46. Andersen KG, Rambaut A, Lipkin WI, Holmes EC, Garry RF. The proximal origin of SARS-CoV-2. *Nat Med*. 2020;26:450–2. <https://doi.org/10.1038/s41591-020-0820-9>

Address for correspondence: Brian R. Amman, Centers for Disease Control and Prevention, 1600 Clifton Rd. NE, Mailstop H18-B, Atlanta, GA 30329-4027, USA; email: cxx1@cdc.gov

Global Phylogeography and Genomic Epidemiology of Carbapenem-Resistant *bla*_{OXA-232}-Carrying *Klebsiella pneumoniae* Sequence Type 15 Lineage

Yuye Wu, Tian Jiang, Xianhong He, Jiayu Shao, Chenghao Wu, Weifang Mao, Huiqiong Jia, Fang He, Yingying Kong, Jianyong Wu, Qingyang Sun, Long Sun, Mohamed S. Draz, Xinyou Xie, Jun Zhang, Zhi Ruan

Prevalence of carbapenem-resistant *Klebsiella pneumoniae* (CRKP) has compromised antimicrobial efficacy against severe infections worldwide. To monitor global spread, we conducted a comprehensive genomic epidemiologic study comparing sequences from 21 *bla*_{OXA-232}-carrying CRKP isolates from China with *K. pneumoniae* sequence type (ST) 15 strains from 68 countries available in GenBank. Phylogenetic and phylogeographic analyses revealed all *bla*_{OXA-232}-carrying CRKP isolates belonged to ST15 lineage and exhibited multidrug resis-

tance. Analysis grouped 330 global *bla*_{OXA-232}-carrying ST15 CRKP strains into 5 clades, indicating clonal transmission with small genetic distances among multiple strains. The lineage originated in the United States, then spread to Europe, Asia, Oceania, and Africa. Most recent common ancestor was traced back to 2000; mutations averaged ≈ 1.7 per year per genome. Our research helps identify key forces driving global spread of *bla*_{OXA-232}-carrying CRKP ST15 lineage and emphasizes the importance of ongoing surveillance of epidemic CRKP.

The global spread of carbapenem-resistant Enterobacterales, particularly carbapenem-resistant *Klebsiella pneumoniae* (CRKP), poses a severe and ongoing public health threat because of high rates of illness and death (1). The production of carbapenemases is the most crucial carbapenem-resistance mechanism in gram-negative bacteria worldwide (2). One of the most prevalent carbapenemase genes, *bla*_{OXA-48} (oxacillin-hydrolyzing β -lactamase), is found predominantly on large and transferable plasmids in bacteria of order Enterobacterales. Prevalence of *K. pneumoniae* strains carrying a *bla*_{OXA-48}-like gene in

China increased during 2018–2022 (3–6). Nosocomial outbreaks, including among pediatric patients, have called attention to the importance of better understanding the transmission potential of CRKP isolates carrying the *bla*_{OXA-48}-like gene (4–6).

*bla*_{OXA-232}, a variant among *bla*_{OXA-48} genes with limited carbapenem hydrolytic activity, was initially identified in France in 2011 (7). Most *bla*_{OXA-232} genes have been discovered on small and nonconjugative ColKP3-type plasmids (8). In China, some strains of sequence type (ST) 15, the predominant lineage of *bla*_{OXA-232}-carrying *K. pneumoniae*, mediate low-level

Author affiliations: Zhejiang University School of Medicine Sir Run Run Shaw Hospital, Hangzhou, China (Y. Wu, T. Jiang, X. He, J. Shao, C. Wu, W. Mao, Y. Kong, X. Xie, J. Zhang, Z. Ruan); Wenzhou Medical University Affiliated Wenling Hospital, Taizhou, China (T. Jiang); Third People's Hospital of Xiaoshan District, Hangzhou (X. He, J. Shao); Shaoxing University Affiliated Hospital, Shaoxing, China (W. Mao); Zhejiang University School of Medicine First Affiliated Hospital, Hangzhou (H. Jia); Key Laboratory of Clinical In Vitro Diagnostic Techniques of Zhejiang Province, Hangzhou (H. Jia); Zhejiang Provincial People's Hospital,

Hangzhou (F. He); Key Laboratory of Precision Medicine in Diagnosis and Monitoring Research of Zhejiang Province, Hangzhou (Y. Kong, X. Xie, J. Zhang, Z. Ruan); Zhejiang University School of Medicine Fourth Affiliated Hospital, Hangzhou (J. Wu); No. 903 Hospital of PLA Joint Logistic Support Force, Hangzhou (Q. Sun); Hangzhou Women's Hospital, Hangzhou (L. Sun); Case Western Reserve University School of Medicine, Cleveland, Ohio, USA (M.S. Draz); Cleveland Clinic, Cleveland (M.S. Draz)

DOI: <https://doi.org/10.3201/eid2911.230463>

carbapenem resistance and many coexist with virulence plasmids (6,9,10). Applying a previously proposed reverse genomic epidemiology strategy enabled us to make genome comparisons of isolates to identify shared sources of infection on the basis of genomic similarity (11). This approach, developed in response to increasing rates of global spread of antimicrobial-resistant bacteria, emphasizes the need to explore transmission of infection from a global rather than a country- or case-specific perspective. Limited data from previous studies on the number and geographic diversity of *bla*_{OXA-232}-carrying *K. pneumoniae* isolates has impeded full understanding of the genomic evolution and transmission dynamics of CRKP (5,12).

We aimed to perform a multicenter molecular epidemiologic study of carbapenem-resistant *bla*_{OXA-232}-carrying *K. pneumoniae* ST15 isolates in China, focusing on the genomic characterization of the lineage and the genetic context of the *bla*_{OXA-232}-carrying plasmids. We performed large-scale comprehensive genomic epidemiologic analysis to investigate the transmission histories, common ancestors, evolution rates, and population structures of all publicly available *bla*_{OXA-232}-carrying *K. pneumoniae* of ST15 lineage. Our study provides data that will help monitor global spread and the epidemic expansion of *K. pneumoniae* ST15 lineage and provide insights for developing new infection control strategies. The ethics committee of Sir Run Run Shaw Hospital, Zhejiang University School of Medicine, approved this study (2022-0227).

Methods

Isolate Collection

We performed a retrospective microbiologic characterization of 21 *bla*_{OXA-232}-carrying CRKP isolates obtained from a collection of 2,398 nonduplicate *K. pneumoniae* clinical isolates recovered from 5 hospitals across 3 areas of Zhejiang Province, China, during August 2018–March 2022. Presence of the *bla*_{OXA-232} gene was detected by PCR and validated by Sanger sequencing (13). We identified bacteria using VITEK 2 (bioMérieux, <https://www.biomerieux.com>) and matrix-assisted laser desorption/ionization-time-of-flight (MALDI-TOF) mass spectrometry (Bruker, <https://www.bruker.com>).

Antimicrobial Susceptibility Testing

We performed antimicrobial susceptibility testing (AST) using a broth microdilution method on antimicrobial agents amikacin, aztreonam, fosfomicin,

cefoxitin, cefepime, cefotaxime, cefiderocol, levofloxacin, imipenem, meropenem, polymyxin, tigecycline, and ceftazidime/avibactam. We determined MICs for cefiderocol using iron-depleted cation-adjusted Mueller-Hinton broth in custom-prepared MIC panels (14). We interpreted antimicrobial susceptibility breakpoints according to Clinical and Laboratory Standards Institute 2020 (<https://clsi.org>) and EUCAST 10.0 (https://www.eucast.org/clinical_breakpoints) guidelines. We used *Escherichia coli* ATCC 25922 as a quality control strain for AST.

Plasmid Conjugation

We used rifampin-resistant *E. coli* EC600 as the recipient. We selected transconjugants on Mueller-Hinton agar supplemented with rifampin (300 mg/L) and imipenem (4 mg/L). We counted numbers of transconjugant colonies after overnight incubation at 37°C and confirmed transconjugants using PCR and Sanger sequencing.

Whole-Genome Sequencing

We performed whole-genome sequencing using the short-read Illumina HiSeq X10 (<https://www.illumina.com>) with 150-bp paired-end protocol. We also sequenced the representative isolate (KP3295) selected from the 21 CRKP isolates on the long-read Oxford Nanopore MinION platform (Nanopore Technologies, <https://nanoporetech.com>). We assembled the derived short Illumina reads and long MinION reads using Unicycler version 0.4.8 (<https://github.com/rrwick/Unicycler>) (15).

Genomic Features and Plasmid Characterization

We annotated genomes using the National Center for Biotechnology Information (NCBI) Prokaryotic Genomes Annotation Pipeline (<https://github.com/ncbi/pgap>). We determined antimicrobial resistance genes using ABRicate version 1.0.1 (<https://github.com/tseemann/abricate>) against the NCBI AMRFinder database (16) and plasmid replicon types using the PlasmidFinder database (17). We detected virulence determinants using Kleborate version 2.1.0 (18) and the 2022 Virulence Factor Database (19). We performed in silico multilocus sequence typing (MLST) analysis and bacterial source tracking using BacWGSTdb 2.0 (20). We used EasyFigure (21) and BLAST Ring Image Generator (22) to analyze genetic context and homologous regions of *bla*_{OXA-232} among the isolates.

Phylogenetic Analysis

On June 3, 2022, we retrieved genome sequences of 43,402 *K. pneumoniae* strains from 114 countries and

related clinical metadata from the NCBI pathogen detection portal (Appendix 1, <https://wwwnc.cdc.gov/EID/article/29/11/23-0463-App1.xlsx>). After conducting in silico MLST analysis and detecting the presence of *bla*_{OXA-232} gene in *K. pneumoniae*, we selected 330 *bla*_{OXA-232}-carrying *K. pneumoniae* ST15 strains for further investigation. On the basis of geographic information for each isolate, we created a minimum-spanning tree based on core genome MLST allelic profiles of *K. pneumoniae* ST15 isolates using chewieSnake (23) and visualized the phylogenetic tree using GrapeTree (24). We considered isolates to be closely related genotypically when separated by a distance of ≤ 20 alleles. We used Snippy version 4.6.0 (<https://github.com/tseemann/snippy>) to align sequences and identify single-nucleotide polymorphisms (SNPs). We parsed genome alignment through Gubbins (<https://github.com/nickjroucher/gubbins>), which identified and removed recombination regions, and inferred and constructed a maximum-likelihood phylogeny from those SNPs. We calculated pairwise SNP distances between the genomes of each isolate to define clades.

Phylogenetic Analysis

We performed root-to-tip regression analysis using TempEst version 1.5.3 (<https://github.com/beast-dev/TempEst>) to confirm that the maximum-likelihood tree had sufficient temporal signal. We used a Bayesian Markov Chain Monte Carlo approach implemented in BEAST2 (25) to analyze alignment of putative substitution mutations identified by Gubbins, on which estimates the time-scaled phylogenetic tree was based, as well as time of most recent common ancestor (tMRCA) and mutation rates. We allowed each run 300 million iterations, sampled from every 20,000th iteration, and discarded the first 10% of the samples as burn-in. We estimated the effective sample size using Tracer version 1.7.1 (<https://github.com/beast-dev/tracer/releases>) to evaluate the operation convergence. We used RhierBAPS version 1.0.1 (26) to analyze the allele frequency parameters of the bacterial population and cluster individual sequences to identify the population structure, then used the resulting clades as input for the SkyGrowth package (<https://github.com/mrc-ide/skygrowth>) to evaluate effective population sizes. We visualized and annotated phylogenetic trees using the interactive Tree of Life (iTOL) V5 web server (27). We analyzed and visualized transmission links for isolates and nodes with spatial phylogenetic reconstruction of evolutionary dynamics using Spread3 (28) under a discrete trait model. We deposited genome sequences of the 21 CRKP isolates in GenBank (BioProject accession nos. PRJNA818898 and PRJNA745926).

Results

Clinical and Microbiologic Characteristics

During August 2018–2022, we recovered *bla*_{OXA-232}-carrying *K. pneumoniae* strains from 21 of 2,398 *K. pneumoniae* patients among 5 hospitals in Zhejiang Province, an incidence rate of 0.87% (Table 1). Most patients with diagnosed *K. pneumoniae* infections experienced pulmonary infections accompanied by respiratory failure. According to AST data (Table 2) most of the *bla*_{OXA-232}-positive isolates were resistant to amikacin, aztreonam, fosfomycin, imipenem, meropenem, ceftazidime, ceftazidime/avibactam, and levofloxacin. Those isolates showed low-level resistance to carbapenems but remained susceptible to colistin, tigecycline, ceftazidime/avibactam, and cefiderocol.

Genomic Features and Plasmid Characterization

To investigate the genetic characteristics of *bla*_{OXA-232}-bearing plasmids, we further subjected isolate KP3295 to whole-genome sequencing using the Oxford Nanopore MinION platform. Whole-genome sequencing data revealed that KP3295 consists of a chromosome of 5,329,783 bp and 10 plasmids (177,848 bp, 133,750 bp, 128,536 bp, 9,730 bp, 6,141 bp, 5,640 bp, 4,510 bp, 3,770 bp, and 3,559 bp). The GC (guanine/cytosine) content of KP3295 was 56.82%; the N50 value was 5,329,783 bp. The *bla*_{OXA-232} gene was carried by a ColKP3-type plasmid (6,141 bp) designated as pKP3295-5-OXA-232. Among the other 20 *bla*_{OXA-232} strains, we identified the *bla*_{OXA-232} gene on ColKP3-type plasmids of comparable sizes (5,934–6,141 bp). The plasmid included 9 open reading frames: *repA*, *mobA*, *mobB*, *mobC*, *mobD*, Δ ISEcp1, *bla*_{OXA-232}, Δ lysR, and Δ ereA (Figure 1). In the conjugation experiment, the *bla*_{OXA-232}-carrying plasmid could not be transferred to *E. coli* EC600, which is consistent with the absence of intact conjugal transfer elements in the backbone structure of that plasmid.

Comparative analysis with the genetic surroundings of the 102 *bla*_{OXA-232}-carrying plasmids in the NCBI nucleotide database revealed that the studied plasmid exhibited 100% coverage and 100% identity to plasmid pOXA-232, originally isolated from *E. coli*, which marked the initial discovery of *bla*_{OXA-232}. When carried by the transposable elements ISEcp1 and Tn1000, the compact 6.1 kb *bla*_{OXA-232}-carrying plasmid could integrate into larger plasmids, such as pOXA-232_30929 (12,351 bp) reported in the Czech Republic and pAI1235M_P5 (9,117 bp) in India. We found the conserved 6.1 kb ColKP3 plasmid structure in association with the transposable element ISEcp1 in

Table 1. Characteristics of 21 infected patients in China investigated in study of global phylogeography and genomic epidemiology of *bla*_{OXA-232}-carrying carbapenem-resistant *Klebsiella pneumoniae* sequence type 15

Isolate	Age, y/sex	Clinical diagnosis	Specimen source	Isolation date
KP3	78/M	Atrial fibrillation, severe pneumonia, respiratory failure	Urine	2020 Nov
KP41	66/M	Cardiac failure, respiratory failure, urinary tract infection	Urine	2020 Nov
KP105	61/F	Cholangiolithiasis	Bile	2020 Nov
KP232	86/M	Cholangiolithiasis	Urine	2020 Dec
KP306	42/M	Severe acute pancreatitis	Excreta	2020 Dec
KP5	61/M	Hydrocephalus	Urine	2021 Jan
KP441	76/F	Lung infection, heart failure	Sputum	2021 Jun
KP68	84/F	Chronic obstructive pulmonary disease	Bronchoalveolar lavage fluid	2021 Sep
KP76	47/F	Posttraumatic brain syndrome	Blood	2021 Sep
KP77	73/M	Multiple brain contusion and laceration	Sputum	2021 Sep
KP79	54/M	Chronic obstructive pulmonary disease	Sputum	2021 Sep
KP81	94/M	Cerebral infarction, hypertension	Sputum	2020 Aug
KP85	56/M	Inhalation lung injury	Sputum	2021 Oct
KP89	56/M	Inhalation lung injury, respiratory failure	Excreta	2021 Nov
KP91	68/M	Respiratory failure, diabetes	Urine	2020 Dec
KP97	55/F	Exogenous injury, motor neuron disease, respiratory failure	Sputum	2021 Dec
KP9112	86/F	Chronic obstructive pulmonary disease	Sputum	2020 Sep
KP135	76/M	Cervical spinal fractures, high paraplegia	Sputum	2021 Jan
KP8474	49/M	Intracranial space occupying lesions	Sputum	2020 Jul
KP12339	65/M	Intracranial injury	Sputum	2019 Jan
KP3295	52/M	Paraplegia	Urine	2018 Aug

IncFIB-ColKP3 (pBio73) and IncFIB-IncHI1B-ColKP3 (pBio45 and pBio3) plasmids from Turkey. Furthermore, with the help of mobile genetic elements, such as ISEcp1 and TnAs1, the Δ ISEcp1-*bla*_{OXA-232}- Δ lysR- Δ dereA structure was integrated into plasmids from Bangladesh, specifically IncFIB-IncFII (p_dm730a_NDM5 and 730a-copy-1-OXA-232). Those Inc-type plasmids also carried other β -lactam resistance genes, including *bla*_{TEM'}, *ble*_M, *bla*_{BL'}, *bla*_{NDM-1'} and *bla*_{CTM-X-15} (Figure 1; Figure 2, panel A).

The 21 CRKP isolates carried several virulence determinants involving yersiniabactin (*fyuA*, *ybtE*, *ybtT*, *ybtU*, *irp1*, *irp2*, *ybtA*, *ybtP*, *ybtQ*, *ybtX*, and *ybtS*), aerobactin (*iutA* and *iucABCD*), and hypermucoidity (*rmpA2*). All 21 isolates belonged to yersiniabactin sequence type 277 (ybST277) and carried *ybt* 16. Except for KP232, KP306, and KP77, all isolates belonged to aerobactin sequence type 1 (AbST1) and contained the aerobactin synthesis

Table 2. MICs for different antimicrobial drugs of 21 *bla*_{OXA-232}-carrying sequence type 15 carbapenem-resistant *Klebsiella pneumoniae* isolates from patients in China*

Isolate	MIC, mg/L												
	AMK	ATM	FOF	FOX	FEP	CTX	LVX	IPM	MEM	CST	TGC	FDC	CZA
KP3	>128	>128	>128	64	>64	>128	64	8	4	<0.0625	1	2	0.25/0.125
KP41	>128	>128	>128	16	>64	>128	16	4	2	<0.0625	0.25	2	0.5/0.25
KP105	>128	>128	>128	128	>64	>128	128	>128	>128	<0.0625	2	1	0.5/0.25
KP232	>128	>128	128	128	>64	>128	>128	8	4	0.0625	2	0.5	0.5/0.25
KP306	>128	>128	>128	64	>64	>128	64	4	4	<0.0625	1	4	0.25/0.125
KP5	>128	>128	>128	64	64	>128	32	2	4	0.5	2	0.25	2/1
KP441	>128	>128	>128	32	>64	>128	16	0.5	2	0.125	2	1	2/1
KP68	>128	>128	>128	64	>64	>128	32	32	32	0.5	1	1	4/2
KP76	>128	>128	>128	32	>64	>128	16	1	1	0.25	1	1	1/0.5
KP77	>128	>128	>128	32	>64	>128	16	0.5	1	0.5	2	0.5	2/1
KP79	>128	>128	>128	32	>64	>128	32	1	1	0.25	1	16	2/1
KP81	>128	>128	>128	128	>64	>128	128	16	32	0.125	4	1	2/1
KP85	>128	>128	>128	32	>64	>128	16	2	1	0.125	1	0.25	2/1
KP89	>128	>128	>128	32	>64	>128	32	1	2	0.125	2	0.25	2/1
KP91	>128	>128	>128	128	>64	>128	64	1	2	0.125	0.5	0.5	1/0.5
KP97	>128	>128	>128	64	>64	>128	128	16	32	0.0625	2	1	2/1
KP9112	>128	>128	>128	64	>64	>128	64	2	2	<0.0625	1	0.5	2/1
KP135	>128	>128	>128	64	64	>128	64	4	2	0.5	2	0.25	2/1
KP8474	>128	>128	>128	>128	>64	>128	64	1	2	0.0625	1	0.5	2/1
KP12339	>128	>128	>128	32	>64	>128	16	1	2	0.125	0.5	0.5	2/1
KP3295	>128	64	>128	>128	>64	>128	>128	32	32	0.25	0.25	0.5	0.25/0.125

*By broth microdilution method for amikacin, aztreonam, fosfomicin, ceftazidime, cefepime, cefotaxime, cefiderocol, levofloxacin, imipenem, meropenem, polymyxin, tigecycline, and ceftazidime/avibactam; iron-depleted cation-adjusted Mueller-Hinton broth in custom-prepared MIC panels (14) method for cefiderocol. Breakpoints are according to Clinical and Laboratory Standards Institute 2020 (<https://clsi.org>) and EUCAST 10.0 (https://www.eucast.org/clinical_breakpoints) guidelines. *Escherichia coli* ATCC 25922 was the quality control strain. AMK, amikacin; ATM, aztreonam; FOF, fosfomicin; FOX, ceftazidime; FEP, cefepime; CTX, cefotaxime; LVX, levofloxacin; IPM, imipenem; MEM, meropenem; CST, colistin; TGC, tigecycline; FDC, cefiderocol; CZA, ceftazidime/avibactam.

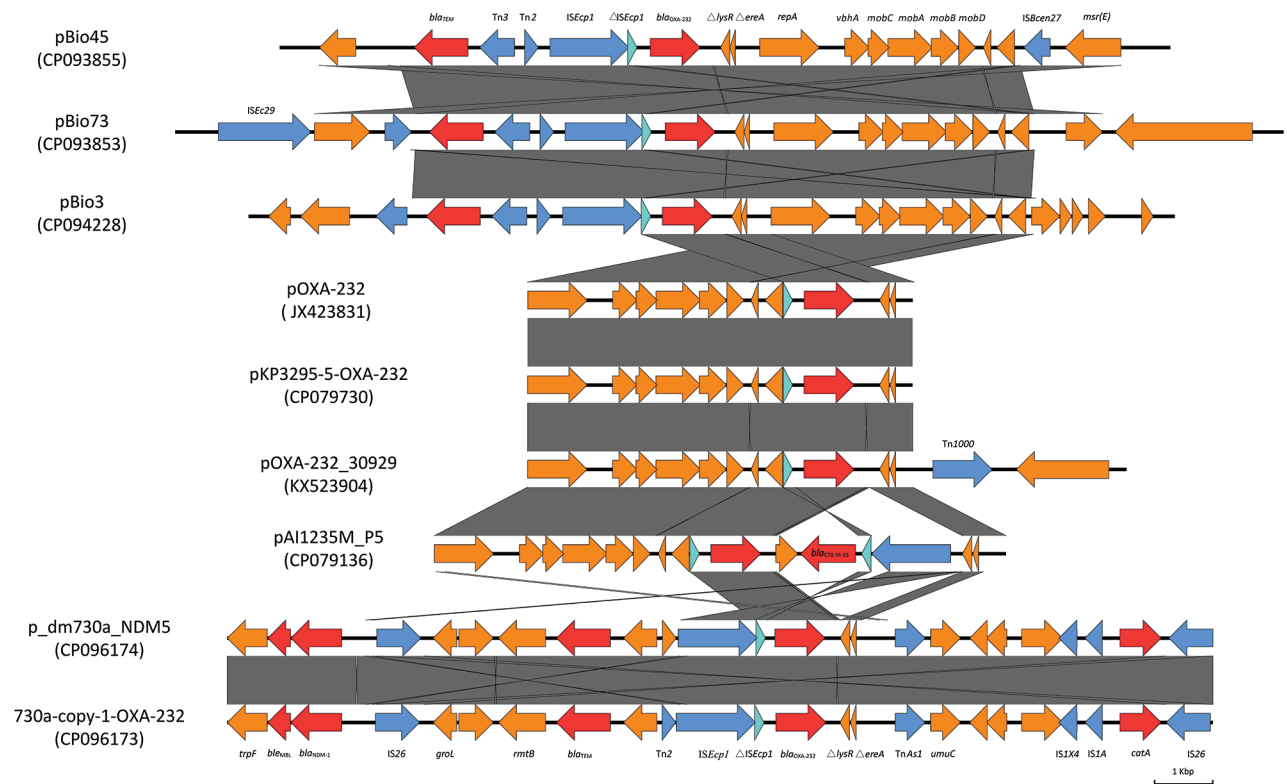


Figure 1. Genetic context of *bla*_{OXA-232} identified in patients in China investigated in study of global phylogeography and genomic epidemiology of *bla*_{OXA-232}-carrying carbapenem-resistant *Klebsiella pneumoniae* sequence type 15. Arrows represent coding sequences (red arrows, antimicrobial resistance genes; yellow or blue arrows, mobile elements) and indicate the direction of transcription. Arrow size is proportional to gene length. GenBank accession numbers are provided.

locus *iuc* 1. Those virulence determinants were all located on an IncFIB/IncHI1B-type plasmid (177,848 bp), pKP3295-1, in KP3295, which exhibits 99% identity and 91% coverage to classic virulence plasmid pLVPK (Figure 2, panel B).

Occurrence and Divergence of ST15 Lineage

We investigated global phylogenetic relationships of 2,118 *K. pneumoniae* ST15 strains using core genome MLST analysis with a cutoff of 20 alleles to define clonality (Appendix 2 Table 1, <https://wwwnc.cdc.gov/EID/article/29/11/23-0463-App2.xlsx>). China, the United States, Ireland, and the United Kingdom emerged as the countries with the highest prevalences of ST15. We identified multiple highly homogeneous strains common between countries, notably United States–China ($n = 317$), China–Nepal ($n = 251$), United Kingdom–United States ($n = 162$), and Vietnam–Thailand ($n = 124$) (Figure 3). Antimicrobial resistance gene testing identified *bla*_{KPC-2} (19.07%), *bla*_{OXA-232} (15.58%), and *bla*_{NDM-1} (10.57%) as the predominant carbapenem-resistance genes carried by global *K. pneumoniae* ST15 strains.

We identified all 21 *bla*_{OXA-232} CRKP isolates collected in this study as ST15. We performed phylogenetic analysis between the 21 *bla*_{OXA-232}-carrying CRKP isolates and 309 *bla*_{OXA-232}-carrying *K. pneumoniae* ST15 isolates obtained from NCBI (Appendix 2 Table 2). The *bla*_{OXA-232}-carrying *K. pneumoniae* ST15 isolates originated from 10 different countries: China, United Kingdom, Nepal, Netherlands, Oman, Thailand, United States, France, India, and Australia. Evaluation of clonal relatedness by core-genome SNPs revealed that the *bla*_{OXA-232}-carrying *K. pneumoniae* ST15 isolates had an average distance of 29 (range 0–208) SNPs. Phylogenetic analysis using hierarchical Bayesian clustering separated ST15 isolates into 2 clusters, I and II, closely corresponding to China and other countries. Cluster I was further divided into clades 1–4, based on SNP distances ≤ 20 . Among 2 clades from Hangzhou, Zhejiang Province, China, clade 1 had distances of 0–14 (median 4) SNPs and clade 2, 0–20 (median 8) SNPs. Clade 3, primarily from Shanghai, China, had distances of 0–18 (median 10) SNPs. Clade 4, from Hangzhou and Taizhou, Zhejiang Province, showed distances of 0–17 (median

5) SNPs. Strains outside those clades scattered across Shandong Province, Jiangsu Province, Jiaxing in Zhejiang Province, and Shanghai, China, as well as in Nepal. Of note, strains SHK022 and SHK012 from China displayed distances of 13 SNPs, and strains 2703 and 2704 from Nepal, 14 SNPs. Strains from the other 9 countries were predominantly found in cluster II (clade 5), with distances 0–202 (median 100) SNPs.

Subsequently, we analyzed effective population size trajectories for each clade. Clade 1 has steadily ascended since its emergence in 2020. Clade 2 exhibited robust population growth beginning in 2017 and clade 3 in 2016, an increase that projects to clades 2 and 3 dominating global distribution of *bla*_{OXA-232}-carrying *K. pneumoniae* ST15 lineage in the future. Clade 4 population sharply declined after emerging, later stabilized, and has increased in recent years. Clade 5 emerged earlier, but its population began to decrease in 2014 (Figure 4).

In-depth phylogenetic analysis revealed details about origins and mutation rates of *bla*_{OXA-232}-carrying *K. pneumoniae* ST15 isolates. The correlation coefficient and R² for the root-to-tip genetic divergence (0.773) compared with time in the TempEst analysis (0.598) indicated a strong linear relationship between accumulated mutations and sampling time, suggesting that enough signal was present to cali-

brate a strict clock model. The median molecular clock rate was estimated to be 3.40×10^{-3} (95% highest posterior density interval [HPD] $3.10\text{--}3.69 \times 10^{-3}$) substitutions/site/year, which translates to ≈ 1.7 mutations/genome/year. The tMRCA for *bla*_{OXA-232}-carrying *K. pneumoniae* ST15 lineage was estimated from the temporal height, which dates to 2000 (95% HPD 1996–2003). Strains from China appeared within a recent time window (after 2015) but have greatly increased, apparently the result of a rapidly expanding epidemic of clonal transmission.

We also compared carriage of antimicrobial resistance genes and virulence genes by *bla*_{OXA-232}-carrying *K. pneumoniae* ST15 strains with strains collected globally. Our findings suggest that the *bla*_{OXA-232}-carrying *K. pneumoniae* ST15 strains in the study were multi-drug-resistant high-risk clones. The ST15 strains carried several genes that confer resistance to β -lactams (*bla*_{OXA-232}, *bla*_{SHV-106}, *bla*_{TEM-1}, and *bla*_{CTX-M-15}), aminoglycosides (*aac*(6')-Ib, *aph*(6)-Id, and *aph*(3'')-Ib), chloramphenicol (*catB*), quinolones (*qnrB1*), sulfonamides (*sul2*), 16S rRNA methylase (*rmtF1*), trimethoprim (*dfrA14*), and rifampin (*arr2*). Most strains also exhibited intrinsic antimicrobial resistance, potentially attributed to genes like *fosA6*, *oqxA6*, and *oqxB20*. Of note, strain KP81 collected in this study harbored

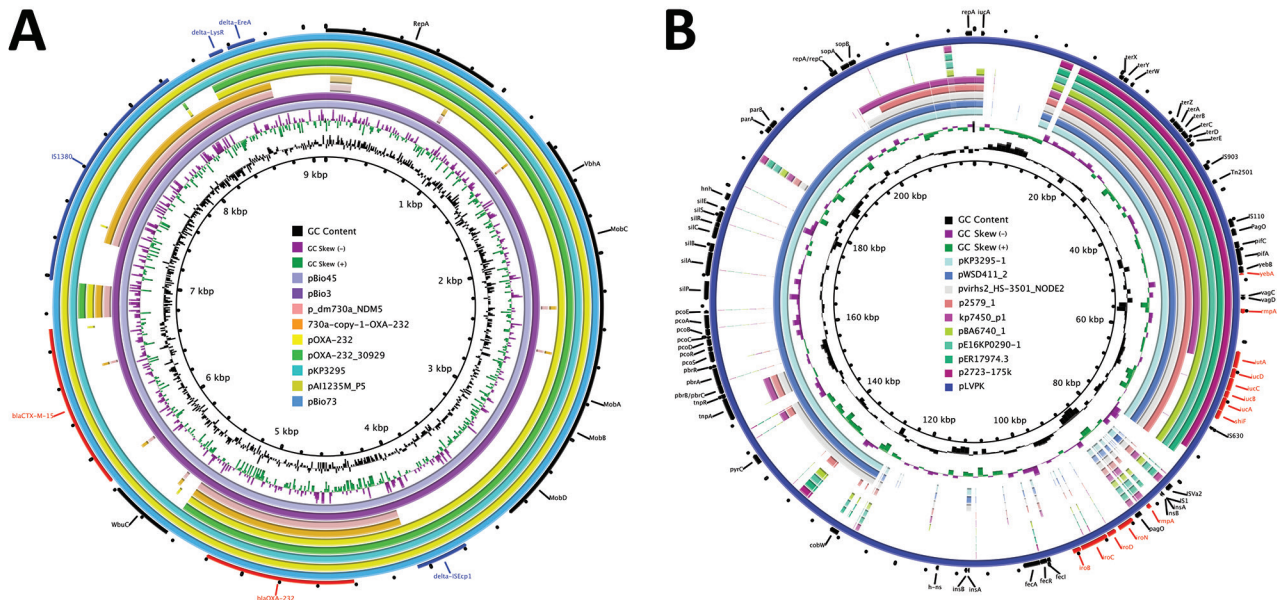


Figure 2. Genetic comparison of *bla*_{OXA-232}-carrying plasmids (A) and virulence plasmids (B) recovered from *Klebsiella pneumoniae* isolate KP3295 from China with reference plasmids. A) Alignment of *bla*_{OXA-232}-carrying plasmids pKP3295-5-OXA-232 (this study), pA11235M_P5 (GenBank accession no. CP079136), pOXA-232_30929 (accession no. KX523904), pOXA-232 (accession no. JX423831), pBio45 (accession no. CP093855), pBio73 (accession no. CP093853), pBio3 (accession no. CP094228), p_dm730a_NDM5 (accession no. CP096174), and 730a-copy-1-OXA-232 (accession no. CP096173). We used pA11235M_P5 as the reference plasmid. Red indicates antimicrobial resistance genes. B) Alignment of virulence plasmids pKP3295-1 (this study), pWSD411_2 (accession no. CP045675), pvirh2_HS-3501_NODE2 (accession no. OM975892), p2579_1 (accession no. MK649822), kp7450_p1 (accession no. CP090469), pBA6740_1 (accession no. MK649823), pE16KP0290-1 (accession no. CP052259), pER17974.3 (accession no. CP059296), p2723–175k (accession no. CP072940), and pLVPK (accession no. AY378100). We used pLVPK as the reference plasmid. Red indicates virulence genes.

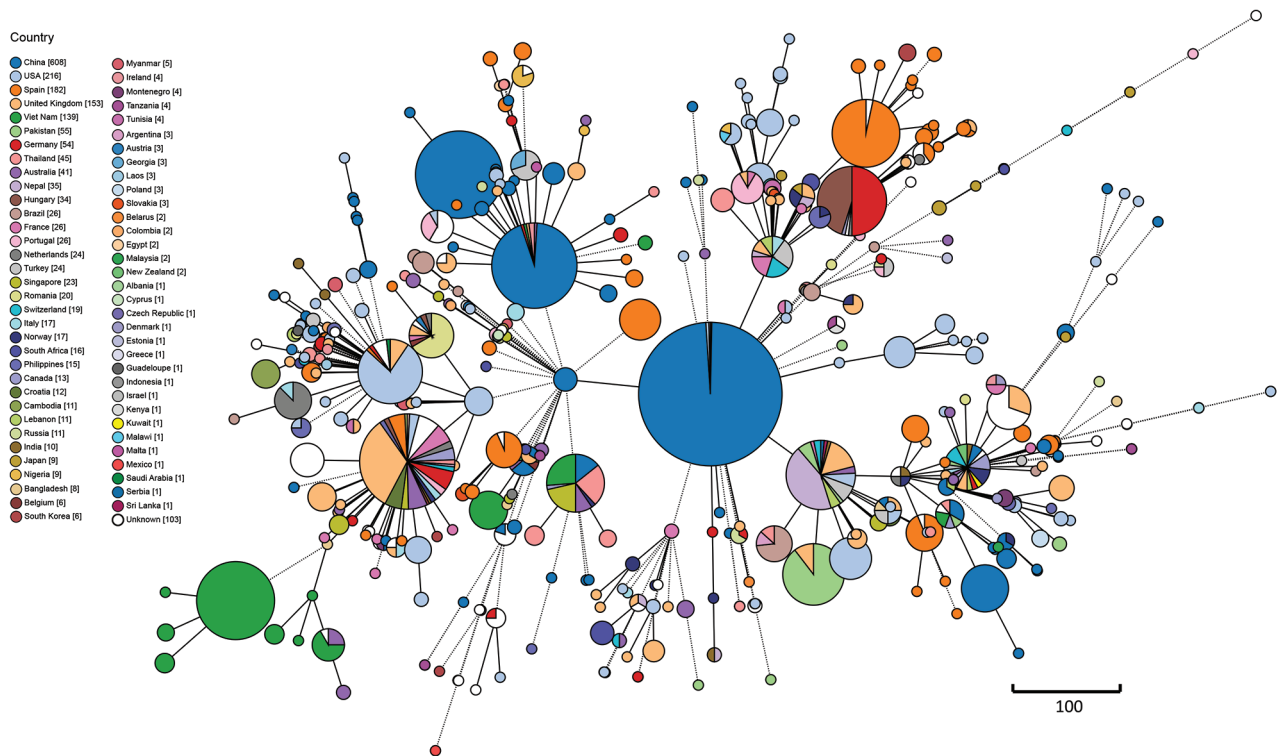


Figure 3. Minimum spanning tree based on core genome MLST analysis of global *bla*_{OXA-232}-carrying carbapenem-resistant *Klebsiella pneumoniae* sequence type 15 isolates. Core genome multilocus sequence typing scheme with clade alert distance set as ≤ 20 alleles. Line lengths connecting each circle depict clonal relationships between isolates. Colors of circles indicate different countries. Numbers in square brackets in the key indicate numbers of isolates recovered from each country. Scale bar represents genetic distance (allelic differences).

2 carbapenemase genes, *bla*_{OXA-232} and *bla*_{KPC-2}. In addition, this lineage carries various virulence determinants, including yersiniabactin, aerobactin, and hypermucoidity (*rmpA2*).

Transcontinental Dissemination of Epidemic ST15 Lineage in the 21st Century

The United States is the likely origin of the ST15 lineage (Figure 5), the offspring of which were introduced into other continents, including Europe, Asia, and Oceania. Transmission from the United States to Europe triggered an epidemic in the United Kingdom. The ST15 lineage was concurrently introduced from the United States to China, where it is the most common strain (93.33%, 308/330 isolates). Epidemic clonal transmissions in China were linked to introductions from the United States (2011–2013), Nepal (2015), and the United Kingdom (2020). Additional global transmission events originated in China and reached the United States, Europe, and Australia. Transmission from China to Australia in 2014 triggered subsequent transmission events from Australia to Europe and Asia. Multiple transmission events occurred from Europe and Australia to Asia in 2015–2016, contributing to complex transmission pathways among countries in Asia. In 2015, strains from

Australia reached Oman and subsequently spread to Nepal. In the same year, strains from Nepal spread to Thailand and China. In 2016, strains from Europe were introduced into Thailand and further disseminated to Nepal. After a local outbreak, strains from China spread to India in 2019.

Discussion

Worldwide spread of CRKP has been accompanied by considerable incidence and death, posing a severe threat to public health (29,30). Multiple nosocomial outbreaks of *bla*_{OXA-232}-carrying *K. pneumoniae* have occurred in China and may have contributed to the prevalence of those strains (5,6,9,31). We analysed the genomic features of 21 CRKP ST15 isolates carrying *bla*_{OXA-232} collected from various regions in China. We integrated the results with global data to investigate the mode of spread and the possible origins of ST15 *bla*_{OXA-232}-carrying CRKP. Our findings provide new insights into the genomic characteristics of *bla*_{OXA-232}-carrying *K. pneumoniae* and transmission dynamics.

Our analysis of *bla*_{OXA-232}-carrying CRKP genomes found *bla*_{OXA-232} on a 6.1 kb ColKP3 plasmid in isolate KP3295 with high similarity and coverage with previously reported plasmids carrying *bla*_{OXA-232} detected

worldwide (6,8,13). Our unsuccessful plasmid conjugation experiment demonstrated the presence of *bla*_{OXA-232} within a nonconjugative plasmid, confirming findings from several previous studies (7,31). Integration of the *bla*_{OXA-232} gene onto IncF-, IncHI1B-, and IncFII-type plasmids through the transposon element *ISEcp1* has been documented. IncF- and IncHI1B-type plasmids serve as crucial carriers for multiple antimicrobial resistance genes, such as extended spectrum β -lactamases and *bla*_{NDM}, that exhibit the ability for interspecies conjugative transfer. Those plasmids are prevalent among members of Enterobacterales and increase risk for wide dissemination (32,33). The integration of ColKP3-type miniplasmid on a larger plasmid suggests that, although not self-transmissible, ColKP3 can be mobilized with the assistance of a self-transmissible plasmid. Of note, plasmids encoding *bla*_{OXA-232} are distributed already in South Asia, Europe, and South

America. The insertion sequence *ISEcp1* was completely lost from the plasmid, which may have inactivated *ISEcp1* transposase and ensured the stability of the *bla*_{OXA-232} gene on the ColKP3 plasmid (9).

Global dissemination of *bla*_{OXA-232} on nonconjugative plasmids, along with escalating outbreaks in China, prompted our investigation into the transmission dynamics and origins of *bla*_{OXA-232}-carrying *K. pneumoniae*. A systematic phylogenetic analysis of 2,118 global ST15 strains revealed a high degree of homogeneity among strains originating from different countries, suggesting the dissemination of *K. pneumoniae* ST15 as a globally prevalent clone. Subsequent genomic epidemiologic analysis revealed distinct regional clustering, primarily within China, characterized by minimal SNP distances, suggesting clonal transmission of *bla*_{OXA-232}-CRKP ST15 lineage. Clonal transmission may also occur between the strains

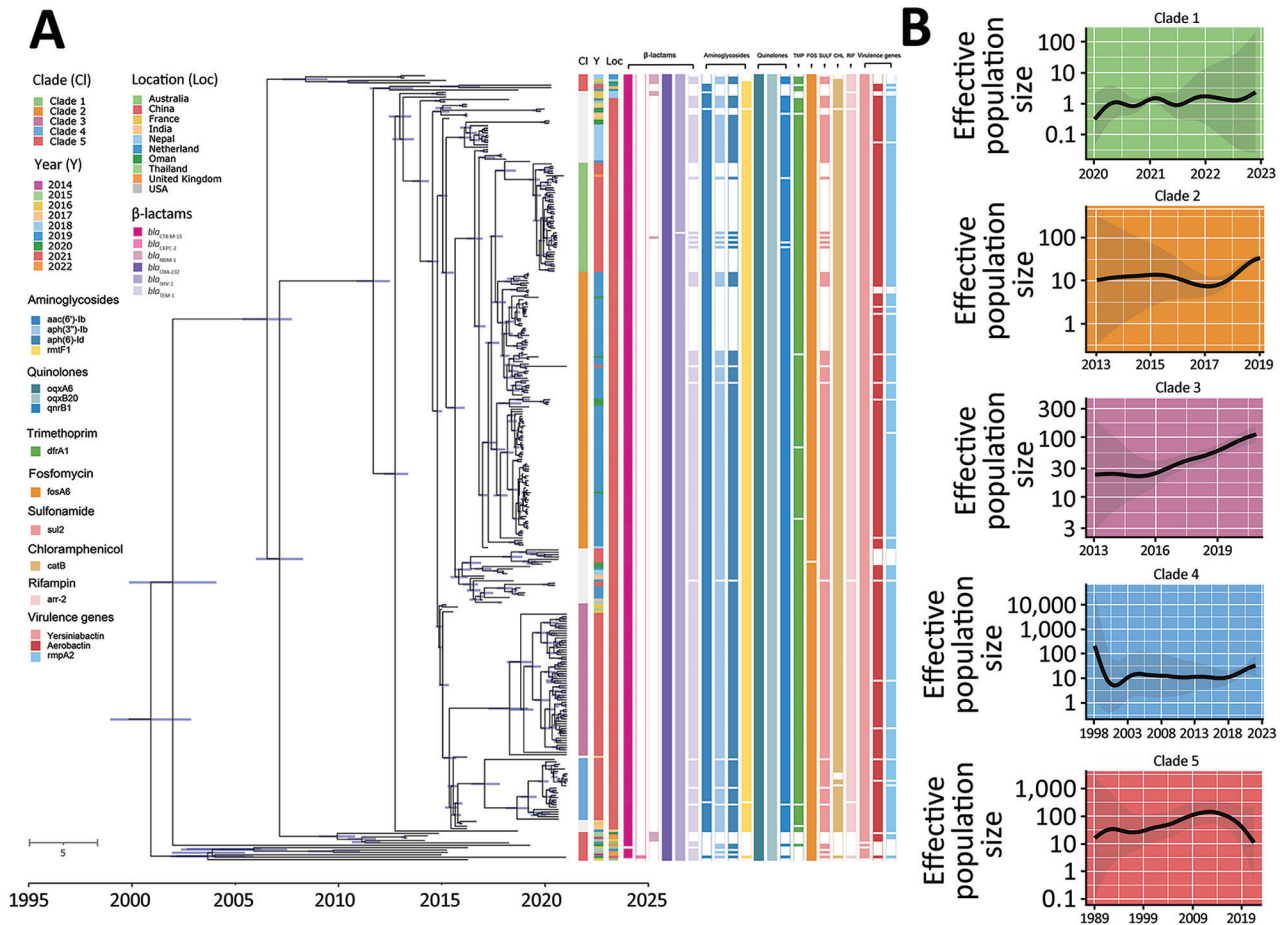


Figure 4. Phylogenetic analysis of global *bla*_{OXA-232}-carrying carbapenem-resistant *Klebsiella pneumoniae* sequence type (ST) 15 isolates. A) Time-calibrated maximum clade credibility Bayesian phylogeny based on 330 *bla*_{OXA-232}-carrying ST15 recombination-filtered core genomes and distribution of antimicrobial resistance genes and virulence genes in the isolates. The cells with colors indicate presence of the gene; blank cells indicate absence. Different colored circles indicate the geographic location and separation time of strains. Blue bars along branches indicate 95% highest posterior probabilities. B) Effective population size of ST15 lineage strains based on the population structure. Shaded areas indicate 95% highest posterior probabilities. Scale bar indicates number of base substitutions per site.

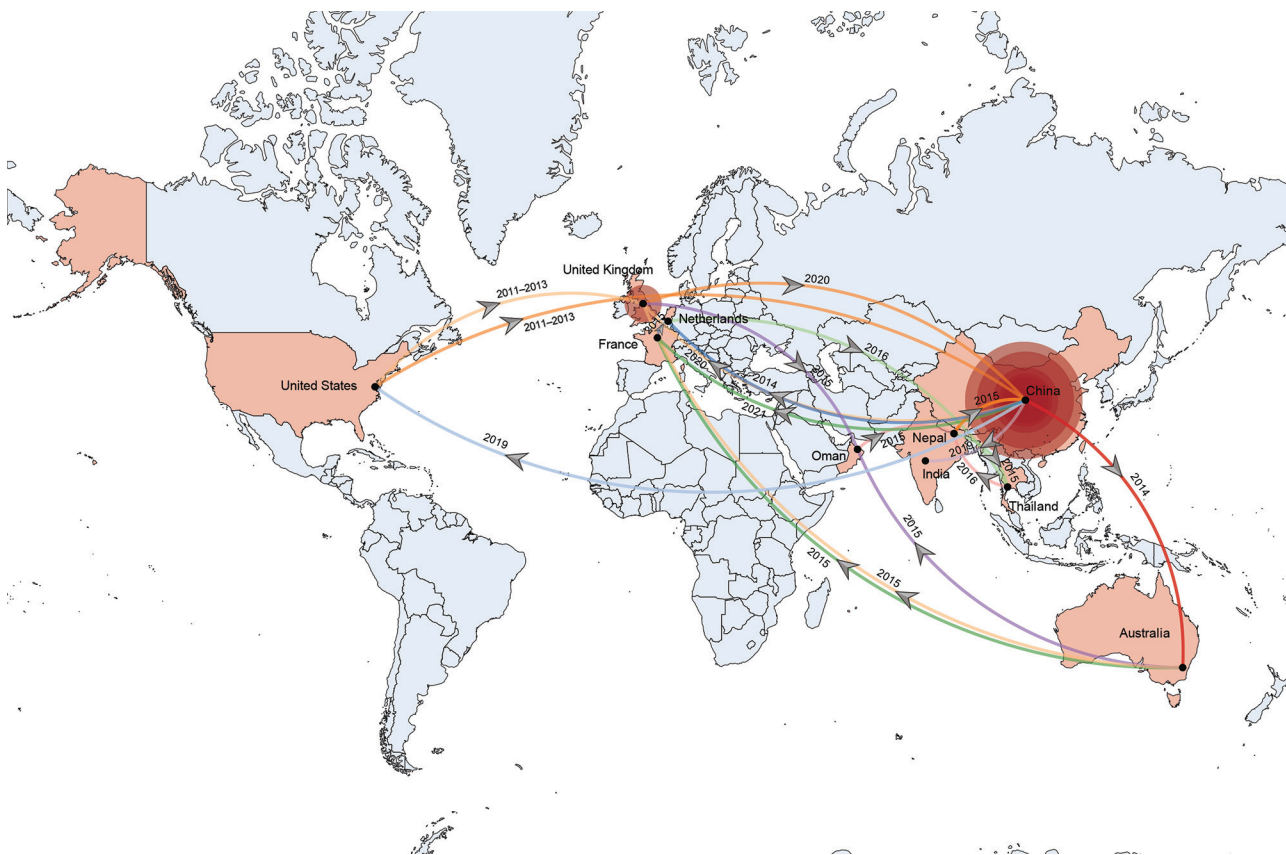


Figure 5. Temporal and spatial transmission trajectory of global *bla*_{OXA-232}-carrying carbapenem-resistant *Klebsiella pneumoniae*. Coral-colored countries on map indicate geographic regions where *bla*_{OXA-232} has occurred; arrows show dates and direction of transmission. The *bla*_{OXA-232}-carrying isolate originated in the United States, initially expanded to the United Kingdom and China, then spread to the rest of the world, with China as its central focus. Red circles represent major outbreak regions in the United Kingdom and China; size of the red circles corresponds to the number of strains analyzed in each country.

from China and Nepal based on pairwise distances ≤ 20 SNPs between these strains. Multiple nosocomial outbreaks of *bla*_{OXA-232}-CRKP ST15 across different geographic regions also provided epidemiologic evidence to support our investigation (5,6,9). We also collected 1 *K. pneumoniae* isolate KP81, carrying both *bla*_{OXA-232} and *bla*_{KPC-2}, also reported in the United States in 2020 (34). Emergence of CRKP ST15 carrying both *bla*_{OXA-232} and *bla*_{KPC-2} in China poses a substantial threat to public health because of its potential for spreading carbapenem resistance internationally through the high-risk clone ST15. *bla*_{OXA-232}-carrying *K. pneumoniae* showed low resistance to imipenem and meropenem in our investigation, also described elsewhere (6,9), possibly attributable to disruption of efficient hydrolytic activity because of loss of a salt bridge between residues D159 and R214 (35).

We used Bayesian phylogeny to elucidate the evolutionary history of *K. pneumoniae* carrying *bla*_{OXA-232} within the ST15 lineage. We estimated that this specific lineage appeared in 2000 (95% HPD interval

1989–1998), approximately the same time the ST147 KL10-O3a (2002) and ST258 (1997) lineages were reported (36,37). On the basis of our analysis, we suggest that the ST15 lineage originated in the United States. In addition, we successfully reconstructed early transmission events from the United States to both Europe and Asia. Imported strains from the United States and Nepal to China catalyzed clonal spread of strains already circulating in China. From China, strains of ST15 lineage were disseminated across multiple continents and eventually became globally dispersed. Introduction and inappropriate use of fourth-generation cephalosporin (38) and carbapenem antimicrobial drugs (39,40), approved in clinical settings in the 1990s, may have influenced the global emergence and transmission of ST15 lineage.

Our study was limited by focusing solely on ST15 *bla*_{OXA-232}-carrying CRKP strains, which we did because those strains have the highest isolation rate in China and have caused multiple nosocomial outbreaks. Future studies are needed to explore global

distribution of other lineages. Second, we might have underestimated prevalence of the *bla*_{OXA-232} gene because of limited carbapenem hydrolysis activity, possibly resulting in false-negative results in antimicrobial susceptibility testing. Finally, although we comprehensively evaluated all publicly available ST15 *bla*_{OXA-232}-carrying CRKP strains worldwide, it is possible that some circulating strains went undetected in some regions with dense strain distribution where isolates were derived from a small number of surveillance sites. Therefore, genomic surveillance should be expanded, especially in countries with low isolation rates, to provide a more comprehensive understanding of the emergence, expansion, and spread of CRKP. In conclusion, our research contributes to the comprehension of the global spread of *bla*_{OXA-232}-carrying CRKP ST15 lineage and emphasizes the need to develop measures for preventing and controlling progression of the CRKP epidemic.

This study was supported by the National Natural Science Foundation of China (82102436, 81871696, 82202565), the Zhejiang Provincial Natural Science Foundation of China (LR23H200001, LY21H190001, LQ22H200001), and the Zhejiang Provincial Medical and Health Science and Technology Plan (2020RC066, 2021RC007, 2022RC299, 2023KY227, 2023KY228).

About the Author

Ms. Wu is a graduate student at Zhejiang University School of Medicine. Her research interests include molecular epidemiology and antimicrobial resistance mechanisms of MDR bacterial pathogens. Dr. Ruan is a principal investigator at Sir Run Run Shaw Hospital, Zhejiang University School of Medicine, China. His primary research interests are microbial genomics and application of bioinformatics to study the genomic epidemiology of multidrug-resistant bacterial infections.

References

- Zhang Y, Wang Q, Yin Y, Chen H, Jin L, Gu B, et al. Epidemiology of carbapenem-resistant Enterobacteriaceae infections: report from the China CRE network. *Antimicrob Agents Chemother.* 2018;62:e01882-17. <https://doi.org/10.1128/AAC.01882-17>
- Nordmann P, Cuzon G, Naas T. The real threat of *Klebsiella pneumoniae* carbapenemase-producing bacteria. *Lancet Infect Dis.* 2009;9:228-36. [https://doi.org/10.1016/S1473-3099\(09\)70054-4](https://doi.org/10.1016/S1473-3099(09)70054-4)
- Karlowsky JA, Lob SH, Kazmierczak KM, Badal RE, Young K, Motyl MR, et al. In vitro activity of imipenem against carbapenemase-positive Enterobacteriaceae isolates collected by the SMART Global Surveillance Program from 2008 to 2014. *J Clin Microbiol.* 2017;55:1638-49. <https://doi.org/10.1128/JCM.02316-16>
- Tian D, Pan F, Wang C, Sun Y, Zhang H. Resistance phenotype and clinical molecular epidemiology of carbapenem-resistant *Klebsiella pneumoniae* among pediatric patients in Shanghai. *Infect Drug Resist.* 2018;11:1935-43. <https://doi.org/10.2147/IDR.S175584>
- Li X, Ma W, Qin Q, Liu S, Ye L, Yang J, et al. Nosocomial spread of OXA-232-producing *Klebsiella pneumoniae* ST15 in a teaching hospital, Shanghai, China. *BMC Microbiol.* 2019;19:235. <https://doi.org/10.1186/s12866-019-1609-1>
- Han X, Chen Y, Zhou J, Shi Q, Jiang Y, Wu X, et al. Epidemiological characteristics of OXA-232-producing carbapenem-resistant *Klebsiella pneumoniae* strains isolated during nosocomial clonal spread associated with environmental colonization. *Microbiol Spectr.* 2022;10:e0257221. <https://doi.org/10.1128/spectrum.02572-21>
- Potron A, Rondinaud E, Poirel L, Belmonte O, Boyer S, Camiade S, et al. Genetic and biochemical characterisation of OXA-232, a carbapenem-hydrolysing class D β -lactamase from Enterobacteriaceae. *Int J Antimicrob Agents.* 2013;41:325-9. <https://doi.org/10.1016/j.ijantimicag.2012.11.007>
- Lutgring JD, Zhu W, de Man TJB, Avillan JJ, Anderson KF, Lonsway DR, et al. Phenotypic and genotypic characterization of Enterobacteriaceae producing oxacillinase-48-like carbapenemases, United States. *Emerg Infect Dis.* 2018;24:700-9. <https://doi.org/10.3201/eid2404.171377>
- Jia H, Zhang Y, Ye J, Xu W, Xu Y, Zeng W, et al. Outbreak of multidrug-resistant OXA-232-producing ST15 *Klebsiella pneumoniae* in a teaching hospital in Wenzhou, China. *Infect Drug Resist.* 2021;14:4395-407. <https://doi.org/10.2147/IDR.S329563>
- Shu L, Dong N, Lu J, Zheng Z, Hu J, Zeng W, et al. Emergence of OXA-232 Carbapenemase-producing *Klebsiella pneumoniae* that carries a pLVPK-like virulence plasmid among elderly patients in China. *Antimicrob Agents Chemother.* 2019;63:e02246-18. <https://doi.org/10.1128/AAC.02246-18>
- Ruan Z, Yu Y, Feng Y. The global dissemination of bacterial infections necessitates the study of reverse genomic epidemiology. *Brief Bioinform.* 2020;21:741-50. <https://doi.org/10.1093/bib/bbz010>
- Shi Q, Han R, Guo Y, Zheng Y, Yang Y, Yin D, et al. Emergence of ST15 *Klebsiella pneumoniae* clinical isolates producing plasmids-mediated RmtF and OXA-232 in China. *Infect Drug Resist.* 2020;13:3125-9. <https://doi.org/10.2147/IDR.S257298>
- Poirel L, Héritier C, Tolün V, Nordmann P. Emergence of oxacillinase-mediated resistance to imipenem in *Klebsiella pneumoniae*. *Antimicrob Agents Chemother.* 2004;48:15-22. <https://doi.org/10.1128/AAC.48.1.15-22.2004>
- Hackel MA, Tsuji M, Yamano Y, Echols R, Karlowsky JA, Sahn DF. Reproducibility of broth microdilution MICs for the novel siderophore cephalosporin, cefiderocol, determined using iron-depleted cation-adjusted Mueller-Hinton broth. *Diagn Microbiol Infect Dis.* 2019;94:321-5. <https://doi.org/10.1016/j.diagmicrobio.2019.03.003>
- Wick RR, Judd LM, Gorrie CL, Holt KE. Unicycler: resolving bacterial genome assemblies from short and long sequencing reads. *PLoS Comput Biol.* 2017;13:e1005595. <https://doi.org/10.1371/journal.pcbi.1005595>
- Feldgarden M, Brover V, Haft DH, Prasad AB, Slotta DJ, Tolstoy I, et al. Validating the AMRFinder tool and resistance gene database by using antimicrobial resistance genotype-phenotype correlations in a collection of isolates. *Antimicrob Agents Chemother.* 2019;63:e00483-19. <https://doi.org/10.1128/AAC.00483-19>
- Carattoli A, Zankari E, García-Fernández A, Voldby Larsen M, Lund O, Villa L, et al. In silico detection and typing of plasmids using PlasmidFinder and plasmid

- multilocus sequence typing. *Antimicrob Agents Chemother.* 2014;58:3895–903. <https://doi.org/10.1128/AAC.02412-14>
18. Lam MMC, Wick RR, Watts SC, Cerdeira LT, Wyres KL, Holt KE. A genomic surveillance framework and genotyping tool for *Klebsiella pneumoniae* and its related species complex. *Nat Commun.* 2021;12:4188. <https://doi.org/10.1038/s41467-021-24448-3>
 19. Liu B, Zheng D, Zhou S, Chen L, Yang J. VFDB 2022: a general classification scheme for bacterial virulence factors. *Nucleic Acids Res.* 2022;50(D1):D912–7. <https://doi.org/10.1093/nar/gkab1107>
 20. Feng Y, Zou S, Chen H, Yu Y, Ruan Z. BacWGSTdb 2.0: a one-stop repository for bacterial whole-genome sequence typing and source tracking. *Nucleic Acids Res.* 2021;49(D1):D644–50. <https://doi.org/10.1093/nar/gkaa821>
 21. Sullivan MJ, Petty NK, Beatson SA. Easyfig: a genome comparison visualizer. *Bioinformatics.* 2011;27:1009–10. <https://doi.org/10.1093/bioinformatics/btr039>
 22. Alikhan NF, Petty NK, Ben Zakour NL, Beatson SA. BLAST Ring Image Generator (BRIG): simple prokaryote genome comparisons. *BMC Genomics.* 2011;12:402. <https://doi.org/10.1186/1471-2164-12-402>
 23. Deneke C, Uelze L, Brendebach H, Tausch SH, Malorny B. Decentralized investigation of bacterial outbreaks based on hashed cgMLST. *Front Microbiol.* 2021;12:649517. <https://doi.org/10.3389/fmicb.2021.649517>
 24. Zhou Z, Alikhan NF, Sergeant MJ, Luhmann N, Vaz C, Francisco AP, et al. GrapeTree: visualization of core genomic relationships among 100,000 bacterial pathogens. *Genome Res.* 2018;28:1395–404. <https://doi.org/10.1101/gr.232397.117>
 25. Bouckaert R, Vaughan TG, Barido-Sottani J, Duchêne S, Fourment M, Gavryushkina A, et al. BEAST 2.5: an advanced software platform for Bayesian evolutionary analysis. *PLOS Comput Biol.* 2019;15:e1006650. <https://doi.org/10.1371/journal.pcbi.1006650>
 26. Tonkin-Hill G, Lees JA, Bentley SD, Frost SDW, Corander J, RhierBAPS: An R implementation of the population clustering algorithm hierBAPS. *Wellcome Open Res.* 2018; 3:93. <https://doi.org/10.12688/wellcomeopenres.14694.1>
 27. Letunic I, Bork P. Interactive Tree Of Life (iTOL) v5: an online tool for phylogenetic tree display and annotation. *Nucleic Acids Res.* 2021;49(W1):W293–6. <https://doi.org/10.1093/nar/gkab301>
 28. Bielejec F, Baele G, Vrancken B, Suchard MA, Rambaut A, Lemey P. Spred3: interactive visualization of spatiotemporal history and trait evolutionary processes. *Mol Biol Evol.* 2016;33:2167–9. <https://doi.org/10.1093/molbev/msw082>
 29. Agyeman AA, Bergen PJ, Rao GG, Nation RL, Landersdorfer CB. A systematic review and meta-analysis of treatment outcomes following antibiotic therapy among patients with carbapenem-resistant *Klebsiella pneumoniae* infections. *Int J Antimicrob Agents.* 2020;55:105833. <https://doi.org/10.1016/j.ijantimicag.2019.10.014>
 30. Xu L, Sun X, Ma X. Systematic review and meta-analysis of mortality of patients infected with carbapenem-resistant *Klebsiella pneumoniae*. *Ann Clin Microbiol Antimicrob.* 2017;16:18. <https://doi.org/10.1186/s12941-017-0191-3>
 31. Yin D, Dong D, Li K, Zhang L, Liang J, Yang Y, et al. Clonal dissemination of OXA-232 carbapenemase-producing *Klebsiella pneumoniae* in neonates. *Antimicrob Agents Chemother.* 2017;61:e00385–17. <https://doi.org/10.1128/AAC.00385-17>
 32. Yamamoto S, Nakano M, Kitagawa W, Tanaka M, Sone T, Hirai K, et al. Characterization of multi-antibiotic-resistant *Escherichia coli* isolated from beef cattle in Japan. *Microbes Environ.* 2014;29:136–44. <https://doi.org/10.1264/jsm2.ME13173>
 33. Villa L, Poirel L, Nordmann P, Carta C, Carattoli A. Complete sequencing of an IncH plasmid carrying the bla_{NDM-1}, bla_{CITX-M-15} and qnrB1 genes. *J Antimicrob Chemother.* 2012;67:1645–50. <https://doi.org/10.1093/jac/dks114>
 34. Palavecino E, Ramirez K, Greene SR, Kilic A. Co-existence of VIM-2-producing *Pseudomonas aeruginosa* and KPC-2 and OXA-232-co-producing *Klebsiella pneumoniae* in the United States. *Ann Lab Med.* 2020;40:267–9. <https://doi.org/10.3343/alm.2020.40.3.267>
 35. Docquier JD, Calderone V, De Luca F, Benvenuti M, Giuliani F, Bellucci L, et al. Crystal structure of the OXA-48 beta-lactamase reveals mechanistic diversity among class D carbapenemases. *Chem Biol.* 2009;16:540–7. <https://doi.org/10.1016/j.chembiol.2009.04.010>
 36. Rodrigues C, Desai S, Passet V, Gajjar D, Brisse S. Genomic evolution of the globally disseminated multidrug-resistant *Klebsiella pneumoniae* clonal group 147. *Microb Genom.* 2022;8:000737. <https://doi.org/10.1099/mgen.0.000737>
 37. Gaiarsa S, Comandatore F, Gaibani P, Corbella M, Dalla Valle C, Epis S, et al. Genomic epidemiology of *Klebsiella pneumoniae* in Italy and novel insights into the origin and global evolution of its resistance to carbapenem antibiotics. *Antimicrob Agents Chemother.* 2015;59:389–96. <https://doi.org/10.1128/AAC.04224-14>
 38. Long TE, Williams JT. Cephalosporins currently in early clinical trials for the treatment of bacterial infections. *Expert Opin Investig Drugs.* 2014;23:1375–87. <https://doi.org/10.1517/13543784.2014.930127>
 39. Zaffiri L, Gardner J, Toledo-Pereyra LH. History of antibiotics. From salvarsan to cephalosporins. *J Invest Surg.* 2012;25:67–77. <https://doi.org/10.3109/08941939.2012.664099>
 40. Lima LM, Silva BNMD, Barbosa G, Barreiro EJ. β -lactam antibiotics: an overview from a medicinal chemistry perspective. *Eur J Med Chem.* 2020;208:112829. <https://doi.org/10.1016/j.ejmech.2020.112829>

Address for correspondence: Zhi Ruan, Jun Zhang, or Xinyou Xie, Department of Clinical Laboratory, Sir Run Run Shaw Hospital, Zhejiang University School of Medicine, 3 East Qingchun Rd, 310016, Hangzhou, China; email: r_z@zju.edu.cn or jameszhang2000@zju.edu.cn or scottxie@zju.edu.cn

SARS-CoV-2 Reinfection Risk in Persons with HIV, Chicago, Illinois, USA, 2020–2022

Richard A. Teran, Alexandra Gagner, Stephanie Gretsches, Jeff Lauritsen, Daniel Galanto, Kelly Walblay, Peter Ruestow, Colin Korban, Massimo Pacilli, David Kern, Stephanie R. Black, Irina Tabidze

Understanding if persons with HIV (PWH) have a higher risk for SARS-CoV-2 reinfection may help tailor future COVID-19 public health guidance. To determine whether HIV infection was associated with increased risk for SARS-CoV-2 reinfection, we followed adult residents of Chicago, Illinois, USA, with SARS-CoV-2 longitudinally from their first reported infection through May 31, 2022. We matched SARS-CoV-2 laboratory data and COVID-19 vaccine administration data to Chicago's Enhanced HIV/AIDS Reporting System. Among 453,587 Chicago residents with SARS-CoV-2, a total of 5% experienced a SARS-CoV-2 reinfection, including 192/2,886 (7%) PWH and 23,642/450,701 (5%) persons without HIV. We observed higher SARS-CoV-2 reinfection incidence rates among PWH (66 [95% CI 57–77] cases/1,000 person-years) than PWOH (50 [95% CI 49–51] cases/1,000 person-years). PWH had a higher adjusted rate of SARS-CoV-2 reinfection (1.46, 95% CI 1.27–1.68) than those without HIV. PWH should follow the recommended COVID-19 vaccine schedule, including booster doses.

HIV can compromise the immune system; persons with HIV (PWH), especially those not receiving antiretroviral therapy (ART), might be vulnerable to SARS-CoV-2 infection. Studies have reported an increased risk for SARS-CoV-2 infection among those with immunocompromising conditions (1–3); older age and underlying health conditions are known to increase the likelihood of severe COVID-19 outcomes (4,5). Understanding how COVID-19 affects PWH is important because approximately half of PWH are ≥ 50 years of age (6) and have higher rates of medical

comorbidities, compared with persons without HIV (PWOH) (7,8). Studies have reported conflicting results regarding SARS-CoV-2 infection among PWH: adverse COVID-19-related outcomes among PWH (9); no association between HIV status and infection risk (10,11); and increased rates of postvaccination infections in PWH (12,13). Repeat SARS-CoV-2 infections among PWH and the risk for SARS-CoV-2 reinfection, compared with PWOH, is less understood.

Recovery from SARS-CoV-2 infection is followed by a period of infection-induced immunity, during which antibody titers persist for several months after infection (14–16). Epidemiologic evidence indicates that infection-induced immunity alone does not provide full protection against subsequent infections and that protection wanes over time (17–22). Observational studies (23–26) also indicate that SARS-CoV-2 reinfections with different strains are possible even when infection-induced immunity is coupled with vaccine-induced immunity; risk is likely compounded in the presence of more transmissible circulating variants (27). We sought to determine whether HIV infection was associated with an increased risk for SARS-CoV-2 reinfection among residents of Chicago, Illinois, USA.

Methods

Data Sources

We abstracted all variables from public health surveillance and information systems. In Illinois, healthcare providers and laboratories are required to report both SARS-CoV-2 and HIV infections among residents to public health. Most SARS-CoV-2 laboratory test results are submitted electronically by testing laboratories directly into the Illinois National Electronic Disease Surveillance System (I-NEDSS). For this analysis, we defined a SARS-CoV-2 case as a positive SARS-CoV-2 nucleic acid amplification or antigen test result

Author affiliations: Centers for Disease Control and Prevention, Atlanta, Georgia, USA (R.A. Teran); Chicago Department of Public Health, Chicago, Illinois, USA (R.A. Teran, A. Gagner, S. Gretsches, J. Lauritsen, D. Galanto, K. Walblay, P. Ruestow, C. Korban, M. Pacilli, D. Kern, S.R. Black, I. Tabidze)

DOI: <http://doi.org/10.3201/eid2911.230577>

from a respiratory specimen collected from a Chicago resident and reported to a public health entity. We considered multiple positive SARS-CoV-2 test results reported to public health occurring within 90 days as part of the same SARS-CoV-2 case; we used the earliest positive specimen collection date as the index date for the infection episode.

The Enhanced HIV/AIDS Reporting System (eHARS) contains records of Chicago residents who have received an HIV/AIDS diagnosis reported to public health. Medical providers must report all new HIV and AIDS diagnoses; laboratories are required to report all positive HIV diagnostic tests, HIV viral load test results, CD4 test results, and nucleotide sequences from HIV genotypic resistance testing.

COVID-19 vaccine doses administered in the state of Illinois must also be reported to Illinois' Comprehensive Automated Immunization Registry (I-CARE). I-CARE data include information about the person receiving the vaccine dose, dose administration date, and vaccine manufacturer.

Surveillance and Information System Matching

The analytic cohort included Chicago residents with a positive SARS-CoV-2 test result reported to I-NEDSS with specimen collection dates on or before March 1, 2022, who were ≥ 18 years of age. We followed cohort members until their second positive SARS-CoV-2 test result or their death, or until May 31, 2022. We matched person-level SARS-CoV-2 data from I-NEDSS to person-level I-CARE data to identify all COVID-19 vaccine doses administered to the analytic cohort. We used a modified standardized 12-key hierarchical deterministic algorithm, described previously (28). The matching algorithm created 12 variables or keys using a variation of character combinations between first name, last name, and date of birth; key 1 (e.g., full last name + first 6 letters of first name + full date of birth) was the strictest and key 12 the least strict. We created keys for each discrete dataset (i.e., data from I-NEDSS and I-CARE). We compared records across datasets by proceeding chronologically through each key. We flagged matched records and appended them to a separate dataset. We then iteratively compared unmatched records across datasets using key 2 through key 12. We then merged the 12 datasets containing matched records for each key to create a matched dataset.

To identify PWH, we compared the matched dataset to a subset of records from eHARS using a separate 12-key hierarchical deterministic algorithm that also used first name, last name, and date of birth. The eHARS subset included PWH reported

in eHARS who were alive as of January 1, 2020, and whose current city of residence was Chicago or whose city of residence at death, HIV diagnosis, AIDS diagnosis, or HIV disease diagnosis was listed as Chicago when current city of residence was unavailable. The final analytic dataset included person-level records containing SARS-CoV-2 data, COVID-19 vaccine data, and HIV data for each person in the analytic cohort.

Category Definitions

We categorized persons with an HIV infection reported to eHARS before their first reported SARS-CoV-2 positive specimen collection date as PWH. For persons with an initial SARS-CoV-2 positive specimen collection date on or after February 1, 2022, we determined HIV status using eHARS data available as of January 31, 2022, because that was the most recent dataset available for analysis. We categorized persons with no evidence of HIV infection as PWOH. We excluded persons with an HIV diagnosis after their first SARS-CoV-2 infection from the analysis. We defined SARS-CoV-2 reinfection as a SARS-CoV-2 case occurring on or before May 31, 2022, and >90 days from an initial SARS-CoV-2 positive test result.

Additional Covariates

We obtained age at first infection, sex at birth, race and ethnicity, and address from SARS-CoV-2 data reported to I-NEDSS. If sex at birth and race and ethnicity data were missing, we examined variables in eHARS and I-CARE and reconciled the data in the analytic dataset. We used address to categorize residence into 1 of 7 Chicago regions to account for differences in SARS-CoV-2 incidence and COVID-19 vaccine distribution and uptake across the city. We categorized persons into 4 distinct infection groups (ancestral variant, Alpha and other pre-Delta variants, Delta variant, and Omicron variant) on the basis of the specimen collection date of their initial SARS-CoV-2 infection. We determined thresholds for each group using local and national molecular surveillance data; the starting threshold for a new infection group indicates when 50% of sequenced specimens were attributed to a variant (29–31).

We evaluated vaccination status at the time of the first SARS-CoV-2 infection, and if applicable, at the time of reinfection. We categorized persons as unvaccinated if they had not received a COVID-19 vaccine dose; partially vaccinated if they received 1 dose of a 2-dose COVID-19 vaccine series; and completed series if they received 2 doses of a 2-dose series or 1 dose of a 1-dose series. We defined an additional

vaccine dose as any vaccine dose administered after completing the primary series. We also characterized vaccination status by vaccine manufacturer of the primary series.

For PWH, we determined years since HIV diagnosis and history of AIDS at initial SARS-CoV-2 infection. We determined history of AIDS on the basis of a clinical opportunistic illness diagnosis or CD4 count <200 cells/mm³ before the first SARS-CoV-2 infection (32). We identified the laboratory CD4 count and HIV viral load test result preceding the first SARS-CoV-2 infection for each PWH. We categorized most recent CD4 count as <200 , 200–349, 350–499, or ≥ 500 cells/mm³. We used HIV viral load results to describe viral suppression status. We classified viral loads <200 copies/mL as suppressed, consistent with the national HIV surveillance definition of viral suppression (33).

The Chicago Department of Public Health Institutional Review Board and the Centers for Disease Control and Prevention reviewed our investigation. We conducted our study in accordance with department policies and applicable federal law (45 C.F.R. part 46.102(l)(2), 21 C.F.R. part 56; 42 U.S.C. §241(d); 5 U.S.C. §552a; 44 U.S.C. §3501 et seq).

Statistical Analysis

We followed persons in the study from the earliest positive SARS-CoV-2 specimen collection date until the earliest specimen collection date of their second positive SARS-CoV-2 infection occurring >90 days from the first infection; until death; or until May 31, 2022, whichever occurred first. We compared characteristics by HIV status to evaluate differences between the subset of persons who had 1 SARS-CoV-2 infection reported to public health and the subset of persons who had >1 SARS-CoV-2 infection. Among PWH, we compared HIV characteristics by reinfection status.

We calculated SARS-CoV-2 reinfection incidence rates and incidence rate differences per 1,000 person-years by HIV status and for each variant phase and calendar quarter. We used nonparametric survival analyses to estimate cumulative incidence of SARS-CoV-2 reinfection during the observation period. We tested for differences in cumulative incidence curves by HIV status by using Gray's tests.

To assess the effect of HIV infection on SARS-CoV-2 reinfection during the observation period, we compared crude and adjusted rate ratios using univariable and multivariable Poisson regression models with the log of person-time as the offset term. To account for overdispersion in the Poisson regression

model, we calculated robust SEs using generalized estimating equations. We adjusted the model for age, sex at birth, race and ethnicity, region of residence, initial SARS-CoV-2 infection group, vaccination status at the time of first SARS-CoV-2 infection, type of first COVID-19 vaccination dose received at the time of first SARS-CoV-2 infection, and number of doses administered after the first SARS-CoV-2 infection. We used SAS version 9.4 (SAS Institute, Inc., <https://www.sas.com>) to conduct record matching and analyses.

Results

A total of 453,587 Chicago residents meeting the analytic cohort criteria had a positive SARS-CoV-2 test result reported to public health during March 2020–March 2022; those persons contributed a total of 473,513 person-years (median 1.1 person-years; interquartile analysis [IQR] 0.4–1.5 person-years) during the 26-month observation period (Appendix Table, <https://wwwnc.cdc.gov/EID/article/29/11/23-0577-App1.pdf>). Median age of the analytic cohort was 39 (IQR 28–53) years, and most (71.0% [321,905/453,587]) were unvaccinated at the time of their first SARS-CoV-2 infection. Among the analytic cohort, 2,886 (0.6%) persons had received an HIV diagnosis before their first SARS-CoV-2 infection. In total, 23,834 (5.3%) persons had a second positive SARS-CoV-2 test result reported to public health >90 days after their first infection, indicating a SARS-CoV-2 reinfection. The percentage having a SARS-CoV-2 reinfection was higher among PWH (6.7% [192/2,886]) compared with PWOH (5.2% [23,642/450,701]; $p<0.01$).

Most (188,155 [41.5%]) persons' first SARS-CoV-2 infection occurred during March–December 2020, which was the ancestral variant phase of the COVID-19 pandemic (Appendix Table 1). Among 131,682 persons who received COVID-19 vaccine before their first SARS-CoV-2 infection, a plurality (71,333 [54.2%]) had completed a primary vaccine series from Pfizer-BioNTech (<https://www.pfizer.com>). Of 23,834 persons who had a SARS-CoV-2 reinfection, 39.6% (9,444/23,834) had completed a primary series but had not received an additional dose at the time of their SARS-CoV-2 reinfection. Among persons who experienced a SARS-CoV-2 reinfection, PWH were older (median 43 years of age, 95% CI 32–57 years of age) than PWOH (median 36 years, 95% CI 27–49 years of age; $p<0.01$). PWH were more likely than PWOH to be male (79.3% vs. 40.9%; $p<0.01$) and non-Hispanic or Latino Black or African American (53.7% vs. 27.0%; $p<0.01$), and to

Table 1. SARS-CoV-2 reinfection incidence rates, by HIV status, Chicago, Illinois, USA, January 1, 2020–May 31, 2022*

Characteristic	No. (%) events	Incidence, % (95% CI)			Incidence rate difference, %
		Analytic cohort	PWH	PWOH	
Total observation period	23,834 (100)	50 (37–66)	66 (57–77)	50 (49–51)	16
Timing of reinfection, by variant phase					
Ancestral variant, 2020 Jan 1–Dec 31	866 (3.6)	16 (9–26)	30 (16–59)	16 (15–17)	14
Alpha and other pre-Delta variants, 2021 Jan 1–Jul 10	1,030 (4.3)	6 (2–13)	8 (4–16)	6 (5–6)	2
Delta variant, 2021 Jul 11–Dec 18	3,039 (12.8)	11 (5–19)	17 (12–25)	11 (10–11)	6
Omicron variant, 2021 Dec 19–2022 Mar 1	18,899 (79.3)	40 (29–55)	50 (42–60)	40 (39–41)	10
Timing of reinfection, by calendar quarter					
2020					
Apr–Jun	14 (0.1)	2 (0–7)	16 (1–209)	2 (1–3)	14
Jul–Sep	268 (1.1)	12 (6–21)	30 (11–82)	12 (10–13)	18
Oct–Dec	584 (2.5)	11 (5–20)	14 (5–37)	11 (10–12)	3
2021					
Jan–Mar	549 (2.3)	5 (2–12)	5 (1–16)	5 (4–6)	0
Apr–Jun	457 (1.9)	3 (1–8)	4 (1–12)	3 (2–3)	1
Jul–Sep	721 (3.0)	3 (1–9)	9 (5–17)	3 (2–3)	6
Oct–Dec	9,477 (39.8)	32 (22–45)	42 (33–53)	32 (31–32)	10
2022					
Jan–Mar	7,750 (32.5)	20 (12–31)	27 (21–35)	20 (19–20)	7
Apr–May	4,014 (16.8)	9 (4–17)	9 (5–13)	9 (8–9)	0

*Incidence is given as percentage of cases per 1,000 person-years. PWH, persons with HIV; PWOH, persons without HIV.

have completed a primary COVID-19 vaccination series plus additional dose (31.8% vs. 22.1%; $p < 0.01$). Also, among persons with a SARS-CoV-2 reinfection, PWH were less likely to be unvaccinated at the time of their first infection, compared with PWOH (87.5% vs. 91.0%; $p < 0.01$).

Among PWH ($n = 2,886$), median time from HIV diagnosis to initial SARS-CoV-2 infection was 12.8 (IQR 6.3–19.7) years. Approximately half (1,359 [47.1%]) met criteria for AIDS before their first SARS-CoV-2 infection. More than half (1,513 [52.4%]) had a CD4 count ≥ 500 cells/mm³, and most (2,213 [76.7%]) had an HIV viral load result < 200 copies/mL, indicating viral suppression. HIV history data and HIV laboratory data were not significantly different ($p \geq 0.05$) when stratified by SARS-CoV-2 reinfection status.

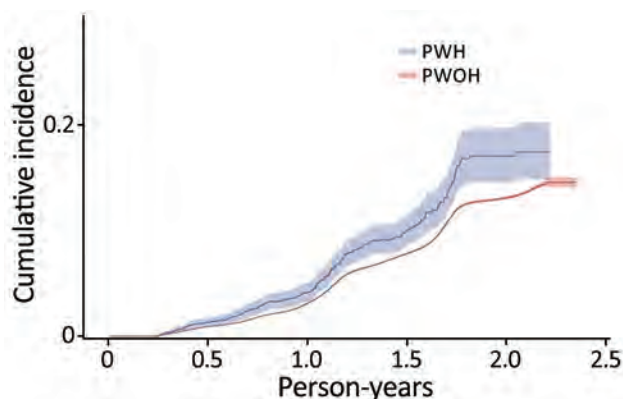


Figure 1. Cumulative incidence (cases/1,000 person-years) of SARS-CoV-2 reinfection by HIV status, Chicago, Illinois, USA, January 1, 2020–May 31, 2022. PWH, persons with HIV; PWOH, persons without HIV.

Incidence rate of SARS-CoV-2 reinfection for the analytic cohort was 50 (95% CI 37–66) cases/1,000 person-years (Table 1). Reinfection incidence was higher among PWH (66 [95% CI 57–77] cases/1,000 person-years) than PWOH during the observation period (50 [95% CI 49–51] cases/1,000 person-years). When we examined SARS-CoV-2 reinfections by variant phase and calendar quarter, PWH consistently had a higher incidence rate of SARS-CoV-2 reinfection, compared with PWOH. We observed the highest incidence rates for PWH during the omicron variant phase (50 [95% CI 42–60] cases/1,000 person-years); by calendar quarter the incidence rates were highest during October–December 2021 (42 [95% CI 33–53] cases/1,000 person-years). Incidence rate differences between PWH and PWOH varied throughout the observation period; overall, an excess of 16 SARS-CoV-2 reinfections/1,000 person-years among PWH were reported. We observed the highest incidence rate difference during July–September 2020, which was an excess of 18 SARS-CoV-2 reinfections/1,000 person-years among PWH compared with PWOH.

SARS-CoV-2 reinfection cumulative incidence rate (CIR) at 1 year after an initial infection was 3.1% (95% CI 3.0%–3.2%); at 1.5 years, 7.8% (95% CI 7.7%–8.0%); at 2 years, 13.1% (95% CI 12.9%–13.3%), and at 2.3 years, the end of observation period, 14.5% (95% CI 14.0%–15.1%). CIR was higher among PWH than PWOH at all time points (Figure 1). Two years after an initial infection, the SARS-CoV-2 reinfection CIR was 17.0% (95% CI 14.5%–19.7%) among PWH, compared with 13.1% (95% CI 12.9%–13.2%) among

PWOH. Persons with HIV who were not virally suppressed had higher SARS-CoV-2 reinfection CIR compared with virally suppressed PWH and PWOH (Figure 2); 1.5 years after an initial SARS-CoV-2 infection, CIR in virally unsuppressed PWH was 12.5% (95% CI 7.6%–18.8%), in virally suppressed PWH was 9.7% (95% CI 8.0%–11.4%), and in PWOH was 7.8% (95% CI 7.7%–7.9%). Similarly, PWH whose most recent CD4 count was <200 cells/mm³ had higher SARS-CoV-2 reinfection CIR (Figure 3). CIR at 1.5 years after initial infection among PWH with CD4 count <200 was 21.2% (95% CI 13.7%–29.7%), among PWH with CD4 of 200–349 was 8.3% (95% CI 4.2%–14.2%), among PWH with CD4 of 350–499 was 9.7% (95% CI 6.2%–14.1%), and among PWH with CD4 ≥ 500 was 9.1% (95% CI 7.2%–11.2%). CIR in PWOH was 7.8% (95% CI 7.7%–7.9%). PWH who had a history of AIDS before their first SARS-CoV-2 infection also had a higher SARS-CoV-2 reinfection CIR (10.8% [95% CI 8.6%–13.2%]) at 1.5 years after initial infection, compared with PWH who had no history of AIDS (9.5% [95% CI 7.5%–11.7%]) and PWOH (7.8% [95% CI 7.7%–7.9%]) (Figure 4).

In unadjusted analyses, compared with PWOH, PWH had a higher rate (rate ratio 1.32 [95% CI 1.15–1.51]) of SARS-CoV-2 reinfection during the observation period (Table 2). After we adjusted for sociodemographic factors, region of residence, initial SARS-CoV-2 infection timing, vaccination status, vaccination type, and number of doses administered after initial SARS-CoV-2 infection, PWH had a higher rate (adjusted rate ratio 1.46 [95% CI 1.27–1.68]) of SARS-CoV-2 reinfection during the observation period compared with PWOH.

Discussion

This population-level analysis of matched records from different public health surveillance and information systems revealed that, among adult Chicago residents who had a reported positive SARS-CoV-2 infection, 5.3% experienced a SARS-CoV-2 reinfection during the observation period. However, incidence of SARS-CoV-2 reinfection was consistently higher among PWH than PWOH. Incidence rate differences fluctuated; differences were greater in SARS-CoV-2 reinfection incidence between PWH and PWOH occurring during periods of high citywide case rates. Moreover, after adjustment for demographic factors, residence, and COVID-19 vaccination, PWH were found to experience a higher rate of SARS-CoV-2 reinfection than were PWOH.

National and local surveillance data distinguishing SARS-CoV-2 reinfections from previous

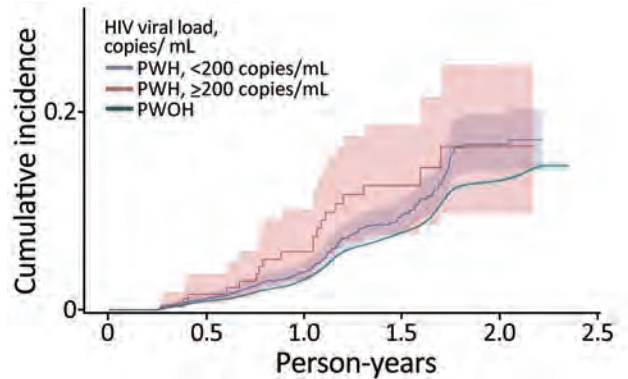


Figure 2. Cumulative incidence (cases/1,000 person-years) of SARS-CoV-2 reinfection by HIV viral suppression status, Chicago, Illinois, USA, January 1, 2020–May 31, 2022. PWH, persons with HIV; PWOH, persons without HIV.

SARS-CoV-2 infections are limited. However, the proportion of persons who experienced a SARS-CoV-2 reinfection in Chicago is consistent with surveillance data from New York state, which reported 5.9% of residents have had a SARS-CoV-2 reinfection (34). Compared with observational studies reporting population-level estimates of SARS-CoV-2 reinfections in other US jurisdictions and in countries in Europe, our analysis identified higher reinfection incidence rates than previously reported (35–37). However, those differences might be attributable to methodological distinctions across studies, including a longer observation period through the Omicron variant phase of the COVID-19 pandemic. Our study also found that reinfection risk increases over time, which is consistent with different studies reporting SARS-CoV-2 infection-induced and vaccine-induced immunity waning over time and immune evasion (18–21).

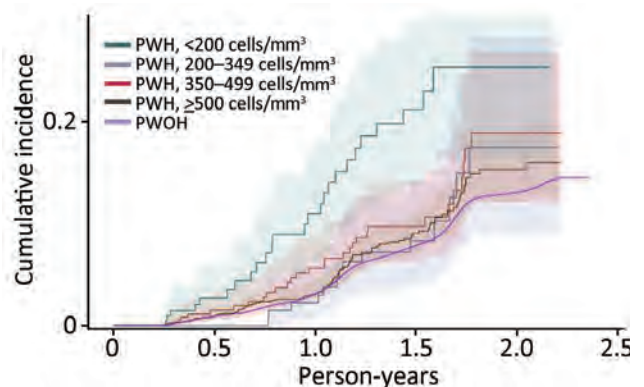


Figure 3. Cumulative incidence (cases/1,000 person-years) of SARS-CoV-2 reinfection by most recent CD4 count, Chicago, Illinois, USA, January 1, 2020–May 31, 2022. PWH, persons with HIV; PWOH, persons without HIV.

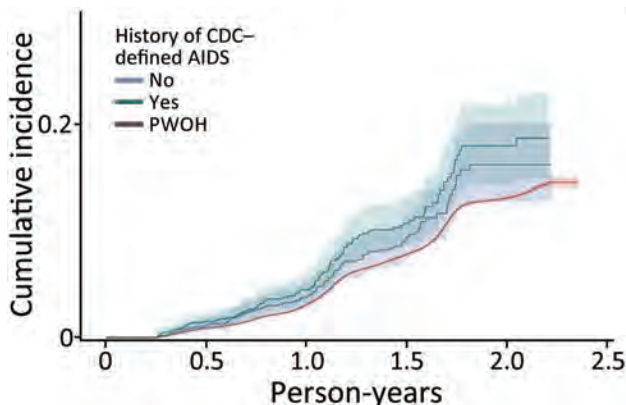


Figure 4. Cumulative incidence (cases/1,000 person-years) of SARS-CoV-2 reinfection by history of AIDS diagnosis, Chicago, Illinois, USA, January 1, 2020–May 31, 2022. CDC, Centers for Disease Control and Prevention; PWH, persons with HIV; PWOH, persons without HIV.

Our analysis found that SARS-CoV-2 reinfection cumulative incidence rates were higher among PWH than PWOH irrespective of most recent CD4 and viral load laboratory results. This finding indicates that even persons with well-controlled HIV infection might have a higher risk for SARS-CoV-2 reinfection compared with PWOH. We observed the highest cumulative incidence rates among PWH with a most recent HIV viral load laboratory result ≥ 200 copies/mL and CD4 laboratory result < 200 cells/mm³, indicating that PWH with laboratory evidence consistent with uncontrolled HIV are at greatest risk for multiple SARS-CoV-2 infections. Similarly, PWH with a history of AIDS had a higher cumulative risk for reinfection, followed by PWH without AIDS; PWOH had the lowest cumulative incidence across the 3 strata. Persons who are immunocompromised are at increased risk for severe COVID-19 illness and death; their immune response to COVID-19 vaccination may not be as strong as in persons who are not immunocompromised. Guidance from the Centers for Disease Control and Prevention recommends that persons with advanced or untreated HIV receive an additional COVID-19 vaccine dose to complete a primary series and receive a booster (38,39). However, our analysis also indicated that PWH with

high CD4 counts, no evidence of a prior AIDS diagnosis, and viral suppression are also at higher risk for SARS-CoV-2 reinfection than PWOH. Additional studies are needed to understand if those with well-controlled HIV also require additional COVID-19 vaccine doses.

Multiple studies have shown that persons who receive COVID-19 vaccine after a SARS-CoV-2 infection have a lower risk for reinfection than do unvaccinated persons (40–42). Most persons in the analytic cohort, regardless of HIV status, were unvaccinated at the time of their first SARS-CoV-2 infection. Most of those infections occurred before COVID-19 vaccine was available. Among persons with a SARS-CoV-2 reinfection, 38.2% (9,039/23,642) of PWOH and 31.8% (61/192) of PWH had either not received any COVID-19 vaccine or had not completed a primary series. All persons, especially PWH, should remain up to date with their COVID-19 vaccines to prevent SARS-CoV-2 reinfections or adverse COVID-19 outcomes.

The first limitation of this study is that we were unable to account for testing practices or healthcare-seeking behaviors in our analysis because surveillance systems do not capture reason for testing. Repeat SARS-CoV-2 infections are more likely to be detected among persons who regularly have access to and participate in SARS-CoV-2 testing, leading to differential SARS-CoV-2 reinfection detection rates among PWH and PWOH. Second, availability of SARS-CoV-2 laboratory and at-home testing evolved over time throughout the observation period. Limited access to testing may lead to unconfirmed infections. Similarly, national distribution of at-home antigen tests starting in January 2022 likely led to underestimation of case counts, because those test results are typically not reported to public health. Therefore, our analysis likely underestimates the true number of SARS-CoV-2 reinfections. Third, our person-time calculations only considered reported positive SARS-CoV-2 test results, death, or the end of the observation period. We were unable to censor persons if they moved out of Chicago or had positive test results not reported to their local public health jurisdiction.

Table 2. Effect of HIV status on SARS-CoV-2 reinfection, Chicago, Illinois, USA, January 1, 2020–May 31, 2022*

HIV status at first SARS-CoV-2 infection	Total no. (%) persons, n = 453,587 (%)	Total no. (%) events, n = 23,834	Unadjusted rate ratio (95% CI)	p value	Adjusted rate ratio (95% CI) [†]	p value
PWH	2,886 (0.6)	192 (0.8)	1.32 (1.15–1.51)	<0.0001	1.46 (1.27–1.68)	<0.0001
PWOH	450,701 (99.4)	23,642 (99.2)	Reference		Reference	

*Estimates describe exponentiated estimates from a Poisson regression model using the logarithm of person-time as the offset term. Bold text indicates statistical significance at $p < 0.05$. PWH, persons with HIV; PWOH, persons without HIV.

[†]Multivariable Poisson regression model controlled for the following covariates: age, sex at birth, ethnicity and race, region of residence, initial SARS-CoV-2 infection group, vaccination status at the time of first SARS-CoV-2 infection, vaccination type, and number of doses administered after the first SARS-CoV-2 infection.

Therefore, our incidence rate estimates are likely underestimates because some persons may have contributed less person-time. Fourth, we were unable to evaluate and adjust for comorbidities and ART use in our analyses because that type of clinical information is not reported to public health through traditional electronic laboratory reporting. Data abstracted from medical records might more fully characterize whether comorbidities influence the association between HIV and SARS-CoV-2 reinfection. Last, this analysis assumed all positive test results separated by >90 days were distinct SARS-CoV-2 infection episodes, consistent with the 2021 COVID-19 case definition (43). Case reports have documented persistent shedding after a single infection spanning >90 days among persons who are immunocompromised (44–46), and SARS-CoV-2 reinfections occurring <90 days from a prior infection (47,48). Because of limited national SARS-CoV-2 whole-genome sequencing capacity and inadequate specimen storage capacity at laboratories, local public health departments are rarely able to verify SARS-CoV-2 reinfections by comparing lineage results from respiratory specimens collected from multiple infection episodes.

All persons, including PWH, should stay up to date with recommended COVID-19 vaccines, including bivalent booster doses (49). Evaluating the association between HIV infection and SARS-CoV-2 reinfections using surveillance data can help strengthen public health recommendations including the need for extra doses as part of a primary series, booster doses of vaccine, and optimized ART in PWH. Tailored guidance and prevention messaging for PWH can help reduce the elevated risk we identified in this analysis and limit continued SARS-CoV-2 transmission. As the COVID-19 pandemic persists, local health jurisdictions can leverage data access and link records across surveillance datasets to monitor SARS-CoV-2 infections and other outcomes among vulnerable populations, including PWH.

Acknowledgments

We thank the staff of the Chicago Department of Public Health (CDPH) and teams of epidemiologists within the Syndemic Infectious Diseases Bureau and Disease Control Bureau who collect, clean, manage, and analyze HIV and COVID-19 data that allow CDPH to respond to outbreaks of disease and prevent transmission across the city of Chicago. We also thank CDPH's Regional Innovative Public Health Laboratory for providing sequencing capacity to understand SARS-CoV-2 variant circulation across Chicago.

About the Author

Dr. Teran is an infectious disease epidemiologist and CDC Epidemic Intelligence Service Officer, assigned to the Chicago Department of Public Health. His research interests include communicable diseases, syndemic infectious diseases, and understanding viral suppression patterns of persons with HIV.

References

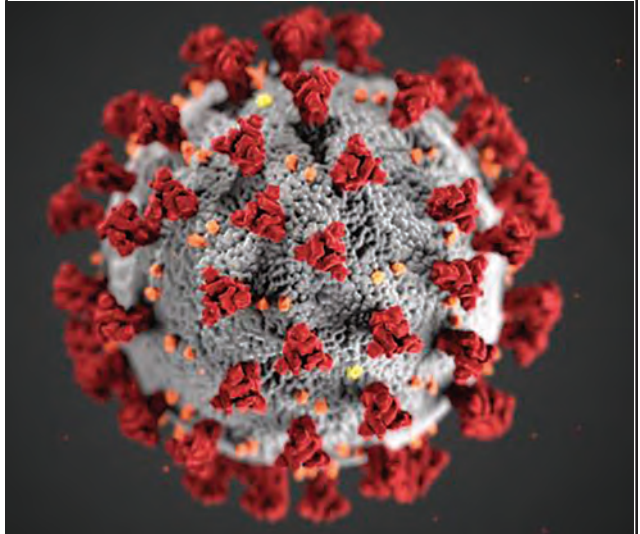
1. Tenforde MW, Patel MM, Gaglani M, Ginde AA, Douin DJ, Talbot HK, et al.; Influenza and Other Viruses in the Acutely Ill (IVY) Network. Effectiveness of a third dose of Pfizer-BioNTech and Moderna vaccines in preventing COVID-19 hospitalization among immunocompetent and immunocompromised adults – United States, August–December 2021. *MMWR Morb Mortal Wkly Rep.* 2022; 71:118–24. <http://dx.doi.org/10.15585/mmwr.mm7104a2>
2. Malinis M, Cohen E, Azar MM. Effectiveness of SARS-CoV-2 vaccination in fully vaccinated solid organ transplant recipients. *Am J Transplant.* 2021;21:2916–8. <https://doi.org/10.1111/ajt.16713>
3. Sun J, Zheng Q, Madhira V, Olex AL, Anzalone AJ, Vinson A, et al.; National COVID Cohort Collaborative (N3C) Consortium. Association between immune dysfunction and COVID-19 breakthrough infection after SARS-CoV-2 vaccination in the US. *JAMA Intern Med.* 2022;182:153–62. <https://doi.org/10.1001/jamainternmed.2021.7024>
4. Kompaniyets L, Pennington AF, Goodman AB, Rosenblum HG, Belay B, Ko JY, et al. Underlying medical conditions and severe illness among 540,667 adults hospitalized with COVID-19, March 2020–March 2021. *Prev Chronic Dis.* 2021;18:210123. <https://doi.org/10.5888/pcd18.210123>
5. Yek C, Warner S, Wiltz JL, Sun J, Adjei S, Mancera A, et al. Risk factors for severe COVID-19 outcomes among persons aged ≥18 years who completed a primary COVID-19 vaccination series – 465 health care facilities, United States, December 2020–October 2021. *MMWR Morb Mortal Wkly Rep.* 2022;71:19–25. <https://doi.org/10.15585/mmwr.mm7101a4>
6. Centers for Disease Control and Prevention. Diagnoses of HIV infection in the United States and dependent areas 2020. *HIV Surveillance Report.* 2022;33 [cited 2022 Jul 5]. <http://www.cdc.gov/hiv/library/reports/hiv-surveillance/vol-33/index.html>
7. Balderson BH, Grothaus L, Harrison RG, McCoy K, Mahoney C, Catz S. Chronic illness burden and quality of life in an aging HIV population. *AIDS Care.* 2013;25:451–8. <https://doi.org/10.1080/09540121.2012.712669>
8. Schouten J, Wit FW, Stolte IG, Kootstra NA, van der Valk M, Geerlings SE, et al.; AGEHIV Cohort Study Group. Cross-sectional comparison of the prevalence of age-associated comorbidities and their risk factors between HIV-infected and uninfected individuals: the AGEHIV cohort study. *Clin Infect Dis.* 2014;59:1787–97. <https://doi.org/10.1093/cid/ciu701>
9. Braunstein SL, Lazar R, Wahnich A, Daskalakis DC, Blackstock OJ. Coronavirus disease 2019 (COVID-19) infection among people with human immunodeficiency virus in New York City: a population-level analysis of linked surveillance data. *Clin Infect Dis.* 2021;72:e1021–9. <https://doi.org/10.1093/cid/ciaa1793>
10. Liu C, Lee J, Ta C, Soroush A, Rogers JR, Kim JH, et al. Risk factors associated with SARS-CoV-2 breakthrough infections in fully mRNA-vaccinated individuals: retrospective

- analysis. *JMIR Public Health Surveill.* 2022;8:e35311. <https://doi.org/10.2196/35311>
11. Butt AA, Khan T, Yan P, Shaikh OS, Omer SB, Mayr F. Rate and risk factors for breakthrough SARS-CoV-2 infection after vaccination. *J Infect.* 2021;83:237–79. <https://doi.org/10.1016/j.jinf.2021.05.021>
 12. Sun J, Zheng Q, Madhira V, Olex AL, Anzalone AJ, Vinson A, et al.; National COVID Cohort Collaborative (N3C) Consortium. Association between immune dysfunction and COVID-19 breakthrough infection after SARS-CoV-2 vaccination in the US. *JAMA Intern Med.* 2022;182:153–62. <https://doi.org/10.1001/jamainternmed.2021.7024>
 13. Coburn SB, Humes E, Lang R, Stewart C, Hogan BC, Gebo KA, et al.; Corona-Infectious-Virus Epidemiology Team (CIVETs) of the NA-ACCORD of IeDEA. Analysis of postvaccination breakthrough COVID-19 infections among adults with HIV in the United States. *JAMA Netw Open.* 2022;5:e2215934. <https://doi.org/10.1001/jamanetworkopen.2022.15934>
 14. Wang H, Yuan Y, Xiao M, Chen L, Zhao Y, Haiwei Zhang, et al. Dynamics of the SARS-CoV-2 antibody response up to 10 months after infection. *Cell Mol Immunol.* 2021;18:1832–4. <https://doi.org/10.1038/s41423-021-00708-6>
 15. Wheatley AK, Juno JA, Wang JJ, Selva KJ, Reynaldi A, Tan HX, et al. Evolution of immune responses to SARS-CoV-2 in mild–moderate COVID-19. *Nat Commun.* 2021;12:1162. <https://doi.org/10.1038/s41467-021-21444-5>
 16. Lumley SF, Wei J, O'Donnell D, Stoesser NE, Matthews PC, Howarth A, et al.; Oxford University Hospitals Staff Testing Group. The duration, dynamics, and determinants of severe acute respiratory syndrome coronavirus 2 (SARS-CoV-2) antibody responses in individual healthcare workers. *Clin Infect Dis.* 2021;73:e699–709. <https://doi.org/10.1093/cid/ciab004>
 17. Babiker A, Marvil CE, Waggoner JJ, Collins MH, Piantadosi A. The importance and challenges of identifying SARS-CoV-2 reinfections. *J Clin Microbiol.* 2021;59:59. <https://doi.org/10.1128/JCM.02769-20>
 18. Hall VJ, Foulkes S, Charlett A, Atti A, Monk EJM, Simmons R, et al.; SIREN Study Group. SARS-CoV-2 infection rates of antibody-positive compared with antibody-negative health-care workers in England: a large, multicentre, prospective cohort study (SIREN). *Lancet.* 2021;397:1459–69. [https://doi.org/10.1016/S0140-6736\(21\)00675-9](https://doi.org/10.1016/S0140-6736(21)00675-9)
 19. Hansen CH, Michlmayr D, Gubbels SM, Mølbak K, Ethelberg S. Assessment of protection against reinfection with SARS-CoV-2 among 4 million PCR-tested individuals in Denmark in 2020: a population-level observational study. *Lancet.* 2021;397:1204–12. [https://doi.org/10.1016/S0140-6736\(21\)00575-4](https://doi.org/10.1016/S0140-6736(21)00575-4)
 20. Sheehan MM, Reddy AJ, Rothberg MB. Reinfection rates among patients who previously tested positive for coronavirus disease 2019: a retrospective cohort study. *Clin Infect Dis.* 2021;73:1882–6. <https://doi.org/10.1093/cid/ciab234>
 21. Lumley SF, O'Donnell D, Stoesser NE, Matthews PC, Howarth A, Hatch SB, et al.; Oxford University Hospitals Staff Testing Group. Antibody status and incidence of SARS-CoV-2 infection in health care workers. *N Engl J Med.* 2021;384:533–40. <https://doi.org/10.1056/NEJMoa2034545>
 22. Wang J, Kaperak C, Sato T, Sakuraba A. COVID-19 reinfection: a rapid systematic review of case reports and case series. *J Investig Med.* 2021;69:1253–5. <https://doi.org/10.1136/jim-2021-001853>
 23. Bozio CH, Grannis SJ, Naleway AL, Ong TC, Butterfield KA, DeSilva MB, et al. Laboratory-confirmed COVID-19 among adults hospitalized with COVID-19-like illness with infection-induced or mRNA vaccine-induced SARS-CoV-2 immunity – nine states, January–September 2021. *MMWR Morb Mortal Wkly Rep.* 2021;70:1539–44. <https://doi.org/10.15585/mmwr.mm7044e1>
 24. Lawandi A, Warner S, Sun J, Demirkale CY, Danner RL, Klompas M, et al. Suspected severe acute respiratory syndrome coronavirus 2 (SARS-CoV-2) reinfections: incidence, predictors, and healthcare use among patients at 238 US healthcare facilities, 1 June 2020 to 28 February 2021. *Clin Infect Dis.* 2022;74:1489–92. <https://doi.org/10.1093/cid/ciab671>
 25. Roskosky M, Borah BF, DeJonge PM, Donovan CV, Blevins LZ, Lafferty AG, et al. Notes from the field: SARS-CoV-2 Omicron variant infection in 10 persons within 90 days of previous SARS-CoV-2 Delta variant infection – four states, October 2021–January 2022. *MMWR Morb Mortal Wkly Rep.* 2022;71:524–6. <https://doi.org/10.15585/mmwr.mm7114a2>
 26. Plumb ID, Feldstein LR, Barkley E, Posner AB, Bregman HS, Hagen MB, et al. Effectiveness of COVID-19 mRNA vaccination in preventing COVID-19-associated hospitalization among adults with previous SARS-CoV-2 infection – United States, June 2021–February 2022. *MMWR Morb Mortal Wkly Rep.* 2022;71:549–55. <https://doi.org/10.15585/mmwr.mm7115e2>
 27. Altarawneh HN, Chemaitelly H, Hasan MR, Ayoub HH, Qassim S, AlMukdad S, et al. Protection against the Omicron variant from previous SARS-CoV-2 infection. *N Engl J Med.* 2022;386:1288–90. <https://doi.org/10.1056/NEJMc2200133>
 28. Drobnik A, Pinchoff J, Bushnell G, Ly S, Yuan J, Varma JK, et al. Matching HIV, tuberculosis, viral hepatitis, and sexually transmitted diseases surveillance data, 2000–2010: identification of infectious disease syndemics in New York City. *J Public Health Manag Pract.* 2014;20:506–12. <https://doi.org/10.1097/PHH.0b013e3182a95607>
 29. Chicago Department of Public Health. SARS-CoV-2 variants. 2022 [cited 2022 Jun 1]. <https://www.chicago.gov/city/en/sites/covid-19/home/sars-cov-2-variants.html>
 30. Centers for Disease Control and Prevention. COVID data tracker: variant proportions. 2022 [cited 2022 Jun 1]. <https://covid.cdc.gov/covid-data-tracker/#variant-proportions>
 31. Centers for Disease Control and prevention. SARS-CoV-2 variant classification and definitions. April 26, 2022 [cited 2022 Jun 1]. <https://www.cdc.gov/coronavirus/2019-ncov/variants/variant-classifications.html>
 32. Selik RM, Mokotoff ED, Branson B, Owen SM, Whitmore S, Hall HI. Revised surveillance case definition for HIV infection – United States, 2014. *MMWR Morb Mortal Wkly Rep.* 2014;63(RR03):1–10. <https://www.cdc.gov/mmwr/preview/mmwrhtml/rr6303a1.htm>
 33. Centers for Disease Control and Prevention. Understanding the HIV care continuum. July 2019 [cited 2022 May 20]. <https://www.cdc.gov/hiv/pdf/library/factsheets/cdc-hiv-care-continuum.pdf>
 34. New York State Department of Health. COVID-19 reinfection data. [cited 2022 Aug 17]. <https://coronavirus.health.ny.gov/covid-19-reinfection-data>
 35. Slezak J, Bruxvoort K, Fischer H, Broder B, Ackerson B, Tartof S. Rate and severity of suspected SARS-Cov-2 reinfection in a cohort of PCR-positive COVID-19 patients. *Clin Microbiol Infect.* 2021;27:1860.e7–10. <https://doi.org/10.1016/j.cmi.2021.07.030>
 36. Nordström P, Ballin M, Nordström A. Risk of SARS-CoV-2 reinfection and COVID-19 hospitalisation in individuals with natural and hybrid immunity: a retrospective, total population cohort study in Sweden. *Lancet Infect Dis.* 2022;22:781–90. [https://doi.org/10.1016/S1473-3099\(22\)00143-8](https://doi.org/10.1016/S1473-3099(22)00143-8)

37. Flacco ME, Acuti Martellucci C, Baccolini V, De Vito C, Renzi E, Villari P, et al. Risk of reinfection and disease after SARS-CoV-2 primary infection: meta-analysis. *Eur J Clin Invest.* 2022;52:e13845. <https://doi.org/10.1111/eci.13845>
38. Centers for Disease Control and Prevention. COVID-19 vaccines for people who are moderately or severely immunocompromised. 2022 [cited 2022 Aug 15]. <https://www.cdc.gov/coronavirus/2019-ncov/vaccines/recommendations/immuno.html>
39. Centers for Disease Control and Prevention. Interim clinical considerations for use of COVID-19 vaccines currently approved or authorized in the United States. 2022 [cited 2022 Aug 15]. <https://www.cdc.gov/vaccines/covid-19/clinical-considerations/interim-considerations-us.html#immunocompromised>
40. Cavanaugh AM, Spicer KB, Thoroughman D, Glick C, Winter K. Reduced risk of reinfection with SARS-CoV-2 after COVID-19 vaccination – Kentucky, May–June 2021. *MMWR Morb Mortal Wkly Rep.* 2021;70:1081–3. <https://doi.org/10.15585/mmwr.mm7032e1>
41. Shrestha NK, Burke PC, Nowacki AS, Terpeluk P, Gordon SM. Necessity of COVID-19 vaccination in persons who have already had COVID-19. *Clin Infect Dis.* 2022.
42. Hall V, Foulkes S, Insalata F, Kirwan P, Saei A, Atti A, et al.; SIREN Study Group. Protection against SARS-CoV-2 after COVID-19 vaccination and previous infection. *N Engl J Med.* 2022;386:1207–20. <https://doi.org/10.1056/NEJMoa2118691>
43. Centers for Disease Control and Prevention. Coronavirus disease 2019 (COVID-19) 2021 case definition. 2022 [cited 2022 Aug 17]. <https://ndc.services.cdc.gov/case-definitions/coronavirus-disease-2019-2021/>
44. Yousaf M, Hameed M, Alsoub H, Khatib M, Jamal W, Ahmad M. COVID-19: prolonged viral shedding in an HIV patient with literature review of risk factors for prolonged viral shedding and its implications for isolation strategies. *Clin Case Rep.* 2021;9:1397–401. <https://doi.org/10.1002/ccr3.3786>
45. Li TZ, Cao ZH, Chen Y, Cai MT, Zhang LY, Xu H, et al. Duration of SARS-CoV-2 RNA shedding and factors associated with prolonged viral shedding in patients with COVID-19. *J Med Virol.* 2021;93:506–12. <https://doi.org/10.1002/jmv.26280>
46. Fontana LM, Villamagna AH, Sikka MK, McGregor JC. Understanding viral shedding of severe acute respiratory coronavirus virus 2 (SARS-CoV-2): Review of current literature. *Infect Control Hosp Epidemiol.* 2021;42:659–68. <https://doi.org/10.1017/ice.2020.1273>
47. Roskosky M, Borah BF, DeJonge PM, Donovan CV, Blevins LZ, Lafferty AG, et al. Notes from the field: SARS-CoV-2 Omicron variant infection in 10 persons within 90 days of previous SARS-CoV-2 Delta variant infection – four states, October 2021–January 2022. *MMWR Morb Mortal Wkly Rep.* 2022;71:524–6. <https://doi.org/10.15585/mmwr.mm7114a2>
48. Nevejan L, Cuyppers L, Laenen L, Van Loo L, Vermeulen F, Wollants E, et al. Early SARS-CoV-2 reinfections within 60 days and implications for retesting policies. *Emerg Infect Dis.* 2022;28:1729–31. <https://doi.org/10.3201/eid2808.220617>
49. Centers for Disease Control and Prevention. Stay up to date with COVID-19 vaccines. [cited 2022 Dec 5]. <https://www.cdc.gov/coronavirus/2019-ncov/vaccines/stay-up-to-date.html>

Address for correspondence: Richard A. Teran, Centers for Disease Control and Prevention, 1600 Clifton Rd NE, Mailstop H21-10, Atlanta, GA 30329-4027, USA; email: RTeran@cdc.gov

EID Podcast: Animal Reservoirs for Emerging Coronaviruses



Coronaviruses are nothing new. Discovered in the 1930s, these pathogens have circulated among bats, livestock, and pets for years.

Most coronaviruses never spread to people. However, because this evolutionary branch has given rise to three high-consequence pathogens, researchers must monitor animal populations and find new ways to prevent spillover to humans.

In this EID podcast, Dr. Ria Ghai, an associate service fellow at CDC, describes the many animals known to harbor emerging coronaviruses.

Visit our website to listen:
<https://go.usa.gov/x6WtY>

**EMERGING
INFECTIOUS DISEASES®**

Evolution of *Klebsiella pneumoniae* Sequence Type 512 during Ceftazidime/Avibactam, Meropenem/Vaborbactam, and Cefiderocol Treatment, Italy

Gabriele Arcari, Federico Cecilia, Alessandra Oliva, Riccardo Polani, Giammarco Raponi, Federica Sacco, Alice De Francesco, Francesco Pugliese, Alessandra Carattoli

In February 2022, a critically ill patient colonized with a carbapenem-resistant *K. pneumoniae* producing KPC-3 and VIM-1 carbapenemases was hospitalized for SARS-CoV-2 in the intensive care unit of Policlinico Umberto I hospital in Rome, Italy. During 95 days of hospitalization, ceftazidime/avibactam, meropenem/vaborbactam, and cefiderocol were administered consecutively to treat 3 respiratory tract infections sustained by different bacterial agents. Those therapies altered the resistome of *K. pneumoniae* sequence type 512 colonizing or infecting the patient during the hospitalization period. In vivo evolution of the *K. pneumoniae* sequence type 512 resistome occurred through plasmid loss, outer membrane porin alteration, and a nonsense mutation in the *cirA* siderophore receptor gene, resulting in high levels of cefiderocol resistance. Cross-selection can occur between *K. pneumoniae* and treatments prescribed for other infective agents. *K. pneumoniae* can stably colonize a patient, and antimicrobial-selective pressure can promote progressive *K. pneumoniae* resistome evolution, indicating a substantial public health threat.

The number of deaths caused by antimicrobial resistance was estimated at 1.27 million worldwide in 2019 (1), mainly attributed to 6 bacterial species: *Escherichia coli*, *Staphylococcus aureus*, *Klebsiella pneumoniae*, *Streptococcus pneumoniae*, *Acinetobacter baumannii*, and *Pseudomonas aeruginosa*. To reinforce the antimicrobial

drug pipeline, the European Union's European Medicines Agency authorized the clinical use of ceftazidime/avibactam (CZA) in 2016, meropenem/vaborbactam (MVB) in 2018, and cefiderocol (FDC) in 2020. Although those drugs all belong to the β -lactams class, substantial differences in mechanisms of action and antimicrobial spectra exist among them. CZA is a third-generation cephalosporin (ceftazidime) combined with a diazabicyclooctane β -lactamase inhibitor (avibactam). Avibactam prevents class A (including *K. pneumoniae* carbapenemase [KPC]), class C, and some class D β -lactamases from hydrolyzing ceftazidime, restoring ceftazidime activity in KPC- and oxacillinase-48-producing Enterobacterales but not in metallo- β -lactamase producers (2). MVB is a carbapenem (meropenem) combined with a boronate β -lactamase inhibitor (vaborbactam); vaborbactam inhibits class A but not class D or B carbapenemases (3). FDC is a siderophore cephalosporin that has a catechol moiety on the C-3 side chain (4), which can form a chelating complex with ferric iron; thus, FDC is subject to active transport through the iron transport system, including TonB-dependent receptors (5). In addition, FDC is highly stable against β -lactamase activity (4,5).

In the past decade, Italy has seen a large increase in cases of carbapenem-resistant *K. pneumoniae* (1), mainly from 3 major KPC-producing (6) sequence types (STs): 101, 307, and 512 (7). In settings highly endemic for KPC-producing Enterobacterales, the selection of CZA-resistant, KPC-producing variants is of great concern (8,9). FDC resistance is not a 1-dimensional phenomenon (10); mutations in siderophore receptors (11), as well as in variants of β -lactamases KPC-2, CMY-2, CTX-M-15, and NDM-1, can con-

Author affiliations: Sapienza University of Rome, Rome, Italy (G. Arcari, F. Cecilia, A. Oliva, R. Polani, G. Raponi, A. De Francesco, F. Pugliese, A. Carattoli); Azienda Ospedaliero-Universitaria Policlinico Umberto I, Rome (A. Oliva, G. Raponi, F. Sacco, F. Pugliese)

DOI: <https://doi.org/10.3201/eid2911.230921>

fer FDC resistance (12). Nonetheless, *cirA* disruption substantially hinders bacterial fitness (13), and β -lactamase evolution contributing to FDC resistance typically comes at the price of functional trade-offs against other β -lactams (12). Under FDC treatment, in vivo resistance has been reported sporadically in *Enterobacter cloacae* (14) and *Escherichia coli* (15).

We describe a patient in Rome, Italy, who was colonized by carbapenem-resistant *K. pneumoniae* ST512. We integrated whole-genome sequencing, clinical, and microbiologic data to reconstruct the evolution of *K. pneumoniae* antimicrobial resistance in this patient after treatments for respiratory tract infections caused by different bacteria.

Methods

Case Report

In February 2022, a 62-year-old patient who was positive for SARS-CoV-2 was transferred from a long-term care facility to Policlinico Umberto I (PUI) in Rome. The patient was hospitalized for 95 days initially in the COVID-19 intensive care unit (ICU) and then in the general ICU until death, which was caused by gastrointestinal bleeding. The patient's medical history was notable for bipolar disorder, obesity, inflammatory bowel disease, type 2 diabetes, respiratory failure, chronic kidney failure, and heart failure. Six months before transfer to PUI, the patient had a percutaneous endoscopic gastrostomy performed because of severe gastrointestinal bleeding caused by underlying inflammatory bowel disease. During the patient's hospitalization at PUI, we isolated a total of 5 different *K. pneumoniae* strains from patient rectal swab samples and respiratory tract specimens.

Isolation of *K. pneumoniae* Strains and Susceptibility Testing

We identified the 5 *K. pneumoniae* strains by matrix-assisted laser desorption/ionization time-of-flight mass spectrometry (Bruker Daltonik GmbH, <https://www.bruker.com>). We identified carbapenamase genes by PCR using the GeneXpert system (Cepheid, <https://www.cepheid.com>) and used the lateral flow immunochromatography systems (NG-Test CARBA 5; Hardy Diagnostics, <https://www.hardydiagnostics.com>). We tested antimicrobial drug susceptibility by using the MicroScan WalkAway system (Beckman Coulter, Inc., <https://beckman.com>). We used gradient strips (Liofilchem, <https://www.liofilchem.com>) to test MVB and CZA MICs and the Compact Antimicrobial Susceptibility Panel (ComASP; Liofilchem) to test FDC MICs.

Whole-Genome Sequencing and Assembly

We performed whole-genome sequencing for each isolate. We purified genomic DNA by using the Isolate II Genomic DNA Kit (Bioline, <https://www.bioline.com>). We sent DNA to an external service to perform short-read Illumina sequencing (Illumina Inc., <https://www.illumina.com>). We obtained long reads by using the MinION Mk1C sequencing platform (Oxford Nanopore Technologies, <https://nanoporetech.com>). We extracted DNA for long reads by using the Wizard HMW DNA Extraction Kit (Promega, <https://www.promega.com>) and prepared libraries by using the Rapid Barcoding Kit 96; we sequenced libraries on R9.4.1 flow cells (Oxford Nanopore Technologies). We performed long-read assemblies by using Flye (16) with standard parameters. We integrated Illumina reads and Oxford Nanopore Technologies assemblies by using the Unicycler tool (17) in normal bridging mode and refined results by using the Bandage tool (18).

Genomic and Phylogenetic Analyses

We analyzed single-nucleotide polymorphisms (SNPs) among the 5 sequenced genomes in this study by using the Snippy tool (<https://github.com/tseemann/snippy>). We annotated the 5 genomes by using Rapid Annotation using Subsystem Technology and compared by using SEED software (19).

We used Prokka software (20) to annotate 133 genomes belonging to ST512: 5 sequences from this study, 12 from a previous study performed at PUI (8), and 116 downloaded from the Pasteur Institute BIGSdb database (<https://bigsdb.pasteur.fr/klebsiella>). We analyzed the resulting general feature formats by using Roary software (21) to build a core genome alignment and generated a consensus phylogenetic tree by using 1,000 ultrafast bootstraps (22) in IQ-TREE 2 (23) and the transversion model plus base frequency plus proportion of invariable sites nucleotide substitution model (24). We visualized tree and metadata by using Microreact (25) and adjusted those data by using open source InkScape software (<https://www.inkscape.org>). We assessed all genomes for replicons by using PlasmidFinder (26), for capsular polysaccharide and lipopolysaccharide loci by using Kaptive (27), and for virulence and resistance gene content by using Kleborate (28) software.

Cloning *bla*_{KPC-154} in pCR-Blunt II TOPO Vector

We cloned the novel β -lactamase *bla*_{KPC-154} allele from isolate 6099 into pCR-Blunt II TOPO-NeoR Vector and transformed TOP10 *E. coli* cells (both

Thermo Fisher Scientific, <https://www.thermo-fisher.com>); we confirmed correctness of the cloned insert by Sanger sequencing. We tested the KPC-154 TOP10 *E. coli* clone for antimicrobial drug susceptibility by using the MicroScan system and measured CZA MICs by gradient tests (Liofilchem) as previously described.

OmpK36 Variant Modeling

We predicted structures of the outer membrane porin (Omp) K36 from isolate 0296 in silico by using AlphaFold2 on the European Galaxy server (<https://usegalaxy.eu>) and analyzed those structures by using UCSF ChimeraX (29) for both the cartoon (ribbon) and surface images. We compared the structures with chain B in the crystal structure of OmpK36 from a *K. pneumoniae* ST258 clinical isolate that has a GD amino acid insertion (30). We used the Orientations of Proteins in Membranes database (31) to obtain spatial arrangements of the protein structures in lipid bilayers.

Data Availability

We submitted the sequences of the strains analyzed in this study to GenBank. Whole-genome sequences are under Bioproject no. PRJNA992043 and complete plasmid sequences under accession nos. OQ096263 (pK-pQIL-6099), OQ282880 (pIncA-6379), and OQ282881 (pIncA-0296).

Ethics Approval

According to the hospital's routine practice, the patient or his relatives gave informed consent to share data for research purposes during hospital admission. The study protocol was approved by the Ethics Committee of Azienda Ospedaliero-Universitaria Policlinico Umberto I (approval no. 109/2020).

Results

K. pneumoniae Strain Descriptions

On the first day of the patient's hospitalization at PUI, surveillance rectal swab samples tested positive for *K. pneumoniae* (strain 6379) that produced both KPC and Verona integron-encoded metallo- β -lactamase (VIM) (Figure 1). The patient had been treated with CZA at the long-term care facility for a previous carbapenem-resistant *K. pneumoniae* bloodstream infection; treatment was discontinued upon admission to PUI.

After 17 days of hospitalization, a respiratory tract infection caused by *Providencia stuartii* (>100,000 CFU/mL in bronchoalveolar lavage fluid) developed in the patient, accompanied by pleural effusion, which we treated with CZA. After 1 week of treatment, we

isolated 2 CZA-resistant, meropenem-susceptible *K. pneumoniae* strains from patient rectal swab samples but not respiratory tract specimens; both strains produced KPC but not VIM and had dimorphic colony phenotypes: white (strain 1186W) and transparent (strain 1186T). Because of potential pleural infection, we maintained CZA therapy for \approx 40 days, resulting in complete eradication of *P. stuartii* from the respiratory tract.

On day 56, the patient was SARS-CoV-2 negative and was transferred to the general ICU at PUI. Respiratory tract samples were negative for *P. stuartii* but positive (>1,000 CFU/mL lavage fluid) for CZA-resistant *K. pneumoniae* (strain 6099) that produced KPC. CZA therapy was stopped, and MVB treatment was begun and continued until day 75. On day 75, respiratory tract samples tested negative for *K. pneumoniae* but positive for carbapenem-resistant *A. baumannii* (1,000 CFU/mL lavage fluid). Because of subsequent worsening respiratory conditions and chest imaging suggestive of new onset pneumonia, we replaced MVB therapy with FDC therapy (day 79) to treat *A. baumannii* pulmonary infection. On day 88, during FDC treatment, respiratory tract samples tested positive for both *A. baumannii* and *K. pneumoniae* (strain 0296) (1,000 CFU/mL lavage fluid each); strain 0296 was positive for KPC and VIM carbapenemases.

Phylogeny, Antimicrobial Resistance, and General Features of ST512

We assigned the 5 *K. pneumoniae* isolates from the patient (6379, 1186W, and 1186T from rectal swab samples, 6099 and 0296 from respiratory tract samples) to ST512 by using in silico multilocus sequence typing of whole-genome sequences. We aligned the complete genomes of those strains against 116 ST512 genomes retrieved from the Pasteur Institute *K. pneumoniae* BIGSdb database (December 7, 2022) and 12 ST512 genomes previously identified at PUI (8,32). Phylogeny of 4,654 core genes showed how isolates from the patient clustered together in the same clade with ST512 strains isolated at PUI during 2018–2020 (Figure 2) and were separated by 0–11 SNPs (Appendix 1 Table 1, <https://wwwnc.cdc.gov/EID/article/29/11/23-0921-App1.xlsx>).

All ST512 isolates are defined by conserved features: the *wzi* allele 154 (assigned to the KL107 capsule), typical of the main clade II of clonal group 258 (33); O1/O2v2 O locus, serotype O2afg; 35Q mutation in the chromosome-encoded SHV-11 β -lactamase (28); premature stop at codon 89 in the OmpK35 protein, in most isolates coupled with a GD amino acid insertion in the OmpK36 eyelet (34); and chromosome

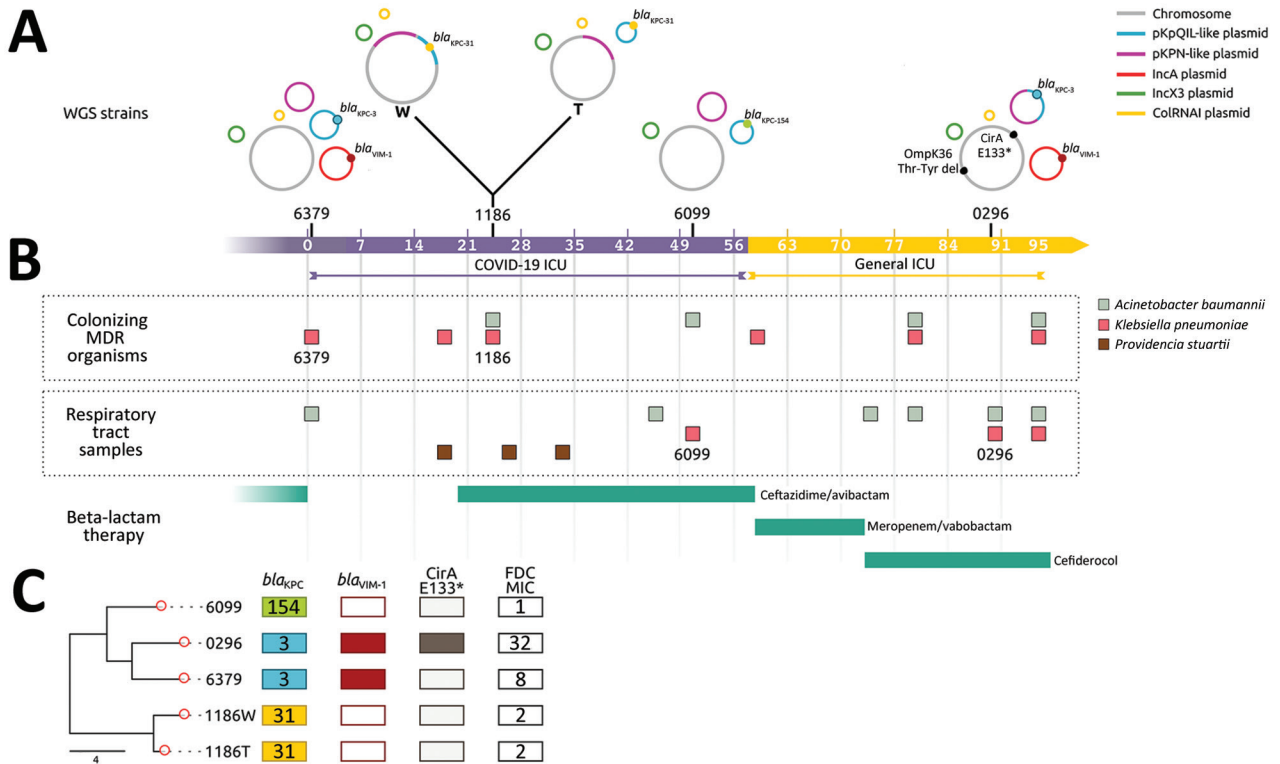


Figure 1. Timeline of colonization and infection of 1 patient by *Klebsiella pneumoniae* clones in study of genotypic evolution of *K. pneumoniae* sequence type 512 during ceftazidime/avibactam, meropenem/vaborbactam, and cefiderocol treatment, Italy. A) Schematic diagram of carbapenemase genes and plasmid content for *K. pneumoniae* strains 6379, 1186, 6099, and 0296; strain 1186 comprised 2 phenotypes: W and T colonies. Isolate collection day is indicated during 95 hospitalization days in either the COVID-19 (purple scale) or general (yellow scale) intensive care unit. Asterisk indicates the premature stop codon at position 133 (E133) in the catechol iron outer membrane transporter CirA. B) Timeline of colonization and infection by *K. pneumoniae*, *Providencia stuartii*, and *Acinetobacter baumannii* as well as β-lactam therapies. C) Phylogenetic analysis used to compare the 5 *K. pneumoniae* strains isolated from the same patient. Core genome alignments were conducted for 5,215 core genes. KPC variants KPC-154, KPC-3, and KPC-31 are shown according to each strain; the *bla*_{VIM-1} gene was present in strains 0296 and 6379. Nonsense mutation in *cirA* was found in strain 0296, producing a premature stop codon (E133), indicated by an asterisk, in the protein. FDC MICs (mg/L) for each strain are shown. Scale bar indicates number of single-nucleotide polymorphisms in the core genome. FDC, cefiderocol; ICU, intensive care unit; KPC, *K. pneumoniae* carbapenemase; MDR, multidrug resistant; OmpK36, outer membrane porin K36; T, transparent; VIM, Verona integron-encoded metallo-β-lactamase; W, white; WGS, whole-genome sequencing.

mutations in the *gyrA* (S83I) and *parC* (S80I) genes potentially conferring quinolone resistance (35). The 5 isolates in this study had additional common features diverging from the average ST512 strain: a SNP in the *mgrB* gene, which stops translation at aa 29 of the MgrB regulator protein, conferring resistance to colistin (36); a SNP in the *uhpB* gene, which stops translation at aa 206 of the UhpB protein (37), conferring resistance to fosfomycin; and the presence of the locus encoding yersiniabactin siderophore, designated as YbST157 (38). The yersiniabactin siderophore is not common in ST512 isolates because this locus could only be found in 31/133 (23%) ST512 genomes from the BIGSdb collection.

The 5 *K. pneumoniae* strains carried multiple acquired resistance genes (Appendix 2 Table 1,

<https://wwwnc.cdc.gov/EID/article/29/11/23-0921-App2.pdf>). Plasmid content of the 5 ST512 strains from the patient was not homogeneous: strains 6379 (first strain isolated) and 0296 (last strain isolated) both carried the pKpQIL plasmid containing the *bla*_{KPC-3} gene and IncA plasmid carrying the *bla*_{VIM-1} gene (Figures 1, 2). Strains 1186W, 1186T, and 6099 lacked the IncA-*bla*_{VIM-1} plasmid.

KPC Variants Conferring Resistance to Ceftazidime/Avibactam

On day 24, *K. pneumoniae* strains 1186W and 1186T colonized the patient (isolated from rectal swab samples). Those strains were negative for VIM-1 (loss of plasmid pIncA-*bla*_{VIM-1}) but reached high levels of CZA resistance through the production

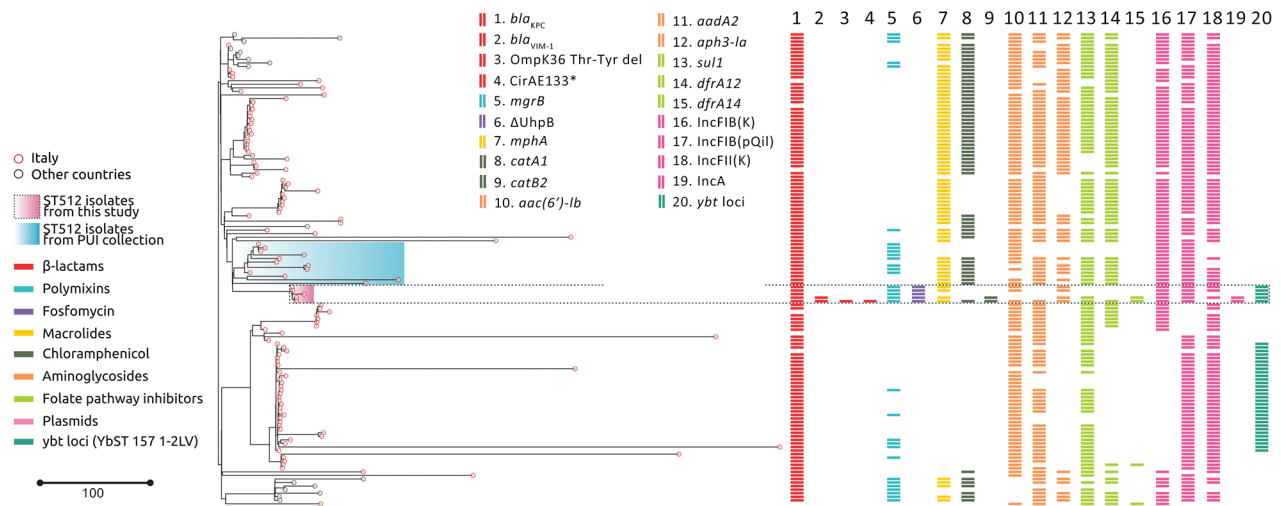


Figure 2. Phylogenetic analysis and genetic features of *Klebsiella pneumoniae* ST512 in study of the strain’s genotypic evolution during ceftazidime/avibactam, meropenem/vaborbactam, and cefiderocol treatment, Italy. Phylogenetic tree was constructed from 4,654 core gene alignments from a total of 133 *K. pneumoniae* ST512 genome sequences: 5 genomes sequenced in this study (pink shading), 12 genomes from the same hospital (pale blue shading), and 116 genomes downloaded from the Pasteur Institute BIGSdb database (<https://bigsd.bpasteur.fr/klebsiella>). Colors indicate resistance and acquired-resistance genes (or corresponding proteins) associated with carbapenemases, yersiniabactin, and chromosomal mutations within the different strains. The same color in the legend on the left indicates the expected resistance phenotype. Asterisk after CirA E133 indicates this mutation produced a premature stop codon. Scale bar indicates number of single-nucleotide polymorphisms in the core genome. Del, deletion; KPC, *K. pneumoniae* carbapenemase; PUI, Policlinico Umberto I; ST, sequence type; VIM, Verona integron-encoded metallo-β-lactamase.

of KPC-31. The *bla*_{KPC-31} gene replaced *bla*_{KPC-3} on an otherwise indistinguishable pKpQIL plasmid; the plasmid was integrated in the chromosome only in strain 1186W. The KPC-31 variant is characterized by a D179Y substitution in the Ω loop, previously shown to confer CZA resistance but restores carbapenem susceptibility (39).

On day 51, CZA-resistant *K. pneumoniae* strain 6099 caused a respiratory tract infection in the patient (Table). This strain hosted a pKpQIL plasmid encoding a novel KPC variant that was assigned by GenBank as KPC-154 (accession no. OQ096263) and was negative for the VIM-encoding IncA plasmid. Compared with KPC-3, KPC-154 has an RAPNKD-

DKYS amino acid duplication in position 263–273, corresponding to the 270 loop (40), but no differences are present in the Ω loop. When compared with an isogenic KPC-31-carrying strain, the strain carrying KPC-154 had higher MICs for several β-lactams (Appendix 2 Table 2).

Cefiderocol Resistance in ST512 Isolates Co-Producing KPC and VIM

K. pneumoniae strain 0296 (pulmonary infectious agent, isolated on day 88) was genotypically related to strain 6379 (colonizer, isolated on day 1). Both strains had similar plasmid content, including pKpQIL carrying *bla*_{KPC-3} and pIncA carrying

Table. MICs of antimicrobial drugs for *Klebsiella pneumoniae* sequence type 512 strains analyzed in study of genotypic evolution of such strains during ceftazidime/avibactam, meropenem/vaborbactam, and cefiderocol treatment, Italy*

Strain	AZT	CZA†	FDC‡	MEM	MVB†	IMI	COL	FOS	AMK	GTM	CIP	SXT	TGC
6379	>4	>256	8	32	1.5	>8	>4	>64	16	≤2	>1	>4/76	2
1186W	>4	32	2	2	0.25	≤1	>4	>64	>16	≤2	>1	≤2/38	≤1
1186T	>4	32	2	4	0.25	≤1	>4	>64	>16	≤2	>1	≤2/38	≤1
6099	>4	16	1	16	0.5	>8	>4	>64	≤8	≤2	>1	≤2/38	≤1
0296	>4	>256	32	32	0.047	>8	>4	>64	≤8	≤2	>1	>4/76	≤1
EUCAST breakpoint	4	8	2	8	8	4	2	32	8	2	0.5	4	ND

*MICs are mg/L. Bold indicates resistance to antimicrobial drugs according to EUCAST breakpoints. AMK, amikacin; AZT, aztreonam; CIP, ciprofloxacin; COL, colistin; CZA, ceftazidime/avibactam; EUCAST, European Committee on Antimicrobial Susceptibility Testing (<https://www.eucast.org>); FDC, cefiderocol; FOS, fosfomycin; GTM, gentamicin; IMI, imipenem; MEM, meropenem; MVB, meropenem/vaborbactam; ND, not done; SXT, trimethoprim/sulfamethoxazole; TGC, tigecycline.

†Tested by using the gradient strip method (Liofilchem, <https://www.liofilchem.com>).

‡Tested by using the Compact Antimicrobial Susceptibility Panel broth microdilution method (Liofilchem).

*bla*_{VIM-1} (Figures 1, 2). However, isolate 0296 carried a pKpQIL-pKPN fused plasmid carrying *catA1*, *dfrA12*, *aadA2*, *aph(3')-Ia* genes, 2 copies of *mph(A)*, *sul1*, and Δ *qacE* genes (Appendix 2 Table 1), and the previously described putative gene involved in iron acquisition (*fec*) (41), all of which were not present in plasmid pKPN from isolate 6379. Within the core genome, strain 0296 had 7 SNPs and 3 deletions when compared with strain 6379 (Appendix 1 Table 2); 1 SNP created a premature stop codon at position 133 in the iron transporter protein CirA (Table 1; Figure 1) (42). Strain 0296 showed 4-fold higher FDC MIC than strain 6379 (6379 FDC MIC = 8 mg/L; 0296 FDC MIC = 32 mg/L). Moreover, in strain 0296, a conservative in-frame deletion resulted in a novel mutation within OmpK36; the deletion was 26 aa (residues Thr263 to Tyr289) according to the reference OmpK36 crystal structure in the Protein Data Bank (no. 6RCP; <https://www.rcsb.org>) (30). The in silico predicted 3-dimensional structure of the mutated OmpK36 porin showed a deep lateral cave, probably favoring MVB permeability from the extracellular site into the periplasmic space (Figure 3). Strain 0296 carrying the mutated OmpK36 protein showed a 5-fold reduction in MVB MICs compared with strain 6379 (6379 MVB MIC = 1.5 mg/L; 0296 MVB MIC = 0.047 mg/L).

Discussion

We report the in vivo evolution of antimicrobial resistance in *K. pneumoniae* high-risk ST512 strains (43) that colonized or infected a critical patient during a 95-day hospitalization. From both phenotypic and genotypic perspectives, each *K. pneumoniae* isolate had univocal characteristics. The rare mutation in the UhpABC signaling pathway conferred fosfomycin resistance by altering expression of the hexose phosphate transporter (44,45). Mutations in the *mgrB* gene, identified in the 5 strains isolated in this study, 8 strains isolated during 2018–2020 at the PUI (8), and globally in 37/133 (27.8%) whole-genome sequences from the Pasteur Institute ST512 collection, conferred colistin resistance. Moreover, the 5 strains from this study carried the yersiniabactin locus, a virulence factor rarely reported in ST512 clones. The yersiniabactin locus was identified in a *K. pneumoniae* ST512 cluster sampled in the framework of the SPARK project from a single city located in northern Italy during 2017–2018 (46). All of those factors support the hypothesis that a single *K. pneumoniae* clone was obtained from the patient first from rectal swab samples and subsequently from the respiratory tract, rather than antimicrobial drug treatment selecting 5 distinct strains.

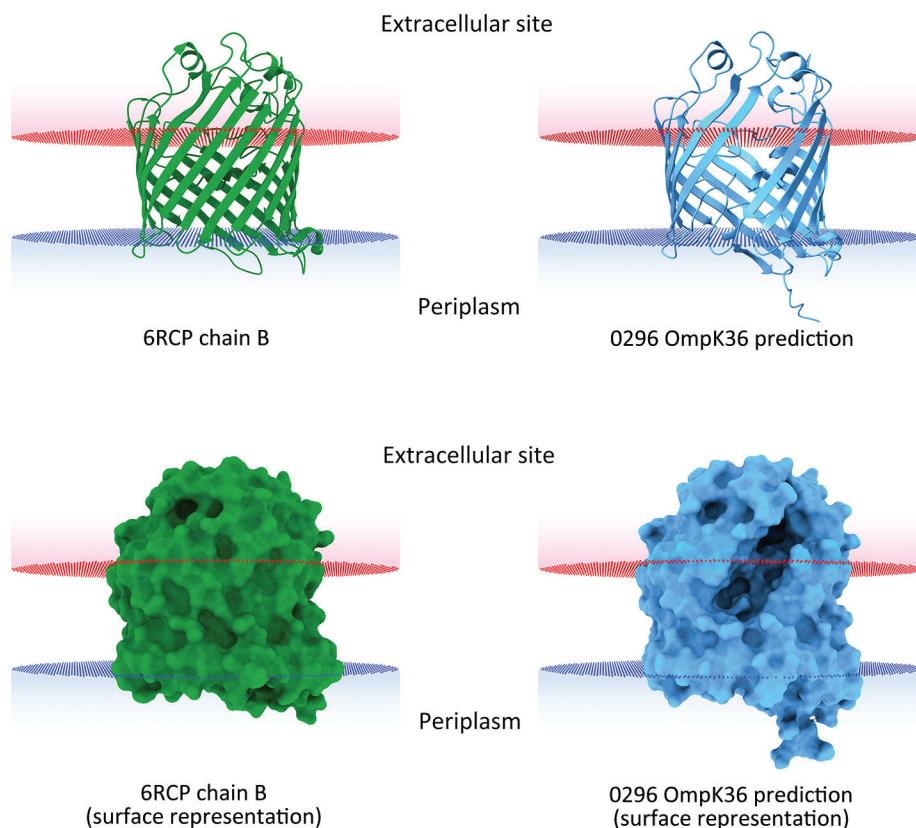


Figure 3. In silico 3-dimensional structure predictions for mutated OmpK36 porin in *Klebsiella pneumoniae* sequence type 512 strain 0296 in study of *K. pneumoniae* genotypic evolution during ceftazidime/avibactam, meropenem/vaborbactam, and cefiderocol treatment, Italy. The outer membrane porin OmpK36 from strain 0296 (blue) containing a 26 aa deletion from residue Thr263 through residue Tyr289 was modeled and compared with the model of reference OmpK36 chain B crystal structure from the Protein Data Bank (no. 6RCP; <https://www.rcsb.org>) (30). Both ribbon cartoon (top) and surface (bottom) models are shown. Structures for strain 0296 were obtained by using AlphaFold2 on the European Galaxy server (<https://usegalaxy.eu>). Spatial arrangements of the porins in lipid bilayers were visualized by using the positioning of proteins in membranes web server in the Orientations of Proteins in Membranes database (31).

The development of β -lactam resistance in *K. pneumoniae* ST512 strains is a critical concern. At the time of transfer to PUI from a long-term care facility, the patient was colonized by a carbapenem-resistant *K. pneumoniae* strain that produced KPC-3 and VIM-1. Although KPC-3 production by *K. pneumoniae* is a persistent phenomenon in Italy (6), the spread of VIM-producing *K. pneumoniae* is less common. However, we previously described an Enterobacterales infection outbreak at PUI caused by IncA plasmids encoding VIM (47). Therefore, we hypothesize that an elusive and untraced spread of VIM-producing Enterobacterales might exist in hospitals and long-term care facilities in Rome.

During the first 3 weeks of hospitalization, the patient was not treated with β -lactams. We introduced CZA therapy to treat a respiratory tract infection sustained by *P. stuartii*, a pathogen more frequently associated with urinary tract infections (48) but also related to respiratory tract infections (49,50). After 3 days of CZA treatment, a KPC-31-producing, CZA-resistant *K. pneumoniae* strain colonized in the patient and then evolved to an infection by a KPC-154-producing CZA-resistant variant. The KPC-154 clone had a wild type Ω loop but a 13 aa insertion in the 270 loop of the enzyme, a feature previously described in other KPC variants (8).

We used MVB to treat the KPC-154-producing *K. pneumoniae* infection, which eradicated the *K. pneumoniae* strain from respiratory tract samples. However, a respiratory tract infection sustained by *A. baumannii* developed in the patient, who we then treated with FDC. Under FDC treatment, the respiratory tract sample tested positive for *K. pneumoniae* ST512 that was identical to the first colonizing strain, producing both KPC-3 and VIM-1 carbapenemases. This result suggests that a mixed population of KPC/VIM-positive and KPC-positive/VIM-negative *K. pneumoniae* was present in the patient during the entire hospitalization period. VIM-1-negative strains prevailed under CZA treatment, whereas MVB and FDC treatments selected the expansion of VIM-1-producing strains, which likely remained in a hidden reservoir within the patient.

The reemerged KPC/VIM producer had a high MIC for FDC because of the loss-of-function mutation in the CirA siderophore receptor. CirA mutations have previously been associated with FDC resistance in an in vitro model of New Delhi metallo- β -lactamase-producing *K. pneumoniae* (11) and in vivo for *E. cloacae* (14) and *E. coli* (15). However, the KPC/VIM-producing *K. pneumoniae* strain showed increased susceptibility to MVB, probably associated

with a novel OmpK36 structure showing a large protein deletion; the 3-dimensional porin structure predicted a large lateral cave that might increase permeability of MVB. Nonetheless, the mutant OmpK36 could also be interpreted as a compensatory mutation that promotes survival of the CirA-defective strain.

We used last resort β -lactam-based antimicrobial drugs (CZA, MVB, and FDC) to treat the patient but only used MVB to treat the respiratory tract infection sustained by the CZA-resistant ST512 *K. pneumoniae*; other antimicrobial drugs were administered to treat infections caused by *P. stuartii* or *A. baumannii*. This case report serves as a warning that cross-selection can occur between *K. pneumoniae* and treatments prescribed against other infective agents and that *K. pneumoniae* can stably colonize a patient for a long period, promoting progressive evolution of the resistome under increasing selective pressure.

This research was supported by European Union funding (to A.C., A.O., and G.A.) from the NextGeneration EU-MUR PNRR Extended Partnership Initiative on Emerging Infectious Diseases (project no. PE00000007, PE13 INF-ACT, Spoke 3).

About the Author

Dr. Arcari is a researcher at Sapienza University of Rome, Italy. His main interests focus on antimicrobial resistance mechanisms and their dissemination in bacterial pathogens.

References

- Murray CJL, Ikuta KS, Sharara F, Swetschinski L, Robles Aguilar G, Gray A, et al.; Antimicrobial Resistance Collaborators. Global burden of bacterial antimicrobial resistance in 2019: a systematic analysis. *Lancet*. 2022;399:629–55. [https://doi.org/10.1016/S0140-6736\(21\)02724-0](https://doi.org/10.1016/S0140-6736(21)02724-0)
- Shirley M. Ceftazidime-avibactam: a review in the treatment of serious gram-negative bacterial infections. *Drugs*. 2018;78:675–92. <https://doi.org/10.1007/s40265-018-0902-x>
- Yahav D, Giske CG, Grāmatniece A, Abodakpi H, Tam VH, Leibovici L. New β -lactam- β -lactamase inhibitor combinations. *Clin Microbiol Rev*. 2020;34:e00115-20. <https://doi.org/10.1128/CMR.00115-20>
- El-Lababidi RM, Rizk JG. Cefiderocol: a siderophore cephalosporin. *Ann Pharmacother*. 2020;54:1215–31. <https://doi.org/10.1177/1060028020929988>
- Ito A, Nishikawa T, Matsumoto S, Yoshizawa H, Sato T, Nakamura R, et al. Siderophore cephalosporin cefiderocol utilizes ferric iron transporter systems for antibacterial activity against *Pseudomonas aeruginosa*. *Antimicrob Agents Chemother*. 2016;60:7396–401. <https://doi.org/10.1128/AAC.01405-16>
- David S, Reuter S, Harris SR, Glasner C, Feltwell T, Argimon S, et al.; EuSCAPE Working Group; ESGEM Study

- Group. Epidemic of carbapenem-resistant *Klebsiella pneumoniae* in Europe is driven by nosocomial spread. *Nat Microbiol*. 2019;4:1919–29. <https://doi.org/10.1038/s41564-019-0492-8>
7. Di Pilato V, Errico G, Monaco M, Giani T, Del Grosso M, Antonelli A, et al.; AR-ISS Laboratory Study Group on carbapenemase-producing *Klebsiella pneumoniae*. The changing epidemiology of carbapenemase-producing *Klebsiella pneumoniae* in Italy: toward polyclonal evolution with emergence of high-risk lineages. *J Antimicrob Chemother*. 2021;76:355–61. <https://doi.org/10.1093/jac/dkaa431>
 8. Carattoli A, Arcari G, Bibbolino G, Sacco F, Tomolillo D, Di Lella FM, et al. Evolutionary trajectories toward ceftazidime-avibactam resistance in *Klebsiella pneumoniae* clinical isolates. *Antimicrob Agents Chemother*. 2021;65:e0057421. <https://doi.org/10.1128/AAC.00574-21>
 9. Hobson CA, Pierrat G, Tenaillon O, Bonacorsi S, Bercot B, Jaouen E, et al. *Klebsiella pneumoniae* carbapenemase variants resistant to ceftazidime-avibactam: an evolutionary overview. *Antimicrob Agents Chemother*. 2022;66:e0044722. <https://doi.org/10.1128/aac.00447-22>
 10. Karakonstantis S, Rousalis M, Kritsotakis EI. Cefiderocol: systematic review of mechanisms of resistance, heteroresistance and in vivo emergence of resistance. *Antibiotics (Basel)*. 2022;11:723. <https://doi.org/10.3390/antibiotics11060723>
 11. McElheny CL, Fowler EL, Iovleva A, Shields RK, Doi Y. In vitro evolution of cefiderocol resistance in an NDM-producing *Klebsiella pneumoniae* due to functional loss of CirA. *Microbiol Spectr*. 2021;9:e0177921. <https://doi.org/10.1128/Spectrum.01779-21>
 12. Fröhlich C, Sorum V, Tokuriki N, Johnsen PJ, Samuelsen Ø. Evolution of β -lactamase-mediated cefiderocol resistance. *J Antimicrob Chemother*. 2022;77:2429–36. <https://doi.org/10.1093/jac/dkac221>
 13. Lan P, Lu Y, Jiang Y, Wu X, Yu Y, Zhou J. Catecholase siderophore receptor CirA impacts cefiderocol susceptibility in *Klebsiella pneumoniae*. *Int J Antimicrob Agents*. 2022;60:106646. <https://doi.org/10.1016/j.ijantimicag.2022.106646>
 14. Klein S, Boutin S, Kocer K, Fiedler MO, Störzinger D, Weigand MA, et al. Rapid development of cefiderocol resistance in carbapenem-resistant *Enterobacter cloacae* during therapy is associated with heterogeneous mutations in the catecholase siderophore receptor cirA. *Clin Infect Dis*. 2022;74:905–8. <https://doi.org/10.1093/cid/ciab511>
 15. Jousset AB, Poignon C, Yilmaz S, Bleibtreu A, Emeraud C, Girlich D, et al. Rapid selection of a cefiderocol-resistant *Escherichia coli* producing NDM-5 associated with a single amino acid substitution in the CirA siderophore receptor. *J Antimicrob Chemother*. 2023;78:1125–7. <https://doi.org/10.1093/jac/dkad004>
 16. Freire B, Ladra S, Parama JR. Memory-efficient assembly using Flye. *IEEE/ACM Trans Comput Biol Bioinform*. 2022;19:3564–77. <https://doi.org/10.1109/TCBB.2021.3108843>
 17. Wick RR, Judd LM, Gorrie CL, Holt KE. Unicycler: resolving bacterial genome assemblies from short and long sequencing reads. *PLOS Comput Biol*. 2017;13:e1005595. <https://doi.org/10.1371/journal.pcbi.1005595>
 18. Wick RR, Schultz MB, Zobel J, Holt KE. Bandage: interactive visualization of de novo genome assemblies. *Bioinformatics*. 2015;31:3350–2. <https://doi.org/10.1093/bioinformatics/btv383>
 19. Overbeek R, Olson R, Pusch GD, Olsen GJ, Davis JJ, Disz T, et al. The SEED and the rapid annotation of microbial genomes using subsystems technology (RAST). *Nucleic Acids Res*. 2014;42:D206–14. <https://doi.org/10.1093/nar/gkt1226>
 20. Seemann T. Prokka: rapid prokaryotic genome annotation. *Bioinformatics*. 2014;30:2068–9. <https://doi.org/10.1093/bioinformatics/btu153>
 21. Page AJ, Cummins CA, Hunt M, Wong VK, Reuter S, Holden MTG, et al. Roary: rapid large-scale prokaryote pan genome analysis. *Bioinformatics*. 2015;31:3691–3. <https://doi.org/10.1093/bioinformatics/btv421>
 22. Hoang DT, Chernomor O, von Haeseler A, Minh BQ, Vinh LS. UFBoot2: improving the ultrafast bootstrap approximation. *Mol Biol Evol*. 2018;35:518–22. <https://doi.org/10.1093/molbev/msx281>
 23. Minh BQ, Schmidt HA, Chernomor O, Schrempf D, Woodhams MD, von Haeseler A, et al. IQ-TREE 2: new models and efficient methods for phylogenetic inference in the genomic era. *Mol Biol Evol*. 2020;37:1530–4. <https://doi.org/10.1093/molbev/msaa015>
 24. Kalyaanamoorthy S, Minh BQ, Wong TKF, von Haeseler A, Jermiin LS. ModelFinder: fast model selection for accurate phylogenetic estimates. *Nat Methods*. 2017;14:587–9. <https://doi.org/10.1038/nmeth.4285>
 25. Argimón S, Abudahab K, Goater RJE, Fedosejev A, Bhai J, Glasner C, et al. Microreact: visualizing and sharing data for genomic epidemiology and phylogeography. *Microb Genom*. 2016;2:e000093. <https://doi.org/10.1099/mgen.0.000093>
 26. Carattoli A, Zankari E, García-Fernández A, Voldby Larsen M, Lund O, Villa L, et al. In silico detection and typing of plasmids using PlasmidFinder and plasmid multilocus sequence typing. *Antimicrob Agents Chemother*. 2014;58:3895–903. <https://doi.org/10.1128/AAC.02412-14>
 27. Lam MMC, Wick RR, Judd LM, Holt KE, Wyres KL. Kaptive 2.0: updated capsule and lipopolysaccharide locus typing for the *Klebsiella pneumoniae* species complex. *Microb Genom*. 2022;8:000800. <https://doi.org/10.1099/mgen.0.000800>
 28. Lam MMC, Wick RR, Watts SC, Cerdeira LT, Wyres KL, Holt KE. A genomic surveillance framework and genotyping tool for *Klebsiella pneumoniae* and its related species complex. *Nat Commun*. 2021;12:4188. <https://doi.org/10.1038/s41467-021-24448-3>
 29. Pettersen EF, Goddard TD, Huang CC, Meng EC, Couch GS, Croll TI, et al. UCSF ChimeraX: structure visualization for researchers, educators, and developers. *Protein Sci*. 2021;30:70–82. <https://doi.org/10.1002/pro.3943>
 30. Wong JLC, Romano M, Kerry LE, Kwong HS, Low WW, Brett SJ, et al. OmpK36-mediated carbapenem resistance attenuates ST258 *Klebsiella pneumoniae* in vivo. *Nat Commun*. 2019;10:3957. <https://doi.org/10.1038/s41467-019-11756-y>
 31. Lomize MA, Lomize AL, Pogozheva ID, Mosberg HI. OPM: orientations of proteins in membranes database. *Bioinformatics*. 2006;22:623–5. <https://doi.org/10.1093/bioinformatics/btk023>
 32. Jolley KA, Bray JE, Maiden MCJ. Open-access bacterial population genomics: BIGSdb software, the PubMLST.org website and their applications. *Wellcome Open Res*. 2018;3:124. <https://doi.org/10.12688/wellcomeopenres.14826.1>
 33. Deleo FR, Chen L, Porcella SF, Martens CA, Kobayashi SD, Porter AR, et al. Molecular dissection of the evolution of carbapenem-resistant multilocus sequence type 258 *Klebsiella pneumoniae*. *Proc Natl Acad Sci USA*. 2014;111:4988–93. <https://doi.org/10.1073/pnas.1321364111>
 34. García-Fernández A, Miriagou V, Papagiannitsis CC, Giordano A, Venditti M, Mancini C, et al. An ertapenem-

- resistant extended-spectrum- β -lactamase-producing *Klebsiella pneumoniae* clone carries a novel OmpK36 porin variant. *Antimicrob Agents Chemother*. 2010;54:4178–84. <https://doi.org/10.1128/AAC.01301-09>
35. Deguchi T, Fukuoka A, Yasuda M, Nakano M, Ozeki S, Kanematsu E, et al. Alterations in the GyrA subunit of DNA gyrase and the ParC subunit of topoisomerase IV in quinolone-resistant clinical isolates of *Klebsiella pneumoniae*. *Antimicrob Agents Chemother*. 1997;41:699–701. <https://doi.org/10.1128/AAC.41.3.699>
 36. Cannatelli A, Giani T, D'Andrea MM, Di Pilato V, Arena F, Conte V, et al.; COLGRIT Study Group. MgrB inactivation is a common mechanism of colistin resistance in KPC-producing *Klebsiella pneumoniae* of clinical origin. *Antimicrob Agents Chemother*. 2014;58:5696–703. <https://doi.org/10.1128/AAC.03110-14>
 37. Verhamme DT, Arents JC, Postma PW, Crielaard W, Hellingwerf KJ. Glucose-6-phosphate-dependent phosphoryl flow through the Uhp two-component regulatory system. *Microbiology (Reading)*. 2001;147:3345–52. <https://doi.org/10.1099/00221287-147-12-3345>
 38. Lam MMC, Wick RR, Wyres KL, Gorrie CL, Judd LM, Jenney AWJ, et al. Genetic diversity, mobilisation and spread of the yersiniabactin-encoding mobile element ICEKp in *Klebsiella pneumoniae* populations. *Microb Genom*. 2018;4:e000196. <https://doi.org/10.1099/mgen.0.000196>
 39. Shields RK, Chen L, Cheng S, Chavda KD, Press EG, Snyder A, et al. Emergence of ceftazidime-avibactam resistance due to plasmid-borne *bla*_{KPC-3} mutations during treatment of carbapenem-resistant *Klebsiella pneumoniae* infections. *Antimicrob Agents Chemother*. 2017;61:e02097-16. <https://doi.org/10.1128/AAC.02097-16>
 40. Tooke CL, Hinchliffe P, Bonomo RA, Schofield CJ, Mulholland AJ, Spencer J. Natural variants modify *Klebsiella pneumoniae* carbapenemase (KPC) acyl-enzyme conformational dynamics to extend antibiotic resistance. *J Biol Chem*. 2021;296:100126. <https://doi.org/10.1074/jbc.RA120.016461>
 41. Villa L, Feudi C, Fortini D, Brisse S, Passet V, Bonura C, et al. Diversity, virulence, and antimicrobial resistance of the KPC-producing *Klebsiella pneumoniae* ST307 clone. *Microb Genom*. 2017;3:e000110. <https://doi.org/10.1099/mgen.0.000110>
 42. Zhang Z, Du W, Wang M, Li Y, Su S, Wu T, et al. Contribution of the colicin receptor CirA to biofilm formation, antibiotic resistance, and pathogenicity of *Salmonella* Enteritidis. *J Basic Microbiol*. 2020;60:72–81. <https://doi.org/10.1002/jobm.201900418>
 43. Wyres KL, Holt KE. *Klebsiella pneumoniae* population genomics and antimicrobial-resistant clones. *Trends Microbiol*. 2016;24:944–56. <https://doi.org/10.1016/j.tim.2016.09.007>
 44. Zheng D, Bergen PJ, Landersdorfer CB, Hirsch EB. Differences in fosfomycin resistance mechanisms between *Pseudomonas aeruginosa* and Enterobacterales. *Antimicrob Agents Chemother*. 2022;66:e0144621. <https://doi.org/10.1128/AAC.01446-21>
 45. Ortiz-Padilla M, Portillo-Calderón I, de Gregorio-Iaria B, Blázquez J, Rodríguez-Baño J, Pascual A, et al. Interplay among different fosfomycin resistance mechanisms in *Klebsiella pneumoniae*. *Antimicrob Agents Chemother*. 2021;65:e01911-20. <https://doi.org/10.1128/AAC.01911-20>
 46. Thorpe HA, Booton R, Kallonen T, Gibbon MJ, Couto N, Passet V, et al. A large-scale genomic snapshot of *Klebsiella* spp. isolates in Northern Italy reveals limited transmission between clinical and non-clinical settings. *Nat Microbiol*. 2022;7:2054–67. <https://doi.org/10.1038/s41564-022-01263-0>
 47. Arcari G, Di Lella FM, Bibbolino G, Mengoni F, Beccaccioli M, Antonelli G, et al. A multispecies cluster of VIM-1 carbapenemase-producing Enterobacterales linked by a novel, highly conjugative, and broad-host-range IncA plasmid forebodes the reemergence of VIM-1. *Antimicrob Agents Chemother*. 2020;64:e02435-19. <https://doi.org/10.1128/AAC.02435-19>
 48. Liu J, Wang R, Fang M. Clinical and drug resistance characteristics of *Providencia stuartii* infections in 76 patients. *J Int Med Res*. 2020;48:300060520962296. <https://doi.org/10.1177/0300060520962296>
 49. Molnár S, Flonta MMM, Almaş A, Buzea M, Licker M, Rus M, et al. Dissemination of NDM-1 carbapenemase-producer *Providencia stuartii* strains in Romanian hospitals: a multicentre study. *J Hosp Infect*. 2019;103:165–9. <https://doi.org/10.1016/j.jhin.2019.04.015>
 50. Akbiyik A, Hepçivici Z, Eşer I, Uyar M, Çetin P. The effect of oropharyngeal aspiration before position change on reducing the incidence of ventilator-associated pneumonia. *Eur J Clin Microbiol Infect Dis*. 2021;40:615–22. <https://doi.org/10.1007/s10096-019-03789-4>

Address for correspondence: Alessandra Carattoli, Department of Molecular Medicine, Sapienza University of Rome, Viale di Porta Tiburtina 28, Rome 00185, Italy; email: alessandra.carattoli@uniroma1.it

Neurologic Effects of SARS-CoV-2 Transmitted among Dogs

Dong-Hwi Kim,¹ Da-Yoon Kim,¹ Kyu-Sung Kim,¹ Sang-Hoon Han, Hyeon-Jeong Go, Jae-Hyeong Kim, Kyu-Beom Lim, Dong-Hun Lee, Joong-Bok Lee, Seung-Yong Park, Chang-Seon Song, Sang-Won Lee, Yang-Kyu Choi, Yeun-Kyung Shin, Oh-Kyu Kwon, Do-Geun Kim, In-Soo Choi

SARS-CoV-2 induces illness and death in humans by causing systemic infections. Evidence suggests that SARS-CoV-2 can induce brain pathology in humans and other hosts. In this study, we used a canine transmission model to examine histopathologic changes in the brains of dogs infected with SARS-CoV-2. We observed substantial brain pathology in SARS-CoV-2-infected dogs, particularly involving blood–brain barrier damage resembling small vessel disease, including changes in tight junction proteins, reduced laminin levels, and decreased pericyte coverage. Furthermore, we detected phosphorylated tau, a marker of neurodegenerative disease, indicating a potential link between SARS-CoV-2–associated small vessel disease and neurodegeneration. Our findings of degenerative changes in the dog brain during SARS-CoV-2 infection emphasize the potential for transmission to other hosts and induction of similar signs and symptoms. The dynamic brain changes in dogs highlight that even asymptomatic individuals infected with SARS-CoV-2 may develop neuropathologic changes in the brain.

Since SARS-CoV-2 was first reported in late 2019, infection has been observed primarily in humans; however, animals of various species have also been infected, partially because their angiotensin-converting enzyme 2 (ACE2) receptor is very similar to that of humans. Infected animals show clinical signs similar to those of humans, raising concerns about potential

transmission of the virus between humans and animals (1,2). SARS-CoV-2 infection in dogs and cats affects the lungs and leads to pathologic changes (Figure 1). However, whether similar pathologic manifestations occur in the brain, as observed in humans, remains unclear.

Close cohabitation of dogs and humans, and their high genetic similarity, has prompted investigations into dogs' susceptibility to SARS-CoV-2 infection (3,4). Wild-type SARS-CoV-2 infection in dogs can induce formation of neutralizing antibodies, and low viral titers in dogs demonstrate seroconversion (5,6). Mutant strains of SARS-CoV-2 in dogs cause histopathologic changes in lung tissues and increased expression of muscle damage markers in the blood (7). ACE2 in dogs can bind to the receptor-binding domain of SARS-CoV-2, implying the possibility of cross-species transmission between humans and dogs (8). Genetic and epidemiologic studies have reported animal-to-human transmission of SARS-CoV-2 (9).

Reportedly, SARS-CoV-2 can cause neurologic signs and symptoms (e.g., headache, fatigue, and cognitive dysfunction) in human patients. Several cohort studies report strong correlations between SARS-CoV-2 and neurologic signs/symptoms (10–13). Furthermore, cortical thickness is reduced in SARS-CoV-2-infected patients, suggesting that SARS-CoV-2 can induce pathologic changes in the brain, which may be linked to the functional deficits noted in those patients. Considering the number of patients infected with SARS-CoV-2, the neurologic signs can lead to a potential wave of neurodegenerative diseases, which could pose an immense burden on society.

The etiology of SARS-CoV-2–induced neuropathologic changes is still elusive. However, clinical and experimental reports suggest that vascular damage and the resultant immune responses in the brain may be a major factor (13–16). Magnetic resonance

Author affiliations: Konkuk University, Seoul, South Korea (D.-H. Kim, D.-Y. Kim, S.-H. Han, H.-J. Go, J.-H. Kim, K.-B. Lim, D.-H. Lee, J.-B. Lee, S.-Y. Park, C.-S. Song, S.-W. Lee, Y.-K. Choi, I.-S. Choi); Korea Brain Research Institute, Daegu, South Korea (K.-S. Kim, D.-G. Kim); Daegu Gyeongbuk Institute of Science and Technology, Daegu (K.-S. Kim, D.-G. Kim); Animal and Plant Quarantine Agency, Gimcheon, South Korea (Y.-K. Shin, O.-K. Kwon); Konkuk University Zoonotic Diseases Research Center, Seoul (D.-H. Lee, J.-B. Lee, S.-Y. Park, C.-S. Song, S.-W. Lee, I.-S. Choi); KU Center for Animal Blood Medical Science, Seoul (I.-S. Choi)

DOI: <https://doi.org/10.3201/eid2911.230804>

¹These authors contributed equally to this article.

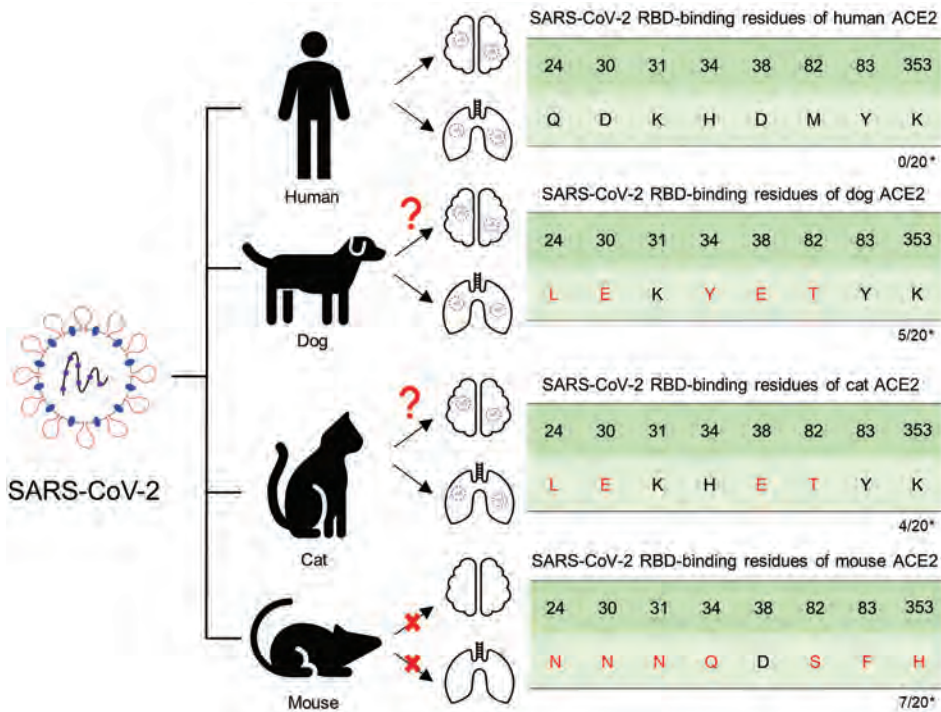


Figure 1. Schematic diagram representing susceptibility to SARS-CoV-2 infection in the lungs and brain of animals with potential for human transmission and homology of ACE2 amino acid sequences in study of the neurologic effects of SARS-CoV-2. *Number of mutations among the key 20 residues involved in interacting with the SARS-CoV-2 RBD. ACE2, angiotensin-converting enzyme 2; RBD, receptor-binding domain.

imaging has detected white matter hyperintensities in SARS-CoV-2-infected patients, indicating damage to the blood-brain barrier (BBB) in this region and that potentially demyelinating pathologic changes can be induced (13). Other studies have revealed signs of neuroinflammatory responses, including activation of microglial cells and astrocytes (14,15). Moreover, damage to the brain vasculature and defects in the coagulation system have been demonstrated (16). The characteristic pathologies observed in human patients (e.g., vascular damage, demyelination, and neuroinflammatory responses) have also been observed in humanized mouse models.

We used a canine transmission model to investigate the susceptibility of dogs to SARS-CoV-2, specifically the Delta variant. The dogs were housed in a Biosafety Level 3 animal facility at Konkuk University Laboratory, Seoul, South Korea, where temperature, humidity, and light were carefully controlled. The study was approved by the Animal Research Center under the supervision of the Institutional Animal Care and Use Committee (accreditation no. KU22065) and the Institutional Biosafety Committee (accreditation no. KUIBC-2022-06) at Konkuk University. The absence of SARS-CoV-2 RNA and SARS-CoV-2 antibodies in dog serum was confirmed.

Materials and Methods

Considering that SARS-CoV-2 infections cause neurologic effects in human and human ACE2 transgenic

mice, and typically follow respiratory system infection, we used models mimicking the natural infection route. We intranasally infected dogs with the Delta variant, and virus subsequently was transmitted to contact dogs. We assessed detection of viruses in the brain and damage to the integrity of the BBB as well as activation of neuroimmune responses in the brain. To test whether SARS-CoV-2 can indeed induce neuropathologic changes in the brain, we also assessed further patterns of demyelination and axonal damage. We describe our methods here in brief; details are provided in the Appendix (<https://wwwnc.cdc.gov/EID/article/29/11/23-0804-App1.pdf>).

We purchased fifteen 6-month-old female conventional beagles from Orient Bio, South Korea (<http://www.orient.co.kr>) and classified them into 3 groups: control (n = 3), infection (n = 6), and contact (n = 6). The dogs in the infection and contact groups were housed in 6 cages, each measuring 800 mm wide × 900 mm deep × 800 mm high.

To mimic natural infection, we implemented 2 infection models: intranasally inoculated dogs and dogs infected via horizontal transmission. We anesthetized 6 dogs in the infection group with 0.3 mg/kg of alfaxalone and then intranasally inoculated each dog with 10⁵ PFU of SARS-CoV-2 Delta variant. After the dogs regained consciousness and acclimated to the environment, each infected dog was placed in a cage with a dog from the contact group. To control

for any potential effects of the inoculation procedure or medium, we intranasally inoculated dogs in the control group with 500 μ L of Dulbecco Modified Eagle Medium. Veterinarians visually examined the dogs for clinical signs, including neurologic signs.

With the infection model established, we next investigated the neuropathologic changes in the brain. First, we confirmed the existence of viral particles in the brain because it is logical to consider that viral particles can migrate to and replicate in the brain, which would directly damage the brain. To confirm the presence of viral nucleic acid we used quantitative reverse-transcription PCR, and to confirm the presence of viral particles we used immunofluorescence assays.

For use in additional experiments, at 4, 7, 11, 14, 18, 21, 25, 28, 32, and 35 days postinfection (dpi), we collected nasopharyngeal, oropharyngeal, and fecal swab and blood samples from all dogs while they were under sedation. At each timepoint in the early (10, 12, and 14 dpi) and late (38, 40, and 42 dpi) periods of infection, dogs were sedated and euthanized by intravenous injection of supersaturated KCl and performed necrop-

sies (only 1 infected and 1 contact dog could be necropsied at each timepoint because of logistical constraints).

Samples underwent quantitative reverse transcription PCR, immunohistochemistry, immunofluorescence staining, ELISA, and plaque reduction neutralization test, as indicated (Appendix). We conducted all experiments in triplicate and express results as mean \pm SD. We plotted dose-response curves, and we performed Student *t*-tests by using Prism 8.0.1 (Graphpad software, <https://www.graphpad.com>). We set statistical significance at $p < 0.05$.

Results

We detected no significant changes in objective measurements of the dogs (body weight and temperature). No dogs exhibited apparent neurologic signs or respiratory signs resembling COVID-19 (Appendix).

Pathologic Changes in the Integrity of the BBB

In this study, we detected viral RNA in the brain during the early infection period only, not during the late infection period (Figure 2, panel A). We confirmed colocalization of the viral particles with neuronal cells

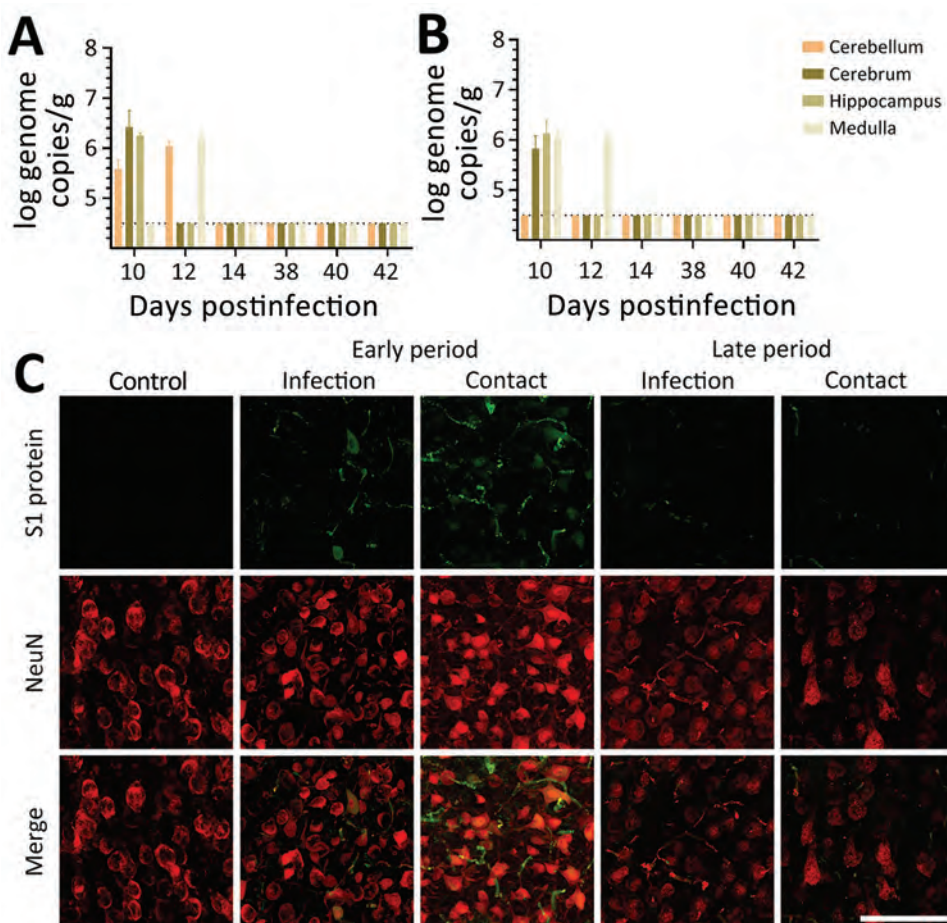


Figure 2. SARS-CoV-2 in the brain of dogs in study of the neurologic effects of SARS-CoV-2, showing transmission at an early stage of infection. A) Quantitative real-time PCR validation of the SARS-CoV-2 gene in the SARS-CoV-2-infected and contact groups of dogs, at each postinfection day. The dashed line indicates the regions where gene copy numbers of SARS-CoV-2 were considered negative. B) Representative fluorescent images of S1 protein (a marker of virus infection) and NeuN (a specific marker of neuronal cells) demonstrated SARS-CoV-2 infection in the canine brain sections of SARS-CoV-2-infected and contact dogs, at early and late days after infection. SARS-CoV-2-infected neuronal cells at the early stage of infection. At the late stage of infection, the presence of the virus appeared to diminish. Scale bars indicate 100 μ m.

by using an immunofluorescence assay with an antibody specific to the spike protein of the virus. As for viral RNA, we also detected viral particles only during the early infection period (Figure 2, panel B). Our observations indicate that SARS-CoV-2 may infect the brain during the early infection period and may be cleared by the later infection period.

Various reports suggest damaged brain vasculature in SARS-CoV-2-infected human patients, which is reported to be associated with the influx of peripheral molecules and activation of immune responses in the brain (13–16). In our study, we tested the pathologic changes in the canine brain vasculature by using an immunofluorescence assay with antibodies specific to the BBB compartments. For dogs infected with the virus, pathologic alterations in the BBB structure were noted, showing decreased signals of matrix proteins (laminin and collagen IV) and tight junction protein (claudin 5) (Figure 3, panel A). In dogs of both groups, those phenomena were prominently observed during late rather than early infection. In addition, PDGFR- β densities, which are markers for pericytes, were decreased in dogs of both groups during the early and late periods, indicating that the cellular components of the BBB were damaged by viral infection. Moreover, the infiltrations of fibrinogen and IgG were found in the parenchyma of the brain, indicating that viral infections breached the functional integrity of the BBB (Figure 3, panel B). Last, infiltration of CD4+ T cells was found in the brain by trespassing into the BBB matrix protein layer, suggesting severe damage to the BBB integrity and subsequent recruitment of these cells into the brain (Figure 3, panels C, D). Those observations indicate that SARS-CoV-2 infection could induce pathologic changes in the structural and functional integrity of the BBB. Such changes may allow entry of peripheral molecules and immune cells into the brain parenchyma during the early infection period. Collectively, the pathologic changes concur with the typical signs of small vessel disease (SVD).

Neuroinflammatory Responses in the Brain

When we tested whether SARS-CoV-2-induced damage of the BBB can induce neuroinflammatory responses, we stained brain sections with markers for glial activation, including glial fibrillary acidic protein and Iba-1, which are markers for activated astrocytes and microglial cells. Glial fibrillary acidic protein showed a statistically significant increase in the brain white matter of dogs in the infection and contact groups at the early and late periods, suggesting potential proinflammatory conditions in the brain (Figure 4, panel A). When we tested activation of microglial

cells (another major component of innate immune responses in the brain) by staining brain sections with an antibody specific to Iba-1 (a marker of activated microglial cells), we observed a significant increase in Iba-1-positive signals in the brain white matter of dogs from both groups during the early and late periods (Figure 4, panel B). However, we did not observe such increases in the gray matter, suggesting that the microglial cell activations were specific for white matter (Figure 4, panel C). Of note, we observed activated microglial cell clustering in several spots in the white matter from dogs in both groups. Overall, those observations suggest that BBB disruption mediated by infection with SARS-CoV-2 could elicit neuroinflammatory responses and further contribute to the progression of neurodegenerative pathology in canine brains.

Typical Signs of SVD-mediated Axonopathy

The early signs of SVD-mediated brain neurodegeneration are pathologic changes in axons and demyelination. To verify whether SARS-CoV-2 can induce these pathologic changes, we stained brain sections with antibodies against the neurofilament light chain (NFL). The intensities of NFL staining were significantly lower in the brain white matter of dogs in both groups at the early and late periods than in the uninfected control dogs (Figure 5, panels A, B). In addition, the pathologic changes in the structure and integrity of the NFL were evidenced by swelling and irregularity. Decreased NFL intensities were more severe in perivascular regions, as typical signs of SVD-mediated axonopathy.

Because demyelination is another hallmark of SVD, we assessed demyelination by using fluomyelin, a fluorescent marker for myelin. We observed a significantly lower intensity of fluomyelin in the brain white matter of dogs in the infection and contact groups during the early and late periods; NFL patterns were similar in both groups (Figure 5, panels C, D). Those changes were more evident in the perivascular area, identical to the NFL lesions. The axonopathy-like changes observed at the perivascular area of the white matter could be a consequence of SVD induction.

Pathologic Signs of Neurodegenerative Diseases, Represented by Tauopathy

To assess production of A β aggregation and test whether SVD-induced neuropathologic changes can further cause neurodegenerative signs, we stained brains with an amyloid β (6E10) antibody. However, we did not observe formation of A β aggregates in the brains of any dogs during the early or late periods (Appendix Figure 10, panel A). Next, to assess

tauopathy in the virus-infected brains, we stained brain sections with different types of phosphorylated tau. Using a p-Tau 181 antibody, we did not observe

positive signals for phosphorylated tau in any dogs (Appendix Figure 10, panel B). However, we detected phosphorylation of tau at Ser202/Thr205 by using an

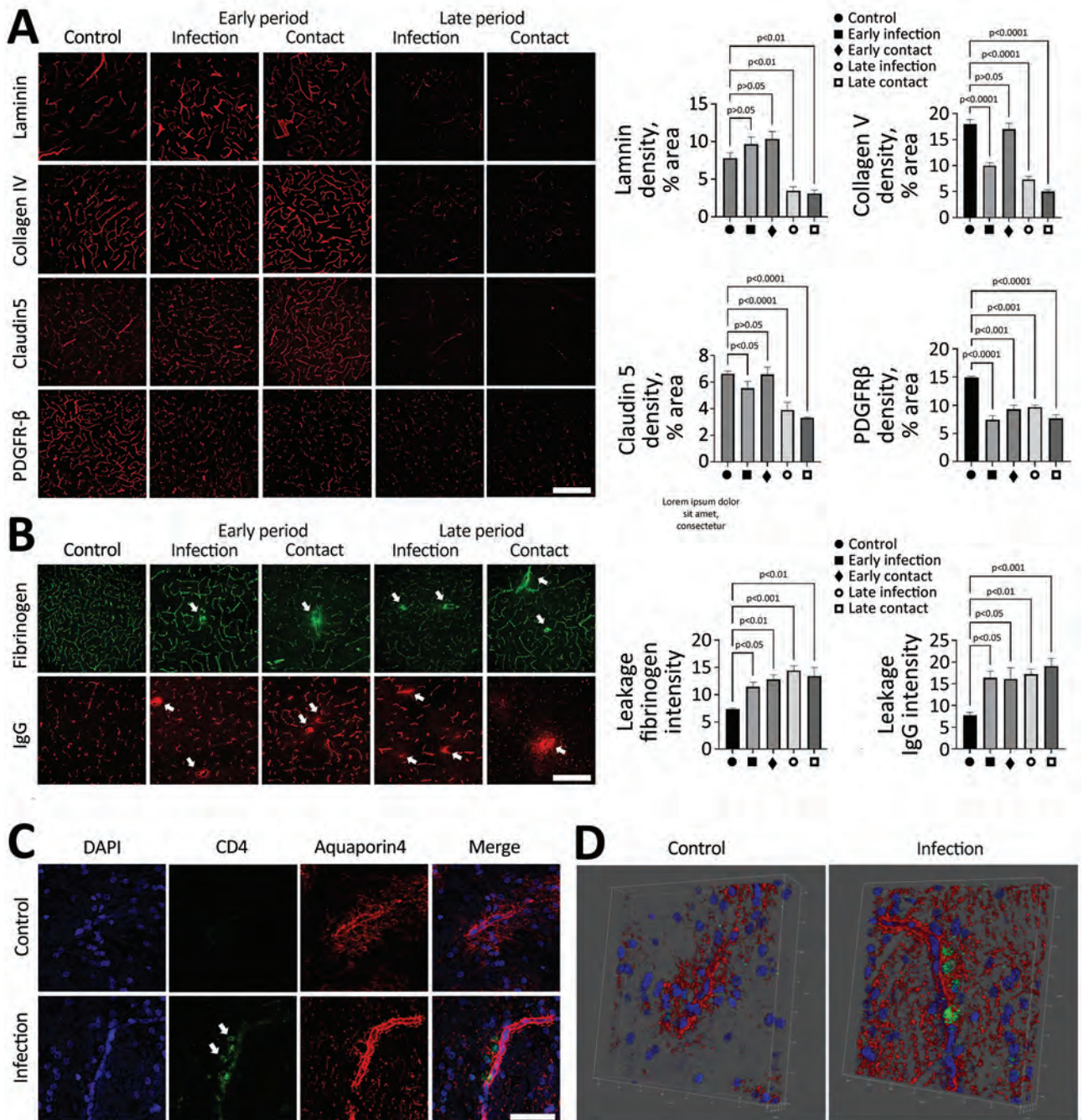


Figure 3. SARS-CoV-2 infection disrupting the blood–brain barrier (BBB) and immune cells infiltrating the brains of infected dogs in study of the neurologic effects of SARS-CoV-2 transmitted among dogs. A) Representative fluorescent images and statistical results of vascular markers including laminin, claudin 5, collagen IV, and PDGFR-β staining of canine brain sections derived from SARS-CoV-2–infected and contact dogs at early and late days after infection. Scale bar indicates 200 μm. B) Brain sections from SARS-CoV-2–infected and contact dogs stained with fibrinogen (green) and IgG (red), which represent BBB leakage staining, at early and late days after infection. Scale bar indicates 200 μm. C) Representative fluorescent images of the brain sections stained with the CD4 (green) and aquaporin 4 (red), which are markers of CD4-positive T cells and astrocytic end foot, respectively. The CD4-positive cells were infiltrated in the brain parenchyma (white arrows) in the SARS-CoV-2–infected group. Scale bar indicates 50 μm. D) Representative 3D images of CD4 (green) and aquaporin 4 (red). Statistical significance was determined using a 1-way analysis of variance. Data are presented as mean ± SEM.

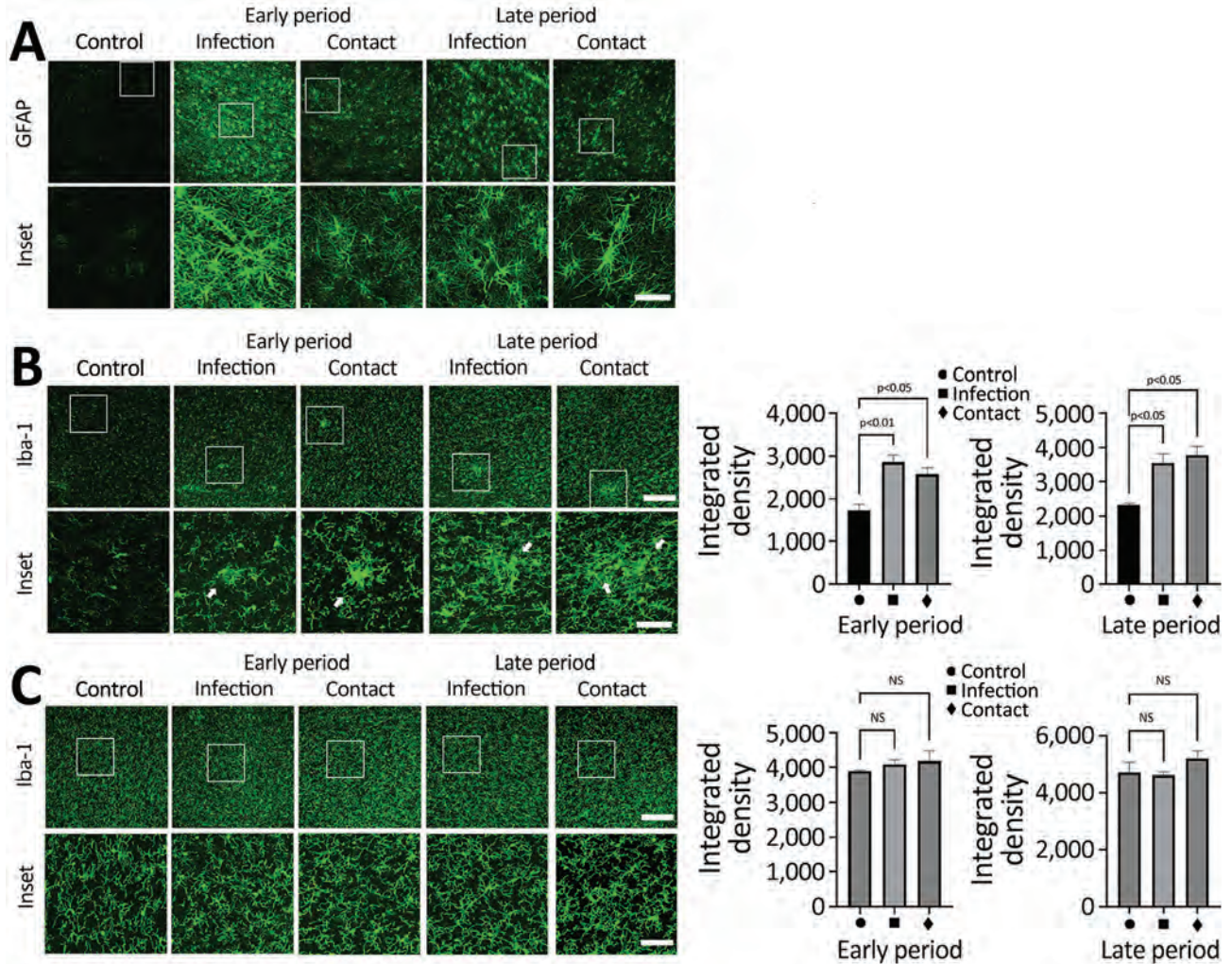


Figure 4. SARS-CoV-2 induces activation of microglial cells in the brain white matter in a region-specific manner in SARS-CoV-2–infected and contact dogs in study of the neurologic effects of SARS-CoV-2 transmitted among dogs. A) Representative fluorescent images of glial fibrillary acidic protein (activation astrocyte marker, green) staining of canine brain sections derived from SARS-CoV-2–infected and contact groups at early and late days after infection. Scale bars indicate 200 μ m; in insets, 50 μ m. B) Representative fluorescent images and statistical results of Iba-1 (a marker of microglia; green) staining of canine brain white matter sections derived from SARS-CoV-2–infected and contact dogs at early and late dpi. Scale bars indicate 200 μ m; in insets, 50 μ m. C) Representative fluorescent images and statistical results of Iba-1 (a marker of microglia, green) staining of canine brain gray matter sections derived from SARS-CoV-2–infected and contact dogs at early and late dpi. Scale bars indicate 200 μ m; in insets, 50 μ m. Statistical significance was determined using a 1-way analysis of variance. Data in graphs are presented as means \pm SEM.

AT8 antibody in the brains of dogs in the infection group during the early period and dogs in the infection and contact groups during the late period. Those results suggest that SARS-CoV-2 infection could induce accumulation of the pathologic form of tau in a site-specific manner (Figure 5, panel E). Last, we used the number of neuronal cells to determine whether those pathologic neurodegenerative signatures are associated with loss of neuronal cells. We did not observe statistically significant changes in the number of cortical neurons in the brains of dogs from the infection and contact groups during the early period

(Figure 5, panels F–H). However, we observed decreased numbers of neuronal cells in the infection and contact groups during the late period. Therefore, degenerative changes such as tauopathy and decreased numbers of neuronal cells in the virus-infected brains seemed to be induced after elicitation of pathologic drivers, including BBB damage, glial activation, and axonopathy, as consequences of SVD.

Discussion

Overall, our study demonstrates solid experimental evidence that SARS-CoV-2 can infect dogs and

be transmitted to others by direct contact, producing pathologic brain changes even without prominent signs. Pathologic changes in the lung and brain were observed in dogs of both groups, providing additional evidence of virus transmission. Of note, SARS-CoV-2 infection has been reported to cause long-term pathologic effects even after the virus is cleared from the main organs of the body (17). Our study provides evidence that SARS-CoV-2 infection can damage the brain as well as the lungs in dogs at early and later stages of infection, suggesting a high potential for a long-lasting COVID-19–like syndrome to develop in affected dogs.

We detected SARS-CoV-2 in secretions from the nasopharynx and oropharynx of dogs in both the infection and contact groups, albeit at a low percentage. Remarkably, we found that the viral titers were higher in the nasal and oral mucosa of dogs in the contact group than in those in the infection group. That finding could

be attributed to the role of the nasal and oral cavities as routes of virus entry for the contact group, resulting in higher replication of the virus at these entry points (18). We observed that during the early stages of infection, dogs in the contact group exhibited more severe inflammatory responses in the trachea and bronchioles than did those in the infection group. Those findings are consistent with results of previous studies that have shown that contact transmission can result in higher levels of virus titers and lead to more rapid onset of pathologic changes in the upper respiratory tract (19,20).

Seroconversion in dogs after SARS-CoV-2 infection was observed as early as 4 dpi; the rapid seroconversion may be associated with the absence of clinical signs (21). Antibody levels peaked a few days later in dogs in the contact group than in dogs in the infection group, suggesting later virus transmission from the virus-infected dogs. Neutralizing

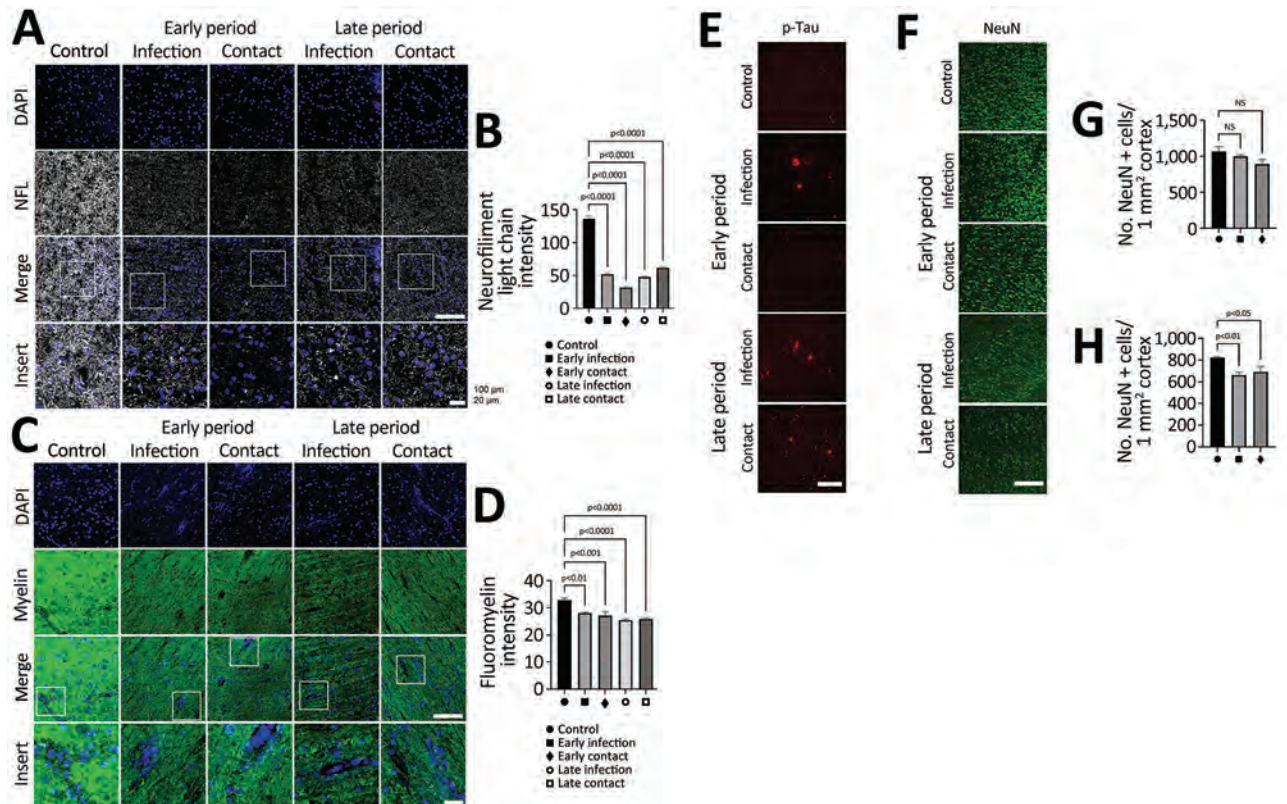


Figure 5. SARS-CoV-2 infection causing perivascular demyelination in the brain in dogs in study of the neurologic effects of SARS-CoV-2 transmitted among dogs. A, B) Representative fluorescent images and statistical analysis results of NFL (a marker of neurofilament light chain; gray) staining of canine brain white matter sections derived from SARS-CoV-2 infected and contact dogs at early and late dpi. Scale bar indicates 200 μ m. Overall images from infected dogs demonstrate irregular axonal morphology compared with that of control dogs. Single-layer slice images. Scale bar indicates 20 μ m. C, D) Representative fluorescent images and statistical analysis results of myelin (fluoromyelin; green) and DAPI (blue) staining of canine brain white matter sections derived from SARS-CoV-2–infected and contact dogs at early and late dpi. Scale bar indicates 200 μ m. E) Representative fluorescent images of p-tau (red) staining of canine brain gray matter sections derived from SARS-CoV-2–infected and contact dogs at early and late dpi. Scale bar indicates 200 μ m. F–H) Representative fluorescent images (F) and statistical analysis results (G, H) of NeuN (a marker of neuron; green) staining of canine brain gray matter sections derived from SARS-CoV-2–infected and contact dogs at early (G) and late (H) infection. Scale bar indicates 200 μ m. Statistical significance was determined using a 1-way analysis of variance. Data are presented as mean \pm SEM. NS, not significant.

antibody titers against SARS-CoV-2 strongly correlate with antibody titers of the spike protein, highlighting the spike protein as a crucial target for the humoral immune response (R value >0.7; $p < 0.001$).

The lung alveolar septum of infected dogs was thickened overall, caused by infiltration of immune cells that indicate interstitial pneumonia (e.g., mononuclear cells, neutrophils, and macrophages) (22,23), associated with the presence of neutrophil elastase-positive cells and Iba-1-positive cells. Neutrophil elastase and Iba-1 levels increase in response to SARS-CoV-2 infection (22,24). Neutrophil elastase-positive and Iba-1-positive cells were found infiltrated around the blood vessels, indicating perivascularitis in SARS-CoV-2 infected dogs as in other hosts (22,25).

Brain damage induced by viral infection has been reported from various nonneurotrophic viruses, including HIV (17,26). Contrary to previous beliefs, accumulating evidence argues that SARS-CoV-2 can induce pathologic changes in the brains of several hosts, including humans, although the detailed mechanisms of those pathologies are still elusive. We analyzed the histopathologic changes in the brains on the basis of those uncertain arguments. Of note, we observed drastic pathologic changes in the dog brains, although the animals did not exhibit any neurologic signs. One of the most prominent features of brain pathology was the BBB damage observed during early infection and maintained until later infection. Typical features of vascular damage observed from SVD were changes in the level of tight junction proteins, decreased levels of laminin, and reduced pericyte coverage (27). SVD involves functional and structural dysfunctions of the brain vasculature, demonstrating white matter hyperintensities, microbleeding, and increased perivascular spaces. Moreover, SVD induces increased influx of peripheral blood factors and immune cells into the brain. Our finding of initial pathologic features of the BBB commonly observed in SVD in the brains of SARS-CoV-2-infected dogs strongly supports our hypothesis that the virus can induce SVD in dog brains. Several human studies supporting our observations also reported these pathologic features of the BBB similarly found in SVD (26,28,29).

SVD induces an influx of peripheral molecules and a favorable environment for producing large amounts of reactive oxygen species that activate microglial cells and astrocytes—hallmarks of neuroinflammatory responses. In our study, we specifically observed activation of glial cells in the white matter of the brains of the SARS-CoV-2-infected dogs, suggesting the neuroinflammatory conditions that SARS-CoV-2-mediated SVD might induce. The activation of

microglial cells has also been observed in humanized ACE2 mice and brains from different animal species, including nonhuman primates (30,31). The marked axonopathy in the white matter and the preferentially increased activity of glial cells in this region strongly suggest correlations between the glial activation and development of axonopathy potentially mediated by development of SVD by SARS-CoV-2 infection. Furthermore, activation of the astrocytes and microglial cells was maintained up to 40 dpi, even when the virus was cleared from the brain. That finding strongly suggests that the glial cells activated by SARS-CoV-2 potentially harm axons or other components of neuronal cells, even when virus is absent in the brain. That topic could be the focus of future research that requires further *in vitro*/*in vivo* studies to reveal the mechanistic link between glial activation and neuronal damage mediated by SARS-CoV-2 infection.

Tau phosphorylation is the hallmark of Alzheimer's disease. Tau is the family of the microtubule-associated protein tau and functions in the delivery of synaptic vesicles required for synaptic transmission; phosphorylation of tau causes loss of this property, but the mechanism remains elusive (32). There are multiple phosphorylation sites on the tau protein, and our study shows the specific phosphorylation of Ser202/Thr205, detected by using the AT8 antibody (33). Detection of phosphorylated tau suggests a high probability of developing signs of neurodegenerative diseases in the SARS-CoV-2-infected brain. A recent study has shown the correlation between the development of SVD and the accumulation of phosphorylated tau, supporting the finding that development of phosphorylated tau could be oriented by SARS-CoV-2-associated SVD (34,35).

Long-term brain damage induced by SARS-CoV-2 has become a major topic for research of long COVID syndromes in humans (36). It has been reported that $\approx 10\%$ of SARS-CoV-2-infected persons experience neurologic signs/symptoms, suggesting potential neurotrophic characteristics of this virus (37). According to recent retrospective studies that used UK Biobank data (<https://www.ukbiobank.ac.uk>), shrinkage in the brain cortex and decreased cognitive function have been reported for human patients after recovery from SARS-CoV-2 infection (38). Moreover, post-mortem human brain tissue analysis demonstrated increased activity of glial cells, proinflammatory immune responses, neuronal damage, and BBB damage, enabling peripheral immune cells to infiltrate, strongly suggesting neuropathologic changes induced by SARS-CoV-2 infection (39). However, those pathologic changes were analyzed mainly in brain samples from patients with severe neurologic sign/symptoms;

neuropathologic changes in asymptomatic patients are still elusive. From that perspective, our study has value as translational research to predict neuropathologic changes in the early phase of asymptomatic SARS-CoV-2 infection in humans because we have observed the kinetic pathologic changes in the brains of dogs that did not show any neurologic signs. Compared with other animal models, dogs are genetically similar to humans and their brain structures are similar to those of humans, making our extrapolation more reliable. According to our results, the brains of dogs infected with SARS-CoV-2 demonstrate severe BBB disruptions and consequent SVD-like pathologic signs, including axonopathy, glial activation, and potential neurodegenerative changes even without neurologic signs. That evidence strongly suggests that even asymptomatic SARS-CoV-2 patients might have neuropathologic changes in their brains, which could develop into severe neurologic disorders later in life.

Among the merits of our study in terms of translational research of SARS-CoV-2-induced neuropathologic changes, we compared 2 infection routes: direct intranasal infection and horizontal transmission models that can mimic more natural infection routes. With that comparison, we determined that neuropathologic changes can be induced via both exposure routes, providing valuable information that owners of companion animals potentially face SARS-CoV-2-associated neurologic disorders. Second, we studied dogs, which are a more advanced species than rodents, to provide neuropathologic data that are closer to data for humans and more relevant. Moreover, our data suggest that neuropathologic changes can be induced in dogs. Last, we found that the neuroinflammatory responses were more prominently observed in the white matter area than the gray matter area, suggesting that the neuroinflammatory responses induced by SARS-CoV-2 differ by brain region. Overall, these data can be used as translational research data to interpret the potential neuropathologic changes that may be observed in humans.

This study was supported by a fund from of Animal and Plant Quarantine Agency, South Korea (project code no. Z-1543085-2022-23-02) and KBRI basic research program through Korea Brain Research Institute funded by the Ministry of Science and ICT (23-BR-04-01 to D.G.K.)

D.-H.K., D.-Y.K., and I.-S.C. conceived and validated the study. Y.-K.S. and O.-K.K. designed the study. D.-H.K., D.-Y.K., K.-S.K., S.-H.H., H.-J.G., J.-H.K., and K.-B.L. contributed to preparing and conducting the experiments. D.-H.L., J.-B.L., S.-Y.P., C.-S.S., S.-W.L., Y.-K.C., and I.-S.C. supervised the experiments. D.-H.K., D.-Y.K., K.-S.K., D.-G.K., and I.-S.C. wrote the main manuscript and prepared

the figures. I.-S.C. contributed to funding acquisition. All authors reviewed the final manuscript and approved the submission. All data are presented in the paper and available from the corresponding authors on request.

About the Author

D.-H. Kim is a PhD candidate at Konkuk University in Seoul. His primary research interests include diagnostics, vaccine development, and antiviral therapeutics, with a particular emphasis on zoonotic viruses.

References

1. Abdel-Moneim AS, Abdelwhab EM. Evidence for SARS-CoV-2 infection of animal hosts. *Pathogens*. 2020;9:529. <https://doi.org/10.3390/pathogens9070529>
2. Mahdy MAA, Younis W, Ewaida Z. An overview of SARS-CoV-2 and animal infection. *Front Vet Sci*. 2020;7:596391. <https://doi.org/10.3389/fvets.2020.596391>
3. Lee DH, Helal ZH, Kim J, Hunt A, Barbieri A, Tocco N, et al. Severe acute respiratory syndrome coronavirus 2 (SARS-CoV-2) in a dog in Connecticut in February 2021. *Viruses*. 2021;13:2141. <https://doi.org/10.3390/v13112141>
4. Sit THC, Brackman CJ, Ip SM, Tam KWS, Law PYT, To EMW, et al. Infection of dogs with SARS-CoV-2. *Nature*. 2020;586:776–8. <https://doi.org/10.1038/s41586-020-2334-5>
5. Bosco-Lauth AM, Hartwig AE, Porter SM, Gordy PW, Nehring M, Byas AD, et al. Experimental infection of domestic dogs and cats with SARS-CoV-2: pathogenesis, transmission, and response to reexposure in cats. *Proc Natl Acad Sci U S A*. 2020;117:26382–8. <https://doi.org/10.1073/pnas.2013102117>
6. Lyoo KS, Yeo YH, Lee SG, Yeom M, Lee JY, Kim KC, et al. Susceptibility to SARS-CoV-2 and MERS-CoV in beagle dogs. *Animals (Basel)*. 2023;13:624. <https://doi.org/10.3390/ani13040624>
7. Lyoo KS, Lee H, Lee SG, Yeom M, Lee JY, Kim KC, et al. Experimental infection and transmission of SARS-CoV-2 Delta and Omicron variants among beagle dogs. *Emerg Infect Dis*. 2023;29:782–5. <https://doi.org/10.3201/eid2904.221727>
8. Zhang Z, Zhang Y, Liu K, Li Y, Lu Q, Wang Q, et al. The molecular basis for SARS-CoV-2 binding to dog ACE2. *Nat Commun*. 2021;12:4195. <https://doi.org/10.1038/s41467-021-24326-y>
9. Oude Munnink BB, Sikkema RS, Nieuwenhuijse DF, Molenaar RJ, Munger E, Molenkamp R, et al. Transmission of SARS-CoV-2 on mink farms between humans and mink and back to humans. *Science*. 2021;371:172–7. <https://doi.org/10.1126/science.abe5901>
10. Xu E, Xie Y, Al-Aly Z. Long-term neurologic outcomes of COVID-19. *Nat Med*. 2022;28:2406–15. <https://doi.org/10.1038/s41591-022-02001-z>
11. Rass V, Beer R, Schiefecker AJ, Lindner A, Kofler M, Ianosi BA, et al. Neurological outcomes 1 year after COVID-19 diagnosis: a prospective longitudinal cohort study. *Eur J Neurol*. 2022;29:1685–96. <https://doi.org/10.1111/ene.15307>
12. Fleischer M, Köhrmann M, Dolf S, Szepanowski F, Schmidt K, Herbstreit F, et al. Observational cohort study of neurological involvement among patients with SARS-CoV-2 infection. *Ther Adv Neurol Disord*. 2021;14:1756286421993701. <https://doi.org/10.1177/1756286421993701>
13. Tsvigoulis G, Palaodimou L, Zand R, Lioutas VA, Krogias C, Katsanos AH, et al. COVID-19 and cerebrovascular diseases:

- a comprehensive overview. Vol. 13. In: *Therapeutic Advances in Neurological Disorders*. Newbury Park (CA): SAGE Publications Ltd; 2020.
14. Mirfazeli FS, Sarabi-Jamab A, Jahanbakhshi A, Kordi A, Javadnia P, Shariat SV, et al. Neuropsychiatric manifestations of COVID-19 can be clustered in three distinct symptom categories. *Sci Rep*. 2020;10:20957. <https://doi.org/10.1038/s41598-020-78050-6>
 15. Shabani Z. Demyelination as a result of an immune response in patients with COVID-19. Vol. 121. In: *Acta Neurologica Belgica*. Berlin: Springer Science and Business Media Deutschland GmbH; 2021. p. 859–66.
 16. Moonis G, Filippi CG, Kirsch CFE, Mohan S, Stein EG, Hirsch JA, et al. The spectrum of neuroimaging findings on CT and MRI in adults with COVID-19. *AJR Am J Roentgenol*. 2021;217:959–74. <https://doi.org/10.2214/AJR.20.24839>
 17. Han C, Duan C, Zhang S, Spiegel B, Shi H, Wang W, et al. Digestive symptoms in COVID-19 patients with mild disease severity: clinical presentation, stool viral RNA testing, and outcomes. *Am J Gastroenterol*. 2020;115:916–23. <https://doi.org/10.14309/ajg.000000000000664>
 18. Huang N, Pérez P, Kato T, Mikami Y, Okuda K, Gilmore RC, et al. SARS-CoV-2 infection of the oral cavity and saliva. *Nature Medicine*. 2021;27:892–903. <https://doi.org/10.1038/s41591-021-01296-8>
 19. Halfmann PJ, Hatta M, Chiba S, Maemura T, Fan S, Takeda M, et al. Transmission of SARS-CoV-2 in domestic cats. *N Engl J Med*. 2020;383:592–4. <https://doi.org/10.1056/NEJMc2013400>
 20. Port JR, Yinda CK, Owusu IO, Holbrook M, Fischer R, Bushmaker T, et al. SARS-CoV-2 disease severity and transmission efficiency is increased for airborne compared to fomite exposure in Syrian hamsters. *Nat Comm*. 2021;12:1–15. <https://doi.org/10.1038/s41467-021-25156-8>
 21. Jonczyk R, Stanislawski N, Seiler LK, Blume H, Heiden S, Lucas H, et al. Combined prospective seroconversion and PCR data of selected cohorts indicate a high rate of subclinical SARS-CoV-2 infections – an open observational study in Lower Saxony, Germany. *Microbiol Spectr*. 2022;10:e0151221. <https://doi.org/10.1128/spectrum.01512-21>
 22. Patania OM, Chiba S, Halfmann PJ, Hatta M, Maemura T, Bernard KA, et al. Pulmonary lesions induced by SARS-CoV-2 infection in domestic cats. *Vet Pathol*. 2022;59:696–706. <https://doi.org/10.1177/03009858211066840>
 23. Clancy CS, Shaia C, Munster V, de Wit E, Hawman D, Okumura A, et al. Histologic pulmonary lesions of SARS-CoV-2 in 4 nonhuman primate species: an institutional comparative review. *Vet Pathol*. 2022;59:673–80. <https://doi.org/10.1177/03009858211067468>
 24. Kinnare N, Hook JS, Patel PA, Monson NL, Moreland JG. Neutrophil extracellular trap formation potential correlates with lung disease severity in COVID-19 patients. *Inflammation*. 2022;45:800–11. <https://doi.org/10.1007/s10753-021-01585-x>
 25. Liu F, Han K, Blair R, Kenst K, Qin Z, Upcin B, et al. SARS-CoV-2 infects endothelial cells in vivo and in vitro. *Front Cell Infect Microbiol*. 2021;11:701278. <https://doi.org/10.3389/fcimb.2021.701278>
 26. Barbosa-Silva MC, Santos LE, Rangel B. The impact of non-neurotropic influenza strains on the brain: a role for microglial priming? *J Neurosci*. 2018;38:7758–60. <https://doi.org/10.1523/JNEUROSCI.1368-18.2018>
 27. Li Q, Yang Y, Reis C, Tao T, Li W, Li X, et al. Cerebral small vessel disease. *Cell Transplant*. 2018;27:1711–22. <https://doi.org/10.1177/0963689718795148>
 28. Gyanwali B, Lui B, Tan CS, Chong EJY, Vrooman H, Chen C, et al. Cerebral microbleeds and white matter hyperintensities are associated with cognitive decline in an Asian memory clinic study. *Curr Alzheimer Res*. 2021;18:399–413. <https://doi.org/10.2174/1567205018666210820125543>
 29. Østergaard L, Engedal TS, Moreton F, Hansen MB, Wardlaw JM, Dalkara T, et al. Cerebral small vessel disease: capillary pathways to stroke and cognitive decline. *J Cereb Blood Flow Metab*. 2016;36:302–25. <https://doi.org/10.1177/0271678X15606723>
 30. Rutkai I, Mayer MG, Hellmers LM, Ning B, Huang Z, Monjure CJ, et al. Neuropathology and virus in brain of SARS-CoV-2 infected non-human primates. *Nat Commun*. 2022;13:1745. <https://doi.org/10.1038/s41467-022-29440-z>
 31. Seehusen F, Clark JJ, Sharma P, Bentley EG, Kirby A, Subramaniam K, et al. Neuroinvasion and neurotropism by SARS-CoV-2 variants in the K18-hACE2 mouse. *Viruses*. 2022;14:1020. <https://doi.org/10.3390/v14051020>
 32. Medeiros R, Baglietto-Vargas D, LaFerla FM. The role of tau in Alzheimer's disease and related disorders. *CNS Neurosci Ther*. 2011;17:514–24. <https://doi.org/10.1111/j.1755-5949.2010.00177.x>
 33. Neddens J, Temmel M, Flunkert S, Kerschbaumer B, Hoeller C, Loeffler T, et al. Phosphorylation of different tau sites during progression of Alzheimer's disease. *Acta Neuropathol Commun*. 2018;6:52. <https://doi.org/10.1186/s40478-018-0557-6>
 34. Kapasi A, Yu L, Petyuk V, Arfanakis K, Bennett DA, Schneider JA. Association of small vessel disease with tau pathology. *Acta Neuropathol*. 2022;143:349–62. <https://doi.org/10.1007/s00401-021-02397-x>
 35. Agrawal S, Yu L, Kapasi A, James BD, Arfanakis K, Barnes LL, et al. Limbic-predominant age-related TDP-43 encephalopathy neuropathologic change and microvascular pathologies in community-dwelling older persons. *Brain Pathol*. 2021;31:e12939. <https://doi.org/10.1111/bpa.12939>
 36. Washington University in St. Louis. COVID-19 infections increase risk of long-term brain problems: strokes, seizures, memory and movement disorders among problems that develop in first year after infection. *Science Daily* [cited 2023 Apr 10]. <https://www.sciencedaily.com/releases/2022/09/220922124408.htm>
 37. Ozel T, Erdem NS, Ünal A, Yalçın AN, İnan D, İlhanlı N, et al. Neurological manifestations and mortality in hospitalized coronavirus disease 2019 patients. *Neurological Sciences and Neurophysiology*. 2022;39:138–145. http://doi.org/10.4103/nsn.nsn_117_21
 38. Douaud G, Lee S, Alfaro-Almagro F, Arthofer C, Wang C, McCarthy P, et al. SARS-CoV-2 is associated with changes in brain structure in UK Biobank. *Nature*. 2022;604:697–707. <https://doi.org/10.1038/s41586-022-04569-5>
 39. Matschke J, Lütgehetmann M, Hagel C, Spherhake JP, Schröder AS, Edler C, et al. Neuropathology of patients with COVID-19 in Germany: a post-mortem case series. *Lancet Neurol*. 2020;19:919–29. [https://doi.org/10.1016/S1474-4422\(20\)30308-2](https://doi.org/10.1016/S1474-4422(20)30308-2)

Address for correspondence: In-Soo Choi, Konkuk University, Veterinary Infectious Diseases, #1 Hwayang-dong Gwanjin-gu, Seoul 143-701, South Korea; email: ischoi@konkuk.ac.kr; Do-Geun Kim, Dementia Research Group, Korea Brain Research Institute, 61 Cheomdaro, Sinseo, Donggu, Daegu, South Korea; email: kimvet0911@kbri.re.kr

Environmental Persistence and Disinfection of Lassa Virus

Marlee Shaffer,¹ Robert J. Fischer,¹ Shane Gallogly, Olivia Ginn, Vincent Munster, Kyle Bibby

Lassa fever, caused by Lassa virus (LASV), is endemic to West Africa, where $\approx 300,000$ illnesses and $\approx 5,000$ deaths occur annually. LASV is primarily spread by infected multimammate rats via urine and fomites, highlighting the need to understand the environmental fate of LASV. We evaluated persistence of LASV Josiah and Sauerwald strains on surfaces, in aqueous solutions, and with sodium hypochlorite disinfection. Tested strains were more stable in deionized water (first-order rate constant [k] for Josiah, 0.23 days; for Sauerwald, k = 0.34 days) than primary influent wastewater (Josiah, k = 1.3 days; Sauerwald, k = 1.9 days). Both strains had similar decay rates on high-density polyethylene (Josiah, k = 4.3 days; Sauerwald, k = 2.3 days) and stainless steel (Josiah, k = 5.3 days; Sauerwald, k = 2.7 days). Sodium hypochlorite was highly effective at inactivating both strains. Our findings can inform future risk assessment and management efforts for Lassa fever.

Lassa fever is an acute viral hemorrhagic illness caused by Lassa virus (LASV), an enveloped RNA virus of the *Arenaviridae* family (1). Lassa fever is endemic to West Africa, causing $\approx 300,000$ illnesses and $\approx 5,000$ deaths annually (1,2). Approximately 80% of Lassa fever cases result in mild symptoms; however, the remaining 20% are serious infections that cause hemorrhaging and vomiting and simultaneously affect several organs, including the kidneys, liver, and spleen, which can have lifelong effects for survivors (3). The overall mortality rate for Lassa fever is 1%; however, patients hospitalized with a severe infection have an increased mortality rate of 15%–20% (1,4).

The natural reservoir of LASV is the multimammate rat, *Mastomys natalensis*, which is found in 50%–98% of households in West Africa and puts ≈ 58 million persons at risk for infection (2,3,5). LASV outbreaks have primarily been limited to 2 distinct

regions, Nigeria and the Mano River Basin, which comprises areas of Liberia, Guinea, and Sierra Leone (3,6). The outbreaks in Nigeria were caused by lineages II and III, and the outbreaks in the Mano River Basin were caused by lineage IV (3,6). Ecologic niche models predicting expansion of suitable environmental conditions for LASV, coupled with population increases in those areas, estimate a 761% increase in the risk for infection among populations in endemic areas (6). During 2012–2022, Lassa fever cases have increased, likely because of an increasing population, urbanization, and environmental changes (7). Concurrently, the range and number of known lineages have also increased; new lineages were discovered in Mali in 2009 and Benin in 2014 (8,9).

Transmission of LASV is primarily through direct contact with fomites contaminated with rat urine or feces or through inhalation (2,10). Secondary person-to-person transmission can occur from direct contact with bodily fluids of infected persons, specifically in healthcare settings that have inadequate infection prevention and control measures (11). Thus, understanding the environmental persistence of LASV is critical for mitigation and control efforts.

The World Health Organization lists LASV as a priority pathogen with pandemic potential because the virus has a relatively long incubation period and populations outside of endemic areas lack prior immunity (12). Infected persons shed the virus in bodily fluids for up to 3 months (10). No standard practice exists for disposing of LASV infectious waste, leading to concerns about further environmental transmission.

Limited research evaluating the environmental persistence and disinfection of LASV is available, creating a critical gap in understanding the potential for continued environmental transmission. We investigated the persistence of 2 LASV strains representing lineages II and IV, on surfaces, and in water and wastewater. We then assessed LASV disinfection

Author affiliations: University of Notre Dame, Notre Dame, Indiana, USA (M. Shaffer, O. Ginn, K. Bibby); National Institutes of Health, Hamilton, Montana, USA (R.J. Fischer, S. Gallogly, V. Munster)

DOI: <https://doi.org/10.3201/eid2911.230678>

¹These first authors contributed equally to this article.

with sodium hypochlorite to assess a potential LASV management approach.

Materials and Methods

We used the Josiah strain to represent lineage IV and the Sauerwald strain to represent lineage II. All experiments were conducted in a Biosecurity Level 4 facility.

Surface Persistence Experiments

We conducted solid surface persistence experiments similar to those previously described (13). In brief, for each time point, we placed three 4-cm diameter disks of either stainless steel or high-density polyethylene (HDPE) into individual wells of a 6-well plate. We evenly distributed 10^6 50% tissue culture infectious dose (TCID₅₀) of either Josiah or Sauerwald LASV isolates in the cell-free medium on the disks, and allowed the plates to air dry at 20°C. At each time point, we placed 450 µL of Dulbecco's Modified Eagle Medium (DMEM; Sigma-Aldrich, <https://www.sigmaaldrich.com>), supplemented with heat-inactivated fetal bovine serum (FBS; GIBCO/ThermoFisher, <https://www.thermofisher.com>) and 2% Pen/Strep (GIBCO) to a final concentration of 50 U/mL penicillin and 50 µg/mL streptomycin, onto the surface and gently agitated to free the surface-bound virus. Then we added L-glutamine (GIBCO) to a final concentration of 2 mmol in an appropriately labeled 2 mL screw top vial and froze at -80°C. We then determined viral titers for each surface.

Aqueous Persistence Experiments

We conducted all experiments in triplicate and at 20°C. We added Josiah and Sauerwald LASV stocks to each replicate of deionized water and primary influent wastewater to achieve a final concentration of 10^6 TCID₅₀/mL (Appendix, <https://wwwnc.cdc.gov/EID/article/23-0678-App1.pdf>). We collected samples daily for 5 days. At each time point, including zero, we added 50 µL of the aqueous matrix from each of the bulk wastewater or deionized water vials into 450 µL of DMEM (Sigma-Aldrich), modified as described above. Then we added L-glutamine (GIBCO) to a final concentration of 2 mmol in an appropriately labeled 2 mL screw top vial and froze at -80°C. We used 50 µL of the nonspiked aqueous matrix for negative controls. We then determined viral titers for each replicate.

Aqueous Disinfection Experiments

We used primary influent wastewater for the aqueous disinfection experiments to replicate the type of wastewater in low- and middle-income countries in which

emergency disinfection for LASV would be used. We assessed the initial chlorine demand of the wastewater matrix by using the Chlorine (Free and Total) Test Kit (Hach, <https://www.hach.com>) (14). We assessed LASV disinfection in triplicate in wastewater for Josiah and Sauerwald isolates at 1 mg/L, 5 mg/L, and 10 mg/L of sodium hypochlorite. In the top row of a deep-well 96-well plate, we spiked virus into wastewater or deionized water to an initial concentration of 1:1,000,000. We removed an initial sample, diluted 1:10 in DMEM, and froze at -80°C. We then added sodium hypochlorite to each well to achieve the desired sodium hypochlorite concentrations. We took the time zero sampling ≈20 seconds after adding chlorine to enable sample mixing. We removed 50-µL samples at 1, 5, 15, and 30 minutes, mixed with 50 µL of sodium thiosulfate (134 nmol), and concentration matched (w:w) with sodium hypochlorite (40 nmol) to quench any remaining free chlorine. We then added that mixture to 400 µL of DMEM to achieve a final 1:10 dilution before freezing at -80°C until titrated.

Virus Titration

To assess the concentration of viable virus, we performed TCID₅₀ by using 4 10× dilution series for each sample. We then incubated Vero E6 cells with the virus dilutions for 1 h at 37°C, then removed the virus from the 2 highest concentrations, rinsed 2 times with PBS, and added 200 µL of fresh culture medium. We also added 100 µL of fresh culture medium to each of the remaining wells in the plate. We incubated the plates at 37°C for 7 days, inspected for cytopathic effect, and scored plates by using the Spearman-Kärber method.

Statistical Analysis

We analyzed the decay of infectious LASV strains for all experiments by using a first-order decay model and excluded data points below the limit of detection for the assay, as previously described (13–16). In the decay models, each plotted point represents the mean of 3 independent experimental replicates run concurrently, and the error bars show the standard deviation. We performed all plotting, regressions, and statistical analyses by using R Studio 2022.07.2 (R Foundation for Statistical Computing, <https://www.r-project.org>).

Results

Persistence of Lassa Virus on Surfaces

Stainless steel and high-density polyethylene (HDPE) are commonly used nonporous materials for hospital

Table 1. First-order decay rate constants and decimal reductions for 2 virus strains on different surfaces in study of environmental persistence and disinfection of Lassa virus*

Measurements	High-density polyethylene		Stainless steel	
	Josiah strain	Sauerwald strain	Josiah strain	Sauerwald strain
<i>k</i> , d	4.3 (3.5–5.1)	2.3 (0.50–4.1)	5.3 (4.3–6.3)	2.7 (2.0–3.4)
D value, d	0.54 (0.45–0.66)	1.0 (0.56–4.6)	0.43 (0.37–0.54)	0.85 (0.68–1.2)

*Values are no. (95% CI). D value, time required to kill 90% of virus; *k*, first-order rate constant.

equipment. In addition, HDPE is a component of common full-body personal protective coveralls and gowns worn in hospitals (13). We deposited LASV on HDPE and stainless steel surfaces, allowed concentration to air dry at 20°C, and measured virus viability over 5 days. We found no statistically significant difference in decay between the HDPE and stainless steel within a single strain (Table 1; Figure 1). Conversely, we noted a small but significant difference between the 2 strains on stainless steel ($p = 0.028$) but not on HDPE.

Persistence of Aqueous LASV

We spiked LASV strains into deionized water and raw municipal wastewater and monitored persistence for 5 days. The decay rate was significantly higher in wastewater than deionized water ($p < 0.002$),

which can be attributed to multiple factors (17). First, microorganisms found in wastewater contribute to viral inactivation (18). Second, RNA genomes experience increased degradation when exposed to higher concentrations of ammonia found in wastewater (19). We noted no statistically significant difference between LASV strains for deionized water or wastewater (Table 2; Figure 2).

LASV Disinfection with Sodium Hypochlorite

Sodium hypochlorite is a widely available disinfectant used for wastewater disinfection (20). Sodium hypochlorite is effective at inactivating microorganisms and produces a disinfectant residual, which would be advantageous for short-term use in a public health emergency (20). Hospitals have also used sodium hypochlorite on site to manage wastewater

Figure 1. First-order decay of Josiah and Sauerwald isolates on surfaces in a study of environmental persistence and disinfection of Lassa virus. A) Josiah strain on high-density polyethylene; B) Josiah strain on stainless steel; C) Sauerwald strain on high-density polyethylene; D) Sauerwald strain on stainless steel. Each plotted point represents the mean of 3 independent experimental replicates run concurrently, and the error bars show the standard deviation. Solid blue and orange lines indicate decay rates; dashed lines indicate the assay's detection limits; hollow circles represent points below the detection limit that were not included in the regression analysis. The equation of the linear regression (*y*) and the *R*² value are shown on the plots. All plotting, regressions, and statistical analyses were performed using R Studio 2022.07.2 (The R Foundation for Statistical Computing, <https://www.r-project.org>). *C*₀, initial concentration of infectious virus; *C*_{*t*}, concentration of infectious virus at time, *t*; TCID₅₀, 50% tissue culture infectious dose.

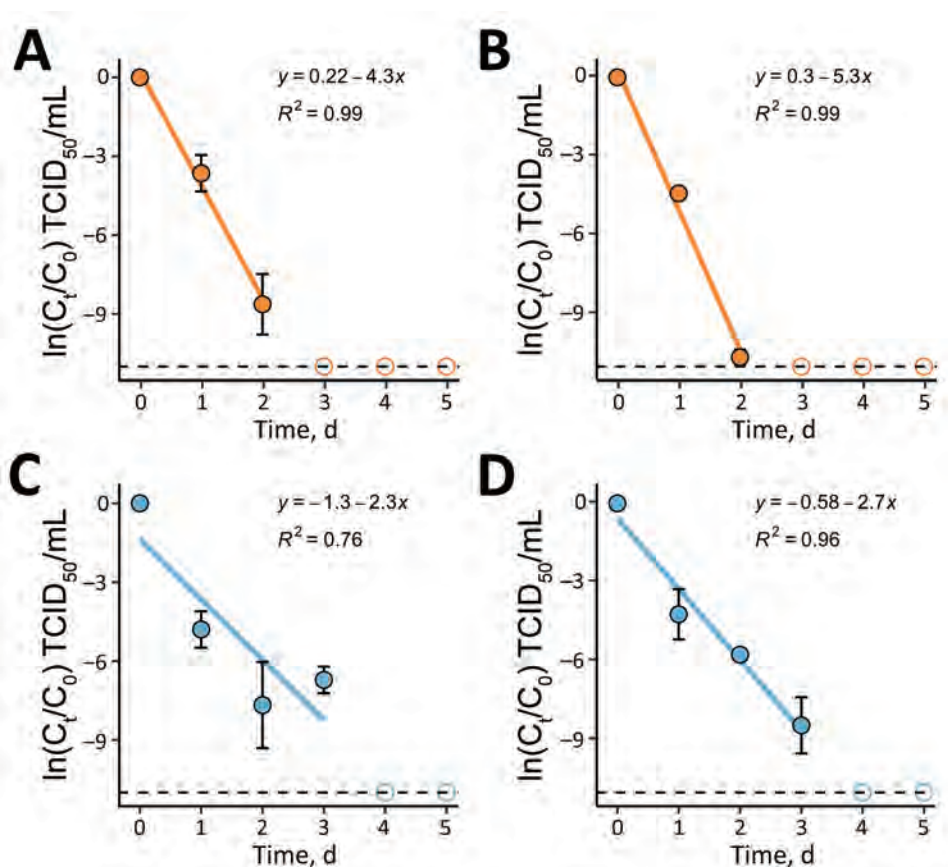


Table 2. First-order decay rate constants and decimal reductions for 2 virus strains in different aqueous solutions in study of environmental persistence and disinfection of Lassa virus*

Measurements	Deionized water		Wastewater	
	Josiah strain	Sauerwald strain	Josiah strain	Sauerwald strain
k , d	0.23 (0.04–0.43)	0.34 (0.15–0.53)	1.3 (0.94–1.6)	1.9 (1.5–2.3)
D value, d	10.0 (5.4–57.6)	6.8 (4.3–15.4)	1.8 (1.4–2.4)	1.2 (1.0–1.5)

*Values are no. (95% CI). D value, time required to kill 90% of virus; k , first-order rate constant.

containing high-consequence pathogens (21). Prior LASV disinfection studies have evaluated thermal inactivation, ultraviolet irradiation, and gamma irradiation in human serum and plasma (22). We assessed the disinfection kinetics Josiah and Sauerwald LASV strains in raw municipal wastewater by using sodium hypochlorite at 0 mg/L, 1 mg/L, 5 mg/L, and 10 mg/L (Figure 3).

Neither strain was removed at 0 mg/L sodium hypochlorite over the experimental timeframe. Increased sodium hypochlorite concentrations resulted in significantly higher decay rates for Josiah ($p = 0.001$ –0.3) and Sauerwald ($p = 0.001$ –0.007) strains of LASV. The Sauerwald strain showed faster inactivation than the Josiah strain for both 5 mg/L and 10 mg/L ($p = 0.04$). Those results indicate that sodium hypochlorite effectively inactivates the LASV strains analyzed in this study.

Discussion

In general, we found LASV persisted longer in aqueous solution than on surfaces. Josiah strain persistence was significantly longer in wastewater than on HDPE and stainless steel ($p < 0.01$). Both Josiah and Sauerwald strains had significantly lower decay rates in deionized water than on HDPE and stainless steel ($p < 0.01$ –0.02), indicating higher stability in deionized water than on either surface (Appendix Tables 2–9).

Contact with potentially contaminated surfaces without proper personal protective equipment, especially in hospitals, is anticipated to be a potential transmission route for LASV (23). However, previous studies have not analyzed the persistence of infectious LASV on surfaces to support that claim. Quantifying LASV persistence is critical to implementing proper control mechanisms and prevention measures (24). The persistence of enveloped viruses on surfaces is

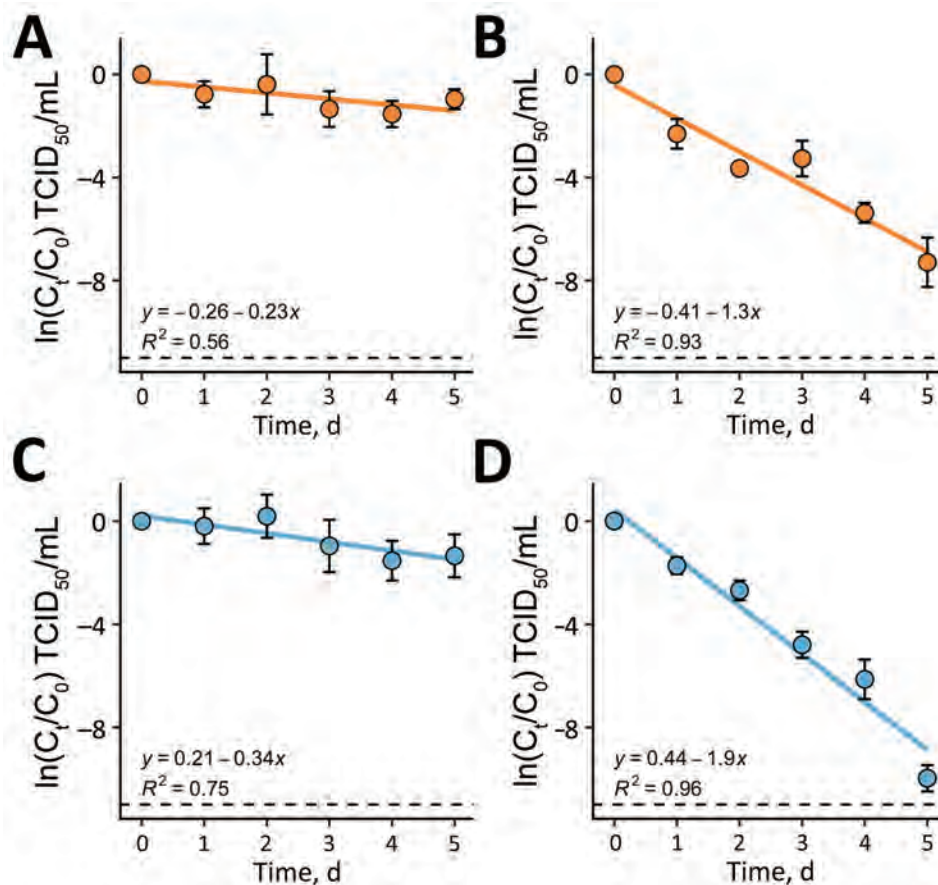


Figure 2. First-order decay of Josiah and Sauerwald strains in water in a study of environmental persistence and disinfection of Lassa virus. A) Josiah strain in deionized water; B) Josiah strain in wastewater; C) Sauerwald strain in deionized water; D) Sauerwald strain in wastewater. Each plotted point represents the mean of 3 independent experimental replicates run concurrently, and the error bars show the standard deviation. Solid blue and orange lines indicate decay rates; dashed lines indicate the assay's detection limits; hollow circles represent points below the detection limit that were not included in the regression analysis. The equation of the linear regression (y) and the R^2 value are shown on the plots. All plotting, regressions, and statistical analyses were performed using R Studio 2022.07.2 (The R Foundation for Statistical Computing, <https://www.r-project.org>). C_0 , initial concentration of infectious virus; C_t , concentration of infectious virus at time, t ; $TCID_{50}$, 50% tissue culture infectious dose.

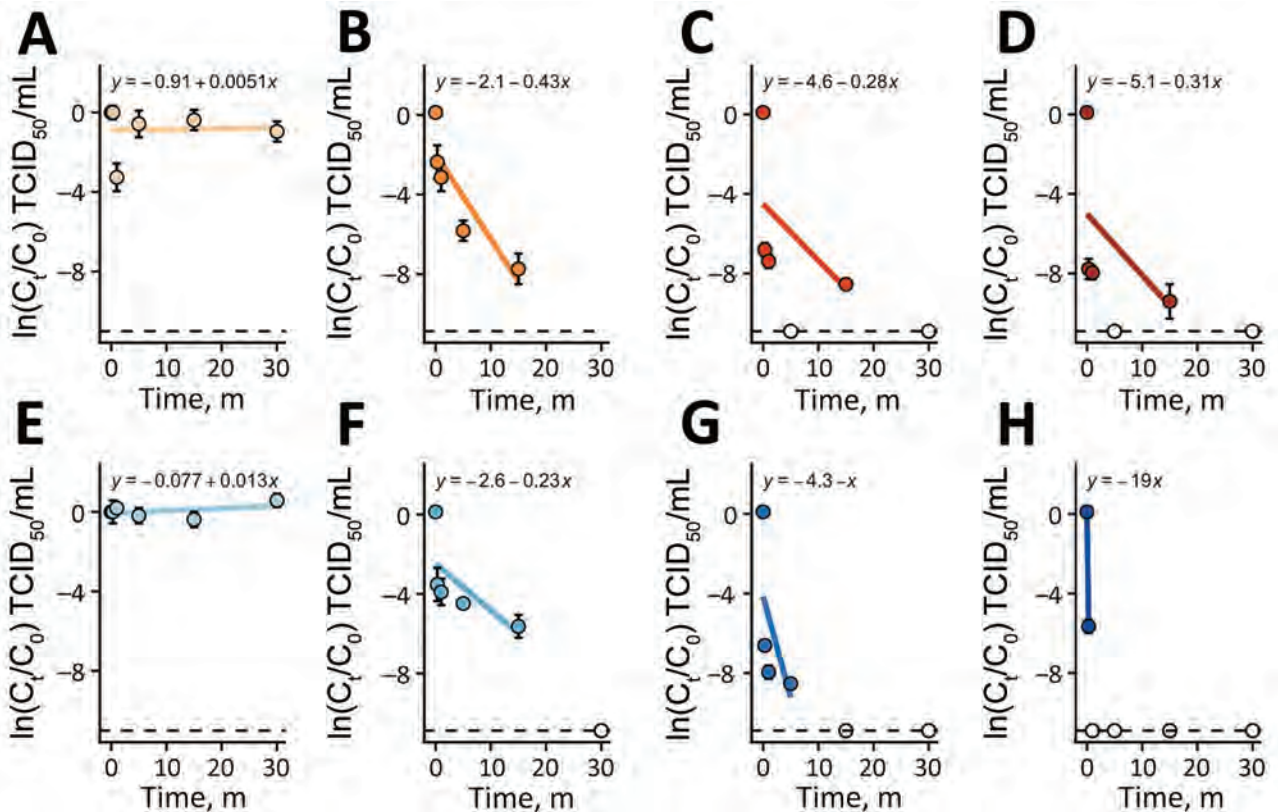


Figure 3. Virus disinfection in a study of environmental persistence and disinfection of Lassa virus. Graphs depict disinfection of Lassa virus with sodium hypochlorite in municipal wastewater. A–D) Josiah strain; E–H) Sauderwald strain. Graphs depict sodium hypochlorite concentrations of 0 mg/L (A, E), 1 mg/L (B, F), 5 mg/L (C, G), and 10 mg/L (D, H). Each plotted point represents the mean of 3 independent experimental replicates run concurrently, and the error bars show the standard deviation. Solid blue and orange lines indicate decay rates; dashed lines indicate the assay's detection limits; hollow circles represent points below the detection limit that were not included in the regression analysis. The equation of the linear regression (y) and the R^2 value are shown on the plots. All plotting, regressions, and statistical analyses were performed using R Studio 2022.07.2 (The R Foundation for Statistical Computing, <https://www.r-project.org>). C_0 , initial concentration of infectious virus; C_t , concentration of infectious virus at time, t ; $TCID_{50}$, 50% tissue culture infectious dose.

specific to the virus, the surface, and the temperature and humidity. A previous study using Ebola virus at 21°C and 40% relative humidity on HDPE and stainless steel found the decay of Ebola was slower than we found for LASV on the same surfaces (15). In contrast, another study found the decay rates of SARS-CoV-1 and SARS-CoV-2 on stainless steel were faster than the Sauderwald strain but slower than the Josiah strain of LASV from this study (25). The slow decay rates and increased LASV persistence in aqueous solution compared with surfaces seen in our data suggests that efforts are best directed at managing fluids containing infectious LASV recently deposited onto surfaces.

Wastewater in LASV endemic locations will likely be more concentrated than the primary influent wastewater we used in our study. Wastewater from a LASV treatment unit will have higher ammonia levels, total suspended solids, and biologic oxygen demand. Those physiochemical changes would be

expected to decrease LASV persistence but increase the amount of sodium hypochlorite needed to reach similar free chlorine levels due to increased chlorine demand. If sodium hypochlorite is used for disinfection, then chlorine residual should be assessed to ensure proper sodium hypochlorite concentrations for LASV inactivation.

Previous research analyzed the persistence of other priority pathogens, including Ebola virus, SARS-CoV-2, and Nipah virus, on representative surfaces or solutions (14,26,27). Ebola virus and SARS-CoV-2 persisted in wastewater similarly to LASV under the same experimental conditions (14,26). A study analyzing Nipah virus in blood and tissue cultures found that decay rates increased in samples that were exposed to the atmosphere, further describing how experimental conditions are critical when discussing the persistence of a virus (27). Compared with disinfection of SARS-CoV-2 and Ebola virus, LASV was inactivated faster

under the same dose of sodium hypochlorite and all 3 viruses have been shown to be highly susceptible to disinfection with sodium hypochlorite (15,16).

Bacteriophage Phi6 and murine hepatitis virus are commonly used as surrogates for enveloped viruses of concern, such as Ebola and SARS-CoV-2, and potentially LASV. Bacteriophage Phi6 and murine hepatitis virus decay rates were previously assessed in wastewater (28). Compared with the LASV decay rates from this study, surrogate decay was 2–5 times faster than LASV (28), indicating surrogate viruses are not representative of LASV persistence in wastewater. Furthermore, in deionized water, the decay rate for bacteriophage Phi6 was faster than we found for LASV, showing lower surrogate virus persistence (17). Conversely, in autoclaved wastewater influent, the decay rate of bacteriophage Phi6 was lower than what we found for LASV strains (17), suggesting potential differences in the decay of viruses based on the specific matrix. Overall, commonly used surrogates for enveloped viruses of concern do not indicate the behavior of LASV in aqueous solutions.

Given the differences in stability between the surrogates and LASV, the differences in stability and susceptibility to chlorine disinfection between the LASV strains were not predicted here. The 2 strains evaluated displayed strain-dependent behavior, suggesting that the potential for environmental transmission might vary by strain. Those differences could have ramifications that affect virus transmission between the zoonotic reservoir and humans, as well as influencing human-to-human transmission. Future transmission studies should incorporate potential differences in stability between lineages into the study design. Additional investigations into the mechanistic basis of those differences could help elucidate potential regional differences of spillover risk in human populations.

In conclusion, LASV is a World Health Organization priority pathogen with pandemic potential. Our findings supply data for the environmental persistence of LASV on representative surfaces, in aqueous solutions, and with sodium hypochlorite disinfection. LASV showed shorter persistence on surfaces than previously assessed enveloped virus surrogates and priority pathogens, and longer persistence in aqueous solution. LASV was rapidly disinfected in the presence of free chlorine from the addition of sodium hypochlorite. The data we provide on the stability and control of LASV in the environment could be used to further LASV management and mitigation efforts.

This article was preprinted at <https://www.biorxiv.org/content/10.1101/2023.05.17.541161v1>.

Acknowledgments

This work was supported by the Intramural Research Program of the National Institute of Allergy and Infectious Diseases (NIAID), National Institutes of Health (NIH), and Water Research Foundation award no. 5029.

About the Authors

Ms. Shaffer is a PhD candidate in engineering at the University of Notre Dame, Notre Dame, Indiana, USA. Her research interests include viral persistence and detection in water and wastewater. Dr. Fischer is a member of the Virus Ecology Section in the Laboratory of Virology at the National Institutes of Health Rocky Mountain Labs, Hamilton, Montana, USA. His research interests center around the ecology of pathogens in their natural foci, the circulation of pathogens within zoonotic host populations, pathogen movement across the landscape, and events leading to cross-species jumps.

References

- Günther S, Lenz O. Lassa virus. *Crit Rev Clin Lab Sci*. 2004;41:339–90. <https://doi.org/10.1080/10408360490497456>
- Yaro CA, Kogi E, Opara KN, Batiha GES, Baty RS, Albrakati A, et al. Infection pattern, case fatality rate and spread of Lassa virus in Nigeria. *BMC Infect Dis*. 2021;21:149. <https://doi.org/10.1186/s12879-021-05837-x>
- Garry RF. Lassa fever – the road ahead. *Nat Rev Microbiol*. 2023;21:87–96. <https://doi.org/10.1038/s41579-022-00789-8>
- Richmond JK, Baglolle DJ. Lassa fever: epidemiology, clinical features, and social consequences. *BMJ*. 2003;327:1271–5. <https://doi.org/10.1136/bmj.327.7426.1271>
- Bonwitt J, Sáez AM, Lamin J, Ansumana R, Dawson M, Buanie J, et al. At home with *Mastomys* and *Rattus*: human-rodent interactions and potential for primary transmission of Lassa virus in domestic spaces. *Am J Trop Med Hyg*. 2017;96:935–43. <https://doi.org/10.4269/ajtmh.16-0675>
- Gibb R, Moses LM, Redding DW, Jones KE. Understanding the cryptic nature of Lassa fever in West Africa. *Pathog Glob Health*. 2017;111:276–88. <https://doi.org/10.1080/20477724.2017.1369643>
- Klitting R, Kafetzopoulou LE, Thiery W, Dudas G, Gryseels S, Kotamarthi A, et al. Predicting the evolution of the Lassa virus endemic area and population at risk over the next decades. *Nat Commun*. 2022;13:5596. <https://doi.org/10.1038/s41467-022-33112-3>
- Safronetz D, Lopez JE, Sogoba N, Traore SF, Raffel SJ, Fischer ER, et al. Detection of Lassa virus, Mali. *Emerg Infect Dis*. 2010;16:1123–6. <https://doi.org/10.3201/eid1607.100146>
- Yadouleton A, Picard C, Rieger T, Loko F, Cadar D, Kouthon EC, et al. Lassa fever in Benin: description of the 2014 and 2016 epidemics and genetic characterization of a new Lassa virus. *Emerg Microbes Infect*. 2020;9:1761–70. <https://doi.org/10.1080/22221751.2020.1796528>
- Centers for Disease Control and Prevention. What you need to know about Lassa fever [cited 2022 Nov 2]. <https://www.cdc.gov/vhf/lassa/pdf/What-you-need-to-know-about-Lassa-508.pdf>
- World Health Organization. Lassa fever – Nigeria [cited 2022 Oct 14]. <https://www.who.int/emergencies/>

- disease-outbreak-news/item/27-may-2016-lassa-fever-nigeria-en
12. Mazzola LT, Kelly-Cirino C. Diagnostics for Lassa fever virus: a genetically diverse pathogen found in low-resource settings. *BMJ Glob Health*. 2019;4(Suppl 2):e001116. <https://doi.org/10.1136/bmjgh-2018-001116>
 13. Fischer R, Judson S, Miazgowicz K, Bushmaker T, Prescott J, Munster VJ. Ebola virus stability on surfaces and in fluids in simulated outbreak environments. *Emerg Infect Dis*. 2015;21:1243–6. <https://doi.org/10.3201/eid2107.150253>
 14. Bivins A, Greaves J, Fischer R, Yinda KC, Ahmed W, Kitajima M, et al. Persistence of SARS-CoV-2 in water and wastewater. *Environ Sci Technol Lett*. 2020;7:937–42. <https://doi.org/10.1021/acs.estlett.0c00730>
 15. Bibby K, Fischer RJ, Casson LW, de Carvalho NA, Haas CN, Munster VJ. Disinfection of Ebola virus in sterilized municipal wastewater. *PLoS Negl Trop Dis*. 2017; 11:e0005299. <https://doi.org/10.1371/journal.pntd.0005299>
 16. Greaves J, Fischer RJ, Shaffer M, Bivins A, Holbrook MG, Munster VJ, et al. Sodium hypochlorite disinfection of SARS-CoV-2 spiked in water and municipal wastewater. *Sci Total Environ*. 2022;807:150766. <https://doi.org/10.1016/j.scitotenv.2021.150766>
 17. Aquino de Carvalho N, Stachler EN, Cimabue N, Bibby K. Evaluation of Phi6 persistence and suitability as an enveloped virus surrogate. *Environ Sci Technol*. 2017;51:8692–700. <https://doi.org/10.1021/acs.est.7b01296>
 18. Sinclair RG, Rose JB, Hashsham SA, Gerba CP, Haas CN. Criteria for selection of surrogates used to study the fate and control of pathogens in the environment. *Appl Environ Microbiol*. 2012;78:1969–77. <https://doi.org/10.1128/AEM.06582-11>
 19. Decrey L, Kazama S, Kohn T. Ammonia as an in situ sanitizer: influence of virus genome type on inactivation. *Appl Environ Microbiol*. 2016;82:4909–20. <https://doi.org/10.1128/AEM.01106-16>
 20. US Environmental Protection Agency. The effectiveness of disinfectant residuals in the distribution system. Washington: The Agency; 2010.
 21. Gautam AK, Kumar S, Sabumon PC. Preliminary study of physico-chemical treatment options for hospital wastewater. *J Environ Manage*. 2007;83:298–306. <https://doi.org/10.1016/j.jenvman.2006.03.009>
 22. Hossain F. Sources, enumerations, and inactivation mechanisms of four emerging viruses in aqueous phase. *J Water Health*. 2022;20:396–440. <https://doi.org/10.2166/wh.2022.263>
 23. Choi MJ, Worku S, Knust B, Vang A, Lynfield R, Mount MR, et al. A case of Lassa fever diagnosed at a community hospital – Minnesota 2014. *Open Forum Infect Dis*. 2018;5:ofy131. <https://doi.org/10.1093/ofid/ofy131>
 24. Wißmann JE, Kirchhoff L, Brüggemann Y, Todt D, Steinmann J, Steinmann E. Persistence of pathogens on inanimate surfaces: a narrative review. *Microorganisms*. 2021;9:343. <https://doi.org/10.3390/microorganisms9020343>
 25. van Doremalen N, Bushmaker T, Morris DH, Holbrook MG, Gamble A, Williamson BN, et al. Aerosol and surface stability of SARS-CoV-2 as compared with SARS-CoV-1. *N Engl J Med*. 2020;382:1564–7. <https://doi.org/10.1056/NEJMc2004973>
 26. Bibby K, Fischer RJ, Casson LW, Stachler E, Haas CN, Munster VJ. Persistence of Ebola virus in sterilized wastewater. *Environ Sci Technol Lett*. 2015;2:245–9. <https://doi.org/10.1021/acs.estlett.5b00193>
 27. Smither SJ, Eastaugh LS, Findlay JS, O'Brien LM, Thom R, Lever MS. Survival and persistence of Nipah virus in blood and tissue culture media. *Emerg Microbes Infect*. 2019;8:1760–2. <https://doi.org/10.1080/22221751.2019.1698272>
 28. Ye Y, Ellenberg RM, Graham KE, Wigginton KR. Survivability, partitioning, and recovery of enveloped viruses in untreated municipal wastewater. *Environ Sci Technol*. 2016;50:5077–85. <https://doi.org/10.1021/acs.est.6b00876>

Address for correspondence: Kyle Bibby, University of Notre Dame Ringgold Standard Institution, Department of Civil and Environmental Engineering and Earth Sciences, 171 Fitzpatrick Hall, Notre Dame, IN 46556, USA; email: kbibby@nd.edu

Simulation Study of Surveillance Strategies for Faster Detection of Novel SARS-CoV-2 Variants

Selina Patel, Fergus Cumming, Carl Mayers, André Charlett,¹ Steven Riley¹

Earlier global detection of novel SARS-CoV-2 variants gives governments more time to respond. However, few countries can implement timely national surveillance, resulting in gaps in monitoring. The United Kingdom implemented large-scale community and hospital surveillance, but experience suggests it might be faster to detect new variants through testing arrivals in England for surveillance. We developed simulations of emergence and importation of novel variants with a range of infection hospitalization rates to the United Kingdom. We compared time taken to detect the variant through testing arrivals at borders in England, hospital admissions, and the general community. We found that sampling 10%–50% of arrivals at borders in England could confer a speed advantage of 3.5–6 weeks over existing community surveillance and 1.5–5 weeks (depending on infection hospitalization rates) over hospital testing. Directing limited global capacity for surveillance to highly connected ports could speed up global detection of novel SARS-CoV-2 variants.

In the current phase of the COVID-19 pandemic, waves of SARS-CoV-2 infection are driven by novel variants and their sublineages, which continue to cause illness and death with potential to disrupt society. Government policies to mitigate those effects are more effective if they are put in place early but have substantial associated costs and therefore should not be implemented unless necessary. Evaluating the threat of an emergent variant to determine a proportionate response requires time to gather evidence. Global surveillance of SARS-CoV-2 and other respiratory pathogen genome sequences aims to contribute to the rapid detection of novel variants so that countries have more time to make policy decisions to

respond. However, few countries have the capacity and resources for timely national surveillance, resulting in gaps in international monitoring.

During the first few years of the pandemic, Hong Kong implemented a strict traveler quarantine protocol (1). Travelers underwent testing for SARS-CoV-2 infection during their quarantine, and 10% of detected imported infections were sequenced. Retrospective sequence data from those travelers reflects the global emergence and spread of variants over time. In some instances, traveler-based testing in Hong Kong detected variant circulation in other nations before it had been domestically sequenced and uploaded to GISAID (<https://www.gisaid.org>). The Hong Kong border screening experience suggests opportunities for traveler-based surveillance to speed up detection of novel variants and compensate for internationally incomplete coverage of domestic genomic surveillance.

To pilot this approach, the United States sampled arrival flights from countries with a high travel volume (India, South Africa, Nigeria, Brazil, France, United Kingdom, Germany) for voluntary surveillance testing (2). During November 2021–January 2022, the United States achieved a 10% response rate and detected Omicron BA.2 seven days earlier and Omicron BA.3 forty-three days earlier than anywhere else in the country.

In the United Kingdom, although traveler-based surveillance was not used when border measures were decreased in 2022, previous traveler-based testing policies required inbound passengers to undergo testing shortly after arrival (3). The United Kingdom also conducted a large community survey of SARS-CoV-2 surveillance, and all patients experiencing symptomatic respiratory disease in hospital undergo testing for SARS-CoV-2 infection (4). Although

Author affiliations: University College London, London, UK (S. Patel); UK Health Security Agency, London (S. Patel, F. Cumming, C. Mayers, A. Charlett, S. Riley); Imperial College London, London (S. Riley)

DOI: <https://doi.org/10.3201/eid2911.230492>

¹These senior authors contributed equally to this article.

reporting times were variable across those testing routes, Omicron was isolated and detected in England from a mandatory day 2 border test in an inbound traveler on November 16, 2021 (5). This test was 5 days earlier than a non-travel-associated sample that was obtained on November 21. Moreover, most of the earliest samples of Delta during the first 2 weeks of detection in the United Kingdom were also collected from travelers, despite the availability of universal testing in the community alongside surveillance at that time (6). To explore the potential utility of border screening for more rapid detection of variants, we simulated the time to obtaining a sample of an imported novel variant for genomic sequencing through sampling arrivals at ports in England, compared with existing large-scale community surveillance and testing of persons who came to a hospital.

Methods

Variants in our scenarios are considered to be imported from a country of a similar level of connectedness as between England and China. Over the most recent winter (December 2022–January 2023), China showed a huge increase in transmission of SARS-CoV-2 and resulting deaths after lifting of regulations that were part of previous Zero-COVID policy (7). This transmission risks the emergence of novel variants that could have a major effect on the epidemiology of COVID-19 elsewhere in the world. We replicated simulations for 4 scenarios of imported novel variants with infection hospitalization rates (IHRs) of 1.0%, 1.5%, 2.0%, and 2.5%. During the initial spread of the Alpha variant, the IHR was estimated at 1.0%–2.0%, which caused major impact and resulted in the reintroduction of national lockdown laws to mitigate its spread (8,9).

We generated a single-wave epidemic curve originating in an area with a total population of 60 million. The index case occurred on day 0. A Poisson distribution with a mean of 2 was assumed as the offspring distribution (i.e., each case, on average, transmits an infection to 2 other persons). The distribution of the generation time (the interval between the infection in a primary case and the infection in a secondary case caused by a transmission from the primary case) was assumed to be a gamma distribution with a shape parameter of 7 and a scale parameter of 1. Thus, the effective reproduction number was 2, and the average doubling time was 7 days. The offspring distribution for the first 2 generations was fixed at exactly 2. We assumed that the epidemic increased unchecked for 16 weeks, after which the mean of the offspring distribution was reduced to represent both control

countermeasures and depletion of susceptible persons in the population. Between the 17th and 26th generations, we reduced the mean by 0.1 at each successive generation, such that the reproduction number was 1 at the 26th generation. From the 27th generation onward, the mean of the offspring distribution was reduced at each generation by 0.01786 (1/56).

The incubation period for each generated infection was drawn from the published pooled lognormal distribution in McAloon et al. (10). This procedure provides an estimated mean of 1.63 and SD of 0.5 for a normal distribution of the logged incubation period distribution. Published estimates of the infectious period before and after symptom onset are extremely heterogeneous, as described in Byrne et al. (11). Thus, the presymptomatic infectious period was fixed at 2 days, and the combined presymptom and postsymptom infectious period for each generated infection was drawn from a normal distribution with a mean of 10 days and an SD of 1.33 days. This procedure provides a relatively small probability of being infectious 10 days after symptom onset, as reported by Singanayagam et al. (12). We rounded those 2 periods to an integer, providing the duration for disease. Daily prevalence as estimated by combining the simulated cases over their duration for all days after the day the index case occurred. In the simulations, the period postinfectiousness in which PCRs could still detect virus was ignored. The simulated epidemic curve was truncated at 300 days.

We obtained the number of incoming travelers on each day that were incubating or infectious by using a draw from a binomial distribution. We assumed that the number of daily travelers was fixed at 250 and a probability equal to the origin areas prevalence on that day (i.e., assuming that persons infected are as equally likely to travel as persons not infected).

For detection at the border, conditional on the simulations having ≥ 1 infected traveler, we selected a representative sample ranging from 10% to 50% of travelers for testing. We further assumed that the percentage who are in an infectious state (detectable) was 73%, the sensitivity of the test 85%, and the percentage of positive test results, 50%. We used those percentages as the probability of draws from independent Bernoulli distributions; a detection was declared if each of those draws were 1.

We assumed growth in the destination country to be the same as growth in the origin area. Incubating or infectious incursions were drawn from a Bernoulli distribution with a probability of 73%. The time remaining in these states was obtained from a uniform distribution and the mean of the offspring distribution

modified to account for this time. We assumed that travelers would spend all of their infectious period in the destination country. Daily incidence and prevalence of cases in the destination country were generated, but with the destination country population being assumed to be 56 million. We simulated 1,000 destination country epidemics.

For detection of a simulated case in the hospital setting, we assumed IHRs of 1.0%–2.5% and allocated simulated cases to presence in a hospital by using a draw from a Bernoulli distribution with a probability of 1%. We assumed that time to seeking care at a hospital because of infection followed a gamma distribution with a shape parameter of 1.4 and a scale parameter of 4 (i.e., giving a mean of 5.6 days, but with substantial variation). The percentage of persons seeking care who were tested was 50%; sensitivity of the test and percentage of positive test results sequenced were set as previously stated. Simulations were applied to each of the 1,000 destination country epidemics.

For detection of a simulated case in a community setting, we used a range of community cohort surveillance sizes from 20,000 ($\approx 0.04\%$ of the population) to 200,000 ($\approx 0.36\%$ of the population). We assumed that each person in this surveillance was tested every 2 weeks. We applied simulations to each of the 1,000 destination country epidemics. The number detected each day obtained from a draw from a binomial distribution by using the number tested each day and the simulated daily prevalence, combined with the sensitivity of the test and the percentage of positive test results.

The time to detecting a case from border, hospital, and community testing has been summarized by using the empirical 5th, 25th, 50th, 75th, and 95th percentiles of the simulation sets. We ran simulations using Stata version 17.0 (StataCorp LLC, <https://www.stata.com>). For all simulation sets, we used a unique random number seed in a 64-bit Mersenne Twister pseudo-random number generator (default pseudo-random number generator in Stata). A detailed technical description of the methods used is available (<https://wwwnc.cdc.gov/EID/article/29/11/23-0492-App1.pdf>).

Results

First, we simulated the time to detection of an imported novel variant through different sampling fractions (10%, 20%, 30%, 40%, and 50%) of traveler arrivals in England. We assumed that the prevalence of infection in the passenger population was equal to that of the epidemic curve generated for the country of origin over time (Appendix 1). In our scenarios, there was a nonlinear relationship between increasing sampling fraction and decreasing days to detection starting from 131 days to detection through sampling 10% of passenger arrivals (Table 1). The greatest reduction in time to detection was gained between sampling fractions 10%–20%, which led to a median 8-day decrease in time to detection. Thereafter, the time gained began to decrease with increasing sampling fraction.

Next, we simulated the time to detection through testing 50% of persons coming to a hospital in England. We assumed that growth in incidence in England (the destination country) was the same as that in the country of origin. We ran simulations for scenarios where variants had IHRs of 1.0%, 1.5%, 2.0%, and 2.5%. Although time to detection in hospitals decreased with increasing IHR, in all 4 scenarios it took >10 days longer to detect a novel variant in hospitals than by sampling 10%–50% of travelers arriving in England (Table 2).

Finally, we simulated the earliest time to obtaining a sample of an imported novel variant through testing a community cohort sampled for surveillance. We ran scenarios implementing a sample size of 0.04% (20,000) to 0.36% (200,000) of the population in England, assuming the same growth in prevalence in the population over time as that assumed for incidence. Increasing the size of the community cohort from 0.04% to 0.36% of the population decreased the time to detection by 3 weeks (175 days reduced to 154 days) (Table 3). For the sample size of existing community surveillance in England, which comprises $\approx 140,000$ tests every 2 weeks, the simulated earliest time to detection was 157 days.

We found that, for border testing, the range of the median time to detection from the index case was 131 days (10% of travelers tested) to 114 days (50% of travelers tested). This result compares with 150

Table 1. Simulated time to detect a novel variant since index case in study of traveler testing for surveillance of novel SARS-CoV-2 variants

Percentage tested	Empirical percentiles of simulated time to detection distribution, d				
	5th	25th	Median	75th	95th
10	104	121	131	140	150
20	96	114	123	131	141
30	94	110	119	126	136
40	89	107	115	123	131
50	86	105	114	121	130

Table 2. Simulated time to detect a novel variant since index case through hospital testing in study of traveler testing for surveillance of novel SARS-CoV-2 variants

Infection hospitalization rate (%)	Empirical percentiles of simulated time to detection distribution, d				
	5th	25th	Median	75th	95th
0.01 (1)	124	141	150	157	167
0.015 (1.5)	122	138	147	154	162
0.02 (2)	117	134	143	151	159
0.025 (2.5)	115	132	142	149	159

days (1% IHR) to 142 days (2.5% IHR) for the median of the earliest time to detection in hospitals, assuming 50% of persons seeking care are tested. Also, we found medians of 175 days (testing a cohort of 0.04% of the population) versus 154 days (testing a cohort of 0.36% of the population) for the earliest time to detection through community surveillance. Detailed study results are provided (<https://wwwnc.cdc.gov/EID/article/29/11/23-0492-App2.pdf>).

Discussion

Our simulations indicate that sampling a relatively small percentage, 10%, of inbound travelers for surveillance could reduce the time to detection of the first case of an imported novel variant of SARS-CoV-2 in the England by 26 days compared with existing community surveillance. Increasing sampling fraction of travelers to 50% could increase this speed advantage to 43 days. Depending on IHR (1.0%–2.5%), sampling 10% of inbound travelers would also detect a variant 11–19 days faster than testing hospital admissions for surveillance. However, sampling 50% of arrivals would lead to detection 4–5 weeks faster than hospital testing.

Our simulated results appear concordant with the closest available observed data. In the United States, testing 10% of passengers on arrival flights from

countries with a high travel volume resulted in Omicron BA.2 being detected 7 days earlier and Omicron BA.3 being detected 43 days earlier than anywhere else in the country (2). In comparison with our scenarios, a 10% sampling fraction resulted in detection of a novel variant 1.5–4 weeks sooner than in other settings. However, the extent to which further comparisons can be drawn between our results and this experience is limited. The scale of community and healthcare surveillance in the United States is much smaller than is assumed in our scenarios, and, unlike in our scenarios, US arrivals were required to present a negative test result before departure. In addition, the time between specimen collection and reporting sequence data can be extremely variable between testing pathways, which makes it challenging to observe the speed advantage gained in this example through sampling strategy alone.

Our findings are also broadly in agreement with more distantly related retrospective data from community testing and policies such as managed quarantine services (MQS) and requirement to test on or shortly after arrival in a country. Testing inbound travelers has detected or collected some of the earliest samples of imported novel variants nationally and globally, even during periods when universal testing has been available in the community. In Hong Kong,

Table 3. Simulated time to detect a novel variant since index case through community testing in study of traveler testing for surveillance of novel SARS-CoV-2 variants

Community testing cohort size (% destination country population)	Time to detection (days since emergence of index case), summaries from 1,000 simulations				
	5th percentile	25th percentile	Median	75th percentile	95th percentile
20,000 (0.04)	145	165	175	183	191
30,000 (0.05)	144	161	170	178	187
40,000 (0.07)	140	158	168	176	185
50,000 (0.09)	138.5	156	166	175	184
60,000 (0.11)	137	155.5	165	172	182
70,000 (0.13)	137	154	163	171	181
80,000 (0.14)	136	153	162	170	179
90,000 (0.16)	133	151	161	169	177
100,000 (0.18)	133.5	150.5	160	168	178
110,000 (0.20)	130	150	159	167	176
120,000 (0.21)	130	148	158	166.5	176
130,000 (0.23)	130.5	149	158	165	174
140,000 (0.25)	129	148	157	164	173
150,000 (0.27)	129	146	156	163	172
160,000 (0.29)	127.5	146	155.5	163	172
170,000 (0.30)	127	146	155	164	173
180,000 (0.32)	126	145	154	162	171
190,000 (0.34)	128	145	154	162	173
200,000 (0.36)	127	144.5	154	162	171

sequence data were collected for 10% of all infections detected through MQS. Retrospective analysis of those records and external data sources indicate that traveler-based testing was either a good reflection, or an early indicator, of the global emergence and spread of novel variants. For example, Omicron (B.1.1.529) was detected in Hong Kong through a sample obtained in an MQS on November 13, 2021 (13), which was uploaded to GISAID on November 23 (13). This upload triggered UK investigations on November 24, resulting in government intervention to delay further introduction and spread (14). Most of the earliest samples of Omicron subsequently collected in the United Kingdom were from persons who had recently traveled (5). Thus, Omicron samples collected through MQS in Hong Kong were able to be used as prospective evidence for policy decisions because of rapid genomic sequencing of samples and data reporting. In the United States, early samples of Omicron were also collected, frequently from persons who had a history of recent travel. However, long lag times from data collection to reporting indicated that this factor was not known until December 1, 2021 (15).

We also report that sampling 50% of persons seeking care at hospitals for surveillance in our scenarios detected a novel variant with an IHR of 2.5% \approx 8 days faster than a variant with an IHR of 1.0%. A lower IHR could either be caused by less severe disease associated with the variant or the availability of effective COVID-19 therapies preventing severe outcomes. An increased number of persons seeking care at hospitals when IHR is greater reduces the speed advantage gained through traveler-based surveillance. However, waves of infection caused by variants that have higher IHRs are more likely to be detected earlier in the country of emergence as a result of increasing hospital visits. This factor often already offers governments outside the country of emergence some advanced warning of the impact of a new wave of infection associated with greater illness and death, despite gaps in global genomic surveillance. Therefore, the greatest potential impact of early detection through genomic surveillance might be for those variants that have an IHR large enough to cause societal disruption but low enough that it is slower to identify through hospital admissions.

To simulate the time to detection of an imported novel variant in England in each of our scenarios, we have made some simplifying assumptions. We have assumed that the prevalence of infection in air passengers is the same as that in the country of origin at the time of the departure of their flight, specimens are collected from a random sample of passengers, and

the variant doubling time in the destination country is the same as that of in country of origin once seeded. A lower reproductive rate across both countries would have extended the time to detection of a novel variant across all surveillance strategies. However, a lower reproductive rate in only the destination country would have increased the speed advantage of border surveillance testing strategies.

We have also considered only direct incursions from the country of emergence of a novel variant to the destination country. We have not considered the effect of indirect incursions linked to infected travelers arriving from other countries where transmission might also be occurring. This decision is a simplification of observed human behavior, population immunity profiles, and transmission dynamics. However, we do not expect that a model comprising more complex representations of those processes would result in greatly different overall conclusions. We have also not attempted to carry out an economic evaluation of each surveillance strategy. Although such an evaluation is a major factor in policy and public health decisions, it would require a detailed cost-effectiveness analysis that is beyond the scope of this study.

In this report, we have focused the results and discussion on simulated scenarios that compare border surveillance with existing surveillance in hospitals and the community in England and the United Kingdom. However, this surveillance in England achieved greater coverage than for most countries. Therefore, as routine testing and surveillance for SARS-CoV-2 is decreasing globally, this study probably provides conservative estimates of the potential speed advantage that could be gained through traveler-based surveillance approaches. Also, if there were concerns about a specific country at any point in time, temporary programs would be able to achieve high sample proportions at the border with only limited numbers of samples compared with other ongoing or potential global programs.

It is useful to recognize that the collection of a sample of a novel variant for detection is the first step to evaluate the threat of a novel variant. In our scenarios, we do not consider the time it takes to sequence and report data obtained from a sample. Sequencing and reporting times are extremely variable across countries which can greatly reduce the time gained through effective sampling approaches (16). In addition, a full threat assessment requires robust estimates of severe outcomes in addition to temporal and geospatial descriptions of variant epidemiology to inform policy decisions.

Global surveillance of SARS-CoV-2 genome sequences contributes to rapid detection of novel variants to give governments more time to respond. However, few countries have capacity to implement national surveillance with timely sequencing and reporting, resulting in major gaps in global coverage of surveillance. In our scenarios, directing limited global capacity for surveillance to the most highly connected ports could provide governments with much more time to respond to future novel variants of SARS-CoV-2 and their sublineages. Beyond informing national approaches to surveillance, this approach also underscores the potential usefulness of international collaboration to achieve high global coverage of surveillance and provide governments with more time to make policy decisions to respond to novel variants of SARS-CoV-2.

About the Author

Ms. Patel is a research scientist at University College London, London, UK, and a principal public health scientist at the UK Health Security Agency, London. Her primary research interests are public health, infectious diseases, and surveillance approaches.

References

- Gu H, Cheng SS, Krishnan P, Ng DY, Chang LD, Liu GY, et al. Monitoring international travelers arriving in Hong Kong for genomic surveillance of SARS-CoV-2. *Emerg Infect Dis.* 2022;28:247–50. <https://doi.org/10.3201/eid2801.211804>
- Wegrzyn RD, Appiah GD, Morfino R, Milford SR, Walker AT, Ernst ET, et al. Early detection of severe acute respiratory syndrome coronavirus 2 variants using traveler-based genomic surveillance at 4 US airports, September 2021–January 2022. *Clin Infect Dis.* 2023;76:e540–3. <https://doi.org/10.1093/cid/ciac461>
- Williams GH, Llewelyn A, Brandao R, Chowdhary K, Hardisty KM, Loddio M. SARS-CoV-2 testing and sequencing for international arrivals reveals significant cross border transmission of high risk variants into the United Kingdom. *EClinicalMedicine.* 2021;38:101021. <https://doi.org/10.1016/j.eclinm.2021.101021>
- Office of National Statistics. COVID-19 infection survey [cited 2022 Oct 3]. <https://www.ons.gov.uk/surveys/informationforhouseholdsandindividuals/householdandindividualsurveys/covid19infectionsurvey>
- UK Health Security Agency. SARS-CoV-2 variants of concern and variants under investigation in England. Technical briefing 32. Report no. 32 [cited 2023 Sep 29]. https://assets.publishing.service.gov.uk/government/uploads/system/uploads/attachment_data/file/1060337/Technical-Briefing-38-11March2022.pdf
- Public Health England. SARS-CoV-2 variants of concern and variants under investigation in England. Technical briefing 14. Report no. 14 [cited 2023 Sep 29]. <https://www.gov.uk/government/publications/investigation-of-novel-sars-cov-2-variant-variant-of-concern-20201201>
- Reuters. China reports 59,938 COVID-related hospital deaths since Dec. 8. January 14, 2023 [cited 2023 Jan 16]. <https://www.reuters.com/world/china/china-reports-59938-covid-related-hospital-deaths-since-dec-8-2023-01-14>
- Public Health England. SARS-CoV-2 variants of concern and variants under investigation in England. Technical briefing 13. Report no. 13 [cited 2023 Sep 2]. https://assets.publishing.service.gov.uk/government/uploads/system/uploads/attachment_data/file/990339/Variants_of_Concern_VOC_Technical_Briefing_13_England.pdf
- Baker C, Kirk-Wade E, Brown J, Barber S. Coronavirus: a history of English lockdown laws. July 1, 2023 [cited 2023 Jan 7]. <https://commonslibrary.parliament.uk/research-briefings/cbp-9068>
- McAloon C, Collins A, Hunt K, Barber A, Byrne AW, Butler F, et al. Incubation period of COVID-19: a rapid systematic review and meta-analysis of observational research. *BMJ Open.* 2020;10:e039652. <https://doi.org/10.1136/bmjopen-2020-039652>
- Byrne AW, McEvoy D, Collins AB, Hunt K, Casey M, Barber A, et al. Inferred duration of infectious period of SARS-CoV-2: rapid scoping review and analysis of available evidence for asymptomatic and symptomatic COVID-19 cases. *BMJ Open.* 2020;10:e039856. <https://doi.org/10.1136/bmjopen-2020-039856>
- Singanayagam A, Patel M, Charlett A, Lopez Bernal J, Saliba V, Ellis J, et al. Duration of infectiousness and correlation with RT-PCR cycle threshold values in cases of COVID-19, England, January to May 2020. *Euro Surveill.* 2020;25:2001483. <https://doi.org/10.2807/1560-7917.ES.2020.25.32.2001483>
- Gu H, Krishnan P, Ng DY, Chang LD, Liu GY, Cheng SS, et al. Probable transmission of SARS-CoV-2 Omicron variant in quarantine hotel, Hong Kong, China, November 2021. *Emerg Infect Dis.* 2022;28:460–2. <https://doi.org/10.3201/eid2802.212422>
- UK Health Security Agency. SARS-CoV-2 variants of concern and variants under investigation in England. Technical briefing 29. Report no. 29 [cited 2023 Sep 29]. https://assets.publishing.service.gov.uk/government/uploads/system/uploads/attachment_data/file/1036501/Technical_Briefing_29_published_26_November_2021.pdf
- CDC COVID-19 Response Team. SARS-CoV-2 B.1.1.529 (Omicron) variant – United States, December 1–8, 2021. *MMWR Morb Mortal Wkly Rep.* 2021;70:1731–4. <https://doi.org/10.15585/mmwr.mm7050e1>
- Brito AF, Semenova E, Dudas G, Hassler GW, Kalinich CC, Kraemer MU, et al.; Swiss SARS-CoV-2 Sequencing Consortium. Global disparities in SARS-CoV-2 genomic surveillance. *Nat Commun.* 2022;13:7003. <https://doi.org/10.1038/s41467-022-33713-y>

Address for correspondence: Selina Patel, UK Health Security Agency, Nobel House, London SW1P 3HX, UK; email: selina.patel.17@ucl.ac.uk

Human Salmonellosis Outbreak Linked to *Salmonella* Typhimurium Epidemic in Wild Songbirds, United States, 2020–2021

Kane Patel,¹ G. Sean Stapleton,¹ Rosalie T. Trevejo, Waimon T. Tellier, Jeffrey Higa, Jennifer K. Adams, Sonia M. Hernandez, Susan Sanchez, Nicole M. Nemeth, Emilio E. Debess, Krysta H. Rogers, Asli Mete, Katherine D. Watson, Leslie Foss, Mabel S.F. Low, Lauren Gollarza, Megan Nichols

Salmonella infection causes epidemic death in wild songbirds, with potential to spread to humans. In February 2021, public health officials in Oregon and Washington, USA, isolated a strain of *Salmonella enterica* serovar Typhimurium from humans and a wild songbird. Investigation by public health partners ultimately identified 30 illnesses in 12 states linked to an epidemic of *Salmonella* Typhimurium in songbirds. We report a multistate outbreak of human salmonellosis associated with songbirds,

resulting from direct handling of sick and dead birds or indirect contact with contaminated birdfeeders. Companion animals might have contributed to the spread of *Salmonella* between songbirds and patients; the outbreak strain was detected in 1 ill dog, and a cat became ill after contact with a wild bird. This outbreak highlights a One Health issue where actions like regular cleaning of birdfeeders might reduce the health risk to wildlife, companion animals, and humans.

More than 1 million human illnesses result from *Salmonella* each year (1); ≈11% are attributed to animal contact (2,3). Humans infected with *Salmonella* can have abdominal pain, diarrhea, and fever that are often self-limiting, but more severe illness and death are possible (4). Animals can carry *Salmonella* in their gastrointestinal tract and the bacteria might shed intermittently in feces.

Among wild songbirds, particularly those within the family Fringillidae (finches), salmonellosis can cause periodic widespread deaths, typically during winter, which can result in the deaths of hundreds to thousands of birds (5–7). Clinical signs in songbirds infected with *Salmonella* include reluctance to fly, anorexia, abnormal mentation, diarrhea, inability to swallow food, and sudden death (8,9). *Salmonella*

enterica serotype Typhimurium is the most common serotype isolated from moribund songbirds during salmonellosis deaths (6,8,10–13). The prevalence of *Salmonella* among North American wild birds is difficult to determine because of species differences in shedding and current lack of standardization in surveillance efforts. A recent meta-analysis estimated an overall prevalence of 6.4% (n = 40,295 birds) based on 102 studies that investigated *Salmonella* in one third of wild bird species that breed in North America (14). However, prevalence can be highly variable, ranging from <1% to 22% depending on the species, habitat, and season examined (5,14,15).

Various host and environmental factors might contribute to the risk for wild bird salmonellosis outbreaks. Gatherings in large numbers at specific

Author affiliations: Oak Ridge Institute for Science and Education, Oak Ridge, Tennessee, USA (K. Patel, G.S. Stapleton); Centers for Disease Control and Prevention, Atlanta, Georgia, USA (K. Patel, G.S. Stapleton, J.K. Adams, M.S.F. Low, L. Gollarza, M. Nichols); Oregon Health Authority, Portland, Oregon, USA (R.T. Trevejo, E.E. Debess); Washington State Department of Health, Shoreline, Washington, USA (W.T. Tellier); California Department of Public Health, Los Angeles and Richmond, California, USA (J. Higa, L. Foss); Association of Public Health Laboratories, Silver Spring,

Maryland, USA (J.K. Adams); University of Georgia, Athens, Georgia, USA (S.M. Hernandez, S. Sanchez, N.M. Nemeth); Wildlife Health Laboratory, California Department of Fish and Wildlife, Rancho Cordova, California, USA (K.H. Rogers); California Animal Health and Food Safety Laboratory, University of California Davis, Davis, California (A. Mete, K.D. Watson)

DOI: <http://doi.org/10.3201/eid2911.230332>

¹These authors contributed equally to this article.

locations such as birdfeeders lead to increased density of birds and fecal contamination of the feeders and surrounding area, increasing transmission probability (7,11,16,17). The type of feeder also matters; platform feeders can result in fecal contamination of food, and the potential for such transmission might be increasing, given the expanding use of birdfeeders (18,19) in urban and suburban environments (20).

There is a strong seasonal component to avian salmonellosis. Most cases appear in the winter, when birds become more reliant on feeders (20) and are more physiologically stressed by colder temperatures. In addition, climate change has affected seasonal migration patterns, which might affect birds' ability to find high-quality food and could introduce or exacerbate environmental stressors that might alter birds' immune system function and increase their susceptibility to disease (21,22). Those factors collectively contribute to concern for the conservation of wild birds (16) and the possibility that infection could spill over to humans, although the magnitude of this risk is not yet well understood (14).

Enteric pathogens can be transmitted from wild birds to humans through multiple routes (7,14). Handling ill or dead birds or touching surfaces contaminated with bird feces, such as birdfeeders, has been linked to outbreaks of *Salmonella* infections in humans in the United Kingdom (11), Norway (23), and New Zealand (8). Indirect transmission through contact with companion animals that bridge the connection between humans and wild birds has also been linked to a human *Salmonella* outbreak in Sweden (24). Cats and dogs can serve as a source of human illness in several ways: bringing bird carcasses or feed into homes; tracking *Salmonella* into the household after contact with birds or contaminated environments; or ingesting birds, bird feces, or bird seed and shedding *Salmonella* in their own feces (24,25). Clinical salmonellosis (also known as songbird fever) in cats and dogs is characterized by fever, abdominal pain, diarrhea, vomiting, or systemic illness resulting from septicemia (25).

In February 2021, public health officials in Oregon and Washington, USA, reported to the Centers for Disease Control and Prevention (CDC) that 8 persons were infected with *Salmonella* Typhimurium; illness onset dates were December 2020–February 2021. Whole-genome sequencing (WGS) determined isolates collected from those patients were genetically related to one another as well as to an isolate from a pine siskin (*Spinus pinus*), a type of finch, collected in Oregon in December 2020 (26). To identify

the source of human illness and conduct further case findings, public health partners initiated a multistate outbreak investigation. We report the findings of this investigation and provide recommendations for preventing salmonellosis as it relates to interaction with wild birds.

Methods

Identification of Human Cases

Cases were defined as patients infected with laboratory-confirmed, genetically related *Salmonella* Typhimurium based on core genome multilocus sequence typing (cgMLST) of WGS data (within 0–12 allele differences) with an illness onset of December 26, 2020–May 19, 2021. WGS was performed by using the Nextera XT library preparation kit (Illumina, <https://www.illumina.com>), followed by sequencing on the Illumina MiSeq. Sequences were shared with CDC for cgMLST analysis (27); all generated sequence data have been deposited in the National Center for Biotechnology Information (<https://www.ncbi.nlm.nih.gov>; Bioproject PRJNA230403). To identify historically related and newly identified cases during the investigation, we queried PulseNet (<https://www.cdc.gov/pulsenet/index.html>), the national molecular subtyping network for enteric disease surveillance at the CDC (28).

Exposure Data

In the United States, state and local health officials routinely interview laboratory-confirmed *Salmonella*-infected patients with a standard questionnaire designed to collect demographic information and general food and animal exposures the week before illness onset. When patients are identified as having isolates matching an ongoing multistate outbreak, those data are shared with CDC. Because isolates from index cases were genetically related to an isolate from a wild bird, health officials collected additional information on patients' exposures to dogs, cats, songbirds, birdfeeders, and bird feed, as well as characterized behaviors of patients' pets, such as wildlife predation that could result in exposure to songbirds or birdfeeders. This information was shared with CDC and analyzed with SAS 9.4 (SAS Institute Inc; <https://www.sas.com>). We conducted descriptive analysis for each interview question, including frequency calculation for each answer on the basis of total number of responses. Using a binomial proportion test, we compared the percentage of patients with songbird, dog, or cat exposure within 7 days of illness onset to the FoodNet Population Survey, which measured the proportion

of healthy persons reporting similar exposures in the 7 days before interview (29). This activity was reviewed by CDC and was conducted in accordance with applicable federal law and CDC policy (see, e.g., 45 C.F.R. part 46, 21 C.F.R. part 56; 42 U.S.C. §241(d); 5 U.S.C. §552a; 44 U.S.C. §3501 et seq).

Animal Testing

Dead songbirds were collected in Oregon, Washington, and California for mortality investigation. In Oregon and Washington, dead songbirds were identified by members of the National Audubon Society with the assistance of the state public health veterinarian and were submitted to the Oregon State Veterinary Diagnostic Laboratory, where aerobic culture was performed. Additional songbirds were identified in Washington by veterinarians and submitted to the Washington State University Animal Disease Diagnostic Laboratory for aerobic culture. In California, incidents of sick and dead wild birds can be reported to California Department of Fish and Wildlife's Wildlife Health Laboratory by the public, wildlife rehabilitation centers, and other agencies by telephone, email, or a web-based mortality reporting application (<https://wildlife.ca.gov>). In addition, the public can report dead birds to the California Department of Public Health for the West Nile virus surveillance program (<https://westnile.ca.gov>). Total reports of songbird deaths in California were compiled from those sources.

The California Department of Fish and Wildlife submitted a total of 15 dead songbirds to the California Animal Health and Food Safety Laboratory System for postmortem examination. In brief, tissue samples of brain, muscle, thyroid/parathyroid glands, peripheral nerves, trachea, lung, heart, esophagus, crop, proventriculus, gizzard, pancreas, intestines, liver, spleen, adrenals, kidneys, and gonads were collected and immersed in 10% neutral buffered formalin, paraffin-embedded, sectioned at 4 μ m, and stained with hematoxylin and eosin for histologic examination by light microscopy. Swabs of pathologic lesions affecting the oral cavity or gastrointestinal tract were collected for *Salmonella* testing by PCR and *Salmonella* culture. In addition, specimens were collected from companion animals when available during this investigation. State and local public health laboratories sequenced animal isolates by using standardized sequencing methods described previously (27).

Concurrently, the Southeastern Cooperative Wildlife Disease Study (SCWDS) at the University of Georgia (Athens, GA, USA) diagnosed salmonellosis in songbirds in the southeastern United States. When *Salmonella* was isolated from samples by means of

aerobic culture at the Athens Veterinary Diagnostic Laboratory, isolation was confirmed and isolates serotyped at the National Veterinary Services Laboratory (30). Isolates from those birds were not available for genetic sequencing.

We conducted a comparison of genetic relatedness of isolates from humans and animals (when available). We consulted with wildlife experts regarding wild bird deaths and the biologic plausibility of *Salmonella* transmission routes between wildlife and humans. CDC, state partners, and wildlife experts jointly developed public communications to share recommendations to reduce illnesses.

Results

Human Cases

In total, we identified 30 human *Salmonella* Typhimurium cases across 12 US states (Figure 1). Twenty patients (67%) resided in the western United States (Oregon, Washington, and California). Known and estimated illness onset dates ranged from December 26, 2020, to May 19, 2021 (Figure 2). Patient ages ranged from <1 to 89 years (median 12 years); 10 patients (33%) were \leq 1 year of age. Of 28 patients with information available, 14 (50%) were hospitalized, and no deaths were reported.

All sequences from clinical isolates were related by cgMLST within 0–12 allele differences (Figure 3). Investigators identified 18 historical clinical isolates that were closely related to the outbreak strain (within 0–10 allele differences), which were collected from Washington (n = 10), Oregon (n = 5), and Minnesota (n = 3) during November 2017–July 2020 (Figure 2). None of those isolates were linked to a specific animal or other type of outbreak, and no exposure information was available for the patients.

Exposure Data

We interviewed 22 patients with additional detailed questions about exposure to dogs, cats, songbirds, birdfeeders, and bird feed. Of those, 14 (64%) reported having a birdfeeder on their property, 8 recalled purchasing bird seed for their feeder within 2 months before illness onset, 7 fed bird seed that contained sunflower seeds, and 1 patient recalled feeding only dried corn. Only 1 patient recalled the brand of seed that they purchased. At the time of interview, no patients reported having any bird seed available for *Salmonella* testing. Seven (32%) patients, 6 of whom also owned birdfeeders, had contact with living or dead songbirds in the week before illness onset, including 1 patient who owned a pet sparrow and 1 who



Figure 1. Geographic locations of human *Salmonella* Typhimurium cases in the United States, 2020–2021. Colored shading indicates number of cases by state; black bird icons indicate states that detected the outbreak strain of *Salmonella* Typhimurium from wild birds (within 0–12 allele differences based on core genome multilocus sequence typing). One isolate was obtained from a dog's mouth wound at a veterinary hospital in Oregon (dog icon) and matched the outbreak strain. Numbers of genetically related isolates obtained from wild birds are indicated within animal icons. *Salmonella* Typhimurium was also detected in wild birds as part of the Southeastern Cooperative Wildlife Disease Study at the University of Georgia (gray bird icons); those isolates were serotyped at the National Veterinary Services Laboratory (30), but whole-genome sequencing was not performed to confirm relatedness to the outbreak strain.

handled a wild finch. This number was higher than the percentage of healthy persons interviewed in the 2018–2019 FoodNet Population Survey who reported contact with pet or wild birds in the 7 days before the interview (4.6% of respondents; $p = 0.001$).

Eighteen (82%) of the 22 patients owned pet dogs, and 7 (32%) owned pet cats. The percentage of patients reporting contact with dogs was significantly higher than for healthy persons interviewed in the FoodNet Population survey (68% of respondents; $p = 0.03$), but the percentage of patients reporting contact with cats was similar to that for healthy persons (39% of respondents; $p = 0.86$). Six patients reported their dog or cat was exposed to birds or birdfeeders. One patient reported their cat caught a wild bird and was subsequently hospitalized at a veterinary clinic with fever, diarrhea, and vomiting within 7 days before the patient's illness onset; no isolates were obtained from either the cat or the bird. All 8 patients reporting no exposure to

birdfeeders had a pet dog or cat. Of those patients, 2 reported their pets might have been exposed to wild birds in the week before illness onset, and 1 was the patient who handled the wild finch. Overall, 16 (73%) of 22 patients could be linked to wild bird exposure, either by direct contact with birds, contact with birdfeeders, or contact with companion animals that might have interacted with birds.

Animal Testing

Environmental health partners and wildlife experts from involved states, academic research colleagues, and representatives from the United States Geological Service and SCWDS noted an increase in reports of sick and dead songbirds on private property and around birdfeeders. State public health officials and environmental health partners similarly indicated that a songbird fatality event, primarily involving finches, was occurring congruently with the outbreak timeline. In California, 2,048 individual reports of sick and dead

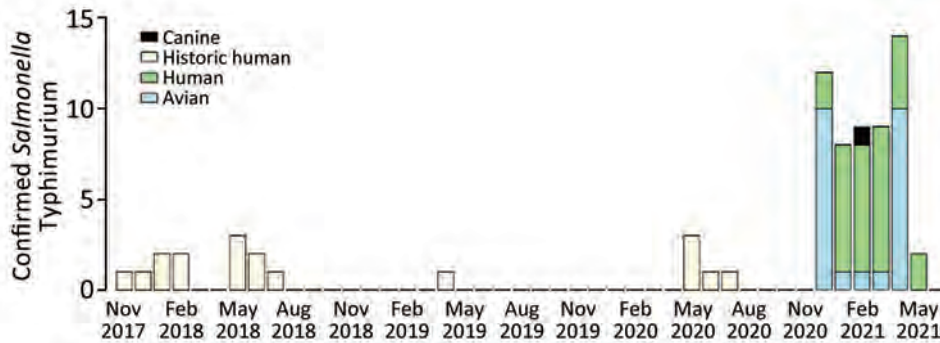


Figure 2. Epidemiologic curve of onset dates of human *Salmonella* Typhimurium illnesses and isolation dates of animal isolates, United States, November 7, 2017–May 19, 2021. Isolates shown are within 0–12 allele differences based on core genome multilocus sequence typing.

birds were provided by the public and wildlife rehabilitation centers during November 1, 2020–May 6, 2021. Those reports included \approx 2,440 sick and dead birds, and more than half were identified as pine siskins.

In total, Oregon, Washington, and California public health officials obtained 23 isolates of the outbreak strain from wild songbirds collected during December 2020–April 2021 (Figures 1, 2). The isolates were related within 0–12 cgMLST allele differences to each other and to the outbreak strain. In California, 66 songbirds from 11 counties were collected by the California Department of Fish and Wildlife’s Wildlife Health

Laboratory. Salmonellosis was identified in 15 birds selected for postmortem examination at California Animal Health and Food Safety Laboratory System, including pine siskins ($n = 9$), Lawrence’s goldfinch (*S. lawrencei*; $n = 1$), lesser goldfinches (*S. psaltria*; $n = 2$), purple finches (*Haemorhous purpureus*; $n = 2$), and yellow-rumped warbler (*Setophaga coronate*; $n = 1$). SCWDS investigators additionally identified salmonellosis in 29 songbirds of 5 species: 15 pine siskins, 11 American goldfinches (*S. tristis*), 1 northern mockingbird (*Mimus polyglottos*), 1 northern cardinal (*Cardinalis cardinalis*), and 1 brown-headed cowbird (*Molothrus ater*). Most birds examined (27/29, 93%) died during January 22, 2021–March 23, 2021; the birds were identified in 8 states (Figure 1). Histopathological findings among birds examined at California Animal Health and Food Safety Laboratory System and SCWDS were similar and included ulcerative esophagitis and ingluvititis, consistent with songbird salmonellosis.

Oregon officials sequenced a *Salmonella* isolate from a wound sample from a pet dog’s mouth that was related within 0–12 cgMLST allele differences to the outbreak strain. The dog was treated at a veterinary hospital for surgical removal of stick fragments from its mouth. The dog’s owner reported that dead birds had been observed on their property and neighboring properties, but no human illnesses were linked to contact with the dog.

A CDC Investigation Notice was posted on April 1, 2021, that detailed the outbreak investigation and provided recommendations on cleaning and maintaining birdfeeders, preventing pets from being exposed to contaminated birdfeeders, how to report dead birds, and how to properly dispose of them (31). The notice was promoted on social media, news media, and through newsletters and partner outreach with wildlife experts and state partners.

Discussion

We report a multistate outbreak of *Salmonella* infections in the United States linked to wild birds; a link

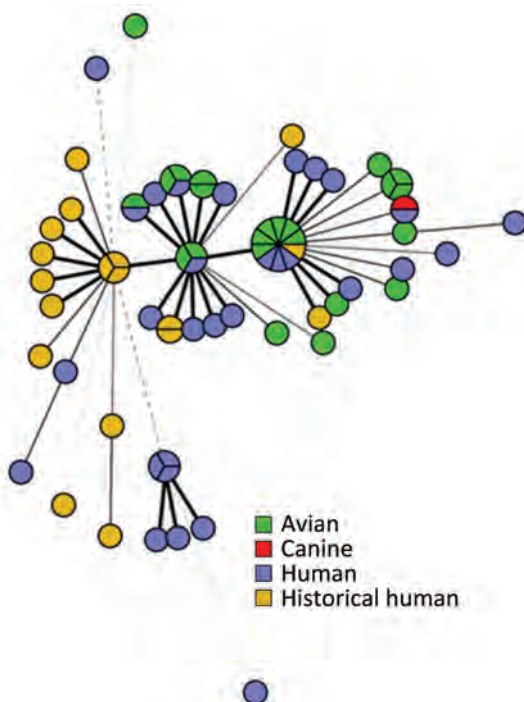


Figure 3. Minimum spanning tree demonstrating the genetic relatedness of human and animal isolates based on core genome multilocus sequence typing from samples obtained in the United States, 2021–2022. All sequences have an allele difference range of 0–12 alleles. Line length is proportionally scaled; the longer the line, the greater the allele difference is between the sequences. Isolates with no allelic variation are represented as slices of the same circle.

was previously suspected to wild birds during another salmonellosis outbreak in 2009 (6). Internationally, human illness outbreaks have been associated with direct contact with wild birds (8,11,23). *Salmonella* has been isolated from healthy and ill wild birds across the United States for decades, and salmonellosis fatality events involving wild songbirds have occurred during that time (6,10,14). However, in the United States, the general prevalence of *Salmonella* in these wild bird populations has been difficult to estimate, presenting challenges in evaluating the magnitude of the risk for *Salmonella* spillover from wild birds to humans (14). The findings of this 2020–2021 outbreak exemplify the potential for spillover. Furthermore, genetically related clinical and wild bird isolates dating back to 2017 suggest sporadic human illnesses associated with wild bird contact might have occurred before the 2020–2021 outbreak (Figure 2), but exposure information is not available from historical patients to corroborate this.

Increased incidence of deaths of songbirds were reported during the course of the 2020–2021 human salmonellosis outbreak, although the outbreak strain was not confirmed in birds in all states with human cases. Environmental health experts speculated that the presence of birdfeeders likely attracted migratory songbirds, providing a source of exposure as the infection spread among individual songbirds. Pine siskins and other irruptive migrants vary their migration pattern partially in response to the seasonal availability of food and the availability of pine crops in their natural wintering grounds in Canada (32). Those migratory variances might contribute to increased congregation of birds around birdfeeders during some winters, which might result in the buildup of fecal material on and under feeders, especially if not routinely cleaned and disinfected. If birdfeeders become contaminated with *Salmonella*, they can serve as a source for human and wild bird infections (11,33). The presence of large numbers of pine siskins at feeders has been associated with avian salmonellosis outbreaks in the past, and as a highly gregarious species, pine siskins might play an important role in the transmission of *Salmonella* at feeders (6). Although recreational supplemental feeding practices might positively affect the health of some wild birds (34), the preponderance of evidence demonstrates that unsafe feeding practices can put birds at risk for infectious diseases, particularly during migration or disease epidemics (16). Factors that could increase infectious disease spread at feeders include feeder type (e.g., platform-style feeders that enable birds to perch on top of food or feeders and are constructed of materials that are difficult to

clean); feeder location (e.g., placed in shady areas); providing various feed types that promote interspecies contact while feeding in close proximity; allowing feeders and surrounding areas to become soiled with feces, food waste, or animal carcasses; and providing food year-round regardless of external circumstances such as disease outbreaks or presence of sick and dead birds at the feeders (33).

Involvement of companion animals in this outbreak demonstrates the potential for illness transmission, either directly or indirectly, from wildlife or contaminated environments to pets and subsequently to humans. Multiple patients reported their pets had access to birdfeeders on their property or had direct contact with wild songbirds through predation. One patient's cat reportedly became ill after catching a wild bird, and the outbreak strain was isolated from the mouth wound of a pet dog during the outbreak. Contact with wildlife is a known risk factor for *Salmonella* infection in companion animals (25), and a previous outbreak of salmonellosis in cats in Sweden was linked to wild bird predation (24). Ill cats in that outbreak also were thought to be the source of human illnesses (24). This situation has similarly occurred in the United States when pets infected with *Salmonella* treated at a single veterinary clinic were subsequently linked to salmonellosis among clinic staff members and owners of those pets (35); no single source of *Salmonella* was identified, but *Salmonella* Typhimurium was the causative serotype, similar to outbreaks previously linked to wild birds (8,11,23,24,35).

Overall, clinical salmonellosis is considered rare in companion animals (25), even though, at least among free-roaming domestic cats, predation of wildlife occurs often (36). Such pets either might be infrequently exposed to *Salmonella* through wildlife predation because of variability in infection prevalence among individual birds or might be *Salmonella* carriers rather than develop clinical signs of infection. Research into the prevalence of *Salmonella* carriage among pets that are in contact with wildlife would aid in measuring the salmonellosis risk that this behavior creates for pet owners.

The first limitation of this investigation is that not all patients were available or agreed to be interviewed, limiting the amount of data on potential *Salmonella* source exposures that could be explored and representativeness of the underlying population. Second, although testing of wild bird carcasses yielded the outbreak strain, no testing of patients' homes, birdfeeders, or pets was performed to determine if the hypothesized links between humans and wildlife were definitively contaminated with the outbreak strain. Third, a limited number

of wild birds reported during this outbreak were examined; thus, cause of death cannot be confirmed as salmonellosis in all cases. Isolating the outbreak strain from individual birds could represent merely the carriage of the organism and not necessarily the cause of disease and death. Fourth, this investigation was not able to determine what factors predominantly contributed to spread of *Salmonella* among wild birds. Additional information from patients (e.g., type of feeders used, feeder location, feeding practices) or testing of feeders or bird feed for *Salmonella* might have elucidated the sources of exposure for wild birds. Finally, identifying patients as part of an outbreak necessitates those ill persons to seek medical care, healthcare providers to order appropriate diagnostic testing, and positive test results to be reported to public health departments. Therefore, our investigation is likely an underestimate of the true number of persons that were affected by the outbreak strain (1) and an overestimate of the severity of illness.

This outbreak of *Salmonella* Typhimurium demonstrates the ongoing need to raise public awareness of the potential to acquire *Salmonella* from wild animals such as songbirds. To prevent birdfeeders and birdbaths from becoming a source of infection for birds and humans, use of birdfeeders and birdbaths should be reduced or eliminated, especially during an active disease outbreak. If birdfeeders and birdbaths are in use, a minimum of monthly cleaning and disinfection is recommended, but more frequent cleaning might be needed when feeders or baths become visibly soiled or when they are placed in shady areas where they remain moist (31,37). Persons should avoid direct contact with wild birds, particularly those that are visibly sick or dead, and should wash their hands after any contact with birds, feeders, or baths, even if wearing gloves (31). Similarly, pet owners should prevent their pets from contacting wild birds, birdfeeders, spilled seed, and birdbaths to reduce the potential for them to bridge the transmission of pathogens between wildlife and humans or to become infected with *Salmonella* themselves (31). Veterinarians and veterinary staff should be aware of the potential health risk for zoonotic pathogens like *Salmonella*, particularly when treating animals that frequently contact wildlife (25). Given the repeated detection of this outbreak strain over time and the periodic deaths associated with *Salmonella* in some wild birds, it is possible for further illness to arise in persons or their pets in the United States. As such, public health officials should continue to provide information about measures to prevent the transmission of illness between persons, pets, and wildlife and should continue to conduct similar investigations by using a One Health approach.

Acknowledgments

We thank the outbreak investigation team members in local and state jurisdictions impacted by this outbreak who contributed data, effort, and time in solving this investigation. We also thank various academic partners and members of United States Geological Survey who provided comments and consultation in solving this outbreak and recommendations of actions to prevent further illnesses. We thank the staff of wildlife rehabilitation centers, members of the public, veterinarians, the Washington Department of Fish and Wildlife, and member state wildlife management agencies of SCWDS for contributing reports and specimens for examination. We thank Richard Lemana for input during development of the patient questionnaire, Julie Hatch for coordination and management of Oregon laboratory data, Karim Morey-Castro for interpretation and management of WGS results of Oregon patients and songbirds, and Katie Haman and Kristin Mansfield for reviewing this manuscript. We thank the Portland Audubon Society for coordination with Oregon Health Authority on their investigation of songbird deaths.

The findings and conclusions in this article are those of the author(s) and do not necessarily represent the views or opinions of the Centers for Disease Control and Prevention or the California Department of Public Health or the California Health and Human Services Agency.

About the Author

Kane Patel completed this analysis while he was an epidemiologist with the Outbreak Response and Prevention Branch, Division of Foodborne, Waterborne, and Environmental Diseases, National Center for Emerging and Zoonotic Infectious Diseases, Centers for Disease Control and Prevention. There, he coordinated responses for multistate outbreaks caused by enteric pathogens, with particular attention to *Salmonella* and *E. coli*. He leads a team at PVM, Inc., in modernizing public health surveillance and outbreak response systems for government agencies.

References

1. Scallan E, Hoekstra RM, Angulo FJ, Tauxe RV, Widdowson MA, Roy SL, et al. Foodborne illness acquired in the United States—major pathogens. *Emerg Infect Dis*. 2011;17:7-15. <https://doi.org/10.3201/eid1701.P11101>
2. Beshearse E, Bruce BB, Nane GF, Cooke RM, Aspinall W, Hald T, et al. Attribution of illnesses transmitted by food and water to comprehensive transmission pathways using structured expert judgment, United States. *Emerg Infect Dis*. 2021;27:182-95. <https://doi.org/10.3201/eid2701.200316>
3. Hale CR, Scallan E, Cronquist AB, Dunn J, Smith K, Robinson T, et al. Estimates of enteric illness attributable

- to contact with animals and their environments in the United States. *Clin Infect Dis*. 2012;54(Suppl 5):S472-9. <https://doi.org/10.1093/cid/cis051>
4. Shane AL, Mody RK, Crump JA, Tarr PI, Steiner TS, Kotloff K, et al. 2017 Infectious Diseases Society of America clinical practice guidelines for the diagnosis and management of infectious diarrhea. *Clin Infect Dis*. 2017;65:e45-80. <https://doi.org/10.1093/cid/cix669>
 5. Hall AJ, Saito EK. Avian wildlife mortality events due to salmonellosis in the United States, 1985-2004. *J Wildl Dis*. 2008;44:585-93. <https://doi.org/10.7589/0090-3558-44.3.585>
 6. Hernandez SM, Keel K, Sanchez S, Trees E, Gerner-Smidt P, Adams JK, et al. Epidemiology of a *Salmonella enterica* subsp. *enterica* serovar Typhimurium strain associated with a songbird outbreak. *Appl Environ Microbiol*. 2012;78:7290-8. <https://doi.org/10.1128/AEM.01408-12>
 7. Tizard I. Salmonellosis in wild birds. *Seminars in avian and Exotic Pet Medicine*. 2004;13:50-66. <https://doi.org/10.1053/j.saep.2004.01.008>
 8. Alley MR, Connolly JH, Fenwick SG, Mackereth GF, Leyland MJ, Rogers LE, et al. An epidemic of salmonellosis caused by *Salmonella* Typhimurium DT160 in wild birds and humans in New Zealand. *N Z Vet J*. 2002;50:170-6. <https://doi.org/10.1080/00480169.2002.36306>
 9. Daoust P, Prescott JF. Salmonellosis. In: Thomas N, Hunter DB, Atkinson CT, editors. *Infectious disease of wild birds*. Ames (IA); Blackwell Publishing, 2007. p. 270-288. <https://doi.org/10.1002/9780470344668>
 10. Hudson CR, Quist C, Lee MD, Keyes K, Dodson SV, Morales C, et al. Genetic relatedness of *Salmonella* isolates from nondomestic birds in southeastern United States. *J Clin Microbiol*. 2000;38:1860-5. <https://doi.org/10.1128/JCM.38.5.1860-1865.2000>
 11. Lawson B, de Pinna E, Horton RA, Macgregor SK, John SK, Chantrey J, et al. Epidemiological evidence that garden birds are a source of human salmonellosis in England and Wales. *PLoS One*. 2014;9:e88968. <https://doi.org/10.1371/journal.pone.0088968>
 12. Mather AE, Lawson B, de Pinna E, Wigley P, Parkhill J, Thomson NR, et al. Genomic analysis of *Salmonella enterica* serovar Typhimurium from wild passerines in England and Wales. *Appl Environ Microbiol*. 2016;82:6728-35. <https://doi.org/10.1128/AEM.01660-16>
 13. Refsum T, Vikøren T, Handeland K, Kapperud G, Holstad G. Epidemiologic and pathologic aspects of *Salmonella* Typhimurium infection in passerine birds in Norway. *J Wildl Dis*. 2003;39:64-72. <https://doi.org/10.7589/0090-3558-39.1.64>
 14. Smith OM, Snyder WE, Owen JP. Are we overestimating risk of enteric pathogen spillover from wild birds to humans? *Biol Rev Camb Philos Soc*. 2020;95:652-79. <https://doi.org/10.1111/brv.12581>
 15. Hamer SA, Lehrer E, Magle SB. Wild birds as sentinels for multiple zoonotic pathogens along an urban to rural gradient in greater Chicago, Illinois. *Zoonoses Public Health*. 2012;59:355-64. <https://doi.org/10.1111/j.1863-2378.2012.01462.x>
 16. Murray MH, Becker DJ, Hall RJ, Hernandez SM. Wildlife health and supplemental feeding: A review and management recommendations. *Biological Conservation*. 2016;204:163-74. <https://doi.org/10.1016/j.biocon.2016.10.034>
 17. Robb GN, McDonald RA, Chamberlain DE, Bearhop S. Food for thought: supplementary feeding as a driver of ecological change in avian populations. *Frontiers in Ecology and the Environment*. 2008;6:476-84. <https://doi.org/10.1890/060152>
 18. Fuller RA, Irvine KN. Interactions between people and nature in urban environments. In: Gaston KJ, editor. *Urban ecology* (Ecological Reviews). Cambridge: Cambridge University Press; 2012. p. 134-171. <https://doi.org/10.1017/CBO9780511778483.008>
 19. Jones DN, James Reynolds S. Feeding birds in our towns and cities: a global research opportunity. *J Avian Biol*. 2008;39:265-71. <https://doi.org/10.1111/j.0908-8857.2008.04271.x>
 20. Marzluff JM. Worldwide urbanization and its effects on birds. In: Marzluff JM, Bowman R, Donnelly R, editors. *Avian ecology and conversation in an urbanizing world*. Boston: Springer; 2011. p. 19-47. https://doi.org/10.1007/978-1-4615-1531-9_2
 21. Fuller T, Bensch S, Müller I, Novembre J, Pérez-Tris J, Ricklefs RE, et al. The ecology of emerging infectious diseases in migratory birds: an assessment of the role of climate change and priorities for future research. *EcoHealth*. 2012;9:80-8. <https://doi.org/10.1007/s10393-012-0750-1>
 22. Mills JN, Gage KL, Khan AS. Potential influence of climate change on vector-borne and zoonotic diseases: a review and proposed research plan. *Environ Health Perspect*. 2010;118:1507-14. <https://doi.org/10.1289/ehp.0901389>
 23. Kapperud G, Stenwig H, Lassen J. Epidemiology of *Salmonella typhimurium* O:4-12 infection in Norway: evidence of transmission from an avian wildlife reservoir. *Am J Epidemiol*. 1998;147:774-82. <https://doi.org/10.1093/oxfordjournals.aje.a009522>
 24. Tauni MA, Osterlund A. Outbreak of *Salmonella* Typhimurium in cats and humans associated with infection in wild birds. *J Small Anim Pract*. 2000;41:339-41. <https://doi.org/10.1111/j.1748-5827.2000.tb03214.x>
 25. Sykes JE, Marks SL. Salmonellosis. In: Sykes JE, editor. *Canine and feline infectious diseases*. St. Louis (MO): Elsevier Inc.; 2014. p. 437-44. <https://doi.org/10.1016/C2009-0-41370-9>
 26. National Center for Biotechnology Information Pathogen Detection Project. [cited 2021 Dec 8] <https://www.ncbi.nlm.nih.gov/pathogens/>
 27. Katz LS, Griswold T, Williams-Newkirk AJ, Wagner D, Petkau A, Sieffert C, et al. A comparative analysis of the lyve-set phylogenomics pipeline for genomic epidemiology of foodborne pathogens. *Front Microbiol*. 2017;8:375. <https://doi.org/10.3389/fmicb.2017.00375>
 28. Centers for Disease Control and Prevention. PulseNet methods and protocols: Whole genome sequencing (WGS). 2016 [cited 2021 Dec 6] <https://www.cdc.gov/pulsenet/pathogens/wgs.html>
 29. Centers for Disease Control and Prevention. Foodborne Disease Active Surveillance Network (FoodNet). 2020 [cited 2021 Dec 8] <https://www.cdc.gov/foodnet/index.html>
 30. Morningstar-Shaw BR, Mackie TA, Barker DK, Palmer EA. *Salmonella* serotypes isolated from animals and related sources. 2016 [cited 2022 Nov 2] <https://www.cdc.gov/nationalsurveillance/pdfs/salmonella-serotypes-isolated-animals-and-related-sources-508.pdf>
 31. Centers for Disease Control and Prevention. *Salmonella* outbreak linked to wild songbirds. 2021 [cited 2021 Dec 8]. <https://www.cdc.gov/salmonella/typhimurium-04-21/index.html>
 32. Newton I. Irruptive migration. In: Breed MD, Moore J, editors. *Encyclopedia of animal behavior*, 1st edition. Academic Press. Oxford: American Press; 2010. p. 221-229.
 33. Lawson B, Robinson RA, Toms MP, Risely K, MacDonald S, Cunningham AA. Health hazards to wild birds and risk factors associated with anthropogenic food provisioning.

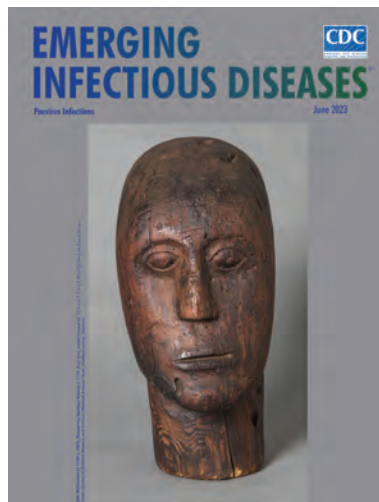
- Phil Trans R Soc Lond B Biol Sci. 2018;373:20170091. <https://doi.org/10.1098/rstb.2017.0091>
34. Wilcoxon TE, Horn DJ, Hogan BM, Hubble CN, Huber SJ, Flamm J, et al. Effects of bird-feeding activities on the health of wild birds. *Conserv Physiol*. 2015;3:cov058. <https://doi.org/10.1093/conphys/cov058>
35. Cherry B, Burns A, Johnson GS, Pfeiffer H, Dumas N, Barrett D, et al. *Salmonella* Typhimurium outbreak associated with veterinary clinic. *Emerg Infect Dis*. 2004;10:2249–51. <https://doi.org/10.3201/eid1012.040714>
36. Loyd KAT, Hernandez SM, Carroll JP, Abernathy KJ, Marshall GJ. Quantifying free-roaming domestic cat predation using animal-borne video cameras. *Biological Conservation*. 2013;160:183–9. <https://doi.org/10.1016/j.biocon.2013.01.008>
37. Feliciano LM, Underwood TJ, Aruscavage DF. The effectiveness of bird feeder cleaning methods with and without debris. *Wilson J Ornithol*. 2018;130:313–20. <https://doi.org/10.1676/16-161.1>

Address for correspondence: Megin Nichols, Centers for Disease Control and Prevention, 1600 Clifton Rd NE, Mailstop A38, Atlanta, GA 30329-4027, USA; email: gpg6@cdc.gov

June 2023

Poxvirus Infections

- Association of Persistent Symptoms after Lyme Neuroborreliosis and Increased Levels of Interferon- α in Blood
- Probable Transmission of SARS-CoV-2 from African Lion to Zoo Employees, Indiana, USA, 2021
- Epidemiologic Characteristics of Mpox among People Experiencing Homelessness, Los Angeles County, California, USA, 2022
- Case Studies and Literature Review of *Francisella tularensis*-Related Prosthetic Joint Infection
- Neurologic Complications of Babesiosis, United States, 2011–2021
- SARS-CoV-2 Seroprevalence Studies in Pets, Spain
- Similar Prevalence of *Plasmodium falciparum* and Non-*P. falciparum* Malaria Infections among Schoolchildren, Tanzania
- Early SARS-CoV-2 Reinfections Involving the Same or Different Genomic Lineages, Spain
- SARS-CoV-2 Vaccine Effectiveness against Omicron Variant in Infection-Naive Population, Australia, 2022
- Increased Incidence of Legionellosis after Improved Diagnostic Methods, New Zealand, 2000–2020



- Risk Factors for Non-O157 Shiga Toxin-Producing *Escherichia coli* Infections, United States
- Evolution of Avian Influenza Virus (H3) with Spillover into Humans, China
- Detection of Novel Poxvirus from Gray Seal (*Halichoerus grypus*), Germany
- Tanapox, South Africa, 2022
- Replication of Novel Zoonotic-Like Influenza A(H3N8) Virus in Ex Vivo Human Bronchus and Lung
- Novel Orthonairovirus Isolated from Ticks near China–North Korea Border
- Risk for Infection in Humans after Exposure to Birds Infected with Highly Pathogenic Avian Influenza A(H5N1) Virus, United States, 2022
- Results of PCR Analysis of Mpox Clinical Samples, Sweden, 2022
- SARS-CoV-2 Seroprevalence and Cross-Variant Antibody Neutralization in Cats, United Kingdom
- Ranid Herpesvirus 3 Infection in Common Frog *Rana temporaria* Tadpoles
- *Baylisascaris procyonis* Roundworm Infection in Child with Autism Spectrum Disorder, Washington, USA, 2022
- MERS-CoV-Specific T-Cell Responses in Camels after Single MVA-MERS-S Vaccination
- High Prevalence of SARS-CoV-2 Omicron Infection Despite High Seroprevalence, Sweden, 2022
- Novel Avian Influenza Virus (H5N1) Clade 2.3.4.4b Reassortants in Migratory Birds, China
- Detection of Leishmania RNA Virus 1 in Leishmania (*Viannia*) *panamensis* Isolates, Panama
- Enterovirus D68 Outbreak in Children, Finland, August–September 2022

**EMERGING
INFECTIOUS DISEASES**

To revisit the June 2023 issue, go to:
<https://wwwnc.cdc.gov/eid/articles/issue/29/6/table-of-contents>

Prevalence of Undiagnosed Monkeypox Virus Infections during Global Mpox Outbreak, United States, June–September 2022

Faisal S. Minhaj, Vijay Singh, Stephanie E. Cohen, Michael Townsend, Hyman Scott, John Szumowski, C. Bradley Hare, Pallavi Upadhyay, Jairus Reddy, Barbara Alexander, Nicolle Baird, Terese Navarra, Lalita Priyamvada, Nhien Wynn, William C. Carson, Solomon Odafe, Sarah Anne J. Guagliardo, Emily Sims, Agam K. Rao, Panayampalli S. Satheshkumar, Paul J. Weidle,¹ Christina L. Hutson¹

Since May 2022, mpox has been identified in 108 countries without endemic disease; most cases have been in gay, bisexual, or other men who have sex with men. To determine number of missed cases, we conducted 2 studies during June–September 2022: a prospective serologic survey detecting orthopoxvirus antibodies among men in San Francisco, California, who have sex with men and a retrospective monkeypox virus PCR testing of swab specimens submitted for other infectious disease testing among

all patients across the United States. The serosurvey of 225 participants (median age 34 years) detected 18 (8.0%) who were orthopoxvirus IgG positive and 3 (1.3%) who were also orthopoxvirus IgM positive. The retrospective PCR study of 1,196 patients (median age 30 years; 54.8% male) detected 67 (5.6%) specimens positive for monkeypox virus. There are likely few undiagnosed cases of mpox in regions where sexual healthcare is accessible and patient and clinician awareness about mpox is increased.

Since May 2022, monkeypox virus (MPXV) infections have been detected in 108 countries without endemic disease. Most cases have been among gay, bisexual, or other men who have sex with men (MSM). Because lesions commonly occur on the genitals, mpox was most frequently diagnosed in clinics conducting sexually transmitted infection (STI) screening (1). The diagnosis can be challenging because the mpox rash has been confused with STIs (e.g., herpes simplex virus infection

and syphilis), hand-foot-and-mouth disease, varicella zoster virus infection, and even arthropod bites (2–4). In addition to cases being undiagnosed because of diminished clinical suspicion, some cases may have been undiagnosed if patients did not seek care (i.e., because the symptoms were mild and self-limiting or because of poor access to a medical provider). As the global outbreak continued, public health authorities continued to increase awareness of mpox. However, clinicians and public health authorities were concerned that if a high number of cases were missed, the outbreak would be difficult to control. To determine the number of undiagnosed MPXV infections in the United States, we conducted 2 studies during June–September 2022: a prospective serologic surveillance study among MSM who sought sexual health services in San Francisco, California, USA, and a retrospective study of molecular testing of specimens tested for other infectious diseases linked to specific codes from the International Classification of Diseases, 10th Revision, Clinical Modification (ICD-10-CM), among all populations. Each study used specimens

Author affiliations: Centers for Disease Control and Prevention, Atlanta, Georgia, USA (F.S. Minhaj, M. Townsend, N. Baird, T. Navarra, L. Priyamvada, N. Wynn, W.C. Carson; S. Odafe, S.A.J. Guagliardo, E. Sims; A.K. Rao, P.S. Satheshkumar, P.J. Weidle, C.L. Hutson); HealthTrackRx, Denton, Texas, USA (V. Singh, P. Upadhyay, J. Reddy, B. Alexander); San Francisco Department of Public Health, San Francisco, California, USA (S.E. Cohen, H. Scott); University of California San Francisco and Zuckerberg San Francisco General Hospital, San Francisco (J. Szumowski); Kaiser Permanente Northern California, San Francisco (C.B. Hare)

DOI: <https://doi.org/10.3201/eid2911.230940>

¹These authors contributed equally to this article.

collected during the peak of the outbreak. Our studies were reviewed by the Centers for Disease Control and Prevention (CDC) and were conducted consistent with applicable federal law and CDC policy (e.g., 45 C.F.R. part 46.102(l)(2), 21 C.F.R. part 56; 42 U.S.C. §241(d); 5 U.S.C. §552a; 44 U.S.C. §3501 et seq.).

Methods

Prospective Serologic Survey

For the primary recruitment sites for this serologic survey, we selected 3 prominent sexual health clinics (clinics A, B, C) in San Francisco that regularly treat MSM

and 1 research clinic in San Francisco (clinic D). Those 4 private and publicly funded clinics encompass an estimated 20,000 MSM patients of varying socioeconomic status, insured rates (2%–85% private, 14%–92% public, 0–40% uninsured), and races and ethnicities within the San Francisco Bay area. Patients entering the 3 sexual health clinics during June 28–August 26, 2022, were given an informational flier in English or Spanish containing a QR code that directed interested patients to a survey to self-screen for inclusion. The flier also stated that participation was voluntary and the decision to enroll would not in any way affect their medical care. Study inclusion was limited to patients who self-reported that

Table 1. Demographics and characteristics of 225 participants in study of prevalence of undiagnosed monkeypox virus infections during the global mpox outbreak, United States, June–September 2022*

Characteristic or demographic	No. (%)
Demographic	
Age, y	34 (29–42)
Race/ethnicity	
Hispanic	42 (18.7)
Non-Hispanic	
Asian	35 (15.6)
Black	20 (8.9)
Native American or Pacific Islander	4 (1.8)
White	119 (52.9)
Prefer not to answer	5 (2.2)
Sexual orientation	
Bisexual	22 (9.8)
Gay	196 (87.1)
Straight	0
A different term	6 (2.7)
Prefer not to answer	1 (0.4)
Clinic	
A	23 (10.2)
B	131 (58.2)
C	52 (23.1)
D	19 (8.4)
Known contact with someone with mpox	26 (11.6)
Travel in the past 3 mo†	77 (34.2)
International	29 (43.3)
Europe	17 (25.4)
Americas	13 (19.4)
Domestic	38 (56.7)
Sex partners in the past 1 mo	
0	22 (9.8)
1–4	135 (60)
5–9	37 (16.4)
10–19	20 (8.9)
≥20	11 (4.9)
Attended a large event (e.g., festivals, parades, weddings, clubs, sex parties)	130 (57.8)
Immunocompromising conditions	
Yes	65 (28.9)
HIV	58 (89.2)
CD4 count, cells/mm ³	
≥200	27 (46.6)
<200	8 (13.8)
Unknown	23 (39.7)
HIV viral load, copies/mL	
≥200	9 (15.5)
<200	34 (58.6)
Unknown	15 (25.9)

*Results of serologic survey (Appendix 1, <https://wwwnc.cdc.gov/EID/article/29/11/23-0940-App1.pdf>).

†Location unknown for 10 persons who had traveled.

they did not have symptoms of mpox (e.g., rash, fever, lymphadenopathy), had never received an mpox diagnosis, were 18–50 years of age (the upper age limit was set to exclude childhood smallpox vaccination in the United States), and did not have a history of smallpox or mpox vaccination. Because most cases detected at that point in the outbreak were in MSM, and to ensure sufficient participation among this population at high risk for mpox, we also excluded cisgender women and persons who did not identify as ever having had male-to-male sexual contact. Participants at clinic D were recruited by a query into the electronic medical record system from HIV and HIV pre-exposure prophylaxis registries; a subset of MSM patients 18–50 years of age were sent an invitation to participate. At clinic arrival, those participants were given the same survey to self-screen. All participants who completed the self-screening questionnaire and were eligible for study inclusion, then completed a brief 7-question electronic survey that asked about factors thought to be associated with risk for mpox during the initial stage of the outbreak that could affect public health action (e.g., travel and exposure history within the past 90 days) (Appendix 1, <https://wwwnc.cdc.gov/EID/article/29/11/23-0940-App1.pdf>) (3). We collected 5 mL of blood from each participant who completed the questionnaire. Peak IgM is detected 2–3 weeks and IgG 3–5 weeks after exposure to an orthopoxvirus (including primary vaccination with ACAM2000 [second-generation live vaccinia virus vaccine] and JYNNEOS [third-generation live, non-replicating, modified vaccinia Ankara Bavarian Nordic vaccine; <https://jynneos.com>] and convalescence has been documented at 7–14 weeks after exposure. Orthopoxvirus IgM is reliably detected 4–56 days and IgG \geq 8 days after rash onset (5). Because IgG persists for several years after orthopoxvirus exposure (6), we chose IgG as the initial screening tool to detect any past orthopoxvirus exposure. To detect recent exposure, we tested positive IgG specimens for IgM. We separated serum by centrifugation, aliquoted the samples, and sent them to CDC for ELISA analysis of orthopoxvirus IgG and, if positive, IgM.

Retrospective Molecular Testing

During the multinational outbreak that began in 2022, mpox was diagnosed by nonvariola orthopoxvirus- and MPXV-specific real-time PCR tests of lesion swab samples (7,8). Before an mpox-specific diagnosis code (B.04) was established, clinical diagnoses and testing were documented with ICD-10-CM codes representing broad symptoms of infection, which were used as a surveillance tool for early identification of potentially undiagnosed infections

Table 2. Clinical signs/symptoms reported by participants in study of prevalence of undiagnosed monkeypox virus infections during the global mpox outbreak, United States, June–September 2022*

Acute illness sign/symptoms in past 3 months	No. (%)
Cough	28 (12)
Rhinorrhea	27(11)
Sore throat	23 (10)
Fever	22 (9)
Chills	21(9)
Headaches	20 (8)
Sweats	15 (6)
Malaise	15 (6)
Shortness of breath	12 (5)
Lymphadenopathy	8 (3)
Diarrhea	7 (3)
Rash	6 (3)
Wheezing	5 (2)
Itchiness	4 (2)
Nausea/vomiting	4 (2)
Abdominal pain	4 (2)
Back pain	4 (2)
Rectal bleeding	3 (1)
Stridor	2 (1)
Rectal pain	2 (1)
Eye lesions	1
Pus in stool	1
Penile discharge	1

*Results of serologic survey (Appendix 1, <https://wwwnc.cdc.gov/EID/article/29/11/23-0940-App1.pdf>).

similar to other diseases (9,10). To evaluate the presence of MPXV within specimens received for other testing, CDC partnered with HealthTrackRx, a private laboratory that receives specimens from a variety of clinics across the United States for infectious disease testing. During June 1–September 2, 2022, CDC deidentified and tested lesion swab specimens associated with ICD-10-CM codes for genital lesions, herpes simplex virus infection, inflammation of the genital region, skin rash, and others that may overlap with symptoms of mpox (Appendix 2, <https://wwwnc.cdc.gov/EID/article/29/11/23-0940-App2.pdf>) for presence of MPXV DNA by using a clade II-specific PCR (8). After June 27, 2022, HealthTrackRx validated its own mpox clade II-specific assay (8) and continued to test specimens for MPXV that fit the ICD-10-CM codes (Appendix 2). No specimens were excluded; only basic demographic and geographic data and pertinent ICD-10-CM codes that may be associated with mpox were available from the initial test request from the submitting clinician. No information about sexual history was included.

Results

Prospective Serologic Survey

During the study period, \approx 8,670 patients were seen at clinics A, B, and C, of which 3,832 (44.2%) were

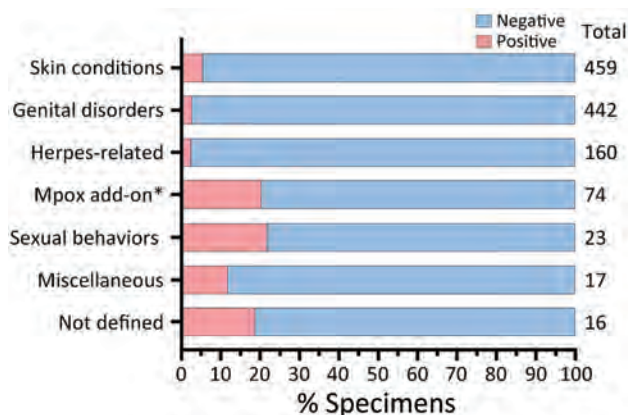


Figure 1. Total numbers and percentages of positive results for specimens tested by monkeypox virus–specific PCR under different code categories by the International Classification of Diseases, 10th Revision, Clinical Modification, United States, June–September 2022. *Mpox add-on is defined as having an initial negative result from other testing, after which a provider requested testing for mpox.

MSM, 18–50 years of age, and may have been eligible for participation. An estimated 6,000 persons from clinic D were eligible for study participation, and 2,400 (40%) were sent an invitation to participate. A total of 398 patients started the survey. Of 358 (87.4%) participants who completed the survey, 133 were excluded for not self-identifying as having male-to-male sexual contact ($n = 67$), reporting previous receipt of smallpox or mpox vaccination ($n = 41$), being >50 years of age ($n = 18$), or reporting a past diagnosis of mpox ($n = 7$). We collected serum samples from the final sample size of 225

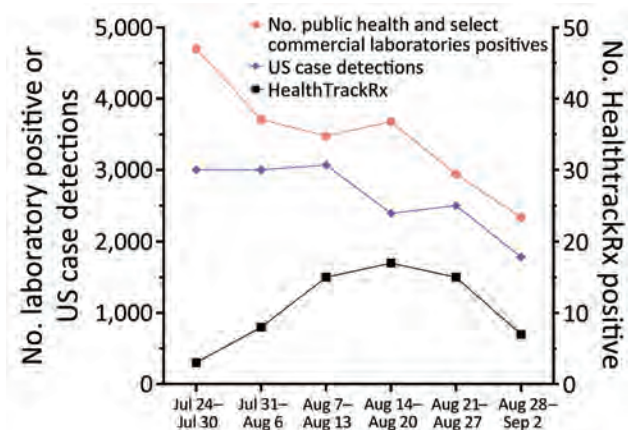


Figure 2. Weekly positive detection of monkeypox virus by PCR testing and US Centers for Disease Control and Prevention case detection (<https://www.cdc.gov/ecr/index.html>), July 24–September 2, 2022. Results are from public health and select commercial laboratories and HealthTrackRx testing and US case detections. The greater number of laboratory positives than US case detections most likely results from testing of multiple samples from a single patient.

participants. Participant median age was 34 (interquartile range [IQR] 29–42) years. Most (52.9%) eligible participants were non-Hispanic White, and most (87.1%) reported sexual orientation as gay (Tables 1, 2). Twenty-six (11.6%) participants reported known contact with someone with mpox. Recent travel (previous 3 months) was reported by 77 (34.2%); among the 67 who reported a location, 38 (56.7%) had traveled in the United States, 17 (25.4%) to Europe, and 13 (19.4%) to other countries within the Americas. A total of 130 (57.8%) participants had attended a large private or public event (e.g., festivals, parades, weddings, clubs, sex parties). Most (203, 91.2%) participants had ≥ 1 sexual contact in the previous month, among which 68 (30.2%) had ≥ 5 partners. A total of 65 (28.9%) participants had an immunocompromising condition, most commonly HIV (89.2%; $n = 58$). Of those who reported HIV, 8 (13.8%) reported a CD4 count <200 cells/mm³ and 9 (15.5%) reported a viral load ≥ 200 copies/mL. Among the 47 (20.9%) who reported being ill in the previous 3 months, the most common signs/symptoms were cough, rhinorrhea, sore throat, fever, and chills (participants could report >1 sign/symptom).

Of 225 serum samples tested for orthopoxvirus IgG, 18 (8.0%) were positive and 3 (1.3%) were also positive for orthopoxvirus IgM. Those 3 participants were 20–49 years of age. Two patients denied prior smallpox or mpox vaccination; vaccination status for the third patient was unknown. All 3 participants had traveled in the previous 3 months (2 internationally and 1 domestically), 1 reported attending a large event, and 1 reported having had contact with someone with mpox. All 3 participants reported having had 3–20 sex partners within the previous month. Two participants reported signs/symptoms consistent with mpox in the previous 3 months, including rash, diaphoresis, and lymphadenopathy. One participant had well-controlled HIV (CD4 count >200 cells/ μ L).

Retrospective Molecular Testing

During the study period, MPXV testing was performed for 1,196 patients (median age 30 [IQR 19–46] years); 656 (54.8%) were men. The most common specimen collection sites were arm (24.8%; $n = 297$), anogenital (18.6%; $n = 222$), leg (10.1%; $n = 121$), and unspecified (14.2%; $n = 170$). The ICD-10-CM codes accompanying specimens were broadly categorized as disorder of the genitals, herpes-related lesions, pruritus, cellulitis, skin conditions, vaginitis, high-risk sexual behavior, mpox, miscellaneous, and not defined. A total of 67 (5.6%) specimens

Table 3. International Classification of Diseases, 10th Revision, Clinical Modification codes associated with PCR-positive specimens in study of monkeypox virus infections, United States, June–September 2022

Code	Description
K13.70	Disease of oral mucosa, unspecified
R36.9	Urethral discharge, unspecified
R19.8	Other specified symptoms and signs involving the digestive system and abdomen
R21, R30	Rash and other nonspecific skin eruption, pain associated with micturition
M79.10	Myalgia unspecified site
B08.8, J02.9, R21	Other specified viral infections characterized by skin and mucous membrane lesions
L98.9, N48.9	Disorder of the skin and subcutaneous tissue, unspecified, disorder of penis, unspecified
Z72.52	High-risk homosexual behavior
A63.8, A64	Other specified predominantly sexually transmitted diseases, unspecified sexually transmitted disease
R21, Z11.3	Rash and other nonspecific skin eruption, encounter for screening for infections with a predominantly sexual mode of transmission
L98.9	Disorder of the skin and subcutaneous tissue, unspecified
N48.5	Ulcer of penis
Z20.828	Contact with and (suspected) exposure to other viral communicable diseases
N50.89, R21	Other specified disorders of the male genital organs, rash and other nonspecific skin eruption
A63.0	Anogenital (venereal) warts
A60.1, A63.0	Herpes viral infection of perianal skin and rectum, anogenital (venereal) warts
L08.9	Local infection of skin and subcutaneous tissue, unspecified
N48.5, N50.89, R22.0	Ulcer of penis, other specified disorders of the male genital organs, localized swelling, mass and lump of skin and subcutaneous tissue
B34.9, R50.9, R53.83, Z20.822	Viral infection, unspecified
N48.5, R36.9, Z72.51	Ulcer of penis, urethral discharge, unspecified, high-risk heterosexual behavior
L30.8, R21	Other specified dermatitis, rash and other nonspecific skin eruption
B89, R21	Unspecified parasitic disease, rash and other nonspecific skin eruption
I88.9, N48.89, R36.9	Nonspecific lymphadenitis, unspecified, other specified disorders of penis, urethral discharge, unspecified
K60.2	Anal fissure, unspecified
N48.9, S30.812A	Disorder of penis, unspecified, abrasion of penis
N50.89	Other specified disorders of the male genital organs
L08.89, L98.8	Local infection of skin and subcutaneous tissue, unspecified, other specified disorders of the skin and subcutaneous tissue
Z11.3, Z20.822	Encounter for screening for infections with a predominantly sexual mode of transmission, contact with and (suspected) exposure to other viral communicable diseases
R07.0, R21	Pain in throat, rash and other nonspecific skin eruption
R50.9, Z20.822	Fever, unspecified, contact with and (suspected) exposure to other viral communicable diseases
Z20.2	Contact with and exposure to infections with a predominantly sexual mode of transmission
L30.8	Other specified dermatitis
B04, Z11.3	Monkeypox, encounter for screening for infections with a predominantly sexual mode of transmission
R23.8, Z20.2	Other skin changes, contact with and exposure to infections with a predominantly sexual mode of transmission
A600	Anogenital herpes viral (herpes simplex) infections
B00.2	Herpes viral gingivostomatitis and pharyngotonsillitis
N48.5, Z11.3	Ulcer of penis, encounter for screening for infections with a predominantly sexual mode of transmission
J03.90, K13.79	Acute tonsillitis, unspecified, other lesions of oral mucosa
L03.818	Cellulitis of other sites
L02.818	Cutaneous abscess of other sites

tested positive for MPXV DNA (Figure 1). The dates that the positive specimens had been obtained corresponded to the increase in mpox epidemic curve in the United States (Figure 2). Most MPXV-positive specimens were associated with skin conditions, including ICD-10-CM codes R21 (rash and other nonspecific skin eruption), L98.9 (disorder of skin and subcutaneous tissue, unspecified), L08.89 (other specified local infections of the skin and subcutaneous tissue), and disorders of the genital regions including N48.5 (ulcer of the penis) (Table 3). Among those categories, all specimens with ICD-

10-CM codes corresponding to signs/symptoms of pruritis, cellulitis, and vaginitis tested negative for MPXV; no positive specimens were from women. Among the 67 MPXV-positive specimens, 5 (7.3%) ICD-10-CM codes were classified under sexual behavior that places someone at increased STI/HIV risk and 4 (5.8%) under herpes-related lesions. Of the 67 positive specimens, 15 (20.3%) were among 74 specimens that were originally submitted for testing of other infectious organisms but after negative results had been submitted for MPXV testing at provider request.

Most specimens received were from Michigan (12.8%), Georgia (12.0%), Colorado (10.4%), and Florida (9.9%); however, the highest proportion of specimens that tested positive for mpox were from Georgia (24.5%, 35 positive), followed by Missouri (25.0%, 5 positive) and Texas (12.9%, 11 positive) (Table 4). Specimens were also tested on the STI and wound infection PCR panels at HealthTrackRx. Among the specimens testing positive for mpox, only 1 tested positive for other etiologies consistent with contamination (*Finegoldia magna*, *Cutibacterium acnes*, and *Peptostreptococcus* spp).

Discussion

A total of 21,798 mpox cases were reported in the United States during the peak of the outbreak, June–September 2022, accounting for 72.0% of the total US cases reported as of March 2023. Despite concerns that some cases could be undetected (particularly in the MSM community), potentially preventing outbreak control, the serologic survey identified only 1.3% of MSM patients at high risk for mpox without a known mpox diagnosis who had orthopoxvirus IgM, indicating recent exposure to mpox. That rate of IgM positivity is similar to the 1.4% rate among persons experiencing homeless-

ness in San Francisco during July–October 2022 (11). Mpox was retrospectively detected by PCR in 5.6% of lesion swab samples obtained across the country, suggesting that mpox was probably undiagnosed in a small subset of symptomatic patients during the height of the mpox outbreak in the United States. The highest percentage positivity was among those who reported sexual behavior that places someone at increased for STI/HIV. However, the second highest percentage positivity was among those for whom mpox testing was retrospectively ordered by the clinician after negative diagnostic test results for other common rash illnesses, suggesting that clinician awareness was higher for mpox during this period. The data from the 2 analyses reported here indicate that as long as persons are aware of mpox and the need to seek medical care, the percentage of undiagnosed cases remains low, as it did during the peak of the outbreak.

The clinical manifestations (especially skin lesions, pustules, and rashes) of mpox patients can be confused with those of varicella zoster virus and STIs (e.g., herpes and syphilis), and mpox can co-occur with other STIs. However, in the molecular study, we did not find any significant levels of co-infections with mpox and other STIs.

Table 4. Positive monkeypox virus PCR detections and case detections by state, United States, June–September 2022*

State	Total tested by HealthTrackRx	MPXV PCR positive, no. (%)	CDC case detections	Mpox cases detected by HealthTrackRx, %
Georgia	143	35 (24.5)	1,602	2.2
Missouri	20	5 (25)	72	6.9
Texas	85	11 (12.9)	2,012	0.5
Nevada	12	1 (8.3)	234	0.4
Illinois	15	1 (6.7)	1,181	0.1
California	31	2 (6.5)	4,389	0
North Carolina	18	1 (5.6)	414	0.2
Michigan	153	7 (4.6)	234	3.0
Florida	119	3 (2.5)	2,269	0.1
Colorado	124	1 (0.8)	268	0.4
Arizona	96	0	386	0
Wisconsin	95	0	74	0
Ohio	90	0	237	0
Arkansas	31	0	40	0
Oklahoma	23	0	29	0
Kentucky	16	0	40	0
Wyoming	16	0	2	0
Alabama	14	0	95	0
Indiana	14	0	195	0
Iowa	10	0	21	0
New Mexico	10	0	35	0
Oregon	10	0	191	0
Idaho	9	0	13	0
Kansas	9	0	7	0
Mississippi	8	0	51	0
Washington	7	0	469	0
Tennessee	6	0	228	0
Maryland	4	0	580	0
New Hampshire	4	0	27	0
New Jersey	2	0	614	0
Rhode Island	2	0	60	0

*CDC, Centers for Disease Control and Prevention; MPXV, monkeypox virus.

That the earliest positive IgM result was obtained in mid-July suggests infection up to 56 days earlier. The lack of IgM detection before that time, in a small sample from 1 region, is suggestive that cases may not have been prevalent before the first detection on May 17. Of the 3 persons with an IgM-positive result, 2 self-reported symptoms consistent with mpox within the previous 3 months.

Among the limitations of our analyses, the response rates to the survey were low. The serologic survey relied on patient self-screening through the survey questionnaire, self-reported symptoms, and travel history. Also, the serologic survey was conducted in San Francisco, where infrastructure and resources may not be reflective of other geographic locations. Because the serologic survey was a point seroprevalence study, no follow-up testing or interviews were conducted among the participants who were positive for orthopoxvirus IgM; it is unknown whether any participants previously had signs/symptoms that were not reported on the survey or if signs/symptoms ultimately developed. Only 3 specimens were positive for both orthopoxvirus IgG and IgM. For the other 15 IgG-positive/IgM-negative specimens, it is unknown whether the participants had been exposed to orthopoxvirus beyond the IgM detection window or whether they did not self-report previous vaccination (many JYNNEOS vaccination campaigns were ongoing during the study period). We did not collect information on military service, which would include persons who may have received ACAM2000, a live-replicating vaccinia virus vaccine that results in production of orthopoxvirus antibodies. Because we used IgG as the initial screening tool, a participant could have been IgM positive and IgG negative; however, because that window of time is small (3–4 days), the likelihood of missing potential cases is low. The major limitations of molecular testing were similar to those of any study relying on ICD-10-CM codes for analysis and for which detailed patient history was not available beyond the ICD-10-CM codes on test requisitions.

In conclusion, the rate of undiagnosed mpox infections during the peak of reported cases in the United States was low among persons at high risk for disease (represented by participants in the San Francisco serosurvey). Mpox diagnosis was probably missed for some persons with rash (represented by retrospective molecular testing at HealthTrackRx), and providers should remain vigilant and conduct mpox testing from lesion swab samples on patients with mpox signs/symptoms. We rapidly collected our data during the peak of the outbreak

to provide information for the epidemiologic response. Ongoing serologic and molecular studies that are underway that use specimens stored before May 2022 will be useful for determining whether mpox was present before the outbreak was identified in the United States.

Acknowledgments

We thank Inger Damon for early constructive conversations with HealthTrackRx, members of the CDC mpox outbreak response (including the Laboratory and Testing and Epidemiology Task Forces), Nathanael Gistand, staff at each participating clinic site, and the patients who volunteered for the serologic study. We also acknowledge Bernadette Aragon, Jon Oskarsson, and Judith Sansone for their research contributions.

Use of trade names and commercial sources are for identification only and do not imply endorsement by the US Department of Health and Human Services.

About the Author

Dr. Minhaj is an emergency medicine pharmacist/toxicologist and an epidemiologist at CDC within the Poxvirus and Rabies Branch, Division of High-Consequence Pathogens and Pathology, National Center for Emerging and Zoonotic Infectious Diseases. His work focuses on medical countermeasures related to orthopoxviruses.

References

1. Thornhill JP, Barkati S, Walmsley S, Rockstroh J, Antinori A, Harrison LB, et al. Monkeypox virus infection in humans across 16 countries. *N Engl J Med*. 2022;387:679–91. <https://doi.org/10.1056/NEJMoa2207323>
2. McCollum AM, Damon IK. Human monkeypox. *Clin Infect Dis*. 2014;58:260–7. <https://doi.org/10.1093/cid/cit703>
3. Minhaj FS, Ogale YP, Whitehill F, Schultz J, Foote M, Davidson W, et al. Monkeypox outbreak – nine states, May 2022. *MMWR Morb Mortal Wkly Rep*. 2022;71:764–9. <https://doi.org/10.15585/mmwr.mm7123e1>
4. Hughes CM, Liu L, Davidson WB, Radford KW, Wilkins K, Monroe B, et al. A tale of two viruses: coinfections of monkeypox and varicella zoster virus in the Democratic Republic of Congo. *Am J Trop Med Hyg*. 2020;104:604–11. <https://doi.org/10.4269/ajtmh.20-0589>
5. Karem KL, Reynolds M, Braden Z, Lou G, Bernard N, Patton J, et al. Characterization of acute-phase humoral immunity to monkeypox: use of immunoglobulin M enzyme-linked immunosorbent assay for detection of monkeypox infection during the 2003 North American outbreak. *Clin Diagn Lab Immunol*. 2005;12:867–72. <https://doi.org/10.1128/CDLI.12.7.867-872.2005>
6. Taub DD, Ershler WB, Janowski M, Artz A, Key ML, McKelvey J, et al. Immunity from smallpox vaccine persists for decades: a longitudinal study. *Am J Med*. 2008;121:1058–64. <https://doi.org/10.1016/j.amjmed.2008.08.019>

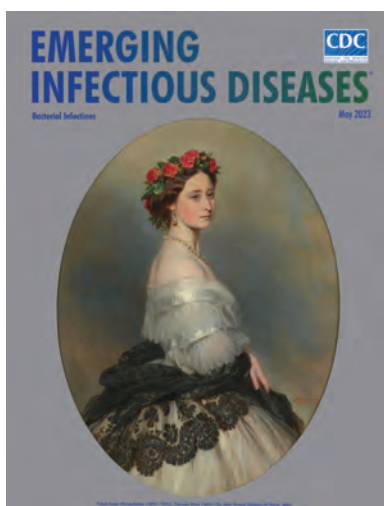
7. Li Y, Olson VA, Laue T, Laker MT, Damon IK. Detection of monkeypox virus with real-time PCR assays. *J Clin Virol*. 2006;36:194–203. <https://doi.org/10.1016/j.jcv.2006.03.012>
8. Li Y, Zhao H, Wilkins K, Hughes C, Damon IK. Real-time PCR assays for the specific detection of monkeypox virus West African and Congo Basin strain DNA. *J Virol Methods*. 2010;169:223–7. <https://doi.org/10.1016/j.jviromet.20107.012>
9. Dixon BE, Rahurkar S, Ho Y, Arno JN. Reliability of administrative data to identify sexually transmitted infections for population health: a systematic review. *BMJ Health Care Inform*. 2019;26. <https://doi.org/10.1136/bmjhci-2019-100074>
10. Mauk KC, Torrone EA, Flagg EW. Can diagnostic codes in health care claims data identify confirmed chlamydial and gonococcal infections? A retrospective cohort study, 2003 to 2017. *Sex Transm Dis*. 2021;48:S26–s31. <https://doi.org/10.1097/OLQ.0000000000001454>
11. Waddell CJ, Filardo TD, Prasad N, Pellegrini GJ Jr., Persad N, Carson WC, et al. Possible undetected mpox infection among persons accessing homeless services and staying in encampments—San Francisco, California. *MMWR Morb Mortal Wkly Rep*. 2023;72:227–31. <https://doi.org/10.15585/mmwr.mm7209a3>

Address for correspondence: Faisal S. Minhaj, Centers for Disease Control and Prevention, 1600 Clifton Rd NE, Mailstop H24-12, Atlanta, GA 30329-4027, USA; email: rhu5@cdc.gov

May 2023

Bacterial Infections

- Trends in and Risk Factors for Recurrent *Clostridioides difficile* Infection, New Haven County, Connecticut, USA, 2015–2020
- Phylogenetic Analysis of Transmission Dynamics of Dengue in Large and Small Population Centers, Northern Ecuador
- Emergence of Erythromycin-Resistant Invasive Group A *Streptococcus*, West Virginia, USA, 2020–2021
- Environmental, Occupational, and Demographic Risk Factors for Clinical Scrub Typhus, Bhutan
- Misdiagnosis of *Clostridioides difficile* Infections by Standard-of-Care Specimen Collection and Testing among Hospitalized Adults, Louisville, Kentucky, USA, 2019–2020
- SARS-CoV-2 Seroprevalence Compared with Confirmed COVID-19 Cases among Children, Colorado, USA, May–July 2021
- Disparities in Implementing COVID-19 Prevention Strategies in Public Schools, United States, 2021–22 School Year
- *Leishmania donovani* Transmission Cycle Associated with Human Infection, *Phlebotomus alexandri* Sand Flies, and Hare Blood Meals, Israel
- Case–Control Study of Long COVID, Sapporo, Japan
- Influence of Sex and Sex-Based Disparities on Prevalent Tuberculosis, Vietnam, 2017–2018 [
- Use of High-Resolution Geospatial and Genomic Data to Characterize Recent Tuberculosis Transmission, Botswana



- *Borrelia miyamotoi* Infection in Immunocompromised Man, California, USA, 2021
- Novel Circovirus in Blood from Intravenous Drug Users, Yunnan, China
- Cystic Echinococcosis in Northern New Hampshire, USA
- Therapeutic Failure and Acquired Bedaquiline and Delamanid Resistance in Treatment of Drug-Resistant TB
- Mpox among Public Festival Attendees, Chicago, Illinois, USA, July–August 2022
- Severe *Streptococcus equi* Subspecies *zooepidemicus* Outbreak from Unpasteurized Dairy Product Consumption, Italy
- Characteristics and Treatment of *Gordonia* spp. Bacteremia, France
- No Substantial Histopathologic Changes in *Mops condylurus* Bats Naturally Infected with Bombali Virus, Kenya
- Comparative Aerosol and Surface Stability of SARS-CoV-2 Variants of Concern
- Poor Prognosis for Puumala Virus Infections Predicted by Lymphopenia and Dyspnea
- Rustrela Virus as Putative Cause of Nonsuppurative Meningoencephalitis in Lions
- Limited Nosocomial Transmission of Drug-Resistant Tuberculosis, Moldova
- *Burkholderia pseudomallei* Laboratory Exposure, Arizona, USA
- Epizootic Hemorrhagic Disease Virus Serotype 8, Italy, 2022
- Spatiotemporal Evolution of SARS-CoV-2 Alpha and Delta Variants during Large Nationwide Outbreak of COVID-19, Vietnam, 2021
- Emerging Invasive Group A *Streptococcus* M1UK Lineage Detected by Allele-Specific PCR, England, 2020
- Cutaneous Leishmaniasis Caused by *Leishmania infantum*, Israel, 2018–2021
- Fatal Case of Heartland Virus Disease Acquired in the Mid-Atlantic Region, United States
- Case Report and Literature Review of Occupational Transmission of Monkeypox Virus to Healthcare Workers, South Korea
- Unknown Circovirus in Immunosuppressed Patient with Hepatitis, France, 2022

**EMERGING
INFECTIOUS DISEASES**

To revisit the May 2023 issue, go to:

<https://wwwnc.cdc.gov/eid/articles/issue/29/5/table-of-contents>

Duration of Enterovirus D68 RNA Shedding in the Upper Respiratory Tract and Transmission among Household Contacts, Colorado, USA

Hai Nguyen-Tran, Careese Thompson, Molly Butler, Kristen R. Miller, Laura Pyle, Sarah Jung, Shannon Rogers, Terry Fei Fan Ng, Janell Routh, Samuel R. Dominguez, Kevin Messacar

Enterovirus D68 (EV-D68) causes cyclical outbreaks of respiratory disease and acute flaccid myelitis. EV-D68 is primarily transmitted through the respiratory route, but the duration of shedding in the respiratory tract is unknown. We prospectively enrolled 9 hospitalized children with EV-D68 respiratory infection and 16 household contacts to determine EV-D68 RNA shedding dynamics in the upper respiratory tract through serial midturbinate specimen collections and daily symptom diaries. Five (31.3%) household contacts, including 3 adults, were EV-D68–positive. The median duration of EV-D68 RNA shedding in the upper respiratory tract was 12 (range 7–15) days from symptom onset. The most common symptoms were nasal congestion (100%), cough (92.9%), difficulty breathing (78.6%), and wheezing (57.1%). The median illness duration was 20 (range 11–24) days. Understanding the duration of RNA shedding can inform the expected rate and timing of EV-D68 detection in associated acute flaccid myelitis cases and help guide public health measures.

Enterovirus D68 (EV-D68) is a nonpolio enterovirus that causes respiratory illness and can result in acute flaccid myelitis (AFM), a devastating polio-like neurologic disease (1–17). This positive-sense single-stranded RNA virus is transmitted primarily through respiratory droplets and is an emerging pathogen of public health concern. EV-D68 has been recognized as a cause of recurrent cyclical outbreaks of asthma-like respiratory disease and AFM since 2014, affecting families, healthcare systems, and society (1,2,5,8,10,11,13,18,19).

Author affiliations: University of Colorado, Aurora, Colorado, USA (H. Nguyen-Tran, K.R. Miller, L. Pyle, S.R. Dominguez, K. Messacar); Children’s Hospital Colorado, Aurora (C. Thompson, M. Butler, S. Jung); Centers for Disease Control and Prevention, Atlanta, Georgia, USA (S. Rogers, T.F.F. Ng, J. Routh)

DOI: <https://doi.org/10.3201/eid2911.230947>

The causal link between EV-D68 and AFM is strong, but EV-D68 is still not identified in most epidemiologically linked AFM cases (3,9,17). Compared with poliovirus and other nonpolio enteroviruses, EV-D68 has properties that more closely resemble rhinovirus (9,13). EV-D68 can be acid labile and is thus less likely to be detected in stool, grows most optimally at 33°C, and is transmitted in the upper respiratory tract (9,13). However, unlike rhinoviruses and some other respiratory viruses, the duration of RNA shedding in the upper respiratory tract and the timeline of clinical manifestations of EV-D68 respiratory illness are unknown.

In this study, we investigated the duration of EV-D68 RNA shedding in the upper respiratory tract and the associated clinical characteristics in children hospitalized with EV-D68 respiratory disease and their household contacts. We hypothesized that the duration of RNA shedding of EV-D68 would be similar to that of rhinovirus at a median of 11.4 days (20). Determining RNA shedding dynamics has implications for expected rates of detection in EV-D68–associated AFM cases that can help inform clinical diagnosis and public health measures.

Methods

Study Description

We performed a prospective observational cohort study during September–November 2022, during an EV-D68 outbreak at Children’s Hospital Colorado in Aurora, Colorado, USA. Children’s Hospital Colorado is a large, freestanding children’s hospital with 444 beds serving a 7-state region. The study was approved by the Colorado Multiple Institutional Review Board. We obtained written informed consent, and assent when applicable, from all participants.

Study Participants and Study Procedures

Patients hospitalized at Children's Hospital Colorado for respiratory illness who were positive for rhinovirus/enterovirus by provider-directed testing on the BioFire Respiratory 2.1 Panel (BioFire Diagnostics, <https://www.biofire.com>) were eligible to be included as primary participants in the study. Household contacts of enrolled primary participants were also eligible for inclusion. We excluded persons <2 months of age or ≥65 years of age, persons who tested positive for SARS-CoV-2 (for infection control purposes), and persons with contraindications to respiratory specimen collection.

For primary participants and household contacts who were present at bedside, we collected a midturbinate flocked swab sample (COPAN Diagnostics, <https://www.copanusa.com>) on the day of enrollment, daily while the primary participant was admitted, and every 3 days after discharge until 21 days after enrollment. Midturbinate swab specimens were collected by study personnel or by the participant, parent, or legal guardians (who were trained by study personnel) during hospital admission and by the participant, parent, or legal guardian during home collections. For household contacts who were not present at the hospital, midturbinate swab samples were collected every 3 days by the participant or a parent or guardian from day of enrollment until 21 days after enrollment.

We collected demographic and patient history by using a standardized questionnaire and verified data through the electronic medical record. We asked participants to recall symptoms, medications, and interventions experienced during the 14 days before enrollment using standardized lists. Prospective symptom diaries including the same list of symptoms, medications, and interventions were completed daily until 21 days after enrollment by the participant, parent, or legal guardian. Assuming a 20% censoring rate and a hypothesized mean duration of 11.4 days, we planned to enroll a minimum of 30 participants to produce a 2-sided 80% CI width of 6.3 days.

Samples and Laboratory Testing

Midturbinate swab samples were stored in PrimeStore Molecular Transport Media (Longhorn Vaccines and Diagnostics, <https://www.lhnvd.com>), which was previously validated by our laboratory for home collection and storage conditions for EV-D68 qualitative detection (21). Samples were stored in a refrigerator, delivered from home after the 21-day collection period, then aliquoted and frozen at -80°C until testing.

An aliquot from each collection day from all participants underwent EV-D68 real-time qualitative

reverse transcription PCR testing. We extracted total nucleic acid, including exogenously added internal positive control DNA (TaqMan Exogenous Internal Positive Control Reagents; ThermoFisher Scientific, <https://www.thermofisher.com>) on the QIAGEN EZ1 Advanced XL platform using the Virus 2.0 Mini Kit (<https://www.qiagen.com>), then performed cDNA synthesis on the ABI Veriti Thermal Cycler platform using TaqMan Reverse Transcription Reagents (ThermoFisher Scientific). We added 5 µL of cDNA to a final PCR reaction volume of 20 µL with the reaction component qScript XLT One-Step RT-qPCR ToughMix Low-Rox (Quantabio, <https://www.quantabio.com>), primers and probes at a final reaction concentration of 250 nM, and internal positive control primers and probe (ThermoFisher Scientific) (22,23). We performed reverse transcription PCR on the ABI 7500 Real-Time PCR System (ThermoFisher Scientific) with the following cycling conditions: 45°C for 10 minutes, then 95°C for 10 minutes, followed by 45 cycles of 95°C for 15 seconds and 60°C for 1 minute. We considered a cycle threshold (Ct) value <40 positive for EV-D68. This laboratory-developed protocol for EV-D68 detection was validated in-house and found to have a limit of detection of 700 genome copies/mL and 100% overall agreement (46/46) with an independent comparator assay specific to EV-D68 (T.F.F. Ng, unpub. data, <https://www.biorxiv.org/content/10.1101/2022.10.06.511205v2>). We performed further sequencing on an EV-D68-positive specimen using an established enterovirus typing method (24) to identify the EV-D68 subclade in the study.

Statistical Analysis

We included primary participants who tested positive for EV-D68 and their household contacts in the analysis (Figure 1). We summarized demographics, medical histories, medications, and interventions using frequency and percentage or median, interquartile range, and range.

We determined the duration of RNA shedding of EV-D68-positive participants from symptom onset to time-of-negativity, defined as the first negative result that was immediately followed by a subsequent negative result. Participants were censored on the last day a specimen was collected that followed the study schedule if they did not complete further collections per the study schedule. We created a Kaplan-Meier curve for RNA shedding for all EV-D68-positive participants and further stratified it by children (<18 years of age) and adults. We used log-rank tests to compare time-to-negativity by group and calculated median and 95% CI for RNA shedding duration from the Kaplan-Meier

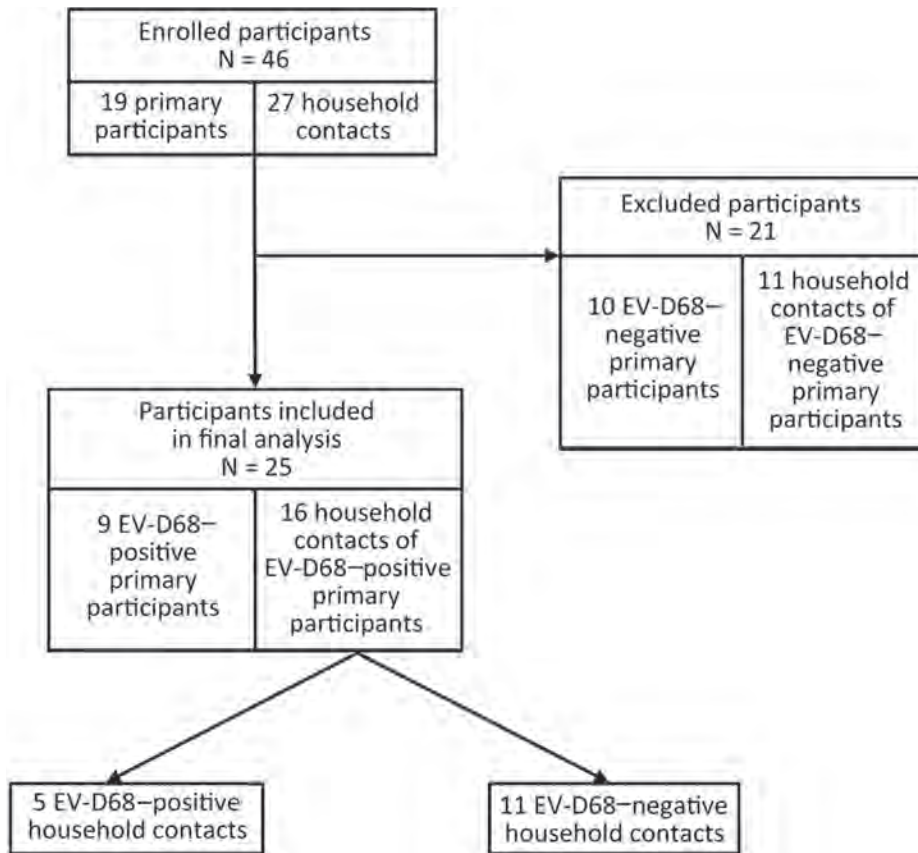


Figure 1. Study flowchart showing selection process of study participants included in the analysis of EV-D68 RNA shedding in the upper respiratory tract and associated clinical characteristics, Colorado, USA. EV, enterovirus.

curve. Because of the small sample size and few events at later time points, the upper limits of the 95% CIs of median survival times were undefined, so the range was also reported from the raw data. We calculated symptom duration from the first day until the last day the symptom was reported during the study period and illness duration from first day of any symptom to last day of any symptom. For each symptom and illness duration, we calculated median and interquartile range for day of onset and day of offset. We used R version 4.2.2 (The R Foundation for Statistical Computing, <https://www.r-project.org>) for analysis.

Results

During September–November 2022, we enrolled 46 participants (19 primary participants and 27 household contacts) in the study. Of the primary participants, 9 (47.4%) were EV-D68-positive; no other co-detections were detected on respiratory pathogen panel. We included the 9 EV-D68-positive primary participants and their 16 household contacts ($n = 25$) in the analysis (Figure 1). We confirmed EV-D68 subclade B3 by sequencing in a study participant, which is consistent with the predominant clade circulating in the United States during 2022 (25,26).

Study Population Characteristics

For the 9 primary participants, the median age was 2.2 years (range 8 months–17 years); 7 (77.8%) were boys and 2 (22.2%) were girls (Table 1). The age range of all household contacts was 4 months–44 years (Table 1). Of the 16 household contacts, 5 (31.3%) persons, each from a different household, were positive for EV-D68. Of the EV-D68-positive household contacts, 2 were sibling children (<5 years) and 3 were mothers of the primary participants. Prematurity, chronic lung disease, and chronic heart disease were reported among the primary participants; only 1 participant (11.1%) reported a history of asthma (Table 2). Of the EV-D68-positive household contacts, 2 (40%) of 5 reported a history of asthma; both were mothers of primary participants.

Medications, Interventions, and Hospitalization

All 9 primary participants received albuterol, antipyretics, and supplemental oxygen support (Table 3), and 7 (77.8%) received steroids. Seven (77.8%) primary participants required noninvasive positive pressure ventilation support during their admission, and 1 (11%) required intubation. Both EV-D68-positive household

Table 1. Demographic characteristics of participants and number of specimens collected in study of EV-D68 RNA shedding in the upper respiratory tract and associated clinical characteristics, Colorado, USA*

Characteristic	All participants, N = 25	EV-D68–positive primary participants, n = 9	EV-D68–positive household contacts, n = 5†	EV-D68–negative household contacts, n = 11
Age, y				
Median (IQR)	17.0 (2.2–35.0)	2.2 (1.5–3.3)	32.0 (4.0–39.3)	34.5 (26.2–39.2)
Range	0.3–44.9	0.7–17.0	0.7–44.9	0.3–40.2
Sex				
F	15 (60.0)	2 (22.2)	4 (80.0)	9 (81.8)
M	10 (40.0)	7 (77.8)	1 (20.0)	2 (18.2)
Race				
American Indian or Alaska Native	0	0	0	0
Asian	0	0	0	0
Black or African American	0	0	0	0
Native Hawaiian or other Pacific Islander	0	0	0	0
White	25 (100)	9 (100)	5 (100)	11 (100)
Ethnicity				
Hispanic or Latino	15 (60)	6 (66.7)	3 (60)	6 (54.5)
Not Hispanic or Latino	10 (40)	3 (33.3)	2 (40)	5 (45.5)
Median household size (IQR)‡				
Overall, all members	6 (5–7)	6 (5–7)	6 (5–7)	6 (5–6)
Household members ≥18 y	2 (2–2)	2 (2–2)	2 (2–2)	2 (2–2)
Household members <18 y	3 (2–4)	3 (3–4)	3 (3–4)	4 (2–4)
No. midturbinate specimens collected per participant during study period				
Median (IQR)	9 (7–10)	9 (8–11)	9 (9–14)	8 (7–10)

*Values are no. (%) except as indicated. EV, enterovirus; IQR, interquartile range.

†Two EV-D68–positive household contacts were children and had onset of symptoms starting 2 d before or on the same day as the primary participant.

The other 3 EV-D68–positive household contacts were adults and had onset of symptoms that started 3–5 d after the primary participant.

‡Including the primary participant.

contacts who were children subsequently required hospital admission and supplemental oxygen support but did not require noninvasive positive pressure ventilation or intubation (Table 3). None of the adult EV-D68–positive household contacts required hospital admission, although 1 person sought outpatient care.

Of the 11 children admitted with EV-D68 respiratory disease (9 primary participants and 2 household contacts), the median length of stay was 4 days (range 1–26 days). Eight (72.7%) required intensive care unit (ICU) admission; median ICU stay was 2.5 days (range 1–17 days). The most common discharge diagnosis was asthma exacerbation/reactive airways (45.5%), followed by viral lower respiratory tract infection (bronchiolitis/pneumonitis) (36.3%); a superimposed bacterial pneumonia was noted in 18.2% (not mutually exclusive).

EV-D68 RNA Shedding and Associated Characteristics

We analyzed RNA shedding of EV-D68 in the upper respiratory tract for all 14 EV-D68–positive participants (Figure 2). One participant was censored at the last day of inpatient collection because dates of home testing were not reported. The median duration of RNA shedding from illness onset was 12 days overall (range 7–15 days; 95% CI lower limit 9, upper limit undefined [because of small sample size; see Methods]). For adults, median duration was 9 days (range 7–9 days; 95% CI lower limit 7, upper limit undefined), and for children, median duration was 12 days (range 7–15 days; 95% CI lower limit 11, upper limit undefined; $p = 0.13$) (Figure 3). By 9 days after illness onset, 25% of participants were no longer shedding detectable RNA; by 14 days, 75% no longer had detectable EV-D68 RNA.

Table 2. Selected medical history of study participants in study of EV-D68 RNA shedding in the upper respiratory tract and associated clinical characteristics, Colorado, USA*

Comorbidity†	No. (%) participants			
	All participants, N = 25	EV-D68–positive primary participants, n = 9	EV-D68–positive household contacts, n = 5	EV-D68–negative household contacts, n = 11
Asthma	4 (16.0)	1 (11.1)	2 (40.0)	1 (9.1)
History of prematurity	3 (12.0)	2 (22.2)	1 (20.0)	0
Chronic heart disease	1 (4.0)	1 (11.1)	0	0
Chronic lung disease	1 (4.0)	1 (11.1)	0	0
Other reported history‡	4 (16.0)	2 (22.2)	1 (20.0)	1 (9.1)
None reported	15 (60.0)	5 (55.6)	1 (20.0)	9 (81.8)

*EV, enterovirus.

†Comorbidities are not mutually exclusive.

‡Other includes Trisomy 21, chromosomal abnormality, developmental delay, cavernous malformation, obesity, hypothyroidism, or nephrolithiasis.

Table 3. Medications and interventions received during the study period for participants in study of EV-D68 RNA shedding in the upper respiratory tract and associated clinical characteristics, Colorado, USA*

Intervention	All participants, N = 25	EV-D68–positive primary participants, n = 9	EV-D68–positive household contacts, n = 5	EV-D68–negative household contacts, n = 11
Medications				
Albuterol	13 (52.0)	9 (100)	3 (60.0)	1 (9.1)
Antipyretic	17 (68.0)	9 (100)	3 (60.0)	5 (45.5)
Steroids	8 (32.0)	7 (77.8)	1 (20.0)	0
No. outpatient visits during study period†				
0	13 (52.0)	1 (11.1)	2 (40.0)	10 (90.9)
1	11 (44.0)	7 (77.8)	3 (60.0)	1 (9.1)
2	1 (4.0)	1 (11.1)	0	0
Hospital course				
Required admission	11 (44.0)	9 (100)	2 (40.0)	0
Required ICU stay	8 (32.0)	8 (88.9)	0	0
Median length of stay (IQR), d	4.0 (3.0–6.5)	5.0 (4.0–7.0)	2.0 (1.5–2.5)	NA
Median ICU length of stay (IQR), d	2.5 (1.8–4.3)	2.5 (1.8–4.3)	NA	NA
Oxygen support at any time during admission				
Supplemental oxygen	11 (44.0)	9 (100)	2 (40.0)	0
Noninvasive positive pressure ventilation	7 (28.0)	7 (77.8)	0	0
Intubation	1 (4.0)	1 (11.1)	0	0

*Values are no. (%) except as indicated. ICU, intensive care unit; IQR, interquartile range; NA, not applicable.

†Includes clinic, urgent care, and emergency department visits.

The most common reported symptom in EV-D68–positive participants was runny nose/nasal congestion (100%), followed by cough (92.9%), difficulty breathing (78.6%), wheezing (57.1%), and fever (57.1%). Less common symptoms included sore throat (21.4%), headache (21.4%), and diarrhea (21.4%). The median illness duration was 20 days (range 11–24 days); cough had the longest median duration (18 days, range 7–30 days), followed by runny nose and nasal congestion (15 days, range 3–30 days) and wheezing (12 days, range 3–26 days). Twelve (85.7%) of the 14 EV-D68–positive participants were still symptomatic after they were no longer shedding detectable RNA. AFM did not develop in any EV-D68–positive participants in the study.

All EV-D68–positive household contacts were symptomatic. The adult household contacts reported mild respiratory symptoms, such as cough, runny nose and nasal congestion, wheezing, fever, and sore throat. Onset of symptoms in household contacts ranged from 2 days before to 5 days after symptom onset in the primary participant.

Discussion

We found that EV-D68 RNA shedding duration is more similar to that of rhinoviruses than of other enteroviruses; the median duration of EV-D68 RNA shedding in the upper respiratory tract was 12 days. Understanding RNA shedding dynamics can inform the expected rate at which EV-D68 could be detected in the upper respiratory tract at various time-points in the course of illness, particularly in EV-D68–associated AFM cases. Insight into the natural

history of EV-D68 from this study also helps inform transmission risk among household members and further defines the range of disease severity and symptoms, which can guide public health measures and management.

Cases of AFM are often preceded by a respiratory or febrile illness; median delay is 5–7 days from prodromal respiratory or febrile illness to onset of neurologic symptoms (1,2,27). Delayed recognition and misdiagnosis of AFM can result in even further delays in specimen collection and testing, leading to many cases going undiagnosed until weeks to months after symptom onset (28). Enterovirus PCR detection in sterile sites (e.g., cerebrospinal fluid [CSF] or blood) is specific for the diagnosis of enterovirus neurologic disease, but detection at those sites in AFM is exceedingly rare; enteroviruses are more commonly detected in nonsterile sites, particularly the respiratory tract (EV-D68) and stool (poliovirus, enterovirus A71) (29). Unfortunately, in many AFM cases, the recommended set of biospecimens is collected late in the course of disease, if at all, and samples from nonsterile sites, particularly the respiratory tract, are often lacking (29). In a 2014 study of AFM cases in the United States, 120 AFM cases were reported, but a respiratory sample was submitted for only 56 (46%) patients. In patients for whom respiratory samples were tested for enterovirus/rhinovirus, 44% were collected ≥ 12 days after symptom onset, and our findings suggest that at least half would no longer have been shedding detectable EV-D68 RNA. Those early data demonstrating that the proportion of EV-D68–positive samples

increased when samples were collected closer to symptom onset (47% positive for EV-D68 if tested ≤ 7 days from onset of respiratory or febrile illness) hinted at the importance of early sample collection and prompted this effort to learn more about shedding dynamics (29).

Our study confirms that timely specimen collection, particularly of respiratory specimens, is critical for detecting EV-D68 in suspected AFM cases (20,30), whereas other enteroviruses can shed for weeks in stool. On the basis of RNA shedding curve in the upper respiratory tract of this study, all participants had detectable EV-D68 RNA at 5 days after symptom onset, reinforcing the goals of prompt recognition and early sampling at the time of neurologic symptom onset in cases of suspected AFM. In EV-D68-associated AFM cases in which recognition is delayed, this study suggests that, by 9 days after prodromal symptom onset, 25% will no longer be shedding detectable RNA; 50% will no longer be shedding by 12 days, and 75% by 14 days. The later a respiratory specimen is collected in the course of

AFM, the less likely it is that EV-D68 will be detected; by 14 days after prodromal symptom onset, EV-D68 is exceedingly unlikely to be detected, even if causing disease. Providers should be encouraged to collect respiratory samples, in addition to stool, CSF, and serum samples, as soon as AFM is suspected on physical examination, without waiting for confirmatory imaging, lumbar puncture, or classification and confirmation by public health authorities (31). Furthermore, this study highlights that, in some AFM cases, EV-D68 RNA detection might not be possible if recognition or sample collection is delayed. That finding speaks to the need for complementary diagnostics, such as EV-D68 antibody testing in CSF samples, to detect intrathecal antibody production as the serologic footprint of neurologic infection when viral RNA is no longer detectable, which has become the standard for diagnosing West Nile virus and other neuroinvasive arboviruses in immunocompetent hosts (32).

Enrolling household contacts in this study, including adult family members with mild disease,

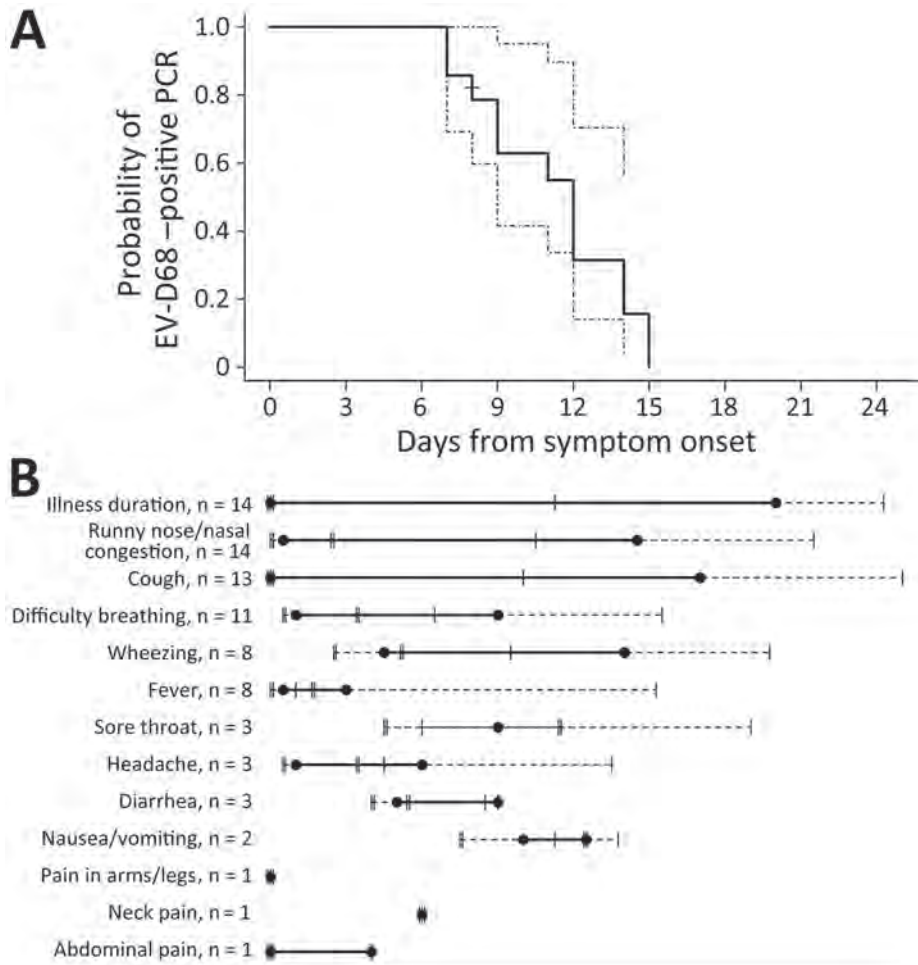


Figure 2. EV-D68 RNA shedding curve (A) and associated symptoms (B) for all EV-D68-positive participants (n = 14), Colorado, USA. A) Dotted line on Kaplan-Meier curve represents 95% CI. The + mark indicates the time at which 1 participant was censored at the last day of inpatient collection because they did not report dates of home testing. B) Number of participants reporting the symptom at any time is indicated. Black dots represent the median onset and median offset time for each symptom; solid horizontal line represents the duration between median onset and median offset time. The double vertical hash lines represent the 25th and 75th quartile for onset time, and the single vertical hash lines represent the 25th and 75th quartile for offset time. Symptoms on standardized list were abdominal pain, back pain, cough, diarrhea, difficulty breathing, difficulty swallowing, difficulty walking, facial droop/weakness, fever, headache, muscle jerks/tremors, nausea/vomiting, neck pain, pain in arms/legs, runny nose/nasal congestion, sore throat, vision changes, weakness in arms/legs, and wheezing. EV, enterovirus.

also provided insight into EV-D68 transmission and epidemiology outside of the hospital setting, where it has been primarily studied. Of the 9 households in the study, 5 (55.6%) had EV-D68-positive household contacts, suggesting transmission within households occurs between children and parents. All EV-D68-infected persons were symptomatic. We found no evidence of asymptotically infected persons shedding RNA to suggest the potential for silent transmission, although brief shedding or transmission before or after the collection period could not be excluded. Additional community studies are needed to further elucidate the burden of EV-D68 respiratory disease.

Both parents and siblings of children hospitalized with EV-D68 were themselves infected with EV-D68, but the severity of disease between adult and child contacts differed. The EV-D68-infected adults had only mild respiratory symptoms and did not require hospitalization, whereas the 2 EV-D68-infected child siblings had more severe respiratory illness that required hospitalization (15). Despite similar exposures, not all household contacts were infected, some had mild disease, and others had more severe disease, suggesting a role for host immunity in infection. Studies have found that, by the time they reach school age, most persons have neutralizing serum antibodies against EV-D68 suggestive of previous infection (33–35). This study demonstrated that adults, who would be expected to have neutralizing antibodies, still could be infected with EV-D68 and experience respiratory symptoms, but their symptoms tended to be milder; the median duration of RNA shedding was 9 days after symptom onset. Thus, having systemic immunity from previous infection might be protective against more severe manifestations but might not provide sterilizing immunity to prevent infection entirely or protect against mild respiratory disease. Future studies should investigate the role of innate and adaptive mucosal and systemic immunity in the development of different EV-D68 disease manifestations (e.g., asymptomatic, mild to severe respiratory disease, or neurologic disease). Clarifying the host immune response to natural EV-D68 infection will be key to developing effective monoclonal antibodies and vaccine candidates for treatment and prevention.

In terms of symptoms, we found that EV-D68 infection caused prolonged illness, including wheezing lasting nearly 2 weeks. As for rhinoviruses, EV-D68 causes upper respiratory symptoms and triggers bronchoreactive symptoms in the lower respiratory tract (7). Most children with EV-D68 respiratory illness in this study were hospitalized with asthma-like bronchoreactive symptoms and received treatment

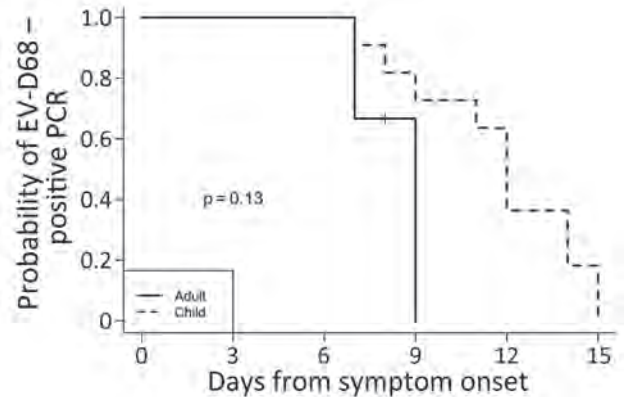


Figure 3. EV-D68 RNA shedding curve for adults ($n = 3$) versus children ($n = 11$) in study of shedding and household transmission, Colorado, USA. All children required hospitalization. The + mark indicates the time at which 1 participant was censored at the last day of inpatient collection because they did not report dates of home testing. The log-rank test statistic was used to test whether the 2 curves were different. EV, enterovirus.

with medications typically used for asthma, such as albuterol and steroids, which are generally not recommended for viral respiratory infections in young children. However, unlike rhinovirus-associated exacerbations occurring predominantly in children with underlying asthma, only 1 child with EV-D68 in our study had asthma. Previous studies have found that EV-D68 induces interleukin-17-dependent airway inflammation and hyperresponsiveness, which might explain the response to bronchodilators and steroids in children without underlying asthma seen in our study and in previous EV-D68 outbreaks (36–38). Long-term longitudinal studies and a better understanding of the mechanisms by which EV-D68 causes respiratory disease are needed to determine optimal management and whether early EV-D68 infection predisposes patients to develop asthma in the future, similar to other respiratory viruses, such as respiratory syncytial virus (39).

The first limitation of our study was the limited time frame in which participants were enrolled, given the small window during which EV-D68 circulation peaks; thus, our sample size was small and might not be fully generalizable to a broader population. Provider-directed respiratory pathogen panel testing in hospitalized children might have biased the primary participant study population toward more severe illness; however, we also enrolled household contacts to capture a broader range of clinical manifestations. We infer that the RNA shedding of EV-D68 in the upper respiratory tract, particularly in those with mild respiratory illness, might be similar to the shedding that precedes EV-D68 neurologic manifestations (i.e.,

AFM). However, that possibility would be extremely challenging, if not impracticable, to investigate without enrolling AFM patients before neurologic disease develops, during the prodromal respiratory/febrile illness. The results of this study cannot be used to evaluate the infectious period of EV-D68 because we relied on detection of viral RNA above our assay's limit of detection and did not perform viral culture because of the difficulty of growing EV-D68 caused by its atypical pH and temperature requirements (13). However, because RNA is typically shed longer than live culturable virus, this study provides upper limits for the longest potential period of infectiousness, which could help inform infection control measures. We spaced sample collection to every 3 days after discharge for ease of home collection, but that timing might have decreased the precision of shedding duration endpoints after hospitalization; conservatively calculating duration from the first negative sample rather than the last positive might slightly overestimate shedding durations. Finally, we used midturbinate swab specimens (instead of nasopharyngeal swabs) to detect RNA shedding, and some of those specimens were collected by the patient or a parent or legal guardian. Nasopharyngeal swab specimens are often used as the standard for upper respiratory pathogen detection, and use of midturbinate swab specimens in this study might have decreased sensitivity; however, midturbinate swab specimens are increasingly being used in practice because of their tolerability and were more practical for this study given the serial nature of sample collection. In addition, although we cannot definitively ensure the quality of home-collected samples, and differences between home-collected samples and those collected by study personnel might exist, studies have shown that parent-collected or self-collected specimens are adequate for pathogen detection and are a feasible convenient option, particularly in studies collecting serial samples (40–42).

Given current epidemiologic patterns, future EV-D68 outbreaks of respiratory disease and AFM are likely. The knowledge generated by this study about RNA shedding, transmission dynamics, and the natural history of EV-D68 can help families, providers, and healthcare systems anticipate frequency of illness, expected disease course, and resource needs to prepare for outbreaks. We found a median duration of EV-D68 RNA shedding in the upper respiratory tract of 12 days after respiratory symptom onset and found that transmission within households, both between children and with parents, occurs. All participants with EV-D68 reported respiratory symptoms, illness duration of EV-D68 was >2 weeks, and most hospi-

talized children with asthma-like respiratory disease required ICU-level care, highlighting the severity of EV-D68 illness. Notably, this study stresses the importance of recognizing illness early and collecting respiratory specimens promptly in suspected AFM cases. Our findings also underscore the importance of diagnostic advances, such as EV-D68-specific CSF antibody testing, to help detect previous infection when viral RNA is no longer present, confirm cases, and enable targeted treatment when EV-D68-specific therapeutics are approved.

Acknowledgments

We thank our study participants, study staff, and Tiffany Mylius, Andrea Lerick, and Aneesa Syed for assisting with sample processing and testing.

This study was funded by the Centers for Disease Control and Prevention. This activity was reviewed by CDC and was conducted consistent with applicable federal law and CDC policy (see e.g., 45 C.F.R. part 46, 21 C.F.R. part 56; 42 U.S.C. §241(d); 5 U.S.C. §552a; 44 U.S.C. §3501 et seq).

H.N.-T., C.T., S.R.D., and K.M. receive funding from the National Institutes of Allergy and Infectious Diseases (NIAID) Vaccine Research Center for the Pandemic Response Repository through Microbial and Immune Surveillance and Epidemiology (PREMISE): Enterovirus D68 (EV-D68) Pilot Study. H.N.-T. received support from the Congenital and Perinatal Infections Consortium for conference attendance. S.R.D. receives grant support from Pfizer and BioFire Diagnostics and is a consultant for BioFire Diagnostics and Karius. M.B. received support from Pfizer for conference attendance. S.J. received support from DiaSorin Molecular LLC, Karius Inc, and bioMérieux for conference attendance. DiaSorin Molecular LLC and Abbott Molecular have partnered with the Children's Hospital Colorado Microbiology Laboratory and have provided reagent and supply support.

About the Author

Dr. Nguyen-Tran is an assistant professor in the Department of Pediatrics Section of Infectious Diseases at the University of Colorado School of Medicine. Her research interests include global health, pandemic preparedness, enterovirus D68, and other emerging infectious diseases.

References

1. Aliabadi N, Messacar K, Pastula DM, Robinson CC, Leshem E, Sejvar JJ, et al. Enterovirus D68 infection in children with acute flaccid myelitis, Colorado, USA, 2014. *Emerg Infect Dis.* 2016;22:1387–94. <https://doi.org/10.3201/eid2208.151949>

2. Ayers T, Lopez A, Lee A, Kambhampati A, Nix WA, Henderson E, et al. Acute flaccid myelitis in the United States: 2015–2017. *Pediatrics*. 2019;144:e20191619. <https://doi.org/10.1542/peds.2019-1619>
3. Dyda A, Stelzer-Braid S, Adam D, Chughtai AA, MacIntyre CR. The association between acute flaccid myelitis (AFM) and enterovirus D68 (EV-D68) – what is the evidence for causation? *Euro Surveill*. 2018;23:17–00310. <https://doi.org/10.2807/1560-7917.ES.2018.23.3.17-00310>
4. Kamau E, Harvala H, Blomqvist S, Nguyen D, Horby P, Pebody R, et al. Increase in enterovirus D68 infections in young children, United Kingdom, 2006–2016. *Emerg Infect Dis*. 2019;25:1200–3. <https://doi.org/10.3201/eid2506.181759>
5. Kujawski SA, Midgley CM, Rha B, Lively JY, Nix WA, Curns AT, et al. Enterovirus D68–associated acute respiratory illness – new vaccine surveillance network, United States, July–October, 2017 and 2018. *MMWR Morb Mortal Wkly Rep*. 2019;68:277–80. <https://doi.org/10.15585/mmwr.mm6812a1>
6. McKay SL, Lee AD, Lopez AS, Nix WA, Dooling KL, Keaton AA, et al. Increase in acute flaccid myelitis—United States, 2018. *MMWR Morb Mortal Wkly Rep*. 2018;67:1273–5. <https://doi.org/10.15585/mmwr.mm6745e1>
7. Messacar K, Abzug M. Nonpolio enterovirus. In: Kliegman RM, St. Geme J, editors. *Nelson textbook of pediatrics*, 21st ed. Amsterdam: Elsevier; 2019. p. 1690–7.
8. Messacar K, Abzug MJ, Dominguez SR. 2014 outbreak of enterovirus D68 in North America. *J Med Virol*. 2016;88:739–45. <https://doi.org/10.1002/jmv.24410>
9. Messacar K, Asturias EJ, Hixon AM, Van Leer-Buter C, Niesters HGM, Tyler KL, et al. Enterovirus D68 and acute flaccid myelitis—evaluating the evidence for causality. *Lancet Infect Dis*. 2018;18:e239–47. [https://doi.org/10.1016/S1473-3099\(18\)30094-X](https://doi.org/10.1016/S1473-3099(18)30094-X)
10. Messacar K, Pretty K, Reno S, Dominguez SR. Continued biennial circulation of enterovirus D68 in Colorado. *J Clin Virol*. 2019;113:24–6. <https://doi.org/10.1016/j.jcv.2019.01.008>
11. Messacar K, Schreiner TL, Van Haren K, Yang M, Glaser CA, Tyler KL, et al. Acute flaccid myelitis: A clinical review of US cases 2012–2015. *Ann Neurol*. 2016;80:326–38. <https://doi.org/10.1002/ana.24730>
12. Midgley CM, Watson JT, Nix WA, Curns AT, Rogers SL, Brown BA, et al.; EV-D68 Working Group. Severe respiratory illness associated with a nationwide outbreak of enterovirus D68 in the USA (2014): a descriptive epidemiological investigation. *Lancet Respir Med*. 2015;3:879–87. [https://doi.org/10.1016/S2213-2600\(15\)00335-5](https://doi.org/10.1016/S2213-2600(15)00335-5)
13. Oberste MS, Maher K, Schnurr D, Flemister MR, Lovchik JC, Peters H, et al. Enterovirus 68 is associated with respiratory illness and shares biological features with both the enteroviruses and the rhinoviruses. *J Gen Virol*. 2004; 85:2577–84. <https://doi.org/10.1099/vir.0.79925-0>
14. Pons-Salort M, Oberste MS, Pallansch MA, Abedi GR, Takahashi S, Grenfell BT, et al. The seasonality of nonpolio enteroviruses in the United States: patterns and drivers. *Proc Natl Acad Sci U S A*. 2018;115:3078–83. <https://doi.org/10.1073/pnas.1721159115>
15. Centers for Disease Control and Prevention. Non-polio enterovirus: enterovirus D68. 2022 [cited 2023 Sep]. <https://www.cdc.gov/non-polio-enterovirus/about/ev-d68.html>
16. Murphy OC, Messacar K, Benson L, Bove R, Carpenter JL, Crawford T, et al.; AFM working group. Acute flaccid myelitis: cause, diagnosis, and management. *Lancet*. 2021; 397:334–46. [https://doi.org/10.1016/S0140-6736\(20\)32723-9](https://doi.org/10.1016/S0140-6736(20)32723-9)
17. Vogt MR, Wright PF, Hickey WF, De Buysscher T, Boyd KL, Crowe JE Jr. Enterovirus D68 in the anterior horn cells of a child with acute flaccid myelitis. *N Engl J Med*. 2022;386:2059–60. <https://doi.org/10.1056/NEJMc2118155>
18. Messacar K, Hawkins SMM, Baker J, Pearce K, Tong S, Dominguez SR, et al. Resource burden during the 2014 enterovirus D68 respiratory disease outbreak at Children’s Hospital Colorado: an unexpected strain. *JAMA Pediatr*. 2016;170:294–7. <https://doi.org/10.1001/jamapediatrics.2015.3879>
19. Schieble JH, Fox VL, Lennette EH. A probable new human picornavirus associated with respiratory diseases. *Am J Epidemiol*. 1967;85:297–310. <https://doi.org/10.1093/oxfordjournals.aje.a120693>
20. Peltola V, Waris M, Kainulainen L, Kero J, Ruuskanen O. Virus shedding after human rhinovirus infection in children, adults and patients with hypogammaglobulinaemia. *Clin Microbiol Infect*. 2013;19:E322–7. <https://doi.org/10.1111/1469-0691.12193>
21. Nguyen-Tran H, Reno S, Mwangi E, Mentel M, Hengartner R, Dominguez SR, et al. Qualitative detection of enterovirus D68 from PrimeStore molecular transport medium: implications for home- and self-collection. *Diagn Microbiol Infect Dis*. 2023;106:115976. <https://doi.org/10.1016/j.diagmicrobio.2023.115976>
22. Ikuse T, Aizawa Y, Takihara H, Okuda S, Watanabe K, Saitoh A. Development of novel PCR assays for improved detection of enterovirus D68. *J Clin Microbiol*. 2021; 59:e0115121. <https://doi.org/10.1128/JCM.01151-21>
23. Selvaraju SB, Nix WA, Oberste MS, Selvarangan R. Optimization of a combined human parechovirus-enterovirus real-time reverse transcription-PCR assay and evaluation of a new parechovirus 3-specific assay for cerebrospinal fluid specimen testing. *J Clin Microbiol*. 2013;51:452–8. <https://doi.org/10.1128/JCM.01982-12>
24. Nix WA, Oberste MS, Pallansch MA. Sensitive, seminested PCR amplification of VP1 sequences for direct identification of all enterovirus serotypes from original clinical specimens. *J Clin Microbiol*. 2006;44:2698–704. <https://doi.org/10.1128/JCM.00542-06>
25. Fall A, Han L, Abdullah O, Norton JM, Eldesouki RE, Forman M, et al. An increase in enterovirus D68 circulation and viral evolution during a period of increased influenza like illness, The Johns Hopkins Health System, USA, 2022. *J Clin Virol*. 2023;160:105379. <https://doi.org/10.1016/j.jcv.2023.105379>
26. Hodcroft E, Neher R, Dyrda K, Albert J. Phylodynamics of enterovirus D68. 2022 [cited 2023 Aug 22]. <https://nextstrain.org/enterovirus/d68/genome?dmin=2022-08-01>
27. Messacar K, Schreiner TL, Maloney JA, Wallace A, Ludke J, Oberste MS, et al. A cluster of acute flaccid paralysis and cranial nerve dysfunction temporally associated with an outbreak of enterovirus D68 in children in Colorado, USA. *Lancet*. 2015;385:1662–71. [https://doi.org/10.1016/S0140-6736\(14\)62457-0](https://doi.org/10.1016/S0140-6736(14)62457-0)
28. Hayes LH, Hopkins SE, Liu S, Pardo CA, Garcia-Dominguez MA, Oleszek J, et al. Challenges in the clinical recognition of acute flaccid myelitis and its implications. *J Pediatr*. 2023;253:55–62.e4. <https://doi.org/10.1016/j.jpeds.2022.09.012>
29. Sejvar JJ, Lopez AS, Cortese MM, Leshem E, Pastula DM, Miller L, et al. Acute flaccid myelitis in the United States, August–December 2014: results of nationwide surveillance. *Clin Infect Dis*. 2016;63:737–45. <https://doi.org/10.1093/cid/ciw372>

30. Messacar K, Abzug MJ. Enteroviruses and parechoviruses. In: Long SS, editor. Principles and practice of pediatric infectious diseases, 6th ed. Philadelphia: Elsevier; 2023. p. 1228–36.
31. Centers for Disease Control and Prevention. Acute flaccid myelitis (AFM): specimen collection. 2022 [cited 2023 Sep 1]. <https://www.cdc.gov/acute-flaccid-myelitis/hcp/specimen-collection.html>
32. Schubert RD, Hawes IA, Ramachandran PS, Ramesh A, Crawford ED, Pak JE, et al. Pan-viral serology implicates enteroviruses in acute flaccid myelitis. *Nat Med*. 2019;25:1748–52. <https://doi.org/10.1038/s41591-019-0613-1>
33. Harrison CJ, Weldon WC, Pahud BA, Jackson MA, Oberste MS, Selvarangan R. Neutralizing antibody against enterovirus D68 in children and adults before 2014 outbreak, Kansas City, Missouri, USA. *Emerg Infect Dis*. 2019;25:585–8. <https://doi.org/10.3201/eid2503.180960>
34. Karelehto E, Koen G, Benschop K, van der Klis F, Pajkrt D, Wolthers K. Enterovirus D68 serosurvey: evidence for endemic circulation in the Netherlands, 2006 to 2016. *Euro Surveill*. 2019;24:1800671. <https://doi.org/10.2807/1560-7917.ES.2019.24.35.1800671>
35. Sun S, Gao F, Hu Y, Bian L, Wu X, Su Y, et al. A cross-sectional seroepidemiology study of EV-D68 in China. *Emerg Microbes Infect*. 2018;7:99. <https://doi.org/10.1038/s41426-018-0103-4>
36. Rao S, Messacar K, Torok MR, Rick AM, Holzberg J, Montano A, et al. Enterovirus D68 in critically ill children: a comparison with pandemic H1N1 influenza. *Pediatr Crit Care Med*. 2016;17:1023–31. <https://doi.org/10.1097/PCC.0000000000000922>
37. Schuster JE, Miller JO, Selvarangan R, Weddle G, Thompson MT, Hassan F, et al. Severe enterovirus 68 respiratory illness in children requiring intensive care management. *J Clin Virol*. 2015;70:77–82. <https://doi.org/10.1016/j.jcv.2015.07.298>
38. Rajput C, Han M, Bentley JK, Lei J, Ishikawa T, Wu Q, et al. Enterovirus D68 infection induces IL-17-dependent neutrophilic airway inflammation and hyperresponsiveness. *JCI Insight*. 2018;3:e121882. <https://doi.org/10.1172/jci.insight.121882>
39. Wu P, Hartert TV. Evidence for a causal relationship between respiratory syncytial virus infection and asthma. *Expert Rev Anti Infect Ther*. 2011;9:731–45. <https://doi.org/10.1586/eri.11.92>
40. Esposito S, Molteni CG, Daleno C, Valzano A, Tagliabue C, Galeone C, et al. Collection by trained pediatricians or parents of mid-turbinate nasal flocked swabs for the detection of influenza viruses in childhood. *Virol J*. 2010;7:85. <https://doi.org/10.1186/1743-422X-7-85>
41. Gangell CL, Shackleton C, Poreddy S, Kappers J, Gaydon JE, Sloots TP, et al. Feasibility of parental collected nasal swabs for virus detection in young children with cystic fibrosis. *J Cyst Fibros*. 2014;13:661–6. <https://doi.org/10.1016/j.jcf.2014.02.009>
42. Thompson MG, Ferber JR, Odouli R, David D, Shifflett P, Meece JK, et al. Results of a pilot study using self-collected mid-turbinate nasal swabs for detection of influenza virus infection among pregnant women. *Influenza Other Respir Viruses*. 2015;9:155–60. <https://doi.org/10.1111/irv.12309>

Address for correspondence: Hai Nguyen-Tran, University of Colorado School of Medicine, Department of Pediatrics, Section of Infectious Diseases, 13123 E 16th Ave, B055, Aurora, CO 80045, USA; email: hai.nguyen-tran@childrenscolorado.org

EID Podcast Rising Incidence of Legionnaires' Disease, United States, 1992–2018



Reported Legionnaires' disease cases began increasing in the United States in 2003 after relatively stable numbers for more than 10 years. This rise was most associated with increases in racial disparities, geographic focus, and seasonality. Water management programs should be in place for preventing the growth and spread of Legionella in buildings.

In this EID podcast, Albert Barskey, an epidemiologist at CDC in Atlanta discusses the increase of Legionnaires' disease within the United States.

Visit our website to listen:
<https://go.usa.gov/xuD7W>

**EMERGING
INFECTIOUS DISEASES®**

Risk Factors for Recent HIV Infections among Adults in 14 Countries in Africa Identified by Population-Based HIV Impact Assessment Surveys, 2015–2019

Dustin W. Currie, Christine A. West, Hetal K. Patel, Jennifer Favaloro, Fred Asiimwe, Felix Ndagije, Rachel Silver, Owen Mugurungi, Judith Shang, Clement B. Ndongmo, Daniel B. Williams, Edington Dzinotyiweyi, Anthony Waruru, Munyaradzi Pasipamire, Harriet Nuwagaba-Biribonwoha, Sindisiwe Dlamini, Natasha McLeod, Eugenie Kayirangwa, Gallican Rwibasira, Peter A. Minchella, Andrew F. Auld, Rose Nyirenda, Yimam Getaneh, Ashenafi Haile Hailemariam, Isabelle Tondoh-Koui, Natacha Kohemun, George S. Mgomella, Prosper Faustine Njau, Wilford L. Kirungi, Ibrahim Dalhatu, Kristen A. Stafford, Stephane M. Bodika, Faith Ussery, Stephen McCracken, Paul Stupp, Kristin Brown, Yen T. Duong, Bharat S. Parekh, Andrew C. Voetsch

Identifying persons who have newly acquired HIV infections is critical for characterizing the HIV epidemic direction. We analyzed pooled data from nationally representative Population-Based HIV Impact Assessment surveys conducted across 14 countries in Africa for recent infection risk factors. We included adults 15–49 years of age who had sex during the previous year and used a recent infection testing algorithm to distinguish recent from long-term infections. We collected risk factor information via participant interviews and assessed correlates of recent infec-

tion using multinomial logistic regression, incorporating each survey's complex sampling design. Compared with HIV-negative persons, persons with higher odds of recent HIV infection were women, were divorced/separated/widowed, had multiple recent sex partners, had a recent HIV-positive sex partner or one with unknown status, and lived in communities with higher HIV viremia prevalence. Prevention programs focusing on persons at higher risk for HIV and their sexual partners will contribute to reducing HIV incidence.

Author affiliations: Centers for Disease Control and Prevention, Atlanta, Georgia, USA (D.W. Currie, C.A. West, H.K. Patel, J. Favaloro, R. Silver, S.M. Bodika, F. Ussery, S. McCracken, P. Stupp, K. Brown, B.S. Parekh, A.C. Voetsch); Centers for Disease Control and Prevention, Maseru, Lesotho (F. Asiimwe); Columbia University, Maseru (F. Ndagije); Zimbabwe Ministry of Health and Child Care, Harare, Zimbabwe (O. Mugurungi); Centers for Disease Control and Prevention, Yaoundé, Cameroon (J. Shang, C.B. Ndongmo); Centers for Disease Control and Prevention, Windhoek, Namibia (D.B. Williams); Republic of Namibia Ministry of Health and Social Services, Windhoek (E. Dzinotyiweyi); Centers for Disease Control and Prevention, Nairobi, Kenya (A. Waruru); Centers for Disease Control and Prevention, Mbabane, Eswatini (M. Pasipamire); Columbia University, Mbabane (H. Nuwagaba-Biribonwoha); Ministry of Health Mbabane, Mbabane (S. Dlamini); Columbia University, New York, New York, USA (N. McLeod, Y.T. Duong); Centers for Disease

Control and Prevention, Kigali, Rwanda (E. Kayirangwa); Republic of Rwanda Ministry of Health, Kigali (G. Rwibasira); Centers for Disease Control and Prevention, Lusaka, Zambia (P.A. Minchella, A.F. Auld); Ministry of Health, Lilongwe, Malawi (R. Nyirenda); Ethiopian Public Health Institute, Addis Ababa, Ethiopia (Y. Getaneh); Zhejiang University, Hangzhou, China (Y. Getaneh); Centers for Disease Control and Prevention, Addis Ababa (A.H. Hailemariam); Cote d'Ivoire Ministry of Health, Abidjan, Côte d'Ivoire (I. Tondoh-Koui); Centers for Disease Control and Prevention, Abidjan (N. Kohemun); Centers for Disease Control and Prevention, Dar es Salaam, Tanzania (G.S. Mgomella); United Republic of Tanzania Ministry of Health, Dodoma, Tanzania (P.F. Njau); Republic of Uganda Ministry of Health, Kampala, Uganda (W.L. Kirungi); Centers for Disease Control and Prevention, Abuja, Nigeria (I. Dalhatu); University of Maryland, Baltimore, Maryland, USA (K.A. Stafford)

DOI: <https://doi.org/10.3201/eid2911.230703>

Sub-Saharan Africa has the highest HIV infection incidence and prevalence in the world (1,2). Although incidence is declining (3), more progress is needed to reduce transmission to a sufficient level that achieves global epidemic control. Several metrics for epidemic control have been proposed, including an incidence:mortality ratio (number of new HIV infections:total number of deaths from all causes among HIV-infected persons), a metric used providing that both new infections and deaths are low and declining (4). In sub-Saharan Africa, the Joint United Nations Programme on HIV/AIDS (UNAIDS) estimates that women and girls accounted for 63% of all new HIV infections in 2021 (2). Determining risk factors for HIV acquisition in countries with generalized HIV epidemics can help identify appropriate groups for tailored prevention programming and can support testing for those at highest risk of acquiring infection.

Methods used to examine risk factors for HIV often compare HIV-negative and HIV-positive persons (prevalence) (5–7) or use longitudinal cohort studies that comprise HIV-negative persons at baseline (8–11). Each of those methods has drawbacks. The prevalence approach does not distinguish recent from long-term infections, making it difficult to determine whether risk factors preceded the infection (12). In addition, risk factors for HIV might change over time, and programmatic efforts need to assess who is at the highest risk of acquiring new infections to prevent transmission. Longitudinal cohorts can establish timing of infection; however, they require long follow-up periods and large sample sizes and are subject to attrition bias that might not be equal across risk factors (12).

Assays that distinguish recent from long-term HIV-1 infections present an opportunity to estimate HIV incidence and assess risk factors in cross-sectional population-based household surveys (12,13). The limiting-antigen (LAG) avidity enzyme immunoassay (EIA) has been well characterized, validated, and used for the detection of recent infections and estimation of HIV-1 incidence as part of a recent infection testing algorithm (RITA) in cross-sectional surveys, including Population-Based HIV Impact Assessment (PHIA) surveys (14,15). Therefore, PHIA surveys can identify risk factors for new HIV infections in the general population across multiple countries in sub-Saharan Africa by using the largest sample of recent infections. We identified demographic and behavioral risk factors for recent HIV infections among sexually active adults across 14 sub-Saharan Africa countries and assessed whether those factors differed between recent and long-term infections.

Methods

Study Design

PHIAs are nationally representative, cross-sectional, population-based surveys of households across each country (16,17). A 2-stage, stratified cluster sample design was used in each survey: enumeration areas were selected within strata (subnational units, such as regions) by using a probability proportional to size method, and households within enumeration areas were randomly selected in the second stage. Weights were calculated to account for unequal probability of household selection, nonresponse, and noncoverage. Within selected households, the household head completed a household survey, and eligible household members completed individual interviews and had blood collected after providing consent for each survey component.

Study Population

We used data from PHIA surveys completed in 14 countries during 2015–2019: Cameroon, Cote d'Ivoire, Eswatini, Ethiopia, Kenya, Lesotho, Malawi, Namibia, Nigeria, Rwanda, Tanzania, Uganda, Zambia, and Zimbabwe. We pooled data across PHIAs in a multicountry analysis because of small sample sizes for recent infections within each country. We included adults 15–49 years of age who reported engaging in sexual activity during the year before their interview. We only included persons who consented to a blood draw and had a valid final RITA classification.

Variable Definitions

We explored demographic and behavioral variables collected during participant interviews to identify potential risk factors. Demographic factors were country, sex, age, marital status, education, and household wealth. Behavioral factors were number of recent sexual partners (during the previous 12 months), age of sexual debut, HIV status of partner(s), age of partner(s), condom usage, and voluntary medical male circumcision status. Age of sexual debut was divided into <18 or ≥18 years categories; 18 years of age was the median. The numbers of partners in the previous year were grouped into categories (0, 1, or ≥2 partners), consistent with previous literature and an examination of the data (12,13). Age groups were 15–24, 25–34, and 35–49 years, according to published precedent.

We calculated community viremia levels within each stratum in each country. We defined participants with long-term HIV infections and detectable viral load of ≥1,000 copies/mL as viremic and all

HIV-negative or HIV-positive participants with an undetectable viral load as nonviremic. We excluded persons with recent HIV infection (as defined in the next paragraph) from community viremia calculations, which were calculated as the weighted number of viremic persons divided by the weighted number of viremic plus nonviremic persons within each stratum. We then categorized each stratum into quantiles representing the percentages of persons with nonsuppressed HIV infection within the stratum.

The 3 primary outcome categories for each participant were recent HIV infection, long-term HIV infection, or HIV negative. All participants were tested for HIV in the household according to each country's national testing algorithm. Confirmatory HIV testing was completed in all countries except Uganda by using the Geenius HIV-1/2 rapid test (Bio-Rad Laboratories, <https://www.bio-rad.com>). We classified HIV according to confirmatory testing and excluded a small number of participants ($n < 25$) who tested positive for HIV-2 but not HIV-1 from recency testing because the LAg-Avidity EIA is meant for HIV-1 recency classification only. Among HIV-positive participants, RITA was used to distinguish recent from long-term infections. The first step of RITA used the LAg-Avidity EIA (Sedia Biosciences Corp., <https://www.sediabio.com>, for plasma specimens or Maxim Biomedical, <https://www.maximbio.com>, for dried blood spot specimens), which assesses development of antibody avidity. We classified participants with a median normalized optical density ≤ 1.5 for plasma samples (or ≤ 1.0 for dried blood spot samples where venous blood could not be collected [$< 5\%$ of participants]) as LAg-recent infections. Next, we categorized participants as recently infected if they had LAg-recent infections, HIV viral loads $> 1,000$ copies/mL, and an absence of antiretroviral drug metabolites in their blood by using RITA (14,15). All HIV-1-positive participants who did not meet the criteria for recent infection were categorized as having long-term HIV infection.

Statistical Analysis

Initial data analysis strategies were bivariate comparisons between HIV-negative participants and those who had a recent HIV infection or long-term HIV infections. We calculated an overall χ^2 test statistic and unadjusted odds ratios for categorical variables. We used Taylor series weights and variables representing strata and units for all analyses. We performed analyses by using SAS version 9.4 (SAS Institute, <https://www.sas.com>) and considered p values < 0.05 statistically significant.

Our model-building strategy incorporated candidate exposure variables with bivariate p values < 0.20 . In cases where variables were colinear, we included only 1 variable or set of variables in the final model. Only variables collected consistently across countries were eligible for the multivariable model. We used multinomial logistic regression to calculate adjusted weighted odds ratios accounting for the complex survey sample design.

Ethics Statement

PHIA surveys were funded by the US President's Emergency Plan for AIDS Relief (PEPFAR) (18); technical assistance was provided by the US Centers for Disease Control and Prevention. The surveys were conducted through cooperative agreements with grantees/federal entities, including country Ministries of Health, ICAP at Columbia University (New York, New York, USA), and the University of Maryland (Baltimore, MD, USA). Each survey was approved by human subject institutional review boards specific for each country, cooperative agreement grantees/federal entities conducting the survey, or the US Centers for Disease Control and Prevention.

Results

Population Description

Across the 14 countries included in this analysis, we identified 16,831 HIV-positive and 241,909 HIV-negative PHIA participants (Figure). Of the 16,831 HIV-positive participants, 264 (1.6% of all HIV-positive participants) had recent infections and 16,567 had long-term infections. Sample sizes of participants who met inclusion criteria ranged from 5,874 in Eswatini to 95,463 in Nigeria (Table 1). Biomarker (blood draw) response rates ranged from 86.7% in Malawi to 99.0% in Uganda for female participants and 85.3% in Namibia to 98.5% in Uganda for male participants.

Bivariate Analysis Findings

We performed weighted bivariate comparisons between HIV-negative and recently infected participants (Table 2, <https://wwwnc.cdc.gov/EID/article/29/11/23-0703-T2.htm>). Region was significantly associated with recent HIV infection; persons living in western Africa represented only 27.1% of persons with recent HIV infections but represented 51.5% of those who were HIV negative. In addition, female sex, age 25–34 years, and divorced or separated marital status were associated with recent HIV infection. Among young adults 15–24 years of age, female participants accounted for 72.1% of

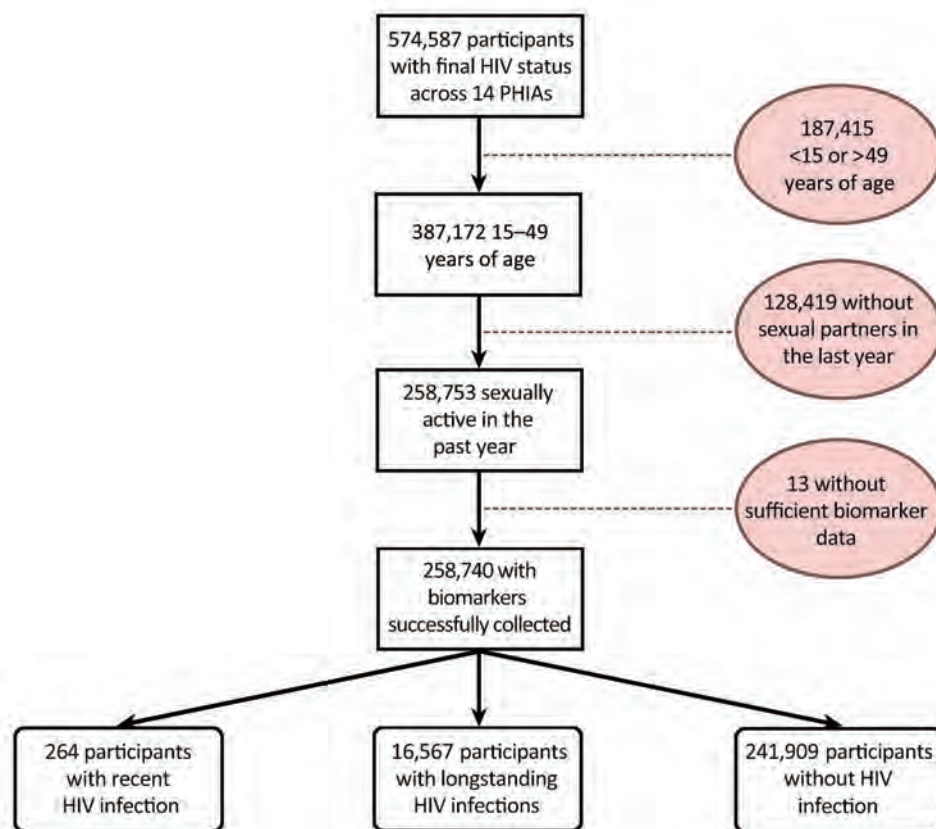


Figure. Inclusion and exclusion criteria and final outcome status in study of population-based assessments of risk factors for recent HIV infections among sexually active adults in 14 sub-Saharan Africa countries, 2015–2019. Shaded circles indicate numbers of excluded participants and reasons for exclusion from the study. Final outcome was categorized into 3 groups of participants: recent HIV infection, long-term HIV infection, and HIV negative. PHIA, Population-Based HIV Impact Assessment.

recent infections. Demographic variables not associated with recent infection were urban and rural locations, household wealth, and working during the previous 12 months.

Behavioral factors were also associated with the prevalence of recent infections. For example, compared with HIV-negative participants, those who had recent HIV infections were more likely to have had

Table 1. Sample sizes of sexually active adults 15–49 years of age in study of risk factors for recent HIV infections among adults in 14 countries in Africa identified by Population-based HIV Impact Assessment surveys, 2015–2019*

Region and country	HIV negative	Long-term HIV infection	Recent HIV infection	Total sample size
Western Africa				
Cameroon	15,747	617	18	16,382
Cote d'Ivoire	11,688	258	4	11,950
Nigeria	93,895	1,537	31	95,463
Subtotal	121,330	2,412	53	123,795
Eastern Africa				
Ethiopia	8,131	265	4	8,400
Kenya	15,084	880	7	15,971
Tanzania	17,113	1,070	27	18,210
Rwanda	15,665	520	4	16,189
Uganda	17,850	1,171	30	19,051
Subtotal	73,843	3,906	72	77,821
Southeastern Africa				
Malawi	9,735	1,428	19	11,182
Zambia	9,762	1,486	30	11,278
Zimbabwe	9,663	1,976	21	11,660
Subtotal	29,160	4,890	70	34,120
Southern Africa				
Eswatini	3,848	2,004	22	5,874
Lesotho	5,480	2,107	31	7,618
Namibia	8,248	1,248	16	9,512
Subtotal	17,576	5,359	69	23,004
Overall total	241,909	16,567	264	258,740

*Sexually active adults are those who reported ≥1 sexual partner in the previous 12 mo.

Table 3. Description of potential risk factors for HIV infection from data collected inconsistently across Population-Based HIV Impact Assessment surveys among adults in 14 countries in Africa, 2015–2019*

Variable	Recent HIV Infections			HIV negative			p value	Long-term HIV infections			
	No.	Weighted		No.	Weighted			No.	Weighted		p value
	No.	No.	%	No.	No.	%		No.	No.	%	
Previous HIV testing†											
Never	29	12,504	13.3	28,497	18,070,566	21.2	0.08	950	12,504	8.7	0.0007
In previous year	120	40,316	42.8	63,272	34,907,993	41.0		4,941	1,852,308	33.3	
>12 mo ago	79	41,334	43.9	54,926	32,071,315	37.7		9,053	3,230,533	58.1	
Hazardous drinking‡											
Yes	23	6,465	12.3	7,687	3,782,225	10.7	0.61	1,286	464,592	14.8	0.38
No	115	46,171	87.7	53,395	31,645,051	89.3		8,038	2,671,216	85.2	
STD diagnosis§											
Yes	7	2,891	10.7	1,239	780,205	4.0	0.02	350	153,294	7.3	0.23
No	68	24,249	89.3	37,007	18,917,995	96.0		4,889	1,939,752	92.6	
STI symptoms¶											
Yes	24	14,602	27.0	9,189	7,347,057	14.3	0.007	1,448	790,794	21.6	0.28
No	81	39,535	73.0	59,901	46,925,388	85.7		5,602	2,865,735	78.4	
Victim of sexual violence by partner in previous 12 mo#											
Yes	2	869	3.8	424	217,821	1.5	0.17	60	20,445	1.4	0.15
No	77	21,816	96.2	33,334	14,227,044	98.5		5,650	1,422,172	98.6	
VMMC status**											
Medical	13	8,262	21.1	31,546	23,295,330	38.2	0.005	976	562,564	26.2	0.004
Traditional	26	16,358	41.7	36,456	26,060,244	42.7		1,028	508,445	23.7	
None	36	14,610	37.2	24,119	11,612,109	19.0		2,797	1,073,815	50.1	

*STD, sexually transmitted disease; STI, sexually transmitted infection; VMMC, voluntary medical male circumcision.

†Excludes Nigeria.

‡Includes Eswatini, Kenya, Malawi, Namibia, Tanzania, Zambia, and Zimbabwe.

§Includes Ethiopia, Kenya, Malawi, Zambia, and Zimbabwe.

¶Includes Ethiopia, Kenya, Malawi, Tanzania, Zambia, and Zimbabwe.

#Includes a single participant per household in Cameroon, Cote D'Ivoire, Ethiopia, Lesotho, Malawi, Namibia, Eswatini, Uganda, Zambia, and Zimbabwe.

**Men only.

a sexual debut at <18 years of age, had >1 partner in the previous 12 months, had sex with a partner with whom they were not living, not used condoms during their last sexual intercourse with a nonregular partner, and had sex within the previous 12 months with a partner who had unknown HIV status or an HIV-positive status (Table 2).

We also performed weighted bivariate comparisons of recently infected participants and those with long-term infections (Table 2). Compared with participants 35–49 years of age, adolescents and young adults (15–34 years of age) had a greater percentage of recent infections than long-term infections. Participants who were never married or were divorced/separated had a greater percentage of recent than long-term infections, whereas those who were widowed were more likely to have long-term infections. Sex, employment, education, household wealth, and urbanicity were not associated with recent versus long-term infections. Behavioral factors more common in participants who had recent HIV infections (compared with those with long-term HIV infections) were sexual debut at <18 years of age, >1 sexual partner in the previous 12 months, having partners other than a spouse or live-in partner in the previous 12 months, not using a condom during their last sexual intercourse, and having a partner in the previous 12 months who had unknown HIV status (Table 2).

We performed bivariate exploratory comparisons of variables that were not collected consistently across all PHIA or were only relevant to population subgroups (Table 3). Participants who had a sexually transmitted disease diagnosis or sexually transmitted infection symptoms and male participants who did not have a medical circumcision were more likely to be recently infected than HIV-negative. In addition, participants who had long-term infections were more likely to have previously been tested for HIV >1 year ago and were more likely to be uncircumcised than those who had a recent HIV infection (Table 3).

Multivariate Analysis Findings

In the adjusted model, the southern, southeastern, and eastern Africa regions and community-level viremia remained significantly associated with recent infections (Table 4). Participants living in countries within eastern, southeastern, and southern Africa had higher odds of recent HIV infection compared with those in western Africa, even after adjusting for community-level viremia. In addition, participants grouped in the third and fourth highest quartiles of community-level viremia were more likely to have a recent HIV infection than those in the lowest quartile; the odds of recent infection increased with each viremia quartile.

Individual demographic characteristics, including sex and marital status, remained significantly

associated with HIV acquisition; female participants had 1.82 times greater odds of recent HIV infection than for male participants. In addition, participants who were divorced, separated, or widowed had 3.58 times greater odds of recent HIV infection than for those who were never married. Age group was not significantly associated with HIV acquisition risk in adjusted models (Table 4). Sexual behavior characteristics that remained significantly associated with recent HIV acquisition were having >1 partner in the previous 12 months (adjusted odds ratio [aOR] 1.92) and having ≥1 partner who thought or was told they were HIV-positive (aOR 7.25) or had unknown HIV status (aOR 2.05).

In the multivariable model, compared to those with longstanding infections, those 15–24 years of age (aOR 4.79) and 25–34 years of age (aOR 2.23) were more likely to have a recently acquired infection than were participants who were 35–49 years of age (Table 5). Participants who used a condom the last time they had sex (aOR 0.46) and had ≥1 partner in the previous 12 months that the participant believed or knew to be HIV-positive (aOR 0.17) were less likely to have a recent infection than a long-term infection. Region, sex, marital status, age of sexual debut, partner age differences, and community-level viremia did not significantly differ between those with recent and long-term infections.

Table 4. Correlates of recent and long-term HIV infections compared with HIV negativity in study of risk factors for HIV infections among adults in 14 countries in Africa identified by Population-Based HIV Impact Assessment surveys, 2015–2019

Category	Recent infection vs. HIV-negative		Long-term infection vs. HIV-negative	
	Crude odds ratio (95% CI)	Adjusted odds ratio (95% CI)	Crude odds ratio (95% CI)	Adjusted odds ratio (95% CI)
Region				
Eastern Africa	2.26 (1.46–3.50)	1.88 (1.18–3.02)	2.74 (2.53–3.00)	1.73 (1.58–1.89)
Southeastern Africa	4.39 (2.86–6.73)	2.74 (1.64–4.57)	7.74 (7.17–8.35)	2.66 (2.42–2.93)
Southern Africa	8.58 (5.54–13.28)	4.73 (2.65–8.44)	15.02 (13.89–16.25)	4.03 (3.63–4.47)
Western Africa	Referent	Referent	Referent	Referent
Sex				
F	1.56 (1.09–2.24)	1.82 (1.11–2.98)	1.62 (1.55–1.70)	1.81 (1.68–1.96)
M	Referent	Referent	Referent	Referent
Age group, y				
15–24	1.60 (1.02–2.51)	1.26 (0.74–2.15)	0.27 (0.25–0.29)	0.26 (0.24–0.29)
25–34	1.68 (1.09–2.58)	1.43 (0.92–2.23)	0.64 (0.61–0.68)	0.64 (0.60–0.68)
35–49	Referent	Referent	Referent	Referent
Marital status				
Married/cohabiting	0.87 (0.58–1.31)	1.16 (0.67–1.99)	1.92 (1.79–2.07)	1.35 (1.21–1.51)
Divorced/separated/widowed	4.24 (2.48–7.26)	3.58 (1.92–6.69)	6.97 (6.37–7.62)	3.28 (2.91–3.70)
Never married	Referent	Referent	Referent	Referent
Age of sexual debut, y				
<18	1.74 (1.23–2.46)	1.42 (0.99–2.04)	1.17 (1.11–1.23)	1.20 (1.13–1.28)
≥18	Referent	Referent	Referent	Referent
No. sexual partners in previous 12 mo				
1 partner	Referent	Referent	Referent	Referent
≥2 partners	1.95 (1.34–2.83)	1.92 (1.23–3.00)	0.99 (0.93–1.06)	1.05 (0.96–1.15)
Condom used at last sex				
Condom used	1.32 (0.88–1.99)	0.97 (0.58–1.62)	2.59 (2.45–2.73)	2.13 (1.97–2.30)
Condom not used	Referent	Referent	Referent	Referent
HIV status of sexual partners in previous 12 mo				
≥1 partner thought/told/tested HIV+	15.15 (6.81–33.69)	7.25 (3.41–15.40)	68.92 (6.80–33.68)	42.74 (38.53–47.42)
≥1 partner with unknown HIV status	1.90 (1.34–2.69)	2.05 (1.38–3.03)	1.41 (1.32–1.49)	1.73 (1.62–1.85)
All partners thought/told/tested HIV–	Referent	Referent	Referent	Referent
Age difference with sexual partners				
All partners <5 years older than participant	Referent	Referent	Referent	Referent
≥1 partner 5–9 years older than participant	1.38 (0.95–2.02)	1.05 (0.67–1.66)	1.27 (1.20–1.35)	0.97 (0.90–1.06)
≥1 partner ≥10 years older than participant	0.98 (0.65–1.48)	0.97 (0.58–1.62)	1.20 (1.13–1.27)	1.15 (1.06–1.25)
Community-level viremia*				
Lowest quartile	Referent	Referent	Referent	Referent
Second quartile	1.42 (0.64–3.13)	1.86 (0.79–4.38)	1.57 (1.38–1.80)	1.85 (1.62–2.11)
Third quartile	2.87 (1.36–6.08)	3.16 (1.38–7.26)	3.99 (3.56–4.48)	3.68 (3.27–4.13)
Highest quartile	6.58 (3.22–13.46)	4.81 (2.10–11.00)	11.38 (10.21–12.68)	6.84 (6.09–7.69)

*Lowest quartile (0–25%), <39.38 viremic persons/10,000 population; second quartile (25%–50%), 39.38–122.51 viremic persons/10,000 population; third quartile (50%–75%), 122.52–297.03 viremic persons/10,000 population; highest quartile (76%–100%), >297.03 viremic persons/10,000 population.

Table 5. Crude and adjusted odds ratios comparing recent and long-term HIV infections in study of risk factors for HIV infections among adults in 14 countries in Africa identified by Population-Based HIV Impact Assessment surveys, 2015–2019

Category	Crude odds ratio (95% CI)	Adjusted odds ratio (95% CI)
Region		
Eastern Africa	0.82 (0.53–1.28)	1.10 (0.68–1.76)
Southeastern Africa	0.57 (0.37–0.88)	1.03 (0.61–1.73)
Southern Africa	0.57 (0.37–0.89)	1.18 (0.66–2.11)
Western Africa	Referent	Referent
Sex		
F	0.96 (0.67–1.38)	1.00 (0.61–1.65)
M	Referent	Referent
Age Group, y		
15–24	6.03 (3.81–9.53)	4.79 (2.79–8.24)
25–34	2.60 (1.69–4.01)	2.23 (1.43–3.47)
35–49	Referent	Referent
Marital Status		
Married/cohabiting	0.45 (0.30–0.68)	0.86 (0.49–1.49)
Divorced/separated/widowed	0.61 (0.35–1.05)	1.09 (0.58–2.06)
Never married	Referent	Referent
Age of Sexual Debut, y		
<18	1.49 (1.05–2.11)	1.19 (0.82–1.71)
≥18	Referent	Referent
No. sexual partners in previous 12 mo		
1	Referent	Referent
≥2	1.96 (1.35–2.85)	1.83 (1.17–2.86)
Condom used at last sex		
Condom used	0.51 (0.34–0.77)	0.46 (0.28–0.74)
Condom not used	Referent	Referent
HIV status of sexual partners		
≥1 partner thought/told/tested HIV+	0.22 (0.10–0.49)	0.17 (0.08–0.36)
≥1 partner with unknown HIV status	1.35 (0.95–1.92)	1.18 (0.80–1.76)
All partners thought/told/tested HIV–	Referent	Referent
Age difference with sexual partners		
Partners <5 years older than participant	Referent	Referent
≥1 partner 5–9 years older than participant	1.09 (0.74–1.59)	1.08 (0.68–1.72)
≥1 partner ≥10 years older than participant	0.82 (0.54–1.24)	0.84 (0.50–1.42)
Community-level viremia*		
Lowest quartile	Referent	Referent
Second quartile	0.90 (0.40–2.01)	1.01 (0.43–2.39)
Third quartile	0.72 (0.34–1.54)	0.86 (0.37–1.99)
Highest quartile	0.58 (0.28–1.19)	0.70 (0.31–1.62)

*Lowest quartile (0–25%), <39.38 viremic persons/10,000 population; second quartile (25%–50%), 39.38–122.51 viremic persons/10,000 population; third quartile (50%–75%), 122.52–297.03 viremic persons/10,000 population; highest quartile (76%–100%), >297.03 viremic persons/10,000 population.

Discussion

We compared persons recently infected with HIV, HIV-negative persons, and persons with long-term HIV infections in 14 countries within sub-Saharan Africa by using large, nationally representative, population-based surveys. Participants living in regions of sub-Saharan Africa with higher HIV prevalence were considerably more likely to have a recent HIV infection. Similarly, participants living in communities with higher prevalence of HIV viremia had higher odds of recent HIV infection. Both associations persisted after controlling for individual risk factors. Treatment as prevention (TasP) is a primary strategy for ending the HIV epidemic and is an essential strategy within the conceptual framework of UNAIDS 95–95–95 goals (that 95% of people living with HIV/AIDS know their status, 95% of those who know their status are on treatment, and 95% of those

on treatment are virally suppressed). Multiple studies have shown that persons with undetectable levels of HIV (i.e., HIV viral load <200 copies/mL blood) have essentially no risk of transmitting HIV through sex (19,20). However, population-based studies that assess the effects of TasP on HIV incidence in communities have had fewer clear outcomes; some studies found a lack of population-level effect of TasP (21). Persons living in areas with higher HIV prevalence or higher prevalence of viremic people living with HIV/AIDS have increased likelihood of acquiring HIV infections (22). This finding reinforces the potential benefits of identifying persons who are unaware of their HIV infection and enrolling them in treatment programs to achieve sustained HIV viral suppression, as well as benefits of prevention interventions, such as scale-up of HIV preexposure prophylaxis according to programmatic need.

Consistent with existing literature from sub-Saharan Africa, we found that recent HIV infection was higher in female than male participants; female participants accounted for 65% of recent infections and had ≈ 2 times the adjusted odds of recent HIV infection compared with male participants (12,23). The estimated proportion of new infections occurring among adolescents and young adults 15–24 years of age (31.4%) was largely consistent with UNAIDS estimates of 2 in 7 new infections occurring among that age group (24). We also found that $>70\%$ of new HIV infections among adolescents and young adults were acquired by female participants, in line with the 60%–80% estimates by UNAIDS (25). Those findings highlight the continued need for HIV prevention programs for women and girls, along with other sexual and reproductive health services. Gender disparities in HIV incidence also highlight the need to engage male patients in treatment uptake and retention efforts to further reduce infections among their female partners (26). Age group was not associated with risk for recent HIV infection in adjusted models, indicating the importance of HIV prevention programming across the age continuum among sexually active adolescents and adults.

Compared with participants having sex only with partners they believed or knew were negative for HIV, having a partner that the participant knew or believed was positive for HIV or a partner with unknown HIV status was associated with acquiring a recent HIV infection. The relationship was stronger for those with a partner known or believed to be positive for HIV. Still, most new infections occurred among those who had a sex partner with unknown HIV status. Very few participants with recent HIV infection had sex only with partners they thought were negative for HIV. Having sex with a partner outside of marriage, a sexual debut before turning 18 years of age, and having multiple partners were also associated with an increased risk for new HIV infection. Those findings are not surprising, because they are broadly consistent with similar analyses completed over the previous 2 decades (12,13). Although HIV incidence has decreased during that period, further declines in incidence and reduction in incidence disparities might rely on continued targeted testing to identify those persons at risk of transmitting HIV, as well as interventions that encourage disclosure of positive status, promote access to antiretroviral therapy to suppress viral load, prevent transmission, reduce the number of sexual partners, and promote safe sex and access to preexposure prophylaxis.

Certain factors could not be included in the final model because those data were collected inconsistently across countries or were applicable only to subpopulations. However, voluntary medical male circumcision has been shown to reduce the risk of HIV acquisition by 38%–66% (27), and our bivariate comparisons of participants with recent infections compared with HIV-negative participants are consistent with those data. Additional analyses of PHIA data from fewer countries but using methods designed to specifically determine the effect of male medical circumcision on HIV incidence have similarly found a substantial protective effect, particularly among younger men and boys 15–34 years of age (28).

Although using RITAs in cross-sectional surveys enables the examination of risk factors for new infections, limitations to this approach exist. PHIA data are designed to estimate national incidence rates by using RITAs and are not powered to examine any specific associations between potential risk factors and recent infections. Even though PHIA data were used in some countries with the highest HIV prevalence worldwide and sample sizes were large, very few (range 4–31) recent infections among the study populations were identified. The rarity of the outcome precluded country-specific analyses of risk factors for recent infections. In addition, cultural context, epidemic dynamics, and responses of governments to the epidemic are not homogenous across the continent. Therefore, we could not examine those nuances across or within countries. The size and scope of PHIA data prevents data being available in near real-time; thus, delays in monitoring HIV-acquisition trends using survey-based approaches exist, and risk factors for new infection might change over time. In addition, previous studies that have used a similar approach within a single country had larger sample sizes of recent infections because a larger proportion of HIV infections were classified as recent, such as 7% in Kenya (13) and 17% in Uganda (12). In contrast, only 1.6% of HIV infections in our study were classified as recent infections, likely because incidence rates have declined; the studies in Uganda (12) and Kenya (13) used data collected during 2007, whereas PHIA data used in our study were collected during 2015–2019. Furthermore, differences in RITAs might have contributed to differences in proportions of HIV infections classified as recent; for example, the Uganda study used a different assay, which might have a higher false recency rate than the LAg-avidity EIA (29). Moreover, PHIA data used in our study were conducted with a revised RITA that

incorporated viral load (>1,000 copies/mL) and absence of antiretroviral drug metabolites.

Because this study used a pooled analysis, we were limited to factors that were collected consistently across each PHIA, reducing our ability to examine potential relationships between recent infections and other factors, such as mobility, violence, stigma, alcohol use, and sexually transmitted infection symptoms or diagnosis, which were not collected consistently across countries. Other potential risk factors, such as education, had to be regrouped into broad categories that might have limited our analysis of their relationship with recent HIV infection. Furthermore, only countries that completed a PHIA were included in the analysis; therefore, results might not be generalizable to other countries in sub-Saharan Africa. Community-level viremia was calculated at the stratum level, which often represented larger geographic or political areas such as regions or provinces. Finally, a potential for misclassification of potential risk factors in PHIA existed because of the self-reported nature of risk factors of interest and potential for outcome misclassification by RITA.

Despite those limitations, we successfully identified key factors associated with recent infections among the adult populations of 14 countries that have high HIV burdens. Focusing prevention resources on persons who are at higher risk of acquiring a recent infection should contribute to the continued decline in HIV incidence and, ultimately, to epidemic control. Additional strategies will be needed to monitor recent infections, such as routine surveillance as part of HIV testing services for rapid case and cluster investigations (30–32) or using testing history-based methods to classify recent infections within surveys that do not require the use of a recency assay (33). Those data will provide actionable information for HIV programs regarding new outbreak locations and where prevention resources might be needed most (30).

This research was supported by the US President's Emergency Plan for AIDS Relief through the Centers for Disease Control and Prevention under the terms of cooperative agreement nos. U2GGH001226 and U2GGH002108.

B.S.P. receives royalties from the sale of LAg-Avidity EIA kits sold by the manufacturer according to US government policy.

About the Author

Dr. Currie is an epidemiologist in the Division of Global HIV and TB, Global Health Center, Centers for Disease

Control and Prevention, Atlanta, Georgia, USA. His research interests focus on HIV surveillance in the general population and relationships between behavioral science and communicable diseases.

References

1. Frank TD, Carter A, Jahagirdar D, Biehl MH, Douwes-Schultz D, Larson SL, et al.; GBD 2017 HIV collaborators. Global, regional, and national incidence, prevalence, and mortality of HIV, 1980–2017, and forecasts to 2030, for 195 countries and territories: a systematic analysis for the Global Burden of Diseases, Injuries, and Risk Factors Study 2017. *Lancet HIV*. 2019;6:e831–59. [https://doi.org/10.1016/S2352-3018\(19\)30196-1](https://doi.org/10.1016/S2352-3018(19)30196-1)
2. UNAIDS. Fact sheet – World AIDS Day 2022 [cited 2022 Apr 11]. https://www.unaids.org/sites/default/files/media_asset/UNAIDS_FactSheet_en.pdf
3. Joshi K, Lessler J, Olawore O, Loevinsohn G, Bushey S, Tobian AAR, et al. Declining HIV incidence in sub-Saharan Africa: a systematic review and meta-analysis of empiric data. *J Int AIDS Soc*. 2021;24:e25818. <https://doi.org/10.1002/jia2.25818>
4. Ghys PD, Williams BG, Over M, Hallett TB, Godfrey-Faussett P. Epidemiological metrics and benchmarks for a transition in the HIV epidemic. *PLoS Med*. 2018;15:e1002678. <https://doi.org/10.1371/journal.pmed.1002678>
5. Nabukenya AM, Nambuusi A, Matovu JKB. Risk factors for HIV infection among married couples in Rakai, Uganda: a cross-sectional study. *BMC Infect Dis*. 2020;20:198. <https://doi.org/10.1186/s12879-020-4924-0>
6. Eilami O, Nazari A, Dousti M, Sayehmiri F, Ghasemi M. Investigation of HIV/AIDS prevalence and associated risk factors among female sex workers from 2010 to 2017: a meta-analysis study. *HIV AIDS (Auckl)*. 2019;11:105–17. <https://doi.org/10.2147/HIV.S196085>
7. Kabapy AF, Shatat HZ, Abd El-Wahab EW. Attributes of HIV infection over decades (1982–2018): a systematic review and meta-analysis. *Transbound Emerg Dis*. 2020;67:2372–88. <https://doi.org/10.1111/tbed.13621>
8. Geis S, Maboko L, Saathoff E, Hoffmann O, Geldmacher C, Mmbando D, et al. Risk factors for HIV-1 infection in a longitudinal, prospective cohort of adults from the Mbeya Region, Tanzania. *J Acquir Immune Defic Syndr*. 2011; 56:453–9. <https://doi.org/10.1097/QAI.0b013e3182118fa3>
9. Olawore O, Tobian AAR, Kagaayi J, Bazaale JM, Nantume B, Kigozi G, et al. Migration and risk of HIV acquisition in Rakai, Uganda: a population-based cohort study. *Lancet HIV*. 2018;5:e181–9. [https://doi.org/10.1016/S2352-3018\(18\)30009-2](https://doi.org/10.1016/S2352-3018(18)30009-2)
10. Nsanzimana S, Remera E, Kanters S, Mulindabigwi A, Suthar AB, Uwizihiwe JP, et al. Household survey of HIV incidence in Rwanda: a national observational cohort study. *Lancet HIV*. 2017;4:e457–64. [https://doi.org/10.1016/S2352-3018\(17\)30124-8](https://doi.org/10.1016/S2352-3018(17)30124-8)
11. Risher KA, Cori A, Reniers G, Marston M, Calvert C, Crampin A, et al.; ALPHA Network. Age patterns of HIV incidence in eastern and southern Africa: a modelling analysis of observational population-based cohort studies. *Lancet HIV*. 2021;8:e429–39. [https://doi.org/10.1016/S2352-3018\(21\)00069-2](https://doi.org/10.1016/S2352-3018(21)00069-2)
12. Mermin J, Musinguzi J, Opio A, Kirungi W, Ekwaru JP, Hladik W, et al. Risk factors for recent HIV infection in Uganda. *JAMA*. 2008;300:540–9. <https://doi.org/10.1001/jama.300.5.540>

13. Kim AA, Parekh BS, Umuro M, Galgalo T, Bunnell R, Makokha E, et al.; 2007 KAIS study group. Identifying risk factors for recent HIV infection in Kenya using a recent infection testing algorithm: results from a nationally representative population-based survey. *PLoS One*. 2016; 11:e0155498. <https://doi.org/10.1371/journal.pone.0155498>
14. Voetsch AC, Duong YT, Stupp P, Saito S, McCracken S, Dobbs T, et al. HIV-1 recent infection testing algorithm with antiretroviral drug detection to improve accuracy of incidence estimates. *J Acquir Immune Defic Syndr*. 2021; 87:S73–80. <https://doi.org/10.1097/QAI.0000000000002707>
15. Federal Ministry of Health, Nigeria. Nigeria HIV/AIDS indicator and impact survey (NAIS) 2018 technical report. October 2019 [cited 2023 Sep 18]. <https://ciheb.org/media/SOM/Microsites/CIHEB/documents/NAIS-Report-2018.pdf>
16. Sachathep K, Radin E, Hladik W, Hakim A, Saito S, Burnett J, et al. Population-based HIV impact assessments survey methods, response, and quality in Zimbabwe, Malawi, and Zambia. *J Acquir Immune Defic Syndr*. 2021; 87:S6–16. <https://doi.org/10.1097/QAI.0000000000002710>
17. Patel HK, Duong YT, Birhanu S, Dobbs T, Lupoli K, Moore C, et al. A comprehensive approach to assuring quality of laboratory testing in HIV surveys: lessons learned from the population-based HIV impact assessment project. *J Acquir Immune Defic Syndr*. 2021;87:S17–27. <https://doi.org/10.1097/QAI.0000000000002702>
18. Justman JE, Mugurungi O, El-Sadr WM. HIV population surveys – bringing precision to the global response. *N Engl J Med*. 2018;378:1859–61. <https://doi.org/10.1056/NEJMp1801934>
19. Cohen MS, Chen YQ, McCauley M, Gamble T, Hosseinipour MC, Kumarasamy N, et al.; HPTN 052 Study Team. Prevention of HIV-1 infection with early antiretroviral therapy. *N Engl J Med*. 2011;365:493–505. <https://doi.org/10.1056/NEJMoa1105243>
20. Rodger AJ, Cambiano V, Bruun T, Vernazza P, Collins S, van Lunzen J, et al.; PARTNER Study Group. Sexual activity without condoms and risk of HIV transmission in serodifferent couples when the HIV-positive partner is using suppressive antiretroviral therapy. *JAMA*. 2016;316:171–81. <https://doi.org/10.1001/jama.2016.5148>
21. Brault MA, Spiegelman D, Abdool Karim SS, Vermund SH. Integrating and interpreting findings from the latest treatment as prevention trials. *Curr HIV/AIDS Rep*. 2020;17:249–58. <https://doi.org/10.1007/s11904-020-00492-4>
22. Jia KM, Eilerts H, Edun O, Lam K, Howes A, Thomas ML, et al. Risk scores for predicting HIV incidence among adult heterosexual populations in sub-Saharan Africa: a systematic review and meta-analysis. *J Int AIDS Soc*. 2022;25:e25861. <https://doi.org/10.1002/jia2.25861>
23. Ramjee G, Daniels B. Women and HIV in sub-Saharan Africa. *AIDS Res Ther*. 2013;10:30. <https://doi.org/10.1186/1742-6405-10-30>
24. Joint United Nations Programme on HIV/AIDS. Young people and HIV [cited 2022 May 25]. https://www.unaids.org/sites/default/files/media_asset/young-people-and-hiv_en.pdf
25. Joint United Nations Programme on HIV/AIDS (UNAIDS). Women and HIV: a spotlight on adolescent girls and young women. 2019 [cited 2022 May 25]. https://www.unaids.org/sites/default/files/media_asset/2019_women-and-hiv_en.pdf
26. Vandormael A, Akullian A, Siedner M, de Oliveira T, Bärnighausen T, Tanser F. Declines in HIV incidence among men and women in a South African population-based cohort. *Nat Commun*. 2019;10:5482. <https://doi.org/10.1038/s41467-019-13473-y>
27. Siegfried N, Muller M, Deeks JJ, Volmink J. Male circumcision for prevention of heterosexual acquisition of HIV in men. *Cochrane Database Syst Rev*. 2009;15:CD003362. <https://doi.org/10.1002/14651858.CD003362.pub2>
28. Hines JZ, Sachathep K, Pals S, Davis SM, Toledo C, Bronson M, et al. HIV incidence by male circumcision status from the population-based HIV impact assessment surveys – eight sub-Saharan African countries, 2015–2017. *J Acquir Immune Defic Syndr*. 2021;87:S89–96. <https://doi.org/10.1097/QAI.0000000000002658>
29. Duong YT, Qiu M, De AK, Jackson K, Dobbs T, Kim AA, et al. Detection of recent HIV-1 infection using a new limiting-antigen avidity assay: potential for HIV-1 incidence estimates and avidity maturation studies. *PLoS One*. 2012;7:e33328. <https://doi.org/10.1371/journal.pone.0033328>
30. Kim AA, Behel S, Northbrook S, Parekh BS. Tracking with recency assays to control the epidemic: real-time HIV surveillance and public health response. *AIDS*. 2019;33:1527–9. <https://doi.org/10.1097/QAD.0000000000002239>
31. Suthar AB, Ouk V, Samreth S, Ngauv B, Bain R, Eng B, et al. Programmatic implications of national recent HIV infection surveillance in Cambodia. *J Infect Dis*. 2023 Apr 1 [Epub ahead of print] <https://doi.org/10.1093/infdis/jiad082>
32. Telford CT, Tessema Z, Msukwa M, Arons MM, Theu J, Bangara FF, et al. Geospatial transmission hotspots of recent HIV infection – Malawi, October 2019–March 2020. *MMWR Morb Mortal Wkly Rep*. 2022;71:329–34. <https://doi.org/10.15585/mmwr.mm7109a1>
33. Gurley SA, Stupp PW, Fellows IE, Parekh BS, Young PW, Shiraishi RW, et al. Estimation of HIV-1 incidence using a testing history-based method; analysis from the population-based HIV impact assessment survey data in 12 African countries. *J Acquir Immune Defic Syndr*. 2023;92:189–96. <https://doi.org/10.1097/QAI.0000000000003123>

Address for correspondence: Dustin Currie, Centers for Disease Control and Prevention, 1600 Clifton Rd NE, Mailstop H16-3, Atlanta, GA 30329-4027, USA; email: pif7@cdc.gov

Systematic Review and Meta-analysis of Deaths Attributable to Antimicrobial Resistance, Latin America

Agustín Ciapponi, Ariel Bardach, María Macarena Sandoval,
María Carolina Palermo, Emiliano Navarro, Carlos Espinal, Rodolfo Quirós

Antimicrobial resistance is a pressing global health concern, leading to 4.95 million deaths in 2019. We conducted a systematic review and meta-analysis to assess the lethality attributed to infections caused by multidrug-resistant organisms (MDROs) in Latin America and the Caribbean. A comprehensive search of major databases retrieved relevant studies from 2000–2022. We included 54 observational studies, primarily from Brazil, Argentina, and Colombia. The most commonly studied organism was methicillin-resistant *Staphylococcus aureus*. The overall unadjusted case fatality rate related to MDROs was 45.0%; higher adjusted lethality was observed in persons infected with MDROs than in those infected with other pathogens (adjusted odds ratio 1.93, 95% CI 1.58–2.37). A higher lethality rate was seen in patients who did not receive appropriate empirical treatment (odds ratio 2.27, 95% CI 1.44–3.56). These findings underscore the increased lethality associated with antimicrobial resistance in Latin America and the Caribbean.

Antimicrobial resistance (AMR) is a growing public health problem that affects health, the economy, and human development (1). A 2016 review of AMR showed that drug-resistant infections will kill 10 million persons annually by 2050 and cause a cumulative economic loss of US \$100 trillion if proactive solutions to slow the rise of drug resistance are not implemented (2). Although some persons have criticized

this forecast, numerous researchers agree that the spread of AMR is an urgent problem, one that will require a global, coordinated action plan to solve (3,4).

Recently, a study using statistical predictive models based on a comprehensive systematic review estimated 4.95 million deaths related to AMR, including 1.27 million deaths attributable to AMR, occurred across 204 countries and territories in 2019 (5). The highest burden of AMR is seen in low-resource settings. AMR was the third leading underlying cause of death for 2019 in the Institute for Health Metrics and Evaluation's Global Burden of Disease study (<https://www.healthdata.org/research-analysis/gbd>). In addition, deaths attributable to AMR surpassed deaths caused by HIV, tuberculosis, and malaria. Understanding the effects of AMR is crucial for building policy resolutions, particularly regarding antimicrobial and diagnostic stewardship and infection prevention and control programs. This study, in which we defined attributable lethality as the excess lethality of patients with infections caused by resistant organisms compared with patients with infections caused by the same susceptible pathogens, represents an essential contribution to knowledge of the effects of AMR on lethality. However, because the estimations were performed for 2019, data related to the effects of the COVID-19 pandemic could not be part of this study. In addition, estimates of attributable lethality for the Latin America region were based principally on data from Brazil, Colombia, and Mexico; information from other countries in the region was limited (5). The incidence of multidrug-resistant organisms (MDROs) increased during the COVID-19 pandemic because of widespread use of antimicrobial drugs and breaches in infection control practices (6–8). During 2020–2021, Latin American and

Author affiliations: Centro de Investigaciones Epidemiológicas y Salud Pública (CIESP), Buenos Aires, Argentina (A. Ciapponi, A. Bardach); Instituto de Efectividad Clínica y Sanitaria (IECS-CONICET), Buenos Aires (A. Ciapponi, A. Bardach, M.M. Sandoval, M.C. Palermo, E. Navarro); Florida International University, Miami, Florida, USA (C. Espinal, R. Quirós); Sanatorio Las Lomas, Buenos Aires (R. Quirós)

DOI: <https://doi.org/10.3201/eid2911.230753>

Caribbean (LAC) countries reported clinical emergence of carbapenemase-producing Enterobacterales that had not been previously characterized locally, increased prevalence of carbapenemases that had been previously detected, and coproduction of multiple carbapenemases in some isolates (9).

Several studies have estimated the effects of antibiotic resistance on incidence, deaths, length of hospital stay, and healthcare costs for MDROs (1,2,10), but systematic research on the effects of AMR in the LAC region for a wide range of bacteria and infections is lacking. We conducted a systematic review to address this evidence gap.

Materials and Methods

Search Strategy and Selection Criteria

We performed a systematic review and meta-analysis using Cochrane methods (11) and the PRISMA (12) statement for reporting systematic reviews and meta-analysis. We searched records published during January 1, 2000–March 29, 2022, in the databases CENTRAL (Cochrane Central Register of Controlled Trials), MEDLINE, Embase, LILACS (Latin American and Caribbean Health Sciences Literature), and CINAHL (Cumulative Index to Nursing and Allied Health Literature), without language restriction and with geographic scope of LAC countries (Appendix, <https://wwwnc.cdc.gov/EID/article/29/11/23-0753-App1.pdf>).

We included cohort studies, case-control studies, cross-sectional and control arms of randomized and quasi-randomized controlled trials, with ≥ 20 inpatient or outpatient participants, irrespective of age and sex, that assessed case-fatality rate (i.e., number of deaths among diagnosed cases only) within 30 days postinfection by any of the following resistant organisms: methicillin-resistant *Staphylococcus aureus* (MRSA), vancomycin-resistant *Enterococcus* spp. (VRE), extended-spectrum β -lactamase producing Enterobacterales (ESBL-E), carbapenem-resistant Enterobacterales (CRE, including *Klebsiella pneumoniae*, *Enterobacter*, *Escherichia coli*, *Proteus*, and *Serratia*), carbapenem-resistant *Pseudomonas aeruginosa* (CR-PA), carbapenem-resistant *Acinetobacter baumannii* (CR-AB), or azole/echinocandin-resistant *Candida* spp. (1). We have incorporated the MDRO category, which encompasses a diverse array of microorganisms (MRSA, VRE, ESBL-E, CRE, CR-PA, CR-AB). MDRO definitions and appropriate empirical treatment varied among primary studies. We accepted the definitions given by each study author.

We planned to include economic evaluations to assess resource use, including hospital stays and loss of health-related quality of life. We considered systematic reviews and meta-analyses only as sources for primary studies. When we found data or data subsets reported in >1 publication, we selected the most recent study or the study with the larger sample size. We searched databases containing proceedings of regional congresses and doctoral theses. We also consulted websites from the main regional medical societies, experts, and associations related to the topic (Appendix).

Statistical Analysis

Pairs of reviewers independently selected articles by evaluating titles and abstracts of identified studies and then performing full-text review using Covidence software (<https://www.covidence.org>). One reviewer performed data extraction and a second verified data by using a prespecified extraction online form previously piloted in 10 studies. The same reviewers independently assessed the risk for bias using a checklist for observational studies developed by the US National Heart, Lung, and Blood Institute (<https://www.nhlbi.nih.gov/health-topics/study-quality-assessment-tools>). All authors resolved discrepancies by consensus.

We extracted study information consisting of type of publication, year of publication, authors, population, geographic location, study design, methods, pathogen-drug combinations, counterfactual data, and outcomes of interest. We classified population risk as high risk if they met ≥ 1 of the following characteristics: intensive care unit (ICU) setting or $>50\%$ of enrolled patients from ICU; median Charlson Comorbidity Index of >3 (if not reported, $>50\%$ of the patients with >1 comorbidity); or patients referred from high-risk wards (i.e., hematology, oncology, burns, transplantation, and infectious diseases, including HIV units). Otherwise, we classified the population as average risk. If study authors provided no data, we categorized the population risk as unknown.

To analyze our data, we used descriptive statistics and performed proportional meta-analysis using the random effects model whenever possible, employing methods to stabilize variance given the degree of expected heterogeneity. We applied the arcsine transformation to stabilize the variance of proportions using inverse arcsine variance weights for the random effects model with the metagen function (13,14). We used the restricted maximum-likelihood estimator to calculate the heterogeneity variance τ^2 across the studies and I^2 statistic as a measure of the proportion

of the overall variation that was attributable to between-study heterogeneity (15,16).

The primary outcome was deaths attributable to AMR. Mortality rates describe the incidence of deaths among a specific population over a specific time. In this study, the population under investigation consisted of infected persons; although the accurate term is lethality (number of deaths among infected patients), we occasionally use the term mortality, which is more commonly used in the literature. We have included adjusted measures, such as odds ratio (OR), relative risk (RR), or hazard ratio (HR), when they were available for ≥ 10 events in the susceptible or resistance group. We included the longest time-point in-hospital lethality reported in each study in the analysis. We also performed a random-effects meta-analysis to estimate the pooled unadjusted OR when possible. Otherwise, we calculated ORs and 95% CIs using the information provided in each study. We report all effects estimates with a 95% CI. We describe the remaining results narratively and in tables.

We performed subgroup analysis by recruitment year and pathogen-drug combination. We performed a sensitivity analysis to assess the effect of risk for bias on the results of the primary analyses by limiting the analysis to a low risk for bias for the primary domains. We also used Knapp-Hartung adjustments to estimate 95% CIs around the pooled effect as a sensitivity analysis (17).

To further explore heterogeneity, we conducted a meta-regression analysis to examine whether adjusted and unadjusted effect estimates differed notably by year of study recruitment, population severity, resistance mechanisms or type of resistance, and appropriate empirical antibiotic treatment. We also planned a sensitivity analysis on the basis of the type of adjustment performed and considered it appropriate if the authors controlled in the final model ≥ 1 variable in each of these categories: variables related to the patients' baseline status, variables related to the infection, and variables related to the treatment (18).

We visually inspected the funnel plot for asymmetry to assess publication bias and performed Begg's test. We used R software version 4.0.3 for all analyses (19). The protocol of this study is registered in PROSPERO (<https://www.crd.york.ac.uk/prospero>; identification no. CRD42022322795).

Results

We identified 1,141 records from databases and 204 records from other sources; after the selection process, 54 studies met our inclusion criteria (Figure 1). The articles were published during January 1, 2000–

March 29, 2022; the inclusion period of participants was 1991–2020. We excluded 19 studies at the extraction stage (Appendix Table 6). Most included studies were cohort studies (50/54 [92.6%]); 36 were retrospective studies. The studies provided data on AMR mainly from Brazil (29 [53.7%]), Argentina (8 [14.8%]), Colombia (6 [11.1%]), and Mexico (6 [11.1%]). Of the 54 included studies, participants in 38 (70.4%) were adults (adults and elderly patients), and 6 (11.1%) studies included only children (neonates and pediatric patients). In the 49 studies that reported the source of patients, all participants were hospitalized, 18 (36.7%) consisted of ICU patients, and 20 (40.9%) included both ICU and non-ICU patients. High-risk populations were included in 43 (79.6%) studies. The most frequently evaluated individual microorganism was MRSA in 16 (29.6%) studies (Appendix Table 12). We identified a fair risk of bias in 24 (44.4%) of 54 studies (Appendix Tables 7, 8). We noted additional characteristics of individual included studies (Appendix Table 9).

We assessed lethality and association measures of the individual studies (Appendix Table 13). The overall unadjusted case-fatality rate related to MDRO was 45.0% (95% CI 40.0–50.0; I^2 85.0%) (Appendix Figure 1). We found higher lethality among participants infected with MDRO than among participants infected with nonresistant organisms, grouped according to the type of resistance (pooled adjusted OR [aOR] 1.93, 95% CI 1.58–2.37; I^2 0%) (Figure 2). Although that trend was maintained in studies that reported RR or HR as adjusted measures, the difference was not statistically significant. We found no evidence of publication bias among studies reporting aOR or adjusted HR (Appendix Figures 2, 3).

Higher lethality was also observed in those who did not receive appropriate empirical treatment (OR 2.27, 95% CI 1.44–3.56) than in those who did (OR 1.59, 95% CI 0.99–2.56), although the test for subgroup differences was not statistically significant ($p = 0.57$). We also found no statistically significant difference ($p = 0.75$) between resistance and lethality in those studies that included appropriate empiric antibiotic treatment as a covariate in the adjusted model (Figure 3; Appendix Figure 4).

We report the association between unadjusted lethality and type of resistance (Table). The pooled unadjusted lethality associated with resistant infections was significantly higher (OR 1.86, 95% CI 1.55–2.23) than that associated with susceptible infections but with high heterogeneity (I^2 71%) (Appendix Figure 5). We identified a downward trend ($p = 0.463$) of this pooled OR of lethality over time (Figure 4). We also

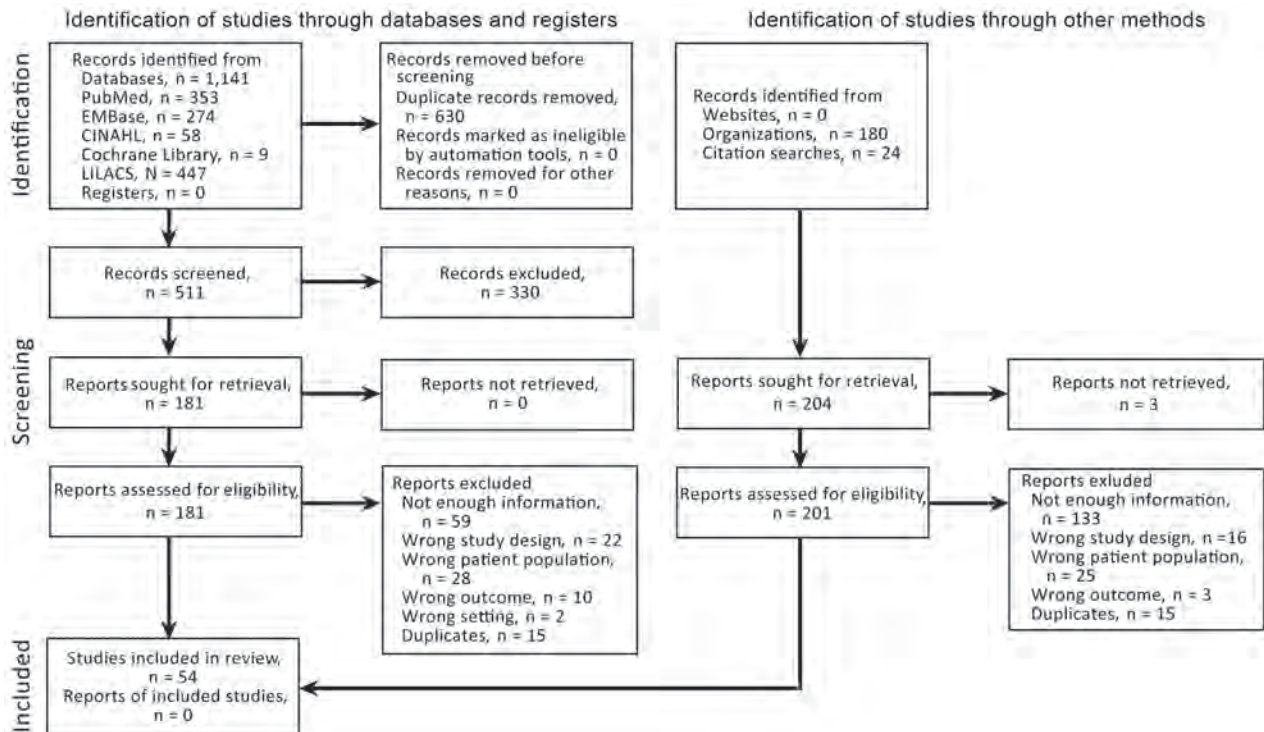


Figure 1. Flowchart demonstrating identification process of studies for systematic review and meta-analysis of deaths attributable to antimicrobial resistance, Latin America. CINAHL, Cumulative Index to Nursing and Allied Health Literature; LILACS, Latin American and Caribbean Health Sciences Literature).

presented a forest plot of unadjusted OR for lethality by year of study recruitment (Appendix Figure 6). The results of a meta-regression analysis showed no significant differences in effect estimates (Appendix Table 10).

We analyzed the difference between the pooled unadjusted and adjusted lethality associated with resistance between studies that reported both measures (Appendix Figure 7). The magnitude of the effect was larger when looking at the unadjusted measures, but the differences between subgroups were not statistically significant ($p = 0.360$).

We performed a sensitivity analysis based on the type of multivariate model adjustment reported in the studies. Although the aOR was larger when the adjustment was appropriate, we found no statistically significant subgroup differences ($p = 0.56$) (Appendix Figure 8). As a sensitivity analysis, we report the 95% CI around the pooled effect with Knapp-Hartung adjustments in those studies that report adjust measures. We found no major differences with or without this method (Appendix Table 11).

In all but 2 reports where hospitalization stay was documented, patients with resistant microorganisms exhibited longer length of stay relative to those with susceptible strains (Appendix Table 9). We did not

find any information related to loss of health-related quality of life attributable to MDRO in the region. Length of stay was not reported because data were scarce and heterogeneous.

Discussion

This systematic review and meta-analysis offers a thorough and current evaluation of how infection with a wide range of antimicrobial-resistant bacteria affects the lethality rates for infectious diseases during hospitalization in LAC countries. We established the unadjusted and adjusted lethality attributable to MDRO within this region. A previous study reported estimations using predictive statistical modeling to produce estimates of AMR burden for all locations, including for locations with no data. However, the methodologic approach used in this study differed substantially (5).

Although unadjusted case-fatality rates varied across different MDROs, the lowest values were observed for ESLB-E. That finding might be because of the increased use of carbapenems as appropriate initial empirical treatments, especially for healthcare-associated infections, which some studies have demonstrated in the region (34).

Similar to previous researchers (35,36), we also report that drug resistance might lead to an increased

attributable risk for death. However, our findings should be interpreted with caution because of substantial heterogeneity in effect estimates across studies and other methodologic limitations. The heterogeneity was partially explained by the fact that some

studies were adjusted for confounding variables, but others were not. When we analyzed studies adjusted for confounding variables separately, the results for each group were no longer heterogeneous. The adjustment decreased the association strength,

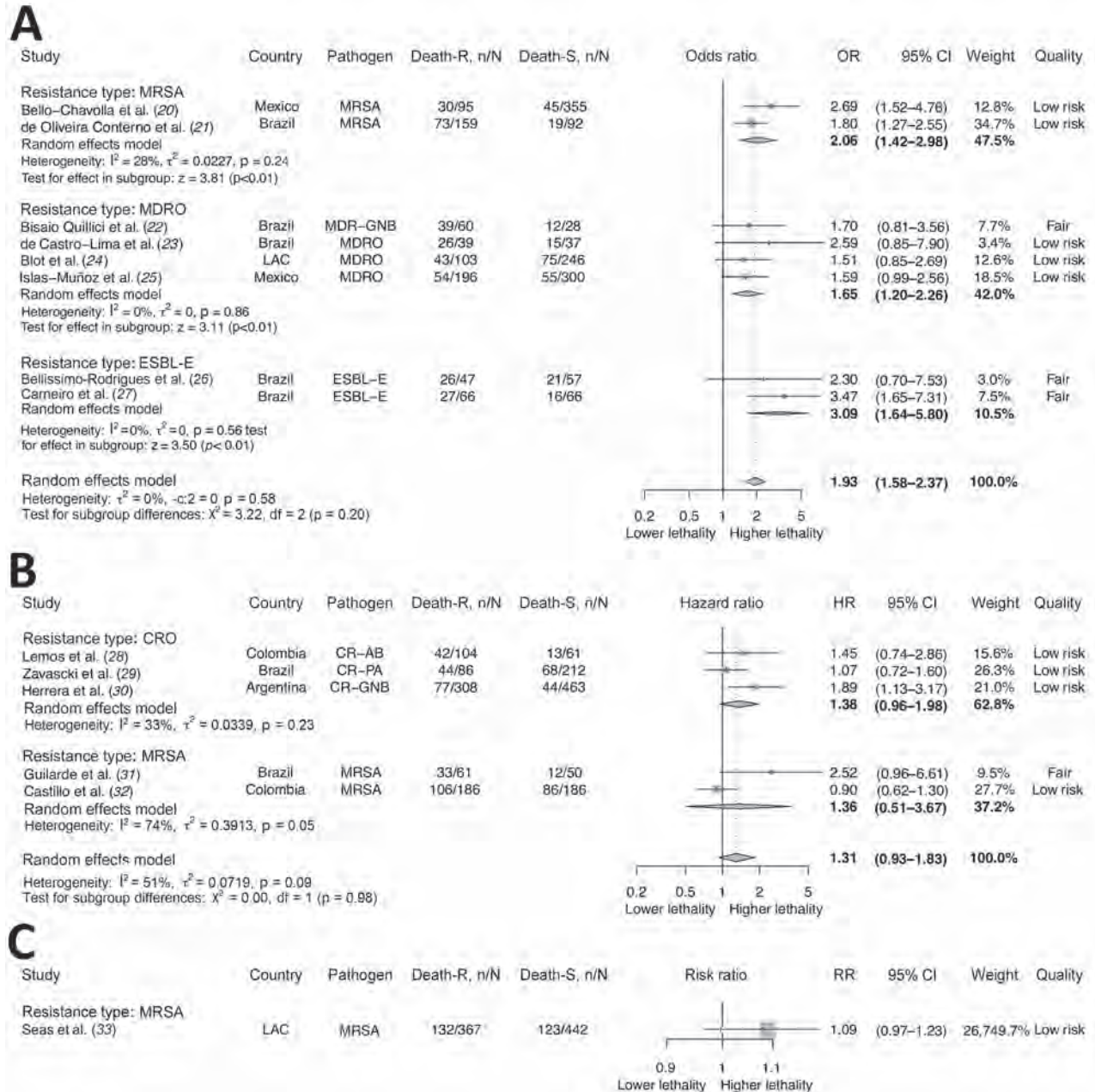


Figure 2. Association between antimicrobial resistance and lethality by the type of resistance in systematic review and meta-analysis of deaths attributable to antimicrobial resistance, Latin America. Adjusted measures are shown as adjusted odds ratio (A), adjusted hazard ratio (B), and adjusted risk ratio (C). Death-R indicates death in the resistant group; Death-S indicates death in the susceptible group. Error bars indicate 95% CIs. CR-AB, carbapenem-resistant *Acinetobacter baumannii*; CRE, carbapenem-resistant Enterobacterales; CR-GNB, carbapenem-resistant gram-negative bacteria (including CRE, CR-PA, CR-AB); CR-PA, carbapenem-resistant *Pseudomonas aeruginosa*; CRO, carbapenem-resistant organisms; ESBL-E, extended-spectrum β -lactamase-producing Enterobacterales; HR, hazard ratio; LAC, Latin American and Caribbean; MDR-GNB, multidrug-resistant gram-negative bacilli (including ESBL-E, CRE, CR-PA, CR-AB); MDRO, multidrug-resistant organisms (including MRSA, vancomycin-resistant *Enterococcus*, ESBL-E, CRE, CR-PA, CR-AB); MRSA, methicillin-resistant *Staphylococcus aureus*; OR, odds ratio; RR, risk ratio.

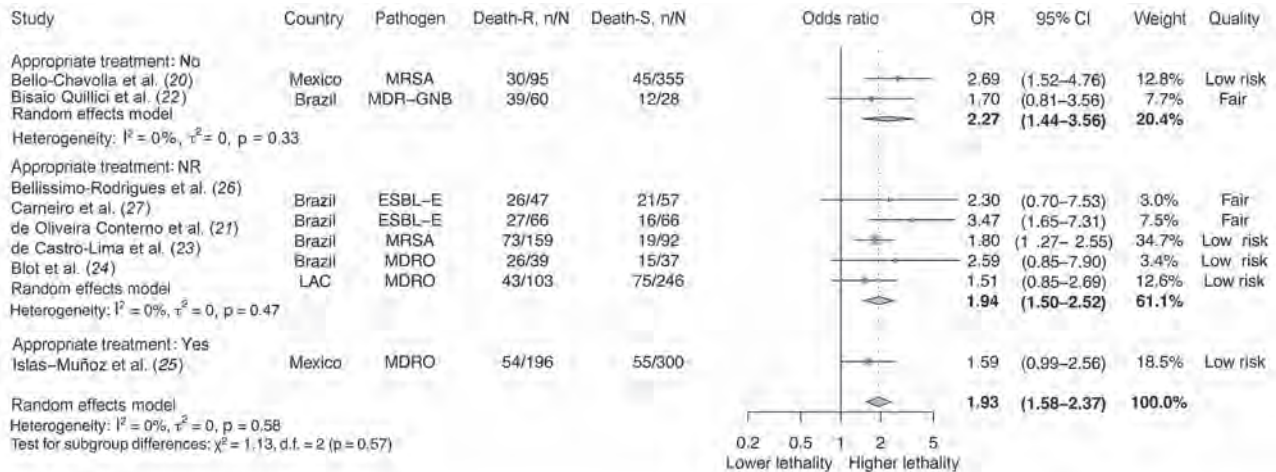


Figure 3. Adjusted odds ratios between antimicrobial resistance and lethality by appropriate empirical antibiotic treatment (considering the definition of appropriate empirical treatment given by each author) in systematic review and meta-analysis of deaths attributable to antimicrobial resistance, Latin America. Death-R indicates death in the resistant group; Death-S indicates death in the susceptible group. Error bars indicate 95% CIs. CR-AB, carbapenem-resistant *Acinetobacter baumannii*; CRE, carbapenem-resistant Enterobacterales; CR-PA, carbapenem-resistant *Pseudomonas aeruginosa*; ESBL-E, extended-spectrum β-lactamase-producing Enterobacterales; MDR-GNB, multidrug-resistant gram-negative bacilli (including ESBL-E, CRE, CR-PA, CR-AB); MDRO, multidrug-resistant organisms (including MRSA, vancomycin-resistant Enterococcus, ESBL-E, CRE, CR-PA, CR-AB); MRSA, methicillin-resistant *Staphylococcus aureus*; NR, not reported; OR, odds ratio.

although the subgroup differences were not statistically significant. The downward trend of pooled unadjusted lethality OR and resistance by calendar recruitment period was not statistically significant, but this finding still might reflect a better understanding of the resistance mechanisms and an improved empirical treatment.

As in previous reports (37,38), our report found 2 times higher attributable lethality associated with MRSA infections than with non-MRSA infections. As in our study, the heterogeneity was explained by the fact that some studies were adjusted for confounding variables, but others were not. When those studies that were adjusted for confounding

variables were analyzed separately from studies that were not adjusted, the results for each group were no longer heterogeneous (Appendix Figure 7). Of note, several studies have identified the association of inappropriate empirical antibiotic treatment with increased lethality among patients with MRSA bacteremia (39,40).

In our study, patients with VRE infections were 4-fold (unadjusted) more likely to die than patients infected with vancomycin-susceptible *Enterococcus* spp. A previous meta-analysis indicated that vancomycin resistance was an independent predictor of death among patients with enterococcal bacteremia (2.5-fold adjusted) (41). Some plausible explanations for this association difference, besides the adjustment of the last estimation, might include type of infection, suboptimal activity, or dosing among the antimicrobials used against VRE, a systematic delay in the initiation of antimicrobial agents active against VRE, and differences in intrinsic virulence among vancomycin-resistant and vancomycin-susceptible species of enterococci.

In our study, infections by ESBL-E were associated with higher lethality than for non-ESBL-E. Other studies have found that ESBL-E bacteremia is associated with higher lethality than bacteremia with non-ESBL-E, although the estimate of this association is affected by adjustment procedures. Adjustment for adequate empirical therapy or delay in effective therapy leads to reduced ORs, indicating that higher

Table. Pooled unadjusted odds ratio for the association between antimicrobial resistance and lethality by type of resistance, Latin America*

Type of resistance	OR (95% CI)	I ²
Carbapenem-resistance	2.86 (2.07–3.95)	61%
Extended-spectrum β-lactamase	1.28 (0.95–1.74)	38%
Methicillin-resistance	1.78 (1.29–2.45)	63%
MDRO†	1.64 (1.16–2.30)	68%
Azol-resistant	1.41 (0.59–3.35)	-
Vancomycin-resistant	4.09 (2.40–6.97)	0%
Random effect model	1.86 (1.55–2.23)	71%

*MDRO, multidrug-resistant organisms; OR, pooled odds ratio.

†Multidrug-resistant organisms include methicillin-resistant *Staphylococcus aureus*, Vancomycin-resistant *Enterococcus* spp, extended-spectrum β-lactamase producing Enterobacterales, carbapenem-resistant Enterobacterales (including *Klebsiella*, *Enterobacter*, *Escherichia coli*, *Proteus*, *Serratia*), carbapenem-resistant *Pseudomonas aeruginosa*, carbapenem-resistant *Acinetobacter baumannii* and azole/echinocandin-resistant *Candida* spp.

lethality is likely to be partly mediated through this phenomenon (42–44).

We found a significant attributable lethality associated with carbapenem-resistant organisms in 11 studies included in our meta-analysis. A previous study showed that KPC-producing *K. pneumoniae* was independently associated with 3 times higher in-hospital lethality (45).

A meta-analysis of 15 studies consisting of 3,201 cases of *P. aeruginosa* infection demonstrated a 2-fold higher lethality rate among patients infected with the multidrug-resistant strain than those with a non-multidrug-resistant strain, especially in patients with bloodstream infection, immunosuppression, and inadequate antimicrobial therapy (35). Other meta-analyses showed that appropriate initial antibiotic therapy was associated with lower unadjusted lethality for *P. aeruginosa* infections than was inappropriate initial antibiotic therapy. The association with lethality persisted in sensitivity meta-analysis of low-risk bias studies (46).

In a meta-analysis that included 16 observational studies, patients with CR-AB had a significantly 2-fold higher risk for lethality than patients with non-carbapenem-resistant strain in the pooled analysis, although substantial heterogeneity was evident. The association remained significant in the pooled aOR of 10 studies. Compared with patients with non-carbapenem-resistant strains, patients with CR-AB were more likely to have a severe underlying illness and to receive inappropriate empirical antimicrobial treatment, which increases the risk for lethality (47).

In our meta-analysis, 4 studies evaluating attributable lethality showed that MDRO had significantly higher lethality than non-MDRO. Although different microorganisms and site infections were represented, we did not find statistical heterogeneity.

For gram-negative infections, a meta-analysis showed that lethality was higher in patients with multidrug-resistant infections than those with non-multidrug-resistant infections (48). The meta-analysis demonstrated that septic shock, ICU stay, pneumonia, isolation of multidrug-resistant gram-negative bacteria, inappropriate empirical and definitive treatment, and male sex were more common in patients who died than patients who survived (48). In addition, several studies have reported inappropriate empirical and definitive treatment as independent variables associated with attributable lethality (35,39–44,46–49)

As the incidence of AMR rises, a corresponding increase in the likelihood of inappropriate empirical treatment occurs. Our meta-analysis revealed that persons who did not receive appropriate empirical treatment had a higher lethality rate than those who

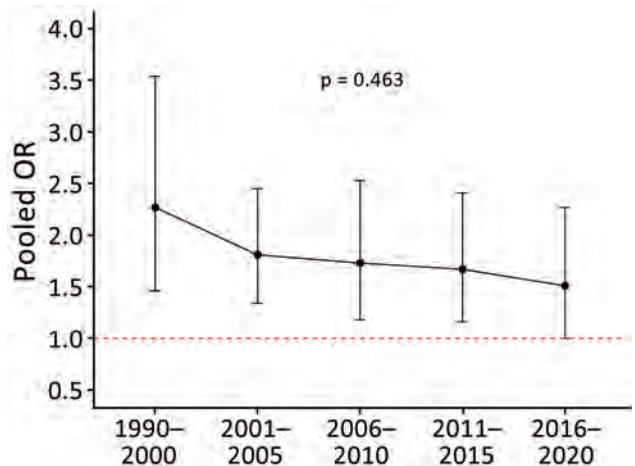


Figure 4. Pooled unadjusted OR between antimicrobial resistance and lethality by calendar recruitment period in systematic review and meta-analysis of deaths attributable to antimicrobial resistance, Latin America. Data points depict pooled lethality estimates from random effects meta-analysis models. Error bars indicate 95% CIs. OR, odds ratio.

did. However, the lack of information regarding the adequacy of antimicrobial therapy in many studies might explain the absence of statistically significant differences between subgroups.

The first limitation of our study is that of the 41 cohort studies included, only 14 were prospective. Incomplete collection in surveys in retrospective cohort studies limits confidence in their estimates. Other limitations include the lack of data for most countries in the LAC region and the number of included studies with small samples. For example, most data were obtained from a few tertiary centers in each country, which are likely to report higher rates of resistance than their national averages. Methods for reporting, collection, and analysis might also differ among laboratories, countries, and surveillance networks. Other limitations included the type of infections (which might vary across included studies), the type of antimicrobial drugs administered for the infection, the type of bacteria, and the mechanism of resistance, which might lead to differences in lethality.

In conclusion, our systematic review and meta-analysis demonstrate that MDROs are associated with higher attributable lethality across different periods in LAC than sensitive organisms, even after adjusting for confounding variables. More studies on AMR-attributable lethality would be needed in the region, with adjustment by confounders and larger sample sizes. Rather than relying solely on new drug development to address the problem of AMR, we should focus efforts on preventing the emergence and transmission of these organisms through the One

Health initiative, principally in low-income settings (50). Future studies that involve many healthcare centers and that adjust for potential confounding variables should be undertaken to address the impact of AMR. In addition, expanding microbiology laboratory capacity and data collection systems are necessary to improve our understanding of this critical human health threat.

Acknowledgments

We thank Daniel Comandé for his support as librarian.

The data used for this analysis can be made available upon reasonable request once all relevant substudies from the consortium are reported and completed. The data dictionary can be made available upon request to the corresponding author.

This work was supported by Department of Global Health/Global Health Consortium, Robert Stempel College of Public Health and Social Work, Florida International University (project ID 800013470). The views expressed in this publication are those of the authors and not necessarily those of Florida International University.

R.Q., A.C., and C.E. conceptualized the study. Data were curated by M.S., E.N., and C.P. Formal analysis was performed by A.C., A.B., M.S., E.N., and C.P., R.Q., and C.E. acquired funding. R.Q., A.C., A.B., M.S., E.N., C.P., and C.E. conducted the investigation. R.Q., A.C., A.B., M.S., E.N., C.P., and C.E. constructed the methodology. Project administration was performed by A.C., A.C., A.B., and R.Q. supervised the study. R.Q., A.C., A.B., M.S., E.N., C.P., and C.E. participated in the writing of the original draft. R.Q., A.C., A.B., M.S., E.N., C.P., and C.E. performed review and editing.

About the Author

Dr. Ciapponi is a family physician and researcher with a focus on evidence synthesis and knowledge translation. He is the director of Cochrane Argentina, a researcher at the Institute of Clinical Effectiveness and Health Policy, CONICET Principal Investigator, and Cochrane Clinical Answers Associated Editor.

References

- World Health Organization. GLASS method for estimating attributable mortality of antimicrobial resistant bloodstream infections [cited 2023 Oct 12]. <https://www.who.int/publications/i/item/9789240000650>
- O'Neill J. Tackling drug-resistant infections globally: final report and recommendations. 2016 [cited 2023 Oct 12]. <https://apo.org.au/node/63983>
- de Kraker MEA, Stewardson AJ, Harbarth S, Harbarth S. Will 10 million people die a year due to antimicrobial resistance by 2050? *PLoS Med*. 2016;13:e1002184. <https://doi.org/10.1371/journal.pmed.1002184>
- National Office of Animal Health. NOAH response to final O'Neill AMR review report July 2016 [cited 2022 Nov 21]. <https://www.noah.co.uk/wp-content/uploads/2016/07/FINAL-NOAH-response-to-final-O-Neill-review-25-07-16-cle.pdf>
- Murray CJL, Ikuta KS, Sharara F, Swetschinski L, Robles Aguilar G, Gray A, et al. Antimicrobial Resistance Collaborators. Global burden of bacterial antimicrobial resistance in 2019: a systematic analysis. *Lancet*. 2022; 399:629–55. [https://doi.org/10.1016/S0140-6736\(21\)02724-0](https://doi.org/10.1016/S0140-6736(21)02724-0)
- Ghosh S, Bornman C, Zafer MM. Antimicrobial resistance threats in the emerging COVID-19 pandemic: where do we stand? *J Infect Public Health*. 2021;14:555–60. <https://doi.org/10.1016/j.jiph.2021.02.011>
- Langford BJ, So M, Raybardhan S, Leung V, Westwood D, MacFadden DR, et al. Bacterial co-infection and secondary infection in patients with COVID-19: a living rapid review and meta-analysis. *Clin Microbiol Infect*. 2020;26:1622–9. <https://doi.org/10.1016/j.cmi.2020.07.016>
- Rawson TM, Moore LSP, Zhu N, Ranganathan N, Skolimowska K, Gilchrist M, et al. Bacterial and fungal coinfection in individuals with coronavirus: a rapid review to support COVID-19 antimicrobial prescribing. *Clin Infect Dis*. 2020;71:2459–68. <https://doi.org/10.1093/cid/ciaa530>
- Thomas GR, Corso A, Pasterán F, Shal J, Sosa A, Pillonetto M, et al. Increased detection of carbapenemase-producing Enterobacterales bacteria in Latin America and the Caribbean during the COVID-19 pandemic. *Emerg Infect Dis*. 2022;28:1–8. <https://doi.org/10.3201/eid2811.220415>
- Naylor NR, Atun R, Zhu N, Kulasabanathan K, Silva S, Chatterjee A, et al. Estimating the burden of antimicrobial resistance: a systematic literature review. *Antimicrob Resist Infect Control*. 2018;7:58. <https://doi.org/10.1186/s13756-018-0336-y>
- Higgins JPT, Thomas J, Chandler J, Cumpston M, Li T, Page MJ, et al. Cochrane handbook for systematic reviews of interventions [cited 2023 Jan 9]. <https://training.cochrane.org/handbook>
- Page MJ, McKenzie JE, Bossuyt PM, Boutron I, Hoffmann TC, Mulrow CD, et al. The PRISMA 2020 statement: an updated guideline for reporting systematic reviews. *Syst Rev*. 2021;10:89. <https://doi.org/10.1186/s13643-021-01626-4>
- DerSimonian R, Laird N. Meta-analysis in clinical trials. *Control Clin Trials*. 1986;7:177–88. [https://doi.org/10.1016/0197-2456\(86\)90046-2](https://doi.org/10.1016/0197-2456(86)90046-2)
- Balduzzi S, Rucker G, Schwarzer G. How to perform a meta-analysis with R: a practical tutorial. *Evid Based Ment Health*. 2019;22:153–60. <https://doi.org/10.1136/ebmental-2019-300117>
- Higgins JPT, Thompson SG, Deeks JJ, Altman DG. Measuring inconsistency in meta-analyses. *BMJ*. 2003; 327:557–60. <https://doi.org/10.1136/bmj.327.7414.557>
- Viechtbauer W. Bias and efficiency of meta-analytic variance estimators in the random-effects model. *J Educ Behav Stat*. 2005;30:261–93. <https://doi.org/10.3102/10769986030003261>
- Knapp G, Hartung J. Improved tests for a random effects meta-regression with a single covariate. *Stat Med*. 2003;22:2693–710. <https://doi.org/10.1002/sim.1482>
- Zavascki AP, Barth AL, Gonçalves ALS, Moro AL, Fernandes JF, Martins AF, et al. The influence of metallo- β -lactamase production on mortality in nosocomial *Pseudomonas aeruginosa* infections. *J Antimicrob Chemother*. 2006;58:387–92. <https://doi.org/10.1093/jac/dkl239>

19. R Core Team. R: a language and environment for statistical computing. 2021 [cited 2023 Oct 12]. <https://www.R-project.org>
20. Bello-Chavolla OY, Bahena-Lopez JP, Garciadiego-Fosass P, Volkow P, Garcia-Horton A, Velazquez-Acosta C, et al. Bloodstream infection caused by *S. aureus* in patients with cancer: a 10-year longitudinal single-center study. *Support Care Cancer*. 2018;26:4057–65. <https://doi.org/10.1007/s00520-018-4275-1>
21. de Oliveira Conterno L, Wey SB, Castelo A. *Staphylococcus aureus* bacteremia: comparison of two periods and a predictive model of mortality. *Braz J Infect Dis*. 2002;6:288–97.
22. Quillici MCB, Resende DS, Gonçalves IR, Royer S, Sabino SS, Almeida VF, et al. Gram-negative bacilli bacteremia: a 7 year retrospective study in a referral Brazilian tertiary-care teaching hospital. *J Med Microbiol*. 2021;70.
23. Castro-Lima VAC, Borges IC, Joelsons D, Sales VVT, Guimaraes T, Ho YL, et al. Impact of human immunodeficiency virus infection on mortality of patients who acquired healthcare associated-infection in critical care unit. *Medicine (Baltimore)*. 2019;98:e15801. <https://doi.org/10.1097/MD.00000000000015801>
24. Blot S, Antonelli M, Arvaniti K, Blot K, Creagh-Brown B, de Lange D, et al.; Abdominal Sepsis Study. (AbSeS) group on behalf of the Trials Group of the European Society of Intensive Care Medicine. Epidemiology of intra-abdominal infection and sepsis in critically ill patients: “AbSeS”, a multinational observational cohort study and ESICM Trials Group Project. *Intensive Care Med*. 2019;45:1703–17. <https://doi.org/10.1007/s00134-019-05819-3>
25. Islas-Muñoz B, Volkow-Fernández P, Ibanes-Gutiérrez C, Villamar-Ramírez A, Vilar-Compte D, Cornejo-Juárez P. Bloodstream infections in cancer patients. Risk factors associated with mortality. *Int J Infect Dis*. 2018;71:59–64. <https://doi.org/10.1016/j.ijid.2018.03.022>
26. Bellissimo-Rodrigues F, Gomes ACF, Passos ADC, Achcar JA, Perdoná GS, Martinez R. Clinical outcome and risk factors related to extended-spectrum beta-lactamase-producing *Klebsiella* spp. infection among hospitalized patients. *Mem Inst Oswaldo Cruz*. 2006;101:415–21. <https://doi.org/10.1590/S0074-02762006000400012>
27. Carneiro IC do RS, Silva DL da. Epidemiology of bloodstream infections caused by ESBL-producing Enterobacteriaceae: case-control study in a neonatal unit in Brazil [in Portuguese]. *Journal of Infection Control*. 2012;1536.
28. Lemos EV, de la Hoz FP, Alvis N, Einarson TR, Quevedo E, Castañeda C, et al. Impact of carbapenem resistance on clinical and economic outcomes among patients with *Acinetobacter baumannii* infection in Colombia. *Clin Microbiol Infect*. 2014;20:174–80. <https://doi.org/10.1111/1469-0691.12251>
29. Zavascki AP, Barth AL, Gonçalves ALS, Moro AL, Fernandes JF, Martins AF, et al. The influence of metallo- β -lactamase production on mortality in nosocomial *Pseudomonas aeruginosa* infections. *J Antimicrob Chemother*. 2006;58:387–92. <https://doi.org/10.1093/jac/dkl239>
30. Herrera F, Laborde A, Jordán R, Berrueto LA, Roccia Rossi I, Valledor A, et al. Current epidemiology of bacteremia in patients with hematological malignancies and hematopoietic stem cell transplantation and the impact of antibiotic resistance on survival. Presented at: 31st European Congress of Clinical Microbiology and Infectious Diseases; 2021 Jul 9–12 [online].
31. Guilarde AO, Turchi MD, Martelli CMT, Primo MGB. *Staphylococcus aureus* bacteraemia: incidence, risk factors and predictors for death in a Brazilian teaching hospital. *J Hosp Infect*. 2006;63:330–6. <https://doi.org/10.1016/j.jhin.2006.02.011>
32. Castillo JS, Leal AL, Cortes JA, Alvarez CA, Sanchez R, Buitrago G, et al. GREBO. Mortality among critically ill patients with methicillin-resistant *Staphylococcus aureus* bacteremia: a multicenter cohort study in Colombia. *Rev Panam Salud Publica*. 2012;32:343–50. <https://doi.org/10.1590/S1020-49892012001100004>
33. Seas C, Garcia C, Salles MJ, Labarca J, Luna C, Alvarez-Moreno C, et al.; Latin America Working Group on Bacterial Resistance. *Staphylococcus aureus* bloodstream infections in Latin America: results of a multinational prospective cohort study. *J Antimicrob Chemother*. 2018;73:212–22. <https://doi.org/10.1093/jac/dkx350>
34. Levy Hara G, Rojas-Cortés R, Molina León HF, Dreser Mansilla A, Alfonso Orta I, Rizo-Amezquita JN, et al.; Latin American Point Prevalent Survey Study Group. Point prevalence survey of antibiotic use in hospitals in Latin American countries. *J Antimicrob Chemother*. 2022;77:807–15. <https://doi.org/10.1093/jac/dkab459>
35. Matos ECO, Andriolo RB, Rodrigues YC, Lima PDL, Carneiro ICDRS, Lima KVB. Mortality in patients with multidrug-resistant *Pseudomonas aeruginosa* infections: a meta-analysis. *Rev Soc Bras Med Trop*. 2018;51:415–20. <https://doi.org/10.1590/0037-8682-0506-2017>
36. Ramos-Castañeda JA, Ruano-Ravina A, Barbosa-Lorenzo R, Paillier-Gonzalez JE, Saldaña-Campos JC, Salinas DF, et al. Mortality due to KPC carbapenemase-producing *Klebsiella pneumoniae* infections: systematic review and meta-analysis: mortality due to KPC *Klebsiella pneumoniae* infections. *J Infect*. 2018;76:438–48. <https://doi.org/10.1016/j.jinf.2018.02.007>
37. Cosgrove SE, Sakoulas G, Perencevich EN, Schwaber MJ, Karchmer AW, Carmeli Y. Comparison of mortality associated with methicillin-resistant and methicillin-susceptible *Staphylococcus aureus* bacteremia: a meta-analysis. *Clin Infect Dis*. 2003;36:53–9. <https://doi.org/10.1086/345476>
38. Shurland S, Zhan M, Bradham DD, Roghmann M-C. Comparison of mortality risk associated with bacteremia due to methicillin-resistant and methicillin-susceptible *Staphylococcus aureus*. *Infect Control Hosp Epidemiol*. 2007;28:273–9. <https://doi.org/10.1086/512627>
39. Paul M, Kariv G, Goldberg E, Raskin M, Shaked H, Hazzan R, et al. Importance of appropriate empirical antibiotic therapy for methicillin-resistant *Staphylococcus aureus* bacteraemia. *J Antimicrob Chemother*. 2010;65:2658–65. <https://doi.org/10.1093/jac/dkq373>
40. Rodríguez-Baño J, Millán AB, Domínguez MA, Borraz C, González MP, Almirante B, et al. GEIH/GEMARA/REIPI. Impact of inappropriate empirical therapy for sepsis due to health care-associated methicillin-resistant *Staphylococcus aureus*. *J Infect*. 2009;58:131–7. <https://doi.org/10.1016/j.jinf.2008.11.003>
41. DiazGranados CA, Zimmer SM, Mitchel K, Jernigan JA; DiazGranados CA, Zimmer SM, Klein M, Jernigan JA. Comparison of mortality associated with vancomycin-resistant and vancomycin-susceptible enterococcal bloodstream infections: a meta-analysis. *Clin Infect Dis*. 2005;41:327–33. <https://doi.org/10.1086/430909>
42. Rottier WC, Ammerlaan HSM, Bonten MJM. Effects of confounders and intermediates on the association of bacteraemia caused by extended-spectrum β -lactamase-producing Enterobacteriaceae and patient outcome: a meta-analysis. *J Antimicrob Chemother*. 2012;67:1311–20. <https://doi.org/10.1093/jac/dks065>

43. Tumbarello M, Spanu T, Di Bidino R, Marchetti M, Ruggeri M, Trecarichi EM, et al. Costs of bloodstream infections caused by *Escherichia coli* and influence of extended-spectrum- β -lactamase production and inadequate initial antibiotic therapy. *Antimicrob Agents Chemother*. 2010;54:4085–91. <https://doi.org/10.1128/AAC.00143-10>
44. Schwaber MJ, Carmeli Y. Mortality and delay in effective therapy associated with extended-spectrum beta-lactamase production in Enterobacteriaceae bacteraemia: a systematic review and meta-analysis. *J Antimicrob Chemother*. 2007;60:913–20. <https://doi.org/10.1093/jac/dkm318>
45. Gasink LB, Edelstein PH, Lautenbach E, Synnvestvedt M, Fishman NO. Risk factors and clinical impact of *Klebsiella pneumoniae* carbapenemase-producing *K. pneumoniae*. *Infect Control Hosp Epidemiol*. 2009;30:1180–5. <https://doi.org/10.1086/648451>
46. Ponce de Leon A, Merchant S, Raman G, Avendano E, Chan J, Tepichin Hernandez G, et al. *Pseudomonas* infections among hospitalized adults in Latin America: a systematic review and meta-analysis. *BMC Infect Dis*. 2020;20:250. <https://doi.org/10.1186/s12879-020-04973-0>
47. Lemos EV, de la Hoz FP, Einarson TR, McGhan WF, Quevedo E, Castañeda C, et al. Carbapenem resistance and mortality in patients with *Acinetobacter baumannii* infection: systematic review and meta-analysis. *Clin Microbiol Infect*. 2014;20:416–23. <https://doi.org/10.1111/1469-0691.12363>
48. Vardakas KZ, Rafailidis PI, Konstantelias AA, Falagas ME. Predictors of mortality in patients with infections due to multi-drug resistant Gram negative bacteria: the study, the patient, the bug or the drug? *J Infect*. 2013;66:401–14. <https://doi.org/10.1016/j.jinf.2012.10.028>
49. Zaïdi M, Sifuentes-Osornio J, Rolón AL, Vázquez G, Rosado R, Sánchez M, et al.; Risk Factors for Mortality in the Intensive Care Unit. Inadequate therapy and antibiotic resistance. Risk factors for mortality in the intensive care unit. *Arch Med Res*. 2002;33:290–4. [https://doi.org/10.1016/S0188-4409\(01\)00380-0](https://doi.org/10.1016/S0188-4409(01)00380-0)
50. Brack W, Barcelo Culleres D, Boxall ABA, Budzinski H, Castiglioni S, Covaci A, et al. One planet: one health. A call to support the initiative on a global science-policy body on chemicals and waste. *Environ Sci Eur*. 2022;34:21. <https://doi.org/10.1186/s12302-022-00602-6>

Address for correspondence: Agustín Ciapponi, Instituto de Efectividad Clínica y Sanitaria (IECS), Dr. Emilio Ravignani 2024 (C1414CPV), Buenos Aires, Argentina; email: aciapponi@iecs.org.ar

etymologia revisited

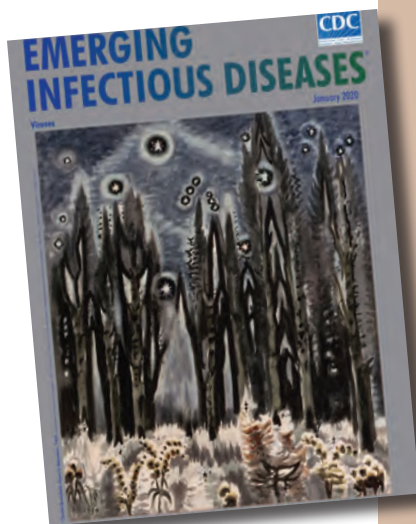
Picobirnavirus [pi-ko-burr'nə-vi"rəs]

Picobirnavirus, the recently recognized sole genus in the family *Picobirnaviridae*, is a small (*Pico*, Spanish for small), bisegmented (*bi*, Latin for two), double-stranded RNA virus. Picobirnaviruses were initially considered to be birna-like viruses, and the name was derived from birnavirus (bisegmented RNA), but the virions are much smaller (diameter 35 nm vs. 65 nm).

Picobirnaviruses are reported in gastroenteric and respiratory infections. These infections were first described in humans and black-footed pigmy rice rats in 1988. Thereafter, these infections have been reported in feces and intestinal contents from a wide variety of mammals with or without diarrhea, and in birds and reptiles worldwide.

Sources

1. Delmas B, Attoui H, Ghosh S, Malik YS, Mundt E, Vakharia VN; ICTV Report Consortium. ICTV virus taxonomy profile: Picobirnaviridae. *J Gen Virol*. 2019;100:133–4. <https://doi.org/10.1099/jgv.0.001186>
2. Malik YS, Kumar N, Sharma K, Dhama K, Shabbir MZ, Ganesh B, et al. Epidemiology, phylogeny, and evolution of emerging enteric Picobirnaviruses of animal origin and their relationship to human strains. *BioMed Res Int*. 2014;2014:780752. <https://doi.org/10.1155/2014/780752>
3. Pereira HG, Flewett TH, Candeias JA, Barth OM. A virus with a bisegmented double-stranded RNA genome in rat (*Oryzomys nigripes*) intestines. *J Gen Virol*. 1988;69:2749–54. <https://doi.org/10.1099/0022-1317-69-11-2749>
4. Smits SL, van Leeuwen M, Schapendonk CM, Schürch AC, Bodewes R, Haagmans BL, et al. Picobirnaviruses in the human respiratory tract. *Emerg Infect Dis*. 2012;18:1539–40. <https://doi.org/10.3201/eid1809.120507>



Originally published
in January 2020

https://wwwnc.cdc.gov/eid/article/26/1/et-2601_article

Monkeypox Virus in Wastewater Samples from Santiago Metropolitan Region, Chile

Manuel Ampuero,¹ Constanza Martínez-Valdebenito,¹ Marcela Ferrés, Ricardo Soto-Rifo, Aldo Gaggero

Sewage surveillance provides useful epidemiologic and public health information on viral infections at the population level. We detected monkeypox virus DNA from sewage samples covering 85% of the population in Santiago Metropolitan Region, Chile. We also isolated infective viruses from those samples. Wastewater surveillance could complement clinical surveillance for monkeypox virus.

On May 13, 2022, the World Health Organization raised an alert caused by a large increase in the number of infections by monkeypox virus (MPXV), which causes mpox, a zoonotic disease endemic to some countries of Central and West Africa that has rapidly expanded to nonendemic countries (1). A case of MPXV infection in Chile was confirmed on July 17, and since then, >1,400 cases and 2 deaths related to mpox have been reported during the outbreak, according to the Chile Ministry of Health (2). The Santiago Metropolitan Region in Chile is the most populated region in the country, accounting for >40% of the total population and most (81%) of the reported MPXV infections (2).

Wastewater surveillance has been demonstrated as a key contributor in monitoring viruses, such as poliovirus and SARS-CoV-2, enabling tracking of new variants and, thus, providing an accurate view of infections at the population level (3–5). In this regard, MPXV detection in sewage samples has also been proposed as a useful complement to clinical surveillance (6–9). Because stigma and discrimination associated with certain infections

limit the willingness of at-risk persons to consult hospital centers, wastewater-based epidemiology (WBE) becomes even more useful because anonymous pooled samples enable visualization of the contributions of a community without revealing individual identities (10).

We report wastewater monitoring of MPXV DNA in sewage samples from 3 wastewater treatment plants (WWTPs), accounting for 85% of the overall sewage from Santiago Metropolitan Region, representative of ≥5.5 million persons. We also report the presence of infective MPXV in those samples.

The Study

We collected 21 raw samples of wastewater during April–September 2022 from the WWTPs El Trebal (n = 6), La Farfana (n = 6), and La Higuera (n = 9). We collected samples in 1,000-mL sterile propylene flasks, transported them to the Laboratory of Environmental Virology at Universidad de Chile Faculty of Medicine, and stored them at 4°C until processing.

We concentrated the samples by ultracentrifugation according to the protocol described by Fumian et al. (11). We resuspended the pellet obtained in 200 μL of phosphate-buffered saline and stored at –80°C until use.

We used 200 μL of concentrated viral particles to isolate DNA with the QIAamp DNA MiniKit (QIAGEN, <https://www.qiagen.com>), according to the instructions provided by the supplier. We mixed 5 μL of DNA with the TaqMan Microbe Detection Monkey-Pox Vi07922155_s1 (ThermoFisher Scientific, <https://www.thermofisher.com>) and the TaqPath 1-Step Multiplex Master Mix (ThermoFisher Scientific) for the specific detection of MPXV DNA in a QuantStudio 5 real-time PCR machine (ThermoFisher Scientific). A pMG-Amp plasmid carrying the synthetic MPXV

Author affiliations: Universidad de Chile, Santiago, Chile (M. Ampuero, R. Soto-Rifo, A. Gaggero); Pontificia Universidad Católica de Chile, Santiago (C. Martínez-Valdebenito, M. Ferrés); Millennium Institute on Immunology and Immunotherapy, Santiago (R. Soto-Rifo)

DOI: <https://doi.org/10.3201/eid2911.230096>

¹These authors contributed equally to this article.

Table. Monkeypox virus detection in wastewater samples from 3 areas, Santiago Metropolitan Region, Chile, 2022*

Date	La Farfana	El Trebal	La Higuera
Apr 11	ND	ND	–
Apr 19	–	–	ND
Apr 22	ND	ND	–
May 5	ND	ND	–
May 16	–	–	ND
May 19	ND	ND	–
Jun 6	–	–	ND
Jun 16	ND	ND	–
Jul 18	36	–	ND
Jul 22	ND	ND	–
Aug 12	ND	ND	–
Aug 16	35	171	ND
Aug 18	ND	ND	–
Sep 15	ND	ND	895
Sep 20	2,231	960	ND

*Values are genome copies/mL. ND, not done; –, negative.

DNA fragment 5'-GTGCTGAATCGTTCGATTACCCAACATCCATTTTCAGATGAATAGAGT-TATCGATTCAGACACATGCTTTGAGTTTT-GTTGAATCGATGAGTGAAGTATCATCGGTTG-CACCTTCAGATGC-3', which contains the target sequence of the primers, was synthesized at Macro-gen Inc. (<https://www.macrogen.com>). We used that plasmid as a positive control and as a template for the calibration curve enabling the quantification of MPXV genome copies per milliliter. We cloned the amplified DNA fragment into pGEM-T Easy Vector (Promega, <https://www.promega.com>) and transformed it into *Escherichia coli* JM109. Five clones from each sample were sequenced at Macro-gen Inc. and compared with MPXV sequences from the 2022 outbreak.

From the 21 sewage samples collected and analyzed from the 3 WWTPs, we detected MPXV DNA in 6 (Table). Consistent with earlier cases of mpox reported in Chile, viral DNA was detected in sewage samples collected in July (La Farfana), August (La Farfana, El Trebal) and September (La Farfana, El Trebal, La Higuera), but not in April or May (Table).

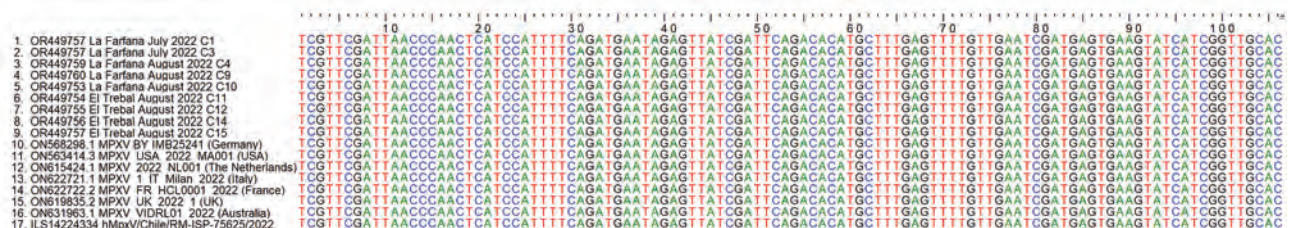
Quantification of MPXV DNA in sewage showed viral loads ranging from 35 to 2,231 genome copies/

mL (Table). Higher viral loads in sewage samples correlated with an increase in the number of cases reported by the Chile Ministry of Health in Santiago. Sequencing of the 106-bp amplified DNA fragment from wastewater samples showed 100% homology with MPXV sequences from the 2022 outbreak reported from Germany, the Netherlands, Italy, France, the United Kingdom, the United States, and Chile (Figure 1).

To determine whether the sewage samples contained viable MPXV, we used the samples that had the highest viral load to inoculate VeroE6 monolayers (ATCC CRL-1586). For this procedure, we infected cells with a mixture of MPXV DNA-positive sewage samples and culture medium and collected the supernatant after 7 days for PCR detection. We stored the remaining supernatant and performed a second round of infection by using the supernatant from the first infection. We used positive and negative controls in separate plates to avoid cross-contamination. At 24- and 48-hours postinfection, we collected supernatant for MPXVDNA detection by PCR.

In addition, we inoculated 300 μ L of sample AF0922 supplemented with 700 μ L of Dulbecco's Modified Eagle Medium plus 2% fetal bovine serum (FBS) into VeroE6 cells in a 6-cm plate. After 2 hours of incubation, we replaced the medium with 5 mL of Dulbecco's Modified Eagle Medium plus 2% FBS. After 7 days, we fixed infected cells with 4% glutaraldehyde and performed negative staining for electron microscopy observation (Appendix Figure, <https://wwwnc.cdc.gov/EID/article/29/11/23-0096-App1.pdf>) All procedures related to viral isolation were performed in a Biosafety Level 3 laboratory at Unidad de Virología Aplicada, Pontificia Universidad Católica de Chile, Santiago.

We detected a high viral DNA load in the supernatant at day 7 postinoculation, suggesting the presence of infective MPXV in sewage samples (Figure 2, panel A). We were not able to detect MPXV DNA from cells inoculated with samples that tested negative for the virus (Figure 2, panel B). Electron

**Figure 1.** Comparison of nucleotide sequences of the MPXV amplicon obtained for wastewater samples from Santiago Metropolitan Region, Chile (sewage samples 1–9), with reference sequences obtained from other countries during the 2022 mpox outbreak.

The 106-bp amplicon generated by quantitative reverse transcription has 100% homology with MPXV sequences obtained in 2022 from cases reported by different countries. GenBank numbers and location and date of isolation are provided for the 9 Chile sample sequences obtained in this study; GenBank or GISAID (<https://www.gisaid.org>) accession numbers and country are provided for reference sequences. MPXV, monkeypox virus.

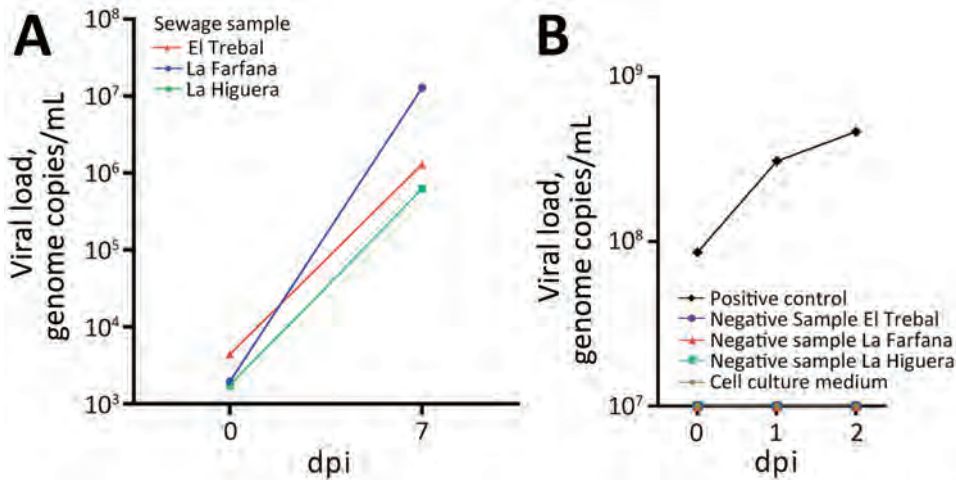


Figure 2. Detection of viral genome of monkeypox virus in wastewater samples from wastewater treatment plants in Santiago Metropolitan Region, Chile. A) PCR results for Vero E6 cell supernatant at 7 dpi. B) PCR results for supernatant samples of Vero E6 cells infected with positive control (cell culture supernatant infected with monkeypox virus) and negative controls (Dulbecco's Modified Eagle Medium plus 2% fetal bovine serum and negative wastewater samples). dpi, days postinfection.

microscopy analyses of VeroE6 cells inoculated with MPXV recovered from sample AF0922 showed intracellular viral particles with an average size of ≈ 300 nm (Appendix Figure).

Conclusions

WBE has acquired an increasingly useful role in surveillance systems that efficiently detect pathogenic microorganisms. It will also be useful as a tool for control and timely prevention of endemic and emerging infectious diseases.

Using WBE as a complement to universal clinical surveillance enables determination of actual pathogen circulation and its load in a population. For example, WBE has become a useful tool worldwide for visualizing the circulation of SARS-CoV-2 and its variants (3–5). Therefore, WBE could also complement clinical surveillance of MPXV, enabling estimation of actual circulation and load of the virus in a community (6,9). However, it will be useful to generate more information regarding virus elimination in an infected person; viral DNA load in stool, urine, semen, saliva, and other secretions; and persistence and infectivity of the virus in the environment and, in particular, in a matrix as complex as wastewater.

In conclusion, we detected MPXV DNA and determined its concentration in wastewater in Santiago, Chile. We were also able to isolate the virus from samples with the highest viral loads. Although detection of viable virus in sewage samples observed in this study generates an alert, there is no information on the risk that this could have for the personnel working in treatment plants. The potential risk for environmental transmission of MPXV is still unknown and thus remains a serious public health issue.

Acknowledgments

We thank Aguas Andinas, WWTP personnel, Sacyr WWTP personnel, and Analisis Ambientales (<https://www.anam.com>) operators for providing sewage samples.

This study was supported by the National Agency for Research and Technology through the Fondecyt Program no. 1181656; Anillo grants ATE220007 and ATE220016 to A.G.; Fondecyt Program no. 1230102; Anillo grants ATE220016 and ANID-ICM, ICN2021_045 to R.S.-R.; Anillo grant ATE220061; and Fondecyt Program no. 1211825 to M.F.

A.G. participated in the study design; M.A. and C.M.-V. performed the experiments; A.G., R.S.-R., and M.F. analyzed the data; and A.G., R.S.-R., and C.M.-V. wrote the manuscript. All authors approved the final version of the manuscript.

About the Author

Mr. Ampuero is a research scientist in the Virology Environmental Laboratory, Universidad de Chile, Santiago, Chile. His primary research interests are identification and characterization of viruses in wastewater.

References

- World Health Organization. Mpox (monkeypox) outbreak: global trends, 2022 [cited 2022 Dec 26]. https://worldhealthorg.shinyapps.io/mpox_global
- Ministry of Health, Department of Epidemiology, Undersecretary of Public Health. Executive report monkeypox, Chile. December 23, 2022 [in Spanish] [cited 2023 Sep 8]. http://epi.minsal.cl/wp-content/uploads/2022/08/Protocolo_vigilancia_viruela_del_mono_22082022.pdf
- Mousazadeh M, Ashoori R, Paital B, Kabdaşlı I, Frontistis Z, Hashemi M, et al. Wastewater based epidemiology perspective as a faster protocol for detecting coronavirus RNA in human populations: a review with specific reference

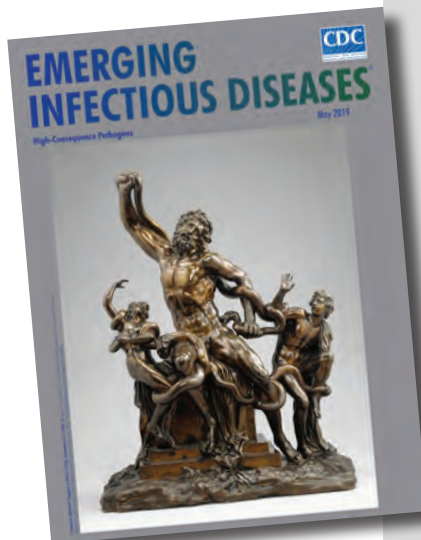
- to SARS-CoV-2 virus. *Pathogens*. 2021;10:1008. <https://doi.org/10.3390/pathogens10081008>
4. Wu F, Lee WL, Chen H, Gu X, Chandra F, Armas F, et al. Making waves: wastewater surveillance of SARS-CoV-2 in an endemic future. *Water Res*. 2022;219:118535. <https://doi.org/10.1016/j.watres.2022.118535>
 5. Karthikeyan S, Levy JL, De Hoff P, Humphrey G, Birmingham A, Jepsen K, et al. Wastewater sequencing reveals early cryptic SARS-CoV-2 variant transmission. *Nature*. 2022;609:101–8. <https://doi.org/10.1038/s41586-022-05049-6>
 6. Chen W, Bibby K. Model-based theoretical evaluation of the feasibility of using wastewater-based epidemiology to monitor monkeypox. *Environ Sci Technol Lett*. 2022;9:772–8. <https://doi.org/10.1021/acs.estlett.2c00496>
 7. Gul I, Liu C, Yuan X, Du Z, Zhai S, Lei Z, et al. Current and perspective sensing methods for monkeypox virus. *Bioengineering (Basel)*. 2022;9:571. <https://doi.org/10.3390/bioengineering9100571>
 8. de Jonge EF, Peterse CM, Koelewijn JM, van der Drift AR, van der Beek RF, Nagelkerke E, et al. The detection of monkeypox virus DNA in wastewater samples in the Netherlands. *Sci Total Environ*. 2022;852:158265. <https://doi.org/10.1016/j.scitotenv.2022.158265>
 9. Tiwari A, Adhikari S, Kaya D, Islam MA, Malla B, Sherchan SP, et al. Monkeypox outbreak: Wastewater and environmental surveillance perspective. *Sci Total Environ*. 2023;856:159166. <https://doi.org/10.1016/j.scitotenv.2022.159166>
 10. Nelson B. What poo tells us: wastewater surveillance comes of age amid covid, monkeypox, and polio. *BMJ*. 2022;378:o1869. <https://doi.org/10.1136/bmj.o1869>
 11. Fumian TM, Leite JP, Castello AA, Gaggero A, Caillou MS, Miagostovich MP. Detection of rotavirus A in sewage samples using multiplex qPCR and an evaluation of the ultracentrifugation and adsorption-elution methods for virus concentration. *J Virol Methods*. 2010;170:42–6. <https://doi.org/10.1016/j.jviromet.2010.08.017>

Address for correspondence: Aldo Gaggero, Laboratorio de Virología Ambiental, Programa de Virología, Instituto de Ciencias Biomédicas, Facultad de Medicina, Universidad de Chile, Independencia 1027, 8380000 Santiago, Chile; email: agaggero@uchile.cl

etymologia revisited

Nipah Virus

[ne ' -pə vī ' -rəs]



Originally published
in May 2019

In 1994, a newly described virus, initially called equine morbillivirus, killed 13 horses and a trainer in Hendra, a suburb of Brisbane, Australia. The reservoir was subsequently identified as flying foxes, bats of the genus *Pteropus* (Greek pteron [“wing”] + pous [“foot”]). In 1999, scientists investigated reports of febrile encephalitis and respiratory illness among workers exposed to pigs in Malaysia and Singapore. (The pigs were believed to have consumed partially eaten fruit discarded by bats.)

The causative agent was determined to be closely related to Hendra virus and was later named for the Malaysian village of Kampung Sungai Nipah. The 2 viruses were combined into the genus *Henipavirus*, in the family *Paramyxoviridae*. Three additional species of *Henipavirus*—Cedar virus, Ghanaian bat virus, and Mojiang virus—have since been described, but none is known to cause human disease. Outbreaks of Nipah virus occur almost annually in India and Bangladesh, but *Pteropus* bats can be found throughout the tropics and subtropics, and henipaviruses have been isolated from them in Central and South America, Asia, Oceania, and East Africa.

References:

1. Centers for Disease Control and Prevention. Outbreak of Hendra-like virus—Malaysia and Singapore, 1998–1999. *MMWR Morb Mortal Wkly Rep*. 1999;48:265–9.
2. Selvey LA, Wells RM, McCormack JG, Ansford AJ, Murray K, Rogers RJ, et al. Infection of humans and horses by a newly described morbillivirus. *Med J Aust*. 1995;162:642–5.

https://wwwnc.cdc.gov/eid/article/25/5/et-2505_article

Three Cases of Tickborne *Francisella tularensis* Infection, Austria, 2022

Florian Heger, Stefanie Schindler, Sonja Pleininger, Astrid Fueszl, Marion Blaschitz, Kathrin Lippert, Patrick Hyden, Peter Hufnagl, David Mutschlechner, Thomas Gremmel, Erwin Hofer, Mateusz Markowicz,¹ Alexander Indra¹

Tularemia is increasing in Austria. We report *Francisella tularensis* subspecies *holarctica* isolated from 3 patients who had been bitten by arthropods. Next-generation sequencing showed substantial isolate similarity. Clinicians should consider bloodstream *F. tularensis* infections for patients with signs/symptoms of ulceroglandular tularemia, and surveillance of potential vectors should be intensified.

Tularemia is a zoonotic disease of the Northern Hemisphere, caused by the highly virulent bacterium *Francisella tularensis*. Although *F. tularensis* subspecies *tularensis* (type A, found only in North America) is associated with severe infections, *F. tularensis* subsp. *holarctica* (type B, found throughout the Northern Hemisphere) causes less severe illness (1,2). Infection occurs after contact with infected animals, transmission via arthropod vectors, or contact with contaminated water or soil (3). Only sporadic infections, detected primarily by serologic testing, have been reported in Austria; therefore, genomic data are scarce (3,4). Recently, cases of tularemia have increased in Austria (Figure 1). We report 3 tularemia cases that developed after arthropod bites in Austria. Ethics approval was not necessary because routine data were processed in the study and personal data were anonymized. The patients gave written consent for publication of the case reports.

Author affiliation: Austrian Agency for Health and Food Safety, Vienna, Austria (F. Heger, S. Schindler, S. Pleininger, A. Fueszl, M. Blaschitz, K. Lippert, P. Hyden, P. Hufnagl, E. Hofer, M. Markowicz, A. Indra); Cardiology and Intensive Care Medicine, Mistelbach, Austria (D. Mutschlechner, T. Gremmel); Institute of Cardiovascular Pharmacotherapy and Interventional Cardiology, St. Pölten, Austria (T. Gremmel); Paracelsus Medical University of Salzburg, Salzburg, Austria (A. Indra)

DOI: <https://doi.org/10.3201/eid2911.230460>

The Cases

Patient 1 was a 64-year-old woman who had received a tick bite in the right inframammary region. After experiencing fever, chills, and a general feeling of discomfort, along with nausea and vomiting, she sought emergency care when symptoms persisted. Clinical examination detected a 20-mm skin lesion surrounded by a reddish hem and central necrotic ulcer. Results of serologic testing for Lyme borreliosis were negative. Stab incision of the skin lesion was performed, and no bacteria grew in culture of the sampled pus. Blood cultures grew *F. tularensis*. Antimicrobial treatment with oral ciprofloxacin (500 mg 2×/d) led to sign/symptom resolution.

Patient 2 was a 5-year-old girl seen at a pediatric outpatient clinic for retroauricular pain after a tick bite 9 days earlier. Clinical examination showed a swollen and reddened pinna, a pus-covered 5-mm retroauricular skin lesion with a central ulcer (Appendix Figure, <https://wwwnc.cdc.gov/EID/article/29/11/23-0460-App1.pdf>), and swollen cervical lymph nodes. After 2 days, fever, increased lymph node swelling, and tonsillitis developed, and the retroauricular wound deteriorated. Therapy was switched from oral amoxicillin/clavuanic acid (250 mg 4×/d) and fucidin ointment to intravenous ceftriaxone (520 mg 1×/d), followed by oral cefixim (64 mg 2×/d), which alleviated signs and symptoms. A wound swab sample culture yielded *F. tularensis*. Antimicrobial treatment, changed to oral ciprofloxacin (250 mg 2×/d), led to substantial signs/symptom improvement.

Patient 3 was a 76-year-old man who was hospitalized after reporting fever, generalized discomfort, nausea, and vertigo. A red, painless skin lesion with central

¹These senior authors contributed equally to this article.

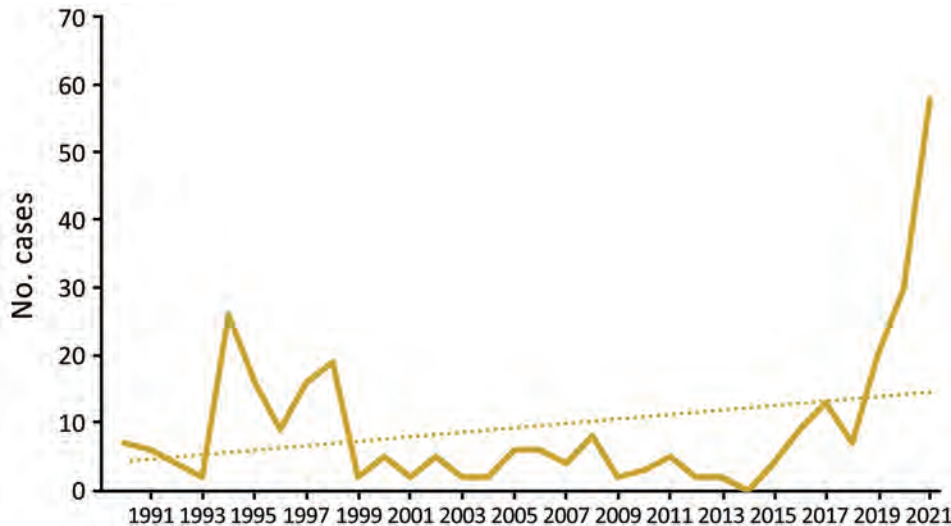


Figure 1. Reported cases (solid line) and trends (dotted line) of tularaemia in Austria, 1990–2021. Data from the Austrian Epidemiologic Reporting System (<https://oecd-opsi.org>).

crust on the left thigh, which probably developed after an arthropod bite, and inguinal lymphadenopathy were noted. Antimicrobial treatment with ampicillin/sulbactam was started because of suspected pneumonia. Eight days after hospitalization, *F. tularensis* grew on anaerobic blood culture. Therapy with ciprofloxacin was initiated and later switched to oral doxycycline (100 mg 2×/d) because of potential allergic reaction to ciprofloxacin, followed by substantial sign/symptom improvement. The findings suggest local transmission of *F. tularensis* after an insect or tick bite.

We used multiplex PCR (Analyticon Instruments GmbH, <https://www.analyticon.eu/de>) to test samples, and all were positive for *F. tularensis*. Real-time PCR (TIB MolBiol, <https://www.tib-molbiol.de>), performed for subspecies determination according to manufacturer instructions, yielded *F. tularensis* subsp. *holarctica* (5). We determined MICs for 6 antimicrobials by Etest (bioMérieux, <https://www.biomerieux.fr>) and interpreted results according to Clinical and Laboratory Standards Institute guidelines (6) (Table). Because of high-level erythromycin resistance, we assigned the isolates to *F. tularensis* subsp. *holarctica* biovar II (genotype B.12), which was later confirmed by whole-genome sequencing (WGS) to be subclade B.34/B.35.

For all *F. tularensis* samples, we performed WGS on a NextSeq 2000 instrument (Illumina, Inc., www.illumina.com), 150-bp paired-end, by using a QIAGEN MagAttract HMW DNA Kit (<https://www.qiagen.com>) for DNA isolation and a Nextera XT DNA Library Prep Kit (Illumina, Inc.) for library preparation.

We assembled whole-genome sequences de novo by using SPAdes (7) version 3.15.2, analyzed them by using ISpecies webserver (8), and corroborated real-time PCR species results by using the TCS (Templeton, Crandall and Sing) calculation method. In a pairwise comparison, the 3 isolates differed in 5 genes: 410015–22 vs. 410016–22 (FTL_0160, FTL_0920, FTL_1212, and FTL_1567); 410015–22 vs. 410041–22 (FTL_0414 and FTL_0920), and 410016–22 vs. 410041–22 (FTL_0160, FTL_0414, FTL_1212, and FTL_1567). Average allelic distance is 3.3 alleles, which is above cluster threshold for this species (1 allele difference). We applied core-genome multilocus sequence typing analysis by using SeqSphere+ version 8.5.1 (Ridom GmbH, <https://www.ridom.de>) with the published core-genome multilocus sequence typing scheme (9) to compare our isolate genomes against genomes from Germany (Bavaria) and Austria from a previous study (PRJEB40963 [10]). We identified clades/subclades by using CanSNPer2 (11). We submitted the following *F. tularensis* subsp. *holarctica* WGS assemblies to the National Center for Biotechnology Information (BioProject PRJNA900077): biosample SAMN31677967 (410015–22, patient 1), accession no. JAPKFK000000000; biosample SAMN31677968 (410016–22, patient 2), accession no. JAPKFJ000000000; and biosample SAMN32382778 (410041–22, patient 3), accession no. JAPZIK000000000 (Figure 2, Appendix).

Table. Antimicrobial MICs for *Francisella tularensis* isolates recovered from 3 patients with tickborne tularemia, Austria*

Patient	MIC, mg/L					
	Gentamicin	Erythromycin	Ciprofloxacin	Tetracycline	Doxycycline	Streptomycin
1	0.25	>256	0.008	0.047	0.094	1.5
2	0.5	>256	0.012	0.032	0.19	3
3	0.19	>256	0.008	0.125	0.125	0.75

*Boldface indicates antimicrobial resistance according to Clinical and Laboratory Standards Institute standards (6).

Conclusions

Outbreaks of *F. tularensis* subsp. *holarctica* in Europe are linked mainly to infected rodents and hares; mosquitoes and ticks serve as arthropod vectors (3). Over the past 30 years (1990–2021), a total of 302 human infections have been reported in Austria, with 2 peaks after outbreaks in hares during 1994–1995 and 1997–1998 (12–14). So far, national reported cases show an upward trend; in 2021 alone, a total of 58 cases were reported (Figure 1).

Biovar I (genotype B.6) is found mainly in western Europe and biovar II (genotype B.12) in northern and eastern Europe (11). Most tularemia cases in Austria are associated with hunting hares and skinning carcasses and are caused by *F. tularensis* subsp. *holarctica* biovar II. Recently, ticks have been identified as

vectors, and *F. tularensis* subsp. *holarctica* biovar I was detected in Austria in 2016 (1,15). Under debate is whether pathogenic potential of biovar I may be higher than that of biovar II (15).

Of the 3 patients, 2 reported removing a tick after spending time in rural areas; the third did not observe a tick or insect bite but had local skin alterations that were highly comparable to those seen on other patients with tickborne tularemia. Isolate sequences were closely related to isolates from Austrian and German hares (10).

Bloodstream infections with *F. tularensis* after arthropod bites are rarely reported in Europe. One reason might be that in Europe only *F. tularensis* subsp. *holarctica* is found, and it is known to cause milder disease than *F. tularensis* subsp. *tularensis* in the United

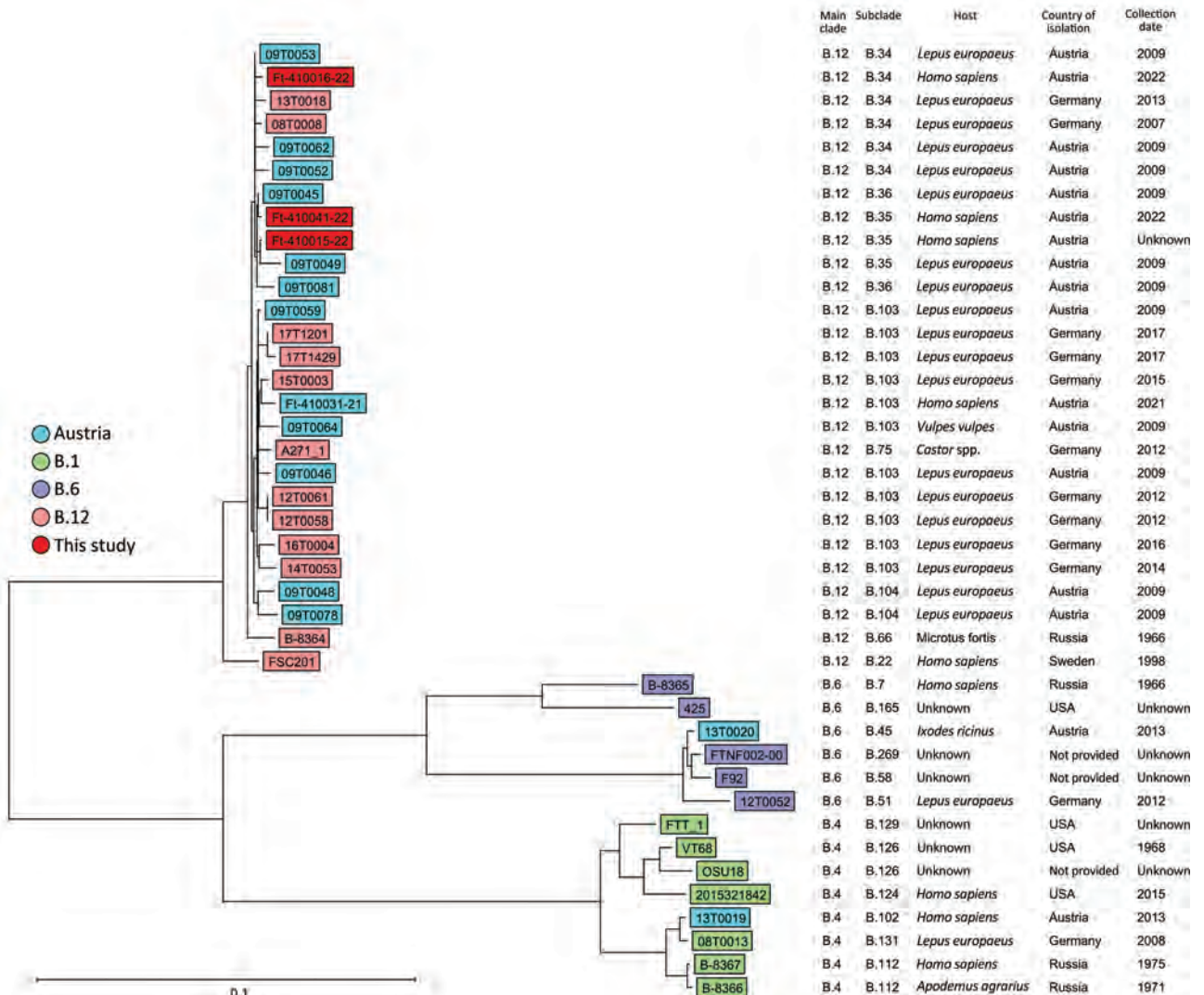


Figure 2. Ridom SeqSphere+ NJ tree (Ridom GmbH, <https://www.ridom.de>) for 41 *Francisella tularensis* samples isolated from 3 patients in Austria, based on 1,147 columns from *F. tularensis* core-genome multilocus sequence typing. Scale bar indicates nucleotide substitutions per site. Metadata are provided in the Appendix Table (<https://wwwnc.cdc.gov/EID/article/29/11/23-0460-App1.pdf>).

States. Thus, we find it remarkable that bacteremia developed in 2 patients in Austria. WGS showed a close relationship between isolates from the patients and isolates found mostly in Germany and Austria, as shown in the neighbor-joining tree for 41 *F. tularensis* complete genomes (Figure 2; Appendix Table), which indicates the wild animal population as a host for *F. tularensis* subsp. *holarctica* biovar II (B.12) and ticks as vectors for tularemia in Austria.

Our findings show that ticks represent underestimated vectors for *F. tularensis* transmission in Austria. Aside from other tickborne diseases endemic to Austria, clinicians should consider tularemia as a cause of signs/symptoms that follow tick bites, especially when combined with fever, enlarged and painful lymph nodes, and skin ulcers. Diagnosis can be achieved by molecular testing. Genomic data are essential for understanding dissemination and invasion of certain genotypes that may cause systemic infections. To confidently declare that certain genetic subpopulations are associated with systemic infections, a larger number of isolates and further research are needed. For that reason, Austria established large-scale monitoring of arthropod vectors for the presence of vectorborne pathogens, including *F. tularensis*, to provide public health authorities with knowledge about infection risk for the exposed population.

Acknowledgments

We thank all persons involved in laboratory work at the Austrian Agency of Health and Food Safety and treating clinicians Gian Farid Monfared, Anna Thell for their cooperation and sharing of the patients' clinical data.

M.M. is an unpaid member of the Executive Committee of ESGBOR, the ESCMID Study Group for Lyme Borreliosis and received honoraria from Pfizer and DiaSorin for obligations unrelated to this study.

F.H. and S.S. undertook the microbiological testing. S.S., M.M., D.M., and T.G. collected the data. M.B., K.L., and P.H. performed molecular testing and analyzed the data. S.P. and A.I. provided laboratory services and supervised the study. F.H. and M.M. wrote the manuscript. All authors reviewed and approved the final version of the manuscript.

About the Author

Mr. Heger is head of the department of Medical Microbiology and Hygiene at the Austrian Agency for Health and Food Safety. His main fields of work are highly pathogenic bacteria, antibiotic resistance, and infectious diseases.

References

- Seiwald S, Simeon A, Hofer E, Weiss G, Bellmann-Weiler R. Tularemia goes west: epidemiology of an emerging infection in Austria. *Microorganisms*. 2020;8:1597. <https://doi.org/10.3390/microorganisms8101597>
- Farlow J, Wagner DM, Dukerich M, Stanley M, Chu M, Kubota K, et al. *Francisella tularensis* in the United States. *Emerg Infect Dis*. 2005;11:1835–41. <https://doi.org/10.3201/eid1112.050728>
- Hestvik G, Warns-Petit E, Smith LA, Fox NJ, Uhlhorn H, Artois M, et al. The status of tularemia in Europe in a one-health context: a review. *Epidemiol Infect*. 2015; 143:2137–60. <https://doi.org/10.1017/S0950268814002398>
- Markowicz M, Schötta AM, Penatzer F, Matscheko C, Stanek G, Stockinger H, et al. Isolation of *Francisella tularensis* from skin ulcer after a tick bite, Austria, 2020. *Microorganisms*. 2021; 9:1407. <https://doi.org/10.3390/microorganisms9071407>
- Kugeler KJ, Pappert R, Zhou Y, Petersen JM. Real-time PCR for *Francisella tularensis* types A and B. *Emerg Infect Dis*. 2006;12:1799–801. <https://doi.org/10.3201/eid1211.060629>
- Clinical and Laboratory Standards Institute. Methods for antimicrobial dilution and disk susceptibility testing of infrequently isolated or fastidious bacteria (M45). 3rd ed. Wayne (PA); The Institute; 2015.
- Bankevich A, Nurk S, Antipov D, Gurevich AA, Dvorkin M, Kulikov AS, et al. SPAdes: a new genome assembly algorithm and its applications to single-cell sequencing. *J Comput Biol*. 2012;19:455–77. <https://doi.org/10.1089/cmb.2012.0021>
- Richter M, Rosselló-Móra R, Glöckner FO, Peplies J. JSpeciesWS: a web server for prokaryotic species circumscription based on pairwise genome comparison. *Bioinformatics*. 2016;32:929–31.
- Antwerpen MH, Prior K, Mellmann A, Höppner S, Spletstoeser WD, Harmsen D. Rapid high resolution genotyping of *Francisella tularensis* by whole genome sequence comparison of annotated genes (“MLST+”). *PLoS One*. 2015; 10:e0123298. <https://doi.org/10.1371/journal.pone.0123298>
- Linde J, Homeier-Bachmann T, Dangel A, Riehm JM, Sundell D, Öhrman C, et al. Genotyping of *Francisella tularensis* subsp. *holarctica* from hares in Germany. *Microorganisms*. 2020;8:1932. <https://doi.org/10.3390/microorganisms8121932>
- Lärkeryd A, Myrtenäs K, Karlsson E, Dwibedi CK, Forsman M, Larsson P, et al. CanSNPer: a hierarchical genotype classifier of clonal pathogens. *Bioinformatics*. 2014; 30:1762–4. <https://doi.org/10.1093/bioinformatics/btu113>
- Federal Ministry of Health. Leaflet on tularemia [in German]. https://www.verbrauchergesundheits.at/tiere/zoosenen/BMG-74600_0201_2012_17_Merkblatt_Tularaemie_Aug2012.pdf
- Federal Ministry for Social Affairs. Epidemiology of communicable diseases in Austria [in German]. <https://www.sozialministerium.at/Themen/Gesundheit/Uebertragbare-Krankheiten/Statistiken-und-Fallzahlen.html>
- Tomaso H, Al Dahouk S, Hofer E, Spletstoeser WD, Treu TM, Dierich MP, et al. Antimicrobial susceptibilities of Austrian *Francisella tularensis holarctica* biovar II strains. *Int J Antimicrob Agents*. 2005;26:279–84. <https://doi.org/10.1016/j.ijantimicag.2005.07.003>
- Faber M, Heuner K, Jacob D, Grunow R. Tularemia in Germany—a re-emerging zoonosis. *Front Cell Infect Microbiol*. 2018;8:40. <https://doi.org/10.3389/fcimb.2018.00040>

Address for correspondence: Florian Heger, Austrian Agency for Health and Food Safety, Medical Microbiology and Hygiene, Waehringer Strasse 25A, Wien, Vienna 1100, Austria; email: florian.heger@ages.at

Racial and Socioeconomic Equity of Tecovirimat Treatment during the 2022 Mpox Emergency, New York, New York, USA

Maura K. Lash,¹ Ned H. Latham,¹ Pui Ying Chan, Mary M.K. Foote, Elizabeth A. Garcia, Matthew F. Silverstein, Marcia Wong, Mark Alexander, Karen A. Alroy, Lovedeep Bajaj, Kuan Chen, James Steele Howard, Lucretia E. Jones, Ellen H. Lee, Julian L. Watkins, Tristan D. McPherson

We assessed tecovirimat treatment equity for 3,740 mpox patients in New York, New York, USA, during the 2022 mpox emergency; 32.4% received tecovirimat. Treatment rates by race/ethnicity were 38.8% (White), 31.3% (Black/African American), 31.0% (Hispanic/Latino), and 30.1% (Asian/Pacific Islander/other). Future public health emergency responses must prioritize institutional and structural racism mitigation.

In May 2022, mpox cases were detected in multiple non-mpox-endemic countries. Increasing numbers of cases worldwide, primarily within sexual networks of gay and bisexual men, prompted the World Health Organization to declare a public health emergency in July 2022 (1). Although mpox-associated deaths have been infrequent (1), mpox can cause considerable illness (2).

No antiviral medications have been approved for mpox treatment in the United States (3). However, an Expanded Access Investigational New Drug (EA-IND) protocol held by the Centers for Disease Control and Prevention enabled health providers to prescribe tecovirimat for persons with mpox in the United States. The New York City (NYC) Department of Health and Mental Hygiene (DOHMH) coordinated the distribution of tecovirimat to hospitals and a single partner pharmacy that delivered medication to

NYC addresses cost-free for patients. DOHMH provided technical support to prescribers and intentional outreach to federally qualified health centers and safety-net health systems.

In the United States, mpox disproportionately affects Hispanic/Latino and Black persons (4,5), consistent with well-established inequities in healthcare access and outcomes because of interpersonal, institutional, and structural racism (6–8). For example, racial inequities in access to HIV preexposure prophylaxis are well-documented and affect similar populations (9). We explored racial and socioeconomic inequities in tecovirimat treatment of mpox in NYC.

The Study

We included all NYC residents who had a positive nonvariola orthopoxvirus (probable case) or mpox (confirmed case) test reported to DOHMH during May 19–October 29, 2022. We collected data on age, gender, race/ethnicity, sexual orientation, and residential addresses during standardized interviews. We obtained tecovirimat treatment data from provider reports via a mandatory REDCap survey and from partner pharmacy dispensing records. We matched cases with treatment data by using names, dates of birth, and postal (ZIP) codes. For persons treated before their first positive test, we used the treatment date instead of diagnosis date. We excluded persons who were treated but never had a reported positive test.

We calculated descriptive statistics for selected demographic characteristics (Table), both overall and according to treatment status. We assessed differences by using χ^2 tests or *t*-tests. We included unknown

Author affiliations: New York City Department of Health and Mental Hygiene, Queens, New York, USA (M.K. Lash, N.H. Latham, P.Y. Chan, M.M.K. Foote, E.A. Garcia, M.F. Silverstein, M. Wong, M. Alexander, K.A. Alroy, L. Bajaj, K. Chen, J.S. Howard, L.E. Jones, E.H. Lee, J.L. Watkins, T.D. McPherson); Columbia University, New York, New York, USA (N.H. Latham)

DOI: <https://doi.org/10.3201/eid2911.230814>

¹These first authors contributed equally to this article.

Table. Characteristics of persons with mpox according to treatment status in study of racial and socioeconomic equity of tecovirimat treatment during 2022 mpox emergency, New York City, New York, USA, May 19, 2022–October 29, 2022*

Characteristics	Overall	Tecovirimat treatment	No treatment	p value
Total no. persons	3,740 (100)	1,213 (32.4)	2,527 (67.6)	NA
Median age (IQR)	35 (12)	36 (11)	35 (12)	ND
Mean age (SD)	37 (9.4)	37 (9)	36 (9.5)	0.004
Age groups, y				<0.001
0–24	255 (6.8)	55 (4.5)	200 (7.9)	
25–34	1,527 (40.8)	471 (38.8)	1,056 (41.8)	
35–44	1,265 (33.8)	449 (37.0)	816 (32.3)	
45–54	507 (13.6)	177 (14.6)	330 (13.1)	
55–64	166 (4.4)	55 (4.5)	111 (4.4)	
≥65	20 (0.5)	6 (0.5)	14 (0.6)	
Gender†				0.01
Men	3,516 (94.2)	1,133 (93.5)	2,383 (94.6)	
Nonbinary/gender queer	52 (1.4)	22 (1.8)	30 (1.2)	
Transgender men or women	70 (1.9)	33 (2.7)	37 (1.5)	
Women	93 (2.5)	24 (2.0)	69 (2.7)	
Unknown	9	1	8	
Sexual orientation				<0.001
LGBQ+	2,409 (64.4)	857 (70.7)	1,552 (61.4)	
Straight	296 (7.9)	61 (5.0)	235 (9.3)	
Unknown‡	1,035 (27.7)	295 (24.3)	740 (29.3)	
Race/ethnicity§				<0.001
Asian/Pacific Islander/other	196 (5.2)	59 (4.9)	137 (5.4)	
Black/African American	1,017 (27.2)	318 (26.2)	699 (27.7)	
Hispanic/Latino	1,294 (34.6)	400 (33.0)	894 (35.4)	
White	847 (22.7)	329 (27.1)	518 (20.5)	
Unknown‡	386 (10.3)	107 (8.8)	279 (11.0)	
Borough of residence				<0.001
Bronx	729 (19.5)	259 (21.4)	470 (18.6)	
Brooklyn	888 (23.7)	299 (24.6)	589 (23.3)	
Manhattan	1,480 (39.5)	504 (41.5)	976 (38.7)	
Queens	596 (15.9)	139 (11.5)	457 (18.1)	
Staten Island	45 (1.2)	12 (1.0)	33 (1.3)	
Unknown	2	0	2	
Neighborhood poverty level¶				0.53
Low	579 (15.5)	177 (14.6)	402 (16.0)	
Medium	1588 (42.6)	508 (41.9)	1080 (42.9)	
High	894 (24.0)	303 (25.0)	591 (23.5)	
Very High	668 (17.9)	223 (18.4)	445 (17.7)	
Unknown#	11	2	9	

*Values are no. (%) except as indicated. IQR, interquartile range; LGBQ, lesbian, gay, bisexual, and queer; NA, not applicable; ND, not done.

†Gender categories are provided as defined by the New York City Department of Health and Mental Hygiene.

‡Because of a substantial number of persons who had unknown sexual orientation or race/ethnicity, those persons were included as a separate category in the χ^2 test. For other characteristics, people with unknown values were excluded from χ^2 test.

§All persons who identified as Hispanic or Latino (Hispanic), regardless of race, were classified as Hispanic; all other race/ethnicity categories were non-Hispanic.

¶Neighborhood poverty level was defined as the percentage of residents in a postal (ZIP) code tabulation area with household incomes of <100% of the federal poverty level according to the American Community Survey 2016–2020 (<https://www.census.gov>). Neighborhoods were categorized into 4 groups: low poverty, <10% of population; medium, 10%–19.9%; high, 20%–29.9%; and very high, ≥30%.

#Unknown because of missing residential or invalid New York ZIP code.

values as separate categories under race/ethnicity and sexual orientation. We calculated cumulative changes in percentages of tecovirimat-treated persons in 2-week intervals according to race/ethnicity and neighborhood poverty level (defined as the percentage of residents in the patient's ZIP code living below the federal poverty level according to the American Community Survey [<https://www.census.gov>]). We categorized neighborhoods into 4 groups: low poverty, <10%; medium, 10%–19.9%; high, 20%–29.9%; and very high, ≥30%. We performed analyses by using SAS version 9.4 (SAS Institute, <https://www.sas.com>) and

R version 4.2.3 (The R Project for Statistical Computing, <https://www.r-project.org>). We considered a p value <0.05 statistically significant. DOHMH's Institutional Review Board deemed this evaluation to be public health surveillance.

Mpox was diagnosed for 3,740 persons during the study period. Most mpox-positive persons were 25–44 years of age (74.7%); men (94.2%); lesbian, gay, bisexual, or queer (64.4%); Hispanic/Latino or Black/African American (61.8%); and lived in medium- or high-poverty neighborhoods (66.6%) (Table). A total of 1,213 (32.4%) persons were treated. Compared

with untreated persons, a larger percentage of treated persons were lesbian, gay, bisexual, or queer (70.7% vs. 61.4%) and White (27.1% vs. 20.5%); a smaller percentage of treated persons were of unknown race/ethnicity (8.8% vs. 11.0%) or resided in Queens (11.5% vs. 18.1%) (Table).

By October 29, 2022, the percentage of treated persons was highest among those identifying as White (38.8%), then Black/African American (31.3%), Hispanic/Latino (31.0%), Asian/Pacific Islander/other (30.1%), and unknown race/ethnicity (27.7%) (Appendix Table, <https://wwwnc.cdc.gov/EID/article/29/11/23-0814-App1.pdf>). Percentages of treated persons were similar (30.6%–33.9%) across neighborhood poverty levels (Appendix Table). Percentages of treated persons increased initially for all racial/ethnic groups, stabilizing by late July 2022, except for White persons, among whom percentages increased an additional month before stabilizing (Figure). In all but one 2-week interval, percentages of tecovirimat-treated White persons were higher than all other groups. The increasing trend was generally consistent across neighborhood poverty levels (Figure).

Conclusions

During our evaluation period, 32.4% of persons in NYC with reported mpox were treated with tecovirimat, compared with <20% nationally (10). The increasing percentages of treated persons during the outbreak was likely related to advocacy by and peer support from affected communities (11), increased prescriber familiarity with tecovirimat, and iterative revisions to the EA-IND protocol that reduced provider administrative requirements. The higher percentage of

persons treated in NYC and our finding that treatment did not substantially vary by neighborhood poverty level might be attributable to the free, at-home delivery approach to tecovirimat distribution, which eliminated pharmacy access as a barrier. DOHMH also established a team to recruit and support providers to prescribe tecovirimat under the EA-IND protocol. Safety net health systems and federally qualified health centers were chosen for early outreach and technical assistance to improve access for underinsured and uninsured patients. In addition, the DOHMH team connected patients to available prescribers, if their initial providers were unable to meet EA-IND requirements.

Although percentages of tecovirimat-treated persons increased over time across all racial/ethnic groups, inequities existed. When we evaluated the cumulative percentages of treated persons in each racial/ethnic category, none approached that of White persons ($\approx 31\%$ for other groups vs. 38.8% for White persons) (Figure 1). Racial inequities and, specifically, lower percentages of treated Black/African American and Hispanic/Latino persons were foreseeable, because similar patterns have been observed for other medical countermeasures (e.g., mpox vaccines, COVID-19 antivirals, and HIV treatment) (5,12,13). Stigma from healthcare providers experienced by Black gay and bisexual men is a known barrier to sex-related healthcare access (14). Furthermore, the regulatory obligations of the EA-IND process limited the number of tecovirimat prescribers, which might have disproportionately affected Black and Hispanic/Latino communities. For example, DOHMH sexual health clinics, safety-net providers of services for Black and

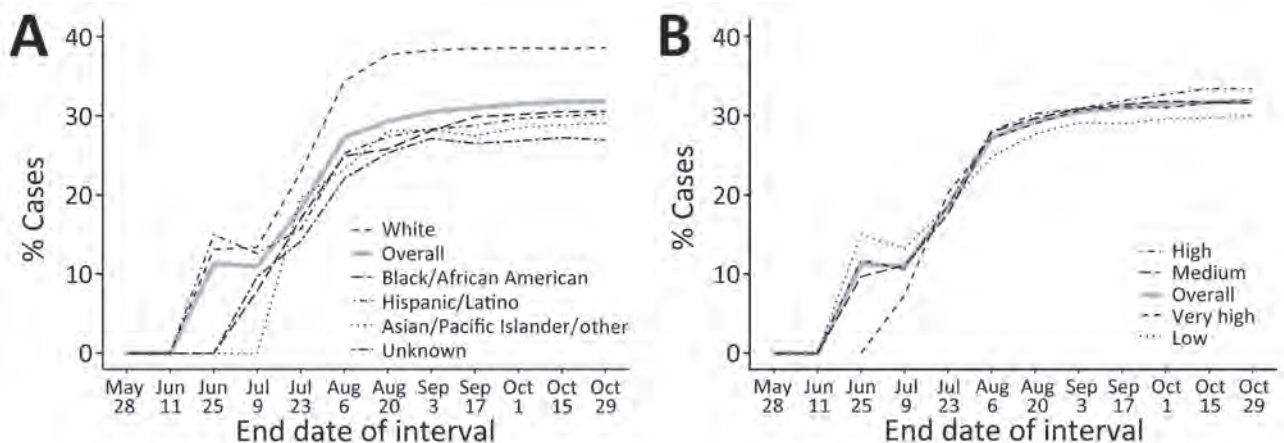


Figure. Comparisons of cumulative percentages of persons with mpox treated with tecovirimat during 2-week intervals in study of racial and socioeconomic equity of tecovirimat treatment during 2022 mpox emergency, New York City, New York, USA. Percentages of mpox cases diagnosed during May 19–October 29, 2022, are indicated. Treated persons who had no prescription date ($n = 22$) were not counted. A) Percentages according to race/ethnicity. B) Percentages according to neighborhood poverty level, defined as: low poverty, <10% of neighborhood population; medium, 10%–19.9%; high, 20%–29.9%; and very high, $\geq 30\%$.

Hispanic/Latino men who have sex with men, did not prescribe tecovirimat until mid-September 2022 because of regulatory issues. In addition, insurance coverage inequities are a major barrier to accessing primary care (15), including mpox testing and treatment. No comprehensive data source identifies healthcare providers serving specific race/ethnicity groups, making interventions to increase equitable access to mpox countermeasures imprecise.

The first limitation of our study is that univariate analysis cannot capture all factors affecting treatment, such as differences in eligibility, healthcare access, and provider prescribing. Second, tecovirimat data were not available if the prescriber did not complete the online form when the drug was prescribed through a clinical trial beginning in mid-September 2022 or was dispensed from an inpatient pharmacy (e.g., some hospitalized patients). Lack of tecovirimat treatment data might have caused treatment undercounting, but we expect minimal effect because crossover between the trial recruitment period and our evaluation was brief, and the reporting form was mandatory for all prescribers.

In conclusion, our findings indicate racial inequity in tecovirimat treatment in NYC during the 2022 mpox emergency. Future responses to public health emergencies must prioritize institutional and structural racism mitigation from the outset to build more resilient communities and healthcare delivery systems. Additional analyses of factors (e.g., clinical characteristics, acceptability of treatment, detailed sociodemographic information) should be prioritized to assess the extent and effect of race/ethnicity on mpox treatment distribution and to inform future efforts to achieve equitable medical countermeasure access. Having comprehensive data for race/ethnicity of populations served by healthcare providers/networks and for characteristics of persons receiving medical countermeasures is critical for improving equity in emergency preparedness and response. Although neither dataset is sufficient to overcome institutional or structural racism, the alternative, a reactive approach, will inevitably perpetuate entrenched inequities.

Acknowledgments

We thank the inspiring care, compassion, and strength of our NYC provider community who confronted a multitude of challenges and the patients and their families who, even in the face of incredible suffering, still sought to contribute to our knowledge amidst the uncertainty of a reemerging disease.

About the Author

Ms. Lash is a research scientist at the New York City Department of Health and Mental Hygiene. Her primary research interests include global health and infectious disease epidemiology.

References

1. World Health Organization. 2022 Mpox outbreak: global trends. 2022 Nov 1 [cited 2022 Nov 1]. https://worldhealthorg.shinyapps.io/mpx_global
2. Philpott D, Hughes CM, Alroy KA, Kerins JL, Pavlick J, Asbel L, et al.; CDC Multinational Monkeypox Response Team. Epidemiologic and clinical characteristics of monkeypox cases – United States, May 17–July 22, 2022. *MMWR Morb Mortal Wkly Rep.* 2022;71:1018–22. <https://doi.org/10.15585/mmwr.mm7132e3>
3. Gessain A, Nakoune E, Yazdanpanah Y. Monkeypox. *N Engl J Med.* 2022;387:1783–93. <https://doi.org/10.1056/NEJMra2208860>
4. Centers for Disease Control and Prevention. Monkeypox cases by age and gender, race/ethnicity, and symptoms. 2022 Oct 26 [cited 2022 Nov 1]. <https://www.cdc.gov/poxvirus/monkeypox/response/2022/demographics.html>
5. New York City Department of Health and Mental Hygiene. Monkeypox (MPV) data. 2022 Nov 1 [cited 2022 Nov 1]. <https://www1.nyc.gov/site/doh/data/health-tools/monkeypox.page#surveillance>
6. Institute of Medicine (US) Committee on Understanding and Eliminating Racial and Ethnic Disparities in Health Care. Smedley BD, Stith AY, Nelson AR, editors. Unequal treatment: confronting racial and ethnic disparities in health care. Washington: National Academies Press; 2003.
7. Bailey ZD, Krieger N, Agénor M, Graves J, Linos N, Bassett MT. Structural racism and health inequities in the USA: evidence and interventions. *Lancet.* 2017;389:1453–63. [https://doi.org/10.1016/S0140-6736\(17\)30569-X](https://doi.org/10.1016/S0140-6736(17)30569-X)
8. Chokshi DA, Foote MMK, Morse ME. How to act upon racism – not race – as a risk factor. *JAMA Health Forum.* 2022;3:e220548. <https://doi.org/10.1001/jamahealthforum.2022.0548>
9. Centers for Disease Control and Prevention. Monitoring selected national HIV prevention and care objectives by using HIV surveillance data United States and 6 dependent areas, 2019 [cited 2022 Nov 1]. <https://www.cdc.gov/hiv/library/reports/hiv-surveillance/vol-26-no-2/index.html>
10. Centers for Disease Control and Prevention. Demographics of patients receiving tecovirimat (TPOXX) for treatment of mpox. 2022 Nov 9 [cited 2023 Jan 18]. <https://www.cdc.gov/poxvirus/monkeypox/response/2022/demographics-TPOXX.html>
11. Gaffney T. With support on monkeypox hard to come by, queer communities turn to one another. *Stat News.* 2022 Aug 11 [cited 2023 Feb 21]. <https://www.statnews.com/2022/08/11/with-support-on-monkeypox-hard-to-come-by-queer-communities-turn-to-one-another>
12. Boehmer TK, Koumans EH, Skillen EL, Kappelman MD, Carton TW, Patel A, et al. Racial and ethnic disparities in outpatient treatment of COVID-19 – United States, January–July 2022. *MMWR Morb Mortal Wkly Rep.* 2022;71:1359–65. <https://doi.org/10.15585/mmwr.mm7143a2>
13. Moore RD, Stanton D, Gopalan R, Chaisson RE. Racial differences in the use of drug therapy for HIV disease in an urban community. *N Engl J Med.* 1994;330:763–8. <https://doi.org/10.1056/NEJM199403173301107>

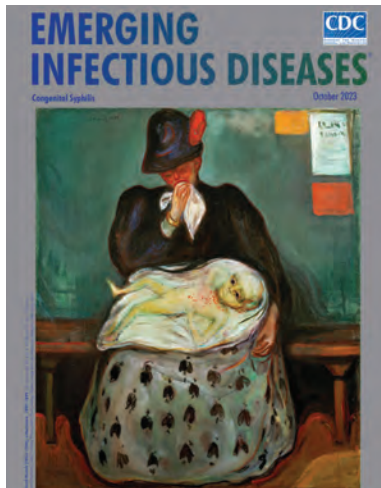
14. Eaton LA, Driffin DD, Kegler C, Smith H, Conway-Washington C, White D, et al. The role of stigma and medical mistrust in the routine health care engagement of black men who have sex with men. *Am J Public Health*. 2015;105:e75–82. <https://doi.org/10.2105/AJPH.2014.302322>
15. Artiga S, Hill L, Damico A. Health coverage by race and ethnicity, 2010–2021. Kaiser Family Foundation. 2022
- Dec 20 [cited 2023 Feb 28]. <https://www.kff.org/racial-equity-and-health-policy/issue-brief/health-coverage-by-race-and-ethnicity>

Address for correspondence: Maura K. Lash, New York City Department of Health and Mental Hygiene, 42-09 28th St, New York, NY, USA; email: mlash@health.nyc.gov

October 2023

Congenital Syphilis

- Serotype Distribution and Disease Severity in Adults Hospitalized with *Streptococcus pneumoniae* Infection, Bristol and Bath, UK, 2006–2022
- Spike in Congenital Syphilis, Mississippi, USA, 2016–2022
- Carbapenem-Resistant *Klebsiella pneumoniae* in Large Public Acute-Care Healthcare System, New York, New York, USA, 2016–2022
- Posttransfusion Sepsis Attributable to Bacterial Contamination in Platelet Collection Set Manufacturing Facility, United States
- Effects of COVID-19 on Maternal and Neonatal Outcomes and Access to Antenatal and Postnatal Care, Malawi
- Emergence of SARS-CoV-2 Delta Variant and Effect of Nonpharmaceutical Interventions, British Columbia, Canada
- Community Outbreak of *Pseudomonas aeruginosa* Infections Associated with Contaminated Piercing Aftercare Solution, Australia, 2021
- Characteristics of and Deaths among 333 Persons with Tuberculosis and COVID-19 in Cross-Sectional Sample from 25 Jurisdictions, United States
- Cycle Threshold Values as Indication of Increasing SARS-CoV-2 New Variants, England, 2020–2022
- Comprehensive Case–Control Study of Protective and Risk Factors for Buruli Ulcer, Southeastern Australia
- *Candida auris* Clinical Isolates Associated with Outbreak in Neonatal Unit of Tertiary Academic Hospital, South Africa



- Human Tularemia Epididymo-Orchitis Caused by *Francisella tularensis* Subspecies *holartica*, Austria
- *Listeria monocytogenes* Transmission from Donated Blood to Platelet Transfusion Recipient, Italy
- Imported Toxigenic *Corynebacterium Diphtheriae* in Refugees with Polymicrobial Skin Infections, Germany, 2022
- Expansion of Invasive Group A *Streptococcus* M1UK Lineage in Active Bacterial Core Surveillance, United States, 2019–2021
- Estimate of COVID-19 Deaths, China, December 2022–February 2023
- Mpox in Children and Adolescents during Multicountry Outbreak, 2022–2023
- Outbreak of Sexually Transmitted Nongroupable *Neisseria meningitidis*–Associated Urethritis, Vietnam
- *Pseudomonas aeruginosa* High-Risk Sequence Type 463 Co-Producing KPC-2 and AFM-1 Carbapenemases, China, 2020–2022
- Seafood-Associated Outbreak of ctx-Negative *Vibrio mimicus* Causing Cholera-Like Illness, Florida, USA
- Influenza A(H5N1) Virus Infections in 2 Free-Ranging Black Bears (*Ursus americanus*), Quebec, Canada
- Limited Outbreak of Highly Pathogenic Influenza A(H5N1) in Herring Gull Colony, Canada, 2022
- Human-to-Human Transmission of Andes Virus Modeled in Syrian Hamsters
- Sporadic Shiga Toxin–Producing *Escherichia coli*–Associated Pediatric Hemolytic Uremic Syndrome, France, 2012–2021
- Stability of Monkeypox Virus in Body Fluids and Wastewater
- Ancestral Origin and Dissemination Dynamics of Reemerging Toxigenic *Vibrio cholerae*, Haiti
- *Treponema pallidum* Detection at Asymptomatic Oral, Anal, and Vaginal Sites in Adults Reporting Sexual Contact with Persons with Syphilis
- Managing Risk for Congenital Syphilis, Perth, Western Australia, Australia
- Estimated Costs of 4-Month Pulmonary Tuberculosis Treatment Regimen, United States
- Antimicrobial Resistance in Slaughterhouses, Kenya

**EMERGING
INFECTIOUS DISEASES®**

To revisit the October 2023 issue, go to:

<https://wwwnc.cdc.gov/eid/articles/issue/29/10/table-of-contents>

Hepatitis C Virus Elimination Program among Prison Inmates, Israel

Lihi Eisen,¹ Zohar Mor,¹ Miriam Madar, Ron Rabinovitch, Yuval Dadon, Rivka Sheffer, Ehud Kaliner, Liav Goldstein

The Israeli Prison Services implemented a hepatitis C virus (HCV) elimination program in 2020. Inmates considered high risk for HCV were offered serology; HCV-seropositive participants were offered HCV RNA testing. Among participants, 7.0% had detectable HCV RNA and were offered antiviral drug therapy. This program reduced HCV burden among incarcerated persons.

In 2019, the Israeli Ministry of Health joined the World Health Organization initiative to eliminate hepatitis C virus (HCV) (1). The national elimination program included HCV testing among 6 high-risk groups: recipients of blood transfusions before 1992; persons who use intravenous drugs; patients treated with improperly sterilization medical equipment or blood products; immigrants from the former Soviet Union and Romania; persons infected with HIV or hepatitis B virus (HBV); and known HCV carriers (2).

HCV seroprevalence among the general population of Israel is estimated to be 1.9% and detectable HCV RNA is estimated to be 0.7% (3,4). In Israel, the prevalence of HCV RNA among migrants from the former Soviet Union is higher than that of the general population, reaching $\approx 5.5\%$ (5); seroprevalence is $\approx 60.0\%$ among intravenous drug users (IVDUs) (6).

In August 2020, the Israeli Prison Service (IPS), which operates 33 prisons and houses $\approx 14,500$ prisoners across the country (7), implemented an HCV screening, testing, and treatment initiative among inmates at high risk for HCV. We estimated HCV prevalence among prison inmates and identified demographic and behavioral characteristics of HCV-infected inmates.

The Study

HCV serology screening tests were offered to all inmates considered to be at high risk for HCV infection if they met ≥ 1 of the following criteria: had a history of illicit drug use or were arrested for a drug-related felony; were born in the former Soviet Union or Romania; or had known HIV or HBV infection. Inmates were screened and followed from August 1, 2020, through July 31, 2021, or prison discharge. We collected data from IPS medical records and only included inmates incarcerated for >30 days to allow sufficient time to complete the screening process.

Willing inmates who were at high risk for HCV were screened for HCV antibodies and, if positive, were screened for HCV RNA. Participants with detectable HCV RNA were offered free, direct-acting antiviral drug treatment after consultation with gastroenterologists. We considered undetectable HCV RNA 12 weeks after treatment to be sustained viral response. Injection drug use is prohibited in prison; thus, we defined IVDUs as inmates who were treated with opiate substitutes.

We compared HCV-seropositive and seronegative participants. We used the Student *t*-test to compare continuous variables and the χ^2 test for categorical variables. We considered $p < 0.05$ statistically significant. We performed multivariate analysis by logistic regression to identify variables associated with being HCV seropositive and calculated odds ratios and 95% CIs. The study was approved by the ethics committee of Ashkelon Academic College in Israel (approval no. 2022–33).

Serologic screening was offered to all 2,824 inmates in the IPS who were at high risk for HCV infection; 1,751 (62.0%) opted to be tested and 1,021 (36.2%) declined (Figure). Of the tested inmates, 21.6% (379) were seropositive. HCV RNA testing was performed in 317 (83.6%) of the positive serology group and

Author affiliations: Tel-Aviv Department of Health, Ministry of Health, Tel Aviv, Israel (L. Eisen, R. Sheffer); Ashkelon Academic College, Ashkelon, Israel (Z. Mor); Central Department of Health, Ministry of Health, Ramla, Israel (Z. Mor, E. Kaliner); Israel Prison Service, Israel (M. Madar, R. Rabinovitch, L. Goldstein); Deputy Director Office, Ministry of Health, Jerusalem, Israel (Y. Dadon)

DOI: <https://doi.org/10.3201/eid2911.230728>

¹These authors contributed equally to this article.

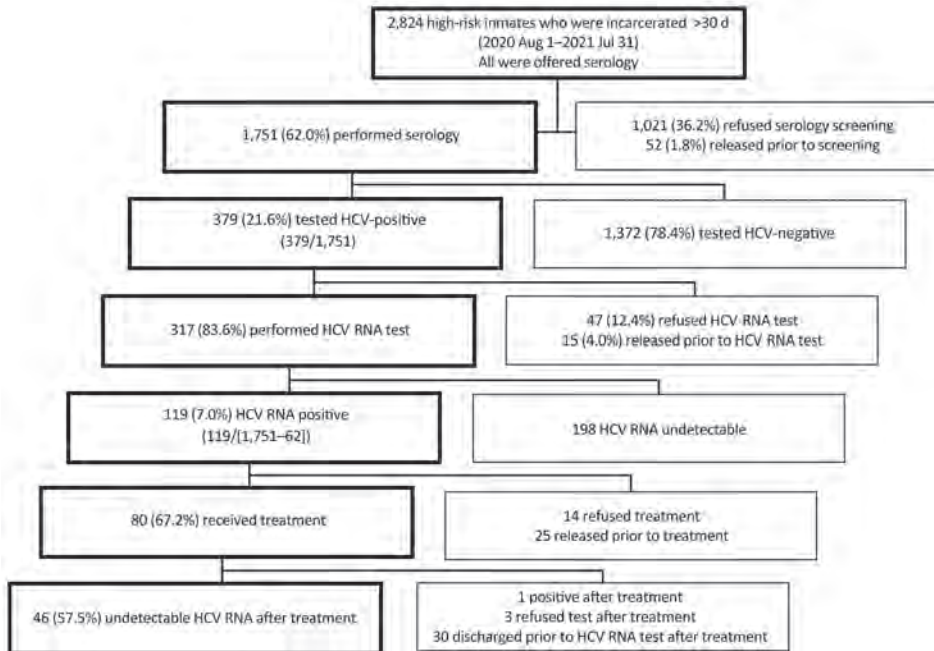


Figure. Flowchart of participant enrollment in a hepatitis C elimination program among high-risk prison inmates, Israel. Bold boxes on left indicate participants. HCV, hepatitis C virus.

119 were positive; 47 declined testing, and 15 were released from prison before testing. Therefore, detectable HCV RNA was found in 7.0% (119/1,689) of all tested participants. Of those, 113 had newly diagnosed cases and 6 had known cases.

Altogether, 80/119 (67.2%) inmates completed antiviral drug treatment during incarceration. Of those followed up after 12 weeks, 97.8% (46/47) had confirmed sustained viral response; the other 33 refused follow-up testing or were discharged from prison.

Table 1. Characteristics of participants and nonparticipants in a hepatitis C virus elimination program among high-risk prison inmates, Israel*

Characteristics	Participated in serology screening, n = 1,751	Did not participate in serology screening, n = 1,021	p value
Gender			0.01
M	1,701 (97.1)	1,009 (98.8)	
F	49 (2.8)	12 (1.2)	
Transgender	1 (<0.1)	0	
Mean age, y (SD)	41.6 (12.2)	36.4 (11.1)	<0.01
Marital status			<0.01
Married	454 (25.9)	193 (18.9)	
Nonmarried†	1,282 (73.2)	812 (79.5)	
Data not available	15 (0.9)	16 (1.6)	
Education level, did not complete high school	1,358 (77.5)	810 (79.3)	0.2
Previously incarcerated	1,471 (84.0)	922 (90.3)	<0.01
Mean number of imprisonments (SD)	8.2 (7.3)	8.7 (6.7)	<0.01
Smoker	1,442 (82.3)	885 (86.6)	0.03
Alcohol user	202 (11.5)	99 (9.7)	0.1
Risk criteria			
Country of birth			<0.01
Former Soviet Union and Romania	651 (37.2)	288 (28.2)	
Israel	876 (50.0)	599 (58.7)	
West Bank and Gaza Strip	115 (6.6)	54 (5.3)	
Other countries	80 (4.6)	62 (6.1)	
Data not available	29 (1.6)	18 (1.7)	
Drug use			
No drug use	371 (21.2)	182 (17.9)	0.03
Non-IV drug use	1,053 (60.1)	718 (70.3)	<0.01
IV drug use	327 (18.7)	121 (11.8)	<0.01
HIV infection	18 (1.0)	2 (0.1)	0.01
Hepatitis B virus infection	71 (4.0)	13 (0.7)	<0.01

*Values indicate no. (%) unless otherwise indicated. IV, intravenous.

†Includes single, divorced, and widowed.

Table 2. Comparison between participants with HCV-positive and HCV-negative serology in a hepatitis C virus elimination program among high-risk prison inmates, Israel*

Characteristics	HCV-positive, n = 379	HCV-negative, n = 1,372	p value	Multivariate analysis	
				OR (95% CI)	p value
Sex					
M	367 (96.8)	1,334 (97.2)	0.8		
F	12 (3.2)	37 (2.7)			
Transgender	0	1 (0.1)			
Mean age, y (SD)	47.6 (9.3)	39.9 (12.4)	<0.01	1.06 (1.05–1.08)	<0.01
Marital status					
Married	77 (20.3)	375 (27.33)	<0.01	Referent	<0.01
Nonmarried†	299 (78.9)	983 (71.65)		1.7 (1.2–2.4)	
Data not available	3 (0.8)	14 (1.02)			
Education level, did not complete high school	299 (78.9)	1,059 (77.2)	0.4		
Previously incarcerated‡	342 (90.2)	1,129 (82.2)	<0.01		
Mean number of imprisonments (SD)	11.6 (8.8)	7.3 ± 6.5	<0.01	1.07 (1.05–1.09)	<0.01
Smoker	324 (85.5)	1,118 (81.5)	0.07		
Alcohol user	33 (8.7)	169 (12.3)	0.05		
Risk criteria					
Country of birth					
Former Soviet Union and Romania	201 (53.0)	450 (32.8)	<0.01	7.4 (5.4–10.3)	
Israel	157 (41.4)	719 (52.4)		Referent	<0.01
West Bank and Gaza Strip	9 (2.4)	106 (7.7)			
Other countries	9 (2.4)	71 (5.2)			
Data not available	3 (0.8)	26 (1.9)			
Drug use					
No drug use	53 (14.0)	318 (23.2)	<0.01	Referent	<0.01
Non-IV drug use	176 (46.4)	877 (63.9)		5.4 (3.5–8.4)	
IV drug use	150 (39.6)	177 (12.9)		12.8 (7.9–20.7)	
HIV infection	11 (2.9)	7 (0.5)	<0.01	NA	NS
Hepatitis B virus infection	31 (8.1)	40 (2.9)	<0.01	3.8 (2.0–7.3)	<0.01

*Values indicate no. (%) unless otherwise indicated. IV, intravenous; NA, not applicable; NS, not significant.

†Includes single, divorced, and widowed.

‡This variable was not included in the multivariate analysis because it is collinear with number of imprisonments.

Compared with nonparticipants, the participant group comprised more female inmates, married persons, nonsmokers, IVDUs, and HIV- or HBV-infected persons; participants were also older and had fewer previous incarcerations (Table 1). Inmates who were HCV seropositive were more likely older, single, had been previously incarcerated, were born in the former Soviet Union or Romania, had used intravenous drugs, or were HIV- or HBV-positive (Table 2). In the multivariate analysis, older age, being single, having a greater number of previous incarcerations, being born in the former Soviet Union or Romania, drug use, and HBV infection were variables predicting HCV-positive serology among participants.

Conclusions

HCV seroprevalence among study participants was 21.6% and detectable HCV RNA was 7.0%. Those prevalences are higher than the estimates of 1.9% seroprevalence and 0.7% HCV RNA-positive in the general population of Israel (3,4). However, HCV seroprevalence among study participants was lower than persons in the general population who use intravenous drugs (60.0%) (6), and close to HCV RNA prevalence (≈5.5%) among male migrants from former Soviet Union in the general population (5).

The rates of HCV infection among inmates vary widely in different prison populations worldwide. A previous meta-analysis (8) explained HCV seroprevalence heterogeneity (2.0%–58.0%) in the correctional system mainly by differences in proportion of inmates who are IVDU (3.0%–69.0%). In our study, seroprevalence was 21.6% and the proportion of IVDUs among inmates who participated in the study was 18.6%.

Older age, being single, having a greater number of previous incarcerations, being born in the former Soviet Union or Romania, and being HBV-positive were risk factors associated with HCV-positive serology among participants in our study. Inmates who had used intravenous drugs had higher rates of HCV-positive serology, as previously published (9). Of note, prisoners who used drugs by other than intravenous routes and those who were incarcerated for drug-related felonies also had higher rates of HCV-positive serology. Because most risk factors can be identified by prison authorities when inmates are admitted to prison, IPS can use a targeted screening policy to improve HCV elimination.

A total of 67.2% of infected inmates completed antiviral drug treatment during their sentences. That completion rate helped lower the overall HCV burden in IPS and highlights the contribution of the screening program to decrease HCV in prison settings among

persons at high-risk for HCV. The IPS plays a critical role in the national efforts to achieve HCV elimination in Israel. In line with the high turnover of inmates who revolve between the community and prisons, the success in reducing HCV burden during incarceration also positively affects the community (10). IPS structural efforts, inmate cooperation (11), and involvement of the medical insurers in the community are all essential to accomplishing HCV elimination in Israel.

The first limitation of this study is that the data were collected from IPS medical files, and we had limited access to community medical records of inmates who were discharged from prison. Thus, antiviral drug treatment outcomes in those cases could not be determined. Second, not all eligible inmates were willing to be screened, which might lead to selection bias. To assess the bias, we compared the characteristics of those refusing to those who were tested and found lower proportions of all individual high-risk criteria among those who declined screening (Table 1). Thus, the bias is conservative if it exists. Third, acute cases of HCV might not have been detected in serologic testing due to a window period. To increase internal validity, only inmates whose incarceration was >1 month were included. Fourth, some of the data, such as smoking history, could be subject to reporting bias. Last, this study did not classify HCV clusters (12) because of lack of available data.

In conclusion, HCV seroprevalence among inmates at high risk was 21.6% and HCV RNA was detectable in 7.0%. The risk factors associated with HCV-positive serology among inmates included older age, being single, and having more previous incarcerations, as well as other HCV risk criteria, such as IV drug use, being born in former Soviet Union or Romania, and being co-infected with HBV. The IPS-led HCV elimination program achieved a decrease in HCV burden among inmates at high risk for HCV. To achieve national HCV elimination, Israel should strengthen cooperation between IPS and medical insurers in the community.

About the Authors

Dr. Eisen is a public health resident with Tel-Aviv Department of Health, Ministry of Health, Tel Aviv, Israel. Her research interests include control and prevention of infectious diseases. Dr. Mor is a public health specialist with the Central Department of Health, Ministry of Health, Ramla, Israel and a professor at Ashkelon Academic College, Ashkelon, Israel. His research interests include special populations, sexually transmitted diseases, and tuberculosis.

References

1. World Health Organization. Global guidance for viral hepatitis B and C elimination [cited 2022 Nov 8]. <https://www.who.int/news/item/25-06-2021-who-releases-first-ever-global-guidance-for-country-validation-of-viral-hepatitis-b-and-c-elimination>
2. Ministry of Health Israel. Press release, July 26, 2016: a program for early detection of viral hepatitis to be promoted [cited 2022 Nov 8]. https://www.health.gov.il/NewsAndEvents/SpokemanMessages/Pages/26072016_1.aspx
3. Cornberg M, Razavi HA, Alberti A, Bernasconi E, Buti M, Cooper C, et al. A systematic review of hepatitis C virus epidemiology in Europe, Canada and Israel. *Liver Int*. 2011;31(Suppl 2):30–60. <https://doi.org/10.1111/j.1478-3231.2011.02539.x>
4. Blach S, Terrault NA, Tacke F, Gamkrelidze I, Craxi A, Tanaka J, et al.; Polaris Observatory HCV Collaborators. Global change in hepatitis C virus prevalence and cascade of care between 2015 and 2020: a modelling study. *Lancet Gastroenterol Hepatol*. 2022;7:396–415. [https://doi.org/10.1016/S2468-1253\(21\)00472-6](https://doi.org/10.1016/S2468-1253(21)00472-6)
5. Weil C, Nwankwo C, Friedman M, Kenet G, Chodick G, Shalev V. Epidemiology of hepatitis C virus infection in a large Israeli health maintenance organization. *J Med Virol*. 2016;88:1044–50. <https://doi.org/10.1002/jmv.24426>
6. Peles E, Schreiber S, Rados V, Adelson M. Low risk for hepatitis C seroconversion in methadone maintenance treatment. *J Addict Med*. 2011;5:214–20. <https://doi.org/10.1097/ADM.0b013e31820e13dd>
7. Israeli Prison Service. Drug and alcohol use by IPS inmates survey report 2013 [cited 2023 April 30]. https://www.gov.il/en/departments/general/about_prison_service
8. Vescio MF, Longo B, Babudieri S, Starnini G, Carbonara S, Rezza G, et al. Correlates of hepatitis C virus seropositivity in prison inmates: a meta-analysis. *J Epidemiol Community Health*. 2008;62:305–13. <https://doi.org/10.1136/jech.2006.051599>
9. Nakitanda AO, Montanari L, Tavoschi L, Mozalevskis A, Duffell E. Hepatitis C virus infection in EU/EEA and United Kingdom prisons: opportunities and challenges for action. *BMC Public Health*. 2020;20:1670. <https://doi.org/10.1186/s12889-020-09515-6>
10. Richter V, Goldstein L, Cohen DL, Bermont A, Zelnik Yovel D, Madar M, et al. The effect of direct-acting antiviral regimens and telemedicine on the treatment of inmates with hepatitis C virus infection in Israeli prisons. *Sci Prog*. 2022;105:00368504221105173. <https://doi.org/10.1177/00368504221105173>
11. Mor Z, Eisenberg JR, Grotto I, Tishler-Aurkin D. HIV/AIDS prevalence in Israeli prisons: is there a need for universal screening? *J Public Health Policy*. 2015;36:484–90. <https://doi.org/10.1057/jphp.2015.21>
12. Hochstatter KR, Tully DC, Power KA, Koepke R, Akhtar WZ, Prieve AF, et al. Hepatitis C virus transmission clusters in public health and correctional settings, Wisconsin, USA, 2016–2017. *Emerg Infect Dis*. 2021;27:480–9. <https://doi.org/10.3201/eid2702.202957>

Address for correspondence: Lihi Eisen, Tel-Aviv Department of Health, 12 Haarba'a St, Tel-Aviv 6473912, Israel; email: lihis28@gmail.com

Trends of Enterovirus D68 Concentrations in Wastewater, California, USA, February 2021–April 2023

Alexandria B. Boehm,¹ Debra A. Wadford,¹ Bridgette Hughes, Dorothea Duong, Alice Chen, Tasha Padilla, Chelsea Wright, Lisa Moua, Teal Bullick, Maria Salas, Christina Morales, Bradley J. White, Carol A. Glaser, Duc J. Vugia, Alexander T. Yu, Marlene K. Wolfe

In this retrospective study, we measured enterovirus D68 (EV-D68) genomic RNA in wastewater solids longitudinally at 2 California, USA, wastewater treatment plants twice per week for 26 months. EV-D68 RNA was undetectable except when concentrations increased from mid-July to mid-December 2022, which coincided with a peak in confirmed EV-D68 cases.

Enterovirus D68 (EV-D68) was recognized as a respiratory virus in 1962 (1). In 2014, unprecedented large outbreaks of EV-D68 infections associated with severe respiratory illnesses occurred in children in the United States (2), coinciding with a subsequent increase in cases of acute flaccid myelitis (AFM) (3). The Centers for Disease Control and Prevention (CDC) began active AFM monitoring in 2014, and as of July 2023, there have been 729 confirmed cases (4). Most patients have AFM develop during August–November. Cyclical peaks in AFM incidence were observed every 2 years (2014, 2016, and 2018) before the COVID-19 pandemic.

CDC began active sentinel surveillance for EV-D68 in 2017 through the New Vaccine Surveillance Network and detected a greater number of EV-D68 cases during July–August 2022 (5). However, there is no formal EV-D68 surveillance at state or local levels. Considering the emergence of wastewater

surveillance (WWS) as a method to monitor pathogens at various population levels (6), we sought to assess the feasibility of applying WWS to elucidate EV-D68 circulation. WWS could provide an early alert system for public health authorities to mitigate possible increases in severe acute respiratory illness and AFM and to enhance physician awareness during times of increased circulation.

EV-D68 is shed in respiratory secretions and feces (7), although data are limited. Two recent studies reported EV-D68 RNA in wastewater in 2021 and concordance with confirmed infections in Israel and the United Kingdom (8,9). In this retrospective, longitudinal study, we developed an EV-D68 assay, deployed it for WWS, and compared WWS results with laboratory-confirmed EV-D68 cases. This study was reviewed by the State of California Health and Human Services Agency Committee for the Protection of Human Subjects and determined to be exempt from oversight.

The Study

We tested the EV-D68-specific primers and probe developed by Wylie et al. (10) for their sensitivity and specificity in silico and in vitro against virus panels, intact viruses, and cDNA gene blocks (Appendix, <https://wwwnc.cdc.gov/EID/article/29/10/23-1080-App1.pdf>). In silico testing indicated no cross-reactivity with non-EV-D68 sequences deposited in GenBank, and in vitro testing indicated no cross-reactivity with nontarget viral gRNA. However, the assay did not detect the EV-D68 variant circulating in fall 2022 in the Northern Hemisphere (EV-D68–2022).

Author affiliations: Stanford University, Stanford, California, USA (A.B. Boehm); California Department of Public Health, Richmond, California, USA (D.A. Wadford, A. Chen, T. Padilla, C. Wright, L. Moua, T. Bullick, M. Salas, C. Morales, C.A. Glaser, D.J. Vugia, A.T. Yu); Verily Life Sciences, South San Francisco, California, USA (B. Hughes, D. Duong, B.J. White); Emory University Rollins School of Public Health, Atlanta, Georgia, USA (M.K. Wolfe)

DOI: <https://doi.org/10.3201/eid2911.231080>

¹These authors contributed equally to this article.

We therefore developed a new set of primers, and modified the probe, to amplify and detect in EV-D68-2022 the same region of the polyprotein region (viral protein 1) gene targeted by Wylie et al. We downloaded EV-D68-2022 genome sequences from GenBank in September 2022, aligned them to identify conserved regions in viral protein 1, and developed primers and probes in silico (Appendix Table 1). We confirmed the new primers and probes were specific and sensitive in silico and in vitro. The EV-D68 assay used in this study uses 2 forward and 2 reverse primers to ensure detection of all EV-D68 variants (Table).

We retrospectively selected wastewater solids grab samples from biobanked samples collected as part of a prospective, longitudinal WWS program in California. We selected samples from wastewater treatment plants in San Jose, serving 1.5 million persons in Santa Clara County and Oceanside, serving 250,000 persons in San Francisco County (Appendix Figure 1). We collected and analyzed 2 samples that were collected from each site per week during February 1, 2021–April 24, 2023.

We thawed wastewater solids overnight and extracted nucleic acids from 10 replicate sample aliquots as described (11). We used RNA as template in 10 replicate digital droplet reverse transcription PCR wells for each sample to measure EV-D68 RNA. We measured pepper mild mottle virus RNA as an endogenous control.

Details of reverse transcription PCR chemistry and data processing are provided (Appendix). We report measurements as copies per gram dry weight of solids (copies/g) with SDs. The lower limit of detection was ≈ 500 copies/g.

During February 2021–April 2023, EV-D68 RNA concentrations in wastewater solids were not detectable except for samples collected during mid-July 2022 to mid-December 2022. During that time, EV-D68 RNA concentrations increased to $\approx 10^5$ cp/g in mid-October at both plants (Figure, panels A, B). Plots of EV-D68 normalized by pepper mild mottle virus were similar (Appendix Figure, panels A, B).

Although there is no active EV-D68 surveillance in California, the California Department of Public

Health Viral and Rickettsial Disease Laboratory (VRDL) accepts enterovirus-reactive specimens from hospitals, clinics, and local public health laboratories for strain typing. Enterovirus typing enables us to know, at a limited level, which enterovirus types are circulating and associated with illness. Since 2020, the VRDL has maintained an AFM surveillance program with CDC (12). This enhanced AFM surveillance captures patient information but is not specific for EV-D68. However, enterovirus testing and typing are conducted when appropriate sample types are submitted. We aggregated the 35 EV-D68 clinical samples confirmed by VRDL during January 2021–April 2023 by week (Figure, panel C). The average time from date of collection to reporting out EV-D68 result was 32 days (range 12–63 days) (data not shown).

Trends in EV-D68 RNA wastewater concentrations at the 2 California communities match the trend in the state-aggregated weekly data on laboratory-confirmed EV-D68 cases (Figure). Weekly mean wastewater EV-D68 RNA concentrations were positively correlated with weekly case counts for both sites (Kendalls $\tau = 0.47$ for San Jose and 0.50 for Oceanside; $p < 0.001$).

Conclusions

Detection of EV-D68 in wastewater over 26 months in 2 California communities corresponded strikingly with the trend in statewide laboratory-confirmed EV-D68 cases, although specific EV-D68 case data were not available from those 2 communities (Appendix Table 3). Passive enterovirus surveillance and sentinel EV-D68 surveillance in the United States do not detect most enterovirus cases and focus primarily on the most severe enterovirus cases causing acute respiratory illness, meningitis, and AFM. Most persons infected with enterovirus are either asymptomatic or have mild symptoms and would not likely be tested. For persons who are tested, enterovirus-specific testing is rare, and a presumptive diagnosis is often based on the rhinovirus/enterovirus test on a respiratory virus panel assay without further characterization. Even in cases where EV-D68 is identified, EV-D68 infection is not a reportable disease and not

Table. Forward and reverse primers and probe used in study of trends of EV-D68 concentrations in wastewater, California, USA, February 2021–April 2023*

Target	Primer/probe	Sequence, 5' → 3'
EV-D68 VP1	Forward	CACYGAACCAGARGAAGCCA and CACTGAACCAGAGGAAGCTA
	Reverse	CCAAAGCTGCTCTACTGAGAAA and CTAAAGCTGCCCTACTAAGRAA
	Probe	TCGCACAGTGATAAATCRACAYGG

*EVD-68, enterovirus D68; VP, viral protein.

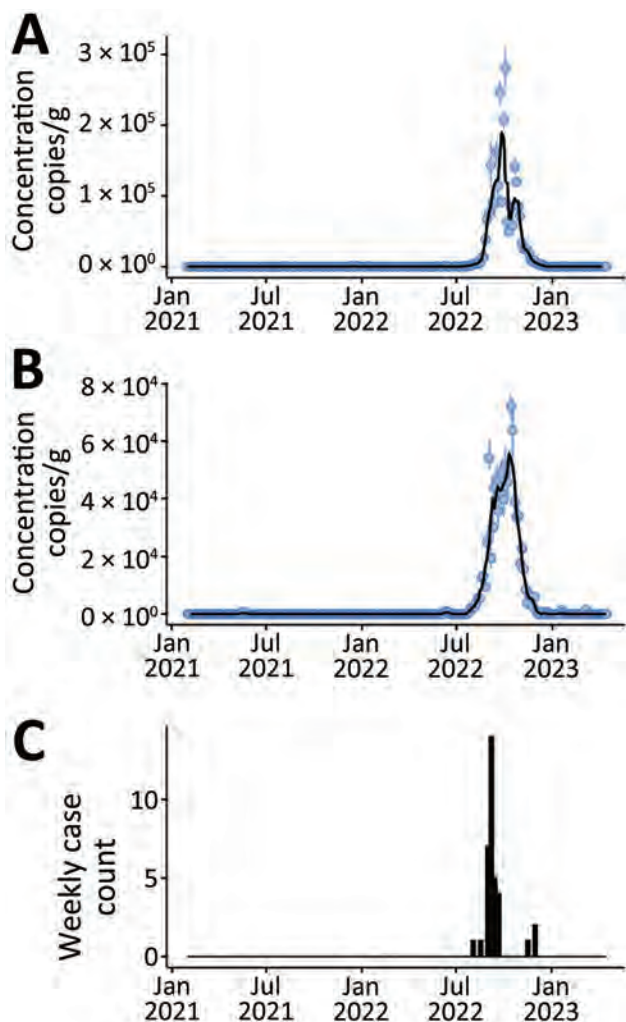


Figure. Enterovirus D68 RNA concentrations in wastewater solids from 2 wastewater treatment plants, California, USA. A, B) San Jose plant (A), serving 1.5 million persons in Santa Clara County, and Oceanside plant (B), serving 250,000 persons in San Francisco County. Error bars indicate SDs. Black lines indicate 5-sample trimmed means and are shown for data visualization purposes only. C) Weekly and state-aggregated laboratory-confirmed enterovirus D68 cases in California.

necessarily captured in public health surveillance systems. During July–December 2022, when EV-D68 RNA was detected and peaked in wastewater, case data were sparse, even when aggregated at the state level (Figure, panel C).

Given that recent EV-D68 surges have been associated with severe pediatric respiratory illness and coincided with increased numbers of AFM cases, there is a benefit to enhancing EV-D68 surveillance so that its circulation dynamics are better understood. Specific testing is rarely done on clinical samples, and surveillance for EV-D68 is limited. When available, EV-D68 typing of clinical cases is seldom timely.

Because WWS results are specific for EV-D68 and available 24 hours after sample collection, early warning of EV-D68 levels could be available irrespective of clinical testing. WWS for EV-D68 can inform public health action, including when to issue alerts to improve clinical recognition of the potential for severe respiratory illnesses and AFM cases. Our findings support routine prospective WWS for EV-D68 to inform public health surveillance. However, monitoring EV-D68 target sequences is necessary to ensure appropriate primers and probes are used for EV-D68 detection in wastewater.

Acknowledgments

We thank Hugo Guevara and Chao-Yang Pan for contributions to EV-D68 case surveillance and Vikram Chan-Herur for support on assay design.

This study was supported in part by a gift from the Sergey Brin Family Foundation to A.B.B.

About the Authors

Dr. Boehm is a professor of environmental engineering at Stanford University, Stanford, California. Her primary research interest is environmental pathogen surveillance. Dr. Wadford is a public health microbiologist at the California Department of Public Health, Richmond, California. Her primary research interests are respiratory and molecular virology.

References

- Schieble JH, Fox VL, Lennette EH. A probable new human picornavirus associated with respiratory diseases. *Am J Epidemiol.* 1967;85:297–310. <https://doi.org/10.1093/oxfordjournals.aje.a120693>
- Brown BA, Nix WA, Sheth M, Frace M, Oberste MS. Seven strains of enterovirus D68 detected in the United States during the 2014 severe respiratory disease outbreak. *Genome Announc.* 2014;2:e01201-14. <https://doi.org/10.1128/genomeA.01201-14>
- Leshem E; Division of Viral Diseases, National Centers for Immunization and Respiratory Diseases, CDC; Division of Vector-Borne Diseases, Division of High-Consequence Pathogens and Pathology, National Center for Emerging and Zoonotic Infectious Diseases, CDC; Children's Hospital Colorado; Council of State and Territorial Epidemiologists. Notes from the field: acute flaccid myelitis among persons aged ≤ 21 years—United States, August 1–November 13, 2014. *MMWR Morb Mortal Wkly Rep.* 2015;63:1243–4.
- Centers for Disease Control and Prevention. Acute flaccid myelitis [cited 2023 Jul 13]. <https://www.cdc.gov/acute-flaccid-myelitis/index.html>
- Centers for Disease Control and Prevention Health Alert Network. Severe respiratory illnesses associated with rhinoviruses and/or enteroviruses Including EV-D68—multistate, 2022 [cited 2023 Jul 17]. <https://emergency.cdc.gov/han/2022/han00474.asp>

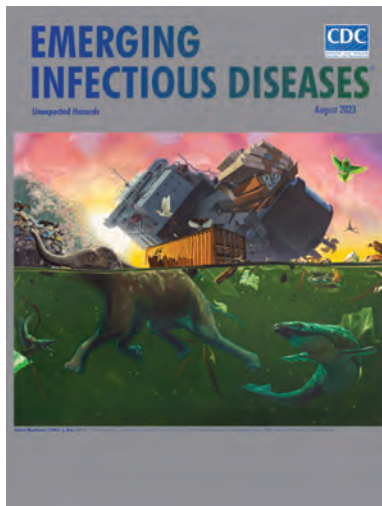
6. Boehm AB, Hughes B, Duong D, Chan-Herur V, Buchman A, Wolfe MK, et al. Wastewater concentrations of human influenza, metapneumovirus, parainfluenza, respiratory syncytial virus, rhinovirus, and seasonal coronavirus nucleic-acids during the COVID-19 pandemic: a surveillance study. *Lancet Microbe*. 2023;4:e340–8. [https://doi.org/10.1016/S2666-5247\(22\)00386-X](https://doi.org/10.1016/S2666-5247(22)00386-X)
7. Zheng H-W, Sun M, Guo L, Wang J-J, Song J, Li J-Q, et al. Nasal infection of enterovirus D68 leading to lower respiratory tract pathogenesis in ferrets (*Mustela putorius furo*). *Viruses*. 2017;9:104. <https://doi.org/10.3390/v9050104>
8. Erster O, Bar-Or I, Levy V, Shatzman-Steuerman R, Sofer D, Weiss L, et al. Monitoring of enterovirus D68 outbreak in Israel by a parallel clinical and wastewater based surveillance. *Viruses*. 2022;14:1010. <https://doi.org/10.3390/v14051010>
9. Tedcastle A, Wilton T, Pegg E, Klapsa D, Bujaki E, Mate R, et al. Detection of enterovirus D68 in wastewater samples from the UK between July and November 2021. *Viruses*. 2022;14:143. <https://doi.org/10.3390/v14010143>
10. Wylie TN, Wylie KM, Buller RS, Cannella M, Storch GA. Development and evaluation of an enterovirus D68 real-time reverse transcriptase PCR assay. *J Clin Microbiol*. 2015;53:2641–7. <https://doi.org/10.1128/JCM.00923-15>
11. Boehm AB, Wolfe MK, Wigginton KR, Bidwell A, White BJ, Hughes B, et al. Human viral nucleic acids concentrations in wastewater solids from central and coastal California USA. *Sci Data*. 2023;10:396. <https://doi.org/10.1038/s41597-023-02297-7>
12. Kidd S, Lopez AS, Konopka-Anstadt JL, Nix WA, Routh JA, Oberste MS. Enterovirus D68-associated acute flaccid myelitis, United States, 2020. *Emerg Infect Dis*. 2020;26:e201630. <https://doi.org/10.3201/eid2610.201630>

Address for correspondence: Alexandria B. Boehm, Department of Civil and Environmental Engineering, Stanford University, 473 Via Ortega, Rm 189, Stanford, CA 94305, USA; email: aboehm@stanford.edu

August 2023

Unexpected Hazards

- Clinical Characteristics of *Corynebacterium ulcerans* Infection, Japan
- Healthcare-Associated Infections Caused by *Mycolicibacterium neoaurum* Response to Vaccine-Derived Polioviruses Detected through Environmental Surveillance, Guatemala, 2019
- Outbreak of NDM-1– and OXA-181–Producing *Klebsiella pneumoniae* Bloodstream Infections in a Neonatal Unit, South Africa
- Spatial Epidemiologic Analysis and Risk Factors for Nontuberculous Mycobacteria Infections, Missouri, USA, 2008–2019
- Waterborne Infectious Diseases Associated with Exposure to Tropical Cyclonic Storms, United States, 1996–2018
- Multidrug-Resistant Bacterial Colonization and Infections in Large Retrospective Cohort of Mechanically Ventilated COVID-19 Patients
- Prospecting for Zoonotic Pathogens by Using Targeted DNA Enrichment
- Omicron COVID-19 Case Estimates Based on Previous SARS-CoV-2 Wastewater Load, Regional Municipality of Peel, Ontario, Canada
- Predicting COVID-19 Incidence Using Wastewater Surveillance Data, Denmark, October 2021–June 2022



- Economic Evaluation of Wastewater Surveillance Combined with Clinical COVID-19 Screening Tests, Japan
- Chromosome-Borne CTX-M-65 Extended-Spectrum β -Lactamase–Producing *Salmonella enterica* Serovar Infantis, Taiwan
- Genome-Based Epidemiologic Analysis of VIM/IMP Carbapenemase-Producing *Enterobacter* spp., Poland
- Pediatric SARS-CoV-2 Seroprevalence, Oregon, USA, November 1, 2020–June 30, 2022
- Human Fecal Carriage of *Streptococcus agalactiae* Sequence Type 283, Thailand
- Emerging *Corynebacterium diphtheriae* Species Complex Infections, Réunion Island, France, 2015–2020
- Increase of Severe Pulmonary Infections in Adults Caused by M1UK *Streptococcus pyogenes*, Central Scotland, UK
- Dengue Outbreak Response during COVID-19 Pandemic, Key Largo, Florida, USA, 2020
- SARS-CoV-2 Variants and Age-Dependent Infection Rates among Household and Nonhousehold Contacts
- Uniting for Ukraine Tuberculosis Screening Experience, San Francisco, California, USA
- Imported Cholera Cases, South Africa, 2023
- *Mycobacterium abscessus* Meningitis Associated with Stem Cell Treatment During Medical Tourism
- Candidatus *Neoehrlichia mikurensis* Infection in Patient with Antecedent Hematologic Neoplasm, Spain
- Elimination of *Dirofilaria immitis* Infection in Dogs, Linosa Island, Italy, 2020–2022
- Detection of Hantavirus during the COVID-19 Pandemic, Arizona, USA, 2020

**EMERGING
INFECTIOUS DISEASES**

To revisit the August 2023 issue, go to:
<https://wwwnc.cdc.gov/eid/articles/issue/29/8/table-of-contents>

Erythema Migrans Caused by *Borrelia spielmanii*, France

Pascal del Giudice, Fabienne Freychet, Lora Kopec, Florence Fenollar, Carole Eldin, Marine Velin, Thomas Hubiche, Didier Raoult, Oleg Mediannikov

We describe a rare case of early Lyme borreliosis in France caused by *Borrelia spielmanii*, which manifested as a large erythema chronicum migrans rash. The patient completely recovered after a 15-day course of amoxicillin. Absence of pathognomonic signs prevented distinguishing *B. spielmanii* from other etiologies as cause in this case-patient.

The causative agents of borreliosis, also known as Lyme disease, in Europe are *Borrelia garinii*, *B. afzelii*, and, more rarely, *B. burgdorferi* sensu stricto. Lyme borreliosis is endemic in France except the southern region. Mean annual incidence of Lyme borreliosis in France may be as high as 84 cases/100,000 persons (1).

B. spielmanii is a rare agent of Lyme borreliosis first isolated in 1993 from a patient with erythema chronicum migrans (ECM) in the Netherlands (2), then well-characterized as a novel genetic variant in 1999 (3). *B. spielmanii* was described as a new species in 2006 with a type strain isolated from *Ixodes ricinus* ticks collected from a garden dormouse in the Petite Camargue Alsacienne region in France (4,5). A few human cases were reported from Germany (4), Hungary (6), Czech Republic (7), Denmark, and Slovenia (8); patients in all reported cases exhibited ECM (9). *B. spielmanii* has been found in a low percentage of ticks feeding on dogs in the United Kingdom, Switzerland, and Belgium and on birds in Poland. Also, ticks in Austria, Denmark, and the Czech Republic (some removed from

humans), *I. ricinus* ticks in the Crimea peninsula (10), as well as in animal tissues from Poland (red fox) (11) and Hungary (hedgehogs), have been shown to carry *B. spielmanii* (12). No infected humans have been identified France.

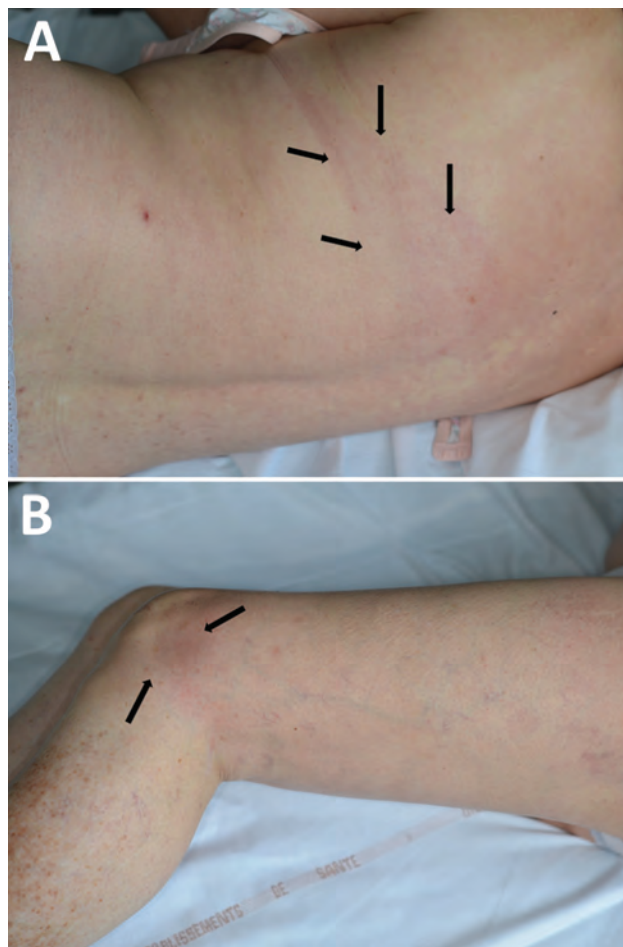


Figure 1. Large erythema chronicum migrans rash on a 60-year-old woman in France that was later determined to be caused by *Borrelia spielmanii*. A) Edges of linear erythema band on patient's back, indicated by arrows. B) End of linear erythema band beginning on patient's knee, indicated by arrows on patient's knee.

Author affiliations: Dermatology Infectiology Unit, CH Fréjus-Saint-Raphaël, France (P. del Giudice, M. Velin, T. Hubiche); Dermatology private practice, Nice, France (F. Freychet); MEPHI, IHU Méditerranée infection, IRD, Aix Marseille Université, Marseille, France (L. Kopec, F. Fenollar, C. Eldin, D. Raoult, O. Mediannikov); VITROME, IHU Méditerranée infection, IRD, Aix Marseille Université, Marseille (L. Kopec, F. Fenollar, C. Eldin, D. Raoult, O. Mediannikov)

DOI: <https://doi.org/10.3201/eid2911.230149>

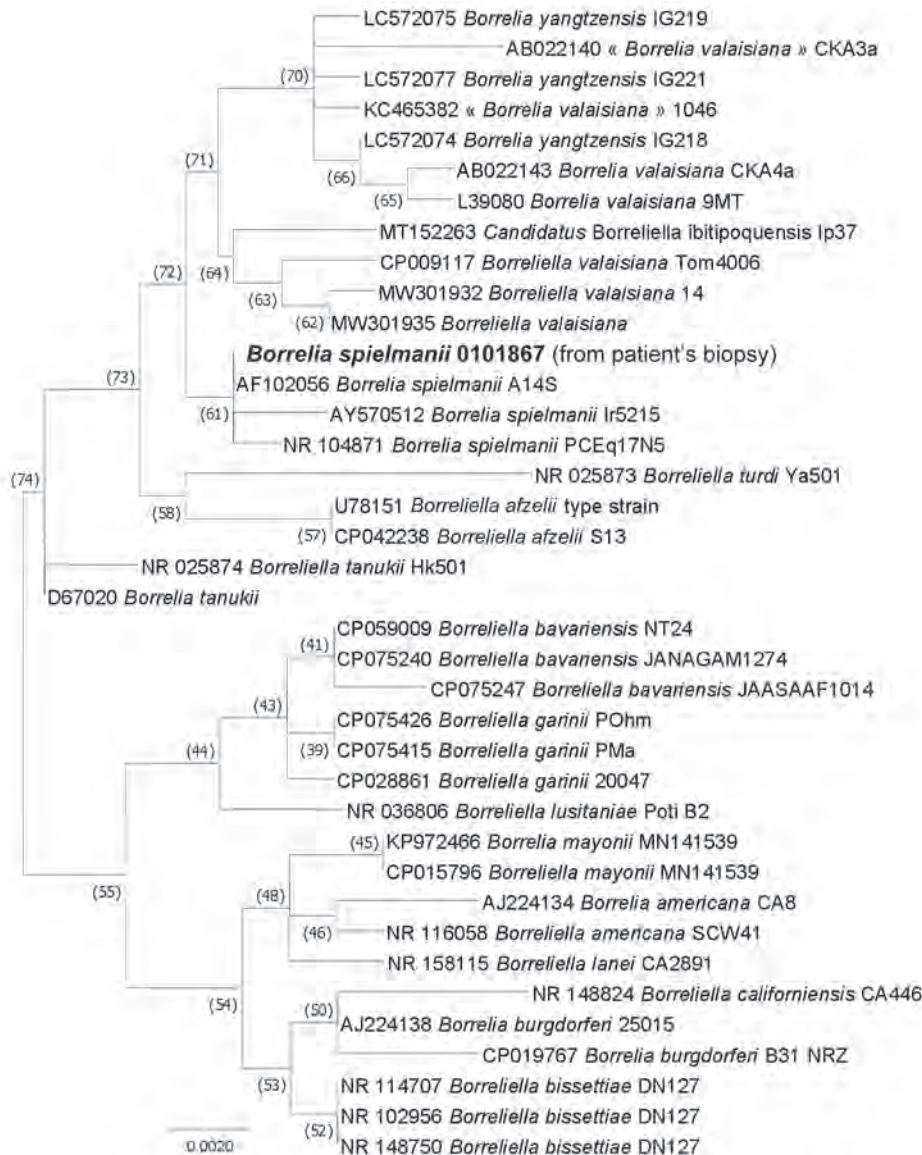


Figure 2. Maximum-likelihood phylogenetic tree of the 16S rRNA gene (rrs) of *Borrelia* genus bacteria showing the position of the *B. spielmanii* sequence obtained from the patient (large bold font). Evolutionary analyses were conducted using TOPALI version 2.5 (<http://www.topali.org>). The sequences of the 16S rDNA amplified in this study with other 12S rDNA tick sequences available on GenBank (910 positions in the final dataset) were aligned using ClustalW (<https://www.genome.jp/tools-bin/clustalw>) implemented on BioEdit version 3 (<https://bioedit.software.informer.com>). The evolutionary history was inferred by using the maximum likelihood method based on the Hasegawa–Kishino–Yano model plus invariate sites plus gamma distribution. The percentage of trees in which the associated taxa clustered together is shown next to the branches. GenBank accession numbers are provided. Scale bar indicates nucleotide sequence divergence.

The Study

A 60-year-old woman sought treatment on November 15, 2017, for 2 erythematous linear asymptomatic and noninfiltrated bands on her left knee and the left side of her thorax. In August 2017, the woman had noticed an annular erythema initially in the middle and on the left side of her back. The annular erythema had gradually extended to the upper left side of her back to form a single erythematous band (Figure 1, panel A) and progressed to the left knee, also forming an erythematous band (Figure 1, panel B). Both general and skin exams were otherwise unremarkable. We hypothesized that the rash might constitute an unusually large ECM. Because Lyme borreliosis is unknown in that area of southeastern France, we

questioned her about her recent travel history. She had spent the week of June 14–20, 2017, in the county of Oise, north of Paris, where Lyme borreliosis is endemic. We performed a punch biopsy on the thoracic erythema band and prescribed oral amoxicillin (1 g 3×/d for 15 d), which resolved the ECM.

We screened a serum sample from the patient using an enzyme-linked immunoassay (Liaison *Borrelia burgdorferi*; DiaSorin, <https://www.diasorin.com>), which revealed presence of IgG and absence of IgM for *B. burgdorferi* sensu lato. Western blotting using LymeCheck Optima IgG & IgM (Biosynex, <https://www.biosynex.com>) revealed presence of *Borrelia* spp.–specific IgG for p100, VlsE, p58, and p41 antigens and a faint band for *B. spielmanii*–specific *ospC* antigen (Appendix Figure,

<https://wwwnc.cdc.gov/EID/article/29/11/23-0149-App1.pdf>). Two weak bands showed IgM for *B. spielmanii* p100 and p41 antigens (Appendix Figure).

We amplified portions of 16S rRNA (13) and *ospA* (5) borrelial genes from the biopsy sample. BLAST search (<https://blast.ncbi.nlm.nih.gov/Blast.cgi>) of sequenced amplicons showed 100% identity of the biopsy sequences with strain A14S of *B. spielmanii* for both the 910 bp-long portion of 16S rRNA gene (Genbank accession no. AF102056) and 260 bps-long amplicon of *ospA* (Genbank accession no. CP001469). We deposited our sequences into Genbank (accession nos. OR192893 and OR234396). The phylogenetic tree (Figure 2) showed that the sequence obtained from the patient clusters with other *B. spielmanii* strains.

Previously, only *B. azfelii*, *B. garinii*, and *B. burgdorferi* sensu stricto had been identified from patients in France (14). Our patient manifested a rare clinical form of ECM, with a large erythema migrans across her body, extending from her upper back to her knee. However, the unusually large size might have resulted from delays in seeking treatment and diagnosis, so that particular clinical manifestation might not be specific to *B. spielmanii*.

We reviewed available literature on clinical descriptions of human cases of *B. spielmanii* infection and found only 2 published case reports. A 69-year-old woman from Slovenia showed skin manifestations described as redness, mild local itching, burning, and pain on the left knee and later a 24 × 20 cm ring-like lesion on the left thigh (8), but she had no identified tick bite. In a second case, a 42-year-old woman from Hungary exhibited an ECM 10 cm in diameter on her knee (6). Clinical manifestations were missing in other case reports (3,9), in which only human isolates were described. In 1 study, *B. spielmanii* was detected in isolates from 4/242 patients with ECM from Germany and Slovenia (9). However, in that study, 3 of the 4 patients infected with *B. spielmanii* lived in Munich where a higher proportion of ticks were positive for that pathogen. This finding argues for sporadic occurrences of the infection in other locations.

In summary, our study has contributed more data on *Borrelia* spp. as potential causes of Lyme disease, prompting need for broader surveillance. However, additional well-documented reports on ECM as a manifestation of *B. spielmanii* are needed to provide new information about the epidemiology of this *Borrelia* in Europe.

Acknowledgment

We thank Mrs. Moussa Hajer for editing the figures, proof-reading, and submitting this manuscript.

About the Author

Dr. Del Giudice is a physician in the Infectious Diseases and Dermatology Unit at Bonnet Hospital, Fréjus, France. His primary research interest is skin infections.

References

- Figoni J, Chirouze C, Hansmann Y, Lemogne C, Hentgen V, Saunier A, et al.; endorsed by scientific societies. Lyme borreliosis and other tick-borne diseases. Guidelines from the French Scientific Societies (I): prevention, epidemiology, diagnosis. *Med Mal Infect*. 2019;49:318–34. <https://doi.org/10.1016/j.medmal.2019.04.381>
- van Dam AP, Kuiper H, Vos K, Widjojokusumo A, de Jongh BM, Spanjaard L, et al. Different genospecies of *Borrelia burgdorferi* are associated with distinct clinical manifestations of Lyme borreliosis. *Clin Infect Dis*. 1993; 17:708–17. <https://doi.org/10.1093/clinids/17.4.708>
- Wang G, van Dam AP, Dankert J. Phenotypic and genetic characterization of a novel *Borrelia burgdorferi* sensu lato isolate from a patient with Lyme borreliosis. *J Clin Microbiol*. 1999;37:3025–8. <https://doi.org/10.1128/JCM.37.9.3025-3028.1999>
- Richter D, Schlee DB, Allgöwer R, Matuschka FR. Relationships of a novel Lyme disease spirochete, *Borrelia spielmani* sp. nov., with its hosts in central Europe. *Appl Environ Microbiol*. 2004;70:6414–9. <https://doi.org/10.1128/AEM.70.11.6414-6419.2004>
- Richter D, Postic D, Sertour N, Livey I, Matuschka FR, Baranton G. Delineation of *Borrelia burgdorferi* sensu lato species by multilocus sequence analysis and confirmation of the delineation of *Borrelia spielmanii* sp. nov. *Int J Syst Evol Microbiol*. 2006;56:873–81. <https://doi.org/10.1099/ijs.0.64050-0>
- Földvári G, Farkas R, Lakos A. *Borrelia spielmanii* erythema migrans, Hungary. *Emerg Infect Dis*. 2005;11:1794–5. <https://doi.org/10.3201/eid1111.050542>
- Richtrová E, Michalová P, Lukavská A, Navrátil J, Kybicová K. *Borrelia burgdorferi* sensu lato infection in *Ixodes ricinus* ticks in urban green areas in Prague. *Ticks Tick Borne Dis*. 2022;13:102053. <https://doi.org/10.1016/j.ttbdis.2022.102053>
- Maraspin V, Ruzic-Sabljić E, Strle F. Lyme borreliosis and *Borrelia spielmanii*. *Emerg Infect Dis*. 2006;12:1177. <https://doi.org/10.3201/eid1207.060077>
- Fingerle V, Schulte-Spechtel UC, Ruzic-Sabljić E, Leonhard S, Hofmann H, Weber K, et al. Epidemiological aspects and molecular characterization of *Borrelia burgdorferi* s.l. from southern Germany with special respect to the new species *Borrelia spielmanii* sp. nov. *Int J Med Microbiol*. 2008;298:279–90. <https://doi.org/10.1016/j.ijmm.2007.05.002>
- Nefedova VV, Korenberg EI, Andreïchuk IV, Gorelova NB, Markov AV, Fadeeva IA, et al. Genetic characterization of pathogenic *Borrelia*, group A14S, isolated in Ukraine [in Russian]. *Zh Mikrobiol Epidemiol Immunobiol*. 2005;4:23–7.
- Wodecka B, Michalik J, Grochowalska R. Red foxes (*Vulpes vulpes*) are exposed to high diversity of *Borrelia burgdorferi* sensu lato species infecting fox-derived *Ixodes* ticks in west-central Poland. *Pathogens*. 2022;11:696. <https://doi.org/10.3390/pathogens11060696>
- Szekeres S, Docters van Leeuwen A, Tóth E, Majoros G, Sprong H, Földvári G. Road-killed mammals provide insight into tick-borne bacterial pathogen communities within urban habitats. *Transbound Emerg Dis*. 2019;66:277–86. <https://doi.org/10.1111/tbed.13019>

13. Raoult D, Ndihokubwayo JB, Tissot-Dupont H, Roux V, Faugere B, Abegbinni R, et al. Outbreak of epidemic typhus associated with trench fever in Burundi. *Lancet*. 1998; 352:353–8. [https://doi.org/10.1016/S0140-6736\(97\)12433-3](https://doi.org/10.1016/S0140-6736(97)12433-3)
14. Lenormand C, Jaulhac B, Debarbieux S, Dupin N, Granel-Brocard F, Adamski H, et al. Expanding the clinico-pathological spectrum of late cutaneous Lyme borreliosis (acrodermatitis chronica atrophicans [ACA]): A prospective

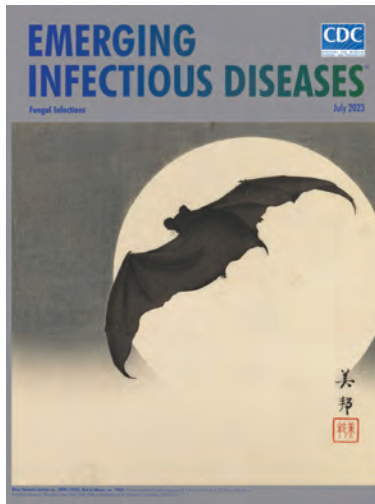
study of 20 culture- and/or polymerase chain reaction (PCR)-documented cases. *J Am Acad Dermatol*. 2016;74:685–92. <https://doi.org/10.1016/j.jaad.2015.10.046>

Address for correspondence: Pascal del Giudice, Infectiology and Dermatology Unit, Centre Hospitalier Intercommunal de Fréjus-Saint-Raphaël, 240 Av. de Saint-Lambert, 83600 Fréjus, France; email: pascal.deljudice@chi-fsr.fr

July 2023

Fungal Infections

- Multicentric Case Series and Literature Review of Coccidioidal Otomastoiditis
- Nationwide Outbreak of *Candida auris* Infections Driven by COVID-19 Hospitalizations, Israel, 2021–2022
- Clinical and Mycologic Characteristics of Emerging Mucormycosis Agent *Rhizopus homothallicus*
- Trajectory and Demographic Correlates of Antibodies to SARS-CoV-2 Nucleocapsid in Recently Infected Blood Donors, United States
- Rising Incidence of *Sporothrix brasiliensis* Infections, Curitiba, Brazil, 2011–2022
- Triplex ELISA for Assessing Durability of *Taenia solium* Seropositivity after Neurocysticercosis Cure
- Effect of Norovirus Inoculum Dose on Virus Kinetics, Shedding, and Symptoms
- Estimating Waterborne Infectious Disease Burden by Exposure Route, United States, 2014
- Highly Pathogenic Avian Influenza Virus (H5N1) Clade 2.3.4.4b Introduced by Wild Birds, China, 2021
- Systematic Review of Hansen Disease Attributed to *Mycobacterium lepromatosis*
- Sensitivity to Neutralizing Antibodies and Resistance to Type I Interferons in SARS-CoV-2 R.1 Lineage Variants, Canada
- Long-Term Epidemiology and Evolution of Swine Influenza Viruses, Vietnam
- Lumpy Skin Disease Virus Infection in Free-Ranging Indian Gazelles (*Gazella bennettii*), Rajasthan, India
- Cutaneous Pythiosis in 2 Dogs, Italy



- Sexually Transmitted *Trichophyton mentagrophytes* Genotype VII Infection among Men Who Have Sex with Men
- Pulmonary Nontuberculous Mycobacteria, Ontario, Canada, 2020
- Evolutionary Formation and Distribution of Puumala Virus Genome Variants, Russia
- *Candida vulturna* Outbreak Caused by Cluster of Multidrug-Resistant Strains, China
- Estimates of Serial Interval and Reproduction Number of Sudan Virus, Uganda, August–November 2022
- Increased Hospitalizations Involving Fungal Infections during COVID-19 Pandemic, United States, January 2020–December 2021
- Nonnegligible Seroprevalence and Predictors of Murine Typhus, Japan
- Spotted Fever and Typhus Group Rickettsiae in Dogs and Humans, Mexico, 2022
- *Nannizzia polymorpha* as Rare Cause of Skin Dermatophytosis
- Fatal Invasive Mold Infections after Transplantation of Organs Recovered from Drowned Donors, United States, 2011–2021
- Surveillance and Genomic Characterization of Influenza A and D Viruses in Swine, Belgium and the Netherlands, 2019–2021
- Detecting, Quantifying, and Isolating Monkeypox Virus in Suspected Cases, Spain
- Tuberculosis Infection among Non-US-Born Persons and Persons ≥60 Years of Age, United States, 2019–2020
- Extensively Drug-Resistant *Shigella flexneri* 2a, California, USA, 2022
- Novel Highly Pathogenic Avian Influenza A(H5N1) Clade 2.3.4.4b Virus in Wild Birds, South Korea
- Long-Term SARS-CoV-2 Antibody Seroprevalence in Blood Donors, Italy
- Reemergence of Dengue Virus Serotype 3, Brazil, 2023
- *Candida auris*-Associated Hospitalizations, United States, 2017–2022
- Isolation of *Elizabethkingia* spp. from Diagnostic Specimens from Dogs and Cats, United States, 2019–2021
- Detection of *Mycobacterium angelicum* in Human Urinary Tract, French Polynesia
- Low Susceptibility of Pigs against Experimental Infection with HPAI Virus H5N1 Clade 2.3.4.4b

**EMERGING
INFECTIOUS DISEASES**

To revisit the July 2023 issue, go to:
<https://wwwnc.cdc.gov/eid/articles/issue/29/7/table-of-contents>

Genetic Characterization of Extensively Drug-Resistant *Shigella sonnei* Infections, Spain, 2021–2022

Camille Jacqueline, Guillermo Ruiz Carrascoso, José Gutiérrez-Fernández, Teresa Vicente Rangel, Lidia Goterris, Fernando Vazquez Valdes, Domingo Fernández Vecilla, Matilde Elía López, Maria Rocío Martínez Ruiz, Carmen Aspiroz Sancho, Ramón Perez Tanoira, Elia Sirvent Quílez, Alba de la Rica Martínez, Nieves Gonzalo Jiménez, Cristina García Salguero, Eva González Barbera, Maria Reyes Sánchez Florez, Francisco J. Merino, Begonia Sagardia Redondo, Enrique Rodriguez Guerrero, Claudia Sanz González, Silvia Herrera-Leon

In 2022, the United Kingdom reported an increase in drug resistance in *Shigella sonnei* isolates. We report 33 cases in Spain genetically related to the UK cases and 4 cases with similar antimicrobial resistance profiles infected with genetically distant strains. Our results suggest circulation of multiple genetic clusters of multidrug-resistant *S. sonnei* in Spain.

On January 27, 2022, the United Kingdom reported an increased number of infections with extensively drug-resistant (XDR) *Shigella sonnei* during September 1, 2021–January 10, 2022 (1). A total of 146 cases were later reported in 9 other countries in Europe, all having either a similar XDR profile or close genetic relationship to the UK cases (2). Most cases were linked to sexual transmission between gay, bisexual, and other men who have sex with men (MSM) (2).

In Spain, information on *S. sonnei* exposure is rarely available (only in 7.2% of cases), but person-to-person transmission is the most frequently observed. Previous studies in Spain reported circulation of lineages of *S. sonnei* resistant to first- and second-line oral treatments among MSM in different autonomous communities (Catalunya, Andalucía, País Vasco, and Madrid) as early as 2015 (3–7). We describe the multidrug-resistant (MDR) isolates of *S. sonnei* circulating in Spain during January 2021–April 2022.

The Study

For this investigation, we defined a suspected case as a patient with laboratory-confirmed *S. sonnei* infection; an MDR profile characterized by nonsusceptibility to ≥ 1 agent in ≥ 3 of the antimicrobial categories tested,

Author affiliations: European Public Health Microbiology Training Program, European Centre for Disease Prevention and Control, Stockholm, Sweden (C. Jacqueline); Centro Nacional de Microbiología, Instituto de Salud Carlos III, Majadahonda, Spain (C. Jacqueline, S. Herrera-Leon); Servicio de Microbiología Clínica, Hospital Universitario La Paz, Madrid, Spain (G.R. Carrascoso, C.S. González); Universidad de Granada, Granada, Spain (J. Gutiérrez-Fernández); Hospital General Universitario Gregorio Marañón, Madrid, Spain (T.V. Rangel); Hospital Universitario Vall d'Hebron, Barcelona, Spain (L. Goterris); Hospital Universitario Central De Asturias, Oviedo, Spain (F.V. Valdes); Hospital Universitario de Basurto, Bilbao, Spain (D.F. Vecilla); Hospital Universitario de Navarra, Pamplona, Spain (M.E. López); Hospital Puerta De Hierro, Majadahonda,

Spain (M.R.M. Ruiz); Hospital Royo Villanova, Zaragoza, Spain (C. Aspiroz Sancho); Hospital Universitario Príncipe de Asturias, Alcalá de Henares, Spain (R.P. Tanoira); Hospital General Universitario de Elche, Alicante, Spain (E.S. Quílez, A.R. Martínez, N.G. Jiménez); Hospital Clínico San Carlos, Madrid, Spain (C.G. Salguero); Hospital Universitario y Politécnico La Fe, Valencia, Spain (E.G. Barbera); C.H.U. Nuestra Señora de Candelaria, Santa Cruz de Tenerife, Spain (M.R.S. Florez); Hospital Universitario Severo Ochoa, Leganés, Spain (F.J. Merino); Laboratorio De Salud Pública, Palma De Mallorca, Spain (B.S. Redondo); Hospital Universitario Virgen de las Nieves, Granada, Spain (E.R. Guerrero)

DOI: <http://doi.org/10.3201/eid2911.221746>

including third-generation cephalosporins, aminoglycosides, sulfamethoxazole, and fluoroquinolones; and a specimen collected in Spain during January 1, 2021–April 1, 2022. Over the study period, hospitals voluntarily sent 51 *S. sonnei* isolates to the National Center of Microbiology in Spain, and epidemiologic data were collected from laboratory request forms or by directly contacting the hospitals. From those cases, we identified 37 (72%) suspected cases across 12 autonomous communities (Appendix 1, <https://wwwnc.cdc.gov/EID/article/29/11/23-1746-App1.xlsx>). This finding represented a dramatic increase compared with 2019 data from Spain, in which only 6% of isolates tested in the National Center of Microbiology were identified as MDR (C. Jacqueline et al., unpub. data). We excluded 2020 from review because of the COVID-19 pandemic.

The median age of the persons with suspected cases was 34 (range 18–75) years (Appendix 2, <https://wwwnc.cdc.gov/EID/article/29/11/23-1746-App2.pdf>). Seventeen (46%) persons reported diarrhea, and 1 person was asymptomatic (tested as contact of another case); for 19 (51%) persons, symptoms were not reported. Eight (22%) persons were hospitalized for fever, enterocolitis, pancolitis, and dehydration; hospitalization status was unknown for 2 (5%) persons. The percentage of hospitalizations was similar to data from 2018 (20%) but higher than data from 2019 (11%). Mean duration of hospitalization was 5.7 (range 2–10) days, and no person died from their infection. When considered appropriate, patients were treated with ertapenem, meropenem, ciprofloxacin, amoxicillin/clavulanic acid, metronidazole, or fosfomycin (alone or in combination). Antibiotic treatment failure was occasionally observed and resolved by a change in treatment (7).

Nineteen (51%) persons from 7 distinct autonomous communities were identified as MSM, and sexual transmission was hypothesized in 4 groups of sexual partners. One person reported sexual contact with persons in France. No person reported exposure to potentially contaminated food or water. Some patients were HIV positive (frequency is omitted to prevent deductive disclosure), and only 2 persons reported using preexposure prophylaxis (18 cases reported not using preexposure prophylaxis; information was unavailable for the 17 other cases).

We performed whole-genome sequencing (WGS; Illumina Inc., <https://www.illumina.com>) on all isolates from suspected cases. Sequences can be accessed on Enterobase (https://enterobase.warwick.ac.uk/uberstrains/ESC_BB1296AA_to_ESC_BB1332AA). Using the *Escherichia/Shigella* scheme of Enterobase, we

performed a core genome multilocus sequence typing analysis. We found 33 (89%) isolates that were within 7 allelic differences (absent alleles were not considered as differences) of the 3 representative outbreak sequences shared by the United Kingdom in the EpiPulse event notification portal (<https://www.ecdc.europa.eu/en/publications-data/epipulse-european-surveillance-portal-infectious-diseases>). We defined all isolates belonging to that genetic cluster as confirmed cases and belonging to sequence type (ST) 152. Two ST152 isolates showed a high number of allelic differences compared with the main cluster, including 1 isolate from a female case-patient. In addition, we identified 2 isolates as belonging to different sequence types, ST3075 and ST5390 (Appendix 1).

We investigated the genetic diversity of ST152 isolates using a single-nucleotide polymorphism analysis (Center for Genomic Epidemiology, <https://cge.food.dtu.dk/services/CSIPhylogeny>). We included all the sequences available on Enterobase that corresponded to *S. sonnei* ST152 cases in Spain during 2019–2022. We found a low genetic diversity overall, especially between the sequences of confirmed cases, but we observed 3 phylogenetical clades (confirmed by hierBAPS, <https://github.com/gtonkinhill/rhierbaps>) (Figure). We observed 1–9 single-nucleotide polymorphisms of difference between cases where sexual transmission was hypothesized.

We determined the genetic determinants of resistance using PlasmidFinder 2.1 (8) and ResFinder 4.1 (9,10). First, we found that all confirmed cases harbored the plasmid replicon IncFII, which carried the gene *bla*_{CTX-M-27} responsible for resistance to ampicillin, cefepime, cefotaxime, and ceftazidime. However, the ST152 isolate from the female case-patient and the ST3075 and ST5390 isolates harbored different extended-spectrum β -lactamase-producing genes (Appendix Table). Resistance to streptomycin was associated with *aadA5*, resistance to sulfamethoxazole was associated with *sul1*, and resistance to trimethoprim was associated with *dfrA1*, all of which were also harbored by the IncFII plasmid. The gene *mphA* conferring resistance to azithromycin was present in all but 2 isolates. We also detected an additional plasmid replicon, IncB/O/K/Z, in 30 isolates. In the core genome, the same point mutation S83L in the *gyrA* gene, conferring fluoroquinolone resistance, was present in all isolates.

Conclusion

We describe the circulation in Spain of a cluster of extended spectrum β -lactamase-producing and MDR *S. sonnei* infections genetically related with those

observed in a contemporaneous UK outbreak. Because most of the isolates harbored the gene conferring azithromycin resistance, we hypothesize that they would be XDR, even though we did not confirm it phenotypically. We also identified strains of MDR *S. sonnei* that belonged to STs other than the one described in the United Kingdom. This finding raises concerns about the ability to manage the spread of MDR and XDR *Shigella* infections and highlights the need to strengthen surveillance of shigellosis.

In the United Kingdom, sexual transmission between MSM was identified as the main factor of

circulation for the strains harboring the IncFII plasmid replicon (1). Although we cannot exclude other confounding factors, our results point in the same direction. Indeed, food exposure was not reported, and 19 confirmed case-patients were MSM, even though the respondent rate for sexual orientation was low in our study. However, identifying a female case-patient and a heterosexual male case-patient suggests circulation of MDR *S. sonnei* outside of the MSM population. In Spain, efforts should be made to obtain information related to exposure and to recommend the use of microbiological culture and WGS to

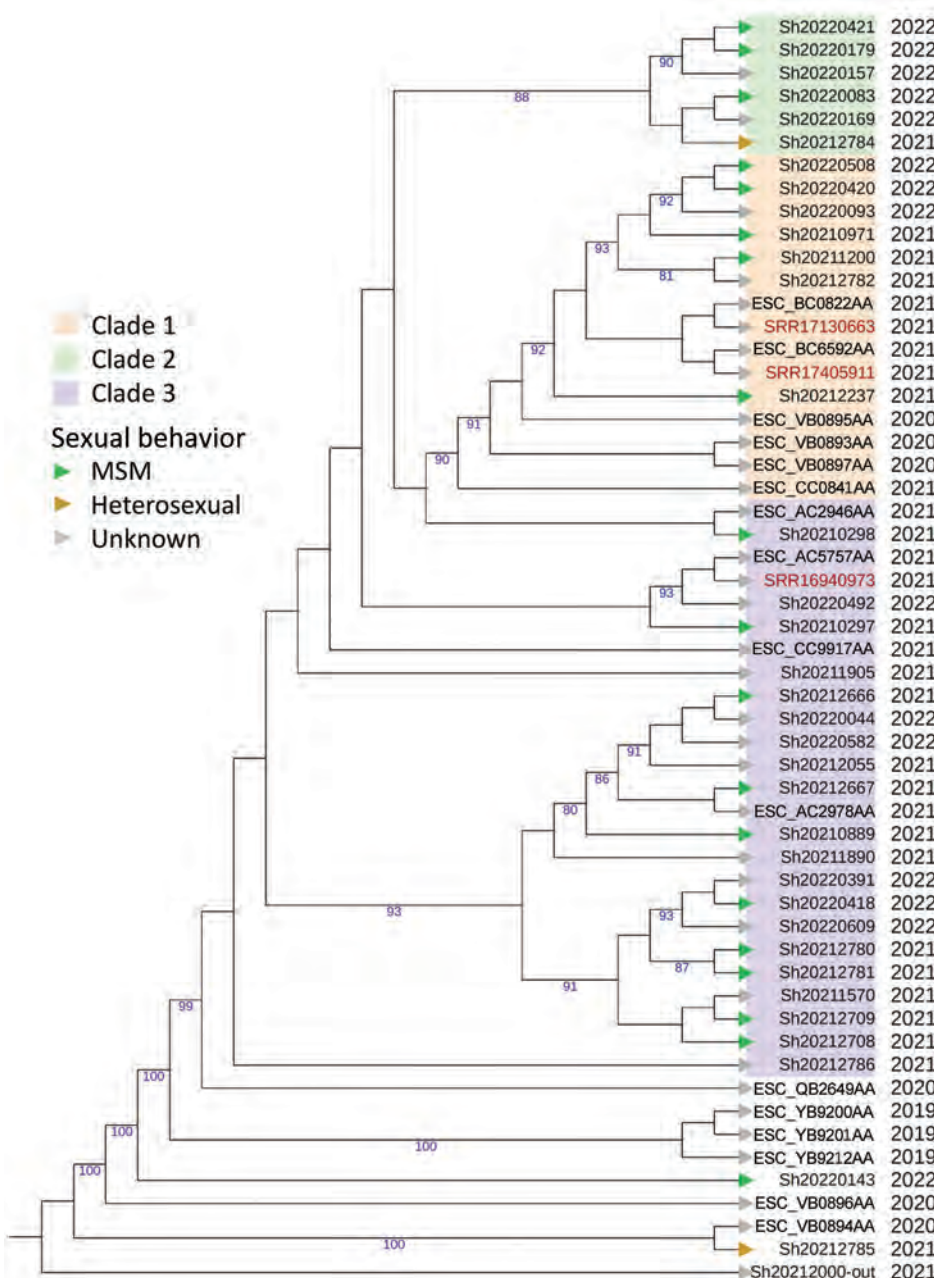


Figure. Phylogenetic analysis of ST152 isolates showing 2 clusters from an investigation of suspected multidrug-resistant *Shigella sonnei* in Spain.

Red text indicates reference sequences from the United Kingdom; blue text indicates assembly barcodes of ST152 feeding sequences available on Enterobase (<https://enterobase.warwick.ac.uk>) from 2019 to 2022. Green arrowheads indicate cases associated with MSM; green brackets connect known sexual partners. Orange arrowheads indicate cases in heterosexual persons (female or male); gray arrowheads indicate sexual behavior was unknown. A sequence from another sequence type was used as an outgroup. Numbers on branches indicate bootstrap values >80%. MSM, men who have sex with men; ST, sequence type.

identify chains of transmission and antibiotic resistance. Such efforts will be crucial in preventing further selection of antimicrobial resistance, avoiding possible treatment failures, and managing what might become a global outbreak.

Further monitoring of the situation in Spain, as well as in Europe, will be necessary to assess the extent of the circulation of XDR *S. sonnei*. Although more studies are needed to confirm the role of sexual transmission in Spain, communication campaigns, notably in HIV and preexposure prophylaxis clinics, could inform MSM on ways to minimize the risk of infection. Finally, alerting healthcare professionals to the role of sexual transmission in *S. sonnei* infections is critical for obtaining information on sexual history and identifying new cases, particularly in adult men with acute diarrhea.

Acknowledgments

We thank the Genomic and Bioinformatic departments of the National Center of Microbiology for their help with WGS and Kristina Zugazaga from the Hospital of Basurto for her technical support.

Financial support for this work came from the National Institute of Health Carlos III with the project Acción Estratégica de Salud Intramural (AESI; PI21CIII/00029).

About the Author

Dr. Jacqueline is a EUPHEM fellow (European Centre for Disease Prevention and Control, Stockholm, Sweden) working at the Instituto de Salud Carlos III in Madrid. Her primary research interests are public health microbiology, epidemiology, and outbreak investigation.

References

1. Charles H, Prochazka M, Thorley K, Crewdson A, Greig DR, Jenkins C, et al.; Outbreak Control Team. Outbreak of sexually transmitted, extensively drug-resistant *Shigella sonnei* in the UK, 2021–22: a descriptive epidemiological study. *Lancet Infect Dis*. 2022;22:1503–10. [https://doi.org/10.1016/S1473-3099\(22\)00370-X](https://doi.org/10.1016/S1473-3099(22)00370-X)
2. European Centre for Disease Prevention and Control. Increase in extensively-drug resistant *Shigella sonnei* infections in men who have sex with men in the EU/EEA and the UK—23 February 2022. Stockholm: The Centre; 2022.
3. Moreno-Mingorance A, Espinal P, Rodriguez V, Goterris L, Fàbrega A, Serra-Pladevall J, et al. Circulation of multi-drug-resistant *Shigella sonnei* and *Shigella flexneri* among men who have sex with men in Barcelona, Spain, 2015–2019. *Int J Antimicrob Agents*. 2021;58:106378. <https://doi.org/10.1016/j.ijantimicag.2021.106378>
4. Ortiz de la Rosa JM, Rodríguez-Villodres Á, Casimiro-Soriguer CS, Ruiz-Pérez De Pipaón M, Briones E, Aznar Fernández M, et al. MDR *Shigella sonnei* in Spain: an ever-evolving emerging threat? *JAC Antimicrob Resist*. 2022;4:dla090. <https://doi.org/10.1093/jacamr/dlac090>
5. González Donapetry P, Pescador Martín P, Gómez-Gil Mira R, Ruiz Carrascoso G. Imported infection by CTX-M-15 extended-spectrum beta-lactamase-producing *Shigella sonnei*. *Enferm Infecc Microbiol Clin (Engl Ed)*. 2019;37:141. <https://doi.org/10.1016/j.eimce.2018.03.009>
6. López-cerero L, Stolz E, Pulido M, Pascual A. Characterization of extended-spectrum β -lactamase-producing *Shigella sonnei* in Spain: expanding the geographic distribution of sequence type 152/CTX-M-27 clone. *Antimicrob Agents Chemother*. 2022;66:e0033422. <https://doi.org/10.1128/aac.00334-22>
7. Vecilla DF, Inchaurrea KZ, Aguirreb IL, del Arco JLD de T. Phenotypic and genotypic characterization of *Shigella sonnei* carrying the extended-spectrum beta-lactamase CTX-M-27. A report of two cases in Spain in men who have sex with men. *Enferm Infecc Microbiol Clin (Engl Ed)*. 2023;41:248–50. <https://doi.org/10.1016/j.eimce.2023.02.003>
8. Carattoli A, Zankari E, García-fernández A, Larsen V, Lund O, Villa L, Aarestrup M, Hasman H. In silico detection and typing of plasmids using Plasmidfinder and plasmid multilocus sequence typing. 2014;58:3895–903. <https://doi.org/10.1128/AAC.02412-14>
9. Bortolaia V, Kaas RS, Ruppe E, Roberts MC, Schwarz S, Cattoir V, et al. ResFinder 4.0 for predictions of phenotypes from genotypes. *J Antimicrob Chemother*. 2020;75:3491–500. <https://doi.org/10.1093/jac/dkaa345>
10. Zankari E, Allesøe R, Joensen KG, Cavaco LM, Lund O, Aarestrup FM. PointFinder: a novel web tool for WGS-based detection of antimicrobial resistance associated with chromosomal point mutations in bacterial pathogens. *J Antimicrob Chemother*. 2017;72:2764–8. <https://doi.org/10.1093/jac/dkx217>

Address for correspondence: Silvia Herrera León, Centro Nacional de Microbiología, Instituto de Salud Carlos III, Pozuelo Road, 28, 28222, Majadahonda, Madrid; email: sherrera@isciii.es

Severe *Rickettsia typhi* Infections, Costa Rica

Diana Chinchilla, Inés Sánchez, Ida Chung, Arlyn N. Gleaton, Cecilia Y. Kato

Author affiliations: Instituto Costarricense de Investigación y Enseñanza en Nutrición y Salud, Cartago, Costa Rica (D. Chinchilla, I. Sánchez); Centers for Disease Control and Prevention, Atlanta, Georgia, USA (I. Chung, A.N. Gleaton, C.Y. Kato)

DOI: <https://doi.org/10.3201/edi2911.221561>

Murine typhus is a febrile, fleaborne disease caused by infection with *Rickettsia typhi* bacteria. Cases can range from mild and nonspecific to fatal. We report 2 cases of murine typhus in Costa Rica, confirming the presence and circulation of *R. typhi* causing severe disease in the country.

Murine typhus is an acute febrile, fleaborne disease caused by infection with *Rickettsia typhi* bacteria. The initial symptoms are nonspecific and resemble those of other common bacterial and viral infections. Murine typhus is generally mild to moderate in severity and has a low case-fatality rate, especially in treated patients (1,2). In untreated patients, the case-fatality rate is reported to be 0.4%, and complications can occur in 6%–30% of patients (1).

In Costa Rica, cases of spotted fever group (SFG) rickettsiosis and Rocky Mountain spotted fever have been reported since 1950, and 6 species of *Rickettsia* have been identified (2,3). In Central America, there is serologic evidence of antibodies in humans against typhus group (TG) *Rickettsia* in El Salvador, Guatemala, Honduras, Nicaragua, and Panamá, but there are no serologic or molecular reports of *R. typhi* in Costa Rica (2). We report 2 cases of murine typhus in Costa Rica.

During 2015–January 2021, a total of 190 acute-phase clinical samples from patients suspected of having rickettsiosis, ehrlichiosis, Lyme disease, and other febrile illnesses were submitted to the Centro Nacional de Referencia de Bacteriología, Instituto Costarricense de Investigación y Enseñanza en Nutrición y Salud, Cartago, Costa Rica, for laboratory diagnosis. For rickettsial disease testing, we extracted DNA from whole blood, serum, swab specimens, or biopsy specimens collected <21 days from symptom onset within 3 days of collection by using the QIAamp DNA Mini Kit (QIAGEN, <https://www.qiagen.com>). We also used automated platforms (Seeprep12 and SGprep 32; Seegene, <https://www.seegene.com>) for extraction of blood and serum, according to the manufacturer's instructions.

We performed the *Rickettsia* genus-specific real-time PCR, PanR8, as described (4). We further



Figure. Location of 2 cases of murine typhus (colored circles), Costa Rica.

Table. Characteristics of 2 patients confirmed to have murine typhus, Costa Rica, 2019

Characteristic	Patient 1	Patient 2
Age, y/sex	30/M	46/F
Presumptive diagnosis upon arrival	Leptospirosis, ehrlichiosis	Lyme disease, brucellosis, dengue fever
Travel history	Visited Cocolos Beach on the Atlantic coast of Costa Rica	Not indicated
Days after onset of symptoms	Sample drawn within 7 d	Sample drawn within 9 d
Early symptoms	Fever, joint pain, myalgia, chills, headache, abdominal pain, dehydration, diarrhea, cough	Fever, chills, headache, vomiting, cough
Late symptoms	Jaundice, gum bleeding, multiple organ failure	Sepsis
Hospital ward	Admitted to intensive care unit, required mechanical ventilation	Admitted to infectious disease ward
Outcome	Recovered after 15 d treatment with doxycycline and tigecycline	Died from nosocomial pneumonia, septic shock, and renal failure (as stated in certificate of death)
Seroconversion in convalescent-phase sample*	No convalescent-phase sample	Titer of IgG against <i>Rickettsia typhi</i> 1:64

*By immunofluorescence for IgG against spotted fever group and typhus group *Rickettsia* (Fuller Laboratories, <http://www.fullerlabs.com>).

analyzed all 8 samples that tested positive with the PanR8 assay by using the RRI6 assay; a real-time PCR assay specific for *R. rickettsii* (causative agent of Rocky Mountain spotted fever) detection (4,5). We assessed amplicon size verification by using gel electrophoresis with the Qiaxcel Automated Platform (QIAGEN). We performed immunofluorescence-IgG (Fuller Laboratories, <http://www.fullerlabs.com>) when second samples were available.

A total of 104 coded samples were sent to the diagnostics laboratory of the Rickettsial Zoonoses Branch, Division of Vector-Borne Diseases, National Center for Emerging and Zoonotic Infectious Diseases, Centers for Control Disease and Prevention, for diagnostic testing to confirm results by using ≥ 1 of the following assays: PanR8 *Rickettsia* spp. real-time PCR (4), RCKr *Rickettsia* spp. real-time reverse transcription PCR (6), and RT27 and RT12 for *R. typhi* (*D. Chinchilla*, unpub. data). We attempted sequencing for all specimens that had positive results by using the 17kDa (TG and SFG) (7,8) and *ompA* (SFG) (9,10) gene targets.

We detected *Rickettsia* spp. nucleic acid in 8 samples (7.7%). Of those, 2 (1 whole blood and 1 serum) were identified as *R. typhi* (GenBank accession no LS992663.1) by sequencing of the 17-kDa gene targeting TG *Rickettsia*. The remaining 6 samples that were positive for *Rickettsia* spp. could not be further identified by sequencing, probably because of low copy numbers (Appendix, <https://wwwnc.cdc.gov/EID/article/29/11/22-1561-App1.pdf>). The samples corresponding to the 2 murine typhus cases were submitted in March and October 2019.

Both murine typhus patients required hospitalization and had severe disease develop. The patients lived in a rural area in Cartago, a province located in the Central Valley of Costa Rica (Figure). Both patients

had fever and moderate symptoms at the early stages but later progressed to severe disease (Table). One of the patients required admission to the intensive care unit and mechanical ventilation, and the other patient died of superimposed nosocomial pneumonia (Table). Neither patient had a rash, which occurs in up to 50% of the patients with murine typhus and is often considered suggestive of rickettsial disease. At hospital admission, both patients had fever of unknown origin, but rickettsiosis was not considered in the clinical diagnosis because of the lack of knowledge of the incidence of rickettsial disease in Costa Rica and the consideration that a rash is expected to occur.

We evaluated samples by using the PanR8 assay as part of the laboratory differential diagnosis assays performed for samples suspected of indicating a tickborne disease. Patient 1 was initially suspected of having leptospirosis or ehrlichiosis, and patient 2 was suspected of having Lyme disease, brucellosis, or dengue; all of those conditions are febrile diseases that have similar symptoms at early stages. Subsequent sequencing using 17-kDa TG primers identified *R. typhi* DNA within each sample. Patient 2 showed seroconversion to TG in a convalescent-phase sample (titer 1:64)

In conclusion, we report 2 cases of murine typhus in Costa Rica, confirm the presence of *R. typhi* by sequencing, and document the occurrence of severe disease. Our findings indicate that *R. typhi* is actively circulating in Costa Rica and is capable of causing severe disease. Early clinical and laboratory diagnosis of SFG and TG rickettsiosis in Costa Rica will ensure timely treatment to prevent complications and deaths. Laboratory confirmation of the specific rickettsial agent is also critical to support epidemiologic interventions, including vector control and community and physician education.

Acknowledgment

We thank Saúl Rodríguez Sánchez for his work in detection of rickettsiosis cases in the province of Cartago and for his collaboration in obtaining clinical information from the patients, which enables improving the epidemiologic surveillance and diagnosis of rickettsial diseases in Costa Rica.

About the Author

Dr. Chinchilla is a microbiologist in the Laboratory of Febrile Zoonotic Diseases of the National Reference Center of Bacteriology, Cartago, Costa Rica. Her primary research interest is implementation of methods and protocols to improve the diagnosis and epidemiologic surveillance of bacterial zoonoses in the country.

References

1. Doppler JF, Newton PN. A systematic review of the untreated mortality of murine typhus. *PLoS Negl Trop Dis.* 2020;14:e0008641. <https://doi.org/10.1371/journal.pntd.0008641>
2. Bermúdez CS, Troyo A. A review of the genus *Rickettsia* in Central America. *Res Rep Trop Med.* 2018;9:103–12. <https://doi.org/10.2147/RRTM.S160951>
3. Troyo A, Moreira-Soto RD, Calderon-Arguedas Ó, Mata-Somarrivas C, Ortiz-Tello J, Barbieri AR, et al. Detection of rickettsiae in fleas and ticks from areas of Costa Rica with history of spotted fever group rickettsioses. *Ticks Tick Borne Dis.* 2016;7:1128–34. <https://doi.org/10.1016/j.ttbdis.2016.08.009>
4. Kato CY, Chung IH, Robinson LK, Austin AL, Dasch GA, Massung RF. Assessment of real-time PCR assay for detection of *Rickettsia* spp. and *Rickettsia rickettsii* in banked clinical samples. *J Clin Microbiol.* 2013;51:314–7. <https://doi.org/10.1128/JCM.01723-12>
5. Kato C, Chung I, Paddock C. Estimation of *Rickettsia rickettsii* copy number in the blood of patients with Rocky Mountain spotted fever suggests cyclic diurnal trends in bacteraemia. *Clin Microbiol Infect.* 2016;22:394–6. <https://doi.org/10.1016/j.cmi.2015.12.019>
6. Chung IH, Robinson LK, Stewart-Juba JJ, Dasch GA, Kato CY. Analytically sensitive *Rickettsia* species detection for laboratory diagnosis. *Am J Trop Med Hyg.* 2022;106:1352–7. <https://doi.org/10.4269/ajtmh.21-0757>
7. Massung RF, Davis LE, Slater K, McKechnie DB, Puerzer M. Epidemic typhus meningitis in the southwestern United States. *Clin Infect Dis.* 2001;32:979–82. <https://doi.org/10.1086/319351>
8. Tzianabos T, Anderson BE, McDade JE. Detection of *Rickettsia rickettsii* DNA in clinical specimens by using polymerase chain reaction technology. *J Clin Microbiol.* 1989;27:2866–8. <https://doi.org/10.1128/jcm.27.12.2866-2868.1989>
9. Regnery RL, Spruill CL, Plikaytis BD. Genotypic identification of rickettsiae and estimation of intraspecies sequence divergence for portions of two rickettsial genes. *J Bacteriol.* 1991;173:1576–89. <https://doi.org/10.1128/jb.173.5.1576-1589.1991>
10. Paddock CD, Sumner JW, Comer JA, Zaki SR, Goldsmith CS, Goddard J, et al. *Rickettsia parkeri*: a newly recognized cause

of spotted fever rickettsiosis in the United States. *Clin Infect Dis.* 2004;38:805–11. <https://doi.org/10.1086/381894>

Address for correspondence: Diana Chinchilla, Centro Nacional de Referencia de Bacteriología National Reference Center of Bacteriology, Instituto Costarricense de Investigación y Enseñanza en Nutrición y Salud, La Unión, Cartago, Costa Rica; email: dchinchilla@inciensa.sa.cr

New SARS-CoV-2 Omicron Variant with Spike Protein Mutation Y451H, Kilifi, Kenya, March–May 2023

Mike J. Mwanga,¹ Arnold W. Lambisia,¹ John Mwita Morobe,¹ Nickson Murunga,¹ Edidah Moraa, Leonard Ndwiwa, Robinson Cheruiyot, Jennifer Musyoki, Martin Mutunga, Laura M. Guzman-Rincon, Charles Sande, Joseph Mwangangi, Philip Bejon, Lynette Isabella Ochola-Oyier, D. James Nokes, Charles N. Agoti, Joyce Nyiro, George Githinji

Author affiliations: Kenya Medical Research Institute Wellcome Trust Research Programme, Kilifi, Kenya (M.J. Mwanga, A.W. Lambisia, J.M. Morobe, N. Murunga, E. Moraa, L. Ndwiwa, R. Cheruiyot, J. Musyoki, M. Mutunga, C. Sande, J. Mwangangi, P. Bejon, L.I. Ochola-Oyier, D.J. Nokes, C.N. Agoti, J. Nyiro, G. Githinji); University of Warwick, Coventry, UK (L.M. Guzman-Rincon, D.J. Nokes); Pwani University, Kilifi (C.N. Agoti, G. Githinji)

DOI: <https://doi.org/10.3201/eid2911.230894>

We report a newly emerged SARS-CoV-2 Omicron subvariant FY.4 that has mutations Y451H in spike and P42L in open reading frame 3a proteins. FY.4 emergence coincided with increased SARS-CoV-2 cases in coastal Kenya during April–May 2023. Continued SARS-CoV-2 genomic surveillance is needed to identify new lineages to inform COVID-19 outbreak prevention.

As of August 2023, >340,000 test-confirmed COVID-19 cases and 5,689 COVID-19-related deaths had been reported in Kenya (1). Seropositivity

¹These authors contributed equally to this article.

rates in rural and urban populations were high, and vaccine uptake was low ($\approx 28\%$ of the adult population received ≥ 1 dose) (2). By August 2022, a total of 69%–81% of rural (Kilifi and Siaya) and 89%–95% of urban (Nairobi and Kisumu) adults in Kenya had IgG against the SARS-CoV-2 spike protein (3).

Genomic surveillance is critical to determine origins of new waves, evolution, and spread patterns of SARS-CoV-2. As of June 2023, a total of 7 distinct waves of SARS-CoV-2 infections have been

observed in Kenya (1; G. Githinji et al., unpub. data, <https://doi.org/10.1101/2022.10.26.22281446>). The last 3 waves were dominated by Omicron BA.1-like, BA.5-like, and BQ-like lineages (in that order), associated with increases in SARS-CoV-2 cases because of virus mutations that conferred transmission advantage or escape from preexisting immunity (4).

In coastal Kenya, the Kenya Medical Research Institute Wellcome Trust Research Programme is conducting SARS-CoV-2 genomic surveillance

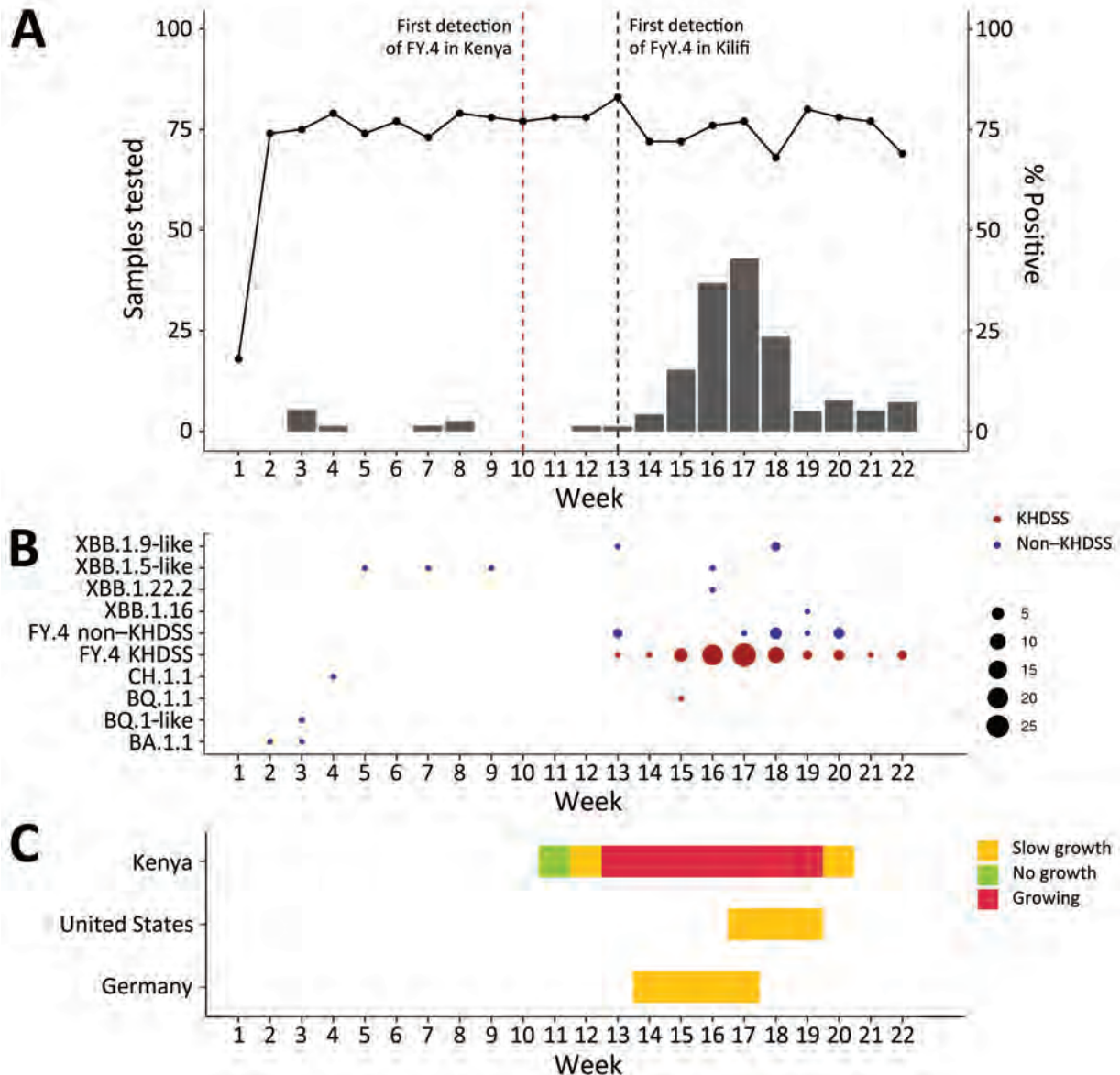


Figure. Number of positive samples, distribution, and growth rate for new SARS-CoV-2 Omicron variant with spike protein mutation Y451H, Kilifi, Kenya, March–May 2023. The x axes indicate calendar weeks beginning on January 1, 2023. A) Weekly number of collected samples (black data line) and positive SARS-CoV-2 cases (data bars) in health facilities within the KHDSS during January–May 2023. Vertical dotted lines indicate the weeks when the FY.4 lineage was first detected in Kenya (red) and Kilifi (black). B) Weekly distribution of SARS-CoV-2 lineages observed in samples processed at the Kenya Medical Research Institute Wellcome Trust Research Programme from KHDSS (red dots) and non-KHDSS (blue dots) health facilities during January–May 2023. C) Growth rate estimates for the Omicron FY.4 variant in Kenya relative to those in the United States and Germany. KHDSS, Kilifi Health Demographic Surveillance System.

Table. Clinical signs and symptoms for patients infected with SARS-CoV-2 Omicron FY.4 variant with spike protein mutation Y451H, Kilifi Health Demographic Surveillance System, Kilifi, Kenya, January–May 2023*

Signs/symptoms	No. (%) patients
Fever	
Yes	57 (78.1)
No	16 (21.9)
Cough	
Yes	72 (98.6)
No	1 (1.4)
Nasal discharge	
Yes	54 (74.0)
No	19 (26.0)
Difficulty breathing	
Yes	5 (6.8)
No	68 (93.2)
Sore throat	
Yes	28 (38.4)
No	45 (61.6)
Body malaise	
Yes	25 (34.2)
No	48 (65.8)
Conscious level	
Alert	73 (100.0)
COVID-19 vaccination status	
Yes	12 (16.4)
No	60 (82.2)
No data	1 (1.4)
COVID19 vaccine doses	
1	3 (4.1)
2	7 (9.6)
No data	63 (86.3)

*Total number of patients was 73.

across 5 health facilities within the Kilifi Health and Demographic Surveillance System (KHDSS) (5). Up to 75 respiratory samples are collected weekly from persons of all ages with acute respiratory illness at participating health facilities. SARS-CoV-2 reverse transcription PCR and sequencing are performed on virus-positive samples from KHDSS health facilities and other collaborating health facilities across Kenya.

SARS-CoV-2 positivity rates in KHDSS health facilities increased from 1.2% during the week beginning March 27, 2023, to 42.9% during the week beginning April 24, 2023 (Figure, panel A). After dropping to 23.5% during the first week of May, rates remained at 5.0%–7.7% over the next 3 weeks.

During January–May, a total of 120 (7.4%) of 1,612 samples collected from KHDSS health facilities were positive for SARS-CoV-2. We sequenced 96 (80%) of 120 samples that had PCR cycle threshold values <35 by using GridION (Oxford Nanopore Technologies, <https://www.nanoporetech.com>) (n = 35) or MiSeq (Illumina, <https://www.illumina.com>) (n = 61) instruments; we recovered 76 (79%) genomes with ≥70% coverage. We also received 39 SARS-CoV-2–positive samples from health facilities

outside the KHDSS and sequenced 32 (82%) of them, yielding 25 (78%) genomes (Appendix Table, <https://wwwnc.cdc.gov/EID/article/29/11/23-0894-App1.pdf>).

We assigned the 76 genomes from KHDSS health facilities to 2 lineages: BQ.1.1 (n = 1) and FY.4 (n = 75). The SARS-CoV-2 infection rate increase observed in late March coincided with detection of the new Omicron FY.4 lineage (Figure, panel B). In Kenya, FY.4 was first observed in Lamu County (n = 6) on March 10, 2023 (Figure, panel A); in KHDSS, FY.4 was first identified from samples collected on March 27 and, in April and May, it became the dominant lineage, representing 98% of all SARS-CoV-2 cases. By May 31, according to the GISAID database (<https://www.gisaid.org>), FY.4 had been detected in 4 other counties: Mombasa (n = 2), Narok (n = 2), Nairobi (n = 7), and Kiambu (n = 31). The FY.4 subvariant has since been detected in Austria, Belgium, Germany, Italy, India, Sweden, Canada, France, China, Australia, Spain, the United Kingdom, and the United States (6).

In KHDSS health facilities, patients infected with FY.4 had cough (98%), fever (78%), and nasal discharge (74%); 7% had difficulty breathing (Table). Only 13 (16%) participants reported receiving ≥1 dose of a COVID-19 vaccine. A serosurveillance study (February–June 2022) found that 67% of unvaccinated KHDSS health facility residents had SARS-CoV-2 IgG, indicating a high percentage of this population might have been naturally infected (3).

Compared with other Omicron lineages, FY.4 had 2 amino acid mutations, Y451H in the spike protein and P42L in the open reading frame (ORF) 3a protein. The effect of the Y451H change is unknown; however, an L452R mutation in the receptor-binding domain of the spike protein (near the Y451H site) increased virus infectivity and fusogenicity by enhancing spike stability and cleavage (7). Changes within ORF3a epitopes can cause complete loss of CD8+ T-cell recognition of ancestral SARS-CoV-2 lineages and Alpha variant (8).

We applied a Bayesian hierarchical model (9) to estimate the growth rate of FY.4-like lineages in Kenya. Growth estimates serve as an epidemic warning system for lineages that have consistent increases in frequency for ≥2 consecutive weeks. We compared growth rate estimates from Kenya with those from Germany and the United States, the only other countries reporting FY.4 cases for ≥2 consecutive weeks during the last weeks of May 2023 (Figure, panel C). The model warned of a high epidemic potential in Kenya from March 26 through May, suggesting continued increases in cases attributed to the FY.4 lineage.

In conclusion, we detected emergence of a new Omicron lineage with unique spike and ORF3a gene mutations in coastal Kenya by using SARS-CoV-2 genomic surveillance. FY.4 subvariant detection coincided with an increase in SARS-CoV-2 cases in Kilifi. FY.4 was also detected in other parts of Kenya, and growth estimates suggest potential for continued spread of the FY.4 subvariant. Continued SARS-CoV-2 genomic surveillance is critical for identifying new lineages to inform COVID-19 prevention measures.

Acknowledgments

We thank the laboratories, hospitals, and organizations that shared specimens for sequencing at the Kenya Medical Research Institute Wellcome Trust Research Programme and submitting laboratories that generated and shared genetic sequence data via the GISAID Initiative (<https://www.gisaid.org>), on which this research is based. Submitting and originating laboratories that generated the GISAID data used in this study are listed at <https://doi.org/10.55876/gis8.230627zw>. Genome sequences generated in this study are available in the GISAID's EpiCoV database. The dataset and analysis scripts used are available in the Harvard Dataverse repository (<https://doi.org/10.7910/DVN/ZMGR5P>). The whole-genome sequencing study protocol was reviewed and approved by the Scientific and Ethics Review Committee at the Kenya Medical Research Institute headquarters in Nairobi, Kenya (SERU no. 4035).

This work was supported by the New Variant Assessment Programme, a UK Health Security Agency program funded by the UK Department of Health and Social Care as a global initiative to strengthen genomic surveillance for pandemic preparedness and response to emerging and priority infectious diseases; the UK National Institute for Health and Care Research (project references 17/63/82 and 16/136/33) that uses aid from the UK government to support global health research; UK Foreign, Commonwealth and Development Office, and The Wellcome Trust, UK (grant nos. 220985/Z/20/Z and 226002/A/22/Z).

The views expressed in this publication are those of the author(s) and not necessarily those of National Institute for Health and Care Research, Department of Health and Social Care, or the Foreign Commonwealth and Development Office, Africa Centers for Disease Control, World Health Organization Africa, or African Society for Laboratory Medicine.

About the Author

Mr. Mwangi is a research assistant at Kenya Medical Research Institute Wellcome Trust Research Programme. His research focuses on leveraging epidemiologic and genomic sequence data to investigate virus evolution, transmission, and spread in human populations to inform effective control and intervention strategies.

References

1. Our World in Data. Coronavirus pandemic (COVID-19) [cited 2023 Aug 24]. <https://ourworldindata.org/coronavirus>
2. World Health Organization. WHO coronavirus (COVID-19) vaccination dashboard. 2023 [cited 2023 Aug 24]. <https://www.afro.who.int/health-topics/coronavirus-covid-19/vaccines>
3. Kagucia EW, Ziraba AK, Nyagwange J, Kutima B, Kimani M, Akech D, et al. SARS-CoV-2 seroprevalence and implications for population immunity: evidence from two Health and Demographic Surveillance System sites in Kenya, February–December 2022. *Influenza Other Respir Viruses*. 2023;17:e13173. <https://doi.org/10.1111/irv.13173>
4. He Q, Wu L, Xu Z, Wang X, Xie Y, Chai Y, et al. An updated atlas of antibody evasion by SARS-CoV-2 Omicron sub-variants including BQ.1.1 and XBB. *Cell Rep Med*. 2023;4:100991. <https://doi.org/10.1016/j.xcrm.2023.100991>
5. Scott JAG, Bauni E, Moisi JC, Ojal J, Gatakaa H, Nyundo C, et al. Profile: the Kilifi Health and Demographic Surveillance System (KHDSS). *Int J Epidemiol*. 2012;41:650–7. <https://doi.org/10.1093/ije/dys062>
6. Shu Y, McCauley J. GISAID: global initiative on sharing all influenza data—from vision to reality. *Euro Surveill*. 2017;22:30494. <https://doi.org/10.2807/1560-7917.ES.2017.22.13.30494>
7. Motozono C, Toyoda M, Zahradnik J, Saito A, Nasser H, Tan TS, et al.; Genotype to Phenotype Japan (G2P-Japan) Consortium. SARS-CoV-2 spike L452R variant evades cellular immunity and increases infectivity. *Cell Host Microbe*. 2021;29:1124–1136.e11. <https://doi.org/10.1016/j.chom.2021.06.006>
8. de Silva TI, Liu G, Lindsey BB, Dong D, Moore SC, Hsu NS, et al.; COVID-19 Genomics UK (COG-UK) Consortium; ISARIC4C Investigators. The impact of viral mutations on recognition by SARS-CoV-2 specific T cells. *iScience*. 2021;24:103353. <https://doi.org/10.1016/j.isci.2021.103353>
9. Guzmán-Rincón LM, Hill EM, Dyson L, Tildesley MJ, Keeling MJ. Bayesian estimation of real-time epidemic growth rates using Gaussian processes: local dynamics of SARS-CoV-2 in England. *J R Stat Soc Ser C Appl Stat*. In press 2023. <https://doi.org/10.1093/jrssc/qlad056>

Address for correspondence: George Githinji, KEMRI-Wellcome Trust Research Programme, Hospital Road, PO Box 230, Kilifi, Kenya; email: ggithinji@kemri-wellcome.org

Genomic Sequencing Surveillance to Identify Respiratory Syncytial Virus Mutations, Arizona, USA

LaRinda A. Holland,¹ Steven C. Holland,¹ Matthew F. Smith, Victoria R. Leonard, Vel Murugan, Lora Nordstrom, Mary Mulrow, Raquel Salgado, Michael White, Efreem S. Lim

Author affiliations: Arizona State University, Tempe, Arizona, USA (L.A. Holland, S.C. Holland, M.F. Smith, V.R. Leonard, V. Murugan, E.S. Lim); Valleywise Health, Phoenix, Arizona, USA (L. Nordstrom, M. Mulrow, R. Salgado, M. White)

DOI: <https://doi.org/10.3201/eid2911.230836>

We conducted surveillance of respiratory syncytial virus (RSV) genomic sequences for 100 RSV-A and 27 RSV-B specimens collected during November 2022–April 2023 in Arizona, USA. We identified mutations within prefusion F-protein antigenic sites in both subtypes. Continued genomic surveillance will be critical to ensure RSV vaccine effectiveness.

Respiratory syncytial virus (RSV), an RNA virus of the family Pneumoviridae, causes acute respiratory infections, primarily in children, adults with severe lung disease, and elderly persons (1). The United States experienced an early surge in RSV cases during the 2022–2023 respiratory pathogen season, coinciding with high levels of influenza and SARS-CoV-2 infections (2). In Arizona, USA, numbers of laboratory-confirmed RSV cases increased beginning in September 2022, peaked in mid-November 2022, and then declined to average levels by March 2023 (Figure, panel A).

The 2 major RSV subtypes, RSV-A and RSV-B, have distinct antigenic characteristics in the P, N, F, and G proteins (1). Each subtype is classified into genotypes based on sequence variability in the G protein (3). According to sequencing data from the GISAID database (4), global distribution of RSV genotypes during 2022–2023 was split between the GA2.3.5 genotype of RSV-A and the GB5.0.5a genotype of RSV-B (Figure, panel B). However, RSV vaccines are based on the prefusion conformation of the F protein. Because surveillance efforts should focus on whole-genome sequencing to better understand the evolution of the virus and its potential effect on vaccine efficacy, we conducted surveillance of genomic sequences from

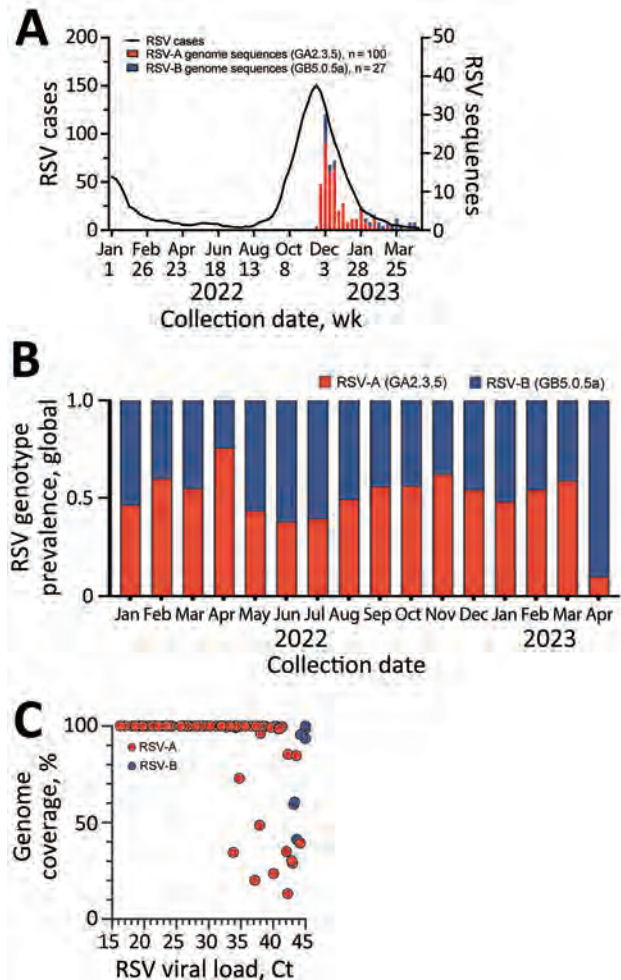


Figure. Genomic sequencing analysis of RSV in Arizona, USA, 2022–2023. A) Five-week moving average of PCR-confirmed RSV detections in Arizona reported to the National Respiratory and Enteric Virus Surveillance System and RSV sequence counts by genotype obtained for specimens used in this study. B) Relative abundance of RSV-A and RSV-B genotypes shown for all RSV genomes (RSV-A, n = 1,047; RSV-B, n = 941) deposited in GISAID (<https://www.gisaid.org>) with collection dates January 1, 2022–May 1, 2023, including genotypes obtained for specimens used in this study (RSV-A n = 100; RSV-B, n = 27). C) Reverse transcription PCR Ct values and genome coverage for RSV-A and RSV-B samples. Ct, cycle threshold; RSV, respiratory syncytial virus.

RSV-A and -B subtypes to identify genetic mutations. This study was approved by the Arizona State University Institutional Review Board (STUDY00011967).

We tested 127 RSV-positive nasopharyngeal swabs from previous standard-of-care respiratory pathogen testing at Valleywise Health Medical Center, which serves Maricopa County, Arizona, USA. Patients were a median of 22 years of age (interquartile range 2–44 years). We performed genomic surveillance to determine RSV strains circulating in Arizona during the 2022–2023 season. We per-

¹These first authors contributed equally to this article.

formed 2 × 150-bp paired-end next-generation sequencing using a hybrid capture enrichment panel (Illumina Respiratory Virus Oligo Panel version 2, <https://www.illumina.com>). We used Trim Galore version 0.6.10 (<https://github.com/FelixKrueger/TrimGalore>) to quality filter and adaptor trim sequencing reads, mapped the reads to RSV-A and RSV-B reference sequences (GISAID accession nos. EPI_ISL_412866 and EPI_ISL_165399) using Burrows-Wheeler Aligner version 0.7.17-r1188 (<https://bio-bwa.sourceforge.net>), and generated consensus sequences using SAMtools version 1.17 (<https://github.com/samtools/samtools/releases>). We assembled 92 RSV-A (GA2.3.5 genotype) and 24 RSV-B (GB5.0.5a genotype) complete genome sequences and 8 RSV-A (GA2.3.5) and 3 RSV-B (GB5.0.5a) partial genome sequences (GenBank accession nos. OR143134–250; GISAID accession nos. EPI_ISL_17808760–814) (Figure, panel A).

To determine RSV viral load, we performed quantitative reverse transcription PCR using pan-HRSV assays that recognize both subtypes RSV-A and RSV-B (5). The mean RSV cycle threshold (Ct) value was 29.83 (SD 7.44). We found that specimens with viral load Ct ≤33 yielded 99%–100% genome coverage (Figure, panel C). Whole-genome phylogenetic analysis (Nextclade version 2.14.1, <https://clades.nextstrain.org>) showed that RSV-A sequences from Arizona clustered in clade GA2.3.5, indicating ≥3 independent introductions of RSV-A into Arizona (Appendix Figure 1, <https://wwwnc.cdc.gov/EID/article/29/11/23-0836-App1.pdf>). RSV-B sequences from Arizona formed a monophyletic group in clade GB5.0.5a, indicating a single introduction of strains locally transmitted within the state (Appendix Figure 1). Our findings were consistent with RSV investigations in Massachusetts (6) and Washington

(7), USA, both of which suggested the atypical increase in cases during the 2022–2023 season resulted from multiple introductions of extant lineages, not a divergent RSV lineage with increased virulence or transmissibility.

The US Food and Drug Administration has approved 2 RSV vaccines for persons ≥60 years of age, both based on the RSV prefusion F protein. Arexvy (GlaxoSmithKline, <https://www.gsk.com>) is monovalent and Abrysvo (Pfizer, <https://www.pfizer.com>), bivalent (8,9). Most host antibodies target 6 antigenic sites (Ø–V) of the F protein (10). Within the F-gene sequences from RSV genomes from Arizona, we identified 7 nonsynonymous substitutions in antigenic sites I, II, IV, and V of RSV-A and 5 nonsynonymous substitutions in antigenic sites Ø, I, II, and V of RSV-B. We found each RSV-A genome mutation in <10% of samples. Most RSV-B genome mutations were more frequent; we found only 1 rare single-nucleotide polymorphism. Mutation frequencies were comparable with trends in recent global RSV genome sequences (Table). RSV-B S190N, S211N, and S389P mutations specifically have become increasingly dominant since 2020. Mutability at residue 389 was shared between subtypes, and each subtype had a preferential amino acid. Finally, we located the mutated residues on the prefusion F-protein crystal structure (protein data bank 7KQD). Many mutated residues were exposed on the F protein surface, suggesting they might interfere with antibody recognition (Appendix Figure 2).

Although RSV remains a substantial clinical burden, approved RSV vaccines reduce the risk of lower respiratory tract illness. By tracking RSV evolution, we can improve design of vaccine formulations to improve effectiveness. Our study was limited because we lacked understanding of potential functional

Table. Nonsynonymous amino acid substitutions in RSV-A and RSV-B F protein antigenic sites found in genome sequences in Arizona, USA, during 2022–2023 compared with GISAID global genome sequences*

Mutation	Antigenic site	Global frequency, no. (%)				Arizona frequency, † no. (%)
		2020	2021	2022	2023†	
RSV-A		n = 967	n = 1,144	n = 740	n = 115	n = 92
I57V	V	0	0	19 (3)	1 (1)	2 (2)
I59V	V	2 (<1)	1 (<1)	0	0	1 (1)
S276N	II	29 (3)	51 (4)	142 (19)	14 (12)	4 (4)
V379A	I	0	0	1 (<1)	0	8 (9)
L381I	I	0	0	0	0	1 (1)
P389S	I	0	5 (<1)	3 (<1)	0	2 (2)
K470R	IV	0	0	0	0	1 (1)
RSV-B		n = 305	n = 812	n = 720	n = 126	n = 24
R42K	I	1 (<1)	15 (2)	61 (8)	16 (13)	18 (75)
S190N	V	9 (3)	191 (24)	400 (56)	116 (92)	24 (100)
S211N	Ø	1 (<1)	195 (24)	399 (55)	116 (92)	24 (100)
E378D	III	1 (<1)	0	0	0	2 (8)
S389P	I	0	193 (24)	412 (57)	116 (92)	24 (100)

*GISAID, <https://www.gisaid.org>; RSV, respiratory syncytial virus.

†Through April 30, 2023.

consequences from mutations in F-protein antigenic sites. Although the G protein is under greater selective pressure and has higher mutation rates (3), observing its evolutionary trajectory in context with the F protein will be critical. Our study demonstrates the value of using whole-genome sequencing to identify genetic mutations in respiratory pathogens, including RSV, to ensure ongoing effectiveness of RSV vaccines.

Acknowledgments

We gratefully acknowledge Sarah Namdarian for assistance with collecting clinical specimens; Alexis Thomas, Gabrielle Hernandez Barrera, Michelle Tan for assistance with specimen processing; and Regan Sullins for assistance with constructing the resource library. We thank the authors from originating laboratories responsible for obtaining the specimens and the submitting laboratories where genetic sequence data were generated and shared through GISAID (<https://www.gisaid.org>) and GenBank.

This study was supported in part by Arizona State University and the Centers for Disease Control and Prevention (CDC BAA 75D30121C11084).

Contributions: conceptualization: E.S.L.; formal analysis: L.A.H., S.C.H., M.F.S., V.R.L.; investigation: L.A.H., S.C.H., M.F.S., V.R.L., E.S.L.; resources: V.M., L.N., M.M., R.S., M.W.; data curation: L.A.H., S.C.H., M.F.S., V.R.L.; writing, original draft: L.A.H., S.C.H., M.F.S., E.S.L.; writing, review and editing: L.A.H., S.C.H., M.F.S., L.N., E.S.L.; supervision: E.S.L.; funding acquisition: E.S.L. All authors reviewed and approved the final manuscript.

About the Author

Mrs. Holland is a research specialist at Arizona State University under the supervision of Dr. Efreim Lim. Her primary research interests are viral diseases and infections and how they influence viromes and microbiomes in human health.

References

1. Tin Tin Htar M, Yerramalla MS, Moisi JC, Swerdlow DL. The burden of respiratory syncytial virus in adults: a systematic review and meta-analysis. *Epidemiol Infect.* 2020;148:e48. <https://doi.org/10.1017/S0950268820000400>
2. Centers for Disease Control and Prevention. Increased respiratory virus activity, especially among children, early in the 2022–2023 fall and winter [cited 2023 Jun 16]. <https://emergency.cdc.gov/han/2022/han00479.asp#print>
3. Muñoz-Escalante JC, Comas-García A, Bernal-Silva S, Robles-Espinoza CD, Gómez-Leal G, Noyola DE. Respiratory syncytial virus A genotype classification based on systematic intergenotypic and intragenotypic sequence analysis. *Sci Rep.* 2019;9:20097. <https://doi.org/10.1038/s41598-019-56552-2>

4. Khare S, Gurry C, Freitas L, Schultz MB, Bach G, Diallo A, et al. GISAID's role in pandemic response. *China CDC Wkly.* 2021;3:1049–51. <https://doi.org/10.46234/ccdcw2021.255>
5. Wang L, Piedra PA, Avadhanula V, Durigon EL, Machabishvili A, López MR, et al. Duplex real-time RT-PCR assay for detection and subgroup-specific identification of human respiratory syncytial virus. *J Virol Methods.* 2019; 271:113676. <https://doi.org/10.1016/j.jviromet.2019.113676>
6. Adams G, Moreno GK, Petros BA, Uddin R, Levine Z, Kotzen B, et al. Viral lineages in the 2022 RSV surge in the United States. *N Engl J Med.* 2023;388:1335–7. <https://doi.org/10.1056/NEJMc2216153>
7. Goya S, Sereewit J, Pfalmer D, Nguyen TV, Bakhsh SAKM, Sobolik EB, et al. Genomic characterization of respiratory syncytial virus during 2022–23 outbreak, Washington, USA. *Emerg Infect Dis.* 2023;29:865–8. <https://doi.org/10.3201/eid2904.221834>
8. Papi A, Ison MG, Langley JM, Lee D-G, Leroux-Roels I, Martinon-Torres F, et al.; AReSVi-006 Study Group. Respiratory syncytial virus prefusion F protein vaccine in older adults. *N Engl J Med.* 2023;388:595–608. <https://doi.org/10.1056/NEJMoa2209604>
9. Kampmann B, Madhi SA, Munjal I, Simões EAF, Pahud BA, Llapur C, et al.; MATISSE Study Group. Bivalent prefusion F vaccine in pregnancy to prevent RSV illness in infants. *N Engl J Med.* 2023;388:1451–64. <https://doi.org/10.1056/NEJMoa2216480>
10. Gilman MS, Castellanos CA, Chen M, Ngwuta JO, Goodwin E, Moin SM, et al. Rapid profiling of RSV antibody repertoires from the memory B cells of naturally infected adult donors. *Sci Immunol.* 2016;1:eaaj1879.

Address for correspondence: Efreim S. Lim, Arizona State University, PO Box 876101, Tempe, AZ 85287, USA; email: Efreim.Lim@asu.edu

Domestically Acquired NDM-1–Producing *Pseudomonas aeruginosa*, Southern California, USA, 2023

Hannah K. Gray, Omer E. Beard, Ethan A. Smith, Joanna M. Schaenman, Shangxin Yang

Author affiliation: University of California, Los Angeles, California, USA

DOI: <https://doi.org/10.3201/eid2911.230646>

We describe a case of New Delhi metallo- β -lactamase 1–producing carbapenem-resistant *Pseudomonas aeruginosa* (CRPA) in a transplant patient with multiple hospitalizations in California, USA. Whole-genome sequencing revealed the isolate was genetically distinctive, despite $\approx 95\%$ similarity to other global strains. The patient's lack of international travel suggests this CRPA was acquired domestically.

Carbapenem-resistant *Pseudomonas aeruginosa* (CRPA) is increasing worldwide and has up to 30% prevalence in US *P. aeruginosa* isolates (1). The Antimicrobial Resistance Laboratory Network reported 280 carbapenemase-producing CRPA in 2021, most commonly Verona integron metallo- β -lactamase (Centers for Disease Control and Prevention, <https://arpsp.cdc.gov/profile/arln/crpa>). New Delhi metallo- β -lactamase (NDM)–producing CRPA is prevalent in Eurasia and the Middle East. Sporadic NDM CRPA cases linked to international travel have been reported in the United States, the earliest of which was identified in Delaware in 2014 (2). We describe a case of NDM CRPA in southern California.

A previously healthy patient in his 50s was admitted to a hospital in Riverside County, California, in 2023 with cardiogenic shock secondary to new onset nonischemic cardiomyopathy. He was briefly admitted to the same hospital a few weeks earlier because of chest pain and dyspnea. He had no other healthcare exposures and had only traveled briefly to Hawaii earlier that year.

Shortly after the second admission, the patient experienced cardiac arrest, was cannulated for extracorporeal life support, and was transferred to Ronald Reagan UCLA Medical Center for heart transplant evaluation. Admission blood cultures grew *Bacillus cereus*, attributed to gastrointestinal translocation. The patient received vancomycin, resulting in bacteremia clearance, and empiric piperacillin/tazobactam for gram-negative bacteria coverage. Four days pretransplant, hypotension and leukocytosis worsened, and antimicrobial therapy was empirically changed to meropenem and amikacin. A urine culture sent during sepsis evaluation grew *P. aeruginosa*. On the basis of susceptibility testing results, cefiderocol was initiated; the patient received heart and kidney transplants the next day. Cefiderocol was continued for 6 days posttransplant; subsequent urine cultures were negative. *P. aeruginosa* was not isolated from other blood or respiratory cultures.

Initial susceptibility testing of the urine isolate revealed extensive resistance to carbapenems,

aminoglycosides, fluoroquinolones, and cephalosporins, except cefiderocol (Appendix, <https://wwwnc.cdc.gov/EID/article/29/11/23-0646-App1.xlsx>). Rapid Carba-5 (Hardy Diagnostics, <https://hardydiagnostics.com>) testing detected NDM. We performed whole-genome sequencing by using MiSeq (Illumina, <https://www.illumina.com>) and assembled reads de novo by using CLC Genomics Workbench (QIAGEN, <https://www.qiagen.com>). We submitted tentative assemblies to the Comprehensive Antibiotic Resistance Database Resistance Gene Identifier tool (<https://card.mcmaster.ca/analyze/rgi>) for resistance gene detection and verified results by using ResFinder (Center for Genomic Epidemiology, <https://genomicepidemiology.org>) (Table). The isolate contained 5 β -lactamase genes: class A extended-spectrum β -lactamase *bla*_{PME-1}, class B carbapenemase *bla*_{NDM-1}, class D oxacillinase *bla*_{OXA-50}-type *bla*_{OXA-488} and *bla*_{OXA-10}, and class C cephalosporinase *bla*_{PDC-35}.

Multilocus sequence typing designated the isolate as sequence type (ST) 235, frequently associated with *bla*_{NDM-1}, including in isolates from Serbia, France, and Italy (3,4). ST235 is considered a high-risk clone, notable for harboring multiple β -lactamases, causing invasive infections and high mortality rates (5). Although most metallo- β -lactamases detected in ST235 are imipenemase variants, NDM CRPA are globally disseminated and have been reported in Asia, Europe, the Middle East, and Africa (5). We also detected other resistance genes reported in ST235 strains, including aminoglycoside-modifying enzyme *aac*(6')-Ib9 and chloramphenicol resistance genes *cmlA* and *catB7* (6). In an outbreak of NDM CRPA in Iran, 86.2% of isolates coharbored *bla*_{OXA-10} (7), which we also detected in the isolate in this case.

Table. Antimicrobial genetic markers detected in a case of domestically acquired NDM-1–producing *Pseudomonas aeruginosa*, southern California, USA, 2023

Resistance mechanism	Genes
Aminoglycoside modifying enzymes	<i>aac</i> (6')-Ib9, <i>ant</i> (3')-IIa, <i>aph</i> (3')-IIb, <i>aph</i> (3')-VIa
β -lactamases	<i>bla</i> _{NDM-1} , <i>bla</i> _{OXA-10} , <i>bla</i> _{OXA-488} , <i>bla</i> _{PDC-35} , <i>bla</i> _{PME-1}
Fluoroquinolone resistance determinant	<i>gyrA</i> (T831), <i>parE</i> (S457R)
Chloramphenicol resistance determinant	<i>catB3</i> , <i>catB7</i> , <i>cmlA9</i>
Fosfomycin resistance determinant	<i>fosA</i>
Tetracycline resistance determinant	<i>tet</i> (D)
Sulfonamide resistance determinant	<i>sul1</i>

*NDM, New Delhi metallo- β -lactamase.

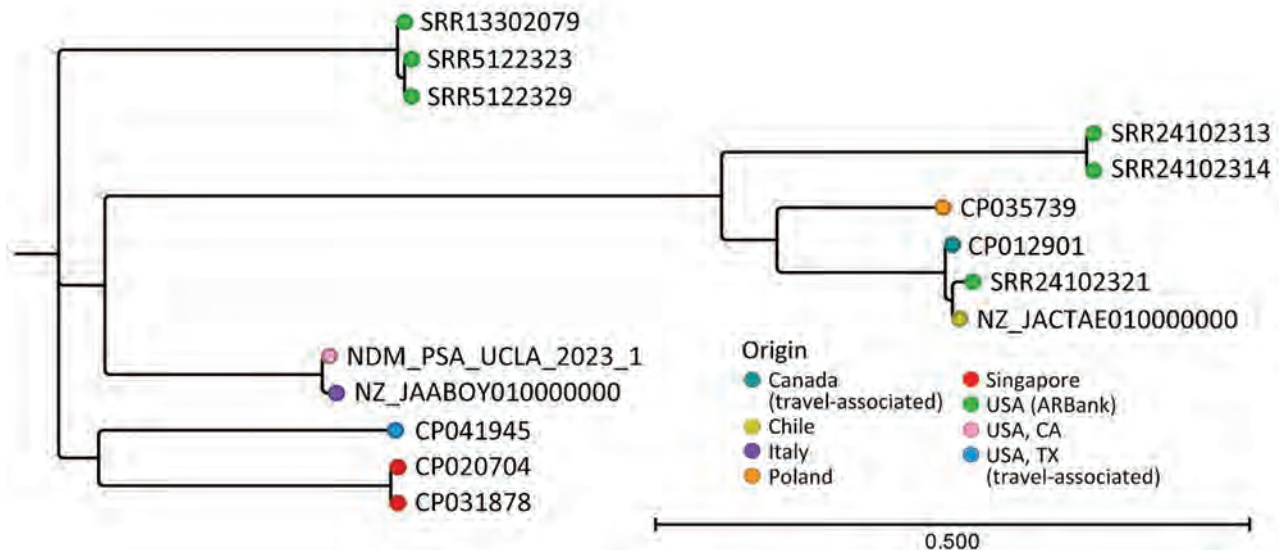


Figure. Phylogenetic tree for domestically acquired NDM-1–producing *Pseudomonas aeruginosa*, southern California, USA, 2023. Node colors indicate geographic location of organism isolation; the isolate described in this case report is designated as NDM_PSA_UCLA_2023_1. Accession numbers are provided for reference sequences. Scale bar indicates nucleotide substitutions per site. ARBank, CDC & FDA Antimicrobial Resistance (AR) Isolate Bank (<https://www.cdc.gov/drugresistance/resistance-bank/>); NDM, New Delhi metallo- β -lactamase; UCLA, University of California Los Angeles.

Consistent with other bla_{NDM-1} -positive isolates, bla_{NDM-1} in this isolate was flanked by IS91-type insertion sequences, indicating mobilizability (8). The isolate also exhibited intermediate susceptibility to colistin, sometimes used to treat carbapenemase-producing CRPA. The isolate lacked an *mcr* gene, indicating mutations in *pmrAB* could be responsible for this phenotype, consistent with other ST235 carbapenemase-producing CRPA (9).

We used CSIPhylogeny (Center for Genomic Epidemiology) to perform single-nucleotide polymorphism (SNP) analysis against other NDM-1-producing ST235 isolates, then CLC Bioinformatics Workbench (QIAGEN) to generate a phylogenetic tree. The isolate from this study exhibited highest homology (≈ 30 SNPs difference) with 2 non-NDM-producing ST235 isolates from Malaysia (Appendix). Among NDM-producing carbapenemase-producing CRPA, the isolate clustered with an NDM CRPA from Italy (147 SNPs distance), suggesting origin in Europe (Figure). Among US strains, the isolate was genetically distinct from all NDM CRPA strains in isolate banks (Appendix Table 3) and a travel-associated strain from Texas ($>20,000$ SNPs distance) (10). That finding, and our patient's lack of international travel, suggest that a domestic NDM CRPA strain is circulating in southern California. The patient received care at multiple institutions, making the precise origin of this strain unknown. Before this isolate, the rate of NDM-pro-

ducing organisms at our institution remained low, <3 carbapenem-resistant Enterobacterales isolated annually, with no NDM CRPA.

The NDM CRPA isolate we report exhibited susceptibility to cefiderocol, which was used to clear the urinary tract infection. Upon phenotypic carbapenem resistance identification, cefiderocol susceptibility testing indicated sensitivity. The rapid availability of susceptibility testing results and preliminary testing performed within 24 hours after isolation were crucial for appropriate clinical management and antimicrobial drug choice, leading to safe heart transplantation and receipt of immunosuppression. Carbapenemase-producing bacteria should not disqualify a patient from transplantation.

In conclusion, high mortality rates of ST235 NDM CRPA in invasive infection and a potential community spread in southern California warrant concern. The mobilization potential of bla_{NDM-1} remains unknown. Infection control measures and expanded surveillance efforts, including routine laboratory screening of all CRPA isolates via carbapenemase tests, could curb the spread of this high-risk genotype.

About the Author

Dr. Gray is a clinical microbiologist at the University of California Los Angeles Medical School, USA. Her research interests include antimicrobial resistance, genomic epidemiology, and healthcare acquired infections.

References

1. Tenover FC, Nicolau DP, Gill CM. Carbapenemase-producing *Pseudomonas aeruginosa* – an emerging challenge. *Emerg Microbes Infect.* 2022;11:811–4. <https://doi.org/10.1080/22221751.2022.2048972>
2. Delaware Health and Social Services. Health alert: first confirmed US case of NDM-producing carbapenem-resistant *Pseudomonas aeruginosa* [cited 2023 Jul 22]. <http://dhss.delaware.gov/dph/php/alerts/dhan324.html>
3. Kocsis B, Gulyás D, Szabó D. Diversity and distribution of resistance markers in *Pseudomonas aeruginosa* international high-risk clones. *Microorganisms.* 2021;9:359. <https://doi.org/10.3390/microorganisms9020359>
4. Hong DJ, Bae IK, Jang IH, Jeong SH, Kang HK, Lee K. Epidemiology and characteristics of metallo- β -lactamase-producing *Pseudomonas aeruginosa*. *Infect Chemother.* 2015;47:81–97. <https://doi.org/10.3947/ic.2015.47.2.81>
5. Recio R, Villa J, Viedma E, Orellana MA, Lora-Tamayo J, Chaves F. Bacteraemia due to extensively drug-resistant *Pseudomonas aeruginosa* sequence type 235 high-risk clone: facing the perfect storm. *Int J Antimicrob Agents.* 2018; 52:172–9. <https://doi.org/10.1016/j.ijantimicag.2018.03.018>
6. Loconsole D, Accogli M, Monaco M, Del Grosso M, De Robertis AL, Morea A, et al. First detection of autochthonous extensively drug-resistant NDM-1 *Pseudomonas aeruginosa* ST235 from a patient with bloodstream infection in Italy, October 2019. *Antimicrob Resist Infect Control.* 2020;9:73. <https://doi.org/10.1186/s13756-020-00734-5>
7. Shahin M, Ahmadi A. Molecular characterization of NDM-1-producing *Pseudomonas aeruginosa* isolates from hospitalized patients in Iran. *Ann Clin Microbiol Antimicrob.* 2021;20:76. <https://doi.org/10.1186/s12941-021-00482-3>
8. Fortunato G, Vaz-Moreira I, Gajic I, Manaia CM. Insight into phylogenomic bias of *bla*_{VIM-2} or *bla*_{NDM-1} dissemination amongst carbapenem-resistant *Pseudomonas aeruginosa*. *Int J Antimicrob Agents.* 2023;61:106788. <https://doi.org/10.1016/j.ijantimicag.2023.106788>
9. Vatansever C, Menekse S, Dogan O, Gucer LS, Ozer B, Ergonul O, et al. Co-existence of OXA-48 and NDM-1 in colistin resistant *Pseudomonas aeruginosa* ST235. *Emerg Microbes Infect.* 2020;9:152–4. <https://doi.org/10.1080/22221751.2020.1713025>
10. Khan A, Shropshire WC, Hanson B, Dinh AQ, Wanger A, Ostrosky-Zeichner L, et al. Simultaneous infection with *Enterobacteriaceae* and *Pseudomonas aeruginosa* harboring multiple carbapenemases in a returning traveler colonized with *Candida auris*. *Antimicrob Agents Chemother.* 2020;64:64. <https://doi.org/10.1128/AAC.01466-19>

Address for correspondence: Shangxin Yang, UCLA Clinical Microbiology Laboratory, 11633 San Vicente Blvd, Los Angeles, CA 90049, USA; email: shangxinyang@mednet.ucla.edu

Plasmodium vivax Prevalence in Semiarid Region of Northern Kenya, 2019

Wendy Prudhomme O'Meara, Linda Maraga, Hannah Meredith, Daniel Esimit, Gilchrist Lokoel, Tabitha Chepkwony, Joseph Kipkoech, George Ambani, Diana Menya, Elizabeth Freedman, Steve Taylor, Andrew Obala

Author affiliations: Duke University, Durham, North Carolina, USA (W. Prudhomme O'Meara, H. Meredith, E. Freedman, S. Taylor); Moi University, Eldoret, Kenya (W. Prudhomme O'Meara, D. Menya, A. Obala); Academic Model Providing Access to Healthcare, Eldoret (L. Maraga, T. Chepkwony, J. Kipkoech, G. Ambani); Turkana County Health Management, Lodwar, Kenya (D. Esimit, G. Lokoel)

DOI: <https://doi.org/10.3201/eid2911.230299>

In urban and rural areas of Turkana County, Kenya, we found that 2% of household members of patients with *Plasmodium falciparum* infections were infected with *P. vivax*. Enhanced surveillance of *P. vivax* and increased clinical resources are needed to inform control measures and identify and manage *P. vivax* infections.

Until recently, little or no endemic transmission of *Plasmodium vivax* has been reported in sub-Saharan Africa outside of the Horn of Africa (1). *P. vivax* was presumed to be largely absent because the Duffy blood group antigen was rare in persons living in the region. However, accumulating evidence of endemic *P. vivax* has indicated that this parasite might be present in many areas of sub-Saharan Africa, albeit at low levels, and Duffy antigen-negative persons can be infected and contribute to transmission (2).

Turkana County is in northwestern Kenya and shares a border with Uganda, South Sudan, and Ethiopia. Turkana county's harsh climate is characterized by an average rainfall of <215 mm/year and daytime temperatures of 40°C. Malaria transmission in this region was predicted to occur in isolated pockets with epidemic potential only after unusual rainfall. However, reactive case detection conducted across central Turkana County documented year-round symptomatic and asymptomatic *P. falciparum* infections and confirmed perennial endemic transmission of malaria (3).

We hypothesized that *P. vivax* might also be circulating in Turkana County because of stable malaria transmission and proximity to Ethiopia, where *P.*

Table. *Plasmodium falciparum* and *P. vivax* infections according to age groups of household members in study of *P. vivax* prevalence in semiarid region of northern Kenya, 2019*

Infection type	Age range, y			
	<5, n = 490	6–15, n = 1,069	16–40, n = 1,324	>40, n = 318
Any <i>Plasmodium</i> sp.	166 (33.9)	368 (34.4)	397 (30.0)	98 (30.8)
<i>P. falciparum</i> only	151 (30.8)	344 (32.2)	373 (28.2)	92 (28.9)
<i>P. vivax</i> only	8 (1.6)	13 (1.2)	13 (0.98)	4 (1.3)
Mixed	7 (1.4)	11 (1.0)	11 (0.83)	2 (0.63)

*Values are no. (%) positive samples for each age group. Total number of samples tested was 3,305. However, 47 tested samples had missing age information, of which 20 were infected with *P. falciparum* and none with *P. vivax*; 57 samples were tested for *P. vivax* but not *P. falciparum*, of which none were positive for *P. vivax*. Therefore, the total number of samples in this table is 3,201. *P. falciparum* PCR methods and results are reported in (3).

vivax infections are endemic. To test this hypothesis, we extracted genomic DNA from 3,305 dried blood spots collected from household members of patients with *P. falciparum* infections; household members were enrolled in the study at their homes in catchment areas surrounding 3 rural and 3 urban health facilities in central Turkana County (3). The study was approved by the Moi University Institutional Research and Ethics Committee and Duke University Institutional Review Board.

We tested each DNA sample for *P. vivax* by using an established nested qualitative PCR protocol (4). Gel electrophoresis bands were identified independently by 2 observers. We randomly selected 15 extracts for retesting by probe-based real-time PCR with the same primer sequences to detect the same target; all PCR products were confirmed. For our analysis, we used nested qualitative PCR results.

The percentage of household members infected with *P. vivax* was 2.1% (69/3,305); of those, 45% (31/69) were co-infected with *P. falciparum* (Table). We detected *P. vivax* infections across our study transect throughout most of the year (Figure; Appendix Figures 1, 2, <https://wwwnc.cdc.gov/EID/>

article/29/11/23-0299-App1.pdf); the highest (5.8%, 28/485) prevalence was recorded near an urban facility in the town of Lodwar. Infections were present across all age groups, but we observed a slightly higher (1.6%, 8/490) percentage of *P. vivax* mono-infections in children <5 years of age (Table). Ten *P. vivax*-infected participants reported malaria-like symptoms when they were screened; 7 of those were co-infected with *P. falciparum*. Only 3 *P. vivax*-infected participants had a malaria-like illness within 1 month before enrollment; none reported taking antimalarial drugs. None of the *P. vivax*-infected participants reported traveling outside of their subcounty within 2 months before enrollment; 16% (11/69) reported having a net for their sleeping space, which was slightly less than uninfected participants (19.7%, 468/2,376) who had a net.

The burden of *P. vivax* infections in sub-Saharan Africa remains unclear; infections are rarely diagnosed in a clinical setting and might often be asymptomatic. The recommended rapid diagnostic test in most countries of sub-Saharan Africa is *P. falciparum*-specific. Consequently, *P. vivax* infections might be underestimated or undocumented.

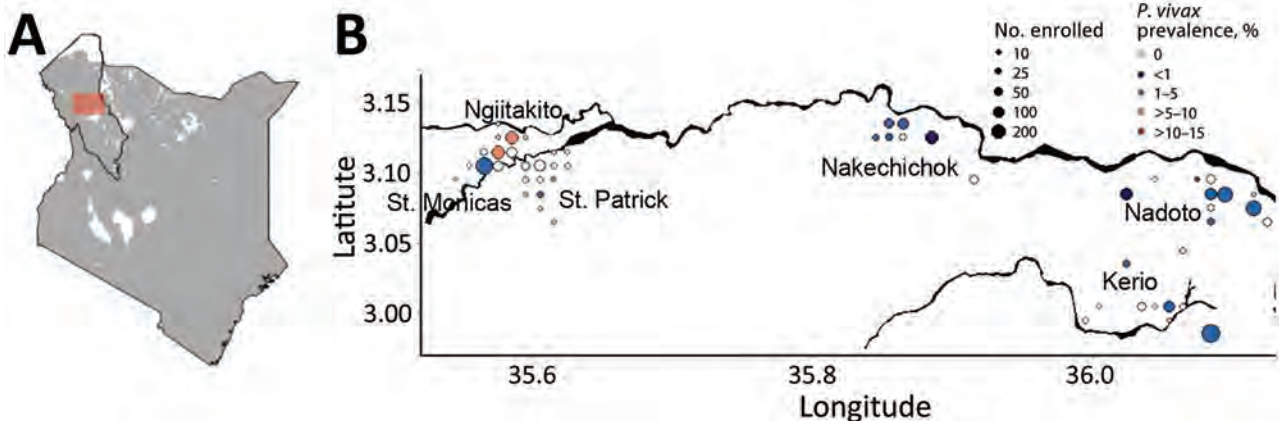


Figure. Prevalence of *Plasmodium vivax* infection in communities along the Turkwel River in study of *P. vivax* prevalence in semiarid region of northern Kenya, 2019. Household members of patients with *P. falciparum* infections were tested for *P. vivax* infection. A) Study area (red box) in Turkana County, northwestern Kenya. Gray shading indicates <0.01% prevalence of *P. vivax* infections; white shading indicates no detected infections. Data from the Malaria Atlas Project. B) Coordinates of different study enrollment sites. Main black line across the graph indicates the Turkwel River in Turkana County. Sizes of dots indicate number of household members enrolled; colors indicate percentages of household members who were positive for *P. vivax* by qualitative PCR.

Strategies designed to eliminate *P. falciparum* are undermined by *P. vivax* because dormant *P. vivax* hypnozoites that can cause relapse and sustain transmission are difficult to detect and treat (5). Furthermore, *P. vivax* infections generate gametocytes before symptom onset, making detection and treatment challenging before onward transmission occurs. *P. vivax* infections could present a growing challenge in Kenya, even as *P. falciparum* is brought under control, a process that has been observed in co-endemic malaria settings in Southeast Asia (6).

We did not test participants for Duffy antigen expression, which could have affected their susceptibility to *P. vivax*. Estimated Duffy antigen positivity in Kenya is 5%–10% (7). *P. vivax* infections in Duffy-negative subjects have been documented in Africa (2). Characterization of Duffy antigen expression will be needed to understand the threat of *P. vivax* infections in Kenya.

Anopheles stephensi mosquitoes have been identified in Kenya (E.O. Ochomo et al., unpub. data, <https://doi.org/10.21203/rs.3.rs-2498485/v1>), and the potential expansion of this highly competent vector, which survives in urban and manmade habitats, could dramatically change malaria transmission patterns. Continued spread of this invasive vector into sub-Saharan Africa would place ≈126 million persons at risk for malaria (8). Identification of *An. stephensi* mosquitoes in Djibouti was linked with a >100-fold rise in malaria cases, including the first autochthonous cases of *P. vivax* reported in 2016 (9).

In conclusion, if emerging *An. stephensi* mosquitoes become established across Kenya in the presence of confirmed *P. vivax* cases, malaria elimination in Kenya will be substantially more difficult to achieve. Enhanced surveillance for both *An. stephensi* mosquitoes and *P. vivax* will be needed to inform control measures, and increased clinical resource allocation will enable detection and effective treatment of patients with *P. vivax* malaria.

About the Author

Dr. Prudhomme O'Meara is a scientist with joint appointments at Duke University and Moi University. Her research interests focus on malaria transmission

dynamics and prevention, control, and elimination strategies in remote communities facing new malaria threats.

References

1. Battle KE, Lucas TCD, Nguyen M, Howes RE, Nandi AK, Twhig KA, et al. Mapping the global endemicity and clinical burden of *Plasmodium vivax*, 2000–17: a spatial and temporal modelling study. *Lancet*. 2019;394:332–43. [https://doi.org/10.1016/S0140-6736\(19\)31096-7](https://doi.org/10.1016/S0140-6736(19)31096-7)
2. Wilairatana P, Masangkay FR, Kotepui KU, De Jesus Milanez G, Kotepui M. Prevalence and risk of *Plasmodium vivax* infection among Duffy-negative individuals: a systematic review and meta-analysis. *Sci Rep*. 2022;12:3998. <https://doi.org/10.1038/s41598-022-07711-5>
3. Meredith HR, Wesolowski A, Menya D, Esimit D, Lokoel G, Kipkoech J, et al. Epidemiology of *Plasmodium falciparum* infections in a semi-arid rural African setting: evidence from reactive case detection in northwestern Kenya. *Am J Trop Med Hyg*. 2021;105:1076–84. <https://doi.org/10.4269/ajtmh.21-0256>
4. Singh B, Bobogare A, Cox-Singh J, Snounou G, Abdullah MS, Rahman HA. A genus- and species-specific nested polymerase chain reaction malaria detection assay for epidemiologic studies. *Am J Trop Med Hyg*. 1999;60:687–92. <https://doi.org/10.4269/ajtmh.1999.60.687>
5. Olliaro PL, Barnwell JW, Barry A, Mendis K, Mueller I, Reeder JC, et al. Implications of *Plasmodium vivax* biology for control, elimination, and research. *Am J Trop Med Hyg*. 2016;95:4–14. <https://doi.org/10.4269/ajtmh.16-0160>
6. Price RN, Commons RJ, Battle KE, Thriemer K, Mendis K. *Plasmodium vivax* in the era of the shrinking *P. falciparum* map. *Trends Parasitol*. 2020;36:560–70. <https://doi.org/10.1016/j.pt.2020.03.009>
7. Howes RE, Patil AP, Piel FB, Nyangiri OA, Kabaria CW, Gething PW, et al. The global distribution of the Duffy blood group. *Nat Commun*. 2011;2:266. <https://doi.org/10.1038/ncomms1265>
8. Sinka ME, Pironon S, Massey NC, Longbottom J, Hemingway J, Moyes CL, et al. A new malaria vector in Africa: predicting the expansion range of *Anopheles stephensi* and identifying the urban populations at risk. *Proc Natl Acad Sci USA*. 2020;117:24900–8. <https://doi.org/10.1073/pnas.2003976117>
9. Seyfarth M, Khaireh BA, Abdi AA, Bouh SM, Faulde MK. Five years following first detection of *Anopheles stephensi* (Diptera: Culicidae) in Djibouti, Horn of Africa: populations established—malaria emerging. *Parasitol Res*. 2019;118:725–32. <https://doi.org/10.1007/s00436-019-06213-0>

Address for correspondence: Wendy Prudhomme O'Meara, Duke Global Health Institute, Duke University, 310 Trent Dr, Durham, NC 27708, USA; email: wpo@duke.edu

Case Report and Literature Review of Prosthetic Cardiovascular Mucormycosis

Baptiste Hoellinger, Louis Magnus, Yvon Ruch, Mickael Ohana, Yves Hansmann, Valérie Letscher-Bru, Anne Lejay, Nabil Chakfé, François Danion

Author affiliations: University Hospital of Strasbourg, Strasbourg, France (B. Hoellinger, L. Magnus, Y. Ruch, M. Ohana, Y. Hansmann, V. Letscher-Bru, A. Lejay, N. Chakfé, F. Danion); University Hospital of Clermont-Ferrand, Clermont-Ferrand, France (L. Magnus); Inserm UMR_S 1109, Strasbourg (F. Danion)

DOI: <http://doi.org/10.3201/eid2911.230837>

We report a rare case of aorto-bi-iliac prosthetic allograft mucormycosis in a 57-year-old immunocompetent patient in France. Outcome was favorable after surgery and dual antifungal therapy with liposomal amphotericin B and isavuconazole. In a literature review, we identified 12 other cases of prosthetic vascular or heart valve mucormycosis; mortality rate was 38%.

Mucormycosis, caused by fungi of order Mucorales, is a rare, life-threatening fungal infection whose incidence has been rising since the late 1990s (1). The main infection locations are pulmonary, rhino-orbito-cerebral, cutaneous, and disseminated. Although the vascular tropism of Mucorales is well described, few cases of cardiovascular infections have been reported (2). We report a rare case of aorto-bi-iliac prosthetic allograft mucormycosis in a 57-year-old immunocompetent patient in France. We obtained written informed consent from the patient for publication of this report.

The patient, who had a history of type B aortic dissection, underwent an open surgical repair of a

right common iliac artery aneurysm with aorto-bi-iliac prosthetic graft reconstruction (day 0). We noted a bowel perforation at the end of the surgery and performed resection-anastomosis. Because of a history of allergy to penicillin, we treated the patient with aztreonam, metronidazole, vancomycin, and amikacin. The patient acquired an early post-operative *Candida albicans* infection diagnosed on periprosthetic collection puncture and treated with caspofungin on day 10. On day 30, he had emergency surgery for proximal anastomosis rupture with hemorrhagic shock (Figure, panels A, B). All the prosthetic material was excised with in situ reconstruction using a silver-coated prosthetic aorto-bi-iliac graft. Three intraoperative samples were positive for *Lactobacillus plantarum* and *Rhizopus microsporus* pathogens. Serum samples were positive by Mucorales PCR for *Rhizopus*, which we confirmed on 5 other samples (3). Histology was not performed. Neither chest computed tomography nor brain magnetic resonance imaging showed another location of infection. We replaced caspofungin with liposomal amphotericin B (5 mg/kg).

We performed surgical revision for recurrence of collection on day 37; the patient had retroperitoneal necrosis with false necrotic membranes, another digestive fistula, and graft exposure (Figure, panel C). We performed tissue debridement, perigraft collection drainage, and irrigation associated with bowel resection-anastomosis and omentoplasty to cover the graft. We administered isavuconazole with liposomal amphotericin B after surgery. Cultures of the peroperative samples found *R. microsporus* and *C. albicans*. Histology showed signs of acute inflammation in contact with the prosthetic fibers, but specific staining was not performed. Serum samples tested by Mucorales PCRs 3 times/week were still positive at day 37 and became negative at day 52. We



Figure. Vascular prosthetic mucormycosis in a 57-year-old immunocompetent patient in France. A, B) Aortic computed-tomography angiogram (A) and 3-dimensional reconstruction (B) show the periprosthetic collection and vascular leak (arrows). C) Intraoperative view shows the graft exposure and false necrotic membranes.

performed surgery again, excising the silver-coated graft and then using a cryopreserved human allograft for in situ aorto-iliac reconstruction, on day 95. Three months later, the patient's clinical and biologic progress was favorable; amphotericin B was discontinued, and isavuconazole was continued on a long-term basis. After 1 year of follow-up, the infection had not recurred.

We performed a literature review of cases of prosthetic vascular or heart valve mucormycosis and identified 13 cases, including our case (Appendix, <https://wwwnc.cdc.gov/EID/article/29/11/23-0837-App1.pdf>). Nine of those patients were male and 4 female; median age was 54 years. Two (15%) of the patients had known immunosuppression, 1 from solid organ transplantation and 1 from hematologic malignancy. Two patients had received steroids in the weeks before illness. Seven patients had a vascular infection. Eight had endocarditis; of interest, 4 of those 8 patients had emboli in the lower limbs, which is usually a rare embolic site in endocarditis (4). Nine (69%) of 13 patients had an early postoperative infection (<4 months after surgery). The mucormycosis infection was monomicrobial in 10 (85%) of the 13 cases. Two patients were co-infected with *Aspergillus*; the patient we report was co-infected with *Candida albicans*. Ten of the 13 patients received treatment with liposomal or deoxycholate amphotericin B; 2 patients died before they could receive any treatment. Surgery was performed in 11/13 patients, and infected prosthesis were explanted in 10 patients. Five (38%) of the 13 patients died.

The main fungal cause of vascular infection and endocarditis is *Candida* spp. Mucormycosis occurs mainly in immunocompromised patients. However, certain forms can occur in immunocompetent patients, particularly posttraumatic and healthcare-associated forms; prosthetic mucormycosis also seems to fall into this category (5). We suggest 2 hypotheses for the mechanism of mucormycosis in our patient: a healthcare-associated mucormycosis, if we consider that the implanted prosthesis could have been contaminated, or a contamination of the prosthesis by digestive perforation (6). As for the second hypothesis, Mucorales are found on many foods; in our patient's case, ongoing treatment with caspofungin and broad-spectrum antimicrobial therapy could have encouraged colonization (7).

Our study and review of the literature suggest a better prognosis for vascular prosthetic mucormycosis than for pulmonary and disseminated mucormycosis, probably because it occurs in immunocompetent patients and the source can be effectively controlled by surgery. However, we acknowledge that reporting cases with favorable outcomes may have introduced

bias. The first-line treatment for mucormycosis is liposomal amphotericin B (5 mg/kg) (8). Surgery is crucial for controlling the infection, particularly in extrapulmonary locations (8). The benefit of amphotericin B/isavuconazole dual therapy has been suggested in a neutropenic mice model and should be explored for difficult-to-treat locations, especially when a prosthesis is involved (9). In conclusion, prosthetic cardiac and vascular mucormycosis are very rare infections that require prompt surgery and antifungal therapy.

F.D. declares personal fees from Gilead and Pfizer.

Y.H. declares personal fees from Pfizer.

Author contributions: B.H. reviewed the literature. B.H., L.M., and F.D. conceived the case report and drafted the manuscript. L.M., A.L., and N.C. were involved in the management of the patient. F.D., L.M., B.H., N.C., A.L., V.L., Y.H., and M.O. provided critical revision of the manuscript for important content. All authors contributed to the article and approved the submitted version.

About the Author

Dr. Hoellinger is an infectious diseases physician working at the University Hospital of Strasbourg in France. His primary research interest is fungal infections.

References

1. Danion F, Coste A, Le Hyaric C, Melenotte C, Lamoth F, Calandra T, et al. What is new in pulmonary mucormycosis? *J Fungi (Basel)*. 2023;9:307. <https://doi.org/10.3390/jof9030307>
2. Ben-Ami R, Luna M, Lewis RE, Walsh TJ, Kontoyiannis DP. A clinicopathological study of pulmonary mucormycosis in cancer patients: extensive angioinvasion but limited inflammatory response. *J Infect*. 2009;59:134–8. <https://doi.org/10.1016/j.jinf.2009.06.002>
3. Millon L, Larosa F, Lepiller Q, Legrand F, Rocchi S, Daguindau E, et al. Quantitative polymerase chain reaction detection of circulating DNA in serum for early diagnosis of mucormycosis in immunocompromised patients. *Clin Infect Dis*. 2013;56:e95–101. <https://doi.org/10.1093/cid/cit094>
4. Millaire A, Leroy O, Gaday V, de Groote P, Beuscart C, Goullard L, et al. Incidence and prognosis of embolic events and metastatic infections in infective endocarditis. *Eur Heart J*. 1997;18:677–84. <https://doi.org/10.1093/oxfordjournals.eurheartj.a015315>
5. Petrikos G, Skiada A, Lortholary O, Roilides E, Walsh TJ, Kontoyiannis DP. Epidemiology and clinical manifestations of mucormycosis. *Clin Infect Dis*. 2012;54(Suppl 1):S23–34. <https://doi.org/10.1093/cid/cir866>
6. Rammaert B, Lanternier F, Zahar JR, Dannaoui E, Bougnoux ME, Lecuit M, et al. Healthcare-associated mucormycosis. *Clin Infect Dis*. 2012;54(Suppl 1):S44–54. <https://doi.org/10.1093/cid/cir867>
7. Paterson RRM, Lima N. Filamentous fungal human pathogens from food emphasising *Aspergillus*, *Fusarium*, and *Mucor*. *Microorganisms*. 2017;5:44. <https://doi.org/10.3390/microorganisms5030044>

8. Cornely OA, Alastruey-Izquierdo A, Arenz D, Chen SCA, Dannaoui E, Hochhegger B, et al.; Mucormycosis ECMM MSG Global Guideline Writing Group. Global guideline for the diagnosis and management of mucormycosis: an initiative of the European Confederation of Medical Mycology in cooperation with the Mycoses Study Group Education and Research Consortium. *Lancet Infect Dis.* 2019;19:e405–21. [https://doi.org/10.1016/S1473-3099\(19\)30312-3](https://doi.org/10.1016/S1473-3099(19)30312-3)
9. Gebremariam T, Gu Y, Singh S, Kitt TM, Ibrahim AS. Combination treatment of liposomal amphotericin B and isavuconazole is synergistic in treating experimental mucormycosis. *J Antimicrob Chemother.* 2021;76:2636–9. <https://doi.org/10.1093/jac/dkab233>

Address for correspondence: François Danion, CHU de Strasbourg, Department of Infectious Diseases, 1 place de l'Hôpital, 67 000, Strasbourg, France; email: francois.danion@chru-strasbourg.fr

Changes in Group A *Streptococcus emm* Types Associated with Invasive Infections in Adults, Spain, 2023

Alba Bellés-Bellés, Núria Prim, Saray Mormeneo-Bayo, Pilar Villalón-Panzano, Mónica Valiente-Novillo, Alfredo Jover-Sáenz, Núria Aixalà, Albert Bernet, Éric López-González, Ivan Prats, Mercè García-González

Author affiliations: Hospital Universitari Arnau de Vilanova, Lleida, Spain (A. Bellés-Bellés, N. Prim, S. Mormeneo-Bayo, A. Jover-Sáenz, N. Aixalà, A. Bernet, É. López-González, I. Prats, M. García-González); Institut de Recerca Biomèdica de Lleida, Lleida (A. Bellés-Bellés, N. Prim, S. Mormeneo-Bayo, A. Jover-Sáenz, A. Bernet, É. López-González, I. Prats, M. García-González); Centro Nacional de Microbiología, Instituto de Salud Carlos III, Madrid, Spain (P. Villalón-Panzano, M. Valiente-Novillo)

DOI: <https://doi.org/10.3201/eid2911.230857>

An increase in invasive group A *Streptococcus* infection was detected in the northeast of Spain in November 2022. A postpandemic decline in the diversity of circulating *emm* types involved in invasive group A *Streptococcus* was observed, along with the emergence of *emm49* in this geographic area.

Streptococcus pyogenes (group A *Streptococcus* [GAS]) can cause a broad range of infections. Although usually associated with streptococcal pharyngitis and skin and soft tissue infections, GAS can also cause life-threatening infections, such as sepsis or necrotizing fasciitis (1).

In December 2022, the World Health Organization issued an alert about increasing rates of invasive GAS (iGAS) infections in children in Europe (2). This warning was followed by a health advisory from the US Centers for Disease Control and Prevention that reported an increase in these infections among children in the United States (3). Since then, several countries in Europe have notified an increase, particularly in the pediatric population (4).

A total of 31 culture-confirmed iGAS cases (incidence 0.0912 cases/1,000 inhabitants) were detected during November 2022–May 2023 in the province of Lleida (catchment of 340,000 inhabitants) in north-east Spain. Invasive cases were defined according to Centers for Disease Control and Prevention definitions (5). The median age was 62 years (range 3–93 years); 4 cases occurred in children. Three deaths in adults were notified during this period. Given that increase, we analyzed the distribution of iGAS in Lleida province during January 2011–May 2023 (Appendix Figure, <https://wwwnc.cdc.gov/EID/article/29/11/23-0857-App1.pdf>). The average number of iGAS cases per year was 5.2 (incidence 0.0153 cases/1,000 inhabitants/year) during 2011–2018. A total of 19 culture-confirmed cases (incidence of 0.0559 cases/1,000 inhabitants/year) were reported in 2019, followed by a decline in incidence during the COVID-19 pandemic (0.0162 cases/1,000 inhabitants/year). The increase detected since November 2022 surpassed 2019 incidence.

Hospital Universitari Arnau de Vilanova (Lleida, Spain) began participating in the iGAS national surveillance program in April 2019. Conducted at Centro Nacional de Microbiología (Majadahonda, Spain), this program performs *emm* typing and toxin gene profiling of iGAS isolates collected from microbiology laboratories. We analyzed the monthly distribution of *emm* types involved in 61 iGAS cases reported during January 2019–May 2023 in our geographic area (Figure). Overall, 19 different *emm* types were detected; *emm1* (n = 18/61) was the most frequent, followed by *emm49* (n = 8/61) and *emm89* (n = 8/61). A decrease in type diversity was observed since November 2022; the 6 *emm* types detected were *emm1* (n = 15/31), *emm12* (n = 5/31), *emm49* (n = 5/31), *emm89* (n = 4/31), *emm77* (n = 1/31) and *emm58* (n = 1/31) (Table).

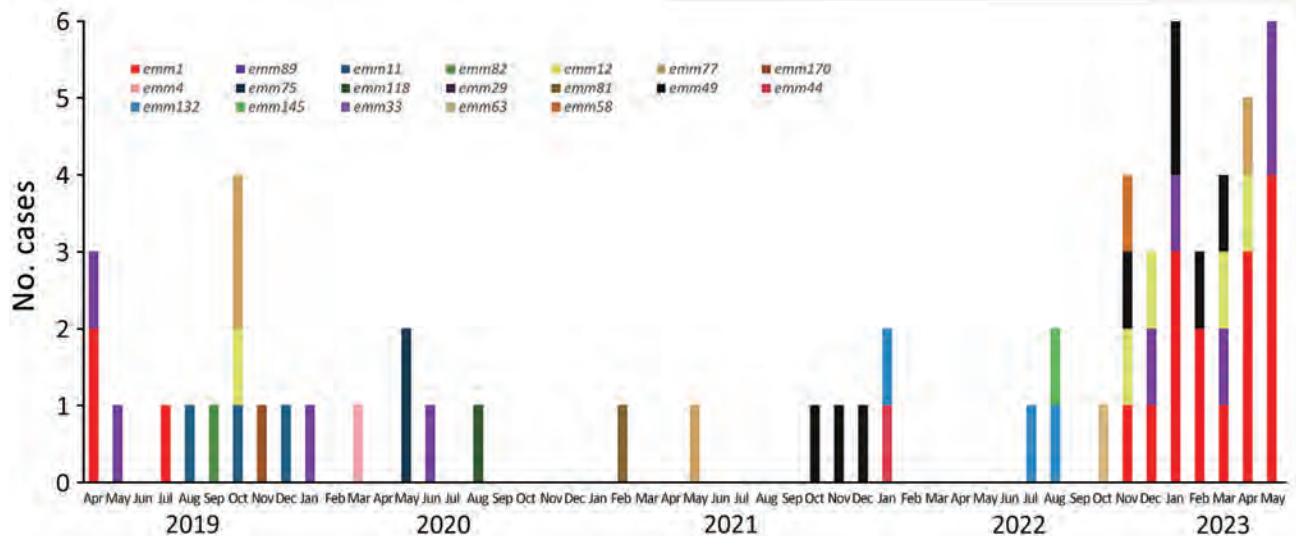


Figure. *emm* type distribution of 61 culture-confirmed invasive group A *Streptococcus* infections, by month, Lleida, northeast Spain, January 2019–May 2023

Table. Phenotypic and genotypic characteristics of 61 *Streptococcus pyogenes* isolates in invasive infections and clinical manifestations, Lleida province, northeast Spain, January 2019–May 2023*

<i>emm</i> type, n = 61	<i>emm</i> cluster†	Exotoxin gene profile	Resistance phenotype	Clinical manifestations
<i>emm1</i> , n = 18	A-C3	A, G, J, <i>smeZ</i> , n = 11 A, C, G, J, <i>smeZ</i> , n = 7	ND	Pneumonia, n = 8‡ Septic shock, n = 3‡ Skin infection, n = 3 UTI / PID, n = 3 AOM, n = 1
<i>emm4</i> , n = 1	E1	C, G, <i>ssa</i> , <i>smeZ</i>	ND	Cellulitis and septic shock
<i>emm11</i> , n = 3	E6	C, G, H, n = 2 C, G, H, J, n = 1	ND	Cellulitis, n = 2 Postoperative fever, n = 1
<i>emm12</i> , n = 6	A-C4	C, G, H, n = 6	ND, n = 5 ERI, CLI, n = 1	Fever, n = 2 Scarlet fever, n = 1 Cellulitis, n = 1 Postchemotherapy fever, n = 1 Odynophagia, n = 1
<i>emm33</i> , n = 1	D4	G, H, J, <i>smeZ</i>	TET	Septic arthritis
<i>emm44</i> , n = 1	E3	A, G, J, <i>ssa</i>	ND	Pneumonia
<i>emm49</i> , n = 8	E3	G, n = 5 G, <i>ssa</i> , n = 1 A, G, n = 1 ND, n = 1	TET, n = 7 ND, n = 1	Cellulitis, n = 6 Postchemotherapy fever, n = 1 Vascular ulcers, n = 1
<i>emm58</i> , n = 1	E3	G, <i>ssa</i>	ERI, TET	Cellulitis
<i>emm63</i> , n = 1	E6	<i>ssa</i>	TET	Cellulitis
<i>emm75</i> , n = 2	E6	C, G, n = 2	ND	Cellulitis
<i>emm77</i> , n = 4	E4	C, G, n = 2 C, n = 2	iMLSB, TET, n = 4	Cellulitis, n = 3 Septic arthritis, n = 1
<i>emm81</i> , n = 1	E6	G	TET	Cellulitis
<i>emm82</i> , n = 1	E3	C, G, H	ND	Septic tenosynovitis
<i>emm89</i> , n = 8	E4	C, G, n = 7 C, G, J, <i>smeZ</i> , n = 1	ND	Cellulitis, n = 3 PID, n = 1 Pneumonia, n = 3 Prosthetic infection, n = 1
<i>emm118</i> , n = 1	E3	G	TET	Cellulitis
<i>emm132</i> , n = 2	Unknown	ND, n = 2	TET, n = 2	Cellulitis
<i>emm145</i> , n = 1	Unknown	G, H	TET	PID
<i>emm170</i> , n = 1	E5	C, G, H	ND	Septic arthritis

*AOM, acute otitis media; CLI, clindamycin; ERI, erythromycin; iMLSB, inducible macrolide-lincosamide-streptogramin B phenotype; ND, not detected; PID, pelvic inflammatory disease; TET, tetracyclin; UTI, urinary tract infection.

†*emm* cluster classification as previously reported (6).

‡Exitus: *emm1* (n = 3) and *emm4* (n = 1).

A large increase in iGAS was detected beginning in November 2022. Decreased exposure to GAS during the COVID-19 pandemic because of mask use and social isolation might have contributed to its low circulation. The decline of masking and social distancing, combined with high rates of respiratory viruses during the winter of 2021–2022, might be behind the increase in iGAS. We found that most iGAS occurred in adults and had a low mortality rate, in contrast with previous reports (4).

Certain GAS *emm* types have been strongly associated with invasive infections. However, a notorious geographic diversity in the circulation of *emm* types exists (7). The most common types involved in iGAS in Spain from 2007–2019 were *emm1*, *emm89*, and *emm3*, according to the GAS Surveillance Program in Spain. In contrast, only 1 *emm49* isolate was detected during that period (6). In our study, *emm1* was predominant in accordance with other reports in Europe (4). After *emm1*, *emm49* and *emm89* were the most frequent *emm* types in our study. A substantial expansion of *emm49* has been recently reported in United States, where it represents the third most common *emm* type associated with iGAS, after *emm1* and *emm89* (8). However, *emm49* was an unusual *emm* type in northeast Spain until recently and was rarely involved in iGAS in Europe (4,9). After *emm49* was first detected in the nationwide surveillance program in Spain in 2011, circulation increased in Spain during 2021–2023 (P. Villalón-Panzano, unpub. data). Including our 8 cases, 11 *emm49* iGAS cases were notified by this program during this period. Despite the lack of a clear epidemiologic link, an outbreak could not be ruled out in this area. The first detection of *emm49* iGAS in Lleida province was in October 2021. The main clinical manifestations of iGAS associated with *emm49* were skin and soft tissue infections, as previously described (8).

A high incidence of iGAS in children during 2019 was recently reported in Spain (10). Our data showed an increasing trend of iGAS in adults in our area that was interrupted by the COVID-19 pandemic. Together with an accumulation of iGAS, a decline in *emm* type diversity has been detected since the World Health Organization alert in late 2022.

In conclusion, this report supports that the increase in iGAS in adults probably began before the COVID-19 pandemic in northeast Spain. The post-pandemic increase was caused by a limited number of *emm* types. Although *emm1* was the most common type, *emm49* is an emergent cause of iGAS in Europe. Continuous surveillance is essential to detect the emergence and spread of *emm* types associated with iGAS in different geographic areas.

About the Author

Dr. Bellés-Bellés is a clinical microbiologist at the Hospital Universitari Arnau de Vilanova de Lleida (Spain) and the Head of the Research Group in Clinical Microbiology at the Biomedical Research Institute (IRBLleida). Her primary research interest are bacterial infections and antibiotic resistance.

References

- Nabarro LE, Brown CS, Balasegaram S, Decraene V, Elston J, Kapadia S, et al. Invasive group A *Streptococcus* outbreaks associated with home healthcare, England, 2018–2019. *Emerg Infect Dis*. 2022;28:915–23. <https://doi.org/10.3201/eid2805.211497>
- World Health Organization. Increased incidence of scarlet fever and invasive Group A *Streptococcus* infection – multi-country. 2022 Dec 15 [cited 2023 Jun 23]. <https://www.who.int/emergencies/disease-outbreak-news/item/2022-DON429>
- Centers for Disease Control and Prevention. Increase in pediatric invasive group A streptococcal infections. 2022 Dec 22 [cited 2023 Jun 23]. <https://emergency.cdc.gov/han/2022/han00484.asp>
- Alcolea-Medina A, Snell LB, Alder C, Charalampous T, Williams TGS. The ongoing *Streptococcus pyogenes* (group A *Streptococcus*) outbreak in London, United Kingdom, in December 2022: a molecular epidemiology study. *Clin Microbiol Infect*. 2023;29:887–90. <https://doi.org/10.1016/j.cmi.2023.03.001>
- Centers for Disease Control and Prevention. Case definitions for infectious conditions under public health surveillance. *MMWR Recomm Rep*. 1997;46(RR-10):1–55.
- Steer AC, Law I, Matatolu L, Beall BW, Carapetis JR. Global *emm* type distribution of group A streptococci: systematic review and implications for vaccine development. *Lancet Infect Dis*. 2009;9:611–6. [https://doi.org/10.1016/S1473-3099\(09\)70178-1](https://doi.org/10.1016/S1473-3099(09)70178-1)
- Villalón P, Sáez-Nieto JA, Rubio-López V, Medina-Pascual MJ, Garrido N, Carrasco G, et al. Invasive *Streptococcus pyogenes* disease in Spain: a microbiological and epidemiological study covering the period 2007–2019. *Eur J Clin Microbiol Infect Dis*. 2021;40:2295–303. <https://doi.org/10.1007/s10096-021-04279-2>
- Li Y, Rivers J, Mathis S, Li Z, Velusamy S, Nanduri SA, et al. Genomic surveillance of *Streptococcus pyogenes* strains causing invasive disease, United States, 2016–2017. *Front Microbiol*. 2020;11:1547. <https://doi.org/10.3389/fmicb.2020.01547>
- Naseer U, Steinbakk M, Blystad H, Caugant DA. Epidemiology of invasive group A streptococcal infections in Norway 2010–2014: a retrospective cohort study. *Eur J Clin Microbiol Infect Dis*. 2016;35:1639–48. <https://doi.org/10.1007/s10096-016-2704-y>
- de Ceano-Vivas M, Molina Gutiérrez MÁ, Mellado-Sola I, García Sánchez P, Grandioso D, Calvo C. *Streptococcus pyogenes* infections in Spanish children before and after the COVID pandemic. Coming back to the previous incidence. *Enferm Infect Microbiol Clín (Engl Ed)*. 2023 Jun 30 [Epub ahead of print]. <https://doi.org/10.1016/j.eimc.2023.04.003>

Address for correspondence: Núria Prim, Clinical Microbiology, Hospital Universitari Arnau de Vilanova, Institut Català de la Salut, Avd Rovira Roure 80, 25198 Lleida, Spain; email: nprimb.lleida.ics@gencat.ca or nuriaprim@gmail.com

Table. Pairwise nucleotide substitutions in comparative genome analysis of SARS-CoV-2 detected in members of national wrestling team after tournaments, Japan, 2021

Patient ID (GISAID ID)	No. 1	No. 3	No. 8	No. 4
No. 1 (EPI_ISL_1927168)	0	14	14	63
No. 3 (EPI_ISL_1927165)	NA	0	16	63
No. 8 (EPI_ISL_13440457)	NA	NA	0	57
No. 4 (EPI_ISL_1927420)	NA	NA	NA	0

*We sequenced a complete genome from patients 1, 3, and 4 and a draft genome from patient 8. GISAID, <https://www.gisaid.org>; ID, identification; NA, not applicable.

We defined cases as persons on the Japanese national wrestling team who participated in tournaments in Almaty, Kazakhstan, and were positive for SARS-CoV-2 according to quantitative antigen test, antigen rapid test, or PCR test at the Japanese airport quarantine station or after entering Japan during April 3–May 29, 2021. We obtained epidemiologic and laboratory information from members and the team doctor on the Japanese national wrestling team, as well as from quarantine station officers and officers at the public health center who investigated the cases and their contacts. We performed whole-genome sequencing (WGS) analysis on available isolates at the National Institute of Infectious Diseases, Japan. We performed comparative genomic analysis as described by Sekizuka et al. (1).

A total of 8 cases were reported in 7 wrestlers (7/30, 23%) and 1 staff member (1/27, 4%). No sparring partners on the team tested positive (0/6, 0%). Among the wrestlers, all case-patients experienced symptoms or tested positive within 10 days (median 5 days, interquartile range 2–7 days) after a match day (Figure). Among the 5 wrestlers for whom we obtained screening PCR results, we identified an N501Y mutated strain in 4 cases and other strains in 1 case. Among 3 wrestlers for whom we obtained WGS results, we identified B.1.1.7 lineage in 2 cases and B.1.617.2 lineage in 1 case; WGS also revealed B.1.1.7 lineage in the case in the staff member. None of the 3 B.1.1.7 lineages were identical to any other sequences in our study based on comparative genome analysis (Table). Moreover, none of the sequences had been previously reported in Japan.

Our investigation found multiple types of SARS-CoV-2, with ≥ 4 types of lineages, including those not previously reported in Japan, in the Japanese wrestling team after participating in international tournaments in Kazakhstan. Although air travel is a possible source of infection (2), we suggest transmission likely occurred during the matches. We base our conclusion on the observation of a higher attack rate in the wrestlers (23%), who followed strict precautionary measures, compared

with the sparring partners (0/6, 0%), whose activities were very similar to those of the wrestlers except that they did not directly participate in matches. The sport of wrestling has been considered to have the highest risk for transmission of SARS-CoV-2 (3,4). Beyond a previous study (5), our study highlighted the possible transmission of SARS-CoV-2 during the matches, based on the combination of epidemiologic information and WGS results.

Preventing transmission of SARS-CoV-2 in international sports events, particularly high-contact competitions like wrestling, is important to ensure the health of the athletes and prevent export of emerging variants of concern to participants' home countries, especially those with vulnerable health systems. In this context, monitoring participants in such settings provides an opportunity both to prevent transmission of the virus among participants and for genomic surveillance, using testing for persons with symptoms, swift case isolation, and timely screening for potential contacts before, during, and after events.

Acknowledgments

We thank the members of the Japanese national wrestling team; Kohei Nakajima and the Japan Wrestling Federation; the staff of Ikebukuro Public Health Center, Toshima city; the staff of Haneda Airport Quarantine Branch, Tokyo Quarantine Station; Bureau of Social Welfare and Public Health, Tokyo Metropolitan Government; Ministry of Education, Culture, Sports, Science and Technology; and Ministry of Health, Labour, and Welfare for their valued assistance in the investigation.

This work was supported by Health, Labour, and Welfare Sciences research grants from the Ministry of Health, Labour and Welfare, Japan (grant no. 21HA2013).

About the Author

Dr. Kuribayashi is a fellow in the Field Epidemiology Training Program at National Institute of Infectious Diseases, Japan. Her interests focus on clinical and epidemiological research to control infectious diseases.

References

1. Sekizuka T, Itokawa K, Hashino M, Kawano-Sugaya T, Tanaka R, Yatsu K, et al. A genome epidemiological study of SARS-CoV-2 introduction into Japan. *mSphere*. 2020;5:e00786-20. <https://doi.org/10.1128/mSphere.00786-20>
2. Hogarth F, Coffey P, Goddard L, Lewis S, Labib S, Wilmot M, et al. Genomic evidence of in-flight SARS-CoV-2 transmission, India to Australia, April 2021. *Emerg Infect Dis*. 2022;28:1527–30. <https://doi.org/10.3201/eid2807.212466>

3. Sparrow AK, Brosseau LM, Harrison RJ, Osterholm MT. Protecting Olympic participants from COVID-19 – the urgent need for a risk-management approach. *N Engl J Med*. 2021;385:e2. <https://doi.org/10.1056/NEJMp2108567>
4. American Academy of Pediatrics. COVID-19 interim guidance: return to sports and physical activity. [cited 2022 Jul 10]. <https://www.aap.org/en/pages/2019-novel-coronavirus-covid-19-infections/clinical-guidance/covid-19-interim-guidance-return-to-sports>
5. Atherstone C, Siegel M, Schmitt-Matzen E, Sjoblom S, Jackson J, Blackmore C, et al. SARS-CoV-2 transmission associated with high school wrestling tournaments – Florida, December 2020–January 2021. *MMWR Morb Mortal Wkly Rep*. 2021;70:141–3. <https://doi.org/10.15585/mmwr.mm7004e4>

Address for correspondence: Munehisa Fukusumi, Center for Field Epidemic Intelligence, Research and Professional Development, National Institute of Infectious Diseases, Japan, J1601 Iidabashi Plano stage Bldg, 2-7-2 Fujimi, Chiyoda-ku, Tokyo 102-0071, Japan; email: munesumi@niid.go.jp

Case of Carbapenem-Resistant *Salmonella* Typhi Infection, Pakistan, 2022

Summiya Nizamuddin, Ejaz Ahmed Khan, Marie Anne Chattaway, Gauri Godbole

Author affiliations: Shaukat Khanum Memorial Cancer Hospital and Research Centre, Lahore, Pakistan (S. Nizamuddin); Shifa International Hospital at Shifa Tameer-e-Millat University, Islamabad, Pakistan (E.A. Khan); UK Health Security Agency, London, United Kingdom (M.A. Chattaway, G. Godbole)

DOI: <https://doi.org/10.3201/eid2911.230499>

Salmonella Typhi infection in a patient in Pakistan initially responded to standard treatment but failed to respond to subsequent treatment. The first strain was susceptible to carbapenems and azithromycin; subsequent strains harbored the NDM-5 gene. Treatment with a combination of intravenous meropenem and colistin was successful. Carbapenem-resistant *Salmonella* Typhi emergence will hinder treatment.

Extensively drug-resistant (XDR) *Salmonella* was first reported in Sindh, Pakistan, in 2016 (1). Since then, several districts have reported cases caused by multiple XDR *S. enterica* serovar Typhi variants belonging to clade H58 and carrying multiple novel genomic integrations of the extended-spectrum β -lactamase gene (2,3). Most cases are managed with meropenem and azithromycin, and most national guidelines recommend those drugs for treating cases of *Salmonella* Typhi in Pakistan (4,5). We report a case of carbapenem-resistant *Salmonella* Typhi infection that required treatment with a last-resort antimicrobial drug.

A 7-year-old girl in Peshawar, Pakistan, visited a government hospital in July 2022 because of fever, chills, rigors, and urinary signs/symptoms. She had Down syndrome with congenital heart disease, including moderate atrial septal defect, large inlet ventricular septal defect, small patent ductus arteriosus defects, ventricular hypertrophy, and severe pulmonary hypertension; and she had a history of reoccurring lower respiratory tract infections, which often required hospitalization and treatment with antimicrobial drugs. Macrolides and carbapenems had been previously prescribed. Specific information regarding previous hospital admissions was not available. The child had received routine childhood vaccinations but not typhoid vaccine.

The patient was hospitalized for suspected enteric fever. At admission, leukocyte count was 7.6×10^9 cells/L and C-reactive protein (CRP) level was 120 mg/dL. Initial empiric treatment was ceftriaxone, but treatment was modified after blood cultures indicated XDR *Salmonella* Typhi, resistant to ampicillin, third-generation cephalosporins, fluoroquinolones, chloramphenicol, and cotrimoxazole but susceptible to azithromycin and meropenem. Treatment was switched to intravenous meropenem (300 mg 3 \times /d) and oral azithromycin (200 mg/5 mL 1 \times /d) for 10 days. The strain from the culture was not saved and was unavailable for additional testing. The patient responded positively to treatment, indicated by decreased CRP levels (7 mg/dL at treatment completion). No clearance blood cultures were obtained before discharge.

One month later, fever and decreased appetite developed; blood was collected at a private laboratory, and cultures were requested. We monitored the blood culture on a BACT/ALERT VIRTUO automated system (bioMérieux, <https://www.biomerieux.com>). When the bottle was flagged as positive for gram-negative rods, we subcultured onto chocolate, blood, and MacConkey agar plates; after 24 hours, oxidase-negative, non-lactose fermenters were identified. *Salmonella* Typhi was identified on the API 20E and Vitek MS (bioMérieux) systems. Antimicrobial

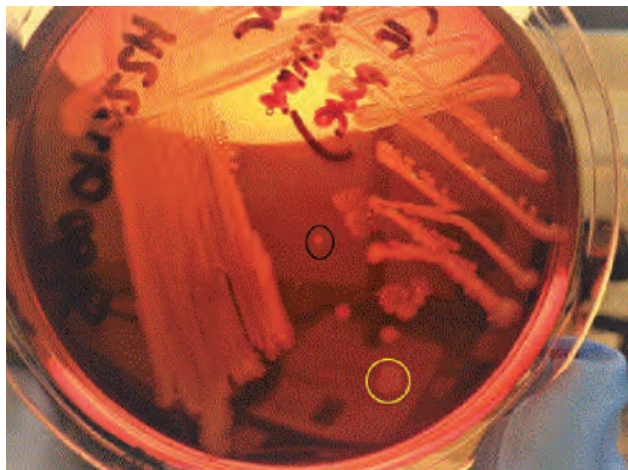


Figure. *Salmonella* Typhi colony on MacConkey agar, isolated from patient during clinical relapse of carbapenem-resistant *Salmonella* Typhi infection, Pakistan, 2022. Variant 1, circled in yellow, is a large gray dull colony. Variant 2, circled in black, is a small whitish shiny colony.

susceptibility testing was initially performed via the disc diffusion Kirby-Bauer method, according to Clinical Laboratory Standards Institute guidelines (<https://www.clsi.org>). The isolate was resistant to ampicillin, third-generation cephalosporins, fluoroquinolones, chloramphenicol, cotrimoxazole, azithromycin, and meropenem. We further confirmed susceptibility results on the Vitek 2 system. MICs for meropenem and azithromycin were >32 $\mu\text{g}/\text{mL}$. We confirmed results by using bioMérieux Etest strips. MIC for colistin, determined by disk-elution method, was 1 $\mu\text{g}/\text{mL}$.

The patient's parents were informed about the pan-resistant nature of the isolate, and the patient was re-

ferred to a private hospital for further management. At admission, she had fever, anorexia, and abdominal pain but was not in distress and was active and alert (Glasgow Coma Scale score 15/15). She had dysmorphic features consistent with Down syndrome. Her chest was bilaterally clear, and respiratory rate was within reference limits. Her abdomen was soft, nontender, and nondistended, with no hepatosplenomegaly. On auscultation of the cardiovascular system, fixed splitting of S2 and grade 3 holosystolic murmur were audible. The patient's extremities exhibited no skin lesions and were well perfused. Initial investigations indicated leukocyte count 7,600 cells/ μL , hemoglobin 14.4 g/dL, platelets 61,000 cells/ μL , and CRP 11.86 mg/L. Chest radiographs revealed mild cardiomeastinal magnification and congestive changes along with right hilar congestion but no consolidation, collapse, or definite pneumothorax. Costophrenic angles were intact.

After admission, treatment with intravenous meropenem (700 mg 3 \times /d infused over 2 h) and intravenous colistin (40 mg 2 \times /d) was initiated. The patient was closely monitored and became afebrile on day 3 of therapy. A 2-dimensional echocardiogram showed no vegetations. Results of repeat blood cultures and fecal cultures were negative. The patient was discharged after completing 11 days of treatment. At a 2-week follow-up visit, she was back to her usual state of health; typhoid vaccination 2 weeks later was recommended.

The isolate obtained during relapse was sent to the UK Gastrointestinal Bacteria Reference Unit, where we confirmed *Salmonella* Typhi by PCR (6) and cultured it on blood and MacConkey agar plates to ensure purity. We isolated 2 distinct morphologic variants: variant

Table. MICs and antimicrobial drug resistance determinants of *Salmonella* Typhi isolated from patient during clinical disease relapse of carbapenem-resistant *Salmonella* Typhi infection, Pakistan, 2022*

Antimicrobial drug	1790097 (variant 1)		1790125 (variant 2)	
	Gene/ mutation	MIC, $\mu\text{g}/\text{L}$	Gene/mutation	MIC, $\mu\text{g}/\text{L}$
Ampicillin	<i>bla</i> _{NDM-5} , <i>bla</i> _{TEM-1}	32	<i>bla</i> _{NDM-5} , <i>bla</i> _{TEM-1} , <i>bla</i> _{CTX-M-15}	32
Azithromycin	<i>mphA</i>	64	<i>mphA</i>	64
Cefoxitin	<i>bla</i> _{NDM-5}	64	<i>bla</i> _{NDM-5}	64
Tetracycline	<i>tetA</i>	32	<i>tetA</i>	32
Tigecycline	NA	0.25	NA	0.25
Ertapenem	<i>bla</i> _{NDM-5}	2	<i>bla</i> _{NDM-5}	2
Imipenem	<i>bla</i> _{NDM-5}	16	<i>bla</i> _{NDM-5}	16
Meropenem	<i>bla</i> _{NDM-5}	16	<i>bla</i> _{NDM-5}	16
Cefotaxime	<i>bla</i> _{NDM-5}	64	<i>bla</i> _{NDM-5} , <i>bla</i> _{CTX-M-15}	64
Ceftazidime	<i>bla</i> _{NDM-5}	128	<i>bla</i> _{NDM-5} , <i>bla</i> _{CTX-M-15}	128
Cefepime	<i>bla</i> _{NDM-5}	32	<i>bla</i> _{NDM-5} , <i>bla</i> _{CTX-M-15}	32
Nalidixic acid	<i>gyrA</i> [83:S-F]	64	<i>gyrA</i> [83:S-F], <i>qnrS1</i>	64
Ciprofloxacin	<i>gyrA</i> [83:S-F]	1	<i>gyrA</i> [83:S-F], <i>qnrS1</i>	8
Chloramphenicol	NA	8	<i>catA</i>	64
Trimethoprim	<i>dfrA-27</i> , <i>dfrA-7</i>	16	<i>dfrA-27</i> , <i>dfrA-7</i>	16
Sulfonamide	<i>sul-1</i>	512	<i>sul-1</i>	512
Amikacin	<i>aac(6')-Ib-cr</i> , <i>aac(6')-Ia</i>	≤ 4	<i>aac(6')-Ib-cr</i> , <i>aac(6')-Ia</i>	8
Gentamicin	<i>aac(6')-Ib-cr</i> , <i>aadA-16</i> , <i>aac(6')-Iy</i>	≤ 0.5	<i>aac(6')-Ib-cr</i> , <i>aadA-16</i> , <i>aac(6')-Iy</i>	≤ 0.5
Temocillin	<i>bla</i> _{NDM-5}	128	<i>bla</i> _{NDM-5}	128
Colistin	NA	1	NA	1

*Boldface indicates additional genes detected and increased MIC values for variant 2. NA, not applicable.

1 (large colony, isolate 1790097) and variant 2 (small colony, isolate 1790125) (Figure). Each variant underwent whole-genome sequencing for single-nucleotide polymorphism typing, core-genome multilocus sequence typing, and antimicrobial resistance determination (7,8). We analyzed phylogeny of both strains in the context of *Salmonella* Typhi reported in England in 2016–2019 (Appendix Figure, <https://wwwnc.cdc.gov/EID/article/29/11/23-0499-App1.pdf>) and visualized them on ITOL (9). We performed MIC testing by using a Thermo Scientific sensititre broth microdilution system (<https://www.thermofisher.com>) on EUVSEC2 and EUVSEC3 plates and confirmed carbapenemase production by Liofilchem metallo- β -lactamase Etest (<http://www.liofilcheminc.com>). Breakpoints and screening concentration criteria used for interpretation were recommended by the European Committee on Antimicrobial Susceptibility Testing (10).

Variants 1 and 2 were XDR *Salmonella* Typhi, resistant to azithromycin and carbapenems; variant 2 had additional antimicrobial resistance determinants (Table). Testing with the metallo- β -lactamase Etest indicated that both variants were carbapenemase producers.

The most likely explanation for the patient's relapse, with *Salmonella* Typhi resistant to carbapenems and azithromycin resulting from acquisition of new resistance determinants *bla*_{NDM-5} and *mphA*, is multiple genetic mutations acquired via a mobile transmissible element such as a plasmid from gut microbiota. Previous receipt of carbapenems and azithromycin for multiple respiratory infections likely led to harboring and selection pressure for carbapenemase-producing strains. Another possibility is a suboptimal host immune response because of Down syndrome, although the patient had not undergone an immunology assessment. Expansion of antimicrobial-resistant strains will make such infections extremely difficult to treat.

Acknowledgments

We thank Amy Gentle for the phenotypic MIC testing.

M.A.C. is affiliated with the National Institute for Health Research, Health Protection Research Unit in Genomics and Enabling Data at University of Warwick in partnership with the UK Health Security Agency. The views expressed are those of the author(s) and not necessarily those of the National Institute for Health Research, the Department of Health and Social Care, or the UK Health Security Agency.

About the Author

Dr. Nizamuddin is the consultant medical microbiologist and section head at the Shaukat Khanum Memorial Cancer

Hospital and Research Centre in Lahore, Pakistan. Her research interests include antibiotic resistance surveillance, antibiotic stewardship, and telepathology.

References

- Klemm EJ, Shakoor S, Page AJ, Qamar FN, Judge K, Saeed DK, et al. Emergence of an extensively drug-resistant *Salmonella enterica* serovar Typhi clone harboring a promiscuous plasmid encoding resistance to fluoroquinolones and third-generation cephalosporins. *MBio*. 2018;9:e00105-18. <https://doi.org/10.1128/mBio.00105-18>
- Kamal R, Ching C, Zaman MH, Sultan F, Abbas S, Khan E, et al. Identification of multiple variant extensively drug-resistant typhoid infections across Pakistan. *Am J Trop Med Hyg*. 2023;108:278–84. <https://doi.org/10.4269/ajtmh.22-0071>
- Nair S, Chattaway M, Langridge GC, Gentle A, Day M, Ainsworth EV, et al. ESBL-producing strains isolated from imported cases of enteric fever in England and Wales reveal multiple chromosomal integrations of *bla*_{CTX-M-15} in XDR *Salmonella* Typhi. *J Antimicrob Chemother*. 2021;76:1459–66. <https://doi.org/10.1093/jac/dkab049>
- Nabarro LE, McCann N, Herdman MT, Dugan C, Ladhani S, Patel D, et al. British infection association guidelines for the diagnosis and management of enteric fever in England. *J Infect*. 2022;84:469–89. <https://doi.org/10.1016/j.jinf.2022.01.014>
- Medical Microbiology & Infectious Diseases Society of Pakistan. Typhoid management guidelines 2022 [cited 2023 Apr 1]. <https://www.mmisp.com/wp-content/uploads/2023/03/Typhoid-Management-Guideline-2022-Jun-22.pdf>
- Nair S, Patel V, Hickey T, Maguire C, Greig DR, Lee W, et al. Real-time PCR assay for differentiation of typhoidal and nontyphoidal *Salmonella*. *J Clin Microbiol*. 2019;57:e00167-19. <https://doi.org/10.1128/JCM.00167-19>
- Dallman T, Ashton P, Schafer U, Jironkin A, Painset A, Shaaban S, et al. SnapperDB: a database solution for routine sequencing analysis of bacterial isolates. *Bioinformatics*. 2018;34:3028–9. <https://doi.org/10.1093/bioinformatics/bty212>
- Chattaway MA, Dallman TJ, Larkin L, Nair S, McCormick J, Mikhail A, et al. The transformation of reference microbiology methods and surveillance for *Salmonella* with the use of whole genome sequencing in England and Wales. *Front Public Health*. 2019;7:317. <https://doi.org/10.3389/fpubh.2019.00317>
- Chattaway MA, Gentle A, Nair S, Tingley L, Day M, Mohamed I, et al. Phylogenomics and antimicrobial resistance of *Salmonella* Typhi and Paratyphi A, B and C in England, 2016-2019. *Microb Genom*. 2021;7:000633. <https://doi.org/10.1099/mgen.0.000633>
- The European Committee on Antimicrobial Susceptibility Testing. Breakpoint tables for interpretation of MICs and zone diameters. Version 13.0, 2023 [cited 2023 Apr 1]. <http://www.eucast.org>

Address for correspondence: Summiya Nizamuddin, Shaukat Khanum Memorial Cancer Hospital and Research Centre Pathology, 7 A, Block R 3, Johar Town Lahore Lahore State 12345, Pakistan; email: summi.niz@gmail.com

Ceftazidime/Avibactam Resistance in Carbapenemase-Producing *Klebsiella pneumoniae*

Qiaozhen Cui,¹ Chen Wang,¹ Qichen Wang, Juanxiu Qin, Min Li, Baixing Ding, Zhen Shen

Author affiliations: Shanxi Provincial People's Hospital, Taiyuan, China (Q. Cui); Renji Hospital at Shanghai Jiao Tong University School of Medicine, Shanghai, China (C. Wang, Q. Wang, J. Qin, M. Li, Z. Shen); Huashan Hospital at Fudan University, Shanghai (B. Ding); Key Laboratory of Clinical Pharmacology of Antibiotics, Ministry of Health, Shanghai (B. Ding)

DOI: <https://doi.org/10.3201/eid2911.230830>

We identified a novel ceftazidime/avibactam resistance mechanism in sequence type 11 *Klebsiella pneumoniae* carbapenemase 2–producing *K. pneumoniae*. Plasmid recombination and chromosomal integration formed a novel virulence plasmid and provided an additional promoter for *bla*_{SHV-12}, leading to *bla*_{SHV-12} overexpression and ceftazidime/avibactam resistance. Genetic rearrangement contributed to convergence of hypervirulence and ceftazidime/avibactam resistance.

Emergence and global dissemination of carbapenem-resistant *Klebsiella pneumoniae* pose therapeutic challenges to public health (1). The most crucial cause of carbapenem resistance in *K. pneumoniae* is carbapenemase production; thus, the novel β -lactamase inhibitor ceftazidime/avibactam (CAZ/AVI) provides an antimicrobial strategy (1–3). However, its increasing use raises resistance concerns. According to the China Antimicrobial Surveillance Network (<http://www.chinets.com/Data/AntibioticdrugFast>), 9.9% of *K. pneumoniae* carbapenemase (KPC) 2–producing *K. pneumoniae* (KPC-KP) displayed CAZ/AVI resistance (4). β -lactamase amino acid substitutions are the dominant mechanisms that lead to CAZ/AVI resistance (5). Mutations in class A β -lactamases, especially KPCs, have been reported (5). Substitutions in KPCs could improve ceftazidime affinity or reduce avibactam inhibition (5). We report a novel CAZ/AVI resistance mechanism in epidemic sequence type (ST) 11 KPC-KP. All study procedures involving human participants and animals were in accordance with the ethics standards of the Institutional Review Board Ethics Committee of Shanxi

Provincial People's Hospital; this type of retrospective study did not require formal consent.

In 2021, a 62-year-old man was transferred from another hospital to a teaching hospital in Shanxi Province, China. Before transfer, a blood culture indicated CAZ/AVI-susceptible carbapenem-resistant *K. pneumoniae*. The patient received 1 week of CAZ/AVI therapy before transfer and another week of CAZ/AVI therapy after admission. In addition to the bloodstream infection, severe pneumoniae, multiple duodenal ulcers, and gastrointestinal hemorrhage de-

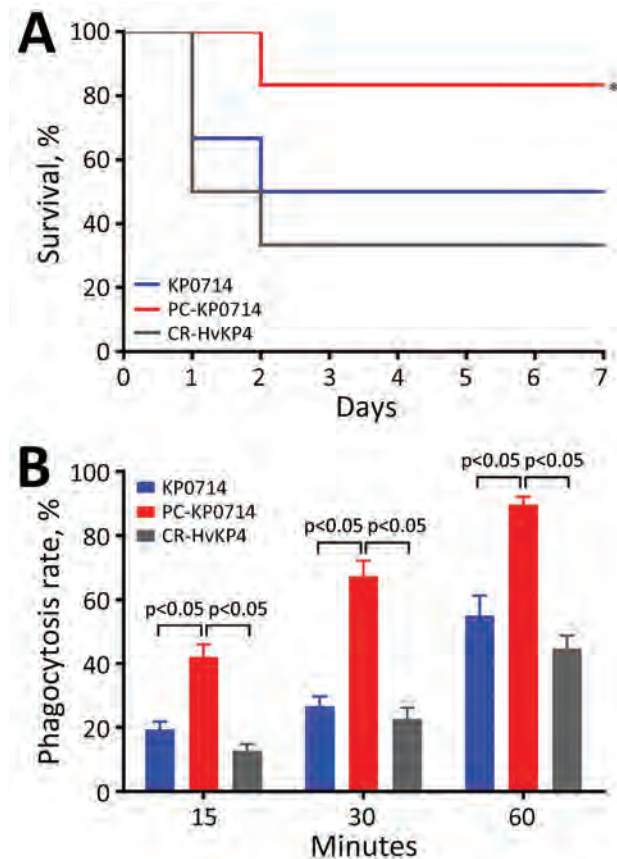


Figure 1. Linear alignment of plasmid pVir-KP0714 and virulence potential determination of *Klebsiella pneumoniae* isolate KP0714 in study of ceftazidime/avibactam resistance in carbapenemase-producing *K. pneumoniae*. A) Virulence potential determination of KP0714 and pVir-KP0714–curing mutant (PC-KP0714) in a mouse infection model. Sequence type 11 carbapenem-resistant hypervirulent *K. pneumoniae* strain CR-HvKP4 was used as a hypervirulence control. Bacterial suspensions in the logarithmic growth phase were diluted in sterile phosphate-buffered saline to 10^7 CFU/mL. Six female BALB/c mice were used as a sample population for each isolate. BALB/c mice were infected intraperitoneally with 0.1 mL of the diluted bacterial suspension. Clinical signs and mortality rates were noted for 7 days. * $p < 0.05$ when compared with PC-KP0714. B) Human neutrophil assays of KP0714. Error bars indicate SDs. p values were computed by 1-way analysis of variance with Bonferroni correction.

¹These first authors contributed equally to this article.

veloped. Two weeks after CAZ/AVI withdrawal, we isolated KP0714, which was resistant to all β -lactams tested but susceptible to tigecycline and polymyxin B (Appendix Table 1, <https://wwwnc.cdc.gov/EID/article/29/11/23-0830-App1.pdf>). We generated the KP0714 complete genome by using the combination of Illumina and PacBio RS sequencing (Appendix Table 2), and it belonged to ST11. The resistance plasmid pKPC-KP0714 carries *bla*_{KPC-2} and several other resistance genes, including *bla*_{TEM-17}, *rmtB*, and *fosA3* (Appendix Table 2), and KPC-2 S130A substitution was constructed in situ. KP0714 and the KPC-2 S130A mutant displayed the same MICs for CAZ/AVI, suggesting that *bla*_{KPC-2} was not involved in CAZ/AVI resistance (Appendix Table 1).

KP0714 possessed a novel IncFIB(K)-type virulence plasmid pVir-KP0714, encoding siderophore aerobactin (*iucABCDiutA*) and capsular polysaccharide regulator RmpA2. pVir-KP0714 was 99.97% identical to reference plasmid pOXA1_020030 (GenBank accession no. CP028791) from *K. pneumoniae* strain WCHKP020030 at 74% coverage. Both ends of pVir-KP0714 were absent from pOXA1_020030 but were highly homologous to another plasmid, pLAP2_020030 (GenBank accession no. CP028792), from WCHKP020030 (Figure 1; Appendix Figure 1). Multiple mobile genetic elements on these plasmids suggested that pVir-KP0714 was generated through genetic recombination between pOXA1_020030 and pLAP2_020030, which not only formed a novel virulence plasmid but also contributed to chromosomal integration of a 45-kb plasmid fragment from pLAP2_020030 (Figure 1; Appendix Figure 1). The 45-kb fragment that had not been integrated into pVir-KP0714 was divided into the upstream 30-kb fragment and a 15-kb genetic context containing *bla*_{SHV-12'} which were independently inserted into the chromosome. The 15-kb genetic context containing *bla*_{SHV-12} was flanked by several IS26 insertion sequences and harbored 3 other resistance genes, *bla*_{LAP-2'}, *qnrS1*, and *aph(3')-Ia*, which exhibited 100% identity and 100% query coverage with the reference plasmid pLAP2_020030 (Figure 2; Appendix Figure 2).

However, we observed substantial structural changes in this chromosomal insertion fragment compared with pLAP2_020030 (Figure 2; Appendix Figure 2). The reversion and rearrangement of IS26-*aph(3')-Ia* provided an additional promoter P2 for *bla*_{SHV-12} (Figure 2; Appendix Figure 2). To determine the role of promoter P2 in CAZ/AVI resistance, we deleted P2 and the original promoter P1 of *bla*_{SHV-12} by using a pConj working vector-based genetic engineering approach

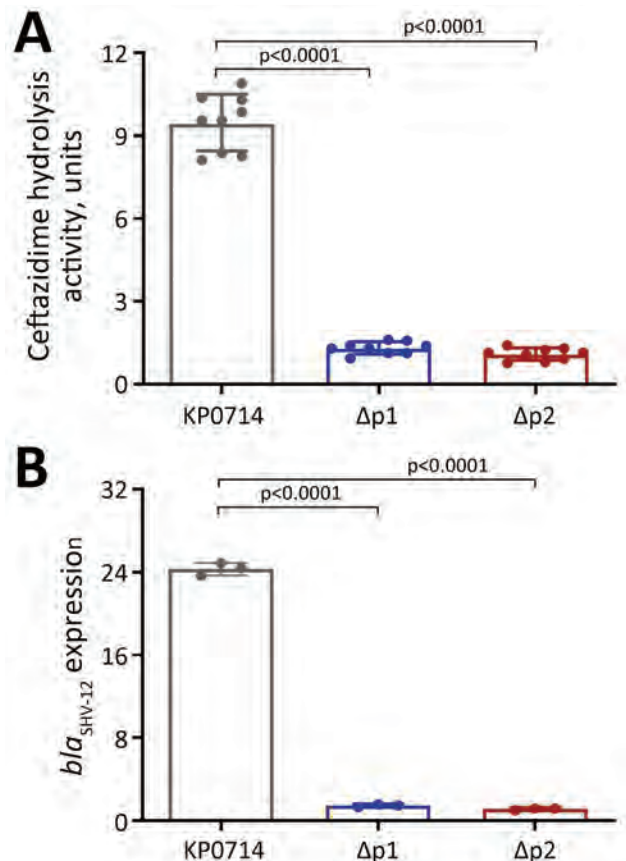


Figure 2. Overexpression of *bla*_{SHV-12} contributing to ceftazidime/avibactam resistance in *Klebsiella pneumoniae* isolate KP0714 in study of ceftazidime/avibactam resistance in carbapenemase-producing *K. pneumoniae*. A) Relative *bla*_{SHV-12} expression level. B) Ceftazidime hydrolysis activity of different *bla*_{SHV-12} promoter deletion mutants. One unit of enzyme activity was defined as the amount of enzyme that hydrolyzed 1 nmol of substrate per min. Error bars indicate SDs. p values were computed by 1-way analysis of variance with Bonferroni correction.

(6). Deletion of P1 or P2 could completely restore KP0714 susceptibility to CAZ/AVI; CAZ/AVI MICs were 2 and 1 $\mu\text{g}/\text{mL}$, respectively (Appendix Table 1). The relative expression of *bla*_{SHV-12} in KP0714 was ≈ 20 -fold higher than in $\Delta P1$ and $\Delta P2$ mutants (Figure 2; Appendix Figure 2). Similarly, the hydrolysis activity of ceftazidime in KP0714 was significantly higher than that of $\Delta P1$ and $\Delta P2$ mutants ($p < 0.0001$). Those results demonstrated that CAZ/AVI resistance in KP0714 was attributed to overexpression of *bla*_{SHV-12} resulting from an additional promoter, and the original promoter P1 was also necessary for the biological function of P2.

Because a novel virulence plasmid pVir-KP0714 was formed through plasmid recombination, we determined the virulence potential of KP0714 by using a mouse infection model and human neutrophil

phagocytosis assay (7). As the hypervirulence control, we used the previously reported ST11 carbapenem-resistant hypervirulent *K. pneumoniae* strain CR-HvKP4 (8). We found no statistical difference regarding mouse survival and neutrophil phagocytosis between KP0714 and CR-HvKP4 (Figure 1; Appendix Figure 2), suggesting convergence of hypervirulence and CAZ/AVI resistance in KP0714. In contrast, mouse survival rates were significantly higher and human neutrophil phagocytosis rates were significantly lower for KP0714 and CR-HvKP4 at each time point when compared with virulence plasmid pVir-KP0714-curing KP0714 (PC-KP0714), demonstrating that KP0714 hypervirulence was attributed to acquisition of virulence plasmid pVir-KP0714.

In conclusion, KP0714 high-level resistance to carbapenems and CAZ/AVI, compensating for decreased carbapenem hydrolyzation activity of KPC variants (5,9), highlights a novel evolution pathway for development of CAZ/AVI resistance in epidemic ST11 KPC-KP, posing a threat to clinical antimicrobial therapy. Emerging CAZ/AVI-resistant and hypervirulent ST11 KPC-KP might be continuously evolving and warrants prospective monitoring.

Acknowledgment

We thank the authority of CR-HvKP4 by Rong Zhang from the Second Affiliated Hospital of Zhejiang University.

This study was supported by National Natural Science Foundation of China (82272374), Shanghai Pujiang Program (22PJ1409600), and a research fund from Renji Hospital for young scholars (RJTJ22-MS-018). The funders had no role in study design, data collection and analysis, decision to publish, or preparation of the manuscript.

The complete genome sequences of KP0714 were deposited in the GenBank (accession nos. CP128191–5).

About the Author

Mrs. Cui is a researcher at Shanxi Provincial People's Hospital of Shanxi Medical University. Her research interests are epidemiology and antimicrobial-resistance mechanisms of carbapenem-resistant *Enterobacteriaceae*.

References

- Dong N, Yang X, Chan EWC, Zhang R, Chen S. *Klebsiella* species: taxonomy, hypervirulence and multidrug resistance. *EBioMedicine*. 2022;79:103998. <https://doi.org/10.1016/j.ebiom.2022.103998>
- Liu C, Dong N, Chan EWC, Chen S, Zhang R. Molecular epidemiology of carbapenem-resistant *Klebsiella pneumoniae* in China, 2016–20. *Lancet Infect Dis*. 2022;22:167–8. [https://doi.org/10.1016/S1473-3099\(22\)00009-3](https://doi.org/10.1016/S1473-3099(22)00009-3)
- Bush K, Bradford PA. Interplay between β -lactamases and new β -lactamase inhibitors. *Nat Rev Microbiol*. 2019;17:295–306. <https://doi.org/10.1038/s41579-019-0159-8>
- Guo Y, Han R, Jiang B, Ding L, Yang F, Zheng B, et al.; China Antimicrobial Surveillance Network (CHINET) Study Group. In vitro activity of new β -lactam- β -lactamase inhibitor combinations and comparators against clinical isolates of gram-negative bacilli: results from the China Antimicrobial Surveillance Network (CHINET) in 2019. *Microbiol Spectr*. 2022;10:e0185422. <https://doi.org/10.1128/spectrum.01854-22>
- Xiong L, Wang X, Wang Y, Yu W, Zhou Y, Chi X, et al. Molecular mechanisms underlying bacterial resistance to ceftazidime/avibactam. *WIREs Mech Dis*. 2022;14:e1571. <https://doi.org/10.1002/wsbm.1571>
- Liu G, Beaton SE, Grieve AG, Evans R, Rogers M, Strisovsky K, et al. Bacterial rhomboid proteases mediate quality control of orphan membrane proteins. *EMBO J*. 2020;39:e102922. <https://doi.org/10.15252/embj.2019102922>
- Shen Z, Gao Q, Qin J, Liu Y, Li M. Emergence of an NDM-5-producing hypervirulent *Klebsiella pneumoniae* sequence type 35 strain with chromosomal integration of an integrative and conjugative element, ICEKp1. *Antimicrob Agents Chemother*. 2019;64:e01675–19. <https://doi.org/10.1128/AAC.01675-19>
- Gu D, Dong N, Zheng Z, Lin D, Huang M, Wang L, et al. A fatal outbreak of ST11 carbapenem-resistant hypervirulent *Klebsiella pneumoniae* in a Chinese hospital: a molecular epidemiological study. *Lancet Infect Dis*. 2018;18:37–46. [https://doi.org/10.1016/S1473-3099\(17\)30489-9](https://doi.org/10.1016/S1473-3099(17)30489-9)
- Shi Q, Yin D, Han R, Guo Y, Zheng Y, Wu S, et al. Emergence and recovery of ceftazidime-avibactam resistance in *bla*_{KPC-33}-harboring *Klebsiella pneumoniae* sequence type 11 isolates in China. *Clin Infect Dis*. 2020;71(Suppl 4):S436–9. <https://doi.org/10.1093/cid/ciaa1521>

Address for correspondence: Zhen Shen, Department of Laboratory Medicine, Renji Hospital, School of Medicine, Shanghai Jiao Tong University, 160 Pujian Rd, Shanghai, China; email: zhenshen@shsmu.edu.cn. Baixing Ding, Institute of Antibiotics, Huashan Hospital, Fudan University, No. 12 Wulumuqi Rd, Shanghai, China; email: dingbaixing@126.com

Refractory *Microascus* Bronchopulmonary Infection Treated with Olorofim, France

Emmanuel Faure, Olivier Brugière, Sylvie Colin de Verdier, Fanny Vuotto, Lucie Limousin, Emilie Cardot, Camille Cordier, Pauline Coulon, Dea Garcia-Hermoso, Olivier Lortholary, Fanny Lanternier

Author affiliations: Université de Lille, Lille, France (E. Faure); Centre Hospitalier Régional Universitaire Lille, Lille (E. Faure, F. Vuotto, C. Cordier, P. Coulon); Hôpital Foch, Suresnes, France (O. Brugière, S. Colin de Verdier, L. Limousin, E. Cardot); Institut Pasteur, Paris, France (D. Garcia-Hermoso, O. Lortholary, F. Lanternier); University Hospital Necker for Sick Children, Assistance Publique-Hôpitaux de Paris, Paris (O. Lortholary, F. Lanternier)

DOI: <https://doi.org/10.3201/eid2911.230984>

We report 3 cases of successful treatment of *Microascus* spp. bronchopulmonary infection in a multiple-traumatized patient and 2 lung transplant recipients in France. We emphasize the promising use of olorofim antifungal therapy in a rising context of intrinsically less-susceptible respiratory infections caused by mold.

The family Microasaceae includes genera *Microascus* and *Scopulariopsis*, opportunistic fungi that have caused respiratory infection associated with poor outcome and an attributable mortality rate of 85%–100% (1,2). Treatment of invasive *Microascus* infection is challenging because of its high resistance to available therapies. Olorofim, a reversible inhibitor of the enzyme dihydroorotate dehydrogenase, has

shown in vitro activity against a variety of mold species, including azole-resistant *Aspergillus* (3,4) and *Microascus* spp. (5). We describe 3 cases of invasive *Microascus* respiratory infection in France that were treated with olorofim (Table). All patients gave informed consent for publication.

Case 1 occurred in a 17-year-old boy with unremarkable medical history who was found unconscious with inhalation pneumonia, bilateral hemothorax, and bilateral thoracic drainage after falling from the top of a rice silo (Appendix Figure 1, <https://wwwnc.cdc.gov/EID/article/29/11/23-0984-App1.pdf>). On day 2, the patient underwent venovenous extracorporeal membrane oxygenation. On day 38, after 5 weeks of adapted antimicrobial treatment, thoracic computed tomography (CT) scan showed worsening of bilateral necrotizing pneumonia with abscess. Bronchoalveolar lavage (BAL) and several bronchial aspirations grew a restricted light-gray fungal colony (Appendix Figure 2), identified through the Paris National Reference Center as compatible with *Microascus melanosporus*; we initiated a combination of olorofim (180 mg 2×/d on day 1, followed by 90 mg 2×/d) and terbinafine (500 mg 2×/d) for 6 weeks (Appendix Table). Radiologic findings and general clinical status improved; we discontinued oxygen support after 2 weeks (day 73). The last CT scan showed complete healing of lung lesions (day 120). The patient was still alive 1 year later.

Case 2 occurred in a 61-year-old lung transplant recipient who sought care for respiratory deterioration and decline in respiratory function. He had recently received isavuconazole for bronchial colonization with *Aspergillus flavus*. Thoracic CT scan at admission showed a new alveolar consolidation in the left upper lobe (Appendix Figure 3); fibroscopy showed a recent-onset yellowish irregular lesion in the culminal bronchus (Figure, panel A). We isolat-

Table. Medical history and keypoints of 3 case-patients with refractory microascus bronchopulmonary infection, France*

Characteristic	Case 1	Case 2	Case 3
Age, y	17	61	65
Immunocompromised status	No	Lung transplant	Lung transplant
Years since transplantation	NA	4	6
Chronic lung allograft dysfunction	NA	Y (for 2 y)	Y (for 5 y)
Intensification of immunosuppressive drug regimen in medical history	NA	Antithymocyte globulin, steroids, rituximab, alemtuzumab, extracorporeal photopheresis	Steroids, rituximab, bortezomib
Maintenance therapy on the onset of <i>Microascus</i> infection	NA	Tacrolimus (C ₀ 4-6 ng/mL), everolimus (C ₀ 4-6 ng/mL), prednisone (5 mg/d)	Tacrolimus (C ₀ 4-6 ng/mL), Everolimus (C ₀ 4-6 ng/mL), prednisone (5 mg/d)
Recent antifungal exposition <3 mo	None	Isavuconazole	Isavuconazole
Tolerance			
Clinical	No SSE	NA	No SSE
Biologic	No ELE	Drug interaction with tacrolimus and everolimus	No ELE

*ELE, elevated liver enzyme; NA, not applicable; SSE, significant side effect.

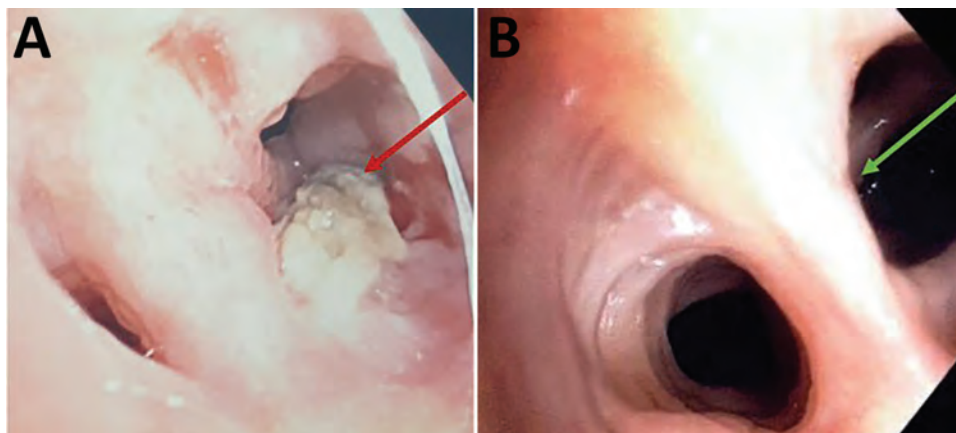


Figure. Macroscopic observation of endobronchial *Microascus cirrosus* lesion in patient in France with refractory microascus bronchopulmonary infection before (A) and after (B) olorofim treatment. Arrows indicate the lesion.

ed *M. cirrosus* from a culture of bronchial aspirate and BAL. We found no other disseminated lesions and retained the diagnosis of invasive pulmonary *M. cirrosus* infection. We initiated olorofim (90 mg 2×/d). We observed, as previously described (6), a moderate increase of both tacrolimus and everolimus blood through levels, which may have been caused by olorofim, a weak inhibitor of CYP 3A4. After 3 months of treatment, lung function slightly improved, CT scan showed a near-complete disappearance of the consolidation, and BAL culture was sterile. After 8 months of olorofim treatment, the endobronchial lesion was gone (Figure, panel B). *M. cirrosus* was found in BAL after 6 months of olorofim, but no more was cultured from BAL 7 months after treatment initiation. The patient was still being treated with olorofim at 9 months.

Case 3 occurred in a 65-year-old lung transplant recipient who sought care for dyspnea. He had experienced progressive decline of respiratory function and had a diagnosis of grade 3 bronchiolitis obliterative syndrome (BOS) linked to obstructive respiratory failure 6 years after transplant. He required permanent oxygen support. At admission, he received isavuconazole that continued for 3 months because of bronchial colonization with *A. fumigatus*. Thoracic CT scan results showed an unchanged pattern of BOS. Nevertheless, bronchial fibroscopy showed a new-onset bronchial lesion, necrotic and blackish in appearance, obstructing the origin of the culminal bronchus (Appendix Figure 4). We isolated *M. cirrosus* samples. Patient received a combination of oral terbinafine (500 mg 2×/d) and olorofim (180 mg 2×/d on day 1 followed by 90 mg 2×/d). After 3 months of treatment, bronchial fibroscopy showed an improvement of the bronchial lesion, and *M. cirrosus* was not found in respiratory specimens. The patient died from respiratory failure attributed to progression of BOS.

Use of olorofim for invasive *Microascus* spp. respiratory infection has not previously been reported with a successful outcome; previous studies were conducted in vitro (4). Miossec et al. (1) reported a series of 9 cases; all 9 patients had a medical history of stem cell or solid organ transplantation, and 8 died. The only survivor was a patient considered immunocompetent with no identified underlying conditions. A fatal *Microascus* sp. lung infection was previously published in a lung transplant recipient (6). Here, we report 2 lung transplant recipients infected with *M. cirrosus*, a ubiquitous mold isolated from soil and moist indoor environments (7). The third case we report was a young immunocompetent adult with no underlying conditions infected with *M. melanosporus*; his exposure by falling in a rice silo and sustaining serious injuries may explain the onset of opportunistic infection.

Microascus spp. and *Scopulariopsis* (8) exhibit a multidrug-resistant phenotype (9). Skóra et al. reported antifungal susceptibility results of several *Microascus* species and confirmed high resistance to ciclopirox, 5-fluorocytosine, amphotericin B, and azoles. However, among echinocandin, lower minimum effective concentrations for caspofungin were reported (10). The highest in vitro activity was observed with terbinafine (10); synergistic activity was observed against some *Scopulariopsis* strains (9). Wiederhold et al. reported promising activity of olorofim on *Scopulariopsis* spp. and *Microascus* spp. fungi (5), but no synergistic in vitro activity was reported between olorofim and terbinafine against *Microascus* spp.

Acknowledgments

We thank F2G laboratory (Manchester, UK) for providing olorofim for compassionate use after reviewing the medical history of the cases with O.L. and F.L.

Author contributions: E.F., O.B., and E.C. were involved in patient care. C.C., P.C., and L.L. were mycologists in charge of laboratory investigations. O.L. and F.L. reviewed the Centre national de référence des mycoses invasives et antifongiques (CNRMA) materials. D.G.H. is responsible for mycological laboratory investigations in the CNRMA and performed identification of strains and extended antimicrobial susceptibility. E.H. managed the compassionate use in F2G laboratory. E.F., O.B., and F.L. wrote the manuscript. All co-authors reviewed the manuscript.

About the Author

Dr. Faure is an associate professor at Lille University and infectious disease specialist at Lille University Hospital. His primary interests include infection in immunocompromised hosts and host–pathogen interactions.

References

- Miossec C, Morio F, Lepoivre T, Le Pape P, Garcia-Hermoso D, Gay-Andrieu F, et al. Fatal invasive infection with fungemia due to *Microascus cirrosus* after heart and lung transplantation in a patient with cystic fibrosis. *J Clin Microbiol*. 2011;49:2743–7. <https://doi.org/10.1128/JCM.00127-11>
- Liu Q, Kong L, Hua L, Xu S. Pulmonary *Microascus cirrosus* infection in an immunocompetent patient with bronchiectasis: a case report. *Respir Med Case Rep*. 2021;34:101484. <https://doi.org/10.1016/j.rmcr.2021.101484>
- Georgacopoulos O, Nunnally NS, Ransom EM, Law D, Birch M, Lockhart SR, et al. In vitro activity of novel antifungal olorofim against filamentous fungi and comparison to eight other antifungal agents. *J Fungi (Basel)*. 2021;7:378. <https://doi.org/10.3390/jof7050378>
- Wiederhold NP. Review of the novel investigational antifungal olorofim. *J Fungi (Basel)*. 2020;6:122. <https://doi.org/10.3390/jof6030122>
- Wiederhold NP, Patterson HP, Sanders CJ, Cañete-Gibas C. Dihydroorotate dehydrogenase inhibitor olorofim has potent in vitro activity against *Microascus/Scopulariopsis*, *Rasamsonia*, *Penicillium* and *Talaromyces* species. *Mycoses*. 2023;66:242–8. <https://doi.org/10.1111/myc.13548>
- Schoeppler KE, Zamora MR, Northcutt NM, Barber GR, O'Malley-Schroeder G, Lyu DM. Invasive *Microascus trigonosporus* species complex pulmonary infection in a lung transplant recipient. *Case Rep Transplant*. 2015;2015:745638. <https://doi.org/10.1155/2015/745638>
- Woudenberg JHC, Meijer M, Houbraken J, Samson RA. *Scopulariopsis* and *scopulariopsis*-like species from indoor environments. *Stud Mycol*. 2017;88:1–35. <https://doi.org/10.1016/j.simyco.2017.03.001>
- Aguilar C, Pujol I, Guarro J. In vitro antifungal susceptibilities of *Scopulariopsis* isolates. *Antimicrob Agents Chemother*. 1999;43:1520–2. <https://doi.org/10.1128/AAC.43.6.1520>
- Cuenca-Estrella M, Gomez-Lopez A, Buitrago MJ, Mellado E, Garcia-Effron G, Rodriguez-Tudela JL. In vitro activities of 10 combinations of antifungal agents against the multiresistant pathogen *Scopulariopsis brevicaulis*. *Antimicrob Agents Chemother*. 2006;50:2248–50. <https://doi.org/10.1128/AAC.00162-06>
- Skóra M, Bulanda M, Jagielski T. *In vitro* activities of a wide panel of antifungal drugs against various *Scopulariopsis* and *Microascus* species. *Antimicrob Agents Chemother*. 2015;59:5827–9. <https://doi.org/10.1128/AAC.00978-15>

Address for correspondence: Emmanuel Faure, CHRU de Lille—Service Universitaire de Maladies infectieuses, 1 rue Michel Polonovski Lille Nord 59037, France; email: emmanuel.faure@univ-lille.fr

Tuberculosis Variant with Rifampin Resistance Undetectable by Xpert MTB/RIF, Botswana

Chawangwa Modongo, Ivan Barilar, Qiao Wang, Tuduetso Molefi, Topo Makhondo, Stefan Niemann, Sanghyuk S. Shin

Author affiliations: Victus Global Botswana Organisation, Gaborone, Botswana (C. Modongo); Forschungszentrum, Borstel, Germany (I. Barilar, S. Niemann); University of California, Irvine, California, USA (Q. Wang, S.S. Shin); University of California, Los Angeles, California, USA (Q. Wang); Botswana Ministry of Health and Wellness, Gaborone (T. Molefi, T. Makhondo); German Center for Infection Research, Partner Site Hamburg-Lübeck-Borstel-Riems, Borstel, Germany (S. Niemann)

GeneXpert MTB/RIF, a tool widely used for diagnosing tuberculosis, has limitations for detecting rifampin resistance in certain variants. We report transmission of a pre-extensively drug-resistant variant in Botswana that went undetected by GeneXpert. The public health impact of misdiagnosis emphasizes the need for comprehensive molecular testing to identify resistance and guide treatment.

DOI: <https://doi.org/10.3201/eid2911.230987>

The GeneXpert (Xpert) MTB/RIF assay (Cepheid, <https://www.cepheid.com>) has enabled rapid molecular diagnosis of tuberculosis (TB) and identification of resistance to rifampin, a critical first-line TB drug (1). Operating with minimal infrastructure in a cartridge-based system, the assay is the primary TB diagnostic method in many countries (2). Xpert

MTB/RIF detects rifampin resistance by identifying mutations in an 81-bp region of the *rpoB* gene but does not detect resistance-conferring mutations outside that region (3,4). We report a case of a multidrug-resistant (MDR) *Mycobacterium tuberculosis* complex (MTBC) strain in Botswana with a rifampin resistance-conferring mutation, *rpoB* I491F, not detected by Xpert MTB/RIF (3,4). Genomic epidemiology suggested that the infection was part of a transmission chain spanning ≥ 5 years.

The patient was a 44-year-old man who, in August 2021, sought treatment at a public health clinic in Botswana for cough, fever, and night sweats. Xpert MTB/RIF detected MTBC, but no rifampin resistance. No additional drug susceptibility testing occurred during diagnosis. The case-patient reported no previous TB history. He had also newly tested positive for HIV at the time of TB diagnosis and had a CD4+ T-cell count of 117 cells/mm³, reflective of advanced HIV-associated immunosuppression. The case-patient completed the 6-month rifampin-containing regimen 2HRZ(E)/4HR and concurrently started antiretroviral therapy of tenofovir disoproxil, lamivudine, and dolutegravir. His

TB signs and symptoms resolved; sputum smear tests became negative, and by February 2022, treatment was successfully completed (Figure).

At time of TB diagnosis, the patient joined an ongoing genomic TB epidemiology study (<https://reporter.nih.gov/project-details/10327709>) involving whole-genome sequencing (WGS) of MTBC strains obtained from sputum cultures from TB-diagnosed persons in Botswana study clinics. We performed WGS using Illumina NextSeq 500/2000 (<https://www.illumina.com>) and analyzed data using MTBseq (https://github.com/ngs-fzb/MTBseq_source), as described elsewhere (5). We used variable single-nucleotide polymorphism alignments of MTBC genomes to generate the maximum likelihood phylogeny in IQ-TREE version 1.6.12 (6).

Our October 2022 analysis found that the patient carried a lineage 4.3.3 MTBC strain with the *rpoB* I491F mutation, causing rifampin resistance not detected by Xpert MTB/RIF (3,7). Moreover, WGS identified the MTBC strain as pre-extensively drug-resistant (pre-XDR), with resistance to isoniazid, ethambutol, pyrazinamide, moxifloxacin, and levofloxacin. Among the 165 study participants enrolled during 2021–2022, no

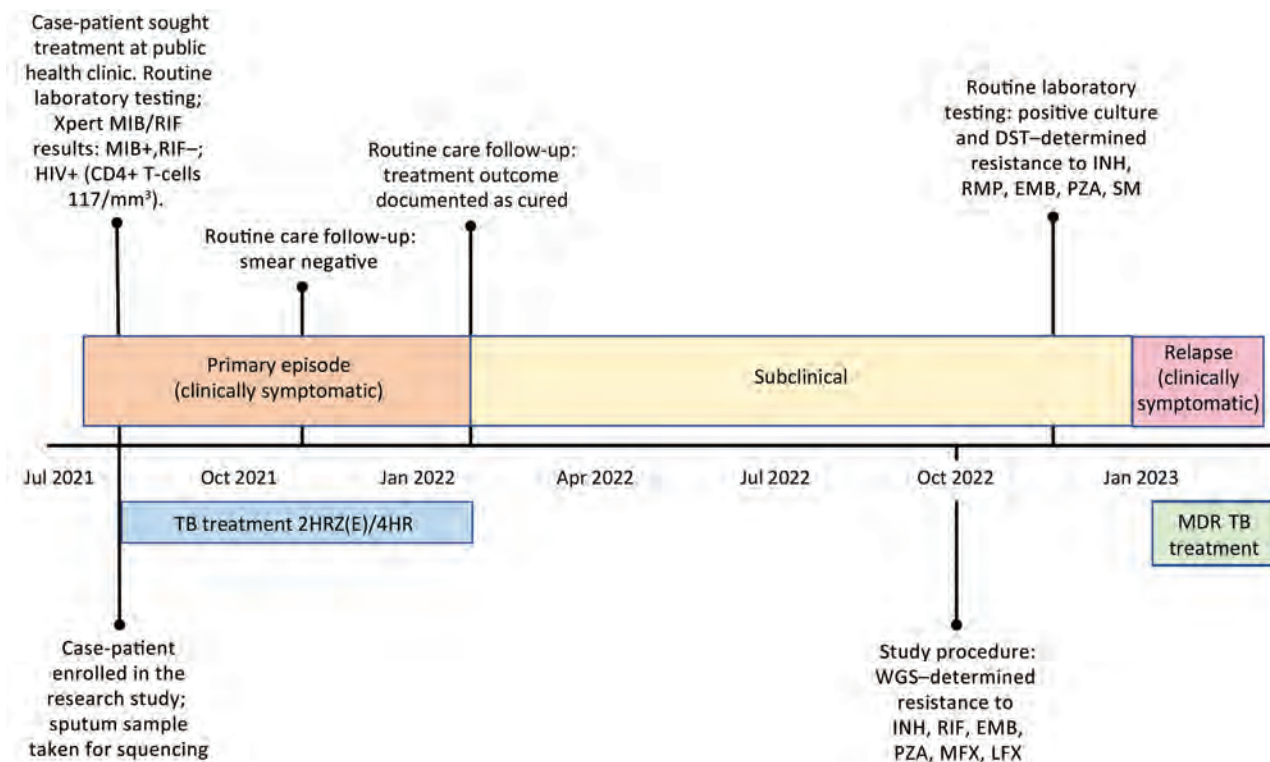


Figure. Timeline of events experienced by case-patient in Botswana from study of a rifampin-resistant TB variant not detectable using Xpert MTB/RIF assay (Cepheid, <https://www.cepheid.com>). Timeline events included routine laboratory procedures, study procedures, and timing of TB treatment. 2HRZ(E)/4HR, standard 6-month tuberculosis treatment regimen (2 months of isoniazid, rifampin and pyrazinamide, with or without ethambutol, followed by 4 months of isoniazid and rifampin); DST, drug susceptibility testing; EMB, ethambutol; INH, isoniazid; LFX, levofloxacin; MDR TB, multidrug-resistant tuberculosis; MFX, moxifloxacin; PZA, pyrazinamide; RMP, rifampin; SM, streptomycin; TB, tuberculosis; WGS, whole-genome sequencing; Xpert, GeneXpert.

other cases were found for which the isolated genome clustered with the MTBC strain from the case-patient. However, examining MTBC sequences from a previous study (8) revealed a clinical MTBC strain, BTB-2087, collected in 2016, in which the genome differed from the present strain, BTC-36, by only 5 single-nucleotide polymorphisms, suggesting that the 2 infections were part of a transmission chain in Botswana that has lasted for ≥ 5 years (Appendix Figure). We identified no epidemiologic links between the 2 persons.

MTBC strains with the *rpoB* I491F mutation have been previously documented in South Africa and Eswatini, and in Eswatini, they constituted $>60\%$ of MDR strains (3,4,7). Of interest, the 2 *rpoB* I491F strains in our study belonged to a different MTBC sublineage (4.3.3) than *rpoB* I491F strains previously identified in Eswatini (4.4.1.1) and South Africa (4.1.1.3), pointing toward convergent evolution and selection of strains that escape diagnosis in the region (3,4).

A public health investigation conducted in November 2022 found that the case-patient remained asymptomatic but was culture positive for MTBC on *Mycobacteria* growth indicator tube 960 medium (Becton Dickinson; <https://www.bd.com>). Drug susceptibility testing indicated resistance to isoniazid, rifampin, pyrazinamide, and fluoroquinolones. We tested 5 members of the patient's household with Xpert MTB/RIF and identified no additional TB cases. In January 2023, the case-patient developed TB symptoms and was placed on an individualized pre-XDR TB treatment of cycloserine, clofazimine, linezolid, bedaquiline, delamanid, pyridoxine, and para-aminosalicylic acid. No mutations linked to bedaquiline and clofazimine resistance were detected. We are conducting additional investigations to explore the extent of the outbreak of undetected MTBC strains.

This case demonstrates the clinical and public health utility of whole-genome sequencing for detecting TB drug resistance missed by conventional molecular tests. Of note, failing to detect the patient's pre-XDR TB resulted in ineffective initial treatment and potentially over a year of infectious TB. Early MDR TB detection could have led to effective initial treatment and reduced the risk of onward transmission. Currently, prevalence of MTBC strains harboring *rpoB* I491F mutation is unknown. Incorporating sequencing into a national TB drug resistance survey and continuing efforts to improve sequencing-based surveillance of drug-resistant TB in Botswana could shed light on the prevalence of MTBC strains harboring the *rpoB* I491F mutation. Those data could be used to inform updates to TB diagnostic guidelines.

In conclusion, our study highlights the utility

of WGS for identifying TB outbreaks and informing public health actions in high-TB burden countries. That approach supports the World Health Organization's recent strategic guidelines for rapidly communicating results from targeted next-generation sequencing combined with conventional tests to inform TB treatment decisions (9). Although Botswana has had remarkable success in improving HIV management, persons not adequately reached by the HIV care system remain at elevated risk of developing TB, including drug-resistant forms (10). Additional efforts are needed to ensure that high-quality HIV and TB care are delivered to underserved communities.

Acknowledgment

We acknowledge the contributions of study participants and the research team involved in data collection who made our study possible.

This work was supported by funding from the National Institute of Allergy and Infectious Diseases (R01AI147336).

About the Author

Dr. Modongo is a physician and the executive director at Victus Global Botswana Organisation in Gaborone, Botswana. Her primary research interests relate to TB and HIV, in particular drug-resistant and complicated TB and TB with adverse effects secondary to HIV or TB drugs.

References

1. Lawn SD, Nicol MP. Xpert® MTB/RIF assay: development, evaluation and implementation of a new rapid molecular diagnostic for tuberculosis and rifampicin resistance. *Future Microbiol*. 2011;6:1067–82. <https://doi.org/10.2217/fmb.11.84>
2. Ismail N, Nathanson C-M, Zignol M, Kasaeva T. Achieving universal access to rapid tuberculosis diagnostics. *BMJ Glob Health*. 2023;8:e012666. <https://doi.org/10.1136/bmjgh-2023-012666>
3. Sanchez-Padilla E, Merker M, Beckert P, Jochims F, Dlamini T, Kahn P, et al. Detection of drug-resistant tuberculosis by Xpert MTB/RIF in Swaziland. *N Engl J Med*. 2015;372:1181–2. <https://doi.org/10.1056/NEJMc1413930>
4. Makhado NA, Matabane E, Faccin M, Pinçon C, Jouet A, Boutachkourt F, et al. Outbreak of multidrug-resistant tuberculosis in South Africa undetected by WHO-endorsed commercial tests: an observational study. *Lancet Infect Dis*. 2018;18:1350–9. [https://doi.org/10.1016/S1473-3099\(18\)30496-1](https://doi.org/10.1016/S1473-3099(18)30496-1)
5. Kohl TA, Utpatel C, Schleusener V, De Filippo MR, Beckert P, Cirillo DM, et al. MTBseq: a comprehensive pipeline for whole genome sequence analysis of *Mycobacterium tuberculosis* complex isolates. *PeerJ*. 2018; 6:e5895. <https://doi.org/10.7717/peerj.5895>
6. Nguyen L-T, Schmidt HA, von Haeseler A, Minh BQ. IQ-TREE: a fast and effective stochastic algorithm for estimating maximum-likelihood phylogenies. *Mol Biol Evol*.

- 2015;32:268–74. <https://doi.org/10.1093/molbev/msu300>
7. Beckert P, Sanchez-Padilla E, Merker M, Dreyer V, Kohl TA, Utpatel C, et al. MDR M. tuberculosis outbreak clone in Eswatini missed by Xpert has elevated bedaquiline resistance dated to the pre-treatment era. *Genome Med.* 2020;12:104. <https://doi.org/10.1186/s13073-020-00793-8>
 8. Zetola NM, Moonan PK, Click E, Oeltmann JE, Basotli J, Wen X-J, et al. Population-based geospatial and molecular epidemiologic study of tuberculosis transmission dynamics, Botswana, 2012–2016. *Emerg Infect Dis.* 2021;27:835–44. <https://doi.org/10.3201/eid2703.203840>
 9. World Health Organization. Use of targeted next-generation sequencing to detect drug-resistant tuberculosis [cited 2023 Aug 22]. <https://www.who.int/publications/i/item/9789240076372>
 10. Thornton J. Botswana's HIV/AIDS success. *Lancet.* 2022; 400:480–1. [https://doi.org/10.1016/S0140-6736\(22\)01523-9](https://doi.org/10.1016/S0140-6736(22)01523-9)

Address for correspondence: Sanghyuk S. Shin, Sue and Bill Gross School of Nursing, UCI Infectious Disease Science Initiative, University of California, Irvine, 854 Health Science Quad, Irvine, CA 92697 USA; email: ssshin2@uci.edu

Scedosporium Infection in Recipients of Kidney Transplants from Deceased Near-Drowning Donor

Devprakash Choudhary, Harsimran Kaur, Vanji Nathan Subramani, Smita Pattanaik, Shivakumar S. Patil, Jasmine Sethi, Manharpreet Kaur, Priya Sreenivasan, Sheetal Thakur, Parul Gupta, Arvind Sekar, Sarbpreet Singh, Muralidharan Jayashree, Deepesh Kenwar, Shivaprakash M. Rudramurthy, Ashish Sharma

Author affiliation: Postgraduate Institute of Medical Education and Research, Chandigarh, India

DOI: <https://doi.org/10.3201/eid2911.231000>

Scedosporium aurianticum infection developed in 2 recipients of kidney transplants in India, acquired from the same deceased near-drowning donor. Given the substantial risk for death associated with *Scedosporium* infection among solid-organ transplant recipients, safety protocols for organ transplantation from nearly drowned donors should be thoroughly reevaluated and refined.

Drowning causes 236,000 deaths annually worldwide and is the third leading cause of accidental child death (1). Hospitalization from near-drowning occurs 2–20 times more frequently than fatal drownings (2). Near-drowning can result in *Scedosporium* spp. fungal infection, which causes pneumonia with a high mortality rate among nearly drowned children and young adults (2). Detecting *Scedosporium* in deceased persons is challenging, and infections thus often remain undetected. Because donor-derived *Scedosporium* infections (DDSI) from nearly drowned donors (NDD) have been linked to substantial allograft loss and increased risk for death among kidney transplant recipients (3–6), undetected *Scedosporium* poses a substantial concern when considering that person for organ donation.

We report on 2 kidney transplant recipients from an NDD, probably infected with *Scedosporium aurianticum*. The Postgraduate Institute of Medical Education and Research ethics committee approved the study. We obtained informed consent from both case-patients to ensure understanding and voluntary participation.

A 2-year-old girl weighing 15 kg was admitted to hospital with hypoxic ischemic encephalopathy and respiratory distress after a nonfatal near-drowning experience in a water tank. Her fever persisted despite antimicrobial treatment for suspected pneumonia but resolved after subsequent liposomal amphotericin B therapy. The girl was declared brain dead after 2 weeks of hospitalization, and her kidneys were retrieved for transplantation (Appendix, <https://wwwnc.cdc.gov/EID/article/29/11/23-1000-App1.pdf>).

Recipient 1, a 42-year-old woman, received 1 kidney from the deceased NDD. However, 10 days after the procedure, thrombosis developed in the graft renal artery, necessitating a graft nephrectomy. The allograft exhibited septate fungal hyphae, and grew *Scedosporium* on culture (Figure). She received a 6-month course of voriconazole and remained symptom-free on hemodialysis while awaiting a second transplant. (Appendix).

Recipient 2, a 23-year-old woman who received the other kidney from the same NDD, developed high-grade fever 3 days after transplantation. We suspected fungal infection on the basis of high β -D-glucan despite sterile blood cultures and initiated liposomal amphotericin B therapy. However, after we identified *S. aurianticum* infection in the first recipient, we switched the second patient's treatment to voriconazole. We briefly halted voriconazole therapy because of a period of elevated liver enzymes, during which the patient experienced occasional headaches and swelling developed in her left leg. The aspirate from the swelling revealed

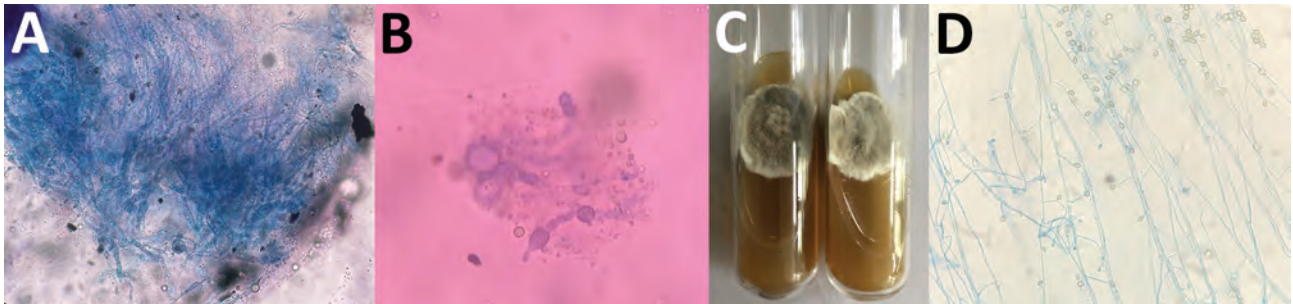


Figure. Testing for *Scedosporium aurianticum* infection in 2 recipients of kidney transplants from deceased near-drowning donor, India. A, B) Potassium hydroxide mount of renal allograft tissue from transplant recipient 1 (A) and skin biopsy from transplant recipient 2 (B) showing septate hyphae. C) Culture on Sabouraud dextrose agar showing a greyish-white colony of *S. aurianticum* from recipients 1 (left) and 2 (right) D) Lactophenol cotton blue mount from a culture from recipient 1 showing smooth-walled sessile conidia on cylindrical or flask-shaped conidiogenous cells.

S. aurianticum mold (Figure), and amplified fragment-length polymorphism molecular typing (Appendix Figure 2) suggested a likely acquisition by kidney donor. After recipient 2 resumed voriconazole therapy, her swelling resolved, and she remained well with stable graft function 12 months after the kidney transplant (Appendix Figure 1).

Donor-derived infection occurs in 0.2%–1.7% of solid organ transplant recipients (7). However, because of the unique characteristics of drowning, ubiquitous fungi of genus *Scedosporium* can permeate the donor's respiratory system, increasing risk of transmission to transplant recipients. We searched transplant literature for additional accounts of probable DDSI cases on the basis of the uniform definition of donor-derived infections from a NDD (7). DDSI from NDD poses an unusually heightened risk of death among solid organ transplant recipients (3–6). Consequently, transplant centers remain cautious about considering organs from NDDs (8).

Scedosporium has emerged as the predominant fungal pathogen causing pneumonia after near-drowning events (2). The International Society for Human and Animal Mycology (<https://www.ish-am.org>) recently introduced a distinct category for fatal cerebral infections after near-drowning incidents linked to *Scedosporium*, which has been documented to precipitate potentially fatal disseminated infections in 70% of immunocompetent and 100% of immunocompromised hosts (9). Addressing *Scedosporium* infection is particularly challenging because of its inherent antifungal resistance, propensity for rapid spread (notably from the lungs to the central nervous system), limited sensitivity of culture based methods, and relatively slow growth of cultured isolates compared to other common saprophytic molds. Those factors collectively lead to delayed diagnoses,

elevated therapeutic failures, and increased relapse rates (10).

The risk of infection transmission during drowning events is influenced by several factors, including the type of drowning. Dry drowning, in which the airways close due to spasms without fluid inhalation to the lungs, often results in better outcomes compared with other types. Water temperature also plays a role; cooler temperatures are often linked to more favorable results. Other considerations affecting risk include volume of aspirated water; occurrence of gastric aspiration, which can harm pulmonary epithelial barriers; and specifics of the drowning location, such as water depth, with shallow water presenting a higher risk (2,8).

Although the Disease Transmission Advisory Committee of the Organ Procurement and Transplant Network/United Network for Organ Sharing (<https://unos.org>) has been operational for more than a decade, specific risk factors for DDSI transmission from NDDs have not yet been defined. The passive reporting system used by the Disease Transmission Advisory Committee and frequent omissions of crucial NDD data in donor medical records impede comprehensive understanding of DDSI transmission risks (7). Furthermore, identifying DDSI from NDDs before transmission poses substantial challenges, such as selecting effective and accurate detection methods and determining the samples needed for testing and optimal time for collection.

Routine PCR screening of organs from NDDs for fungi would ensure accurate identification, timely detection, prompt management, and well-informed decision-making. In addition, uniform international guidelines regarding use of organs from NDDs are needed to address critical technical and procedural issues essential for mitigating risk for DDSI transmission.

About the Author

Dr. Choudhary is a distinguished alumnus of PGIMER Chandigarh's Renal Transplant Surgery Department. His primary interests include integrating a holistic, patient-centered philosophy into patient care in transplantation medicine.

References

1. United Nations. World Drowning Prevention Day [cited 2023 Sep 16]. <https://www.un.org/en/observances/drowning-prevention-day>
2. Katragkou A, Dotis J, Kotsiou M, Tamiolaki M, Roilides E. *Scedosporium apiospermum* infection after near-drowning. *Mycoses*. 2007;50:412-21. <https://doi.org/10.1111/j.1439-0507.2007.01388.x>
3. Wu K, Annambhotla P, Free RJ, Ritter JM, Leitgeb B, Jackson BR, et al. Fatal invasive mold infections after transplantation of organs recovered from drowned donors, United States, 2011-2021. *Emerg Infect Dis*. 2023;29:1455-8.
4. Kim SH, Ha YE, Youn JC, Park JS, Sung H, Kim MN, et al. Fatal scedosporiosis in multiple solid organ allografts transmitted from a nearly-drowned donor. *Am J Transplant*. 2015;15:833-40. <https://doi.org/10.1111/ajt.13008>
5. van der Vliet JA, Tidow G, Kootstra G, van Saene HFK, Krom RAF, Sloof MJ, et al. Transplantation of contaminated organs. *Br J Surg*. 1980;67:596-8. <https://doi.org/10.1002/bjs.1800670822>
6. Leek R, Aldag E, Nadeem I, Gunabushanam V, Sahajpal A, Kramer DJ, et al. Scedosporiosis in a combined kidney and liver transplant recipient: a case report of possible transmission from a near-drowning donor. *Case Rep Transplant*. 2016;2016:1879529. <https://doi.org/10.1155/2016/1879529>
7. Wolfe CR, Ison MG; AST Infectious Diseases Community of Practice. Donor-derived infections: guidelines from the American Society of Transplantation Infectious Diseases Community of Practice. *Clin Transplant*. 2019;33:e13547. <https://doi.org/10.1111/ctr.13547>
8. Pasupneti S, Patel K, Mooney JJ, Chhatwani L, Dhillon G, Weill D. Lung transplantation following death by drowning: a review of the current literature. *Clin Transplant*. 2016;30:1195-7. <https://doi.org/10.1111/ctr.12822>
9. Ramirez-Garcia A, Pellon A, Rementeria A, Buldain I, Barreto-Bergter E, Rollin-Pinheiro R, et al. *Scedosporium* and *Lomentospora*: an updated overview of underrated opportunists. *Med Mycol*. 2018;56(suppl_1):102-25. <https://doi.org/10.1093/mmy/myx113>
10. Hoenigl M, Salmanton-García J, Walsh TJ, Nucci M, Neoh CF, Jenks JD, et al. Global guideline for the diagnosis and management of rare mould infections: an initiative of the European Confederation of Medical Mycology in cooperation with the International Society for Human and Animal Mycology and the American Society for Microbiology. *Lancet Infect Dis*. 2021;21:e246-57. [https://doi.org/10.1016/S1473-3099\(20\)30784-2](https://doi.org/10.1016/S1473-3099(20)30784-2)

Address for correspondence: Shivaprakash M. Rudramurthy, WHO Collaborating Center and Center of Advanced Research in Medical Mycology, National Culture Collection of Pathogenic Fungi, Department of Medical Microbiology, Postgraduate Institute of Medical Education and Research, Chandigarh 160012, India; email: mrshivprakash@yahoo.com, mrshivprakash@gmail.com; Shivakumar S. Patil, Department of Renal Transplant Surgery, Postgraduate Institute of Medical Education and Research, Chandigarh 160012, India; email: drshivpgi@gmail.com

Investigation of Possible Link between Interferon- α and Lyme Disease

Armin Alaedini, Mary K. Crow, Brian A. Fallon, Elzbieta Jacek, Gary P. Wormser

Author affiliations: Columbia University, New York, New York, USA (A. Alaedini, B.A. Fallon); New York Medical College, Valhalla, New York, USA (A. Alaedini, G.P. Wormser); Hospital for Special Surgery, New York (M.K. Crow); The New York State Psychiatric Institute, New York (B.A. Fallon); Lehigh Valley Health Network, Allentown, Pennsylvania, USA (E. Jacek)

DOI: <http://doi.org/10.3201/eid2911.230839>

To the Editor: We were intrigued by Hernandez et al.'s recent important study linking persistent subjective symptoms after Lyme neuroborreliosis in Europe with increased interferon (IFN) α levels in blood (1). Their findings align with our earlier study in the United States, which showed an association between persistent objective neurocognitive deficits, despite antibiotic treatment for Lyme disease, and elevated blood IFN- α activity (2). In our study, we decided to evaluate the potential role of IFN- α in this particular group of patients with posttreatment Lyme disease symptoms (PTLDS), based on the extensive animal and human data that connect IFN- α with adverse cognitive, neuropsychiatric, and behavioral manifestations.

A noteworthy difference between the 2 studies is the method of IFN- α detection. Hernandez et al. (1) relied on a bead-based immunoassay to directly measure IFN- α levels, whereas we used a functional cell-based assay and quantitative real-time PCR to assess IFN- α activity (2,3). Direct quantitation of IFN- α can be challenging, as highlighted by the fact that concentrations for some study participants in the Hernandez et al. article appeared to fall below the limit of quantitation, thus complicating the analysis and interpretation of the data. However, newer ultrasensitive assays recently made available might be useful in detecting even very low concentrations of IFN- α in controls and in patients with PTLDS (4).

The observations linking PTLDS with increased IFN- α strengthen the growing evidence for the involvement of innate and adaptive immune-mediated

pathways in post-Lyme disease sequela. Future studies can use newer ultrasensitive assays for IFN- α detection and be extended to include a more diverse population of persons with PTLDS, including those without a history of neuroborreliosis and those without cognitive dysfunction (5). The findings might have important implications for establishing biomarkers and even for potentially finding effective therapies for PTLDS, with possible relevance to other post-infection conditions.

A.A. reports participation on advisory boards for the National Institutes of Health, Global Lyme Alliance, Roche, Everlywell, and Veravas; he is founder and director of Gut-Immune Research Group. M.K.C. reports serving as a consultant for AMPEL BioSolutions, AstraZeneca, Bristol Myers Squibb, GlaxoSmithKline, and Lilly; she holds a research grant from Gilead Sciences. G.P.W. reports receiving research grants from Biopeptides, Corp., and Pfizer, Inc. He has been an expert witness in malpractice cases involving Lyme disease and babesiosis and is an unpaid board member of the nonprofit American Lyme Disease Foundation. Other authors report no disclosures.

References

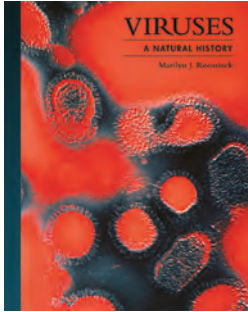
- Hernández SA, Ogrinc K, Korva M, Kastrin A, Bogovič P, Rojko T, et al. Association of persistent symptoms after Lyme neuroborreliosis and increased levels of interferon- α in blood. *Emerg Infect Dis*. 2023;29:1091–101. <https://doi.org/10.3201/eid2906.221685>
- Jacek E, Fallon BA, Chandra A, Crow MK, Wormser GP, Alaedini A. Increased IFN α activity and differential antibody response in patients with a history of Lyme disease and persistent cognitive deficits. *J Neuroimmunol*. 2013;255:85–91. <https://doi.org/10.1016/j.jneuroim.2012.10.011>
- Hua J, Kirou K, Lee C, Crow MK. Functional assay of type I interferon in systemic lupus erythematosus plasma and association with anti-RNA binding protein autoantibodies. *Arthritis Rheum*. 2006;54:1906–16. <https://doi.org/10.1002/art.21890>
- Rodero MP, Decalf J, Bondet V, Hunt D, Rice GI, Werneke S, et al. Detection of interferon alpha protein reveals differential levels and cellular sources in disease. *J Exp Med*. 2017;214:1547–55. <https://doi.org/10.1084/jem.20161451>
- Kaplan RF, Trevino RP, Johnson GM, Levy L, Dornbush R, Hu LT, et al. Cognitive function in post-treatment Lyme disease: do additional antibiotics help? *Neurology*. 2003;60:1916–22. <https://doi.org/10.1212/01.WNL.0000068030.26992.25>

Address for correspondence: Armin Alaedini, Columbia University Irving Medical Center; 1130 Saint Nicholas Ave., New York, NY 10032, USA; email: aa819@columbia.edu

Viruses: A Natural History

Marilyn J. Roossinck; Princeton University Press, Princeton, New Jersey, USA, 2023; ISBN-10: 069123759X; ISBN-13: 978-0691237596; Pages: 288; Price: US \$35.00 (hardcover)

Because of the COVID-19 pandemic that claimed ≈ 7 million lives worldwide, it is easy to lose sight of the great variety and many roles of viruses in the world and just view them as sinister agents of disease. Fortunately, Dr. Marilyn Roossinck, professor emerita of virus ecology at Pennsylvania State University, is here to restore our perspective and redress the balance in *Viruses: A Natural History*. Clearly, viral diseases often have the most dramatic effects and receive the greatest attention, and Dr. Roossinck does not neglect them. However, she elegantly demonstrates that viruses are far more than causes of disease. Viruses are enormously varied and indispensable to our global ecology; they drive many essential biological processes, including maintaining the carbon cycle in the oceans. She notes that many, perhaps most, viruses do not cause observable disease in their hosts and addresses the often asked question of whether viruses can be beneficial, providing examples of benefits. Many other aspects of the virus universe are explored by using clear prose and stunning graphics.



The stunning graphic design is one of the outstanding features of the book, and, although it might cause distraction, I think it is a powerful way to engage the reader. The illustrated vignettes are also a way to begin for persons who prefer to wade into the material more gradually before plunging into deeper technical details. The graphic design is carried throughout the 9 sections of the book: Introduction, The Depth and Breadth of Viruses, Viruses Making More Viruses, How Viruses Get Around, Evolution, The Battle Between Viruses and Hosts, Viruses in

Ecosystem Balance, The Good Viruses, and The Pathogens. Dr. Roossinck considers whether viruses have colors, setting the stage for the visually impressive graphics to come, many of which are false-color representations of virus structures. Whether viruses have color is also a preview of the thought-provoking points she brings up along the way. Given Dr. Roossinck's background as a plant virologist, the plant kingdom receives its share of attention, as do viruses of bacteria, archaea, and fungi.

This is not your conventional virology textbook, although the reader does get a solid foundation in virology. I would recommend it especially for students, young adults, and curious general readers, but nuggets of information are there for even the seasoned virologist. For example, RNA viruses, so common and concerning in eukaryotes, oddly seem exceedingly rare in prokaryotes, notwithstanding greater diversity and evolutionary history. A virus might even have been responsible for our own existence; placental mammals might have evolved through integration of an endogenous retrovirus gene (actually a gene family). Speak of a virus changing the world!

The integration of arresting images and text, especially technical detail, is always a challenge and works better in some places than others. The book ends rather abruptly with a vignette of African swine fever virus and might have benefited from a concluding section. However, those are small quibbles for a book that offers us a rare portal into the complexity and subtlety of the world of viruses.

Stephen S. Morse

Author affiliation: Columbia University Mailman School of Public Health, New York, New York, USA

DOI: <https://doi.org/10.3201/eid2911.231225>

Address for correspondence: Stephen S. Morse, Department of Epidemiology, Columbia University Mailman School of Public Health, 722 W 168th St, New York, NY 10032, USA; email: ssm20@columbia.edu

Correction: Vol. 29, No. 3

The author order was incorrect in Multicenter Retrospective Study of Vascular Infections and Endocarditis Caused by *Campylobacter* spp., France (Tinéz C et al.). The article has been corrected online (https://wwwnc.cdc.gov/eid/article/29/3/22-1417_article).



Ralph Steadman (1936–) *Viral Menace*, 2020 (detail). Water, ink, and paint on paper, 35.25 in x 24.5 in/89.5 cm x 62.23 cm.
© Ralph Steadman Art Collections Ltd. Maidstone, Kent, England.

A Turbulent Cloud, a Viral Menace

Byron Breedlove

A passage from the biographical information on the Ralph Steadman Art Collection website for the British artist and illustrator is revealing. “One of Ralph’s favourite pastimes growing up was to make model aeroplanes. He would rush home from school and would always complete any outstanding homework before allowing himself to indulge in his hobby. This work ethic has remained with him and later, when he began working with Hunter S. Thompson, would lead to no end of irritation to his tall, trans-Atlantic

friend when Ralph would often have completed his drawings before Hunter had written a word.”

After publication of their best known collaboration, *Fear and Loathing in Las Vegas* (first published as a two-part article in Rolling Stone magazine in 1971 and then as a book in 1972), Steadman and Thompson (who was an American journalist and writer who became a counterculture icon) were together catapulted into the popular zeitgeist. A short biographical note on the Tate Museum website states that Steadman “is a British illustrator best known for his collaboration with the American writer Hunter S. Thompson.”

However, Steadman’s voluminous portfolio reveals a restless creativity extending well beyond his

Author affiliation: Centers for Disease Control and Prevention, Atlanta, Georgia, USA

DOI: <https://doi.org/10.3201/eid2911.AC2911>

illustrations linked to Thompson's "gonzo journalism." Steadman has created political cartoons for various magazines; scathing caricatures of politicians; British postal stamps; product labels; artwork for album, CD, and DVD covers; and a pair of books on what he calls "boids" (one depicting extinct birds and the other endangered ones). He also illustrated many other books, including a 1967 edition of *Alice in Wonderland* and an out-of-print (in English) 1995 edition of *Animal Farm*.

Steadman himself is the subject of the 2012 documentary *For No Good Reason*. In her review for National Public Radio, the late film and art critic Pat Dowell wrote, "Steadman's drawings are a ferocious tangle of ink blotches and lines that famously distort but also reveal their subjects." His most recent book, *Ralph Steadman: A Life in Ink*, is a curated retrospective that spans much of his career. Steadman's website describes the 300-page book as "a pandemic project," which was started in November 2019, just before the world learned about the emergence of COVID-19, and which was completed in the fall of 2020 via the online conferencing platforms and file-sharing technologies that provided lifelines for so many people during sustained lockdowns and isolation.

Viral Menace, featured on this month's cover, comes from a small group of works labeled as Steadman's "Lockdown Portfolio" (S. Williams, Ralph Steadman Art Collection, pers. comm., 2023 Jan 23). In a review of Steadman's book from the *Guardian*, journalist Nadja Sayej wrote, "It's the very last image in the book that sums up 2020. It's a drawing called *Viral Menace*, a portrait of COVID-19. It looks like an ink-splattered demon over a sea of blood. A walking nightmare, if there ever was one."

This drawing of a so-called walking nightmare could be seen as a somewhat realistic, if unintentional, depiction of how respiratory viruses, such as SARS-CoV-2, are spread through coughing and sneezing. In a 2021 article about how airborne pathogens are transmitted, researchers Linsey C. Marr and Julian W. Tang describe "the transfer of pathogens in respiratory fluid from 1 person to another" via respiratory droplets of various sizes "emitted as part of a turbulent cloud." In Steadman's drawing, the viewer is confronted by a distorted, twisted visage, barely recognizable as human, with eyes askew and an arm extended. This central shape floats in a miasmic turbulent cloud, and the malevolent red mist dominates the lower portion of the image.

Steadman achieves this splattered effect through his "dirty water technique," as described by Sayej and others, which involves flinging the leftover water

used to clean his paintbrushes onto a clean sheet of paper and letting it dry. He then revisits the splattered paper, which at that point looks like a first pass by Jackson Pollock or an image for a Rorschach test, but it provides a jumping off point for the artist. According to Dowell, Steadman remarked, "You don't pencil in anything; you just start going and see where it leads you."

Steadman's drawing was an artistic reaction to the COVID-19 pandemic in 2020. The world is in a different place in 2023, but respiratory viruses, such as SARS-CoV-2, influenza virus, and respiratory syncytial virus, still circulate globally, causing substantial morbidity and mortality. Some populations, including older people, young children, pregnant women, and people with underlying health conditions, are more vulnerable to severe disease from those three respiratory viruses. Key public health actions to help mitigate the combined impact of those current viral menaces include vaccinations that protect against COVID-19, influenza, and respiratory syncytial virus, combined with proven nonpharmaceutical measures such as handwashing, wearing masks, and improving indoor ventilation.

Bibliography

- Centers for Disease Control and Prevention. CDC respiratory virus updates [cited 2023 Oct 5]. <https://www.cdc.gov/respiratory-viruses/whats-new/index.html>
- Centers for Disease Control and Prevention. Protect yourself from COVID-19, flu, and RSV [cited 2023 Oct 5]. <https://www.cdc.gov/respiratory-viruses/index.html>
- Dowell P. Artist Ralph Steadman: a nice man, for a pictorial assassin. [cited 2023 Sep 25] <https://www.npr.org/2014/04/27/307285367/artist-ralph-steadman-a-nice-man-for-a-pictorial-assassin>
- Marr LC, Tang JW. A paradigm shift to align transmission routes with mechanisms. *Clin Infect Dis*. 2021;73:1747-9. <https://doi.org/10.1093/cid/ciab722>
- Munkstrup C, Lomholt FK, Emborg H-D, Møller KL, Krog JS, Trebbien R, et al. Early and intense epidemic of respiratory syncytial virus (RSV) in Denmark, August to December 2022. *Euro Surveill*. 2023;28:2200937. <https://doi.org/10.2807/1560-7917.ES.2023.28.1.2200937>
- Ralph Steadman Art Collection. A life in ink—a pandemic project [cited 2023 Sep 25]. <https://www.ralphsteadman.com/news/a-life-in-ink>
- Ralph Steadman Art Collection. Ralph Steadman's biography [cited 2023 Sep 25]. <https://www.ralphsteadman.com/biography>
- Sayej N. Ralph Steadman: "We're really living in a hell of a year, aren't we?" [cited 2023 Sep 25]. <https://www.theguardian.com/books/2020/nov/24/ralph-steadman-interview-artist-book>
- Tate Museum. Ralph Steadman. [cited 2023 Sep 26]. <https://www.tate.org.uk/art/artists/ralph-steadman-1988>

Address for correspondence: Byron Breedlove, EID Journal, Centers for Disease Control and Prevention, 1600 Clifton Rd NE, Mailstop HI16-2, Atlanta, GA 30329-4027, USA; email: wbb1@cdc.gov

EMERGING INFECTIOUS DISEASES®

Upcoming Issue Zoonotic Infections

- Invasive *Nocardia* Infections across Distinct Geographic Regions, United States
- Risk Factors for Enteric Pathogen Exposure among Children in Black Belt Region of Alabama, USA
- Detection of *Anopheles stephensi* by Molecular Surveillance, Kenya
- Molecular Detection and Characterization of *Mycoplasma* spp. in Marine Mammals, Brazil
- Work Attendance with Acute Respiratory Illness Before and During the COVID-19 Pandemic, United States, 2018–2022
- Divergent Genotype of Hepatitis A Virus in Alpacas, Bolivia, 2019
- Human Lobomycosis Caused by *Paracoccidioides (Lacazia) loboi*, Panama, 2022
- Neurotropic Highly Pathogenic Avian Influenza A (H5N1) Virus in Red Foxes, Northern Germany
- Microfilaremic *Dirofilaria repens* Infection in Patient from Serbia
- Detection of African Swine Fever Virus from Wild Boar, Singapore, 2023
- Crimean-Congo Hemorrhagic Fever Virus Seropositivity among Dromedary Camels, Algeria, 2020–2021
- Zoonotic Marine Nematode Infection of Fish Products in Landlocked Country, Slovakia
- SARS-CoV-2 Variants BQ.1 and XBB.1.5 in Wastewater of Aircraft Flying from China to Denmark, 2023
- Characterization of Highly Pathogenic Avian Influenza A(H5N1) from Wild Birds, Poultry, and Mammals, Peru
- Anthropogenic Transmission of SARS-CoV-2 from Humans to Lions, Singapore, 2021
- Genome-Based Characterization of *Listeria monocytogenes*, Costa Rica
- Nonnegligible Seroprevalence and Predictors of Murine Typhus, Japan

Complete list of articles in the December issue at
<https://wwwnc.cdc.gov/eid/#issue-305>

Earning CME Credit

To obtain credit, you should first read the journal article. After reading the article, you should be able to answer the following, related, multiple-choice questions. To complete the questions (with a minimum 75% passing score) and earn continuing medical education (CME) credit, please go to <http://www.medscape.org/journal/eid>. Credit cannot be obtained for tests completed on paper, although you may use the worksheet below to keep a record of your answers.

You must be a registered user on <http://www.medscape.org>. If you are not registered on <http://www.medscape.org>, please click on the “Register” link on the right hand side of the website.

Only one answer is correct for each question. Once you successfully answer all post-test questions, you will be able to view and/or print your certificate. For questions regarding this activity, contact the accredited provider, CME@medscape.net. For technical assistance, contact CME@medscape.net. American Medical Association’s Physician’s Recognition Award (AMA PRA) credits are accepted in the US as evidence of participation in CME activities. For further information on this award, please go to <https://www.ama-assn.org>. The AMA has determined that physicians not licensed in the US who participate in this CME activity are eligible for *AMA PRA Category 1 Credits™*. Through agreements that the AMA has made with agencies in some countries, AMA PRA credit may be acceptable as evidence of participation in CME activities. If you are not licensed in the US, please complete the questions online, print the AMA PRA CME credit certificate, and present it to your national medical association for review.

Article Title

***Campylobacter fetus* Invasive Infections and Risks for Death, France, 2000–2021**

CME Questions

1. What was the most common *Campylobacter* species isolated in the current study?

- A. *C. coli*
- B. *C. fetus*
- C. *C. upsaliensis*
- D. *C. jejuni*

2. Which of the following characteristics was more associated with *C. fetus* bacteremia vs. *C. fetus* infection without bacteremia in the current study?

- A. Bacteremia was associated with higher rates of abdominal pain
- B. Bacteremia was associated with higher rates of diarrhea
- C. Bacteremia was positively associated with immunosuppression
- D. Bacteremia was associated with higher levels of C-reactive protein

3. What was the most common anatomical site of secondary localization of *C. fetus* infection in the current study?

- A. Bone and joint
- B. Vascular system
- C. Gastrointestinal tract
- D. Upper respiratory tract

4. Which of the following statements regarding the outcomes of cases of *C. fetus* infection in the current study is most accurate?

- A. Most cases were treated with quinolone antibiotics
- B. 90% of patients with *C. fetus* were treated with dual antibiotic therapy
- C. 30-day mortality was ≈30%
- D. Bacteremia was associated with a 3-fold increase in the risk for mortality in cases of *C. fetus* bacteremia vs no bacteremia

Earning CME Credit

To obtain credit, you should first read the journal article. After reading the article, you should be able to answer the following, related, multiple-choice questions. To complete the questions (with a minimum 75% passing score) and earn continuing medical education (CME) credit, please go to <http://www.medscape.org/journal/eid>. Credit cannot be obtained for tests completed on paper, although you may use the worksheet below to keep a record of your answers.

You must be a registered user on <http://www.medscape.org>. If you are not registered on <http://www.medscape.org>, please click on the "Register" link on the right hand side of the website.

Only one answer is correct for each question. Once you successfully answer all post-test questions, you will be able to view and/or print your certificate. For questions regarding this activity, contact the accredited provider, CME@medscape.net. For technical assistance, contact CME@medscape.net. American Medical Association's Physician's Recognition Award (AMA PRA) credits are accepted in the US as evidence of participation in CME activities. For further information on this award, please go to <https://www.ama-assn.org>. The AMA has determined that physicians not licensed in the US who participate in this CME activity are eligible for *AMA PRA Category 1 Credits™*. Through agreements that the AMA has made with agencies in some countries, AMA PRA credit may be acceptable as evidence of participation in CME activities. If you are not licensed in the US, please complete the questions online, print the AMA PRA CME credit certificate, and present it to your national medical association for review.

Article Title

Group A *Streptococcus* Primary Peritonitis in Children, New Zealand

CME Questions

- 1. Which one of the following statements regarding clinical characteristics of cases of group A *Streptococcus* (GAS) primary peritonitis in the current study is most accurate?**
 - A. 90% of cases of GAS primary peritonitis were boys
 - B. The median symptom duration before hospitalization was 3.5 days
 - C. Most children had a positive pharyngeal source of GAS
 - D. Most children had a positive skin source of GAS
- 2. Which one of the following statements regarding the microbiology of cases of GAS primary peritonitis in the current study is most accurate?**
 - A. 90% of cases had a positive peritoneal culture for GAS
 - B. 95% of cases had a positive peritoneal or blood culture for GAS
 - C. Most cases had positive cultures from both blood and peritoneal samples
 - D. Most cases had a positive culture for GAS at their original hospital of presentation
- 3. Which one of the following statements regarding the outcomes of cases of GAS primary peritonitis in the current study is most accurate?**
 - A. Half of cases were admitted to the pediatric intensive care unit (PICU) and required ventilation
 - B. 90% of cases met criteria for streptococcal toxic shock syndrome (STSS)
 - C. The average duration of antibiotic therapy was 10 days
 - D. The mortality rate was 20%

2024 CDC YELLOW BOOK

Health Information for
International Travel



CS 330909-P

Launch of CDC Yellow Book 2024 – A Trusted Travel Medicine Resource

CDC is pleased to announce the launch of the CDC Yellow Book 2024. The CDC Yellow Book is a source of the U.S. Government's recommendations on travel medicine and has been a trusted resource among the travel medicine community for over 50 years. Healthcare professionals can use the print and digital versions to find the most up-to-date travel medicine information to better serve their patients' healthcare needs.

The CDC Yellow Book is available in print through Oxford University Press
and online at www.cdc.gov/yellowbook.